Hahn-Meitner-Institut Berlin
in der Helmholtz-Gemeinschaft

Berlin Neutron Scattering Center

BENSC

phason

incommensurate

Ni_2MnGa

martensite - austenite

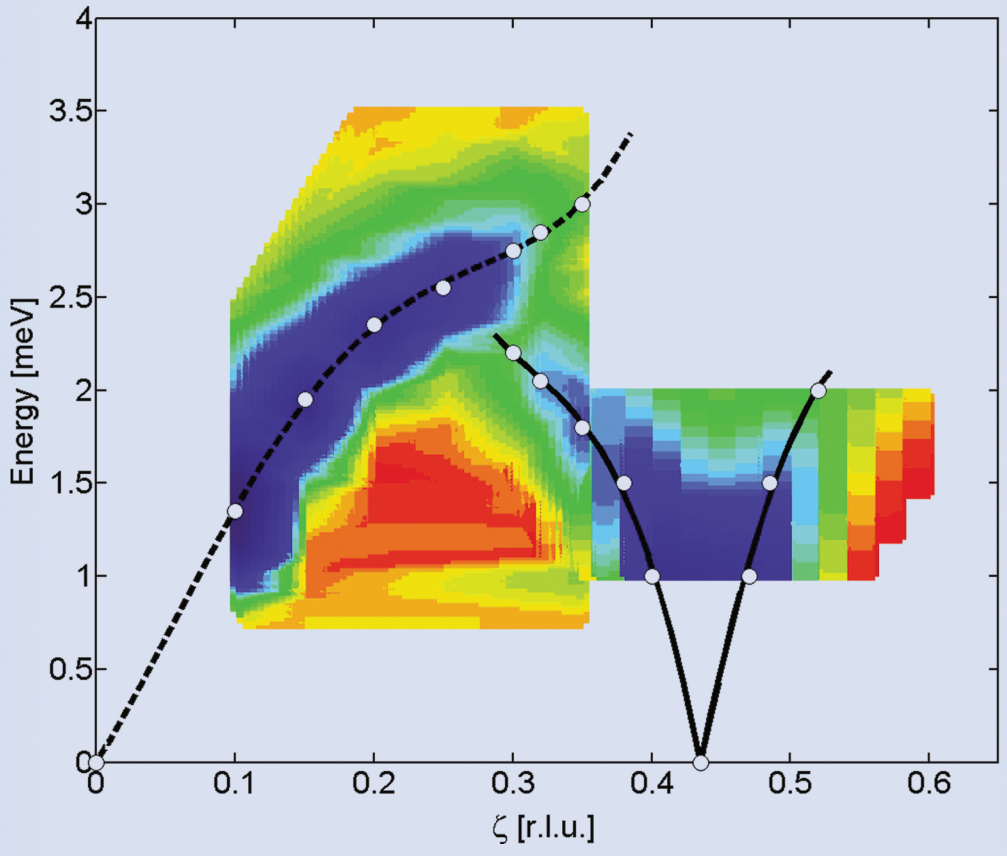

BENSC EXPERIMENTAL REPORTS 2005

BENSC
EXPERIMENTAL REPORTS
2005

edited by

K. Denzer, A. Brandt,
M. Tovar and H.A. Graf

Berlin Neutron Scattering Center
Hahn-Meitner-Institut Berlin
in der Helmholtz Gemeinschaft

Juni 2006

Berichte des Hahn-Meitner-Instituts Berlin

HMI - B 607

ISSN 0936 - 0891

Cover pictures: Phonon anomalies in the martensitic phase of Ni_2MnGa

The cover picture shows the [110] acoustic phonon dispersion in the martensite phase of the ferromagnetic shape-memory alloy Ni_2MnGa. Beside the conventional acoustic phonon branch originating from the Brillouin zone center, a phason mode is observed which is centered at an incommensurate wave vector and produced by a charge-density wave. Further details are given in the experimental report EF p. 77.

The cover was designed by *screenworks*, Leibnizstraße 59, 10629 Berlin, www.screenworks.de

---

Editorial:

The *Berlin Neutron Scattering Center* (BENSC) is a department of *the Hahn-Meitner-Institut Berlin* GmbH. BENSC develops and runs the Neutron Scattering Instruments at the Berlin Research Reactor BER II and is responsible for the service to external users.
The *Hahn-Meitner-Institut Berlin in der Helmholtz-Gemeinschaft* (HMI) is a national research institution financed by the Federal Republic of Germany and the City State of Berlin.

Address:

Berlin Neutron Scattering Center
BENSC
The Scientific Secretary
Dr. Hans-Anton Graf
Hahn-Meitner-Institut
in der Helmholtz-Gemeinschaft
Glienicker Strasse 100
D – 14109 Berlin

Phone: +49-30-8062 2778, -2304

FAX: +49-30-8062 2523

Email: bensc@hmi.de

Net: http://www.hmi.de/bensc

CONTENTS

Introduction	**IV**
List of BENSC Instruments	**VII**
How to apply for BENSC Beam Time	**XII**
Acknowledgement for Support by the European Commission	**XIII**
List of Contributed Reports	**XV**

Part I: EXPERIMENTAL REPORTS 2005

Magnetism		**1**
Magnetic Structure and Phase Transitions	1	
Magnetic Excitations	46	
Structure		**56**
Chemical Structure	56	
Structural Excitations	75	
Biology & Soft Matter		**86**
Biology	86	
Soft Matter	100	
Material Science		**115**
Structures and Phases	115	
Nanostructures	119	
Stress Analysis	130	
Cultural Heritage		**143**
Fundamental Physics and Others		**155**
Development of Instruments and Methods		**157**
BESSY		**172**

Part II: LIST OF BENSC PUBLICATIONS

Theses	**196**
Papers 2005 (and Supplement 2004, 2003, 2001)	**197**
Conference Contributions, Seminar Talks and Posters	**207**
Contributions to the BENSC Users' Meeting 2005	**220**

AUTHOR INDEX	**223**

Introduction

The present volume of the Experimental Reports gives an overview on the research performed with neutrons at BENSC during the year 2005. In addition – starting with this volume – we have also included reports on experiments performed with synchrotron radiation at the five HMI-BENSC instruments of BESSY, the Berlin Synchrotron Radiation Source. The 15 synchrotron reports included represent only a small part of the experiments performed. A complete coverage, however, is intended in the near future, when the administrative structures for incorporating the user service at these five instruments into BENSC will be fully developed.

The neutron experiments performed at BENSC are described by 173 reports - 129 from external users and 44 from BENSC staff members. The reactor was running on 194 days. Two out of 14 user instruments could not be operated in 2005 (reflectometer V6 and spin-echo spectrometer V5), because the cold neutron guide 4 had to be replaced in connection with the important upgrade project of BENSC, the “Neutron Guide Hall II”. The diffractometer E6 was not scheduled for user operation in 2005, because of severe detector problems.

BENSC User Service

BENSC is open to the national and international scientific community. About 70% of the beam time is available to external users, 30% to in-house researchers. A part of the beam time for external users (up to 20% of the total beam time of an instrument) can be given to long term collaborating groups from German universities and other research institutions, the rest (at least 50% of the total beam time) is given to short term projects via a peer-review selection process.

An up-to-date description of the BENSC neutron scattering instrumentation can be found on the BENSC webpages:

http://www.hmi.de/bensc/instrumentation/instrumentation_en.html

An updated colour-printed instrument brochure will be available on request later in 2006. It replaces the brochure HMI-B 577 from March 2001.

BENSC has an outstanding tradition in providing sample environment for extreme conditions. A special emphasis is put on high magnetic fields and low and ultra low temperatures. Sample environment for high pressures and high temperatures is equally available and presently an advanced and highly specialised instrumentation for adsorption experiments is being built up. The sample environment group has published a detailed technical handbook on the BENSC sample environment. The handbook is being updated continuously and available on the internet under

http://www.hmi.de/bensc/sample-env/index_en.html

Scientific Selection Panel

The beam-time allocation for the short-term projects is decided by the Scientific Selection Panel of BENSC which meets twice a year, in November and in May. In 2005 the Selection panel consisted of the following twelve external and two in-house members:

External members:

Dr. M. Enderle
ILL Grenoble, France

Dr. Bela Farago
ILL Grenoble, France

Dr. G. Auffermann
MPI CPfS Dresden, Germany

Dr. K. Clausen
Paul-Scherrer-Institute, Switzerland

Prof. Dr. J. Lu
UMIST, Manchester, U.K**.**

Dr. R. May
ILL Grenoble, France

Prof. Dr. K. McEwen
University College of London, U.K.

Prof. Dr. D.K. Ross
Salford University, Greater Manchester, U.K.

Prof. Dr. J. Texeira
CEA/CNRS/LLB Saclay, France

Internal members:

Prof. Dr. F. Mezei,
HMI Berlin

Prof. Dr. A. Tennant
HMI Berlin

Support for European Access to BENSC from the European Commission

Right from the beginning of the BENSC user program in 1993, the access of European research groups to BENSC was generously supported by the European Commission under framework programmes FP3, FP4, FP5 and FP6 of the European Commission - with funds for the BENSC access programme increasing from contract to contract.

The successful European Access programme of BENSC is presently continued under the 6th EU Framework Programme (FP6), however, with a slightly modified contractual situation: BENSC is now a partner in the ***Integrated Infrastructure Initiative for Neutron Scattering and Muon Spectroscopy (NMI3).*** NMI3 brings together 23 partners from 14 countries, including 11 research infrastructures, together with other interested organisations.

The most important branch of NMI3 includes 12 different Access Activities offering European users approximately 5000 beam days of access to 150 instruments at different facilities with support for travel and subsistence. Under NMI3, BENSC will provide a minimum access of 1040 instrument days, distributed over four years.

In 2005, the second year under NMI3, over 60 projects of European user groups have been completed. BENSC delivered 360 instrument days. A total of 119 users from 56 groups from 16 countries were involved. A list of the respective experimental reports included in this volume can be found on page XIII.

Since the start of NMI3, BENSC has already delivered more than 800 days for the European user community.

BENSC User Meeting 2005

The BENSC User Meeting held in September 2005 attracted more than 100 participants. One half of them came from national and foreign research institutions. 15 invited talks and 46 posters gave ample opportunity for lively discussions and scientific exchange on the latest results from experiments performed at BENSC.

New Neutron Guide Hall

The building of the new neutron guide hall II was finished end of 2004. Beginning of 2005, the multi-spectral beam extraction system replacing the old neutron guide 4 had been installed and reactor operation could start again. Further during the year 2005 the first part of the guide system for the new hall was mounted and connected to the extraction system. This novel extraction system feeds cold as well as thermal neutrons into the guide providing neutrons for the new time-of-flight diffractometer EXED. Two other guides serve for the new high resolution SANS-instrument (VSANS) which is presently constructed and for the spin-echo instrument SPAN which is shifted from the old neutron guide hall to the new one. Some pictures displayed on the following pages show the progress made in this important upgrade project of BENSC.

The “Extreme Environment Diffractometer” EXED was especially designed for investigations using the new planned 25T magnet which shall ensure the leading position of BENSC in neutron scattering experiments at high magnetic fields. In 2005 a redesign of this magnet has been launched with the objective to open up the possibility for later upgrades to even higher fields above 30 T.

HMI instruments at BESSY – new developments

To promote the complementary use of neutrons and synchrotron radiation, HMI has initiated an upgrade project for the synchrotron source BESSY including the development and installation of two new insertion devices: the undulator UE46 providing soft X-rays with worldwide highest brightness and flux density and the 7T wiggler 7T-MPW shifting the photon energies to the hard X-ray regime. HMI-BENSC has built and operates 3 beamlines with four instruments S1 – S4 at these devices and a further instrument, the X-ray tomography station S5, at a none-HMI beamline. Access to these instruments is organised via the BESSY proposal system,

http://www.bessy.de/boat/www/

while the user service is performed by HMI-BENSC personnel.

The instrument S1 at the undulator beamline is in routine user operation since 2003. In 2005 a second experimental station in addition to the spectroscopy chamber has been commissioned: a reflectometer with a magnet providing a field of 7T at the sample position. This high-field reflectometer opens up exciting new possibilities, in particular for investigating thin magnetic films and nanostructures.

Two beamlines are installed at the 7T wiggler: a monochromatic beamline providing photons with energies between 4 keV and 40 keV for the instruments S2 and S3 and a white beamline providing photons of energies up to 150 keV for the materials science instrument S4. The instrument S2 is specialised on resonant magnetic scattering and high resolution diffractometry, the instrument S3 on anomalous small-angle scattering (ASAXS) and grazing incidence scattering (GISAXS). S2 and S3 are operated alternatively at the monochromatic beamline.

The instrument S4 at the white beamline is dedicated to materials science and engineering investigations, in particular to stress analysis using energy dispersive methods. All three wiggler instruments have been commissioned in 2005. S2 and S3 are in full user operation since April 2005, S4 since beginning of 2006.

The X-ray tomography instrument S5 operated by HMI-BENSC at the 7T wavelength-shifter beamline of the Bundesanstalt für Materialprüfung (BAMline) at BESSY is in full user operation since 2004.

A detailed description of these five instruments is given in the new instrument brochure of BENSC which will be available later in 2006 and on the BENSC web pages.

Short user statistics for HMI-BENSC instruments at BESSY in 2005

	Main instrument characteristics	External groups	External beam time	In-house groups	In-house beam time
S1 at UE46	Spectroscopy / reflectometry	16	24 weeks	6	14 weeks
S2 at 7T-MPW	Res. magn. scatt. / high-resol. diffract.	5	7 weeks	3	11 weeks
S3 at 7T-MPW	ASAXS/GISAXS (commissioning)	-	-	1	4 weeks
S4 at 7T-MPW	Materials Science / stress analysis	6	10 weeks	5	6 weeks
S5 at BAM-line	Tomography	20	24 days	5	6 days

Scientific Selection Panel

The beam-time allocation for the short-term projects is decided by the Scientific Selection Panel of BENSC which meets twice a year, in November and in May. In 2005 the Selection panel consisted of the following twelve external and two in-house members:

External members:

Dr. M. Enderle
ILL Grenoble, France

Dr. Bela Farago
ILL Grenoble, France

Dr. G. Auffermann
MPI CPfS Dresden, Germany

Dr. K. Clausen
Paul-Scherrer-Institute, Switzerland

Prof. Dr. J. Lu
UMIST, Manchester, U.K**.**

Dr. R. May
ILL Grenoble, France

Prof. Dr. K. McEwen
University College of London, U.K.

Prof. Dr. D.K. Ross
Salford University, Greater Manchester, U.K.

Prof. Dr. J. Texeira
CEA/CNRS/LLB Saclay, France

Internal members:

Prof. Dr. F. Mezei,
HMI Berlin

Prof. Dr. A. Tennant
HMI Berlin

Support for European Access to BENSC from the European Commission

Right from the beginning of the BENSC user program in 1993, the access of European research groups to BENSC was generously supported by the European Commission under framework programmes FP3, FP4, FP5 and FP6 of the European Commission - with funds for the BENSC access programme increasing from contract to contract.

The successful European Access programme of BENSC is presently continued under the 6th EU Framework Programme (FP6), however, with a slightly modified contractual situation: BENSC is now a partner in the ***Integrated Infrastructure Initiative for Neutron Scattering and Muon Spectroscopy (NMI3).*** NMI3 brings together 23 partners from 14 countries, including 11 research infrastructures, together with other interested organisations. The most important branch of NMI3 includes 12 different Access Activities offering European users approximately 5000 beam days of access to 150 instruments at different facilities with support for travel and subsistence. Under NMI3, BENSC will provide a minimum access of 1040 instrument days, distributed over four years.

In 2005, the second year under NMI3, over 60 projects of European user groups have been completed. BENSC delivered 360 instrument days. A total of 119 users from 56 groups from 16 countries were involved. A list of the respective experimental reports included in this volume can be found on page XIII.

Since the start of NMI3, BENSC has already delivered more than 800 days for the European user community.

BENSC User Meeting 2005

The BENSC User Meeting held in September 2005 attracted more than 100 participants. One half of them came from national and foreign research institutions. 15 invited talks and 46 posters gave ample opportunity for lively discussions and scientific exchange on the latest results from experiments performed at BENSC.

New Neutron Guide Hall

The building of the new neutron guide hall II was finished end of 2004. Beginning of 2005, the multi-spectral beam extraction system replacing the old neutron guide 4 had been installed and reactor operation could start again. Further during the year 2005 the first part of the guide system for the new hall was mounted and connected to the extraction system. This novel extraction system feeds cold as well as thermal neutrons into the guide providing neutrons for the new time-of-flight diffractometer EXED. Two other guides serve for the new high resolution SANS-instrument (VSANS) which is presently constructed and for the spin-echo instrument SPAN which is shifted from the old neutron guide hall to the new one. Some pictures displayed on the following pages show the progress made in this important upgrade project of BENSC.

The “Extreme Environment Diffractometer” EXED was especially designed for investigations using the new planned 25T magnet which shall ensure the leading position of BENSC in neutron scattering experiments at high magnetic fields. In 2005 a redesign of this magnet has been launched with the objective to open up the possibility for later upgrades to even higher fields above 30 T.

HMI instruments at BESSY – new developments

To promote the complementary use of neutrons and synchrotron radiation, HMI has initiated an upgrade project for the synchrotron source BESSY including the development and installation of two new insertion devices: the undulator UE46 providing soft X-rays with worldwide highest brightness and flux density and the 7T wiggler 7T-MPW shifting the photon energies to the hard X-ray regime. HMI-BENSC has built and operates 3 beamlines with four instruments S1 – S4 at these devices and a further instrument, the X-ray tomography station S5, at a none-HMI beamline. Access to these instruments is organised via the BESSY proposal system,

http://www.bessy.de/boat/www/

while the user service is performed by HMI-BENSC personnel.

The instrument S1 at the undulator beamline is in routine user operation since 2003. In 2005 a second experimental station in addition to the spectroscopy chamber has been commissioned: a reflectometer with a magnet providing a field of 7T at the sample position. This high-field reflectometer opens up exciting new possibilities, in particular for investigating thin magnetic films and nanostructures.

Two beamlines are installed at the 7T wiggler: a monochromatic beamline providing photons with energies between 4 keV and 40 keV for the instruments S2 and S3 and a white beamline providing photons of energies up to 150 keV for the materials science instrument S4. The instrument S2 is specialised on resonant magnetic scattering and high resolution diffractometry, the instrument S3 on anomalous small-angle scattering (ASAXS) and grazing incidence scattering (GISAXS). S2 and S3 are operated alternatively at the monochromatic beamline. The instrument S4 at the white beamline is dedicated to materials science and engineering investigations, in particular to stress analysis using energy dispersive methods. All three wiggler instruments have been commissioned in 2005. S2 and S3 are in full user operation since April 2005, S4 since beginning of 2006.

The X-ray tomography instrument S5 operated by HMI-BENSC at the 7T wavelength-shifter beamline of the Bundesanstalt für Materialprüfung (BAMline) at BESSY is in full user operation since 2004.

A detailed description of these five instruments is given in the new instrument brochure of BENSC which will be available later in 2006 and on the BENSC web pages.

Short user statistics for HMI-BENSC instruments at BESSY in 2005

	Main instrument characteristics	External groups	External beam time	In-house groups	In-house beam time
S1 at UE46	Spectroscopy / reflectometry	16	24 weeks	6	14 weeks
S2 at 7T-MPW	Res. magn. scatt. / high-resol. diffract.	5	7 weeks	3	11 weeks
S3 at 7T-MPW	ASAXS/GISAXS (commissioning)	-	-	1	4 weeks
S4 at 7T-MPW	Materials Science / stress analysis	6	10 weeks	5	6 weeks
S5 at BAMline	Tomography	20	24 days	5	6 days

List of BENSC-Photons Instruments

Instruments at HMI-BESSY **March 2006**

N°.	Instrument	Instrument Scientists		Phone	Room
S1	UE46 - PGM Beamline for Magnetic Nanostructures and Magnetic Thin Films 6392-4717	Detlef Schmitz	(Adlershof:) (Wannsee:)	6392-5689 8062-2925	AHB 6317 A 225
		Paolo Imperia	(Adlershof:) (Wannsee:)	6392-5689 8062-3080	AHB 6317 LR 147
		Elizabeta Holub-Krappe	(Wannsee:)	8062-2557	KH 201
		Hermann Rossner	(Adlershof:) (Wannsee:)	6392-5762 8062-2914	AHB 6316 KH 203
	High Field Reflectometry option *(commissioning phase)*				
S2	7T-MPW - MagS Beamline for Resonant Magnetic Scattering and High-resolution Diffraction 6392-3163	Ralf Feyerherm	(Adlershof:) (Wannsee:)	6392-5750 8062-3082	AHB 6319 LR 139
		Esther Dudzik	(Adlershof:) (Wannsee:)	6392-5687 8062-2925	AHB 6319 A 224
		Nora Darowski	(Adlershof:) (Wannsee:)	6392-5756 8062-2400	AHB 6415 P 122
S3	ASAXS option and GISAXS option *(commissioning phase)*	Armin Hoell (SF3)	(Adlershof:) (Wannsee:)	6392-4678 8062-3181	AHB 6414 LR 214
		Ivo Zizak (SF4)	(Adlershof:) (Wannsee:)	6392-5756 8062-2400	AHB 6415 P 122
S4	7T-MPW – EDDI (white beam) Materials Science Diffractometer for Residual Stress and Texture Analysis / *BENSC-ZET* 6392-3164	Christoph Genzel	(Adlershof:) (Wannsee:)	6392-5751 8062-3097	AHB 6318 A 136
		Jens Gibmeier	(Adlershof:)	6392-5686	AHB 6315
		Ingwer Denks	(Adlershof:) (Wannsee:)	6319-5751 8062-3097	AHB 6318 A 136
S5	Tomography @ BAMline HMI Tomography set-up at the BAMline 6392-3159	Astrid Haibel	(Adlershof:) (Wannsee:)	6392-5760 8062-2507	AHB 6411 LR 239

List of BENSC-Neutrons Instruments

Instruments in the BER2 Experiment Hall (Thermal Neutrons)

N°.	Instrument	ext	Tube	Instrument Scientists	ext.	Room
E 1	Thermal 3-Axis Spectrometer with Polarization Analysi	3101	D 1N	Vadim Sikolenko	2847	LR 135
E 2	Flat-Cone- and Powder Diffractomete (/ E2 a: Neutron Photography)	3102	R 1	[Univ. Tübingen, Verbundforschung] Jens-Uwe Hoffmann Uwe Amann	2185 2708	A 241 A 239
E 3	Residual Stress Analysis and Texture Diffractomete	3103	T 2	Rainer Schneider Tobias Poeste (co-op. Uni Kassel Robert Wimpory	3096 3237 3098	A 132 A 131 A 133
E 4	2-Axis Diffractomete (/ E4a: Test Device)	3104	R 2	Karel Prokes Andrew Podlesnyak	2804 2768	LR 138 LR 144
E 5	4-Circle Diffractomete	3104	R	Manfred Reehuis (co-op. MPI-FKF Stuttgart	2692	A 343
E 6	Focusing Single Crystal Diffractomete	3105	T 4	Norbert Stüßer Anthony Arulraj	3171 2793	LR 142 LR 129
E 7	Residual Stress Analysis Diffractometer / *BENSC-ZE*	3107	D 1S	Rainer Schneider Florian Henkel	3096 3098	A 132 A 133
E 9	Fine Resolution Powder Diffractometer (FI RE PO D)	3106	T 5	Dimitri Argyriou Olexandr Prokhnenko Michael Tovar	3016 2847 2768	LR 137 LR 135 LR 144
E 10	^{3}He - Diffractometer (HELI N E)		D 1S	Konrad Siemensmeyer	2757	LS 132

Instruments in the BER2 Cold Neutron Guide Halls

N°.	Instrument	ext	Tube	Instrument Scientists	ext.	Room
V 1	Membrane Diffractometer	3121	NL 1A	Thomas Hauß (co-op. TU Darmstadt) Silvia Dante	2071 2071	LS 333 LS 333
V 2	3-Axis Spectrometer for Cold Neutrons (FLEX)	3122	NL 1B	Klaus Habicht Kirrily Rule	2807 3067	A 333 A 331
V 3	Time-of-Flight Spectrometer (NEAT)	3123	NL 2°	Margarita Russina Alexander Schnegg Alexandra Buchsteiner	3159 3073 3179	A 351 A 348 A 349
V 4	Small Angle Scattering Instrument (SANS)	3124	NL 3A	Albrecht Wiedenmann Uwe Keiderling André Heinemann Sylvain Prevost (co-op. TU Berlin)	2283 2339 2769 2339	LR 211 LR 209 LR 208 LR 209
V 5	Spin-Echo Spectrometer with Time of Flight Option (SPAN) *(open for friendly users)*	3125	NL 4B	Catherine Pappas Carlos Fehr	2046 3072	A 346 A 344
V 6	Reflectometer	2806	NL 4B	Roland Steitz Elena Maltseva (co-op. MPI KGF Golm)	2149 3077	A 221 A 223
V 7	Cold n Tomography (CONRAD)		NL 1B$_u$	Nikolay Kardjilov Andre Hilger	2298 2490	A 317 A 316
B8	n-Autoradiography	3121	NL 1A	Birgit Schröder Smeibidl Lee-Ann Mertens	2337 2292	GE 145 V 122
V 12a	Double-Crystal Diffractometer / (Tomography)	3131	NL 3B	Wolfgang Treimer (TFH Berlin) Markus Strobl (TFH Berlin)	2221 2490	A 319 A 316
V 12 b	Double-Crystal Diffractometer /Tomograph	3131	NL 3B	Wolfgang Treimer (TFH Berlin) Markus Strobl (TFH Berlin)	2221 2490	A 319 A 316
V 13	Fundamental Physics position		NL 3B	Margarita Russina	3159	A 351
V 14	Mirror Test Device		NL 1B°	Thomas Krist	2045	A 233
V 15	EXED *(under construction)*		NL 4A	Judith Peters	3068	A 336
V 16	VSANS *(under construction)*		NL 4C	Daniel Clemens	2280	V 131

Sample Environment	Michael Meißner	2204	LS 131
	Peter Smeibidl	3080	LR 147
	Sebastian Gerischer	3133	LS 113
	Klaus Kiefer	3141	LS 130

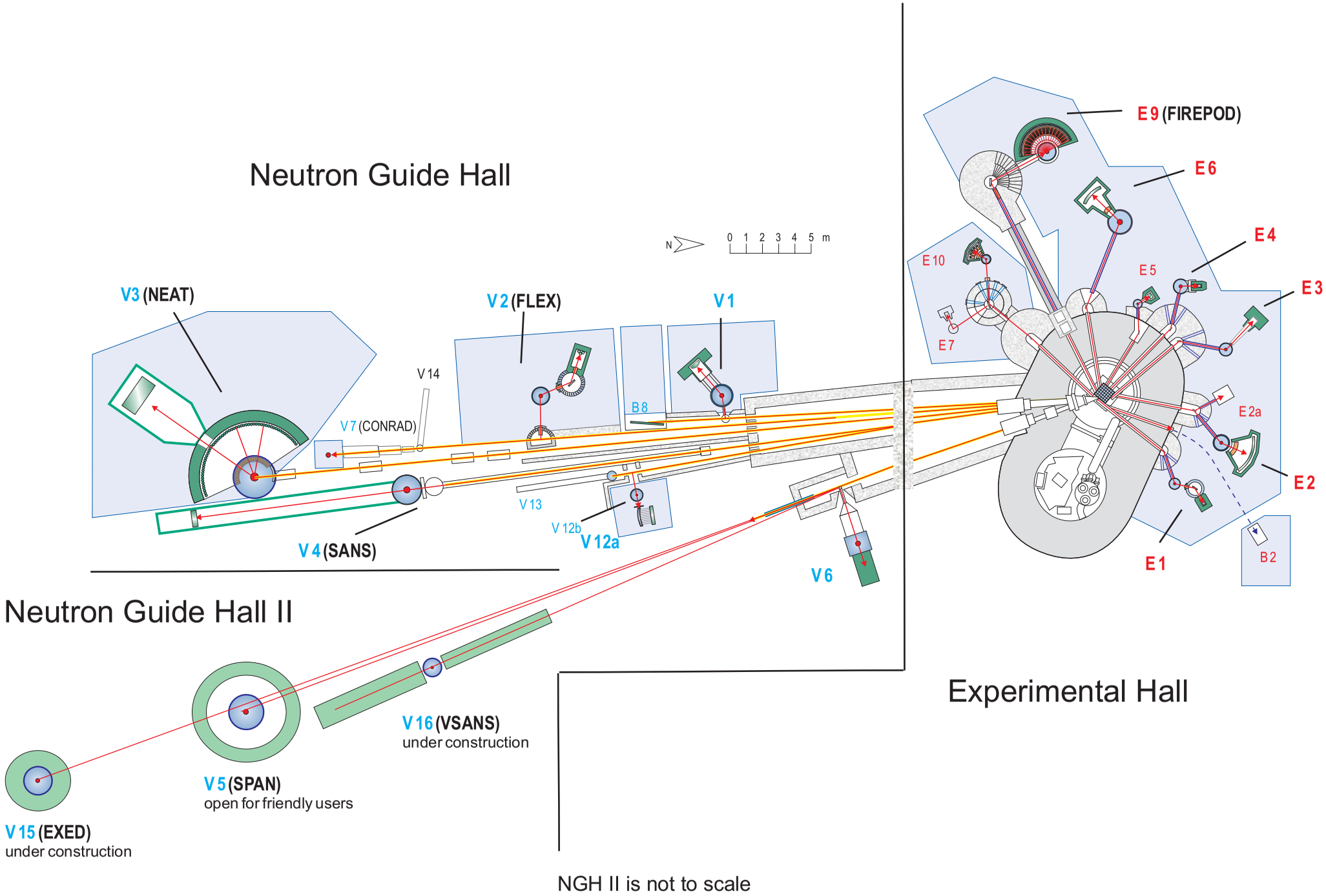
Neutron Guide Hall
N
0 1 2 3 4 5 m
V3 (NEAT)
V2 (FLEX)
V1
V14
V7 (CONRAD)
B8
V13
V12b
V12a
V4 (SANS)
V6
E9 (FIREPOD)
E6
E4
E10
E5
E3
E7
E2a
E2
E1
B2
Neutron Guide Hall II
V16 (VSANS)
under construction
V5 (SPAN)
open for friendly users
V15 (EXED)
under construction
Experimental Hall
NGH II is not to scale

News from the Instrumentation Project in Neutron Guide Hall II

By the end of 2004 important milestones for the integration of the new second neutron guide hall (NGH II) into the Berlin Neutron Scattering Center (BENSC) were reached: The building structure was completed as an extension to Neutron Guide Hall I, where experiments have been performed since 1992. Particular challenges related to this project were the deep foundation in the neighborhood of existing buildings, the unusual condition to use only hardly magnetizable reinforcement steel for this type of constructions in an area of approximately 750 m . Another problem was the opening to NGH I, where valuable instrumentation sensitive to dust is installed in a radiation protection area. The replacement of the old neutron guide elements by a conceptionally new extraction guide at a tight schedule of approximately 6 weeks was a logistical challenge, in particular because manifold technical and radiological safety requirements had to be fulfilled. An innovative design of the extraction guide are implemented at a neutron source for the first time ever. The exchange of the neutron guide was the general prerequisite to resume the highly demanded user operation at all instruments except for the three that were located on the old NL4 guide. Hence, the thermal beam ports and the experiments using cold neutrons on the remaining guides NL1–3 were operational again by January 2005.

The neutron guides leading from the reactor to the instruments in Neutron Guide Hall 2 are being installed.

In 2005, the construction and delivery of the components of the complex neutron guide system at continued operation of the neutron source made good progress. The most prominent achievement in the guide section was the completion of the common initial section which then splits into three individual guides.
The necessary biological shielding, which has the function to guarantee for safe top quality working conditions, was installed subsequently. This set the stage for successful tests and a swift resumption of the user operation of the upgraded (increased flux) neutron reflectometer at the beginning of 2006.

By the end of 2005, the infrastructure components were completed to a large extent. In the future the guest groups will cooperate with their local contacts in spacious cabins that host control units and computer equipment for the experiments.

Experimental Cabins in the Neutron Guide Hall II

The Spin Echo Spectrometer SPAN is already in its new position

Neutron choppers which will be implemented into the neutron guides will define the velocity of the neutrons before they hit the sample under investigation. Infrastructure systems required to accommodate the three big instruments in NGH II, i.e. a Very Small Neutron Scattering Instrument (VSANS) for soft matter investigations, e.g. biosytems, polymers, etc., a Wide Angle Neutron Spin Echo Spectrometer (SPAN), for the investigation of slow dynamics in matter, and a versatile Extreme Environment Diffractometer (EXED) have been prepared and the instruments have partially been installed.

It is planned to combine the EXED instrument with a 25–35 Tesla magnet, which will provide the highest magnetic field world wide available in neutron scattering techniques, strengthen the leading role of HMI in this area of research and provide exciting new information on magnetic structures.

The disc choppers will select the neutrons for the instrument EXED

By Daniel Clemens, HMI Berlin

How to Apply for BENSC-Neutrons Beam Time

BENSC is open to both the national and the international user community with up to 70% of the beam time available to external users. The main portion of this beam time is foreseen for short term research proposals. Applications for short term beam time will be examined by an international scientific selection committee twice each year,

deadlines for submission of proposals are 15 March and 15 September.

The instrument responsibles of BENSC are asked to comment on the technical feasibility of the proposed experiments and have access to the submitted proposals for this purpose.

Requests for urgent or confidential experiments (Directors's discretionary time) and for industrial use may be submitted at any time.

Applications for BENSC-Neutrons beam time should be made by using the BENSC Online Proposal Submission (OPS) system, which is available at the **BENSC VISITORS CLUB**

http://www.hmi.de/pubbin/bensc_club.pl

Further information on BENSC-Neutrons instrumentation can be obtained from the internet via

http://www.hmi.de/bensc/instrumentation/instrumentation_en.html

The latest four-colour printed version of the instrumentation brochure (HMI-B 577) was issued in March 2001 and available on request**:**

Hahn-Meitner-Institute Berlin
BENSC Guest office
Glienicker Str. 100
D - 14109 Berlin (Wannsee)
Germany
Phone +49 - 30 - 8062 2304
Fax: +49 - 30 - 8062 2523
Email: **bensc@hmi.de**

An updated version of the instrumentation brochure will be available later this year.

The BENSC Experimental Reports are intended as interim summaries. In view of the short time available between the termination of certain experiments and the deadline for this report, the results presented here have to be considered as preliminary. The inclusion of reports in this volume does not constitute a publication in the usual sense. Final results will be submitted for publication in regular scientific journals.

Acknowledgement for Support by the European Commission

The access of BENSC users from European Community Member States and Associated States to BENSC has been substantially supported by the European Community under the Framework Programme FP6.

BENSC is a partner in the EU supported network of European neutron facilities – the **Neutron and Muon Integrated Infrastructure Initiative (NMI3),** an action within the EU FP6 activity 'Structuring the European Research Area: Research Infrastructures'. NMI3 brings together 23 partners from 14 countries, including 11 research infrastructures.

The BENSC Access contract under NMI3 is effective for 4 years, from 01/2004 until 12/2007, the relevant EU contract number (NMI3) for acknowledgements is ***RII3-CT-2003-505925***

Results of EU supported groups are contained in **61** reports of this volume.

NMI3-nº	*p.*	*authors*	*affiliation*
1015	55	Alba *et al.*	LLB, CNRS-CEA, F
1051	5	Frontera *et al.*	CSIC-ICMAB Barcelona, E
1052	127	De La Prida *et al.*	Univ. Oviedo, E
1056	39	Fak *et al.*	CEA Grenoble, F
1064	101	Aliotta *et al.*	IPCF CNR Messina, I
1065	47	Moze *et al.*	Univ. Modena, I
1072	131	Ohms *et al.*	EC-JRC-IE Petten, NL
1081	6	Coldea *et al.*	Univ. Bristol, UK
1083	137	Iakoubovskii *et al.*	KU Leuven, B
1084	135	Sittner *et al.*	ASCR IP Prague, CZ
1085	20	Kamarad *et al.*	ASCR IP Prague, CZ
1087	138	Morales-Flórez *et al.*	Univ. Cádiz, E
1088	43	Herrero-Albillos *et al.*	Univ. Zaragossa, ICMA, E
1089	133	Heczko *et al.*	HUT (TKK), FIN
1091	141	U. Dahlborg *et al.*	CNRS-INPL-UHP, F
1092	108	Gummel *et al.*	CNRS-LLB Saclay, F
1093	57	Ross *et al.*	Univ. Salford, UK
1094	100	Arrighi *et al.*	HWU Edinburgh, UK
1095	73	Hall *et al.*	Univ. Strathclyde, UK
1096	110	Cosgrove *et al.*	Univ. Bristol, UK
1097	31	Gamari-Seale *et al.*	NCSR Demokritos, Athens, GR
1098	32	Pissas *et al.*	NCSR Demokritos, GR
1099	64	Christides *et al.*	Univ. Patras, GR
1100	99	Panayiotou *et al.*	AU Thessaloniki, GR
1101	95	Garab *et al.*	HAS BRC Szeged, H
1102	104	Bianco-Peled *et al.*	Technion Haifa, IL
1103	29	Moze *et al.*	Univ. Modena, I
1104	48	Moze *et al.*	Univ. Modena, I
1105	124	Baglioni *et al.*	Univ. Firenze, I
1106	105	Berti *et al.*	Univ. Firenze, I
1107	109	Paduano *et al.*	Univ. Napoli, I
1108	8	Borowiec *et al.*	PAS IP Warsaw, PL
1109	65	Wolska *et al.*	AMU Poznan, PL
1110	33	Szymczak *et al.*	PAS IP Warsaw, PL
1111	28	Wawrzynska *et al.*	Univ. Bristol, UK
1112	83	Tripadus *et al.*	NIPNE-HH Bucharest, RO
1113	136	Smrcok *et al.*	SA Bratislava, SK
1114	118	Zrnik *et al.*	TU Ko ice, SK
1115	44	Yusuf *et al.*	Univ. Zaragoza, ICMA, E
1116	67	Werner *et al.*	TU Wien, A
1117	69	Neov *et al.*	ASCR NPI Rez, CZ
1118	21	Kamarad *et al.*	ASCR IP Prague, CZ
1119	140	Strunz *et al.*	ASCR NPI Rez, CZ
1121	37	Bartolomé *et al.*	Univ. Zaragossa, ICMA, E
1123	11	Chatterji *et al.*	ILL, Grenoble, F
1124	81	Mançois *et al.*	Univ. Bordeaux, F
1125	90	Bradshaw *et al.*	Univ. Edinburgh, UK
1127	51	Rüegg *et al.*	UCL, UK
1129	91	Garab *et al.*	HAS BRC Szeged, H
1130	91	Garab *et al.*	HAS BRC Szeged, H
1131	132	Fiori *et al.*	UPM Ancona, I
1132	149	Manescu *et al.*	UPM Ancona, I
1132	153	Manescu *et al.*	UPM Ancona, I
1133	96	Cantu *et al.*	Univ. Milano, I
1134	111	Triolo *et al.*	IPCF CNR Messina, I
1136	148	Triolo *et al.*	Univ. Palermo, I
1136	150	Triolo *et al.*	Univ. Palermo, I
1136	152	Triolo *et al.*	Univ. Palermo, I
1137	151	Lo Celso *et al.*	Univ. Palermo, I
1140	129	Erne *et al.*	Univ. Utrecht, NL
1143	68	Wolska *et al.*	AMU Poznan, PL

Notice:

The quality of figures in the electronic versions, CD and WEB (http://www.hmi.de/bensc) – especially in colour presentation – is remarkably higher than in the print version

List of Contributed Experimental Reports

PAGE	TITLE	TEAM			PROPOSAL
	Magnetic Structure and Magnetic Phase Transitions				
1	**Magnetic structure of $CsCuCl_3$ at high pressures**	N. Stüßer[1] A. Hoser[2+3] R. Sadykov[4] V.V. Sikolenko[1]	[1]HMI Berlin [2]RWTH Aachen [3]FZ Jülich [4]RAS IHPP Troitsk, RU	E1	**PHY-02-0475-EF**
2	**Magnetic clusters in UPt_2Si_2**	S. Süllow[1] J. Klenke[2] A. Rupp[2]	[1]TU Braunschweig [2]HMI Berlin	E1	**PHY-02-0460**
3	**Impurity- and field-induced magnetic ordering in the doped spin dimer system $TlCu_{1-x}Mg_xCl_3$**	H. Tanaka[1] M. Fujisawa[1] T. Ono[1] V.V. Sikolenko[2] H.A. Graf[2] S. Gerischer[2]	[1]TIT, JP [2]HMI Berlin	E1	**PHY-02-0492**
4	**Dimensionality crossover in hcp cobalt**	U. Köbler[1] A. Hoser[1+2] J. Klenke[3+4] V.V. Sikolenko[4]	[1]FZ Jülich [2]RWTH Aachen [3]Uni Mainz [4]HMI Berlin	E1 E2	**PHY-01-1643** **02-0490**
5	**Magnetic order coexistence and magnetization steps in Ni and Ti substituted manganites**	C. Frontera[1] J.L. García-Muñoz[1] B. Natalia[1] J. Hernández-Velasco[2+] J.-U. Hoffmann[3]	[1]CSIC-ICMAB Barcelona, E [2]UC Madrid, E [3]HMI Berlin	E2	**PHY-01-1552**
6	**Field-dependence of magnetic order in an Ising magnet in transverse field**	R. Coldea[1] E. da Silva Wheeler[1] D.A. Tennant[2] J.-U. Hoffmann[2] P. Smeibidl[2]	[1]Univ. Oxford, UK [2]HMI Berlin	E2	**PHY-01-1555**
7	**Investigation of magnetic interactions in $TbCu_2$ by paramagnetic diffuse scattering**	S. Raasch[1] M. Frontzek[1] J.-U. Hoffmann[2]	[1]TU Dresden [2]HMI Berlin	E2	**PHY-01-1642**
8	**The spontaneous and induced phase transitions for $ARe(WO_4)_2$;** **A = K, Rb; Re = Er, Nd, Dy**	M.T. Borowiec[1] J.-U. Hoffmann[2] T. Lonkai[2]	[1]PAS IP Warsaw, PL [2]HMI Berlin	E2	**PHY-01-1647**
9	**Coexistence of ferro- and anti-ferromagnetic ordering in Ni-Mn-Ga MSMA martensites**	I. Glavatskyy[1] I. Urubkov[1] J.-U. Hoffmann[2]	[1]NAS IMP Kiev, UA [2]HMI Berlin	E2	**PHY-01-1650**
10	**$NdAl_2$, a one-dimensional bulk ferromagnet**	U. Köbler[1] A. Hoser[1+2] J.-U. Hoffman[3+4] U. Amann[3+4]	[1]FZ Jülich [2]RWTH Aachen [3]Uni Tübingen [4]HMI Berlin	E2	**PHY-01-1748**
11	**AF fluctuations in $La_{1.2}Sr_{1.8}Mn_2O_7$**	T. Chatterji[1] J.-U. Hoffman[2] U. Amann[2]	[1]ILL Grenoble, F [2]HMI Berlin	E2	**PHY-01-1753**
12	**Magnetoelectric correlations in multiferroic $DyMnO_3$** **Exchange interactions and multiple magnetic ordering in $DyMnO_3$**	M. Fiebig[1] J.-U. Hoffmann[2]	[1]MBI Berlin [2]HMI Berlin	E2	**PHY-01-1640** **01-1641**
14	**Magnetic structure of Er_2PdSi_3 and Tm_2PdSi_3**	A. Kreyßig[1] E. Faulhaber[1] M. Frontzek[1] J.-U. Hoffmann[2] U. Amann[2]	[1]TU Dresden [2]HMI Berlin	E2	**PHY-01-1747**
16	**Diffuse neutron scattering from TmB_{12}**	K. Siemensmeyer[1] S. Matas[2] K. Flachbart[2]	[1]HMI Berlin [2]SAS Kosice, SK	E2	**PHY-01-1695-EF**

List of Contributed Experimental Reports

PAGE	TITLE	TEAM			PROPOSAL
17	**Magnetic structure of U_4PdGa_{12}**	K. Prokeš[1] R. Jardin[2] J.-C. Griveau[2] J. Rebizant[2]	[1]HMI Berlin [2]ITU Karlsruhe	E2 E4	**EF**
18	**Magnetic order in CePdAl single crystal: effect of magnetic field**	K. Prokeš[1] P. Manuel[2] D.T. Adroja[2]	[1]HMI Berlin [2]RAL ISIS, UK	E4	**EF**
19	**Elastic response of HoB_{12} in external magnetic field**	K. Siemensmeyer[1] S. Matas[2] K. Flachbart[2] K. Prokeš[1]	[1]HMI Berlin [2]SAS Kosice, SK	E4	**PHY-01-1709-EF**
20	**Helical magnetic structures in Y_2Fe_{17} under high pressure**	J. Kamarád[1] O. Prokhnenko[1+2] K. Prokeš[2]	[1]ASCR IP Prague, CZ [2]HMI Berlin	E4	**PHY-01-1670**
21	**Pressure-induced low-temperature helimagnetic structure in R_2Fe_{17} (R = Y, Lu)**	J. Kamarád[1] O. Prokhnenko[1+2] K. Prokeš[2]	[1]ASCR IP Prague, CZ [2]HMI Berlin	E4	**PHY-01-1781**
22	**Quadrupole structures in high magnetic fields in the AFQ material $PrPb_3$**	T. Onimaru[1] N. Aso[1] K. Prokeš[2]	[1]Univ. Tokyo, ISSP, JP [2]HMI Berlin	E4	**PHY-01-1782**
23	**Quantitative analysis of anisotropic domain growth in $CoNb_2O_6$**	S. Mitsuda[1] T. Nakajima[1] K. Prokeš[2] S. Kausche[2]	[1]Tokyo US, JP [2]HMI Berlin	E4	**PHY-01-1783**
24	**Structural and magnetic phase transitions in $Sr_4Fe_4O_{11}$**	M. Reehuis[1+2] C. Ulrich[1] B. Keimer[1] D. Sheptyakov[3]	[1]MPI Stuttgard [2]HMI Berlin [3]ETHZ & PSI, CH	E5	**PHY-01-1724-LT**
25	**Single crystal neutron diffraction study of $La_{0.85}Sr_{0.15}VO_3$ and $La_{0.90}Sr_{0.10}VO_3$**	M. Reehuis[1+2] C. Ulrich[1] B. Keimer[1]	[1]MPI Stuttgard [2]HMI Berlin	E5	**PHY-01-1724-LT**
26	**Magnetic structure of $CeVO_3$**	M. Reehuis[1+2] C. Ulrich[1] B. Keimer[1]	[1]MPI Stuttgard [2]HMI Berlin	E5	**PHY-01-1724-LT**
27	**Relevant and non relevant crystal field interactions (Cr_2O_3, FeO)**	U. Köbler[2] A. Hoser[1+2] N. Stüßer[3]	[1]FZ Jülich [2]RWTH Aachen [3]HMI Berlin	E6	**PHY-01-1585**
28	**Neutron diffraction study of $Ce_3Ag_4X_4$ (X = Ge, Sn)**	E. Wawrzynska[1] J. Hernández-Velasco[2] N. Stüßer[2] S. Baran[3] D. Kaczorowski[4]	[1]Univ. Bristol, UK [2]HMI Berlin [3]JU Krakow, PL [4]PAS ILTSR Wroclaw, PL	E6	**PHY-01-1680**
29	**Magnetic structure of nanocrystalline Tb**	O. Moze[1] C. Vecchini[1] D. Argyriou[2]	[1]Univ. Modena, I [2]HMI Berlin	E9	**PHY-01-1645**
30	**Neutron diffraction study of $LaMn_{0.3}Co_{0.7}O_3$**	K. Bärner[1] A. Sazonov[2] I.O. Troyanchuk[2] D. Karpinsky[2] V.V. Sikolenko[3]	[1]Uni Göttingen [2]ISSSP NAS Minsk, BY [3]HMI Berlin	E9	**PHY-01-1654**
31	**Neutron diffraction study of the $TbCo_{0.47}Mn_{0.53}O_3$ Perovskite**	H. Gamari-Seale[1] A. Sazonov[2] I.O. Troyanchuk[2] K.L. Stefanopoulos[1] V.V. Sikolenko[3]	[1]NCSR Demokritos, GR [2]ISSSP NAS Minsk, BY [3]HMI Berlin	E9	**PHY-01-1661**
32	**Continious or integer period modulations in $La_{1-x}Ca_xMnO_3$ for x>0.5?**	M. Pissas[1] D. Stamopoulos[1] D. Argyriou[2]	[1]NCSR Demokritos, GR [2]HMI Berlin	E9	**PHY-01-1662**

List of Contributed Experimental Reports

PAGE	TITLE	TEAM			PROPOSAL
33	**Magnetic properties of $LaCo_{0.5}Fe_{0.5}O_3$**	H. Szymczak[1] D. Karpinsky[2] M. Tovar[3]	[1]PAS IP Warsaw, PL [2]NAS Minsk, BY [3]HMI Berlin	E9	**PHY-01-1665**
34	**Structure and magnetism in UPd_2Sb**	S. Süllow[1] O. Prokhnenko[2] M. Tovar[2]	[1]TU Braunschweig [2]HMI Berlin	E9	**PHY-01-1756**
35	**Oxygen vacancy ordering in layered double perovskite $NdBaCo_2O_{5.72}$**	K. Bärner[1] I.O. Troyanchuk[2] L. Lobanovsky[2] O. Prokhnenko[3] M. Tovar[3] D. Argyriou[3]	[1]Uni Göttingen [2]ISSSP NAS Minsk, BY [3]HMI Berlin	E9	**PHY-01-1758**
36	**Investigation of nuclear and magnetic structure of Cylindrite $FeSn_4Pb_3Sb_2S_{14}$**	R. Kaden[1] S. Schorr[1] M. Tovar[2]	[1]Uni Leipzig [2]HMI Berlin	E9	**PHY-01-1762**
37	**Crystal and magnetic structure of $Nd_3Co_{13}B_2$ and the Nickel substituted derivatives**	J. Bartolome[1] J. Campo[1] N. Plugaru[2] J. Rubin[2] O. Prokhnenko[3] M. Tovar[3]	[1]Univ. Zaragoza, ICMA, E [2]Univ. Zaragoza, CPS, E [3]HMI Berlin	E9	**PHY-01-1770**
38	**Neutron powder diffraction study of Sr_2CrOsO_6**	Y. Krockenberger[1+2] L. Alff[2] M. Reehuis[1+3] M. Tovar[3]	[1]MPI FKF Stuttgart [2]TU Darmstadt [3]HMI Berlin	E9	**PHY-01-1778-DT**
39	**Study of the magnetic phase diagram in a field-induced non-Fermi liquid**	B. Fak[1] C. Rüegg[2] P. Niklowitz[1] D. McMorrow[2] K. Habicht[3]	[1]CEA Grenoble, F [2]UCL, UK [3]HMI Berlin	V2	**PHY-02-0452**
40	**Kondo Scattering in Heavy Fermion $Ce_3Co_4Sn_{13}$**	A. Christianson[1] K. Habicht[2]	[1]UC Irvine & LANL [2]HMI Berlin	V2	**PHY-02-0469**
41	**Out-of-Plane Magnetism in Underdoped $La_{2-x}Sr_xCuO_4$ (x=0.1)**	A.B. Lake[1+2] G. Aeppli[3] K. Habicht[2]	[1]Iowa State Univ., Ames, US [2]HMI Berlin [3]UCL, UK	V2	**PHY-02-0497**
42	**SANS study of the vortex lattice of the FFLO phase in $CeCoIn_5$**	A.D. Bianchi[1] M. Kenzelmann[2] R. Movshovich[3] P. Smeibidl[4] M. Kammel[4] J. Haug[4] A. Wiedenmann[4]	[1]FZ Rossendorf [2]ETHZ & PSI, Zürich, CH [3]LANL, Los Alamos, US [4]HMI Berlin	V4	**PHY-04-1095**
43	**Searching for ferromagnetic clusters in paramagnetic phase**	J. Herrero-Albillos[1] J. Campo[1] E. Garcia-Matres[2]	[1]Univ. Zaragoza, ICMA, E [2]HMI Berlin	V4	**PHY-04-1099**
44	**Field induced spin-spin correlation length in amorphous Fe_2O_3**	S.M. Yusuf[1+2] J.M. de Teresa Nogueras[2] A. Heinemann[3] A. Wiedenmann[3]	[1]BARC, IN [2]Univ. Zaragoza, ICMA, E [3]HMI Berlin	V4	**PHY-04-1114**
45	**Magnetic properties evolution of $LaMn_{1-x}Co_xO_3$ ($0.5 \leq x \leq 0.7$)**	H. Szymczak[1] D. Karpinsky[2] A. Heinemann[3]	[1]PAS IP Warsaw, PL [2]NAS Minsk, BY [3]HMI Berlin	V4	**PHY-04-1155**

List of Contributed Experimental Reports

PAGE	TITLE	TEAM			PROPOSAL
Magnetic Excitations					
46	**Inelastic neutron response from HoB_{12} single crystal**	K. Siemensmeyer[1] S. Matas[2] K. Flachbart[2] V.V. Sikolenko[1]	[1]HMI Berlin [2]SAS Kosice, SK	E1	**PHY-02-0478-EF**
47	**Magnetic excitations in nanocrystalline Tb**	O. Moze[1] C. Vecchini[1] J. Klenke[2]	[1]Uni. Modena, I [2]HMI Berlin	E1	**PHY-02-0447**
48	**Magnetic excitations in nanocrystalline Tb**	O. Moze[1] C. Vecchini[1] V.V. Sikolenko[2]	[1]Univ. Modena, I [2]HMI Berlin	E1	**PHY-02-0462**
49	**Field dependence of magnetic excitations in $La_{7/8}Sr_{9/8}MnO_4$**	D. Senff[1] M. Braden[1] K. Habicht[2]	[1]Uni Köln [2]HMI Berlin	V2	**PHY-02-0466**
50	**Study of inelastic response to enhancement of the quasi-2D antiferromagnetic phase in superconducting $(Pr_{0.88}La)Ce_{0.12}CuO_4$ (T_c = 21K)**	S. Wilson[1] P. Dai[1] S. Li[1] K. Habicht[2]	[1]Univ. Tennessee, USA [2]HMI Berlin	V2	**PHY-02-0471**
51	**Quantum phase transitions in the organic quantum magnet $(C_5H_{12}N)_2CuBr_4$**	C. Rüegg[1] B. Thielemann[2] K. Habicht[3]	[1]UCL, UK [2]ETHZ & PSI, CH [3]HMI Berlin	V2	**PHY-02-0495**
52	**Field dependence and quantum criticallity in the spin fluctuations of an electron-doped high-T_c cuprate, $Pr_{1-x}LaCe_xCuO_4$**	S. Wilson[1] P. Dai[1] S. Li[1] K. Habicht[2]	[1]Univ. Tennessee, USA [2]HMI Berlin	V2	**PHY-02-0501**
53	**Investigation of antiferromagnetic spin fluctuations in $CePt_3Si$**	J.-G. Park[1] J.-Y. So[1+2] D.T. Adroja[3] E.A. Bauer[4] M. Russina[5]	[1]SKKU Suwon, KP [2]Seoul Nat. Univ., KP [3]RAL ISIS, UK [4]TU Wien, A [5]HMI Berlin	V3	**PHY-03-0380**
54	**The ground state of Pr^{3+} ion in PrB_6 : singlet or triplet?**	N. Tiden[1] E. Nefeodova[1] K. Siemensmeyer[2] A. Buchsteiner[2]	[1]KIAE Moscow, RU [2]HMI Berlin	V3	**PHY-03-0407**
55	**Shape crossover and time scaling of the critical dynamics of an Heisenberg ferromagnet**	M. Alba[1] C. Pappas[2]	[1]LLB, CNRS-CEA, F [2]HMI Berlin	V5	**PHY-03-0331**
Chemical Structure					
56	**Diffuse scattering of cation-doped zirconia-oxinitrides**	I. Kaiser-Bischoff[1] J.-U. Hoffmann[2+3]	[1]LMU München [2]HMI Berlin [3]Uni Tübingen	E2	**CHE-01-1749**
57	**Microstructural twinning characteristics in $YBa_2Cu_3O_{6+x}$ high-temperature superconductor at room temperature**	K. Ross[1] L.F. Zhang[1] J.-U. Hoffmann[2]	[1]Univ. Salford, UK [2]HMI Berlin	E2	**PHY-01-1683**
58	**Neutron powder diffraction of Diindenoperylene**	F. Schreiber[1] U. Amann[1+2] J.-U. Hoffmann[1+2] B. Maier[2]	[1]Uni Tübingen [2]HMI Berlin	E2	**PHY-01-1815-LT**
59	**Neutron diffraction on birch wood for studying the space orientation of the crystalline areas of cellulose**	J. Peters[1] J.T. Bonarski[2] W. Olek[3] M. Reehuis[1]	[1]HMI Berlin [2]InstMetMatSci, Krak., PL [3]Univ. of Poznan, PL	E5	**PHY-01-1723-EF**

List of Contributed Experimental Reports

PAGE	TITLE	TEAM			PROPOSAL
60	**Crystal structure of $CaCu_2O_3$**	A.B. Lake[1+2] M. Reehuis[2+3] D.A. Tennant[2] H.J. Bleif[2]	[1]ORNL,US [2]HMI Berlin [3]MPI FKF Stuttgart	E5	**PHY-01-1838-EF**
61	**X-ray and neutron diffraction study of $YTiO_3$**	M. Reehuis[1+2] C. Ulrich[1] B. Keimer[1] H.J: Bleif[2]	[1]MPI Stuttgard [2]HMI Berlin	E5	**PHY-01-1724-LT**
62	**High temperature structure and phase transition of $CuCr_2O_4$**	M. Tovar	HMI Berlin	E9	**EF**
63	**New nitrogen and hydrogen metal compounds**	G. Auffermann[1] P. Höhn[1] A. Mehta[1] R. Kniep[1] M. Tovar[2]	[1]MPI CPfS Dresden [2]HMI Berlin	E9	**CHE-01-1653**
64	**Investigation of the crystal structure of deuterated Hydrocerussite**	C. Christides[1] V. Psycharis[2] D. Argyriou[3]	[1]Univ. Patras, GR [2]NCSR Demokritos, Ath., GR [3]HMI Berlin	E9	**CHE-01-1663**
65	**Structural and magnetic studies of spinel oxides** **Part 3: Lithium ions distribution in the $Li_xMn_{3-x-y}Fe_yO_4$ system**	E. Wolska[1] J. Darul[1] W. Nowicki[1] M. Tovar[2]	[1]AMU Poznan, PL [2]HMI Berlin	E9	**CHE-01-1664**
66	**New nitrogen and hydrogen metal compounds**	G. Auffermann[1] P. Höhn[1] R. Niewa[1] R. Kniep[1] D. Argyriou[2]	[1]MPI CPfS Dresden [2]HMI Berlin	E9	**CHE-01-1757**
67	**Determination of structural stabilising OH-species in cubic $Ba_2Mg_3F_{10}$**	F. Werner[1] M. Tovar[2]	[1]TU Wien, A [2]HMI Berlin	E9	**CHE-01-1765**
68	**Structural and magnetic studies of spinel oxides** **Part 4: Ferrimagnetic spinel phase in the $Li_xMn_{3-x-y}Fe_yO_4$ system**	E. Wolska[1] W. Nowicki[1] J. Darul[1] O. Prokhnenko[2] M. Tovar[2]	[1]AMU Poznan, PL [2]HMI Berlin	E9	**CHE-01-1773**
69	**Structural study of $(LaSr)_{n+1}Fe_nO_{3n+1}$ and $La_2Ni_{1-x}Cu_xO_4$ solid solutions**	S. Neov[1] O. Prokhnenko[2] N. Velinov[3] V. Kozhukharov[3]	[1]BAS INRNE Sofia, BG [2]HMI Berlin [3]UCTM Sofia, BG	E9	**MAT-01-1767**
70	**Structural phase transitions in $CaTaOAlO_4$**	T. Malcherek[1] M. Tovar[2]	[1]Uni Hamburg [2]HMI Berlin	E9	**OTH-01-1655**
71	**Investigation of lattice deformation in segregations in $(2ZnSe)_x(CuInSe_2)_{1-x}$**	S. Schorr[1] M. Tovar[2]	[1]Uni Leipzig [2]HMI Berlin	E9	**PHY-01-1657**
72	**Structural disorder study on UPt_2Si_2**	S. Süllow[1] O. Prokhnenko[2] M. Tovar[2]	[1]TU Braunschweig [2]HMI Berlin	E9	**PHY-01-1755**
73	**Ananysis of hydrogen forms on nanocrystalline $LiBFeH_x$**	P.J. Hall[1] J. Gil Posada[1] M. Russina[2]	[1]Univ. Strathclyde, UK [2]HMI Berlin	V3	**OTH-03-0378**
74	**Small-angle neutron scattering investigation of the disproportionation process in silicon sub-oxides**	A. Hohl[1] U. Keiderling[2]	[1]TU Darmstadt [2]HMI Berlin	V4	**CHE-04-1093**

List of Contributed Experimental Reports

PAGE	TITLE	TEAM			PROPOSAL
	Structural Excitations				
75	**Defect induced phase transition in doped GaAs**	A. Naberezhnov[1] V.V. Sikolenko[2] S. Borisov[1]	[1]PTI St-Petersburg, Ru [2]HMI Berlin	E1	**PHY-02-0448**
76	**Anisotropic Debye Waller factors of $La_{0.7}Sr_{0.3}MnO_3$ from powder diffraction**	D. Reznik[1] F. Weber[1] O. Prokhnenko[2] D. Argyriou[2]	[1]FZ Karlsruhe [2]HMI Berlin	E9	**PHY-01-1759**
77	**Phonon anomalies in the martensitic phase of Ni_2MnGa**	P. Vorderwisch[1] S.M. Shapiro[2] K. Habicht[1]	[1]HMI Berlin [2]Brookhaven Nat. Lab.	V2	**EF**
78	**NRSE investigation of phonon life times in the conventional superconductor Nb**	K. Habicht[1+2] F. Mezei[1] T. Keller[3+4] B. Keimer[3]	[1]HMI Berlin [2]TU Darmstadt [3]MPI FKF Stuttgart [4]FRM-II Garching	V2	**PHY-02-0484-LT**
79	**Temperature dependence of the phonon-dispersion in Nb at low q**	K. Habicht	HMI Berlin TU Darmstadt	V2	**PHY-02-0485-LT**
80	**Influence of polaron localization on G(ε) in intercalation compounds M_xTiSe_2**	O. Sobolev[1] S. Titova[2] A.N. Skomorokhov[3] J. Pieper[1]	[1]HMI Berlin [2]RAS Ekaterinburg, RU [3]RF SSC IPPE Obninsk, RU	V3	**PHY-03-0388-EF**
81	**Guest molecules dynamics in iodomethane hydrate**	F. Mançois[1] A. Desmedt[1] M. Prager[2] M. Russina[3]	[1]Univ. Bordeaux, F [2]FZ Jülich [3]HMI Berlin	V3	**CHE-03-0400**
82	**Determination of diffusion mechanism and position of Nitrogen in quaternary oxide Hexaluminate at temperatures up to 1200K**	B. Saruhan-Brings[1] M. Stranzenbach[1] C.G. Mondragon Rodriguez[1] A. Buchsteiner[2]	[1]DLR Köln [2]HMI Berlin	V3	**MAT-03-0397**
83	**Molecular dynamics in Tryglicine Sulphate (TGS) using TOF neutron spectroscopy**	V. Tripadus[1] A. Buchsteiner[2] A. Radulescu[1] D. Aranghel[1] M.Gugiu[1] M. Statescu[1] J. Pieper[2]	[1]NIPNE-HH Bucharest, RO [2]HMI Berlin	V3	**PHY-03-0376**
84	**Dynamic study on superionic phosphate glasses $(AgI)_x(AgPO_3)_{1-x}$ x=0.0, 0.3, 0.5**	E. Kartini[1] F. Mezei[2] M. Arai[3+4] M. Nakamura[4] M. Russina[2]	[1]BATAN, ID [2]HMI Berlin [3]KEK Tsukuba, JP [4]JAERI, JP	V3	**PHY-03-0379**
85	**Low energy dynamics of superionic conductor $AgI-Ag_2S-AgPO_3$ glass**	M. Arai[1+2] M. Nakamura[2] E. Kartini[3] M. Russina[4]	[1]KEK Tsukuba, JP [2]JAERI, JP [3]BATAN, ID [4]HMI Berlin	V3	**PHY-03-0381**

List of Contributed Experimental Reports

Biology

PAGE	TITLE	TEAM			PROPOSAL
86	**Interaction of Dicynthaurin with lipid model membranes**	F. Bringezu[1] M. Majerowicz[1] T. Hauß[2] S. Dante[2]	[1]Uni Leipzig [2]HMI Berlin	V1	**BIO-01-1689**
87	**Investigation of deuterium labelled model stratum corneum lipid membranes**	M. Kiselev[1] D. Otto[2] B. Dobner[2] R. Neubert[2] N. Ryabova[1] S. Dante[3] T. Hauß[3+4]	[1]JINR Dubna, RU [2]MLU Halle [3]HMI Berlin [4]TU Darmstadt	V1	**BIO-01-1690**
88	**Effect of cholesterol on the penetration of Alzheimer's peptide Aβ(25-35) into lipid membranes**	S. Dante[1] T. Hauß[1+2] N. Dencher[2]	[1]HMI Berlin [2]TU Darmstadt	V1	**BIO-01-1727-LT 1841-LT**
89	**Lamellar diffraction of spin-labelled membrane protein Colicin A**	K. Lieutenant[1] E. Bordignon[2] V.L.P. Pulagam[2] T. Hauß[3+4]	[1]ILL Grenoble, F [2]Uni Osnabrück [3]HMI Berlin [4]TU Darmstadt	V1	**BIO-01-1731-DT**
90	**Membrane-binding of the N-terminus of annexin A1**	J. Bradshaw[1] A. Hofmann[1] N.-J. Hu[1] T. Hauß[2+3]	[1]Univ. Edinburgh, UK [2]HMI Berlin [3]TU Darmstadt	V1	**BIO-01-1797**
91	**Orientation dependence of the structural flexibility of granal thylakoid sample: thylakoid membranes (isolated from plant leaves)**	G. Garab[1] S. Krumova[1] S. Dante[2+3]	[1]HAS BRC Szeged, H [2]HMI Berlin [3]TU Darmstadt	V1	**BIO-01-1798** **01-1799**
92	**The interaction of the antibiotic peptide KLA1 with neutral model membranes**	B. Klösgen[1] M. Dathe[2] T. Hauß[3+4]	[1]Univ. Odense, DK [2]FI Mol. Pharm. Buch [3]HMI Berlin [4]TU Darmstadt	V1	**PHY-01-1599**
93	**Negative solubility coefficient and dynamics of hydrophobic interactions in aqueous solutions of native and methylated Cyclodextrins**	R. Lechner[1+2] T. Aree[1+3] A. Kouzmine[1] W. Saenger[1] A. Buchsteiner[2]	[1]FU Berlin [2]HMI Berlin [3]Univ. Bern, CH	V3	**BIO-03-0370**
94	**Protein dynamics in the light-harvesting complex II of green plants**	K.-D. Irrgang[1] J. Pieper[2]	[1]TU Berlin [2]HMI Berlin	V3	**BIO-03-0371**
95	**Thermo-optical rearrangements in the thylakoid membrane of green plants**	G. Garab[1] S. Krumova[1] K.-D. Irrgang[2+3] J. Pieper[4]	[1]HAS BRC Szeged, H [2]Max-Volmer-Institut [3]TU Berlin [4]HMI Berlin	V3	**BIO-03-0372**
96	**Directional dynamics in DMPC membranes containing gangliosides**	L. Cantu[1] F. Natali[2] A. Deriu[3] J. Pieper[4]	[1]Univ. Milano, I [2]ILL, Grenoble, F [3]Univ. Parma, I [4]HMI Berlin	V3	**BIO-03-0403**
97	**Hydrophobic interactions: Aggregation behaviour of native and methylated Cyclodextrins in aqueous solutions**	R. Lechner[1+2] T. Aree[1+3] A. Kouzmine[1] W. Saenger[1] M. Kammel[2]	[1]FU Berlin [2]HMI Berlin [3]Univ. Bern, CH	V4	**BIO-04-1090**
98	**Neutron imaging of water uptake in plants**	U. Matsushima[1] N. Kardjilov[2] W. Herppich[3] A. Hilger[2]	[1]Iwate Univ., JP [2]HMI Berlin [3]ATB Potsdam	V7	**BIO-04-1170**
99	**Characterisation of composite microporous bone substitutes**	C. Panayiotou[1] C. Ritzoulis[1] M. Strobl[2+3]	[1]AU Thessaloniki, GR [2]TFH Berlin [3]HMI Berlin	V12a	**BIO-04-1119**

List of Contributed Experimental Reports

Soft Matter

PAGE	TITLE	TEAM			PROPOSAL
100	**Local dynamics of polyethylene and its oligomers**	V. Arrighi[1] J. Tanchawanich[1] A. Buchsteiner[2]	[1]HWU Edinburgh, UK [2]HMI Berlin	V3	**CHE-03-0377**
101	**IQENS on monohydric alcohols/CCl_4 mixtures**	F. Aliotta[1] C. Vasi[1] F. Saija[1] A. Buchsteiner[2]	[1]IPCF-CNR-Messina, I [2]HMI Berlin	V3	**PHY-03-0358**
102	**Microscopic dynamics of a glass-forming liquid in soft confinement**	R. Zorn[1] M. Mayorova[1] M. Russina[2]	[1]FZ Jülich [2]HMI Berlin	V3	**PHY-03-0396**
103	**Quasielastic measurements on liquid n-tetracosane in oriented, tubular silicon mesopores**	P. Huber[1] R. Zorn[2] M. Mayorova[2] M. Russina[3] D. Wallacher[1] T. Hofmann[1] P. Kumar[1]	[1]Uni Saarland [2]FZ Jülich [3]HMI Berlin	V3	**PHY-03-0399**
104	**Heterogeneous polymer micelles and their interactions with proteins**	H. Bianco-Peled[1] K. Shamai[1] E. Garcia-Matres[2]	[1]Technion Haifa, IL [2]HMI Berlin	V4	**BIO-04-1104**
105	**Nucleic acid inclusion in water in oil microemulsions formed by phosphatidylnucleosides**	D. Berti[1] F. Betti[1] A. Brandt[2]	[1]Univ. Firenze, I [2]HMI Berlin	V4	**BIO-04-1107**
106	**Mechanism of cryoprotection of lipid bilayers by simple sugars**	C.J. Garvey[1] T. Lenné[2] G. Bryant[2] U. Keiderling[3]	[1]ANSTO, Aus [2]RMIT Univ. Melbourne, Aus [3]HMI Berlin	V4	**BIO-04-1116**
107	**Self-aggregation and solubilisation properties of a novel type of amphiphilic terblock copolymers in aqueous solution**	M. Gradzielski[1] A. Boschetti de Fierro[2] D. Fierro[2] P. Simon[2] V. Abetz[2] A. Heinemann[3]	[1]TU Berlin, Stranski Lab [2]GKSS Geesthacht [3]HMI Berlin	V4	**CHE-04-1010**
108	**Internal composition of polyelectrolyte-protein complexes**	J. Gummel[1] F. Cousin[1] F. Boue[1] D. Clemens[2]	[1]CNRS-LLB Saclay, F [2]HMI Berlin	V4	**CHE-04-1103**
109	**Structural study of new contrast agents for Magnetic Resonance Imaging**	L. Paduano[1] G. Mangiapia[1] A. Brandt[2]	[1]Univ. Napoli, I [2]HMI Berlin	V4	**CHE-04-1108**
110	**Pluronic micelles swollen with homopolymer**	A. Woodward[1] M. Sharp[1] T. Cosgrove[1] D. Clemens[2]	[1]Univ. Bristol, UK [2]HMI Berlin	V4	**CHE-04-1112**
111	**Micelles in room temperature ionic liquids**	A. Triolo[1] O. Russina[2] U. Keiderling[2]	[1]CNR IPCF Messina, I [2]HMI Berlin	V4	**PHY-04-1149**
112	**Aggregate structure of cationic surfactants in the pores of SBA-15 silica**	G.H. Findenegg[1] T. Shin[1] A. Brandt[2]	[1]TU Berlin, Stranski Lab [2]HMI Berlin	V4	**CHE-04-1091**
114	**Effect of PEI as a first layer and treatment of PAH/PSS films on their structure**	M. Kolasińska[1] R. Krastev[2+3] P. Warszyński[1]	[1]ICSC PAS, Cracow, PL [2]MPI, Golm [3]HMI Berlin	V6	**EF**

List of Contributed Experimental Reports

PAGE	TITLE	TEAM			PROPOSAL
	Structures and Phases				
115	**Neutron diffraction measurements on micro- and nano-sized precipitates embedded in a Ni-base superalloy and after their extraction from the alloy**	R. Gilles[1] M. Hölzel[1+2] D. Mukherji[3] P. Strunz[4] M. Tovar[5]	[1]TUM FRM II [2]TU DA [3]ETH Zürich, CH [4]ASCR NPI Rez, CZ [5]HMI Berlin	E9	**MAT-01-1763**
116	**Evolution of pore microstructure in thermal barrier coatings**	J. Haug[1] A. Wiedenmann[1] B. Saruhan-Brings[2]	[1]HMI Berlin [2]DLR Köln	V4	**MAT-04-1127-EF**
117	**Contrast variation method to reduce the open porosity in thermal barrier coatings**	A. Wiedenmann[1] J. Haug[1] B. Saruhan-Brings[2]	[1]HMI Berlin [2]DLR Köln	V4	**MAT-04-1180-EF**
118	**Solution treatment optimization in SX-CM186LC superalloy using in-situ SANS**	J. Zrnik[1] P. Strunz[2] J. Haug[3]	[1]TU Kosice, SK [2]ASCR NPI Rez, CZ [3]HMI Berlin	V4	**MAT-04-1111**
	Nanostructures				
119	**Reordering dynamics in Co-ferrofluids studied by stroboscopic SANS**	A. Wiedenmann[1] U. Keiderling[1] R. Gähler[2] K. Habicht[1]	[1]HMI Berlin [2]ILL Grenoble, F	V4	**MAT-04-1125-EF**
120	**Field-dependent relaxation behaviour of Co-ferrofluid investigated with stroboscopic time-resolved SANS and SANSPOL**	A. Wiedenmann U. Keiderling	HMI Berlin	V4	**MAT-04-1130-EF**
121	**$Nd_{60}Fe_{20}Co_{10}Al_{10}$ alloys measured by SANSPOL at high magnetic field**	A. Wiedenmann O. Perroud	HMI Berlin	V4	**MAT-04-1177-EF**
122	**Reordering in magnetic colloids induced by variation of magnetic fields**	A. Wiedenmann A. Heinemann M. Kammel	HMI Berlin	V4	**MAT-04-1178-EF**
123	**The nanostructure of encapsulated magnetite nanoparticles – a SANSPOL study**	A. Wiedenmann A. Heinemann M. Kammel	HMI Berlin	V4	**MAT-04-1179-EF**
124	**SANSPOL investigation of magnetic particles for medical applications**	P. Baglioni[1] M. Bonini[1] A. Wiedenmann[2]	[1]Univ. Firenze, I [2]HMI Berlin	V4	**CHE-04-1106**
125	**Investigation of the microstructure of ferrofluids using Small Angle Neutron Scattering**	S. Odenbach[1+2] L.M. Pop[1+2] T. Gerdes[2] M. Kammel[3] A. Wiedenmann[3]	[1]TU Dresden [2]Uni Bremen [3]HMI Berlin	V4	**MAT-04-1092**
126	**Nanoclusters in oxide-dispersion-strenghened steel**	X.-L. Wang[1] A.D. Stoica[1] C.-T. Liu[2] U. Keiderling[3]	[1]ORNL-SNS, USA [2]ORNL-MCD, USA [3]HMI Berlin	V4	**MAT-04-1159**
127	**SANS experiments on self-ordered arrays of electrodeposited FeNi nanowires**	V. De La Prida[1] J.A. Blanco[1] J. Campo[2] E. Garcia-Matres[3]	[1]Univ. Oviedo, E [2]Univ. Zaragoza, ICMA, E [3]HMI Berlin	V4	**PHY-04-1019**
128	**Small angle neutron scattering studies on FeCo ferrofluids.**	W. Kleemann[1] S. Bedanta[1] O. Petracic[1] A. Hütten[2] M. Kammel[3] A. Heinemann[3]	[1]Uni Duisburg - Essen [2]Uni Bielefeld [3]HMI Berlin	V4	**PHY-04-1094**

List of Contributed Experimental Reports

PAGE	TITLE	TEAM			PROPOSAL
129	**Nanostructures in colloidal dispersions of nearly monodisperse Magnetite**	B. Erne[1] M. Klokkenburg[1] A. Wiedenmann[2]	[1]Univ. Utrecht, NL [2]HMI Berlin	V4	**PHY-04-1154**

Stress Analysis

130	**Correlation of defect distribution and twinning stress in Ni_2MnGa MSMAs**	H. Schmidt[1] M. Köhl[2] J. Ihringer[2] R. Schneider[3] J.-U. Hoffmann[3]	[1]Bosch Stuttgart [2]Uni Tübingen [3]HMI Berlin	E2	**MAT-01-1750**
131	**Cladding stresses by sin2 psi method**	C. Ohms[1] T. Poeste[2] R. Wimpory[2]	[1]EC-JRC-IE Petten, NL [2]HMI Berlin	E3	**MAT-01-1607**
132	**Influence of residual stresses on fatigue crack propagation in Al 6056 laser-welded specimens**	F. Fiori[1] A. Manescu[1] V. Calbucci[1] R. Wimpory[2]	[1]UPM Ancona, I [2]HMI Berlin	E3	**MAT-01-1805**
133	**Structural studies of the magnetic shape memory compound Ni-Mn-Ga**	O. Heczko[1] K. Proke_[2]	[1]HUT (TKK), FIN [2]HMI Berlin	E4	**MAT-01-1671**
134	**Study of crystalline phases (microlites) in natural obsidian**	G. Klöß[1] S. Schorr[1] M. Tovar[2]	[1]Uni Leipzig [2]HMI Berlin	E9	**GEO-01-1656-DT**
135	**Structures and textures of martensitic phases in deformed polycrystalline shape memory alloys**	P. Sittner[1] V. Novak[1] P. Molnar[1] M. Tovar[2]	[1]ASCR IP Prague, CZ [2]HMI Berlin	E9	**MAT-01-1660**
136	**In situ study of the phase composition in the Na_3AlF_6-Al_2O_3 within 930°C - 1350°C**	L. Smrcok[1] O. Pritula[1] M. Kucharik[1] M. Tovar[2]	[1]SAS Bratislava, SK [2]HMI Berlin	E9	**MAT-01-1666**
137	**Neutron diffraction studies of the relaxor PLZT 8/65/35 powder irradiated by high-current pulsed electron beam**	K. Iakoubovskii[1] A. Sternberg[2] A. Kuzmin[2] V. Efimov[3] V.V. Sikolenko[4]	[1]KU Leuven, B [2]ISSP, Latvia, LV [3]JINR Dubna, Ru [4]HMI Berlin	E9	**PHY-01-1659**
138	**Hibrid organic/inorganic silica aerogel: control of mechanical behaviour**	V. Morales-Flórez[1] N. de la Rosa-Fox[1] U. Keiderling[2]	[1]Univ. Cádiz, E [2]HMI Berlin	V4	**MAT-04-1098**
139	**In-situ SANS- isothermal ageing measurements of EB – PVD thermal barrier coatings**	B. Saruhan-Brings[1] A. Flores Renteria[1] J. Haug[2] A. Wiedenmann[2]	[1]DLR Köln [2]HMI Berlin	V4	**MAT-04-1143**
140	**Solution treatment of the single-crystal Ni-base superalloy CMSX4: a detail view**	P. Strunz[1] D. Mukherji[2] J. Rösler[3] R. Gilles[4] J. Haug[5]	[1]ASCR NPI Rez, CZ [2]ETH Zürich, CH [3]TU Braunschweig [4]TU München [5]HMI Berlin	V4	**MAT-04-1144**
141	**Isothermal development of the microstructure in molten AlSi alloys**	U. Dahlborg[1] J. Haug[2]	[1]CNRS - INPL –UHP [2]HMI Berlin	V4	**PHY-04-1101**
142	**Formation of liquid water and carbon dioxide in fuel cells**	C. Hartnig[1] I. Manke[2] M. Grünerbel[1] J. Kaczerowski[1] A. Hilger[2] N. Kardjilov[2]	[1]ZSW Ulm [2]HMI Berlin	V7	**MAT-04-1172-DT**

List of Contributed Experimental Reports

PAGE	TITLE	TEAM			PROPOSAL
Cultural Heritage					
143	**Neutron pre-examination of "Portrait – Amedeo Modigliani" attributed to Amedeo Modigliani, 55 x 46 cm^2**	B. Schröder-Smeibidl[1] C. Laurenze-Landsberg[2] C. Schmidt[2] L.A. Mertens[1]	[1]HMI Berlin [2]Gemäldegalerie Berlin (GMB)	B8	**ART-05-0010**
144	**Neutron autoradiographs of "*Ceres, sitting on the rim of a fountain"* by Sebastiano del Piombo, 74,5 x 45,5 cm^2**	C. Laurenze-Landsberg[1] C. Schmidt[1] L.A. Mertens[2] B. Schröder-Smeibidl[2]	[1]Gemäldegalerie Berlin (GMB) [2]HMI Berlin	B8	**ART-05-0011**
145	**Neutron autoradiographs of "*The Repudiation of Hagar" by* Govert Flinck, 110 x 138,7 cm^2**	C. Laurenze-Landsberg[1] C. Schmidt[1] L.A. Mertens[2] B. Schröder-Smeibidl[2]	[1]Gemäldegalerie Berlin (GMB) [2]HMI Berlin	B8	**ART-05-0012**
146	**Neutron autoradiographs of "*Picture of a young Roman lady"* (~1512/13) by Sebastiano del Piombo, 78x 61 cm^2**	C. Laurenze-Landsberg[1] C. Schmidt[1] L.A. Mertens[2] B. Schröder-Smeibidl[2]	[1]Gemäldegalerie Berlin (GMB) [2]HMI Berlin	B8	**ART-05-0013**
147	**Neutron autoradiographs *of "The festival in nature"* by Jean-Baptiste Pater**	J. Bartoll[1] B. Jackisch[1] C. Laurenze-Landsberg[2] L.A. Mertens[3] A. Niemann[3] B. Schröder-Smeibidl[3]	[1]Stiftung Preussische Schlösser und Gärten Berlin-Brandenburg (SPSG) [2]Gemäldegalerie Berlin (GMB) [3]HMI Berlin	B8	**ART-05-0014**
148	**Texture and morphology of ancient wooden artcraft**	R. Triolo[1] U. Keiderling[2]	[1]Univ. Palermo, I [2]HMI Berlin	V4	**CHE-04-1153**
149	**SANS investigation of Cu/Zn alloys for applications to technology for the restoration of ancient European organs**	A. Manescu[1] V. Calbucci[1] M. Kammel[2]	[1]UPM Ancona, I [2]HMI Berlin	V4	**MAT-04-1148**
150	**Texture and morphology of ancient wooden artcraft**	R. Triolo[1] D.I. Donato[1] N. Kardjilov[2] A. Hilger[2]	[1]Univ. Palermo, I [2]HMI Berlin	V7	**CHE-04-1169**
151	**Texture and morphology of marble artefacts from Villa Adriana (Tivoli, Rome)**	F. Lo Celso[1] R. Triolo[1] N. Kardjilov[2]	[1]Univ. Palermo, I [2]HMI Berlin	V7	**OTH-04-1168**
152	**Texture and morphology of ancient wooden artcraft**	R. Triolo[1] I. Ruffo[1] M. Strobl[2]	[1]Univ. Palermo, I [2]HMI Berlin	V12a	**CHE-04-1164**
153	**SANS investigation of brass reed tongues taken from historical and modern organs**	A. Manescu[1] M. Strobl[2]	[1]UPM Ancona, I [2]HMI Berlin	V12a	**MAT-04-1162**
154	**Texture and morphology of marble artefacts from Villa Adriana (Tivoli, Rome)**	F. Lo Celso[1] R. Triolo[1] M. Strobl[2]	[1]Univ. Palermo, I [2]HMI Berlin	V12a	**OTH-04-1163**

List of Contributed Experimental Reports

PAGE	TITLE	TEAM			PROPOSAL
Fundamental Physics and Others					
155	**Neutron deflection by a single crystal prism**	A.G. Wagh[1] S. Abbas[1] M. Strobl[2] W. Treimer[2]	[1]BARC, IN [2]HMI Berlin	V12b	**PHY-04-1165**
156	**Evaluation of the scission neutron fraction in U-235 fission**	G.V. Danilyan[1] V.S. Pavlov[1] P. Shatalov[1] E.V. Brakhman[1] V.A. Krakhotin[1] A.S. Danilyan[1] M. Russina[2] T. Wilpert[2]	[1]RF SSC ITEP Moscow, RU [2]HMI Berlin	V13	**PHY-05-0009** **05-0015**
Development of Instruments and Methods					
157	**Lamor-phase corrections for NRSE**	K. Habicht	HMI Berlin TU Darmstadt	V2	**PHY-02-0457-LT**
158	**Time-resolved SANS studies (TISANE) of field induced ordering in Ferrofluids**	A. Wiedenmann[1] R. Gähler[2] U. Keiderling[1] K. Habicht[1] M. Russina[1] N. Thillosen[2]	[1]HMI Berlin [2]ILL, Grenoble, F	V3	**PHY-03-0413-EF**
159	**Test of the polarised ^{3}He refilling device in combination with a sample magnet**	A. Wiedenmann[1] A. Rupp[1] U. Keiderling[1] W. Heil[2] J. Klenke[1+2]	[1]HMI Berlin [2]Uni Mainz	V4	**MAT-04-1126-EF**
160	**Stroboscopic time-resolved SANS technique for dynamical studies of Co-ferrofluid relaxation with SANSPOL**	A. Wiedenmann U. Keiderling	HMI Berlin	V4	**MAT-04-1182-EF**
161	**The new neutron tomography instrument CONRAD**	N. Kardjilov[1+2] A. Hilger[1+2]	[1]TFH Berlin [2]HMI Berlin	V7	**EF**
162	**A double-monochromator device for CONRAD**	M. Strobl[1+2] N. Kardjilov[1+2] A. Hilger[1+2] M. Rimke[1+2] W. Treimer[1+2]	[1]TFH Berlin [2]HMI Berlin	V7	**EF**
163	**Bragg-edge radiography using the monochromatic option at CONRAD**	N. Kardjilov[1+2] M. Strobl[1+2] A. Hilger[1+2]	[1]TFH Berlin [2]HMI Berlin	V7	**EF**
164	**Neutron scattering effects in cold neutron radiography**	F. de Beer[1] N. Kardjilov[2] A. Hilger[2]	[1]NECSA, Pretoria, ZA [2]HMI Berlin	V7	**OTH-04-1171-LT**
165	**New V12a set-up**	M. Strobl[1+2] W. Treimer[1+2]	[1]HMI Berlin [2]TFH Berlin	V12a	**BIO-04-1134-LT**
166	**Towards quantitative refraction contrast tomography**	M. Strobl[1+2] W. Treimer[1+2] K. Staak[2]	[1]HMI Berlin [2]TFH Berlin	V12a	**BIO-04-1134-LT**
167	**The V12b monochromatic neutron tomography set-up and applications**	M. Strobl[1+2] I. Manke[2+3] O. Neumann[1] W. Treimer[1+2]	[1]TFH Berlin [2]HMI Berlin [3]TU Berlin	V12b	**PHY-04-1135-LT**

List of Contributed Experimental Reports

PAGE	TITLE	TEAM			PROPOSAL
168	**Quantitative tomography with monochromatic neutrons**	M. Strobl[1+2] W. Treimer[1+2] O. Neumann[1]	[1]TFH Berlin [2]HMI Berlin	V12b	**PHY-04-1135-LT**
169	**The new V12b double crystal diffractometer**	M. Strobl[1+2] W. Treimer[1+2]	[1]TFH Berlin [2]HMI Berlin	V12b	**PHY-04-1135-LT**
170	**Test of multi-pinhole grids for VSANS**	D. Clemens L. Mokrani F. Mezei M. Russina	HMI Berlin	V13	**EF**
171	**Focusing lens and polarising supermirror**	T. Krist N. Behr J.-E. Hoffmann	HMI Berlin	V14	**EF**

BESSY

172	**Mass-filtered cobalt clusters on non-magnetic surfaces**	J. Bansmann[1] P. Imperia[2] A. Kleibert[1] K.H. Meiwes-Broer[1] F. Bulut[3] M. Getzlaff[3] C. Boeglin[4] A. Barla[4]	[1]Uni Rostock [2]HMI Berlin [3]Uni Düsseldorf [4]IPCMS Strasbourg, F	S1	**BESSY**
174	**Reading magnetism of one layer of Single Molecule Magnets**	D. Gatteschi[1] M. Mannini[1] R. Sessoli[1] A. Cornia[2] L. Zobbi[2] C. Cartier dit Moulin[3] P. Sainctavit[4] P. Imperia[5]	[1]Univ. Florence, I [2]Univ. Modena, I [3]LCIMM-UPMC Paris, F [4]LMC-UPMC Paris, F [5]HMI Berlin	S1	**BESSY**
176	**Magnetic anisotropy of triangular shaped, hexagonally arranged Co nanostructures**	P. Imperia[1] W. Kandulski[2] A. Kosiorek[2] H. Głaczyńska[2] D. Schmitz[1] H. Maletta[1] M. Giersig[2]	[1]HMI Berlin [2]CAESAR Bonn	S1	**BESSY**
178	**Exchange bias and the role of uncompensated Fe spins in epitaxially grown fcc Fe_xMn_{1-x} at the interface to Co**	D. Schmitz[1] H. Maletta[1] M. Gruyters[2] H. Winter[2]	[1]HMI Berlin [2]HU Berlin	S1	**BESSY**
179	**Determination of magnetization depth profiles of V/Fe/V(110) with X-Ray Resonant Magnetic Reflectometry**	D. Schmitz[1] P. Imperia[1] H. Maletta[1] D.A. Tennant[1] U. Grüner[2] M. Harlander[2] S. Macke[2] E. Goering[2]	[1]HMI Berlin [2]MPI MF Stuttgart	S1	**BESSY**
181	**Depth resolved X-ray residual stress analysis in CVD multi-layer hard coatings on WC-substrates (2005-I)**	E. Dudzik M. Klaus	HMI Berlin	S2	**BESSY**
182	**Depth resolved X-ray residual stress analysis in CVD multi-layer hard coatings on WC-substrates (2005-II)**	E. Dudzik M. Klaus	HMI Berlin	S2	**BESSY**

List of Contributed Experimental Reports

PAGE	TITLE	TEAM		PROPOSAL	
183	**Lock-in transition of sodium ordering in single crystal $Na_{0.48}CoO_2$**	R. Feyerherm E. Dudzik D. Argyriou N. Aliouane	HMI Berlin	S2	**BESSY**
184	**Structural distortion induced by magnetic ordering in $TbMnO_3$ and $DyMnO_3$**	R. Feyerherm E. Dudzik D. Argyriou N. Aliouane	HMI Berlin	S2	**BESSY**
185	**ASAXS investigation of gold nanoparticles in glass**	A. Hoell[1] I. Zizak[1] S. Haas[1] J. Banhart[1] D. Tatchev[2] M. Eichelbaum[3] K. Rademann[3]	[1]HMI Berlin [2]BAS IPC Sofia, BG [3]HU Berlin	S3	**BESSY**
187	**Energy-dispersive diffraction analysis of non-uniform near surface residual stress fields induced by mechanical surface processing - I. Evaluation of the Laplace stress profiles sigma_ij(tau)**	C. Genzel I. Denks	HMI Berlin	S4	**BESSY**
188	**Energy-dispersive diffraction analysis of non-uniform near surface residual stress fields induced by mechanical surface processing - II. Evaluation of the real space stress profiles σ_{ij} (z)**	C. Genzel I. Denks	HMI Berlin	S4	**BESSY**
189	**Locally resolved residual stress analysis in individual sublayers of CVD multilayer systems by means of energy dispersive diffraction**	C. Genzel I. Denks	HMI Berlin	S4	**BESSY**
190	**Improvement on stem cell cultivation in 3D artificial bone structures by pore size optimization using synchrotron tomography**	A. Haibel[1] H. Freidank[1] J. Banhart[1] A. Berthold[2] H. Schubert[2]	[1]HMI Berlin [2]TU Berlin	S5	**BESSY**
192	**High-resolution tomography investigations of cmicro-cracks in hard rocks**	K. Thermann[1] B. Kremmin[1] I. Manke[1] J. Tiedemann[1] S. Zabler[2] A. Haibel[2]	[1]TU Berlin [2]HMI Berlin	S5	**BESSY**

	EXPERIMENTAL REPORT **Magnetic structure in $CsCuCl_3$ at high pressures**	Proposal N° PHY-02-0475-EF Instrument **E1** Local Contact Vadim Sikolenko
Principal Proposer: Experimental Team:	N. Stüßer - HMI Berlin R. Sadykov - RAS IHPP Troitsk, RU A. Hoser – FZ Jülich + RWTH Aachen	Date(s) of Experiment 15.04.-23.04.2005

Date of Report: 07.12.2005

$CsCuCl_3$ belongs to the family of frustrated magnetic systems with a triangular lattice of antiferromagnetically coupled $S = 1/2$ spins of Cu^{2+}-ion in the *ab*-plane ("120° structure"); the dominating magnetic interaction along the *c*-axis is ferromagnetic and there is an additional antisymmetric interaction favouring a state with adjacent spins perpendicular to each other. The competition of both leads to an incommensurate long wavelength magnetic spiral along *c*. The magnetic structure forming below 10.6 K has a propagation vector (1/3 1/3 0.085).

In the past $CsCuCl_3$ was investigated intensively in particular because quantum fluctuations lead to its rich phase diagram.

Here we continued to study the pressure dependence of the magnetic structure which we started recently. In the past it was found that the application of a hydrostatic pressure up to 1.5 GPa affects significantly the turning angles of spins along *c*.

At 2 K the turning angle between adjacent spins along *c* changes from 5.1° at zero pressure to more than 7° at 15 kbar. This could indicate that the structure under pressure has changed in a way which increases the relative strength of the antisymmetric exchange with respect to the ferromagnetic coupling.

A thorough study of the crystal structure under pressure at low temperatures is needed in the future to get a clearer understanding of this behaviour. Main motivation to come to higher pressures is the observation that $CsCuCl_3$ undergoes a structural phase transition at pressure between 1.65 and 3.1 GPa [1]. The transition temperature is lower for powder than for single crystals.

For the experiments we used a clamp cell made of a NiCrAl alloy in the inner part and of Al in the outer part. The cell was loaded with a single crystal of $CsCuCl_3$ together with a NaCl for pressure determination. Fluorinert was used as pressurizing medium.

The experiments were successful until a pressure of about 2.3 GPa. At this value the magnetic propagation vector was determined to be (1/3 1/3 0.142). This means that the turning angle of adjacent spins along c changes from 5.1° at zero pressure to 8.5°at 2.3 GPa.

During our efforts to increase the pressure to higher values one piston made from NiCrAl alloy was broken and we could not continue with the experiment.

According to the reference cited above a pressure about 3 GPa is needed for a single crystal of $CsCuCl_3$ to get the phase transition.

Future plans are to change material of piston to WC in order to come closer to the desired pressure. Below we show the observed change of the magnetic (1/3 1/3 l) with applied pressure.

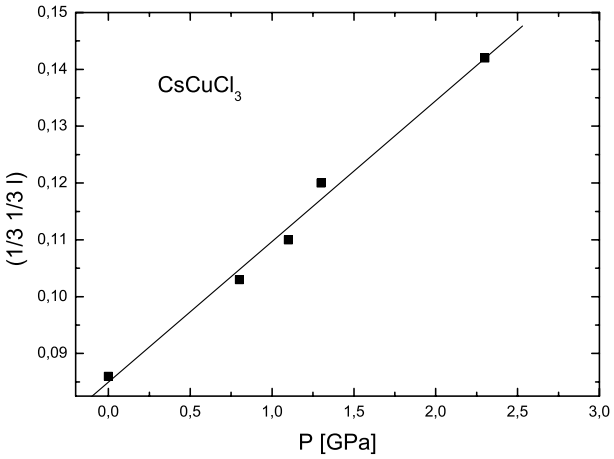

Reference

[1] Christie et al.: J. Phys.: Condens Matter 6 (1994) 3125-3136

	EXPERIMENTAL REPORT **Magnetic Clusters in UPt_2Si_2**	Proposal N° PHY-02-0460 Instrument **E1** Local Contact Jens Klenke
Principal Proposer: Experimental Team:	S. Süllow - TU Braunschweig S. Süllow - TU Braunschweig J. Klenke - HMI Berlin A. Rupp - HMI Berlin	Date(s) of Experiment 10.03. - 23.03.2005

Date of Report: 27.01.2006

Recently, we initiated a reinvestigation of the structural and magnetic properties of the moderately mass enhanced heavy fermion compound UPt_2Si_2 [1], in order to determine the effect of crystallographic disorder on the material properties. In our neutron scattering investigation, utilizing the bright elemental contrast between U, Pt and Si, we have established the presence of crystallographic disorder in this compound in form of strained layers consisting of Pt(2) and Si(2) ligand atoms within the tetragonal $CaBe_2Ge_2$ structure (space group *P4/nmm*; lattice parameters: a = 4.1857Å; c = 9.6301Å).

With respect to the magnetic properties, for our newly prepared annealed single crystal we detect a bulk antiferromagnetic phase transition at T_N = 32.4K. Moreover, between T_N and the irreversibility temperature T_{irr} ~ 35K we detect neutron scattering intensity, with the associated Bragg peaks being not resolution limited. The temperature dependence of the [1 0 0] Bragg peak line width, which is depicted in Fig. 1, can be related to the size of the magnetically correlated areas, yielding clusters sizes down to 100Å along this crystallographic direction (indicated in the figure). It implies that the magnetic state between T_N and T_{irr} consists of magnetic clusters embedded in a non-magnetic matrix, this as result of the crystallographic disorder on the Pt(2) and Si(2) sites. The existence of this cluster glass like state explains the anomalous magnetic domain pinning observed in recent susceptibility studies [2,3].

In order to determine if the shape of the magnetic clusters correlates with the type of crystallographic disorder in the compound, we have performed a polarized neutron scattering study on UPt_2Si_2. The basic idea is to measure the temperature dependence of the line width of a second Bragg peak along an inequivalent direction in reciprocal space (here, the [1 0 2] peak), in order to deduce the correlation length in this direction. As the [1 0 2] peak has a structural scattering component, polarized neutrons are used for suppression of this structural component. Still, even under these conditions the analysis turns out to be very difficult because of a remaining residual structural signal in the polarized neutron data. In effect, in the temperature range of interest, that is between T_N and T_{irr}, it is much larger than the magnetic scattering component, causing a rather small signal-to-noise ratio of the magnetic signal. Presently, further analysis is carried in order to resolve this issue.

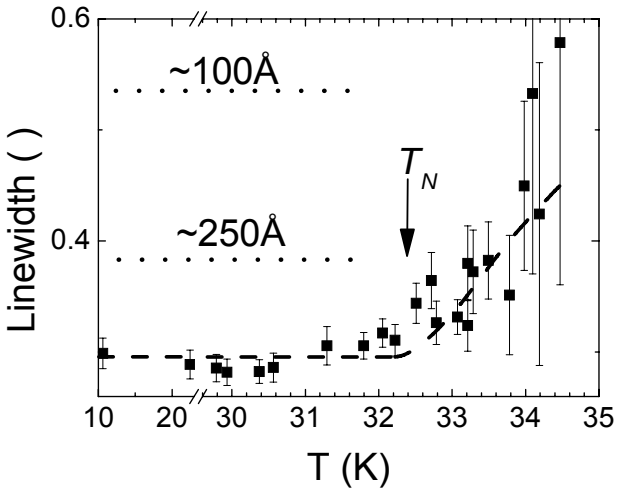

Fig. 1: The temperature dependence of the line width of the [1 0 0] magnetic Bragg peak of UPt_2Si_2; for details see text.

References:

[1] R. Steeman *et al.*: J. Phys.: Condens. Matter **2** (1990) 4059
[2] A. Otop *et al.*: J. Appl. Phys. **95** (2004) 6702
[3] S. Süllow *et al.*: J. Appl. Phys., in print (2006)

	EXPERIMENTAL REPORT **Impurity- and field-induced magnetic ordering in the doped spin dimer system $TlCu_{1-x}Mg_xCl_3$**	Proposal N° PHY-02-0492 Instrument **E1** Local Contact Hans Anton Graf
Principal Proposer: Experimental Team:	H. Tanaka - Tokyo Institute of Technology M. Fujisawa, T. Ono - Tokyo Inst. of Tech. V.V. Sikolenko, H.A. Graf, S. Gerischer - HMI Berlin	Date(s) of Experiment 18.08. - 28.08.2005

Date of Report: 14. Sept. 2005

$TlCuCl_3$ is a 3D coupled spin dimer system with a gapped ground state. The magnitude of the gap is J/k_B=7.5 K. The small gap compared with the intradimer exchange interaction J/k_B=65.9 K is attributed to the strong interdimer exchange interactions [1,2]. Magnetization measurement and neutron scattering experiment [3,4] revealed that $TlCu_{1-x}Mg_xCl_3$ undergoes the impurity-induced magnetic ordering. When nonmagnetic ions are substituted for magnetic ions, the singlet ground state is partially destroyed, so that staggered moments are induced around the impurities. The induced moments interact through effective exchange interactions mediated by intact dimers, which leads to the 3D long-range order. In order to investigate both impurity- and field-induced phase transitions in $TlCu_{1-x}Mg_xCl_3$, we performed specific heat measurements in various magnetic fields, and found that there is no boundary separating impurity- and field-induced ordered phases. When the impurity- and field-induced ordered phases are identical, then the order parameter should be the same. Therefore, it is expected that the sublattice magnetization corresponding to the order parameter exhibit unusual field and temperature dependence. In order to clarify the impurity- and field-induced phase transitions in $TlCu_{1-x}Mg_xCl_3$, we performed neutron elastic scattering.

Measurements were carried out at E1 spectrometer installed in the experimental hall with the vertical field cryomagnet VM1. The incident neutron energy was fixed at E_i=13.9 meV, and the horizontal collimation sequence was chosen as 40'-80'-40'. Single crystal for x≈0.01 with a volume of approximately 0.4 cm^3 was used. The sample was mounted in the cryostat with its cleavage (0,1,0) plane parallel to the scattering plane, so that the reflections in the a^*-c^*-plane were investigated. The external magnetic field up to 12 T was applied along the b-axis. Temprature of the sample was lowered to 0.4 K using ^{3}He cryostat.

The magnetic peaks were observed at $\boldsymbol{Q}$=(h,0,l) with integer h and odd l. These reciprocal points are the same as those for the magnetic Bragg peaks indicative of the field-induced transverse Néel ordering were observed in $TlCuCl_3$. Figure 1 shows the intensity of the magnetic Bragg peak for $\boldsymbol{Q}$=(1,0,-3) as a function of magnetic field. With increasing magnetic field, the Bragg intensity decreases up to 3.5 T and then increases rapidly. The similar field dependence of the intensity was also observed for the Bragg reflection at $\boldsymbol{Q}$=(0,0,1). This field dependence of the Bragg intensity is due not to the change in the spin direction, but to the change in the magnitude of the ordered moment, i.e., the order parameter has a minimum at H≈3.5 T. It is considered that this unusual behavior of the order parameter results from the competition between magnetic ordering and spin gap, the latter of which acts to separate the impurity- and field-induced phases, as discussed by Mikeska *et al*. [5].

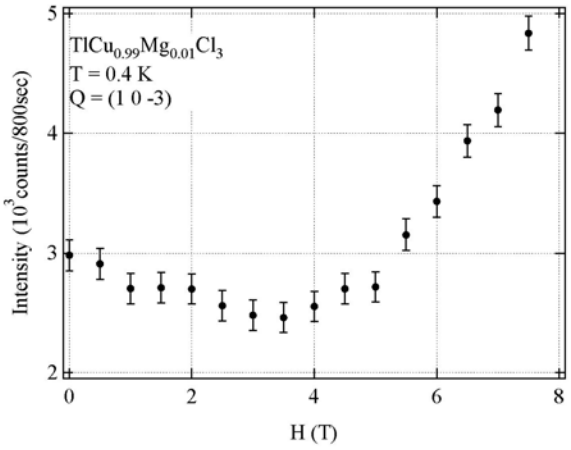

Fig. 1: Bragg peak intensity for $\boldsymbol{Q}$=(1,0,-3) as a function of magnetic field at T=0.4 K. The external field is parallel to the b-axis.

References

[1] A. Oosawa, M. Ishii, H. Tanaka:
J. Phys. Condensed Matter **11** (1999) 265.

[2] A. Oosawa, T. Kato, H. Tanaka, K. Kakurai, M. Müller, H.-J. Mikeska: Phys. Rev. B. **65** (2002) 094426.

[3] A. Oosawa, T. Ono, H. Tanaka:
Phys. Rev. B **66** (2002) 020405.

[4] A. Oosawa, M. Fujisawa, K. Kakurai, H. Tanaka:
Phys. Rev. B **67** (2003) 184424.

[5] H.-J. Mikeska, A. Ghosh, A.K. Kolezhuk:
Phys. Rev. Lett. **93** (2004) 217204.

	EXPERIMENTAL REPORT	Proposal N° PHY-01-1643 PHY-02-0490
BENSC	**Dimensionality crossover in hcp cobalt**	Instrument **E2 / E1** Local Contact Vadim Sikolenko
Principal Proposer: Experimental Team:	U. Köbler - IFF, FZ-Jülich U. Köbler - IFF, FZ-Jülich A. Hoser - Inst. f. Kristallogr. RWTH-Aachen J. Klenke - Inst. f. Physik, Uni Mainz	Date(s) of Experiment 23.02. - 27.02.2005 09.09. - 18.09.2005

Date of Report: 12.12.2005

One dimensional (1D) magnetic behaviour can occur in crystals with axial lattice symmetry if the interactions between the magnetic moments along this axis are much stronger than perpendicular to this axis. The transverse interactions need not to be zero. The condition for 1D behaviour is that the transverse interactions are sufficiently small such that the transverse correlation length remains finite at the magnetic phase transition. The phase transition is then driven by the longitudinal interactions. Speaking in terms of renormalization group theory, the transverse interactions are not relevant.

This characteristic behaviour of 1D magnets has been demonstrated in pioneering neutron scattering studies on MnF_2 with the tetragonal rutile structure [1]. It was shown in [1] that only the longitudinal correlation length diverges at the Néel transition but that the transverse correlation length has a temperature independent finite value for $T \leq T_N$.

Identification of 1D behaviour on account of a finite transverse correlation length is very laborious. It is more convenient to identify the dimensionality on account of the universal power function of the magnetic order parameter at the stable fixed point T=0. For 1D magnets such as MnF_2 with a half-integer spin (S=5/2) the magnetic order parameter approaches saturation according to a $T^{5/2}$ function [2].

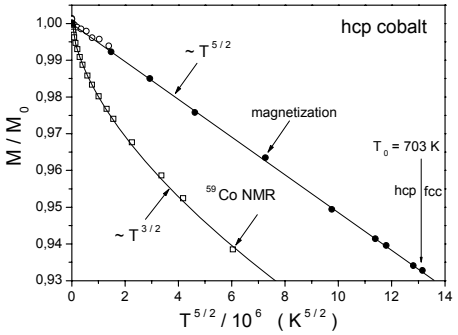

The $T^{5/2}$ universality class is observed also in hcp cobalt but only in the magnetically saturated state with all moments aligned parallel to the hexagonal c-axis. In the zero field state in which the magnetization is split into magnetic domains a $T^{3/2}$ power function is observed as is typical for anisotropic 3D interactions. Fig. 1 demonstrates the different power functions for spontaneous magnetization and for zero field ^{59}Co NMR [3].

The result of Fig. 1 indicates that a crossover between two universality classes occurs upon magnetic saturation. Note that the macroscopic magnetization shows normal saturation as a function of field. In order to specify this field induced crossover, investigations on a single crystal sphere using polarized neutron was planned. Unfortunately it was not possible to achieve a reasonable flipping ratio. The results on Fig. 2 are obtained therefore with non-polarized neutrons. A magnetic field was applied parallel to the c-axis which was perpendicular to the scattering plane.

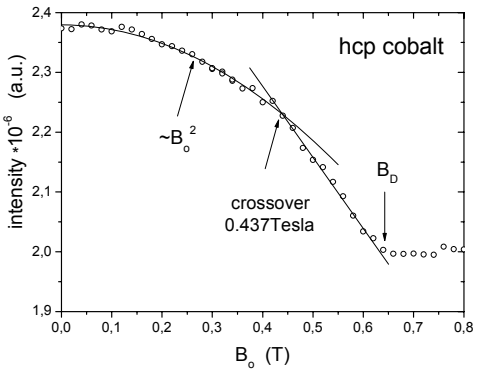

The unusual decrease of the intensity with field (see Fig.2) is explained by a shrinking transverse correlation length. Note that conventional Bragg scattering relies on a finite transverse correlation length. The initial decrease of the scattering intensity is according to B_o^2. At B_o=0.437 T an anomaly is observed. We identify this anomaly as dimensionality crossover from 3D to 1D, i.e. from $T^{3/2}$ to $T^{5/2}$. This anomaly in the transverse correlation length is not observed in the macroscopic magnetization.

References

[1] M. P. Schulhof, R. Nathans, P. Heller, A. Linz: Phys. Rev. 4 (1971) 2254.

[2] U. Köbler, A. Hoser, M. Kawakami, S. Abens: Physica B 307 (2001) 175.

[3] U. Köbler, A. Hoser, J.-U. Hoffmann, C. Thomas: to appear in Solid State Commun.

BENSC	**EXPERIMENTAL REPORT** **Magnetic order coexistence and magnetization steps in Ni and Ti substituted manganites.**	Proposal N° PHY-01-1552 Instrument **E2** Local Contact Jens-Uwe Hoffmann
Principal Proposer: Experimental Team:	C. Frontera - ICMAB-CSIC, Barcelona, E J.L. García-Muñoz - ICMAB-CSIC, Barcelona, E B. Natalia - ICMAB-CSIC, Barcelona, E J. Hernández-Velasco - HMI Berlin	Date(s) of Experiment 26.01.-30.01.2005

Date of Report: 09.01.2006

Besides the technological interesting colossal magnetoresistance, manganese oxides display other amazing phenomena. Between them, charge ordering and phase separation have been studied and, in most of the cases, a strong relation between them has been established.[1]
One of the families of compounds that combines both phenomena very strongly are the B-substituted manganites ($Ln_{1/2}A_{1/2}$-$Mn_{1-y}M_yO_3$, M=Fe, Cr, Co, Ni, Ti, Mg, Al, Ga, In, Sn,…). The effect of this substitution, at surprisingly low levels (y), has revealed to be dramatic: a 3% percent of Cr-substitution is enough to induce ferromagnetism in $Pr_{1/2}Ca_{1/2}$-MnO_3. [2][3][4]
Previous works indicate that the effect of the substituting metal strongly depends on its electronic structure. Ions with active delectrons induce a ferromagnetic and metallic state (at low temperature) while those with closed or empty d-shell (d0 or d10) keep the low temperature state as antiferromagnetic and insulating.[2][3][4] As a second amazing effect, it has been reported that the low temperature magnetization or resistivity vs. magnetic field curves display a series of sharp transitions remembering the avalanches of, for instance, martensitic transformations.[5] These "avalanches" are attributed to sharp transitions of certain regions of the compound from one coexisting phase to the other. In this context, we have performed neutron powder diffraction studies of $Pr_{0.5}Ca_{0.5}Mn_{1-y}M_yO_3$ with M=Ni and Ti (Ni^{2+}-d^8; Ti^{4+}-d^0) and y ranging between 0.005 and 0.05 under magnetic fields up to 6.5T with mainly two goals. The first one was to study the magnetic nature of the lowtemperature coexisting phases. The second one was to characterize magnetic changes taking place at the mentioned "avalanches" under field. Obtained NPD, jointly analyzed with synchrotron X-ray data, revealed the coexistence of different magnetic ordered structures, on one hand a CE-type AFM structure and on the other hand: i) a FM phase in the case of M=Ni and a pseudo-CE one in the case of M=Ti. Under the application of an
applied field, integrated intensity of FM peaks enhances and that of AFM peaks decreases when an "avalanche" occurs.

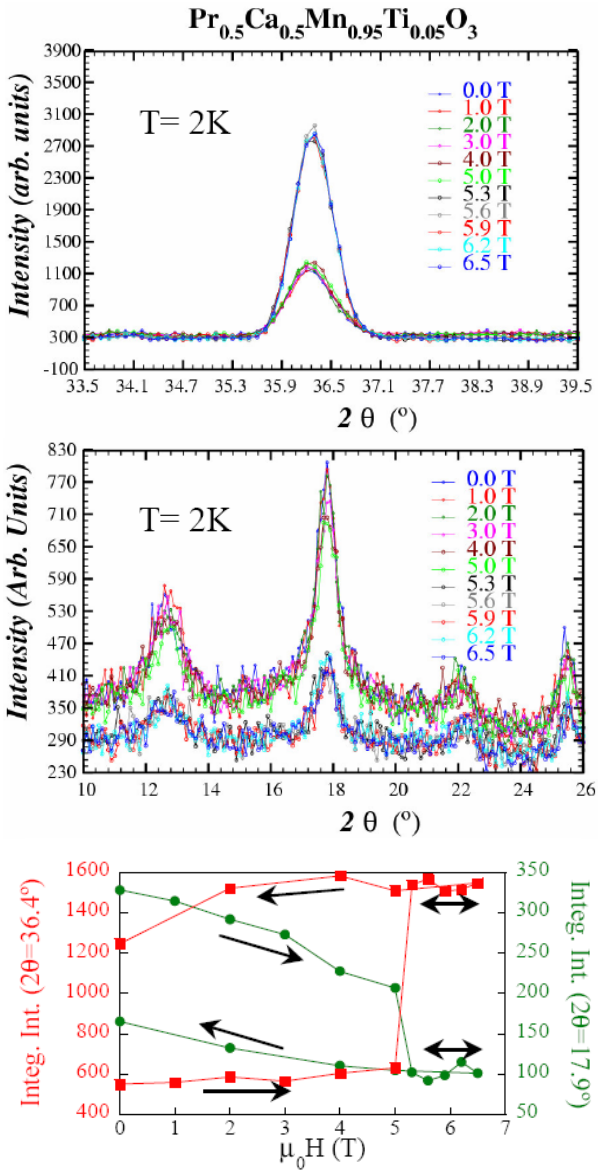

Figure: Variation with applied field of the diffracted patterns and regions correspondending to a FM peak (top panel) and the AFM peaks (middle panel). (Bottom panel) Integrated intensities of a FM and AFM peak under different applied fields. Data correspondend to $Pr_{0.5}Ca_{0.5}Mn_{0.95}Ti_{0.05}O_3$ at T= 2K.

References

[1] E. Dagotto et al.: Phys. Rep. **344**, 1 (2001)
[2] F. Damay et al.: Appl. Phys. Lett. **73**, 3772 (1998)
[3] S. Hérbert et al.: Solid State Comm. **121**, 229 (2002)
[4] S. Hérbert et al.: J. Solid State Chem. **165**, 6 (2002)
[5] R. Mahendiaran et al.: Phys. Rev. Lett. **89**, 286602 (2002)

	EXPERIMENTAL REPORT **Field-dependence of magnetic order in an Ising magnet in transverse field**	Proposal N° PHY-01-1555 Instrument **E2** Local Contact Jens-Uwe Hoffmann
Principal Proposer: Experimental Team:	R. Coldea - Oxford University, UK E. Wheeler, R. Coldea - Oxford University, UK D.A. Tennant, J.-U. Hoffmann, P. Smeibidl - HMI Berlin	Date(s) of Experiment 16.02. - 21.02.2005

Date of Report: 03.06.2005

We have identified the Ising magnet $CoNb_2O_6$ as a suitable system to study the physics of quantum phase transitions as it has a relatively low exchange interaction J~1.5 meV, such that the expected transition from the low-field ferromagnetically-ordered phase to the highfield paramagnetic phase should be experimentally accessible below 6 T. The mechanism of the transition is ultimately quantum fluctuations introduced by the transverse field becoming strong enough to "melt" longrange order and the overall aim of this project is to characterize the physics near the critical point and gain a microscopic understanding of the physics. The purpose of the present E2 experiment was to observe how the magnetic structure transformed upon approaching the critical point. Fields up to the maximum available 4T were applied, and significant changes were observed indicating a large suppression of the magnetic order by the field, however higher fields above 4T would be required to reach the critical point.

Measurements were made on a 6.7g single crystal of $CoNb_2O_6$ mounted in the (*h*0*l*) horizontal plane. Magnetic fields were applied along the *b*-axis transverse to the Ising axis and a dilution fridge insert with a base temperature of 50 mK provided the cooling. The E2 diffractometer was operated in flat cone geometry with tilted magnet and multi detector bank to access the out-of-horizontal scattering plane reflections. The diffraction pattern was measured in the (*h*,*k*,*l*) layers for *k*=0 and to monitor both structural and magnetic peaks. A germanium monochromator was used to give an incident wavelength of λ=0.121nm and the scattered beam was detected in the 80º-wide 400-channel multidetector bank. Counting times for an (ω,2θ) map of the (*h*,1/2,*l*) plane at 0T was 3 hours and an (ω,2θ) map of one magnetic reflection was between 0.5-1 hours at 4T as magnetic intensities decreased significantly, see Fig. 2. Typical scans are shown in Fig. 1. Complete data sets of the magnetic structure were made at zero field, 4T and a few intermediate fields. Measurements were also made at 0T at high temperature (5K) in the paramagnetic phase and no peaks above background level were detected at the magnetic (*h*,1/2,*l*) locations rulling out the possibility that the observed low temperature peaks were contaminated by λ/2 or secondary nuclear Bragg scattering. Preliminary analysis of the measured diffraction intensities at 0T showed good agreement with the structure of ferromagnetic chains coupled antiferromagnetically along b-axis found earlier[1] and measurements at 4T could be described by the same structure but with a much reduced ordered spin moment. Some time-dependent relaxation was observed and its quantitative characterization would require more experiments. A quantitative analysis of the data to determine the magnetic structures is currently in progress.

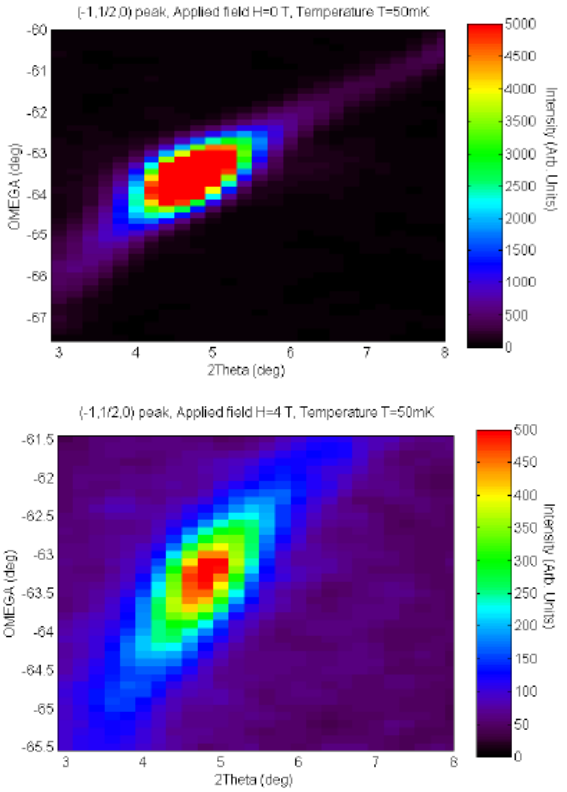

Fig. 1: Intensity of the (-1,1/2,0) magnetic Bragg peak observed in an (w,2q) scan at zero field (top) and at 4T (bottom).

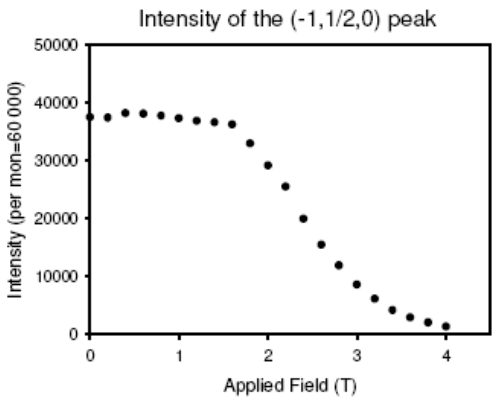

Fig. 2: Intensity of the (-1,1/2,0) magnetic Bragg peak as a function of applied magnetic field along the b-axis.

Reference

[1] Heid et al.: J. Magn. Magn. Mater. **151** 123 (1995).

BENSC	**EXPERIMENTAL REPORT** **Investigation of magnetic interactions in $TbCu_2$ by paramagnetic diffuse scattering**	Proposal N° PHY-01-1642 Instrument **E2** Local Contact Jens-Uwe Hoffmann
Principal Proposer: Experimental Team:	S. Raasch - TU Dresden, HMI-Berlin S. Raasch - TU Dresden, HMI-Berlin M. Frontzek - TU Dresden J.-U. Hoffmann - HMI-Berlin	Date(s) of Experiment 15.06. - 23.06.2005

Date of Report: 31.01.2006

The aim of the performed experiment was to get high statistic diffuse neutron data in order to be able to determine a complete set of exchange interaction constants. A cylindrical $TbCu_2$ sample (8x20mm) was available, grown by Dr. Behr of the IFW Dresden. The sample was 28 times bigger than in the previous experiment, providing an optimal condition for high neutron statistic.
The diffuse neutron data has to be taken slightly above the Néel temperature T_N. At first, a proper temperature for the diffuse measurements had been chosen by observing the magnetic (1/3 0 4) satellite reflection between 30 and 60 K.

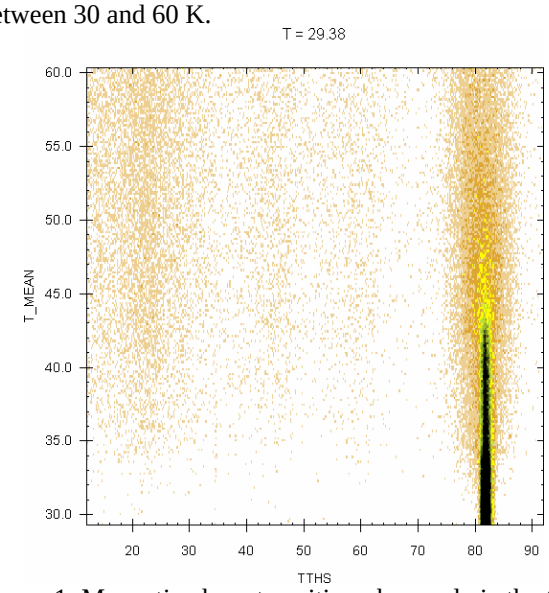

Figure 1: Magnetic phase transition observed via the (1/3 0 4) satellite reflection.

The disappearance of the (1/3 0 4) reflection at about 45 K indicates the magnetic phase transition. From the measurement shown in figure 1 we have chosen T = 55 K for our investigation of the diffuse scattering. A large region of the reciprocal space had been measured, which are in detail the (*h k* 0), (*h k* ½) (0 *k l*), (0.2 *k l*), (0.4 *k l*), (*h* 0 *l*), (*h* 1/6 *l*), (*h* 2/6 *l*), (*h k* 0) and the (*h k* ¼) planes, where the (0 *k l*) plane is shown in figure 2.
Concentrating on the low intensity range of the diffuse scattering planes, as shown in figure 3, curious weak bragg reflections at 1/3*k*, 1/2*k*, 2/3*k* as well as at 1/3*l* and 2/3*l* positions get visible. Those reflections have never seen before at $TbCu_2$ and demand an explanation.

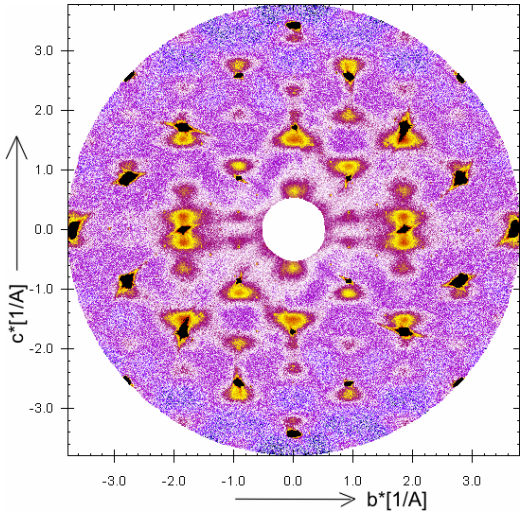

Figure 2: Various diffuse scattering features found at the (0 *k l*) plane at T = 55 K.

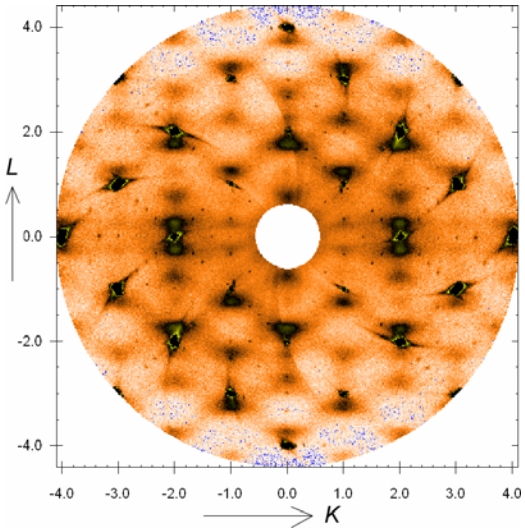

Figure 3: Emphasizing of low the scattering intensity of the (0 *k l*) plane. Strange weak reflections appear.

The measured diffuse scattering will be analysed with the software TVtueb using the meanfield method. Another aim of the experiment had been the verification of the direction of the magnetic moment. Earlier diffuse scattering measurements suggest the moment direction along *a* since no diffuse scattering had been seen in (*h* 0 0) direction. As far as this high statistic experiment is able to tell, still no diffuse scattering along (*h* 0 0) exists. Therefore no tilt of the moment away from the *a* direction can be concluded.

BENSC	**EXPERIMENTAL REPORT** **The spontaneous and induced phase transitions for $ARe(WO_4)_2$; A=K,Rb; Re=Er,Nd,Dy**	Proposal N° PHY-01-1647 Instrument **E2** Local Contact Jens-Uwe Hoffmann
Principal Proposer: Experimental Team:	M.T. Borowiec - PAS IP Warsaw, PL J.-U. Hoffmann - HMI Berlin T. Lonkai - HMI Berlin	Date(s) of Experiment 23.06.-30.06.2005

Date of Report: 09.01.2006

The neutron scattering experiment was directed to solve the problems of existence and conditions of the spontaneous/induced MPT for KErW single crystal and to determine the structure of the magnetic state for it. The neutron scattering measurements were made on powdered KErW single crystal. For experiments the set of selected temperatures and magnetic fields was following: T= 100, 200, 400. 500. 700, 800, 1500mK,40K, for H=0T, and T=200, 700, 1500 mK for H=1T, 2T. The choice of above temperature and magnetic field values is connected with earlier experimental results of specific heat and susceptibility experiments on oriented single crystals. But conclusions were not clear: the magnetic phase transitions (MPT) take place below 0.8K in specific heat and at 0.42K in susceptibility experiment.

The results obtained for powdered KErW single crystal for wavelength 2.4A indicate on existence of spontaneous magnetic phase transitions with phase transition temperature at about 0.75K and antiferro- and ferro- ordering type (simultanously) Figs.1 and 2 (differences between x and 40K, arrows antiferro reflexes). This complex ordering is a reason of the divergence of the earlier experiments. The existence of induced magnetic phase transitions is confirmed too (without change of the ordering type). The strong shift of phase transition temperature to the higher temperature range is observed. The last conclusion explains the behaviour of specific heat in magnetic field-Fig.3

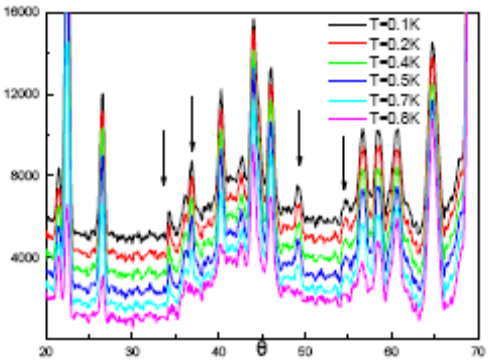

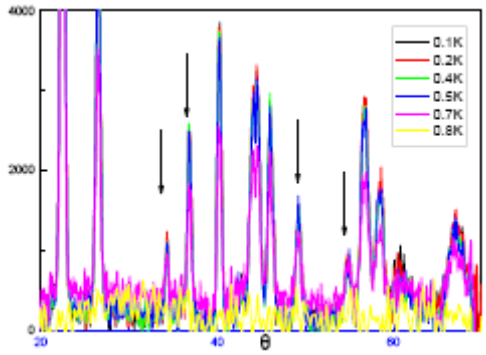

Preliminary results of the neutron scattering experiment for powdered RbNdW in the temperature range below 1500mK indicate that the spontaneous magnetic phase transition was not observed in these conditions. But the induced magnetic phase transition to state with ferromagnetic component of ordering is not excluded. The last conlusion is in agreement with the results of specific heat experiment in magnetic field - Fig. 4.

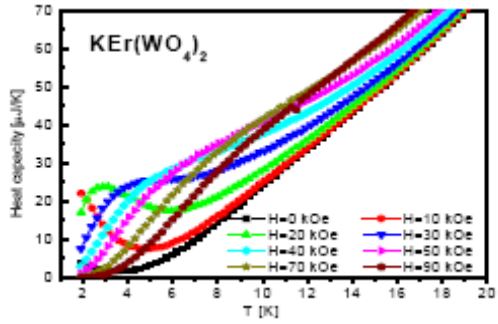

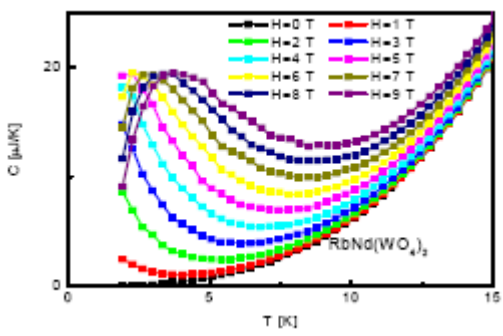

	EXPERIMENTAL REPORT **Coexistence of ferro- and anti-ferromagnetic ordering in Ni-Mn-Ga MSMA martensites**	Proposal N° PHY-01-1650 Instrument **E2** Local Contact Jens-Uwe Hoffmann
Principal Proposer: Experimental Team:	I. Glavatskyy - Inst. f Metal Phys., Kiev, Ukraine I. Urubkov - Inst. f Metal Phys., Kiev, Ukraine	Date(s) of Experiment 12.04. - 20.04.2005

Date of Report: 09.09.2005

Present investigation concerns neutron diffraction study of magnetic structure evolution in off–stoichiometric single crystal $Ni_{2.053}Mn_{1.105}Ga_{0.842}$ martensite during heating and cooling from room temperature down to 40K.

Experiment: During the experiment performed on E2 diffractometer the ƒÉ=0.239nm wavelength was used. Investigations were performed at T=295K, 200K, 100K and 40K in two crystal orientations. VM3 was used for magnetic field application (H=3T) to achieve saturated single variant martensite. Studies were performed in two orientations of single crystal to the scattering plane: 1 – [001] as the zone axis; 2 – [110] as zone axis.

Results: The unit cell in martensite in the studied single crystal is determined as body-centered orthorhombic with „p=0.421 nm, b=0.419 nm and c=0.561 nm at 295K. 5-layered superstructure is observed in <100> diretion. Studied specimen has temperatures of martensite transformation Ms= 307K, Mf= 305K, and Curie point Tc= 375K.

Due to previous studies of magnetic structure evolution with temperature and crystal lattice dynamics of martensite as well as magnetic properties performed for this alloy, it was found that there are few critical temperatures, namely 200K, 140K and 45K, at which the strong anomalies of magnetic scattering contribution are observed.

Fig. 1 illustrates the temperature evolution of strongest magnetic and structural peaks (in (002) the magnetic contribution is killed due to scattering geometry). At 200K, the anomalous increase in martensite twin boundary mobility is found. Thus we concentrated on magnetic scattering studies at these temperatures.

On Fig.2 some examples of the temperatre evolution of the scattering pattern of strong magnetic reflexes are presented. As the lattice parameters changes very slightly in this region, nevertheless the corrections were made, the changes are attributed to purely to the magnetic contribution. In Ni-Mn-Ga alloy system, the magnetic system consists of two subsystems, related to Ni and Mn atoms, which are the carriers of the magnetic moment, and evolves due to Ni-Ni, Ni-Mn and Mn-Mn exchange interaction.

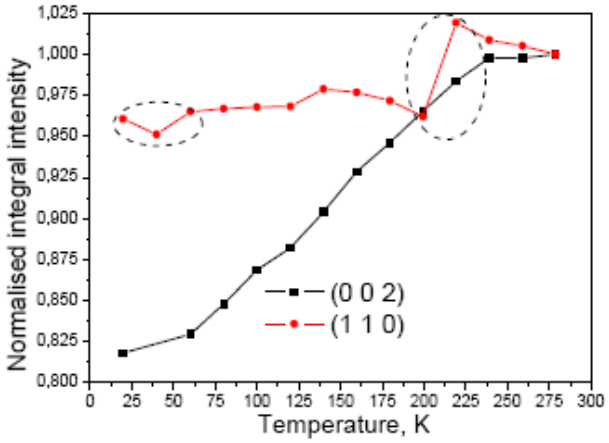

Fig.1: Comparson of normaliyed integral intensities of strongest magnetic (110) and structural (002) reflexes.

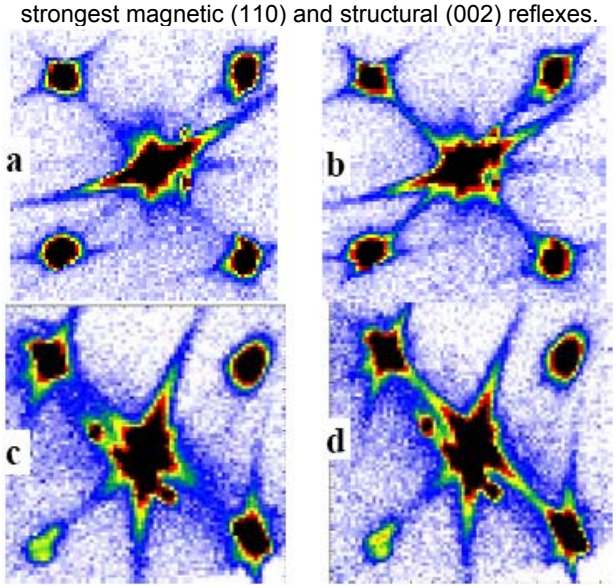

Fig.2: Fragments f the reciprocal space, strong magnetic peaks (200) – a,b & (220) – c,d, at T=220K (a,c) and 200K (b,d).

The diffuse contribution, attributed mainly to the magnon damping decreases abruptly with cooling from 220K to 200K. The magnetic structure becomes more correlated. Further analysis, with combination to the FMR, P-SANS and magnetometry studies, suggests the noncollinear ferrimagnetic ordering.

At 40K, the signs of narrow ~10K metastable spinglass state are observed, which collapses with further cooling to the ferrimagnetic state.

Article is prepared and submitted for publication.

	EXPERIMENTAL REPORT **$NdAl_2$, a one-dimensional bulk ferromagnet**	Proposal N° PHY-01-1748 Instrument **E2** Local Contact Jens-Uwe Hoffmann
Principal Proposer: Experimental Team:	U. Köbler - IFF, FZ - Jülich A. Hoser - Inst. F. Kristallographie, Aachen J.-U. Hoffmann - Inst. f. Kristallogr., Tübingen U. Amann - Inst. f. Kristallogr., Tübingen	Date(s) of Experiment 09.-16.08.2005

Date of Report: 14.12.2005

T = 0 and T = T_C are two stable fixed points. In contrast to the universal (critical) exponents at T=T_C the universal exponents at T=0 are not generally known. Extensive experimental analyses have lead to a six-fold scheme of empirical exponents for T→0. Table 1 displays the six universality classes in dependence of the dimensionality of the relevant interactions and of the spin quantum number [1].

Table 1

exchange interactions	integer spin	half-integer spin
3D	$T^{\frac{9}{2}}$	T^{2}
2D 3D aniso	T^{2}	$T^{\frac{3}{2}}$
1D 2D aniso	T^{3}	$T^{\frac{5}{2}}$

Different universality classes for integer and half-integer spin values in the long range ordered state is in sharp contrast to the paramagnetic phase. This is explained by the different length scales of the dynamics. The length scale in the paramagnetic phase is defined by the near neighbour distance. In the Curie-Weiss regime of the paramagnetic susceptibility the relevant fluctuations are those between nearest neighbours. Under these conditions are the short range Heisenberg interactions the relevant interactions.

Upon expansion of the correlation length at the critical point the length scale of the dynamic grows dramatically. As a consequence, new types of long range interactions can now become relevant. In fact, Table 1 suggests that the relevant interactions in the long range ordered state are no longer the Heisenberg interactions. In Ref. [2] arguments were given that the associated excitations are magneto-elastic modes. Note in particular that the magnetic excitation spectra as observed with inelastic neutron scattering are material specific. They show in contrast to the order parameter no universality.

Table 1 includes universality classes for one-dimensional interactions. Because of the finite band width of the universality classes this does not mean that the transverse interactions are exactly zero. It is sufficient that they are small enough to be not relevant, i.e. not able to induce a crossover to a higher symmetry class.

In order to elaborate the characteristics of a one-dimensional bulk ferromagnet in more detail we have investigated $NdAl_2$. In the paramagnetic phase $NdAl_2$ is cubic. From the observed T^3 dependence of the spontaneous magnetization it can be concluded that strong axial lattice distortions occur at T_C.

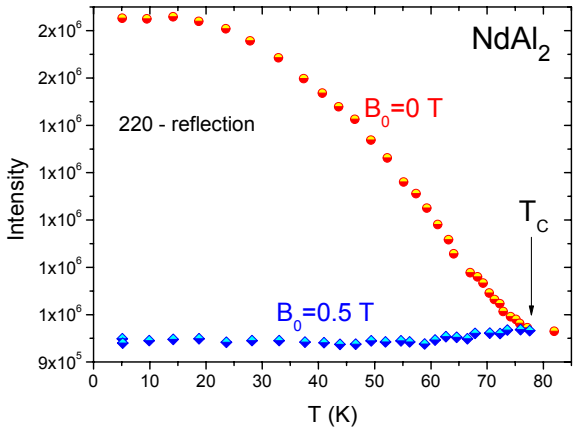

In contrast to a 3D ferromagnet the magnetic scattering intensities drop to zero if the moments are aligned vertically by a magnetic field which is larger than the demagnetization field. Fig.1 shows the temperature dependence of the (220) Bragg reflection for B=0 and B=0.5 Tesla. It can be seen that there are only nuclear intensities for the measurement with B=0.5 Tesla. In other words, there is no long range magnetic order in scattering planes which contain the vertical magnetization. Although a detailed understanding of this result is not trivial it clearly demonstrates the reduced dimensionality of interactions and magnetic order in the 1D ferromagnet $NdAl_2$.

References

[1] U. Köbler, A. Hoser, D. Hupfeld: Physica B 328 (2003) 276.

[2] U.Köbler, M. Kawakami, W. Schnelle: Physica B 367 (2005) 255.

	EXPERIMENTAL REPORT AF fluctuations in $La_{1.2}Sr_{1.8}Mn_2O_7$	Proposal N° PHY-01-1753 Instrument **E2** Local Contact Jens-Uwe Hoffmann
Principal Proposer: Experimental Team:	T. Chatterji - ILL Grenoble, F T. Chatterji - ILL Grenoble, F J.-U. Hoffmann - HMI Berlin U. Amann - HMI Berlin	Date(s) of Experiment 17.10. - 25.10.2005

Date of Report: December 2005

We have determined the magnetic field dependence of the AF correlations in $La_{1.2}Sr_{1.8}Mn_2O_7$ on the flat-cone diffractometer E2 of the Berlin Neutron Scattering Centre (BENSC). The crystal was placed inside a superconducting cryomagnet capable of generating a maximum field of 6.5 Tesla. The vertical axis of the crystal was [010] and the magnetic field was applied parallel to this direction.

Fig. 1 shows the diffuse scattering in the (hol) at H = 0 and 6.5 Tesla at T = 145 K. The relatively weaker diffuse intensity due to antiferromagnetic correlations are clearly seen in between the modulated strong intensity due to ferromagnetic correlations at H = 0. Also seen is the diffuse scattering due to around the 200 Bragg position which also shows peaks at (2+- 0.3,0,+-1). This diffuse scattering arises from lattice distortion or polarons and the satellite peaks are due to short-range correlations between the polarons. At H = 6.5 Tesla intensity due to AF and polaron correlations disappear completely. We determined the integrated intensity of the broad peak at Q = (0.5,0,0) arising due to AF correlations at T = 130 K. We measured the intensity in both increasing and decreasing field up to 6 Tesla but detected no appreciable hysteresis.

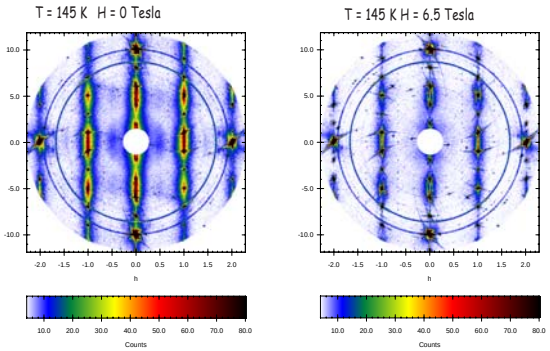

Fig. 1: Diffuse scattering from $La_{1.2}Sr_{1.8}Mn_2O_7$ in the (hol) at H = 0 and 6.5 Tesla at T = 145 K.

Fig. 2 shows the scattered neutron intensity due to the AF correlations at Q = (0.5,0,0) as a function of the increasing magnetic field applied parallel to [010] along with the magnetic field dependence of the resistivity in the a-b plane measured by Moritomo et al. [1]. The AF correlations and resistivity have a very similar magnetic field dependence suggesting that the AF correlations may be related to the CMR effect. The resistivity is expected to be related to antiferromagnetic fluctuations, which imply that adjacent Mn moments are antiparallel. The antiparallel arrangement of spins reduces hopping of the electrons and therefore increases resistivity. The application of magnetic field along the b axis reduces the AF correlations and also causes the reduction in resistivity.

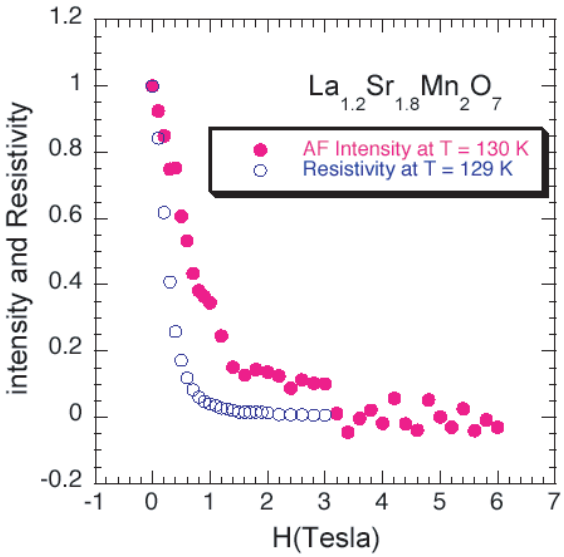

Fig. 2: Magnetic field dependence of the intensity at Q=(0.5,0,0) of $La_{1.2}Sr_{1.8}Mn_2O_7$ along with the magnetic field dependence of resistivity in the a-b plane, measured by Moritomo et al. [1].

Reference:

[1] Moritomo et al., Science **380**, 141 (1996).

BENSC	**EXPERIMENTAL REPORT** **Magnetoelectric correlations in multiferroic $DyMnO_3$ Exchange interactions and multiple magnetic ordering in $DyMnO_3$**	Proposal N° PHY-01-1640 PHY-01-1641 Instrument **E2** Local Contact Jens-Uwe Hoffmann
Principal Proposer: Experimental Team:	M. Fiebig – MBI Berlin M.Fiebig – MBI Berli J.-U. Hoffmann HMI Berlin	Date(s) of Experiment 19.05. – 30.05.2005

Date of Report: Nov. 2005

The scope of the proposed experiments is investigation of the competing sublattice interactions of hexagonal $DyMnO_3$ and the effects of the competition for the magnetic phase diagram and the magnetoelectric effect (ME effect: induction of a polarization by a magnetic field and of a magnetization by an electric field). For this purpose measurements with the Orange Cryostat and the ^{3}He Cryostat insert HS-1 on E2 were done in the range down to 0.15 K. Special emphasis was put on the temperature range from 0.15 to 8 K since in this range the compound is fully ordered, exhibiting ferroelectricity, antiferromagnetic Mn^{3+} ordering and magnetic ordering at the two Dy^{3+} sites.

Our experiments revealed that the $DyMnO_3$ sample available for our experiment was thicker than the absorption length of the neutron beam. Therefore the intensity and the number of the observable diffraction peaks were found to depend on the orientation of the sample in the neutron beam. Many of the allowed low-index reflexes were not observed or much weaker than in other compounds of the hexagonal $RMnO_3$ series. Therefore we restricted our measurements to a selected part of the reciprocal space. We chose the reflexes indexed (31l) with l = 0 to 3 and (21l) with l = 2 to 4, because this limited set already provides access to all the magnetic sublattices. Furthermore, the (h1l) reflexes were found to have the strongest intensity.

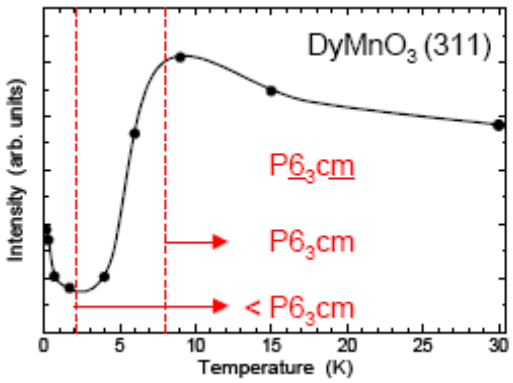

Fig. 1: Temperaturedependence of the intensityof the (311) peak. The (311)peak probes the zcomponent of the Dy^{3+}moment at the 2a site. Theline is a guide to the eye.See Fig. 2 for magneticstructures associated with the given point symmetries.

A detailed quantitative analysis of the data is still in progress. However, Fig. 1 already answers one of the key questions which gave rise to our proposal. The figure displays the intensity of the (311) reflex in the range from 0.15 to 30 K. The intensity is exclusively determined by the magnetic moment along z at the Dy(2a) site. Down to about 8 K the (311) intensity increases continuously. This is followed by a decrease reaching its minimum at 2 K. Below 2 K a renewed increase of intensity is observed.

→

This observation points to ordering, disordering, and reordering at the Dy(2a) site with decreasing temperature. As depicted in Fig. 2, the initial ordering process at >8 K points to a phase with $P6_3cm$ symmetry with antiferromagnetic Dy^{3+} ordering at the 2a and 4b sites along the z axis, but ferromagnetic in-plane correlations between ions at the respective sites. The transient disordering is quite unusual. It points to a change of magnetic structure from $P6_3cm$ to $P6_3cm$ with antiferromagnetic coupling between Dy(4b) ions along the z axis and in the plane. However, the $P6_3cm$ symmetry does not allow ordering at the 2a site which explains the transient disordering evidenced by the decrease of the (311) intensity. The recovery of the (311) peak points to a reduction of symmetry, presumably from $P6_3cm$ to P3c, which allows the system to reorder antiferromagnetically at the 2a site.

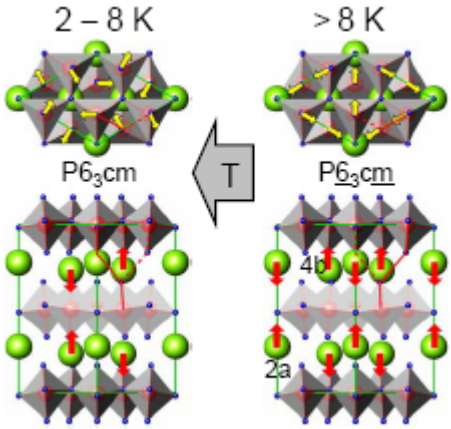

Fig. 2: Magnetic phasesand phase transitionsproposed for $DyMnO_3$ on the basis of our data.

It therefore seems that towards lower temperatures the magnetic structure of $DyMnO_3$ is dominated by Dy-Dy correlations and the competition between the ions at the 2a and 4b sites. Near 0 K full, that is, in-plane and out-of-plane antiferromagnetic Dy^{3+} ordering is preferred. The triangular spin structure of the magnetic Mn^{3+} lattice is maintained at all times because of the strong antiferromagnetic exchange. However, the Mn^{3+} spins change their in-plane orientation repeatedly in order to adopt to the varying magnetic symmetries of the Dy^{3+} sublattices.

Future experiments will be devoted to three aspects:

1. Clarification of the precise symmetry of the magnetic phase below 2 K. A structure with P3c symmetry is most likely and will be tested by including additional reflexes from the reciprocal space in further temperature dependent measurements.

2. Preparation and measurement of thinner samples. If the thickness of the samples is reduced to the absorption length of the neutron beam the low-index reflections will become visible. This will allow us to observe the complete reciprocal space which will lead to more details about the magnetic fine structure and the interaction between sublattices.

3. According to literature data on the magnetic and dielectric properties of the hexagonal $RMnO_3$ series the magnetic low-temperature structure for rare-earth ions from Er to Yb may be quite different from that of $DyMnO_3$ with $HoMnO_3$ acting as borderline compound. Therefore experiments on $ErMnO_3$ will be included in the next step.

BENSC	**EXPERIMENTAL REPORT** **Magnetic structure of Er_2PdSi_3 and Tm_2PdSi_3**	Proposal N° PHY-01-1747 Instrument **E2** Local Contact Jens-Uwe Hoffmann
Principal Proposer: Experimental Team:	M. Frontzek - IFP, TU Dresden E. Faulhaber, A. Kreyssig - IFP, TU Dresden J.-U. Hoffmann - HMI Berlin U. Amann - HMI Berlin	Date(s) of Experiment 06.09. - 15.09.2005

Date of Report: 28.11.2005

The compounds of the isostructual hexagonal R_2PdSi_3 series seem to be strongly influenced by crystal electric field effects (CEF) and the according magnetocrystalline anisotropy. The interplay between CEF and magnetic exchange interaction seem to be of competing type for some compounds, while for others CEF and magnetic exchange seem to favour the same magnetic structure [1]. The neutron scattering experiment on the E2 diffractometer was focused on the magnetic structure of Er_2PdSi_3 and Tm_2PdSi_3. In this experiment we also used the possibility of in-situ ac-susceptibility measurements, developed in our institute to probe both macroscopic and microscopic magnetic properties simultaneously. The ^{3}He insert HS-1 provided temperatures down to 400 mK.

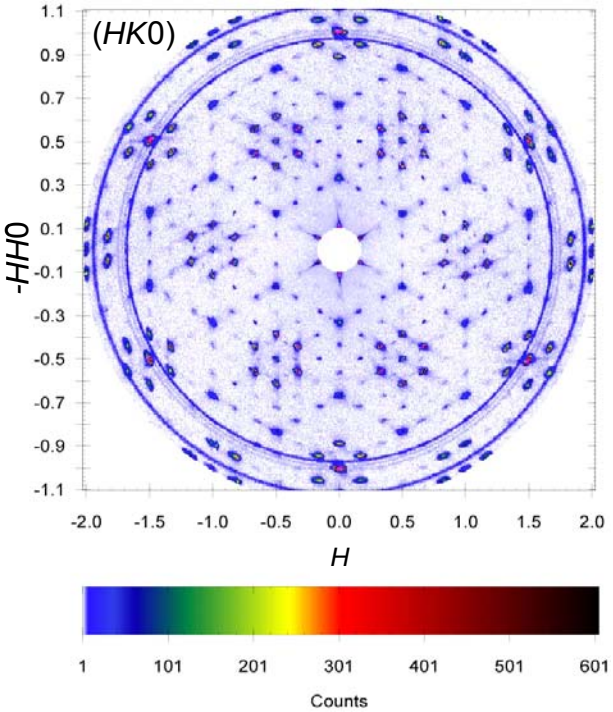

Figure 1: Reciprocal *HK*0-plane of Er_2PdSi_3 at T = 400 mK.

Er_2PdSi_3 orders antiferromagnetically at T_N = 7 K [2] and features a second phase transition below T = 2 K. The second phase transition shows a strong frequency dependence in ac-susceptibility measurements and was therefore assigned to be of spin-glass type by several authors [2]. Figure 1 shows the reciprocal (*HK*0)-plane of Er_2PdSi_3 at T = 400 mK. The position of the magnetic reflections is close to but does not match the commensurate value of 1/9. The propagation is along the (110) direction. The magnetic moments are aligned along the ***c***-axis. The magnetic structure at low temperatures is "squared up" as higher harmonics up to 7th order appear.

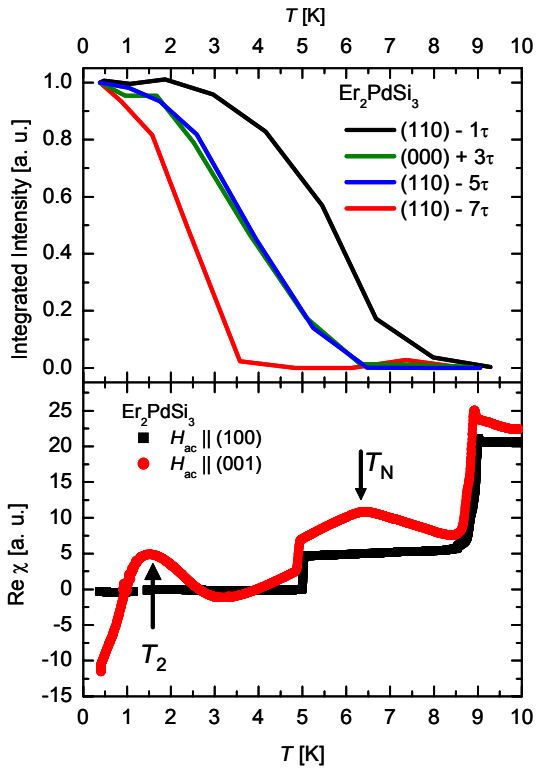

Figure 2: Intensity of magnetic reflections and in-situ measured ac-susceptibility. The two jumps in the susceptibility result from superconducting T_c of Vanadium (5K) and the coil wire (9K).

The temperature dependence of the magnetic intensities is shown in Figure 2 as well as the in-situ measured ac-susceptibility. →

These results strongly suggest that the phase transition at T_2 is a transition to the full squared-up antiferromagnetic structure. Thus, the assumption of a spin-glass like phase in Er_2PdSi_3 could be falsified.

Tm_2PdSi_3 orders antiferromagnetically at T_N = 1.8 K. In the experiment a second phase transition below T_N could not be observed down to 400 mK either in the ac-susceptibility or in the magnetic scattering intensity. The reciprocal (*HK*0) and (*HHL*) planes of Tm_2PdSi_3 are shown in Figure 3 and 4, respectively. In the hexagonal reciprocal (*HK*0) plane the first order magnetic satellites around nuclear peaks are at positions (1/8 1/8 0).

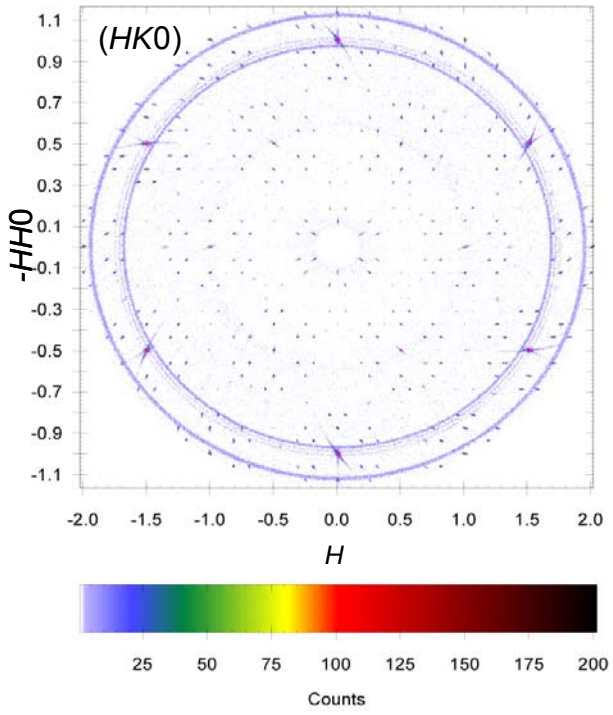

Figure 3: Reciprocal *HK*0-plane of Tm_2PdSi_3 at T = 400 mK.

The next order magnetic satellites are at positions (2/8 1/8 0) and (1/8 2/8 0) thus forming an equilateral triangle with the first order magnetic satellite. These equilateral triangles are positioned on a hexagon around the nuclear peaks due to the crystal symmetry. In the measured (*HHL*)-plane the first order magnetic satellites are on positions (1/8 1/8 ±1/16). Comparing the reciprocal (*HHL*) and (*HK*0) plane it becomes evident that the magnetic satellites at (1/8 1/8 0) in the measured (*HK*0) plane could only be seen due to the relaxed vertical resolution (no magnetic intensity on (*HH*0) positions). With the vertical focused PG monochromator the vertical resolution is about 3 degrees while the flat cone angle to reach the (*HK*1/16) plane is only 2.1 degrees with the used two theta angle.

The next order magnetic satellites can be found on positions (1/8+1/16 1/8+1/16 ±1/16) in the (*HHL*) plane. Along the perpendicular direction to the (*HHL*) plane the *HK* indices running opposite in sign. Thus, the relaxed vertical resolution includes the (*H*+1/16 *H*-1/16 *L*) and (*H*-1/16 *H*+1/16 *L*) reflections. Therefore, the real position of the next order magnetic satellite should be at (2/8 1/8 1/16) and (1/8 2/8 1/16) in reciprocal space. The experimental verification

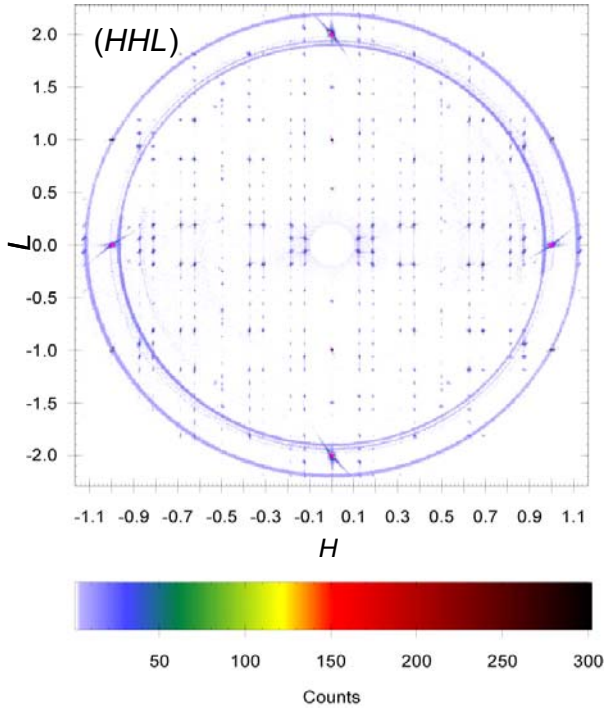

Figure 4: Reciprocal *HK*0-plane of Tm_2PdSi_3 at T = 400 mK.

of this conclusion is planned.

Including the results of the previously studied Tb_2PdSi_3 compound, the similarities of the series became obvious. The modulation of the magnetic moments is along *L* in the case of Tb_2PdSi_3, along *HH* for Er_2PdSi_3 and along both directions for Tm_2PdSi_3.

Acknowledgement

We gratefully acknowledge the financial and technical support from the HMI, Berlin. The realization of the ac-susceptibility was possible by the great support of the sample environment group.

References

[1] M. Frontzek, A. Kreyssig, M. Doerr, M. Rotter, G. Behr, W. Löser, I. Mazilu, M. Loewenhaupt: JMMM *accepted for publication*

[2] K. K. Iyer, P. L. Paulose, E. V. Sampathkumaran, M. Frontzek, A. Kreyssig, M. Doerr, M. Loewenhaupt, I. Mazilu, G. Behr, W. Löser: Physica B **355** (2005) 158-163

	EXPERIMENTAL REPORT **Diffuse neutron scattering from TmB_{12}**	Proposal N° PHY-01-1695-EF Instrument **E2** Local Contact Hans-Peter Nabein
Principal Proposer: Experimental Team:	K. Siemensmeyer - HMI Berlin S. Matas - IEP SAS, Kosice, Slovakia K. Flachbart - IEP SAS , Kosice, Slovakia	Date(s) of Experiment 9.3-14.3.2005

Date of Report: 24.3.2005

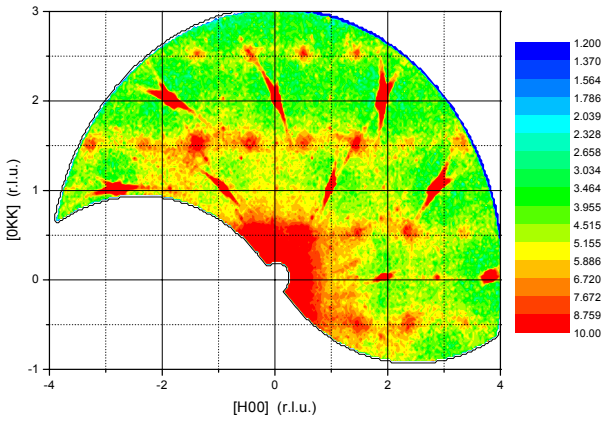

Fig. 1: TmB_{12} neutron response at T= 5 K.

An isotopically enriched TmB_{12} single crystal was used. The crystal of cylindrical shape with 3 mm in diameter and 37 mm length was mounted with the (022) direction perpendicular to the spectrometer plane. Data were taken with an open collimation 60' at a wavelength of 2.386 Å close to the Néel temperature, in the ordered state at 3.1 K and at temperatures above T_N, 3. 7 K, 5 K, 7 K, 10 K and 20 K. The PG filter we used to reject high order contamination. The magnetic structure of TmB_{12} at low temperatures resembles the HoB_{12} type of structure, i.e. an amplitude modulated, incommensurate magnetic structure with wave vector **q**=($\pm\ \delta$ $\pm\delta$ $\pm\ \delta$). Above the Néel temperature T_N a strong diffuse scattering is observed, in a reciprocal space mapping (figure 1) one can see that the diffuse scattering appears in the quadrants around, say (011), (211) etc. and no diffuse signal is seen at the reciprocal lattice positions e.g. (200), (220), (111). Again this behaviour is similar to HoB_{12}. As the temperature decreases and approaches the Néel temperature the diffuse signal localizes around the magnetic reflection positions (Fig.2). Both samples HoB_{12} and TmB_{12} show similar behavior, however, in case of the thulium sample the temperature scale is reduced, probably due to the lower ordering temperature. Thus, the diffuse signal at T=20 K becomes isotropic character and does not show the "chessboard" pattern.

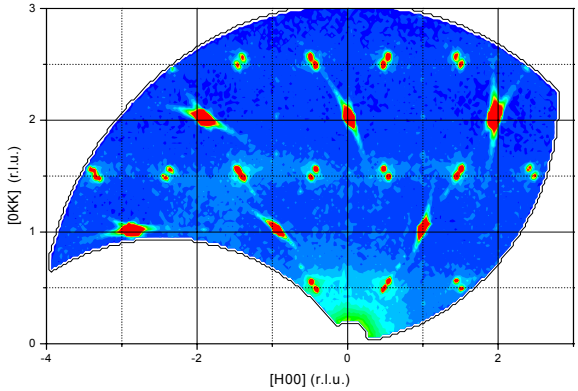

Fig. 2: The TmB_{12} response in the ordered state at a temperature of 3 K.

The origin of the diffuse signal is not clear. In fact, in the asymmetric unit there are four rare-earth atoms occupying (0 0 0), (0 0.5 0.5), (0.5 0.5 0) and (0.5 0.5 0.5). At least two neighbors are required to be parallel, to generate the signal, however, such a correlation can only be thermally activated. For frustrated fcc antiferromagnets systems many single or multiple **q**- structures have been already suggested [2]. The origin of diffuse contribution to scattering could be related to the frustration in the system, but also the multiple q- structure and the underlying magnetic interactions.

Acknowledgements

S.M. acknowledges the support by INTAS 03-51-3036 and APVT-51-031704.

References

[1] A. Kohout, I. Bat'ko, A. Czopnik, K. Flachbart, S. Mat'aš, M. Meissner, Y. Paderno, N. Shitsevalova and K. Siemens-meyer.: Phys. Rev B **70**, 224416 (2004)

[2] M.W. Long: International Journal of Mod.Phys. 7, No. 16 & 17, (1993) 2981

	EXPERIMENTAL REPORT **Magnetic structure of U_4PdGa_{12}**	Proposal N° EF Instrument **E2** & **E4** Local Contact Karel Prokes
Principal Proposer: Experimental Team:	K. Prokes - HMI Berlin R. Jardin - ITU Karlsruhe J.-C. Griveau - ITU Karlsruhe J. Rebizant - ITU Karlsruhe	Date(s) of Experiment 25.08. - 26.08.2005 (E2) 09.09. - 11.09.2005 (E4)

Date of Report: 28.Sept. 2005

The newly discovered cubic ternary U_4PdGa_{12} compound adopts the space group Im-3m. It orders antiferromagnetically at T_N = 43 K. In the paramagnetic state, the magnetic susceptibility can be accounted for by a linear Curie-Weiss law with an effective moment μ_{eff} = 3.4 μ_B and paramagnetic Curie temperature θ_p =-350K.

Neutron-diffraction patterns were collected at temperatures between 1.5 and 60 K using E2 diffractometer with λ=1.21 Å. For the temperature dependence study of the magnetic signal we have used the double-axis diffractometer E4 with λ=2.44 Å has been used. For these measurements about 8 g of U_4PdGa_{12} was powderized. The data were analyzed by means of the Rietveld profile procedure using the program Fullprof.

Inspection of the neutron diffraction pattern recorded at 60 K, in the paramagnetic state of U_4PdGa_{12} is in accord with the cubic space group Im-3m. In this cubic body-centered structure, eight magnetic U atoms that are the only magnetic species occupy the 8(c) ¼,¼,¼ Wyckoff position. There are two Pd atoms in the 2(a) 0,0,0 position, twelve Ga atoms in the 12(d) ¼,0,½ position and another twelve Ga atoms in the 12(e) x,0,0 position with the only free positional parameter x ≈ 0.29.

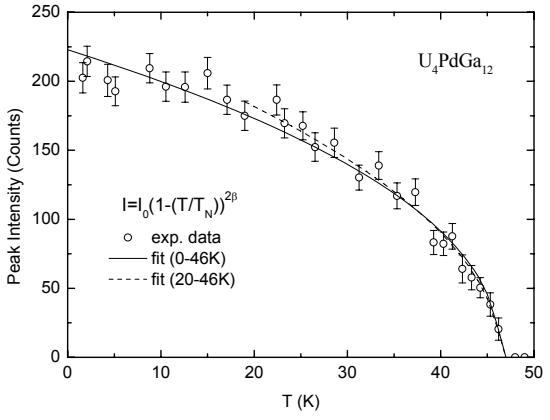

Fig 1: Temperature dependence of (111) Bragg reflections intensity originating from magnetic order in U_4PdGa_{12} as measured on the E4 diffractometer The full and dashed lines represent the best fit to the mean-field type dependence in the full temperature range and for data above 20 K, respectively.

As the temperature is lowered below the antiferromagnetic phase transition temperature, two, small but clearly observable, new Bragg reflections indexable as (111) and (311), that are forbidden for the parent paramagnetic space group appear indicating that the symmetry of the magnetic structure is lower. The temperature dependence of the (111) Bragg reflection peak intensity as measured at E4 is shown in fig. 1 together with fits (in two temperature regions) to a mean-field type dependence of the form $I = I_0(1-T/T_N)^{2\beta}$. In both cases is the value of T_N about 3 K higher as value indicated by the bulk measurements.

Magnetic reflections can be indexed either with propagation vector $\boldsymbol{q_1}$ = (0 0 0) or $\boldsymbol{q_2}$ = (0 0 1). The possible mutual orientations of magnetic moments within each cell were derived for both propagation vector models with the help of computer code MODY. Checking all the possible models the best agreement has been achieved for a simple antiferromagnetic collinear structure shown in fig 2. The model belongs to the propagation vector $\boldsymbol{q_2}$ = (0 0 1).

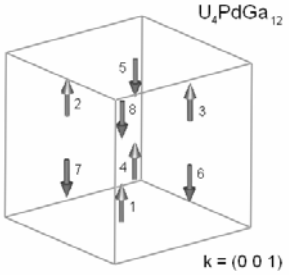

Fig 2: Schematic representation of the simplest magnetic structure of U_4PdGa_{12} that is in accord with experimental data taken at low temperatures. Only U magnetic moments of 0.98 (6) μ_B are shown.

Unfortunately, the nature of present experiment does not allow to determine whether the magnetic structure of U_4PdGa_{12} is described solely by one propagation vector or by combination of symmetrically equivalent propagation vectors and thus also not whether are U moments oriented along one of the principal axes, along one of the face diagonals or along the body diagonal. This can be answered merely in a single crystal experiment planned for the future.

BENSC	**EXPERIMENTAL REPORT** **Magnetic order in CePdAl single crystal: effect of magnetic field**	Proposal N° EF Instrument **E4** Local Contact Karel Prokes
Principal Proposer: Experimental Team:	K. Prokes - HMI Berlin K. Prokes - HM Berlin P. Manuel - RAL ISIS, UK D.T. Adroja - RAL ISIS, UK	Date(s) of Experiment 11.-24.4.2005

Date of Report: 19.Jan. 2006

CePdAl is reported to order antiferromagnetically below 2.7 K with a propagation vector $\boldsymbol{q}$=(0.5 0 τ), τ ≅ 0.35. Two, of the three Ce atoms (Ce1 at x 0 0, with x=0.58 and Ce3 at –x –x 0) in the hexagonal unit cell cary magnetic moment of about 1.6 μ_B while the remaining one at 0 x 0 seems to be paramagnetic [1]. There are three metamagnetic-like transitions in fields applied along the c axis [2].

The crystal has been prepared by a Czocralski method and mounted on the ^{3}He insert that was placed in the HM1 cryomagnet. In this geometry we have been unable to check for the systematic absence/presence of the (-h/2 h k±τ) reflections that are directly linked to magnetic moment on the Ce2 site. The incident neutron wavelength was 2.44 Å.

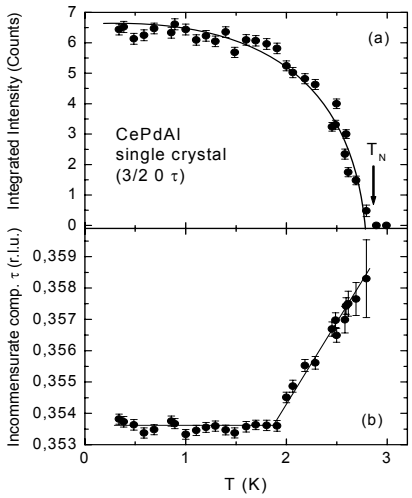

Fig. 1: The temperature dependence of one of the magnetic reflection (3/2 0 τ) **(a)** and the incommensurate component of the propagation vector τ **(b)**. The solid lines through the points are guides for the eye.

As can be seen in fig. 1a, the second-order magnetic phase transition takes place at T_N = 2.78(4) K. The incommensurate component of the propagation vector linearly decreases and around 1.9 K locks-in to τ = 0.3536(2) r.l.u. Ce magnetic moment magnitudes have been determined by fitting to a generally accepted model in which the Ce2 site remains paramagnetic. The refined value of 1.83 (4) μ_B has been obtained. This is 12% higher than value reported for powder sample at 1.5 K [1] but 15% lower than the Ce^{3+} ion moment with J=5/2.

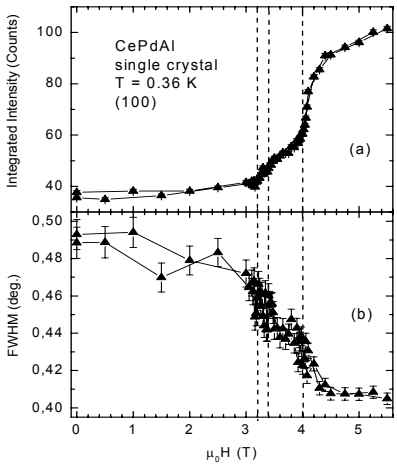

Fig 2: Magnetic field dependence of the (100) nuclear reflection **(a)** and the full width at the half maximum (FWHM) of the (100) reflection **(b)**. Field is parallel to the c axis. The dashed lines represent positions of the metamagnetic transitions at T=0.51K (after [2]).

In fig. 2a and 2b we show the magnetic field dependence of the integrated intensity and the FWHM of the nuclear (100) reflection measured at 0.36 K, respectively. As can be seen, all three transitions are visible. The lower panel documents that upon transition to the field-induced magnetic state the width of (100) reflection gets narrower. This indicates that the frustration present in the ground state phase leading to a strain in the sample is at least partially lifted. This might indicate that the high field state is uniform, having all three Ce atoms magnetic and aligned along the c axis. Refinement to a model with equal Ce moments leads a value of 1.85 (4) μ_B/Ce which is by 0.5 μ_B/Ce higher than it follows from the magnetization measurements [2].

References

[1] A. Dönni et al.: J. Phys. CM **8** (1996) 11213

[2] T. Goto et al.: J. Phys. Chem. of Solids **63** (2002) 1159

BENSC	**EXPERIMENTAL REPORT** **Elastic response of HoB_{12} in external magnetic field**	Proposal N° PHY-01-1709-EF Instrument **E4** Local Contact Karel Prokes
Principal Proposer: Experimental Team:	K. Siemensmeyer - HMI Berlin S. Matas - IEP SAS, Kosice, Slovakia K. Flachbart - IEP SAS , Kosice, Slovakia	Date(s) of Experiment 15.3 - 25.3.2005

Date of Report: Jan. 2006

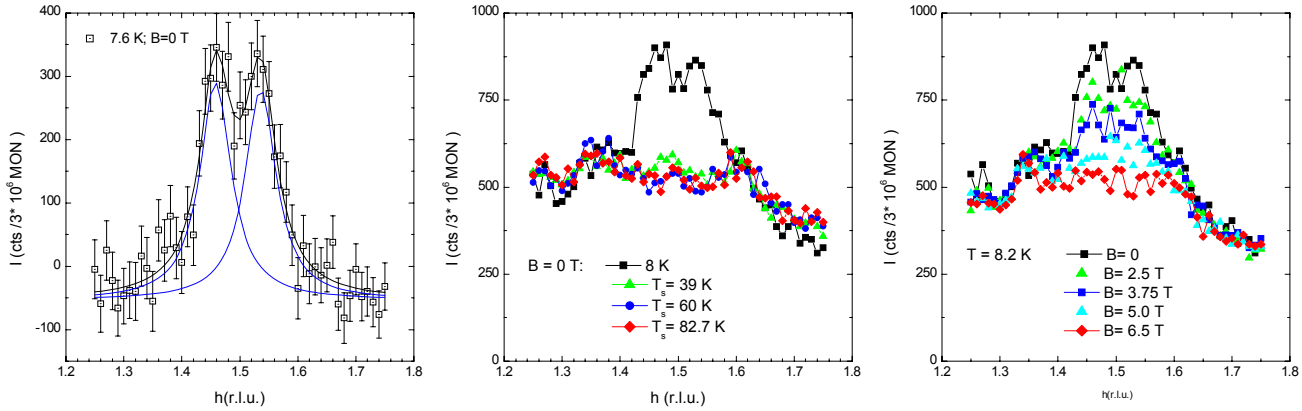

Fig. 1 shows an H- scan on HoB_{12} single crystal at 7.6K in zero magnetic field with background subtracted. The lines are guides to the eye, the blue lines are best fits to measured data.

Fig. 2 and 3 show the same type of scan across the (3/2 3/2 3/2) reciprocal node for different temperature and fields.

Borides of ReB_{12} type crystallise in fcc symmetry, they order antiferromagnetic with an incommensurate magnetic structure. With regard to the high symmetry and isotopic interaction mechanisms they show a surprisingly complex behaviour e.g. for HoB12 three different magnetic phases are observed in an external magnetic field [1]. An isotopic enriched HoB_{12} single crystal was used. The crystal of cylindrical shape with 3 mm in diameter and 22 mm length was mounted with the (022) direction perpendicular to the spectrometer plane. Data were taken with an open collimation 60' and 40' collimation at a wavelength of 2.45 Å close to the Néel temperature, at 8 K in external field up to 6.5 T and at temperatures well above T_N, 10 K, 15 K, 20 K, 40 K, 60K and 90 K The PG filter we used to reject high order contamination.

The magnetic structure of HoB_{12} at low temperatures is an incommensurate magnetic modulated structure with wave $_{vector}$ **q**=(± δ, ± δ, ± δ), δ=0.035. We checked a set of magnetic reflections close to reciprocal node (0.465,0.465 0.465) in order to experimentally prove whose belong to scattering plane (220) and whose are out the plane. Due to big vertical opening of detectors they were observed in previous elastic experiment at E2 spectrometer. Our results simplify and reduce a number of magnetic models which should be taken in consideration.

Above the transition temperature T_N strong diffuse magnetic scattering is observed, in a reciprocal window frame it appears as a „chessboard" pattern where areas with higher and lower contribution to the diffuse signal are observed. In this experiment we probed the diffuse signal from a HoB_{12} single crystal in high magnetic field. A few cuts across reciprocal space for example: from (111) to (-111), across (1/2 1/2 1/2) and (3/2 3/2 3/2) reciprocal nodes were taken with good counting statistics. The field dependence of the diffuse signal (see fig.1 & 2) shows changes in amplitude, however, no change of the correlation length has been observed. Thus the applied field changes only the number of correlated spins (moments), but not the correlation length.

Acknowledgements

S.M. acknowledges the support by INTAS 03-51-3036 and APVT-51-031704.

Reference

[1] A. Kohout, I. Batko, A. Czopnik, K. Flachbart, S. Mataš, M. Meissner, Y. Paderno, N. Shitsevalova and K. Siemens-meyer.: Phys. Rev B **70**, 224416 (2004)

	EXPERIMENTAL REPORT **Helical magnetic structures in Y_2Fe_{17} under high pressure**	Proposal N° PHY-01-1670 Instrument **E4** Local Contact: Karel Proke
Principal Proposer: Experimental Team:	J. Kamarád - ASCR IP Prague, CZ O. Prokhnenko - ASCR IP Prague, CZ K. Proke – HMI Berlin	Date(s) of Experiment 14.02. - 27.02. 2005

Date of Report: 05.03.2005

Recently, the ferromagnetic ground state of Y_2Fe_{17} intermetallic compound has been completely suppressed by pressures above 1 GPa [1]. During the last experiment, we revealed two helimagnetic structures in the Y_2Fe_{17} single crystal under hydrostatic pressures up to 1.05 GPa, using the reciprocal scans along *l*-direction [2]. The incommensurate helical structures (similar to one in Lu_2Fe_{17} compound) were characterized namely by a different temperature dependence of a propagation vector $(00\tau_z)$.

An observed ferrimagnetic character of temperature dependence of saturated magnetization of Y_2Fe_{17} suggests a presence of a non-collinear arrangement of Fe-moments even in basal planes at low temperatures under pressure above 0.8 GPa. [3] Using the 2-axis E4 diffractometer, the VM2 cryomagnet and the CuBe pressure cell, we tried to find a modulation of the pressure induced helimagnetic structure of Y_2Fe_{17} in the basal plane. The Y_2Fe_{17} single crystal ($P6_3/mmc$) was oriented in the CuBe cell with *c*-axis || *H* || axis of neutron diffractometer and with beam in the basal *ab*-plane.

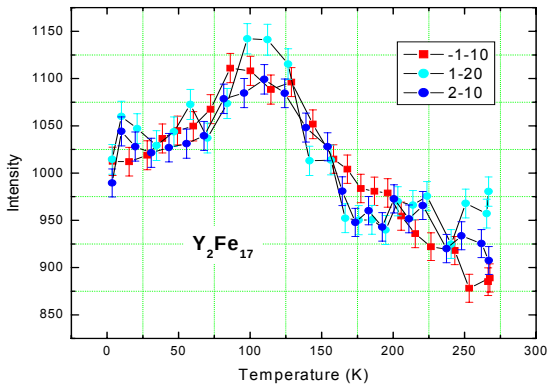

Fig.1: Temperature dependence of integral intensities of (110)-set of reflections under pressure of 1.02 GPa.

The presence of two helimagnetic structures in Y_2Fe_{17} under pressure of 1.02 GPa can be seen in Fig. 1. A large magnetic contribution to integral intensities of (110)-set reflections indicates a presence of the separating ferromagnetic phase between 70 K and 150 K. However, no modulation of the helimagnetic structure has been found by *h*- and *k*-scans at 5 K under pressure 1.02 GPa, see Fig.2.

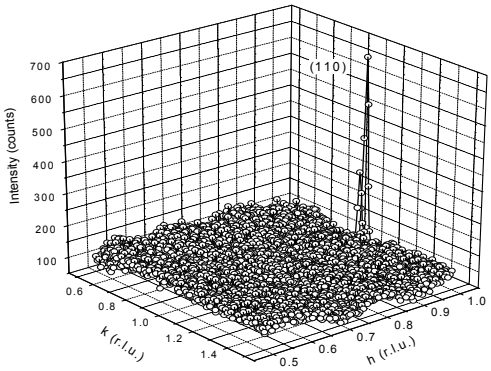

Fig.2: Intensity of *h*- and *k*-scans in vicinity of (110) reflection under pressure 1.02 GPa at 5 K.

On the other hand, intensities of (300)-set reflections (Fig.3) indicate a presence of some Fe-moments antiparallel to others even in fields up to 6.5 T. Unfortunately, none of the used simple models of a moment arrangement satisfies the observed data. A more detailed study of the pressure induced magnetic structures is desirable in the future.

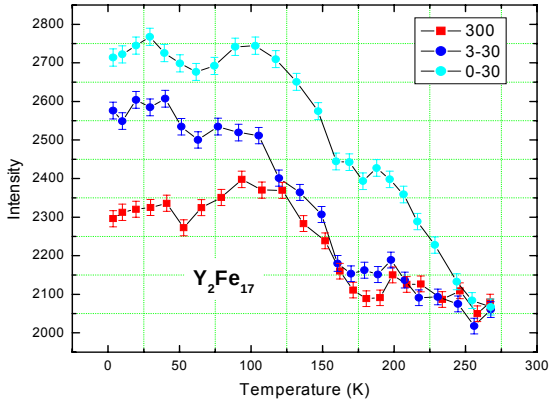

Fig.3: Temperature dependence of integral intensities of (300)-set of reflection under pressure 1.02 GPa.

References

[1] Z.Arnold et al., High Pressure Res. **23** (2003) 165
[2] O. Prokhnenko et al., Phys.Rev.Lett. - accepted
[3] A.V. Andreev et al., Physica **B 348** (2004) 141

	EXPERIMENTAL REPORT **Pressure-induced low-temperature helimagnetic structure in R_2Fe_{17} (R = Y, Lu)**	Proposal N° PHY-01-1781 Instrument **E4** Local Contact Karel Proke
Principal Proposer: Experimental Team:	J. Kamarád - Institute of Physics, Prague O. Prokhnenko - Institute of Physics, Prague K. Proke - HMI Berlin	Date(s) of Experiment 07.08. - 21.08.2005

Date of Report: 20.12.2005

Recently, we have revealed two helimagnetic structures (LTP below 70 K and HTP above 150 K) in the Y_2Fe_{17} single crystal under hydrostatic pressures up to 1.05 GPa, analyzing a set of neutron diffraction reflections (reciprocal scans along *l*-direction) at a wide temperature range [1]. Incommensurate helical structures are characterized by a propagation vector $(00\tau_z)$ and by a metamagnetic transition at the critical field H_C. Temperature dependence of magnetization of the intermetallics at low temperatures and fields above H_C exhibits a ferrimagnetic character (see Fig. 1). This suggests a presence of a non-collinear arrangement of Fe-moments in LTP even at fields above H_C under pressure [2].

Fig.1: Temperature dependence of saturated magnetization

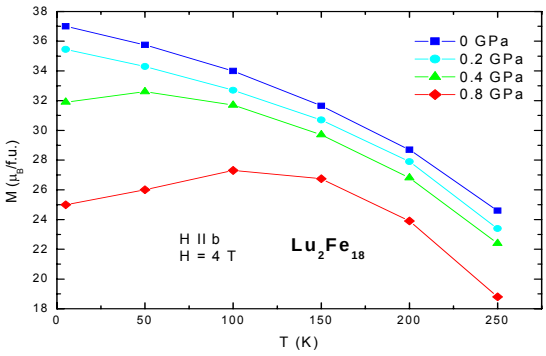

of Lu_2Fe_{17} under different pressures.

We studied the Y_2Fe_{17} and Lu_2Fe_{17} intermetallics under pressure 1.01 GPa and 0.9 GPa, respectively, using two CuBe pressure cells and E4 diffractometer. The Y_2Fe_{17} single crystal was oriented in pressure cell with c-axis || axis of diffractometer ⊥ H (in HM2). No modulation of the helimagnetic LTP structure has been found by *h*- and *k*-scans at temperature range from 2.5 K up to 100 K.

The Lu_2Fe_{17} single crystal was oriented with a-axis || axis of diffractometer || H (in VM1). Using the *l*-scans, a splitting of the $(000)^+$ (see Fig. 2) and $(002)^+$ satellites has been discovered at fields above H_C = 1.7 T !

The new satellite (with larger value of propagation vector $(00\tau_z)$ than the original one) was observed in fields up to 7 T.

Fig.2: Intensity of $(000)^+$ reflections (*l*-scans) at fields

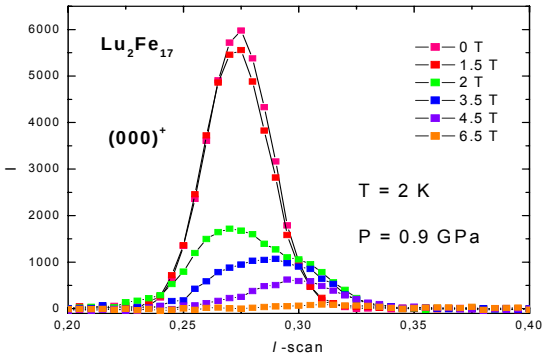

up to 6.5 T under pressure 0.9 GPa at 2 K.

Fig.3: Field dependence of integral intensity of $(000)^+$

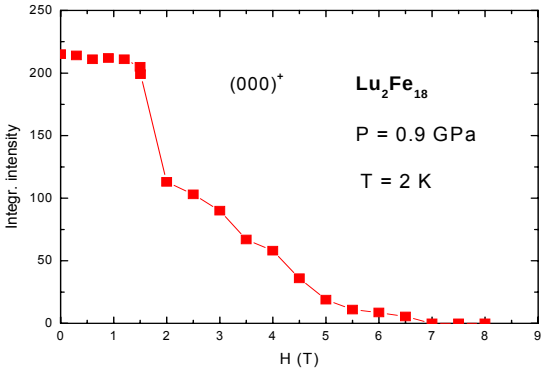

reflection in Lu_2Fe_{17} at 2 K under pressure 0.9 GPa.

The field dependence of an integral intensity of $(000)^+$ reflection in Lu_2Fe_{17} verifies a presence of new non-collinear arrangement of Fe-moments at low temperatures far above H_C (see Fig. 3). A more detailed study of the pressure induced magnetic structures is desirable in the future to test a new model of the magnetic LTP structure.

References

[1] O. Prokhnenko et al., Phys. Rev. Lett. **94,** 107201 (2005)

[2] J. Kamarád et al., J. Phys.: Condens. Matter. **17** (2005) S3069

	EXPERIMENTAL REPORT **Quadrupole structures in high magnetic fields in the AFQ material $PrPb_3$**	Proposal N° PHY-01-1782 Instrument **E4** Local Contact Karel Prokes
Principal Proposer: Experimental Team:	T. Onimaru - SORST JST, ISSP Univ. Tokyo, JP N. Aso - ISSP Univ. of Tokyo, Japan K. Prokes - HMI Berlin	Date(s) of Experiment 17.10. - 01.11.2005

Date of Report: 25.Jan. 2006

Antiferroquadrupolar (AFQ) ordering in the intermetallic *f* electron compounds has been attracting much attention in these years. $PrPb_3$ crystallizes in a simple $AuCu_3$-type cubic structure, and it has a Γ_3 non-Kramers doublet in the crystalline-electrical-field (CEF) ground state. There is a second order transition at 0.4 K with a lambda type anomaly in the specific heat.[1] From various macroscopic experiments, it is considered that an AFQ ordering of Γ_3 type quadrupolar moments occurs. Very recently, we have firstly observed the quadrupole ordered state on the material by neutron diffraction technique in magnetic field. To our surprise, the quadrupole are aligned with modulated structures, although quadrupoles are distributed alternatively in the other AFQ materials.[2]

In the present work, we used a $10x6x5mm^3$ single crystal grown by the Bridegeman method with using a Molybdenum crucible. Neutron diffraction measurements were performed using the two-axis spectrometer E4 installed at the research reactor in the Hahn Meitner Institut. The wave length of neutrons was 2.44 Å and a 40'-40'-(sample)-40' collimation was used. We chose the (*hhk*) scattering plane, and the magnetic field was applied along the [1-10] direction which is perpendicular to the scattering plane. The sample was attached on a copper holder, and mounted on a mixing chamber of a ^{3}He-^{4}He dilution refrigerator. Magnetic field was applied vertically up to 14.5 T with a superconductor magnet.

Fig. 1 shows the results of ***Q***-scans along the line with ***Q***=(*h h* 0.5) at the temperature of *T*=0.1 K and in various magnetic fields up to *H*=14.5 T. Above 7 T, we observed magnetic reflections at ***Q***=(0.02 0.02 0.5) and its equivalents, although we could not observe any superlattice reflections below 6 T. We also confirmed that these magnetic reflections disappear above 0.55 K in the magnetic field of *H*=8 T. These results are very consistent with the *H*-*T* phase diagram determined by our magnetization measurements.[3] From the ***Q*** dependence of the intensity of the magnetic reflections, we can understand that the direction of the magnetic moments is perpendicular to the magnetic field. It strongly suggests that the quadrupole order parameter in the ordered phase should be O_2^2- type. Therefore, the quadrupole order parameter probably changes from O_2^0 to O_2^2 at around 6.5 T when we applied magnetic field along the <110> direction. Moreover, at small region around the field of *H*=6.5 T, the magnetic structure changes variously with changing magnetic field.

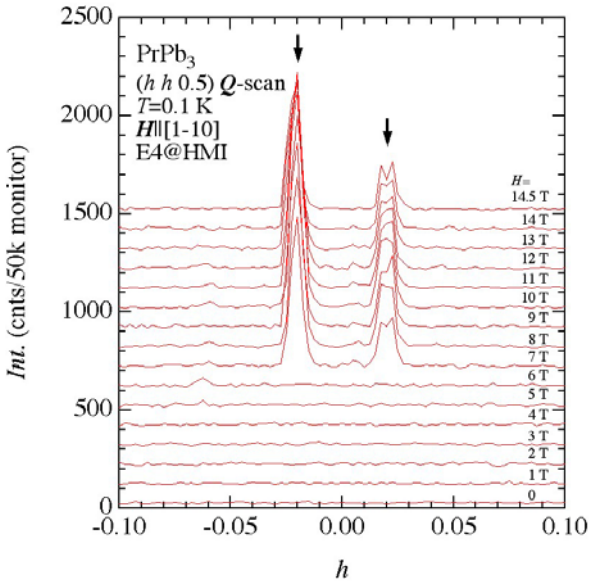

Fig.1: ***Q***-scan along (*h h* 0.5) at the temperature of *T*=0.1 K and in the magnetic fields up to 14.5 T which was applied along [1-10].

References

1) E. Bucher *et al*., J. Low Temp. **2** (1972) 322
2) Onimaru *et al*., Phys. Rev. Lett. **94** (2005) 197201
3) Onimaru *et al*., in preparation

BENSC	**EXPERIMENTAL REPORT** **Quantitative analysis of anisotropic domain growth in $CoNb_2O_6$**	Proposal N° PHY-01-1783 Instrument **E4** Local Contact Karel Prokes
Principal Proposer: Experimental Team:	S. Mitsuda - Tokyo Univ. of Science S. Mitsuda, T. Nakajima - Tokyo Univ. of Sci. K. Prokes, S. Kausche - HMI Berlin	Date(s) of Experiment 13.9. - 19.9.2005

Date of Report: 09.Jan. 2006

Geometrically frustrated isosceles triangular lattice Ising antiferromagnet $CoNb_2O_6$ exhibits slow anisotropic domain growth in the four-fold degenerate antiferromagnetic(AF) phase below $T_{N2}=1.9K$[1,2]. Previous neutron diffraction studies and magnetic susceptibility measurements[1,2] revealed that the time evolution of correlation length $\xi(t)$ is well fitted by the power law as $\xi(t) = \xi_0 + C(T)t^n$ with universal growth exponent is $n\sim0.2$, while that of conventional Ising system with two-fold degenerate ground states is $n=0.5$. Moreover, previous neutron experiments at HMI(2003)[3] reveals the temperature dependence of this domain growth; the pre-factor of the power law $C(T)$ shows 'Arrhenius-law'-like temperature dependence expressed by $C(T)=C_0\exp(-\Delta E/k_BT)$, suggesting some kind of activation energyΔE.

These experimental finding is based on 3D convolution analysis which convolutes the scattering function $S(q)$ with the measured resolution function, and a product of a Lorentzian and two Gaussians is assumed as the form of $S(q)$ in previous studies[2]. However, we can not obtain the absolute value of correlation length in this analysis. Thus, in present experiments, we determined the functional form of $S(q)$ more accurately using 'Multi-Profile-Deconvolution(MPD)' which simultaneously fits numerically-convoluted $S(q)$ to measured profiles along more than 2 directions(as shown in Fig. 1(e)). Trying several functional form of $S(q)$, we found that the $S(q)$ of AF peak is well described by the sum of squared-Lorentzian and Lorentzian with anisotropic width as follows:

$$S(q) \propto \frac{1}{\left(1+(\frac{h-q_a}{\kappa_a})^2+(\frac{k-q_b}{\kappa_b})^2+(\frac{l-q_c}{\kappa_c})^2\right)^2} + \frac{\alpha}{1+(\frac{h-q_a}{\kappa_a})^2+(\frac{k-q_b}{\kappa_b})^2+(\frac{l-q_c}{\kappa_c})^2}$$

Fig. 1(a)-(d) show the results of MPD fitting. The MPD enable us to evaluate the anisotropic spin correlation accurately. We re-analyzed AF domain growth using MPD, and confirmed the 'Arrhenius-law'-like behavior of pre-factor $C(T)$ again. In addition, we obtained temperature-independent growth exponent $n=0.18\pm0.02$ from the results of present neutron diffraction measurements, although, in previous analysis, we fixed exponent n to 0.2 which confirmed by ac-susceptibility measurements. We also found that the squared-Lorentzian term is dominant ($\alpha\sim0.05$) during AF domain growth. The squared-Lorentzian-type of $S(q)$ is also seen in the studies of Random Field Ising Model, and suggest the system consists of large number of domains. By detailed analysis of functional form of $S(q)$, we experimentally confirmed existence of AF domains which grow with time.

We also analyzed the functional form of $S(q)$ in field-induced three-fold degenerated ferromagnetic(FR) phase where field-induced domain growth was reported[1,3]. As a result of MPD, we found that the $S(q)$ of FR peak is also described by the same functional form as that of AF phase. Adopting this $S(q)$ to analysis of FR domain growth, we obtained the external-field dependence of growth as shown in Fig. 1(f), and it is consistent with the results of previous ac-susceptibility measurements[1]. Moreover, we found that the time evolution of correlation length in FR domain growth is also fitted by the power law, and the growth exponent is $n=0.19\pm0.04$. Therefore, it can be said that this growth exponent $n\sim0.2$ is universal constant for the domain growth kinetics in $CoNb_2O_6$.

Noted that ^{3}He refrigerator with VM-3 cryomagnet was invaluable in present experiments to provide access to the temperature region of $T=1.0K\sim2.0K$.

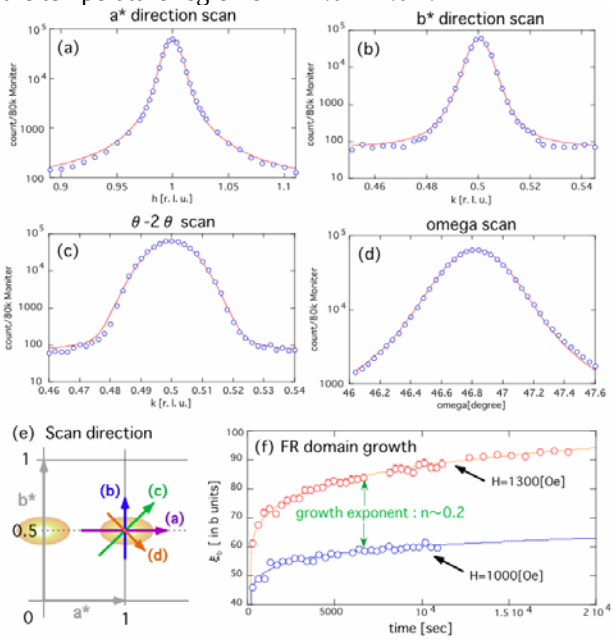

Fig. 1 (a)-(d)The results of MPD for (1,1/2,0) AF peak. The open circles denote observed data and solid lines denote fitting lines.
(e)The scan directions for (1,1/2,0) AF peak. The colored arrows correspond to Fig.1 (a)-(d).
(f)The Time evolution of correlation length in b direction in FR domain growth.

References:

[1] S. Kobayashi, H. Okano, T. Jogetsu, J. Miyamoto and S. Mitsuda Phys. Rev. B **69** 144430(2004)
[2] S. Kobayashi, S. Mitsuda, T. Jogetsu, J. Miyamoto and H. Katagiri Phys. Rev. B **60** R9908(1999)
[3] S. Mitsuda, Y. Inomoto and K. Prokes, BENSC Experimental report **2003**, (2004), 19 (PHY-01-1128)

	EXPERIMENTAL REPORT **Structural and magnetic phase transitions in $Sr_4Fe_4O_{11}$**	Proposal N° PHY-01-1724-LT Instrument **E5** Local Contact Manfred Reehuis
Principal Proposer: Experimental Team:	M. Reehuis, C. Ulrich, B. Keimer - MPI Stuttgart M. Reehuis - MPI Stuttgart C. Ulrich - MPI Stuttgart D. Sheptyakov - ETH Zürich, PSI Villingen, CH	Date(s) of Experiment 14.02. - 27.02.2005 07.03. - 21.03.2005

Date of Report: 05.01.2006

$SrFeO_3$ crystallizes in a simple cubic perovskite-type structure with the space group *Pm*–3*m*. An oxygen vacancy leads to ordered crystal structures in the series $Sr_nFe_nO_{3n-1}$. (n = 2, 4, 8, and ∞) [1]. Large single crystals of these compounds could be grown by the travelling-solvent floating-zone technique [2]. Stoichiometric $SrFeO_3$ could be prepared by postannealing under high pressure, whereas an O-deficiency often results in crystals containing fractions of different phases. But for this experiment a twinned single crystal of $Sr_4Fe_4O_{11}$ (n = 4) was available. This compound crystallizes in the orthorhombic space group *Cmmm* with the lattice constants a = 10.974 Å, b = 7.702 Å and c = 5.473 Å ($2\sqrt{2}a_p \times 2\sqrt{2}a_p \times 2a_p$ supercell; a_p denotes the cubic unit-cell edge) [1]. From electrical resistivity and susceptibility measurements a phase transition could be observed at 55 K that exhibits a hysteresis [3]. Another magnetic transition already sets in at the Néel temperature T_N = 230 K [1]. Mössbauer measurements showed that $Sr_4Fe_4O_{11}$ is a mixed-valence compound, containing the two components Fe^{3+} and Fe^{4+} [1].

Elastic neutron scattering experiments were performed at the four-circle diffractometer E5 using the neutron wavelength λ = 2.34 Å (PG). Complementary high-resolution powder patterns have been recorded at the PSI. Our single-crystal experiment showed a magnetic phase transition at the Néel temperature T_N = 230 K. This is in a perfect agreement with that one observed earlier [1]. Magnetic intensity appeared for the reflections *hkl* with *h*,*l* = odd. The temperature dependence of the reflection (111) is shown in Fig. 1. From the data analysis it could be seen that the magnetic moments of the Fe^{3+}-ions in the positions (¼,¼,½) and (¼,¾,½) (in 4*f* of *Cmmm*) are coupled antiparallel. The same could be found for the Fe^{4+}-ions in the positions (½,~¼, 0) and (½,~¾,0) (in 4*i*), respectively. The moments are aligned parallel to the *b*-axis.

In Fig. 2 it can be seen that additional magnetic intensity appears at 65 K on the positions of (1/4 0 0), (3/4 0 0) and (1/4 1/2 1/2) using the cubic notation. Here it could be seen that these magnetic reflections were strongly broadened indicating the presence of short-range order. The first reflection (1/4 0 0) can be assigned in the orthorhombic representation either with the index (0 1/2 0) or with (3/2 0 3/4), respectively. A determination oft the low-temperature magnetic structure is still in progress. The thermal variation of the nuclear peak (4 0 2) also showed an increase indicating significant shifts of the structural parameters. In order to give a detailed description of the crystal and magnetic structure of $Sr_4Fe_4O_{11}$ further experiments have to be carried out in the next future.

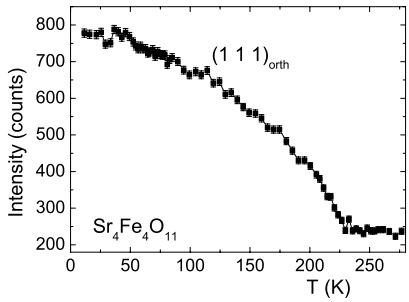

Fig. 1. Temperature dependence of the intensity of the reflections (111) and (202) for $Sr_4Fe_4O_{11}$.

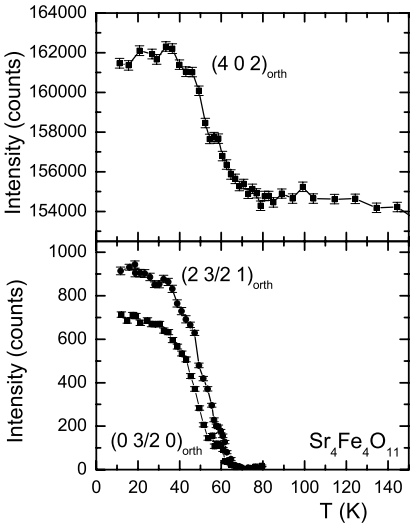

Fig. 2. Temperature dependence of the magnetic reflections (0 3/2 0)$_M$ and (2 3/2 1)$_M$ as well as the nuclear reflections (4 0 2) or (0 4 0) for $Sr_4Fe_4O_{11}$.

References

[1] J.P. Hodges, S. Short, J.D. Jorgensen, X. Xiong, B. Dabrowski, S.M. Mini, C.W. Kimball: Solid State Chem. **151** (2000) 190.

[2] A. Maliuk, J. Strempfer, C. Ulrich, A. Lebon, C.T. Lin: J. Cryst. Growth **257** (2003) 427..

[3] A. Lebon, P. Adler, C. Bernhard, A.V. Boris, A.V. Pimenov, A. Maljuk, C.T. Lin, C. Ulrich, B. Keimer: Phys. Rev. Lett. **92** (2004) 037202.

	EXPERIMENTAL REPORT	Proposal N° PHY-01-1724-LT
BENSC	**Single crystal neutron diffraction study of $La_{0.85}Sr_{0.15}VO_3$ and $La_{0.90}Sr_{0.10}VO_3$**	Instrument **E5** Local Contact Manfred Reehuis
Principal Proposer: M. Reehuis, C. Ulrich, B. Keimer - MPI Stuttgart Experimental Team: M. Reehuis - MPI Stuttgart		Date(s) of Experiment 09.08.-16.08.05 16.11.-30.11.05

Date of Report: 05.01.2006

An extensive investigation of insulating vanadates by neutron scattering has led to the discovery of unusual magnetic ground states and excitations due to the interplay of spin an orbital degrees of freedom. Building on this study, we investigated the magnetic order and crystal structure of vanadates in which a metallic state is generated by doping. The material $La_{1-x}Sr_xVO_3$ becomes metallic at a threshold Sr-doping level of x = 0.176, and the structural transition abruptly disappears [1].

A single-crystal neutron diffraction study of the insulators $La_{0.90}Sr_{0.10}VO_3$ and $La_{0.85}Sr_{0.15}VO_3$ has been carried out on the four-circle diffractometer E5, using the neutron wavelength λ = 2.34 Å (PG). For $La_{0.90}Sr_{0.10}VO_3$ it could be shown that the investigated single crystal was almost detwinned. Therefore we were able to determine the static spin arrangement of the vanadium sublattice. In Fig. 1 it can be seen that a relative strong magnetic intensity has been found on the position of the 100 and a much weaker intensity on the 010. This suggests a *C*-type ordering of the V-moments with a strong component parallel to the *b*-axis. Assuming a component only parallel *c* the intensities of both the 100 and 010 should be almost the same. So we expect a second but weaker component parallel to the *a*-axis, resulting in a magnetic structure with the modes C_xC_y. This structure type was already observed for $NdVO_3$ and $TbVO_3$ [2]. From our data analysis we could deduce for the V-atom a magnetic moment μ_{exp} = 1.39(2) μ_B; the components are μ_x = 0.49(3) μ_B and μ_y = 1.30(2) μ_B. Unfortunately the measured crystal of $La_{0.90}Sr_{0.10}VO_3$ was not single-domain. But we were able to deduce from our data analysis a magnetic moment μ_{exp} = 0.92(2) μ_B, that is considerably smaller than that of $La_{0.90}Sr_{0.10}VO_3$.

In Fig. 2 the temperature dependence of the magnetic and nuclear reflections 100 and 202 are shown. The magnetic intensities of both $La_{0.90}Sr_{0.10}VO_3$ and $La_{0.85}Sr_{0.15}VO_3$ disappear at the Néel temperatures T_N = 110 K and T_N = 75 K, respectively, and they are considerably smaller than the value T_N = 143 K of the undoped $LaVO_3$ [1]. The magnetic and structural transitions of the doped compounds appear practically at the same temperatures, whereas $LaVO_3$ shows a gap of 2 K. Further, it can be seen in Fig. 2 that the phase transitions are much sharper for the vanadate with the lower content of strontium.

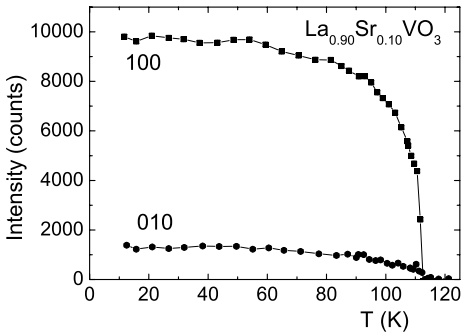

Fig. 1. Temperature dependence of the intensity of the reflections of the magnetic 100 and 010 for $La_{0.90}Sr_{0.10}VO_3$.

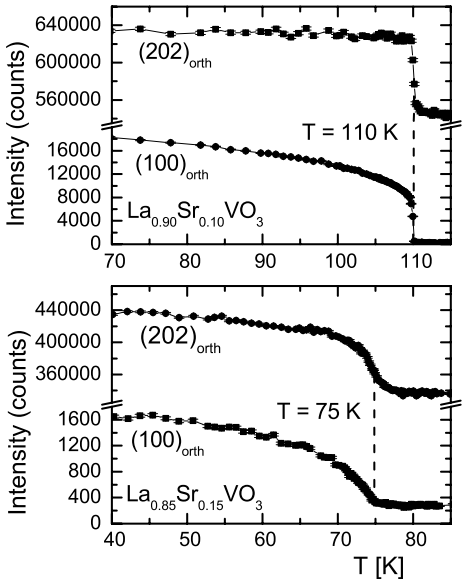

Fig. 2. Temperature dependence of the magnetic intensity of the magnetic and nuclear reflections 100 and 202 for $La_{1-x}Sr_xVO_3$ with x = 0.90 and x = 0.85.

References

[1] S. Miyasaka, T. Okuda and Y. Tokura, Phys. Rev. Lett. **85** (2000) 5388.

[2] M. Reehuis, C. Ulrich, P. Pattison, B. Ouladdiaf, M.C. Rheinstädter, M. Ohl, L.P. Regnault, M. Miyasaka, Y. Tokura, B. Keimer, submitted to Phys. Rev. B.

	EXPERIMENTAL REPORT **Magnetic structure of $CeVO_3$**	Proposal N° PHY-01-1724-LT Instrument **E5** Local Contact Manfred Reehuis
Principal Proposer: Experimental Team:	M. Reehuis, C. Ulrich, B. Keimer - MPI Stuttgart M. Reehuis - MPI Stuttgart	Date(s) of Experiment 29.11. - 10.12.2005

Date of Report: 05.01.2006

Only recently we have started to study the magnetic order of the vanadates YVO_3, $NdVO_3$ and $TbVO_3$ [1]. They show a structural phase transition at about 200 K from an orthorhombic (*Pbnm*) into a monoclinic structure ($P2_1/b$) followed by an antiferromagnetic transition at about 120 K. The magnetic ordering pattern in the *ab*-plane can be described with the basis function [C_x,C_y]. In the present work we have reinvestigated the magnetic order of $CeVO_3$ by single-crystal neutron diffraction because of inconsistencies given in Ref. [2]. The experiment has been performed on the four-circle diffractometer E5 [λ = 2.34 Å (PG)]. In Fig. 1 it can be seen that the thermal variation of the nuclear reflection 022 shows anomalies at 124 K and 136 K indicating spontaneous shifts of structural parameters. The thermal variation of the reflections 100, 010, 102 and 012 finally shows that the magnetic order of the V-sublattice sets in at the Néel temperature T_N = 124 K (Figs. 1 and 2). This is in agreement with YVO_3, $NdVO_3$ and $TbVO_3$, where the structural phase transition also occurs at the higher temperature. In contrast, the onset of the magnetic order was found in Ref. [2] already at the higher temperature. The presence of the reflections 100 and 010 suggests a *C*-type ordering of the V-moments in the *ab*-plane. This is in agreement with Ref. [3] but in contrast to Ref. [2], where a *G*-type order was found. From our data analysis we could deduce for the V-atoms a magnetic moment μ_{exp} = 1.33(2) μ_B; the components are μ_x = 0.57(3) μ_B and μ_y = 1.21(2) μ_B. So the magnetic structure of $CeVO_3$ is very similar to that of $NdVO_3$ [2]. Due to the fact that no other phase transitions occur for both $CeVO_3$ and $NdVO_3$ the monoclinic structure and the *C*-type structure is stable down to low temperature. But Fig. 1 and 2 show at lower temperature a decrease of the reflections 100, 010, 012 and an increase of 102. This clearly suggests an induced magnetic *C*-type order of the Ce-atoms in the *ab*-plane. From the refinements we obtained a magnetic moment μ_{exp} = 0.40(2) μ_B for the Ce-atoms with the components μ_x = 0.20(3) μ_B and μ_y = 0.34(2) μ_B. In Fig. 2 it can be seen that the nuclear reflection 002 also shows a magnetic contribution at lower temperature. This we ascribe to an additional induced ferromagnetic order of the Ce-atoms in the *ab*-plane, resulting in a magnetic structure with the basis functions [F_x,C_y] and [C_x,F_y] that are compatible with Bertaut's representation analysis for the Ce-atoms in the space group *Pbnm*. The ferromagnetic components are μ_x = 0.77(2) μ_B and μ_y = 0.46(2) μ_B resulting in the total moment μ_{exp} = 0.40(2) μ_B.

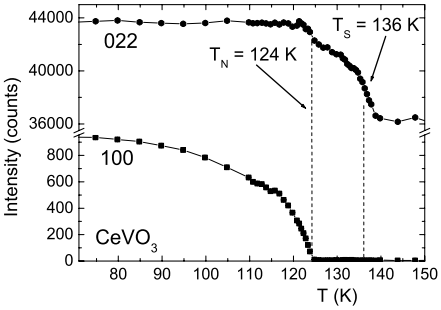

Fig. 1. Temperature dependence of the magnetic and nuclear reflections 100 and 022 of $CeVO_3$.

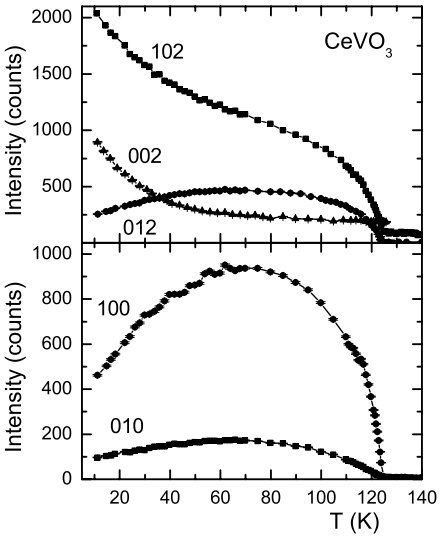

Fig. 2. Temperature dependence of the magnetic intensity of some prominent reflections 100 and 202 of $CeVO_3$.

References

[1] M. Reehuis, C. Ulrich, P. Pattison, B. Ouladdiaf, M.C. Rheinstädter, M. Ohl, L.P. Regnault, M. Miyasaka, Y. Tokura, B. Keimer, submitted to Phys. Rev. B.

[2] A. Muñoz, J.A. Alonso, M.T. Casáis, M.J. Martínez-Lope, J.L. Martínez, M.T. Fernández-Díaz, S, Phys. Rev. B. **68** (2003) 144429.

[3] V.G. Zubkov, G.V.Bazuev, G.P. Shveĭkin, Sov. Phys. Solid State **18** (1976) 1165.

	EXPERIMENTAL REPORT **Relevant and non relevant crystal field interactions (Cr_2O_3, FeO)**	Proposal N° PHY-01-1585 Instrument **E6** Local Contact Norbert Stüßer
Principal Proposer: Experimental Team:	U. Köbler - IFF, FZ-Jülich U. Köbler - IFF, FZ-Jülich A. Hoser - Inst. f. Kristallogr. RWTH-Aachen N. Stüßer - HMI Berlin	Date(s) of Experiment 15.02.-20.02.2005

Date of Report: 12.12.2005

The crystal electric field is a local phenomenon on the length scale of the inter-atomic distance. In the long range ordered state the length scale of the dynamics is, practically, infinite. On this large length scale are all atomistic details averaged out and universality is observed. Universality is well known from the critical exponents that are in-dependent of spin structure and lattice symmetry. A similar universality holds at the stable fixed point T=0 [1].

If the crystal field interaction is much smaller than the exchange interaction the crystal field is not relevant. This is noticed by an observed saturation magnetic moment that corresponds to the full magnetic moment as is observed by the high temperature Curie-Weiss susceptibility. Prominent examples for a non relevant crystal field are the heavy rare earth (RE) elements [2]. In spite of rather strong crystal electric fields the theoretical saturation moment of the free RE^{3+} ion is observed for $T \rightarrow 0$.

In the 3d transition metal compounds the crystal field is mostly not relevant. Exceptions are CoF_2, MnO and Cr_2O_3 [3]. Verification of a reduced saturation moment is, however, ambiguous because the deviations of the Landé g-factor from the pure spin value of g=2 are not known. In this experiment we use as a criterion the fact that saturation of the magnetic order parameter for $T \rightarrow 0$ is according to stable universality classes. These universality classes are represented by the power functions of temperature by which the order parameter approaches saturation for $T \rightarrow 0$. Surprisingly, different universal exponents ε hold for an even or odd number of states per magnetic particle [1]. Note that the number of states, N, and the spin quantum number are equivalent through N=2S+1. In other words, the decrease of the saturation magnetic moment with increasing crystal field interaction is in discrete thermodynamic steps and can alternatively be described either by a reduced number of states or by an effective spin which is smaller than the Hund´s rule value of the free ion.

In FeO the crystal field is not relevant. This reveals from the universal exponent of ε=3 fitted to the sublattice magnetization (see Fig. 1). The T^3 universality class holds for axial magnets with integer spins [1]. As a conclusion, it can be assumed that all states are relevant and that the spin is S=2 as is characteristic for the free Fe^{2+} ion.

For Cr_2O_3 the situation is different. Fig. 2 proves that the universal exponent is again ε=3. The effective spin therefore is integer. Practically, it can be only S_{eff}=1. The number of states therefore is reduced from N=4 (S=3/2) to N=3 (S_{eff}=1) by the action of the crystal field. A reduced saturation moment conforms to earlier neutron scattering investigations [4].

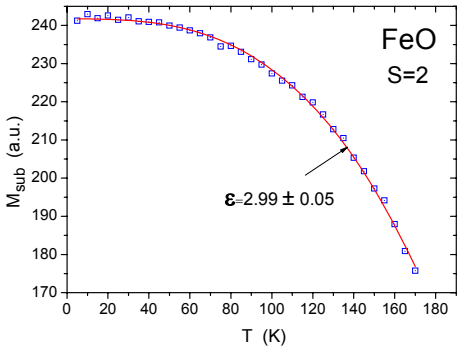

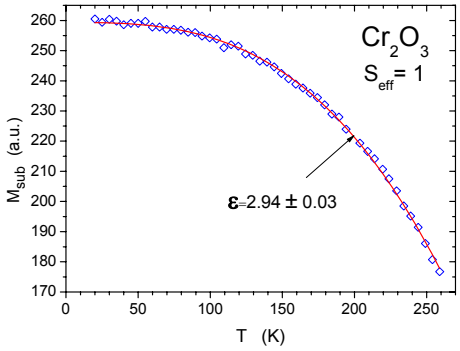

References

[1] U. Köbler, A. Hoser: Physica B 362 (2005) 295.

[2] U. Köbler, A. Hoser: J. Magn. Magn. Mater. 299 (2006) 145.

[3] U. Köbler, A. Hoser, J.-U. Hoffmann: submitted to Physica B.

[4] L.M. Corliss, J.M. Hastings, R. Nathans, G. Shirane: J. Appl. Phys. 36 (1965) 1099.

	EXPERIMENTAL REPORT **Neutron diffraction study of $Ce_3Ag_4X_4$ (X= Ge, Sn)**	Proposal N° PHY-01-1680 Instrument **E6** Local Contact Norbert Stüßer
Principal Proposer: Experimental Team:	E. Wawrzyńska - M. Smoluchowski Inst. of Physics, PL J. Hernández-Velasco, N. Stüßer - HMI Berlin S. Baran, B. Penc, A. Szytuła - JU Krakow, PL D. Kaczorowski - PAS ILTSR Wroclaw, PL	Date(s) of Experiment 20.02. - 28.02.2005

Date of Report: 18.12.2005

Magnetometric, transport properties, XPS and neutron diffraction measurements were performed on polycrystalline samples of $Ce_3Ag_4X_4$ (X = Ge, Sn) that crystallize in the orthorhombic structure of the $Gd_3Cu_4Ge_4$-type. The magnetometric data reveal a ferromagnetic-like behaviour below 10 K in the case of $Ce_3Ag_4Ge_4$ and a weak antiferromagnetic-like maximum at 9 K for $Ce_3Ag_4Sn_4$, not confirmed by the neutron diffraction data. Temperature variations of the electrical resistivity and thermoelectric power suggest their metallic character. The Ce 3d x-ray photoemission spectra show that both compounds are mixed valence systems. Analysis of the f^2 peak weight using the Gunnarsson-Schönhammer theory suggests a hybridization constant of 169 meV for the germanide and 82 meV for the stannide. The valence band spectra are dominated by contributions from the Ag 4d states. Broad and very weak peaks extending between 0 and 4 eV correspond to the Ce $5d6s^2$ states.

Neutron diffraction experiments were carried out for both compounds investigated. For $Ce_3Ag_4Ge_4$ the measurements were made at 1.5 and 25 K whereas for $Ce_3Ag_4Sn_4$ – at 1.5 and 15 K. The results are shown in Fig. 1. The high temperature patterns confirm the crystal structure indicated by x-ray diffraction data. The difference patterns plotted in Fig. 1 as well do not really evidence long range magnetic ordering. The magnetic contribution, if any at all, is very small at 1.5 K in both cases. An experiment in mK-temperatures would be necessary to determine the magnetic structures of the two intermetallics studied.
The details of the experiments mentioned here are described in [1].

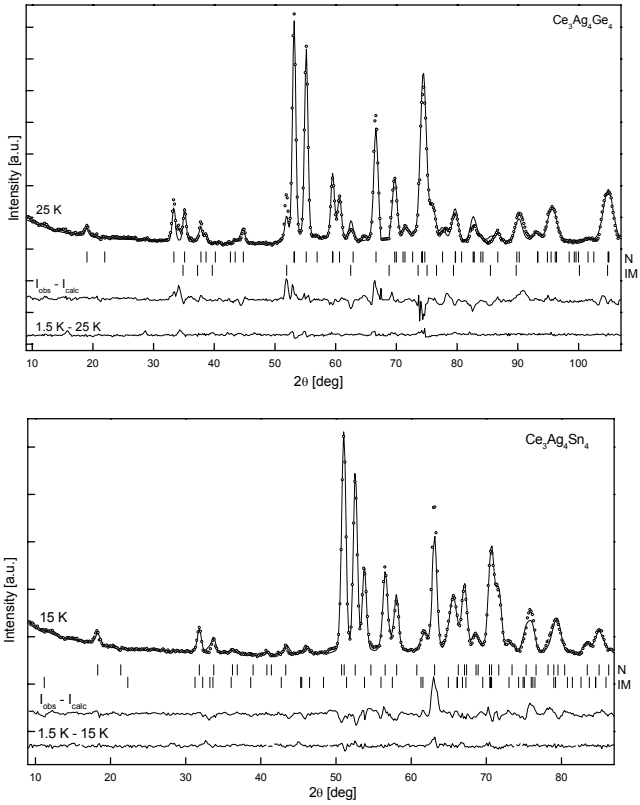

Fig 1: Neutron diffraction patterns of $Ce_3Ag_4Ge_4$ (top) and $Ce_3Ag_4Sn_4$ (bottom). The upper patterns in each section were collected at 25 and 15 K, respectively, the middle ones are differences between the observed and calculated intensities and the difference patterns (1.5 K – 25 K and 1.5 K – 15 K, respectively) are shown at the bottom of each section. The circles represent the experimental points; the solid curves are the calculated profiles for the model crystal structure and the vertical bars indicate the nuclear Bragg peaks originating from $Ce_3Ag_4Ge_4$ (N) and from the impurity phase (CeAgGe, IM) (top) and from $Ce_3Ag_4Sn_4$ (N) and from the impurity phase (Ce_3Sn_7, IM) (bottom).

Reference

[1] A. Szytuła, D. Kaczorowski, S. Baran, J. Hernández-Velasco, B. Penc, N. Stüßer, E. Wawrzyńska: Intermetallics, in print.

	EXPERIMENTAL REPORT **Magnetic structure of nanocrystalline Tb**	Proposal N° PHY-01-1645 Instrument **E9** Local Contact Dimitri Argyriou
Principal Proposer: Experimental Team:	O. Moze - Physics Dept, Modena Uni, Italy O. Moze - Univ. Modena,I C. Vecchini - Univ. Modena,I D. Argyriou - HMI Berlin	Date(s) of Experiment 15.04. – 21.04.2005

Date of Report: 10 May 2005

Nanocrystalline composites are quickly attracting attention becouse of the very different properties they show compared to their coarse counterparts. The only measurement to our knowledge performed on nanocrystalline (grain size of 13 nm) Terbium is by Weissmueller et al. [1] with SANS. We have attempted to measure the anisotropy gap via inelastic neutron scattering. We have also performed a neutron diffraction measurement on E9. Coarse Tb shows 2 magnetic transitions from ferromagnetic at low temperatures to antiferromagnetic at 221K and another one, from antiferro to paramagnetic at 228K. Previous measurements showed the suppression of the antiferromagnetic phase and a rearrangement of the ordering temperature to 226K. We wanted to make scans changing the temperature and to confirm the suppression of the antiferromagnetic phase. We used an incident wavelengh of 1.797 Ang. With the sample mounted inside a Vanadium can to prevent spurious contributions and to maximize the scattering signal due to the 1 gm nano Tb. Different temperatures were investigated, starting from T = 250 K , above the ordering temperature and scans were also done on 18K, 175K, 200K and 220K. Due to the low intensity scattering, measurement times were necessarily long, of the order of 20 hours per run. Fig. 1 shows the low temperature diffraction pattern. From a magnetic structure analysis with GSAS we obtained the Tb moment value for different temperatures. Coarse Tb exibits a moment of 9.2 Bohr Magnetons at low temperature. We obtained a value of 5.9 Bohr Magneton at 18K. Fig. 2 shows the high temperature pattern, from which the intensity difference due to the magnetic contribution is evident. From the data analysis we found that the magnetic moments do not lie totally in the basal plane but have also a component along the c axis. Fig. 3 shows the pattern at 220K in which there is no evidence of an antiferromagnetic phase. Further measurements are naturally desirable in order to measure the magnetic moment dependence with temperature.

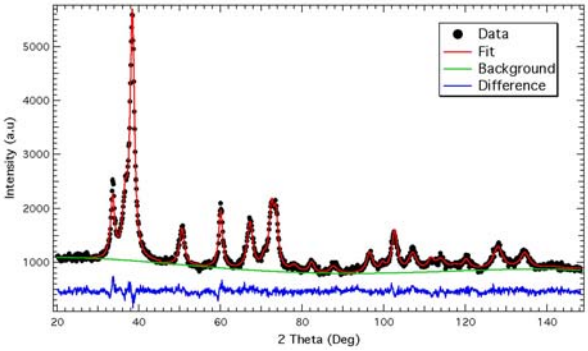

Fig. 1 Observed and calculated diffraction pattern for nano Tb at 18K

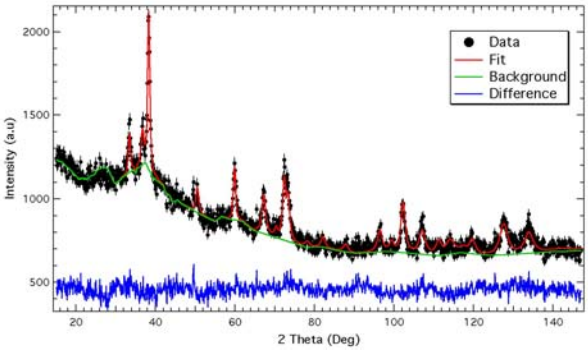

Fig. 2 Observed and calculated diffraction pattern for nano Tb at 250K

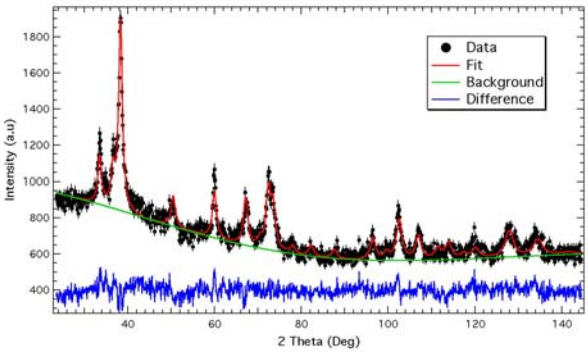

Fig. 3 Observed and calculated diffraction pattern for nano Tb at 220K.

Reference

[1] Weissműller et al: Phys. Rev. B **69**, 054402 (2004)

BENSC	**EXPERIMENTAL REPORT** **Neutron diffraction study of $LaMn_{0.3}Co_{0.7}O_3$**	Proposal N° PHY-01-1654 Instrument **E9** Local Contact Vadim Sikolenko
Principal Proposer: Experimental Team:	K. Bärner - IV. PI UG, Göttingen A.P. Sazonov - ISSSP NAS, Minsk, Belarus I.O. Troyanchuk - ISSSP NAS, Minsk, Belarus D.M. Karpinsky - ISSSP NAS, Minsk, Belarus	Date(s) of Experiment 07.03 - 11.03.2005

Date of Report: Jan. 2006

Lately, the solid solutions with chemical formula $LnMn_{1-x}M_xO_3$ (Ln notes lanthanide, M – alkali earth element) are of considerable interest because of their peculiar magnetic properties [see [1] and Reff. therein]. Such materials show high-temperature ferromagnet-paramagnet transitions and exhibit metamagnetic transformations. The origin of the complex magnetization behavior of the $LaMn_{1-x}Co_xO_3$ system is still a challenge. We should note that a $LaMn_{0.5}Co_{0.5}O_3$ compound is a ferromagnet with a Curie temperature (T_C) above 200 K [1]. On the other hand, Mn enriched compound $LaMn_{0.8}Co_{0.2}O_3$ exhibits maximum magnetic moment of 3.4 μ_B/f.u. [2] among the $LaMn_{1-x}Co_xO_3$ series. Such a strong ferromagnetic coupling leads to the rather low Curie temperature – about of 150 K. The properties of Co enriched compounds, however, were not investigated precisely, especially by means of NPD method. Therefore, we would like to study $LaMn_{0.3}Co_{0.7}O_3$.

The $LaMn_{0.3}Co_{0.7}O_3$ composition was synthesized by the conventional ceramic method at T = 1320 °C. After synthesis the sample was slowly cooled to room temperature. The neutron powder-diffraction experiments were carried out on FIREPOD with incident neutrons of wavelength λ = 1.7973 Å. Data were collected on warming from 1.3 to 300 K.

It is known that LaCoO3 a rhombohedrally distorted unit cell. Therefore, the Rietveld refinement of the NPD data was performed in a rhombohedral space group R-3c. The results of Rietveld refinement is presented in figure. Structural parameters at 1.3 and 300 K are listed in table.

Results of the Rietveld refinement of the NPD pattern of $LnMn_{0.3}Co_{0.7}O_3$ measured at 1.3 and 300 K. Atomic positions: La – 6a(0, 0, 0.25); Co/Mn – 6b(0, 0, 0); O – e(0, y_O, 0.25).

T (K)	1.3	300
a, Å	5.4704(1)	5.4767(1)
c, Å	13.1172(3)	13.1670(3)
y_O	0.4465(2)	0.4477(2)

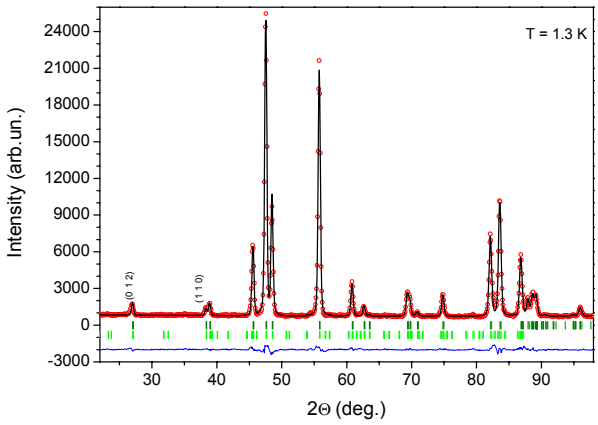

Results of the Rietveld refinement of the NPD pattern of $LnMn_{0.3}Co_{0.7}O_3$ measured at 1.3 K. The measured data (open circles) is shown together with the resulting fit (continuous line) and their difference plot (cont. line below). The ticks show the predicted 2Θ positions for the Bragg peaks of the monoclinic crystal phase (upper row) and the magnetic phase (lower row).

According to our data, the sample exhibit long-range magnetic order. The magnetic contribution is most evident for the peaks which correspond to (0 1 2) and (1 1 0) reflections, and the whole set of data indicates ferromagnetic type of order. To refine the average magnetic moment of the Co-Mn sublattice ($M_{Co/Mn}$) we performed the calculations in a model assumed that the magnetic moment vector parallel to one of the crystallographic axes. This model was successfully used for La_2CoMnO_6 [1]. Thus, we have obtained next value: $M_{Co/Mn}$ ~ 0.5 μB at 1.3 K.

References

[1] I.O. Troyanchuk, A.P. Sazonov, H. Szymczak, D.M. Tobbens, H. Gamari-Seale: JETP **99**, 363 (2004).

[2] I.O. Troyanchuk, L.S. Lobanovsky, D.D. Khalyavin, S.N. Pastushonok, H. Szymczak: J. Magn. Magn. Mater. **210**, 63 (2000).

	EXPERIMENTAL REPORT **Neutron diffraction study of the $TbCo_{0.47}Mn_{0.53}O_3$ Perovskite**	Proposal N° PHY-01-1661 Instrument **E9** Local Contact Vadim Sikolenko
Principal Proposer: Experimental Team:	H. Gamari-Seale - IMS NCSR Demokritos, GR A.P. Sazonov - ISSSP NAS, Minsk, Belarus I.O.Troyanchuk - ISSSP NAS, Minsk, Belarus K.L. Stefanopoulos - IPC NCSR Demokritos, GR	Date(s) of Experiment 11.03 - 16.03.2005

Date of Report: Jan. 2006

Rare-earth (RE) cobaltites and manganites are the model objects to study the interactions between magnetic, electronic and structural phases in strongly correlated systems. Mixed oxides based on both the cobalt and manganese ions exhibit varieties of the magnetic properties. For instance, a $LaCo_{0.5}Mn_{0.5}O_3$ compound is a ferromagnet with a Curie temperature (T_C) above 200 K. This is unexpected because $LaCoO_3$ and $LaMnO_3$ are the paramagnetic and antiferomagnetic materials, respectively. It is known, however, that the properties of the compounds with the perovskite structure change noticeably with replacement of the La ion by another rare-earth element with smaller ionic radius. Therefore, we would like to study Tb_2CoMnO_6 compound, which was not studied by NPD method before.

The $TbCo_{0.47}Mn_{0.53}O_3$ composition was synthesized by the conventional ceramic method at $T = 1320$ °C. After synthesis the sample was slowly cooled to room temperature. The neutron powder-diffraction experiments were carried out on FIREPOD with incident neutrons of wavelength $\lambda = 1.7973$ Å. Data were collected on warming from 1.6 to 300 K.

To test the possibility of partial ordering of the Co and Mn ions we performed the refinement in a monoclinic space group $P2_1/n$ by analogy to the La_2CoMnO_6 [1] and Y_2CoMnO_6 compounds. This group have already two non-equivalent crystallographic *B*-position, B(1): 2d(½,0,0) and B(2): 2c(0,½,0). Our calculations shown that there are ~ 25 % of antisite defects, i.e. the fractional occupancy of the B(1)-site consist of 75 % of Co and 25 % of Mn. The opposite is true for the B(2)-site. The results of Rietveld refinement is presented in figure.

According to our data the sample exhibit long-range magnetic order. The magnetic contribution is most evident for the peaks which correspond to (1 1 0) and (0 0 2) reflections, and the whole set of data indicates ferromagnetic type of order. To refine the average magnetic moment we performed the calculations in a model assumed that the magnetic moment vector parallel to one of the crystallographic axes. This model was successfully used for La_2CoMnO_6 [1].

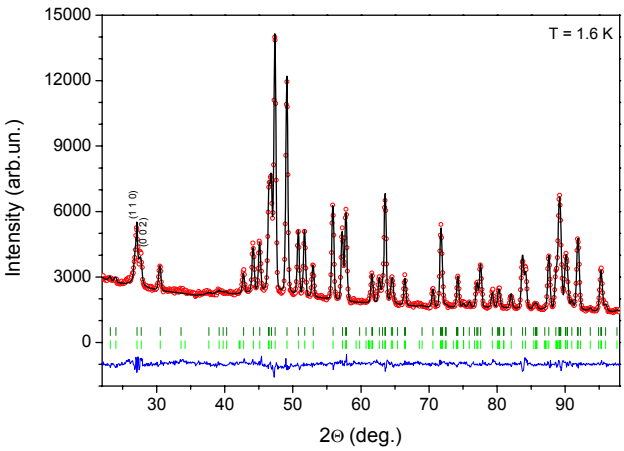

Results of the Rietveld refinement of the NPD pattern of $TbCo_{0.47}Mn_{0.53}O_3$ measured at 1.6 K. The measured data (open circles) is shown together with the resulting fit (continuous line) and their difference plot (cont. line below). The ticks show the predicted 2Θ positions for the Bragg peaks of the monoclinic crystal phase (upper row) and the magnetic phase (lower row).

The magnetic moment of Co/Mn sublattice ($M_{Co/Mn}$) is difficult to determine because the negative *f-d* magnetic interaction orienting the magnetic moment of the Tb sublattice (M_{Tb}) in the opposite direction to that of the Co/Mn one. Nevertheless, we have obtained next values: $M_{Co/Mn} \sim 2$ μB and $M_{Tb} \sim 0.7$ μB at 1.6 K.

According to our data the Co and Mn ions are predominantly placed at the B(1) and B(2) sites, respectively. The average B(1)-O distance is about 1.92 Å, indicating the valence of the Co ions to be more likely 2+. The average B(2)-O distance is about 2.05 Å, suggesting the presence of Mn^{4+}.

Reference

[1] I.O. Troyanchuk, A.P. Sazonov, H. Szymczak, D.M. Tobbens, H. Gamari-Seale: JETP **99**, 363 (2004).

BENSC	**EXPERIMENTAL REPORT** **Continuous or integer period modulations in $La_{1-x}Ca_xMnO_3$ for x>0.5?**	Proposal N° PHY-01-1662 Instrument **E9** Local Contact Dimitri Argyriou
Principal Proposer: Experimental Team:	M. Pissas, NCSR Demokritos, GR D. Stamopoulos, NCSR Demokritos, GR	Date(s) of Experiment 04.04. - 08.04.2005

Date of Report: 01.02.2006

In this experiment we have measured neutron powder diffraction patterns at E9 instrument, using high quality $La_{1-x}Ca_xMnO_3$ ($0.5 \le x \le 0.8$) samples aiming to display how the magnetic reflections of the Mn^{4+}/Mn^{3+} sublattices change with x. Special emphases has been given in studying samples into regime $0.5 \le x \le 0.6$ with $\Delta x = 0.01$.

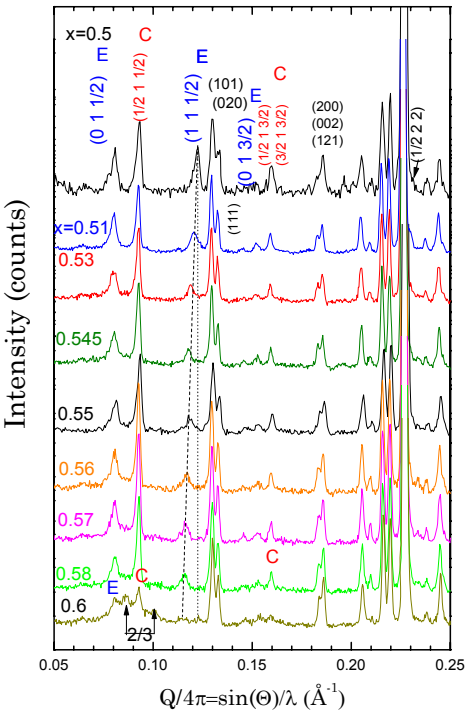

Fig.1 Selected region of the low-angle neutron powder diffraction profile of the $La_{1-x}Ca_xMnO_3$ ($0.5 \le x \le 0.6$) compound

Fig. 1 illustrates the evolution of the neutron diffraction patterns, at T=2 K, for $0.5 \le x \le 0.6$. The first interesting characteristic seen in these patterns is the most intense structural satellite Bragg peak, with indices $(1/2-\varepsilon_s,2,2)$, located at the right foot of the strongest doublet (022)/(420) ($Q/4\pi=0.23$ Å^{-1}), marked by an arrow at the pattern with x=0.5. Other crystal-structure satellites are much weaker or obscured by fundamental reflections. As x increases, incommensurability parameter, ε_s, increases, pushing the satellite Bragg peek towards the (022)/(420) doublet. The next interesting characteristic of the NDP is the appearance of two families of magnetic Bragg peak known as E and C type. As far as the E-type magnetic Bragg peaks are concerned, a pronounced shifting of the (1,1,1/2) magnetic peak, in respect to the one corresponding to the x=0.5 compound, is observed (see dashed line in Fig. 1). This peak-shifting can be accounted for by using an incommensurate parameter $\varepsilon_m(x)$ which modifies the Miller's indices as $(1-\varepsilon_m,1,1/2)$. It should be emphasized that, it is impossible to account for this shifting using the nuclear unit cell parameters describing the crystal structure. In addition, to the shifting, the E-type magnetic peaks, with $h \neq 0$ are accompanied with significant broadening. On the other hand, the C-type magnetic Bragg peaks remain practically steady, although we can not theoretically reproduce the experimental (1/2,1,3/2) peaks intensity by means of the C-type magnetic structure which has been adopted for the x=0.5 compound.

Fig. 2 shows the phase diagram of the $La_{1-x}Ca_xMnO_3$ compound deduced from neutron diffraction data, and the ε_m variation with x. The ε_m increases with x for $0.5<x<0.56$. For $0.56<x\le0.61$ the sample enters in a two magnetic-phase regime. As x further increases only the 3a magnetic structure is present. For $0.7 \le x \le 0.78$ three phases coexist (3a, 4a and C), while at x=0.8 only the C structure is present.

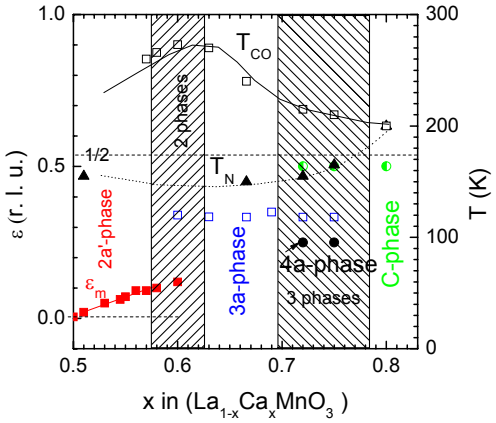

Fig. 2 Phase diagram of the $La_{1-x}Ca_xMnO_3$ ($0.5 \le x \le 0.8$) (right axis) and concentration variation of the ε_m (left axis).

	EXPERIMENTAL REPORT **Magnetic properties of $LaCo_{0.5}Fe_{0.5}O_3$**	Proposal N° PHY-01-1665 Instrument **E9** Local Contact Michael Tovar
Principal Proposer: Experimental Team:	H. Szymczak - Institute of Physics PAN, Warsawa D. Karpinsky - ISSSP NAS, Minsk, Belarus H. Szymczak - Institute of Physics PAN, Warsawa M. Tovar - HMI Berlin	Date(s) of Experiment 21.04. - 25.04.2005

Date of Report: 26.12.2005

Magnetic and transport properties of cobaltites with perovskite structures are known to depend strongly on the electronic configuration of the transition metal ions [1-4]. Particularly the spin state of the cobalt ions is a key factor for the $LaCo_{1-x}M_xO_3$ (M=Co, Ni, Fe) systems which affects on its physical properties. The magnetic and crystal structure investigations were the main objects of the high resolution neutron diffraction measurements.

The neutron diffraction studies have been carried out using the E9 instrument (λ=1.7971 .). The structures have been refined by the full- pattern Rietveld method using the program "FullProf" [5]. The diffraction patterns of the $LaCo_{0.5}Fe_{0.5}O_3$ sample have been recorded at the different temperatures.

The crystal structure refinement of the diffraction pattern recorded at 300 K (Fig. a), revealed that the best reliability factors were obtained assuming the *R*-3*c* space group. Besides rhombohedral peaks, additional ones appear in the neutron powder pattern with a temperature decrease. Such reflections, like (111), (101) are forbidden for the *R*-3*c* space group, but allowed for the orthorhombic one. With a further temperature decrease the rhombohedral peak intensities become quite low and they vanish at 200K. Below this temperature the $LaCo_{0.5}Fe_{0.5}O_3$ sample has a pure orthorhombic structure (Pbnm space group) (Fig. b). Such a behavior suggests a two-phase crystal structure in the temperature range 200 K < *T* < 300 K.

According to the low temperature neutron powder measurements one can conclude that the most noticeable magnetic contribution is observed from the (101), (011) and (013), (121) reflections, which are close to the 23,2° and 45,5° angles correspondingly (Fig. b). One can see, that the observed reflections indicate a magnetic structure similar to that of the $LaFeO_3$ [6]. The spatial orientation of the antiferromagnetic vector can be concluded from the (101), (011) peaks intensities. Because of extremely close allocation of these reflections it is difficult to evaluate their intensities, but from the peak shape we can conclude that they are almost equal. Therefore the antiferromagnetic vector has most probably a spatial orientation G_z.

So extracted from the neutron diffraction data the magnetic moment per B ion is about 1.6 μ_B at 6 K. Assuming a low spin state of the Co^{3+} ions, only Fe^{3+} would carry a magnetic moment, which yield about 3.2 μ_B. It has been found that at low temperatures the Co–O bond lengths in the CoO_6 octahedron differ from each other insignificantly, indicating very small oxygen octahedron distortions. At higher temperatures the situation is more complicated. Since the best reliability factors for the $LaCo_{0.5}Fe_{0.5}O_3$ sample were obtained with the *R*-3*c* space group, we can suppose that if a difference in bond lengths really exists, it is insignificant.

The magnetic properties of the $LaCo_{0.5}Fe_{0.5}O_3$ compound can be described using a model according to which Co^{3+} ions are predominately in the low spin state and do not participate actively in the magnetic interactions, whereas the Fe^{3+} ions interact antiferromagnetically causing a weak ferromagnetism.

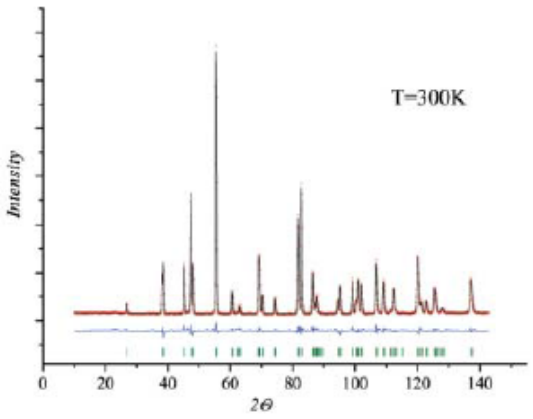

Fig. a

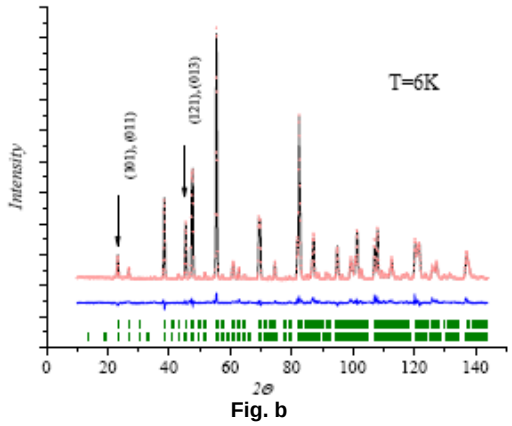

Fig. b

References

[1] K. Asai, O. Yokokura, M. Suzuki, T. Naka, T. Masumoto, H. Yakahashi, N. Mori, K. Kohn: J. Phys. Soc. Jpn. **66**, 967 (1997)

[2] K. Asai, A. Atsuro, O. Yokokura, J.M. Tranguada, G. Shirane, K. Kohn: J. Phys. Soc. Jpn. 67, 290 (1998)

[3] P.M. Raccah, J.B. Goodenough: J. Appl. Phys. 39, 1209 (1968)

[4] M. Itoh, I. Natori, S. Kubota, K. Motoya: J. Phys. Soc. Jpn. 63, 1486 (1994)

[5] T. Roisnel, J. Rodríguez-Carvajal: Proceedings of the Seventh European Powder Diffraction Conference (EPDIC 7), 118-123 (2000)

[6] T. Peterlin-Neumaier, E. Steichele: J. Magn. Magn. Mater. 59, 351 (1986)

	EXPERIMENTAL REPORT **Structure and magnetism in UPd_2Sb**	Proposal N° PHY-01-1756 Instrument **E9** Local Contact Michael Tovar
Principal Proposer: Experimental Team:	S. Süllow - IPKM, TU Braunschweig O. Prokhnenko - HMI Berlin M Tovar - HMI Berlin	Date(s) of Experiment 22.09. - 23.09.2005

Date of Report: 05.01.2006

Recently, the uranium based heavy fermion compound UPd_2Sb has been synthesized and physically characterized for the first time [1]. It has been found that the system crystallizes in the cubic Mn_2CuAl structure (space group *Fm3m*), with a lattice parameter of 6.766(2)Å. Further, a study of the bulk properties [1] indicated the presence of structural disorder [2]. To test UPd_2Sb for the presence of crystallographic disorder we have carried out a structural study using the E9 spectrometer, with a neutron wave length of $\lambda = 1.797429$Å.

In Fig. 1 we plot the overall spectrum taken at a low temperature of 60K. In the figure we include the result of a Rietveld refinement of the data, using a derivative of the fully ordered Mn_2CuAl lattice. With this structure we reproduce the peak positions observed experimentally, using a lattice parameter of 6.7407(3)Å, in agreement with previous work. The refinement value R_{Bragg}, however, is rather poor. Assuming a fully ordered Mn_2CuAl lattice we obtain $R_{Bragg} \sim 28\%$, and improve this value somewhat by allowing for about 10% site exchange between U and Pd ions to $R_{Bragg} \sim 19\%$. Moreover, for our disordered structure model we obtain an unusually large thermal displacement factor $B_{iso} = 4.25$ for all atoms. The large R_{Bragg} value reflects that in the fit we do not adequately describe the experimental peak form.

This is illustrated in Fig. 2, where we enlarge the area around the [2 2 0] peak at ~44º. As can be seen, aside from intensity in the central region of the peak there are broad tails on both sides. These tails indicate that there are structurally short range ordered regions in the sample.

Altogether, our structural study shows that crystallographically UPd_2Sb is disordered on an atomic scale, in a very similar fashion as various other uranium based Heusler compounds [2].

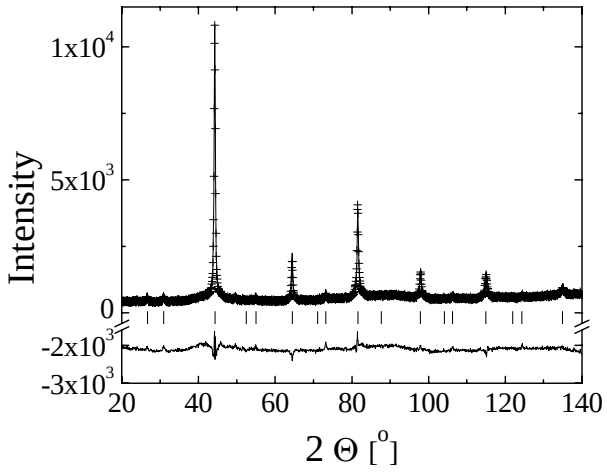

Fig. 1: Neutron powder diffraction spectrum taken on UPd_2Sb at 60K: (+) experimental data, solid line and tics indicate the result of a Rietveld refinement of the data, the lower panel visualizes the difference between fit and data; for details see text.

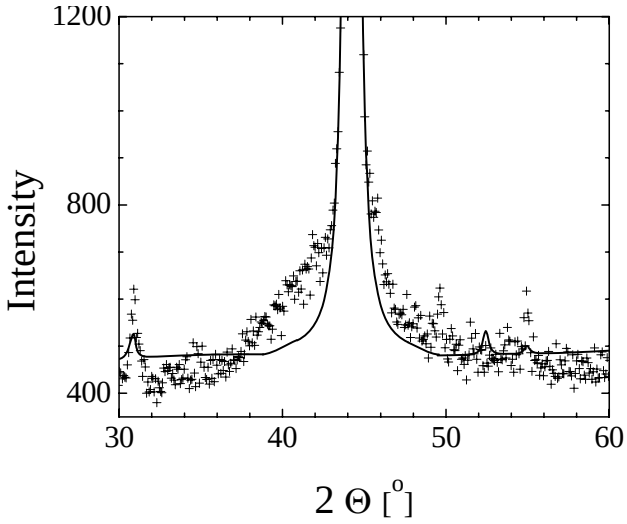

Fig. 2: Enlarged region of the neutron powder diffraction spectrum of UPd_2Sb; for details see text.

References:

[1] K. Gofryk, D. Kaczorowski, and A. Czopnik: Solid State Comm. **133** (2005) 625

[2] I. Maksimov et al.: Phys. Rev. B **67** (2003) 104405

	EXPERIMENTAL REPORT **Oxygen vacancy ordering in layered double perovskite $NdBaCo_2O_{5.72}$**	Proposal N° PHY-01-1758 Instrument **E9** Local Contact Dimitri Argyriou
Principal Proposer: Experimental Team:	K. Bärner - Physik. Institut der Uni Göttingen I.O. Troyanchuk - ISSSP NAS, Minsk, BY L.S. Lobanovsky - ISSSP NAS, Minsk, BY O. Prokhnenko, M. Tovar - HMI Berlin	Date(s) of Experiment 09.08. - 15.08.2005

Date of Report: 05.01.2006

An effect of oxygen vacancies ordering in $REBaCo_2O_{6-\delta}$ layered double perovskite cobaltites has been intensively studied in recent years [1-4]. In these compounds has been found different kind of oxygen vacancy ordering at the δ close to 1 and 0.5 [2-3]. During last two years new type of oxygen vacancy ordering has been found in $REBaCo_2O_{5.75}$ (δ=0.25) [4]. An attempt has been made to receive this type of oxygen vacancy ordering in another (Nd-based) compound.

The neutron diffraction studies of the compound $NdBaCo_2O_{5.72}$ have been carried out using E9 instrument ($<\lambda>$=1.7974 Å) at the temperatures 5 and 250 K. The refinement of the unit cell parameters and accurate determination of the oxygen content of the sample were performed by the full-profile analysis of the neutron powder diffraction pattern (NDP) using the Rietveld method with the Fullprof program.

During refinement of NDP in different models, we found that the best agreement between the experimental and theoretical curves was observed in the rhombic system (space group *Pmmm*, (47)) with the parameters $\sim 2a_p \times 2a_p \times 2a_p$ (a_p is the unit cell parameter of perovskite). Direct evidence of such a structure formation is the presence of slight (111) Bragg reflection (fig.1). In this model, we established that the oxygen vacancies are mainly (~73%) formed in the 1c (0, 0, ½) Wyckoff position of the *Pmmm* space group. Another part of oxygen vacancies is formed in 1d, 1g and 1h Wyckoff positions. The oxygen content obtained by processing the neutron diffraction pattern within the selected model was 5.72. The structural details of the unit cell are: Nd (4y: x=0.2569, y=0.7527); Ba(4y: x=0.2525, y=0.7512); Co1 (2q: z=7489); Co2 (2s: z=0.7509); Co3 (2r: z=0.7480); Co4 (2t: z=0.7544); O1 (1a); O2 (1b); O3 (1c); O4 (1d); O5 (1e); O6 (1f); O7 (1g); O8 (1h); O9 (4u: y=0.7558, z=0.7128); O10 (4v: y=0.7580, z=0.7404); O11 (4w: x=0.2417, z=0.7177); O12 (4x: x=0.2425, z=0.7090).

According to the low temperature neutron diffraction pattern (fig.2), one can conclude that magnetic contributions in Bragg reflections exist. The most noticeable contribution is observed in (111) reflection pointing the G-type antiferromagnetic ordering of magnetic moments of cobalt ions, and in [2 0 0] reflections set. Such a behaviour may indicate, that the magnetic structure is either canted G-type antiferromagnetic structure or mixture of pure antiferromagnetic and ferromagnetic ones. In our assumption, the last model is more realizable. The calculation with the Rietveld method yields the better result for mixed phases model. Calculation of the magnetic moments per cobalt ions for each of phases yields ~0.82 μ_B/Co for G-type antiferromagnetic phase, and 2.16 μ_B/Co for ferromagnetic one.

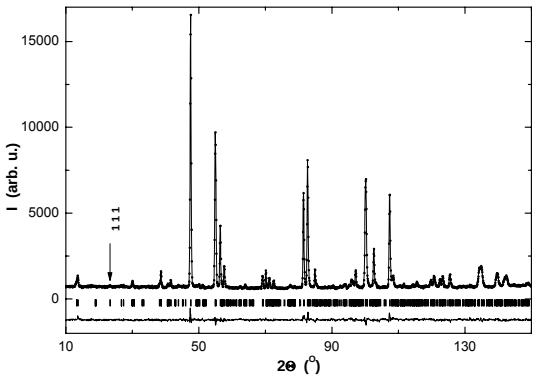

Fig.1. NDP for $NdBaCo_2O_{5.72}$ collected at 250 K.

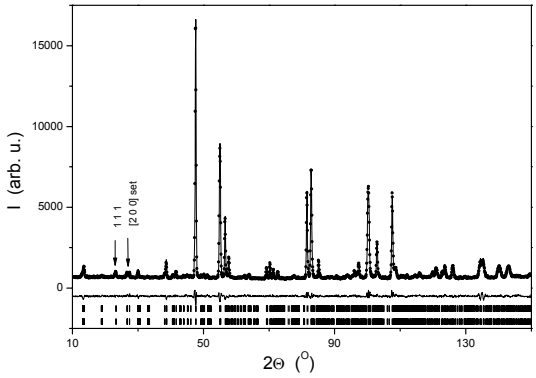

Fig.2. NDP for $NdBaCo_2O_{5.72}$ collected at 5 K.

Thus, one may conclude that a new crystallographic phase is formed in the $NdBaCo_2O_{5.72}$ compound in which oxygen vacancies are ordered in the plane of rare-earth ions in position 1c. Detailed interpretation of the magnetic structure is under refinement.

References

[1] A. Maignan et al.: J. Sol. St. Chem., **142**, 247 (1999).
[2] E. Suard et al.: Phys. Rev. **B61**, R11871 (2000).
[3] M. Soda et al.: J. Phys. Soc. Jpn., **73**, 2857 (2004); H.D. Zhou et al.: J. Sol. St. Chem., **177**, 3339 (2004).
[4] C. Frontera et al.: Phys. Rev. **B70**, 184428 (2004); C. Frontera et al.: J. Appl. Phys. **97**, 10C106 (2005).

	EXPERIMENTAL REPORT **Investigation of nuclear and magnetic structure of Cylindrite $FeSn_4Pb_3Sb_2S_{14}$**	Proposal N° PHY-01-1762 Instrument **E9** Local Contact Michael Tovar
Principal Proposer: Experimental Team:	S. Schorr - University Leipzig R. Kaden - University Leipzig	Date(s) of Experiment 21.10. - 25.10. 2005

Date of Report: 09.01.2006

The sulfosalt cylindrite, naturally grown as cylindrical crystals and platelets, has an incommensurate modulated misfit-layer structure (SG P1), consisting of the pseudotetragonal T-slab (PbS-type) and the pseudohexagonal H-slab (SnS_2). Whereas, the crystallographic a-axis lies perpendicular to the layers, the b-axis follows the curvature of the cylindrical shape, the c-axis aligns the "rolling axis" and shows a wavelike modulation. Up to now, a complete structure model does not exist.

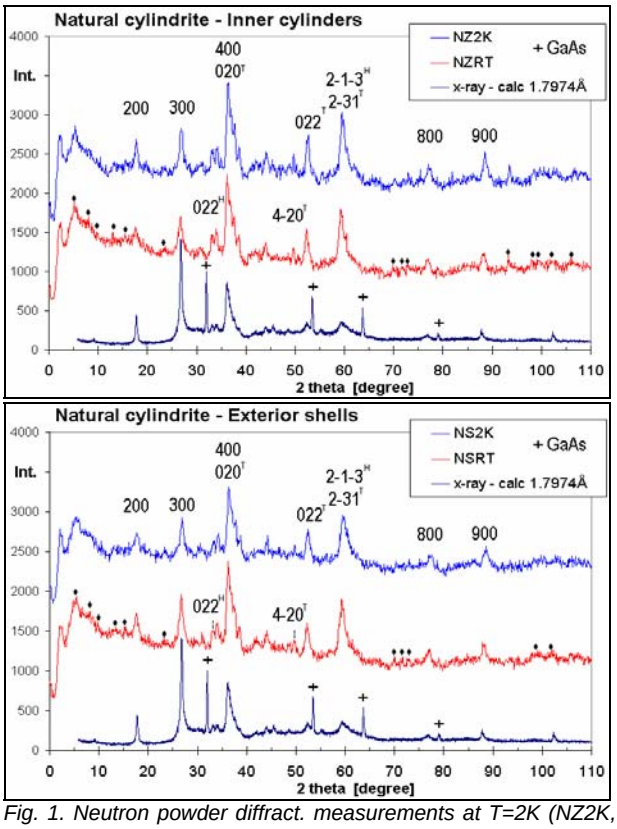

Fig. 1. Neutron powder diffract. measurements at T=2K (NZ2K, NS2K) and T=295K (NZRT, NSRT). A x-ray powder data (Cu-Anode) is calculated for the neutron wavelength of 1,7974 Å.

	NZ2K	NZRT	Δ %	NS2K	NSRT	Δ %
T K	2	295		2	295	
$a_0^{I,H}$ Å	11,61	11,69	0,7	11,62	11,68	0,5
b_0^{I} Å	5,77	5,79	0,3	5,77	5,79	0,3
c_0^{I} Å	5,79	5,76	-0,5	5,79	5,75	-0,7
c_0^{H} Å	6,29	6,30	0,2	6,28	6,31	0,5
γ^{T}	95,5°	94,9°	-0,6	95,5°	94,7°	-0,8

Tab. 1. Selected lattice parameters calculated from fitted peaks. Deviation of the values: 0,02Å, 0,5°, 0,1%

In this neutron powder diffraction experiments, at T = 2K and 295K, wavelength 1,7974Å, two samples of natural cylindrite cylinders were examined: small cylinders (cores) (∅ < 1mm) and exterior cylinder shells (∅ 7-10 mm).
Comparing to the x-ray data, the neutron diffraction reveal additional reflexes (marked in Fig. 1), probably caused by the better differentiation between Sb and Sn and an expected ordering of the Sb-distribution or a magnetic structure, regarding to an ordering of the Fe. Apparently, the reflexes and the high background up to ca. 13° 2ϑ correspond to superstructures and diffuse scattering, we only discovered by electron diffraction or found by lattice *modelling: $1{,}5b_0^T$, $2{,}5b_0^T$, $*3{,}5b_0^T$, $3a_0$, $2a_0$. But this range of the neutron spectra contains some more new reflexes and information, which interpretations are in progress. Moreover, that high background may indicate a frustrated or an undirected magnetic spin orientation of the Fe(II) ions. Sayler and ter Haar [1] described the paramagnetic behaviour of natural cylindrite cylinders and ferromagnetic behaviour below T=30 K with magnetic phase transitions at 8K and 28K. But a stronger directed ordering of the magnetic structure at T=2K not clearly arises from the differences of intensity to 295K.
However, the super structural reflex of $1{,}5b_0^T$ at 11,8(2)° 2ϑ is nearly missing at T=2K, and in the other hand reflexes e.g. at 35,1°, 42,9°, 46,6°, 47,5° 2ϑ appear or are more distinct.
Owing to the week intensity, caused by the triclinic incommensurate structure, only some lattice parameters could be calculated (Tab.1). They are nearly equal for both samples at the same temperatures. The comparison between T=2K and 295K reveal anisotropic thermal expansion. While a_0 increases to higher temperatures, more than b_0^T and c_0^H, the parameters c_0^T and γ^T degrease clearly. The complete interpretation of the data in correlation with additional methods is currently in progress.

Reference

[1] P.A. Sayler, W. L. ter Haar, J. Appl. Phys. 81 (1997) 5163

	EXPERIMENTAL REPORT **Crystal and magnetic structure of $Nd_3Co_{13}B_2$ and the Nickel substituted derivatives**	Proposal N° PHY-01-1770 Instrument **E9** Local Contacts Michael Tovar Oleksandr Prokhnenko
Principal Proposer: Experimental Team:	J. Bartolomé - Univ. Zaragoza, ICMA, E J. Campo - Univ. Zaragoza, ICMA, E N. Plugaru, J. Rubín - Univ. Zaragoza, CPS, E	Date(s) of Experiment 17.10 - 21.10.2005

Date of Report: 05.01. 2006

The new compounds $Nd_3Co_{13-x}Ni_xB_2$ (members of the $R_{m+n}T_{5m+3n}B_{2n}$ series, with m=2 and n=1, $Nd_3Ni_{13}B_2$-type structure) exhibit a linear decrease of the Curie temperature when Ni concentration increases, $x \leq 13$, and a spin reorientation transition (SR) from the c-axis direction to an undetermined direction with macroscopic basal anisotropy, below the SR. We intend to investigate the effect of B on Co moment in this series and relate it to the m=1 series previously studied [1]. Ni substitution for Co dilutes magnetically the 3d sublattice, but the origin of the macroscopically observed Co moment variation has not been determined. Our objective in this system has been: *i)* To determine the magnetic structures in the different phases of the *T-x* diagram; *ii)* To determine the occurrence of a preferential site occupancy of the Ni substitution for Co; *iii)* To determine the local magnetic moments in $Nd_3Co_{13}B_2$ and the Ni-substituted derivatives.

$Nd_3Co_{13-x}Ni_xB_2$ samples were prepared by induction melting the pure elements and subsequent annealing at 720 °C under Ar gas, for three weeks. The crystal structure was investigated by powder x-ray diffraction at room temperature (RT). The structural parameters and phase contents were determined by Rietveld refinement

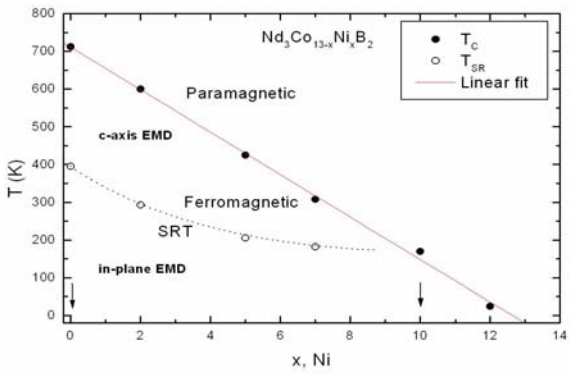

Figure 1: Magnetic phase diagram of $Nd_3Co_{13-x}Ni_xB_2$. Arrows indicate the compositions measured in E9.

Powder samples of two compositions (x=0 and 10) were measured at the E9 Instrument (working with a wavelength 1.79 Å) at three temperatures, corresponding to paramagnetic, ferromagnetic axial and low temperature phases, see the magnetic phase diagram displayed in figure 1. To reach those measure temperatures it was necessary to employ the HTF furnace and the Orange Cryostat OC as ancillary equipment.

Five good quality diffractograms were measured at RT and 650 K, and 1.5, 100 and 200 K for x=0 and 10 samples, respectively. Preliminary data analysis indicates the presence of 1:5 - and 1:4:1 -type secondary phases in each of the samples. Rietveld refinement of the nuclear scattering at 1.5 K is shown in figure 2 for the x=10 composition.

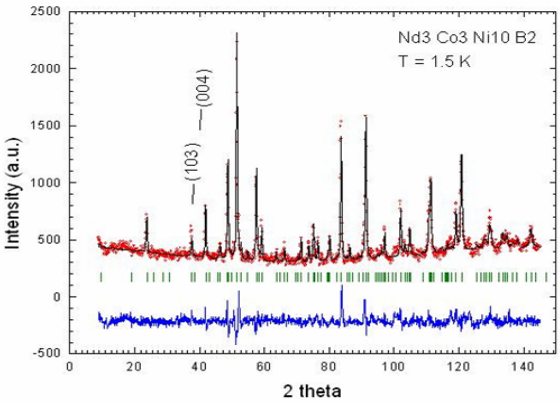

Figure 2: Diffractogram measured at 1.5 K and the refinement of the nuclear scattering for x=10 compound.

A magnetic signal is observed at the (1 0 3) and (0 0 4) lines, similarly at 1.5 and 100 K, originated presumably by a conical magnetic structure. This fact indicates that the SR temperature should be higher than 100 K, in agreement with our macroscopic magnetic measurements [2]. The possible conical structure could explain the average Nd magnetic moment, μ_{Nd}=2.3 μ_B/at. determined from the *M(H)* curve of the *x*=13 compound, which is smaller than the free ion value. Co preferential occupancy of the 3g and 6i lattice sites and Ni of the 4h ones was derived.

References

[1] C. Zlotea, C. Chacon and O. Isnard, J. Appl. Phys. **92** (2002) 7382.

[2] N. Plugaru, J. Rubín, J. Bartolomé and C. Piquer, J. Magn. Magn. Mat., **290-291** (2005) 1563-1566.

	EXPERIMENTAL REPORT **Neutron powder diffraction study of Sr_2CrOsO_6**	Proposal N° PHY-01-1778-DT Instrument **E9** Local Contact Michael Tovar
Principal Proposer: Experimental Team:	Y. Krockenberger - MPI Stuttgart L. Alff - TU Darmstadt Y. Krockenberger - MPI Stuttgart, TU Darmstadt M. Reehuis - MPI Stuttgart	Date(s) of Experiment 26.08. - 28.08.05

Date of Report: 24.01.2006

The double perovskites of the composition $A_2BB'O_6$ (with *A* an alkaline earth, *B* a 3*d*-transition metal ion, and *B*' a 4*d*- or 5*d*-transition metal ion) are interesting materials, both due to their rich physics and their promising properties for applications in spintronics. For the compounds containing iron and chromium a ferromagnetic order of the 3*d*-transition metal ion sets in at relatively high Curie temperatures. The double perovskites with the highest T_C known so far is Sr_2CrReO_6 with T_C = 635 K [1]. Here we report on the structural and magnetic properties of the new compound Sr_2CrOsO_6. SQUID-measurements showed that a ferromagnetic order sets in at an even higher Curie temperature T_C = 700 K (Fig. 1).

The neutron powder diffraction patterns of Sr_2CrOsO_6 were collected with the instrument E9. This instrument uses a germanium monochromator selecting the neutron wavelength λ = 1.7971 Å. For this compound data sets were recorded at 540 K and 770 K between 2θ values of 5 and 155°. The nuclear and the magnetic structures of both compounds were refined from the powder diffraction data with the program *FullProf*. The crystal structure could be refined for both data sets in the cubic space group *Fm*–3*m*. Here the atoms Sr, Cr, Os and O atoms are on the Wyckoff positions 8*c* (¼,¼,¼), 4*a* (0,0,0), 4*b* (½,½,½) and 24*e* (*x*,0,0), respectively. From the Rietveld refinements we have obtained the positional parameters of the oxygen atom *x* = 0.2513(4) at 540 K and *x* = 0.2506(4) at 740 K. It has to be mentioned that our data did not show any broadening or splitting of reflections. Therefore we were not able to find a Bravais lattice with a lower symmetry. Taking into account the group-subgroup relations a tetragonal symmetry with the space group *I*4/*mmm* could be assumed.

In order to investigate the magnetic order of the metal ions we collected a data set well above the Curie temperature T_C = 700 K and a data set at 540 K, where the magnetic order is well established. The magnetic contribution of the reflections could be detected from the difference pattern shown in Fig. 2. Here it can be seen that weak intensities could be observed on the positions of the reflections 111 and 311. Our data analysis finally could show that below T_C the chromium ions are ferromagnetically ordered with a moment value μ_{exp} = 0.9(1) μ_B at 540 K. Fig. 1 shows that at lower temperature the magnetic moment decreases again. Here the magnetic moments of the osmium ions are gradually induced by the ferromagnetic chromium sublattice resulting in a ferrimagnetic structure.

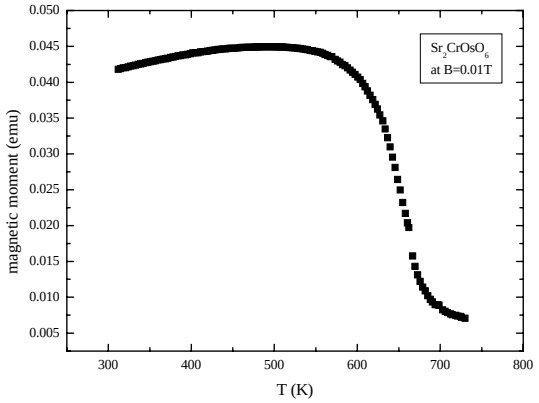

Fig. 1. Temperature dependence of the magnetic moment of Sr_2CrOsO_6 measured at the magnetic flux density *B* = 0.01 T.

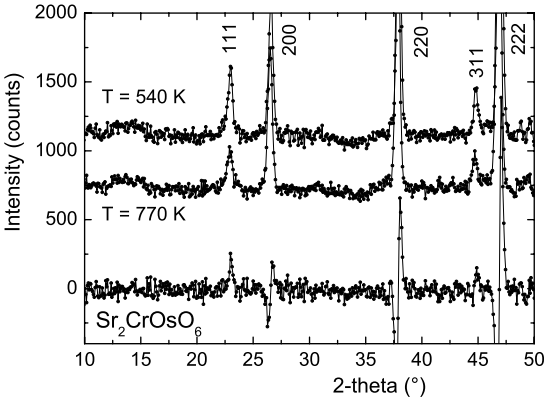

Fig. 2. Neutron powder diffraction patterns of Sr_2CrOsO_6 recorded at 540 K and 770 °C. From the difference plot additional magnetic intensities could be observed on the positions of the reflections 111 and 311.

References

[1] H. Kato, T. Okuda, Y. Okimoto, Y. Tomioka, Y. Takenoya, A. Ohkubo, M. Kawasaki, Y. Tokura, Phys. Rev. Lett. **81** (2002) 328.

	EXPERIMENTAL REPORT **Study of the magnetic phase diagram in a field-induced non-Fermi liquid**	Proposal N° PHY-02-0452 Instrument **V2** Local Contact Klaus Habicht
Principal Proposer: Experimental Team:	B. Fåk - CEA/DSM/DRFMC/SPSMS, Grenoble, F C. Rüegg - UCL, London, UK P.G. Niklowitz - DRFMC/SPSMS, Grenoble, F D. McMorrow - UCL, London, UK	Date(s) of Experiment 08.02.-15.02.2005 05.04.-12.04.2005

Date of Report: 31. May 2005

YbAgGe is a new heavy fermion compound that shows field-induced non-Fermi liquid behavior at low temperatures. The aim of the present experiment was to determine the magnetic phase diagram and to characterize the spin fluctuations. The experiment was rescheduled and split into two parts because of the delay of the reactor start-up.

Part I:
Due to the small dimension of the dilution refrigerator used in the 15 T magnet, a smaller sample than initially foreseen had to be used. A 1.13 g single crystal was oriented with the **a*** and **c*** axes in the horizontal scattering plane and glued with black stycast to a Cu support, which was connected to the mixing chamber. FLEX was operated in long-chair configuration with an incident wave vector of 1.50 Å-1 and 60' collimation throughout. After some initial problems with the control of the sample temperature and an unscheduled one-day reactor shut-down, we determined the firstorder phase transition line for the low-T low-H phase characterized by the propagation vector $\mathbf{k_1}$=(1/3,0,1/3) by scanning temperature and magnetic field applied along the **b** direction. The resulting H-T phase diagram is shown in Fig. 1, and has a more conventional form than that deduced from resistivity measurements.

In addition, we found the magnetic propagation vector in the second phase by scanning one quarter of the Brillouin zone in the **a*-c*** plane near the (101) nuclear Bragg reflection, at H//b=2 T and T=0.4 K.

A limited number of inelastic scans in zero and applied field were made to explore the magnetic field dependence of the quasielastic spin fluctuations. This work will continue at a later stage.

Part II:
In the second part of the experiment, we determined the second-order phase transition line for the second phase by scanning temperature and magnetic field applied along the **b** direction. This magnetic structure has an incommensurate propagation vector $\mathbf{k_2}$= (0,0,z) where z=0.324 is slightly field and temperature dependent. Due to the lack of inversion symmetry and hence the absence of a Lifshitz point, symmetry arguments do not require that the propagation vector becomes commensurate in the zero-temperature limit. Instead, the $\mathbf{k_2}$ structure is replaced by the $\mathbf{k_1}$ structure with a first-order transition with hysteresis. We found, e.g., that on lowering the field, the $\mathbf{k_2}$ phase goes over into the $\mathbf{k_1}$ phase at high temperatures (T=400 mK), but not at lower temperatures (T=62 mK), where the system remains in the $\mathbf{k_2}$ phase even at zero field. The second-order phase line is also shown in Fig. 1.

We also studied the magnetic field dependence of the (101) "nuclear" Bragg peak for magnetic fields between 0 and 13 T at T=65 and 600 mK. The intensity of this peak has a highly unusual field dependence.

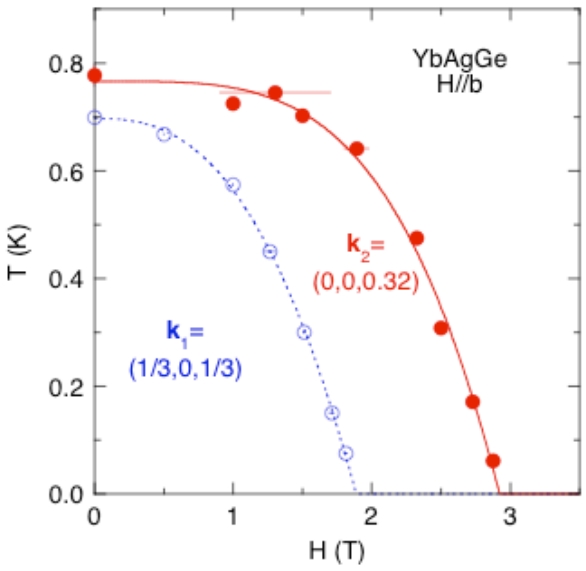

Fig. 1: Magnetic phase diagram of YbAgGe for H//b.

	EXPERIMENTAL REPORT **Kondo Scattering in Heavy Fermion $Ce_3Co_4Sn_{13}$**	Proposal N° PHY-02-0469 Instrument **V2** Local Contact Klaus Habicht
Principal Proposer: Experimental Team:	A. Christianson - UC Irvine & LANL K. Habicht - HMI Berlin	Date(s) of Experiment 08.08. - 15.08.2005

Date of Report: Feb. 2006

The compound $Ce_3Co_4Sn_{13}$ [1] is an extremely heavy cubic heavy fermion $Ce_3Co_4Sn_{13}$ with a low temperature electronic specific heat of order ~4 J/mol-K^2.[2] If the compound is nonmagnetic, it would be the heaviest nonmagnetic Ce-based heavy fermion reported to date, and therefore would be expected to lie *extremely* close to a QCP. However, a peak is observed at 0.8 K in the specific heat [2] and susceptibility [3], suggesting antiferromagnetic order. Nevertheless, the peak in the specific heat is too broad to be explained by a long range magnetic phase transition, and a neutron diffraction measurement on BT-1 does not indicate any sign of long range magnetic order.[4]

Furthermore, if this were an antiferromagnetic transition as suggested by the magnetic susceptibility, the temperature of the specific heat peak would decrease with magnetic field, rather than increase, as observed. In addition, frequency dependent magnetic susceptibility measurements indicate that this feature is not of glassy origin (i.e. no frequency dependence is observed).[3] Preliminary inelastic neutron scattering experiments[4] on PHAROS at Los Alamos indicate crystal field levels at 8 and 30 meV negating the possibility that the peak is due to a Schottky anomaly produced by low lying crystal field levels. The most probable explanation consistent with these observations is that the peak in specific heat and susceptibility are due to antiferromagnetic fluctuations, which should be large near a QCP.

Recently, we have performed inelastic neutron scattering experiments on the cold triple-axis spectrometer FLEX. Constant Q-scans at various points in reciprocal space do not show the typical quasielastic scattering expected for a heavy fermion system. However, there appears to be a broad response at low energy transfers that is independent of Q consistent with a localized response as expected for the quasielastic scattering in a Heavy Fermion systems. One possibility is that we have observed the trail of the quasielastic scattering and a higher resolution experiment is required to elucidate this behavior.

Further experiments are underway to further clarify the behavior of $Ce_3Co_4Sn_{13}$.

References

[1] C. Israel, et al., accepted to Physica B.

[2] A.L. Cornelius, et al., unpublished.

[3] P.G. Pagliuso, et al., unpublished.

[4] A.D. Christianson, et al., unpublished.

	EXPERIMENTAL REPORT **Out-of-Plane Magnetism in Underdoped $La_{2-x}Sr_xCuO_4$ (x=0.1)**	Proposal N° PHY-02-0497 Instrument **V2** Local Contact Klaus Habicht
Principal Proposer: Experimental Team:	B. Lake - Iowa State University / Ames Lab B. Lake - Iowa State University / Ames Lab G. Aeppli - University College London	Date(s) of Experiment 15.08. - 28.08.2005

Date of Report: 23. Jan. 2005

Neutron scattering measurements of $La_{2-x}Sr_xCuO_4$ were carried out on V2/Flex. The aim was to examine the magnetism as a function of wavevector perpendicular to the CuO_2 plane. Within the CuO_2 plane the magnetic peak is resolution limited suggesting long-range magnetic correlations. Our previous results [1] suggest that correlation between the planes extend over only a few planes.

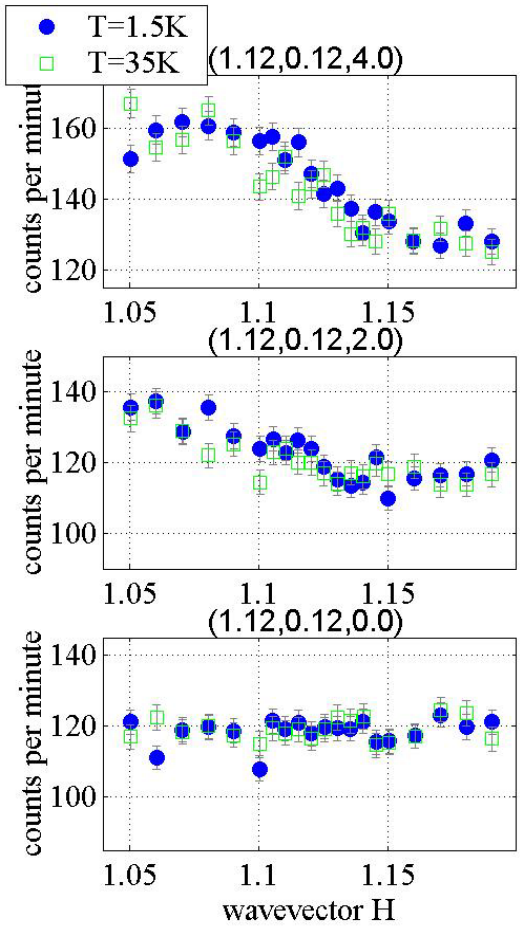

Fig 1: *Magnetic signal at wavevector L=n (n is integer) for T=1.5K and T=35K.*

To carry out this measurement we made in-plane scans at different values of out-of-plane wavevctor at T=1.5K. The scans show a sharp peak whose amplitude varies with out of plane wavevector. These scans were repeated above the superconducting transition temperature at T=35K where the magnetism is lost to give the background.

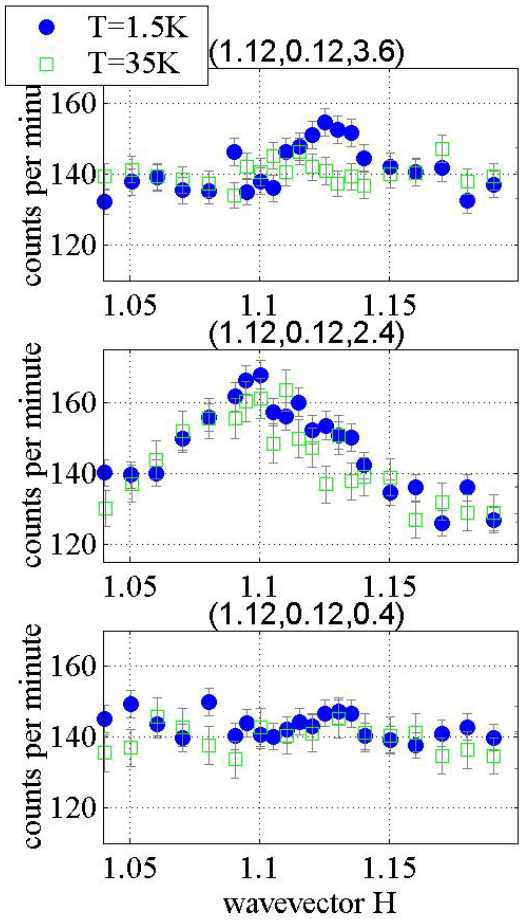

Fig 2: *Magnetic signal at wavevector L=n+/-0.4 (n is integer) for T=1.5K and T=35K.*

The amplitude of the magnetic signal was found to vary significantly with out-of-plane wavevector suggesting the existence of correlations between the planes in particular, at out-of-plane wavevector L=n (n is integer) the magnetic intensity was weakest (see fig.1) while at L=n+/-0.4 (see fig. 2), the magnetic intensity was strongest.

Reference

[1] B.Lake, *et al. Nature Materials* **4**, 658-662 (2005).

	EXPERIMENTAL REPORT SANS study of the vortex lattice of the FFLO phase in $CeCoIn_5$	Proposal N° PHY-04-1095 Instrument **V4** Local Contact Albrecht Wiedenmann
Principal Proposer: Experimental Team:	A.D. Bianchi - FZ Rossendorf, Dresden M. Kenzelmann - ETHZ & PSI, Zürich, CH R. Movshovich - LANL, Los Alamos, US P. Smeibidl, M. Kammel, J. Haug - HMI Berlin	Date(s) of Experiment 17.06. - 23.06.2005

Date of Report: 06. Jan. 2006

Fermionic superfluidity requires paring of particles of half-integer spin, be it in ^{3}He, superconductors, ultra-cold atomic gases, or even inside neutron stars. For a population of fermions with equal number of spin-up and -down particles the pairing can be complete and the system can become superfluid. Even more interesting is the case for an uneven number of spin-up and -down particles, and the resulting question if superfluidity can exist in a system with leftover unpaired fermions has interested physicists since the 1960's [1,2].

With the discovery of a second phase transition inside the superconducting region of the magnetic field (H) –temperature (T) phase diagram of tetragonal CeCoIn5 the search for an FFLO phase [1,2] in solid state physics gained new momentum [3]. Particularly, as $CeCoIn_5$ meets all the prerequisites [3] for the observation of such a FFLO phase. The order parameter of the FFLO state is modulated, and the flux lines may acquire a longitudinal modulation, as the superconducting energy gap becomes modulated along the field direction, which could be detected with neutron scattering. Ultrasound attenuation measurements in $CeCoIn_5$ indicate that the additional phase is indeed the realization of a flux state with a single wave vector modulation $q \sim 0.18$ nm^{-1} [4].

Traditionally, SANS experiments are carried out in a geometry, where the beam of the incoming neutrons is parallel to the applied H [5]. Here we were conducting an experiment, where the incoming beam was perpendicular to H, and we were trying to detect additional reflexes associated with the modulation of the vortex lattice, giving for the first time direct evidence for the FFLO state.

For this we were using the V4 SANS beamline. The sample was aligned in the dilution stick and the VM1 magnet with its bc plane in the horizontal scattering plane. The vertical field was along the crystallographic a axis, allowing us to reach the high-field phase above 10 T which exists over an extended field and temperature range. The sample itself consisted of an oriented mosaic of single crystals of ~ 500 mg with an average thickness of ~ 0.5 mm, screened by a 8 x 8 mm Gd aperture.

Unfortunately, an aluminium plate inside the magnet with a thickness of about 15 mm in the incoming beam led to a large background signal (~ 300:1), preventing us from observing the weak signals associated with the vortex lattice.

Using spin polarized neutrons and a collimator-sample and sample-detector length of 8 m, we were able to observe a magnetic signal from the sample by calculating the difference between the up- and down polarization. We scanned the phase diagram with a field scan at 50 mK, and temperature scans at 6, 11, and 11.8 T. After radially averaging the signal of the field scan at 50 mK for fields above 4 T we found a magnetic signal which increases strongly with increasing field, and is strongest at the lowest scattering angles. For all fields the T-scans showed below 0.4 K an increasing signal with decreasing temperatures getting more pronounced for higher fields. However, we did not observe sharp features at neither the phase boundary to the normal state nor at the boundary between the FFLO and homogenous superconducting phase. Interestingly, the shape of the signal showed a twofold anisotropy, being stronger along the field direction. We are in the process of trying to understand these results and analyze them in detail.

References

[1] P. Fulde and R.A. Ferrell:
Phys. Rev. **135**, A550 (1964).

[2] A. I. Larkin and Y. N. Ovchinnikov:
Zh. Eksp. Teor. Fiz. **47**, 1136 (1964).

[3] A. Bianchi, R. Movshovich, C. Capan,
P.G. Pagliuso, and J.L. Sarrao:
Phys. Rev. Lett. **91**, 187004 (2003).

[4] T. Watanabe, Y. Kasahara, K. Izawa, T. Sakakibara,
Y. Matsuda, C.J. van der Beek, T. Hanaguri,
H. Shishido, R. Settai, and Y. Onuki:
Phys. Rev. B **70**, 020506 (2004).

[5] M.R. Eskildsen, C.D. Dewhurst, B.W. Hoogenboom,
C. Petrovic, and P.C. Canfield:
Phys. Rev. Lett. **90**, 187001 (2003).

	EXPERIMENTAL REPORT **Searching for ferromagnetic clusters in paramagnetic phase**	Proposal N° PHY-04-1099 Instrument **V4** Local Contact Elvira Garcia-Matres
Principal Proposer: Experimental Team:	J. Herrero-Albillos - Universidad de Zaragoza, E J. Campo - Universidad de Zaragoza, ICMA, E E. Garcia-Matres - HMI Berlin	Date(s) of Experiment 19.03. - 22.03.2005

Date of Report: 07. Apr. 2005

$ErCo_2$ is a ferrimagnet with a first order para to ferri transition at $T_c = 32$ K. When a magnetic field is applied, the Er magnetic moment is parallel to the applied field at all temperatures. The Co sublattice is polarized parallel to the applied field at high temperatures and it orders antiparallel below T_c. Results from X-ray Magnetic Circular Dichroism and magnetic measurement made us to propose the development of ferimagnetic clusters in the paramagnetic phase. The aim of our proposal was to use SANSPOL in order to prove the existence of such clusters and to determine its correlation length. In this experiment we have completed the previous data taken in August 2004, where only experiments with an external magnetic field of 1 T were performed. Consequently, zero-field data were taken in March 2005 in order to check the magnetic origin of the SANS signal.

A horizontal cryomagnet was employed to achieve the temperature (5-300 K) and field (0-1 T) environment required on the powered sample and the sample holder was a thin quartz cell of 13 mm in diameter. Measurements were performed on V4 instrument, using the polarization option SANSPOL when working under applied magnetic field.

Neutron absorption of the sample is very high, making necessary to increase the accumulation time especially in the paramagnetic phase. To acquire good statistics on the sample, around six hours were needed for each temperature above T_c. The experiment run reasonably well allowing us to measure SANS at zero field in all the regions of interest as well as to complete the SANSPOL measurements at 1 T.

Preliminary data treatment of the new data as well as the results from August 2004 have shown us interesting features in both the paramagnetic region and in the ferrimagnetic phase. Currently we are working in the data treatment as well as in the interpretation of the results. The SANSPOL intensities at 1 T for two polarization states $I^{on}(q\perp H)$ and $I^{off}(q\perp H)$ are presented in the figure.

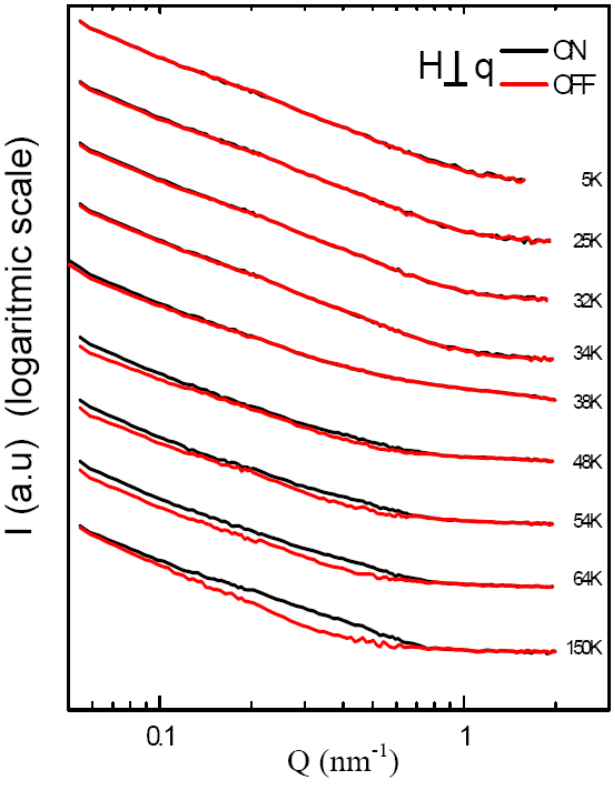

During the performance of the experiment M. Kamel and A. Heinemann supported us as well.

	EXPERIMENTAL REPORT **Field induced spin-spin correlation length in amorphous Fe_2O_3**	Proposal N° PHY-04-1114 Instrument **V4** Local Contact Albrecht Wiedenmann
Principal Proposer: Experimental Team:	S.M. Yusuf - SSPD, BARC, IN S.M. Yusuf - Univ. Zaragoza, ICMA, E J.M. De Teresa - Univ. Zaragoza, ICMA, E A. Heinemann - HMI Berlin	Date(s) of Experiment 15-18.03.2005

Date of Report: 09.12.2005

The aim of the present polarized neutron small angle scattering (SANS) investigation was to study the formation of spin clusters under application of magnetic field in amorphous Fe_2O_3 in its "paramagnetic phase'' above 110 K [1, 2]. It was aimed to have confirmation of dc magnetization results of Langevin function behaviour with a log-normal number distribution of the size of the field induced spin-clusters with a mean diameter of ~30 Å for the regime $125 \leq T \leq 225$ K and with reduced size at higher temperatures above 225 K [1]. The experiments were also aimed to study the temperature dependence of the spatial correlation between magnetic moments at temperatures below about 35 K [2].

We measured I^+ and I^- SANS intensities with two polarization states of the incident neutron beam in the SANSPOL mode under horizontal applied magnetic field of 0, 0.03, 0.1, 0.5, 1.0 and 4 Tesla at 5 and 65 K, 0, 0.03, 0.1, 1.0 and 4 Tesla at 140 K and, 0, 0.04, and 1 Tesla at 300 K. The horizontal field was applied perpendicular to the forward beam direction. A sample thickness of 1 mm was used to avoid multiple scattering. Data were collected by placing the x-y detector at a position of 1, 4 and 12 m from the sample position. Background, transmission and, scattering from plexi were also measured for obtaing the background corrected absolute scattering crosssection for the sample.

Figure 1 shows the two-dimensional pattern measured at 5 K under 4 Tesla applied field when the x-y detector was placed at a distance (from the sample) of 4 m and with spin flipper off. Data reduction shows that there is very small asymmetric (I^+-I^-) scattering arising from the interference between the nuclear and magnetic form factors (Fig. 2). Detailed data analysis is underway.

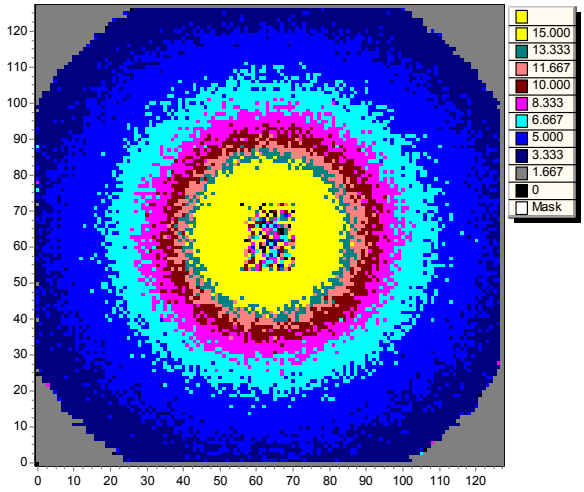

Fig. 1: Two-dimensional pattern measured at 5 K under 4 Tesla field at 4 m detector position.

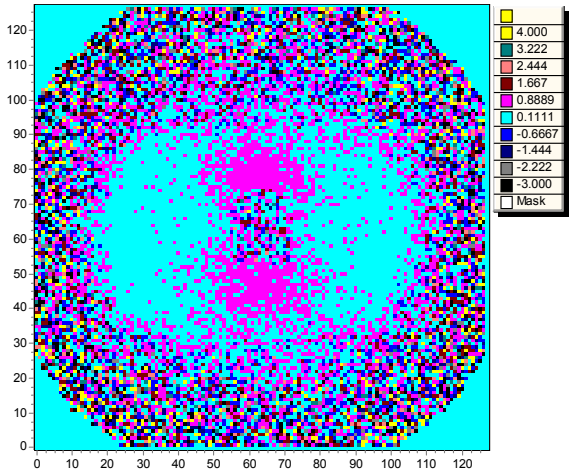

Fig. 2: Difference between the I^+ and I^- neutron counts measured at 140 K under 4 Tesla applied field at 1 m detector position.

References

[1] M.D. Mukadam, S.M. Yusuf, P. Sharma and S.K. Kulshreshtha: J. Magn. Magn. Mater. **269**, 317,(2004)

[2] M.D. Mukadam, S.M. Yusuf, P. Sharma, S.K. Kulshreshtha, G.K. Dey: Phys. Rev. B **72**, 174408, (2005)

	EXPERIMENTAL REPORT **Magnetic properties evolution of $LaMn_{1-x}Co_xO_3$ ($0.5 \leq x \leq 0.7$)**	Proposal N° PHY-04-1155 Instrument **V4** Local Contact André Heinemann
Principal Proposer: Experimental Team:	H. Szymczak - Institute of Physics PAN Warsaw, PL D. Karpinsky - ISSSP NAS Minsk, BY A. Heinemann - HMI Berlin	Date(s) of Experiment 25.08. - 28.08.2005

Date of Report: 23. Dec. 2005

The solid solutions with chemical formula $LnMn_{1-x}Co_xO_3$ (Ln notes lanthanide) are of considerable interest because of their peculiar magnetic properties [1-8]. Such materials show high-temperature ferromagnetparamagnet transition [5-8], exhibit metamagnetic transformation [6-8]. The origin of the complex magnetization behavior of the $LaMn_{1-x}Co_xO_3$ system is still a challenge.

The aim of this experiment was to clarify an origin of the low-temperature magnetic phases in the $LaMn_{1-x}Co_xO_3$ ($x = 0.5, 0.7$) system using the V4 SANS instrument. The SANS investigations were performed with a wavelength 6.05 A covering the range of the momentum transfer of 0.05 $nm^{-1} < q < 3\ nm^{-1}$. The SANS data were corrected concerning background scattering and absorption as well as normalized to absolute scale with a help of a water standard. The data reduction was performed using the HMI-standard "BerSANS" software package.

The scattering patterns were measured in the different ranges of temperatures: 5 - 200 K for the $LaMn_{0.5}Co_{0.5}O_3$ sample and 5 – 150 K for the $LaMn_{0.3}Co_{0.7}O_3$ one. All scattering curves for both samples were calculated assuming homogeneous size distribution of the particles.

The measured scattering curves can be well fit by nearly the same size of the spherical shape particles. One should note that average particle size for the $LaMn_{0.3}Co_{0.7}O_3$ sample is slightly smaller than that for the $LaMn_{0.5}Co_{0.5}O_3$ one - 80 and 100 Å, correspondingly. In the Guinier region of the scattering curves both samples show a $I(Q) \sim Q^{-4}$ behavior (Porod scattering) assuming a scattering from the outer surface of the grains.

In order to separate the magnetic scattering contribution from the nuclear one the samples were placed in a homogeneous magnetic field perpendicular to the direction of the primary neutron beam. The magnetic flux density was turned up to 2 T at which the specific magnetization of this type of ceramics shows nearly saturation.

Fig. shows typical scattering curves depending on a magnetic field applied. The scattering intensities vary with a magnetic field increasing at constant temperature causing by a decrease of the magnetic scattering length mainly for a small particle size for the $LaMn_{0.3}Co_{0.7}O_3$ sample. It can be seen that the largest variation of the scattering cross section as a function of the applied magnetic field corresponds to the q range of 0.1 – 2 nm^{-1} for the $LaMn_{0.5}Co_{0.5}O_3$ sample, thus testifying the more magnetic susceptibility of the inhomogeneous particles for this sample. Above 200 K and 150 K for $LaMn_{0.5}Co_{0.5}O_3$ and $LaMn_{0.3}Co_{0.7}O_3$ samples correspondingly the difference between scattering curves measured with and without a magnetic field is almost negligible, thus confirming the results of the magnetization measurements performed.

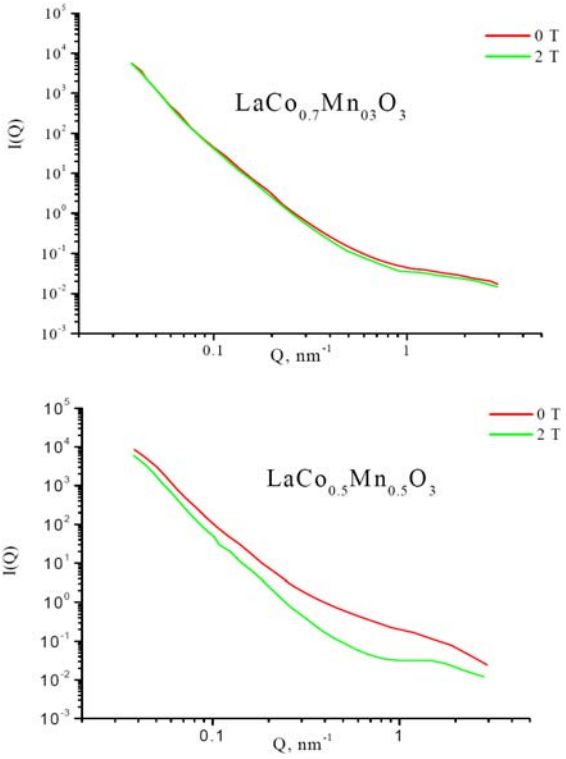

Qualitatively, the results can be interpreted in terms of a formation of the homogeneously distributed spherical magnetic clusters, which size is caused by Mn content in the $LaCoO_3$ rich matrix. The magnetic interactions between clusters in the $LaMn_{0.5}Co_{0.5}O_3$ compound are rather strong whereas they are weak for $LaMn_{0.3}Co_{0.7}O_3$ one even at the low temperatures. The more detailed analysis requires careful investigations which are in progress.

References

[1] J.B. Goodenough, A. Wold, R.J. Arnott, and N. Menyuk: Phys. Rev. **124**, 373.384 (1961)

[2] S. Hebert, C. Martin, A. Maignan, R. Retoux, M. Hervieu, N. Nguyen and B. Raveau: Phys. Rev. B **65**, 104420 (2002)

[3] M.C. Sanchez, J. Garcia, J. Blasco, G. Subias and J. Perez-Cacho: Phys. Rev. B **65**, 144409 (2002)

[4] G.H. Jonker: J. Appl. Phys. **37**, 1424 (1966)

[5] R.I. Dass and J.B. Goodenough: Phys. Rev. B **67**, 014401 (2003)

[6] J. Blasco, M.C. Sanchez, J. Perez-Cacho, J. Garcia, G. Subias and J. Campo: J. Phys. Chem. Solids **63**, 781 (2003)

[7] J.-Q. Yan, J.-S. Zhou and J.B. Goodenough: Phys. Rev. B **70**, 014402 (2004)

[8] I.O. Troyanchuk, L.S. Lobanovsky, D.D. Khalyavin, S.N. Pastushonok and H. Szymczak: JMMM **210**, 63 (2000)

	EXPERIMENTAL REPORT **Inelastic neutron response from HoB_{12} single crystal**	Proposal N° PHY-02-0478-EF Instrument **E1** Local Contact Vadim Sikolenko
Principal Proposer: Experimental Team:	K. Siemensmeyer - HMI Berlin S. Matas - IEP SAS, Kosice, Slovakia K. Flachbart - IEP SAS , Kosice, Slovakia	Date(s) of Experiment 14.02. - 27.02.2005

Date of Report: 01.03.2005

Borides of ReB_{12} type crystallise in fcc symmetry, they order antiferromagnetic with an incommensurate magnetic structure. With regard to the high symmetry and isotopic interaction mechanisms they show a surprisingly complex behaviour e.g. for HoB_{12} three different magnetic phases are observed in an external magnetic field [1,2]. Previous powder neutron diffraction [1] on HoB_{12} in a zero magnetic field reveals an incommensurate amplitude-modulated magnetic structure below T_N, the basic

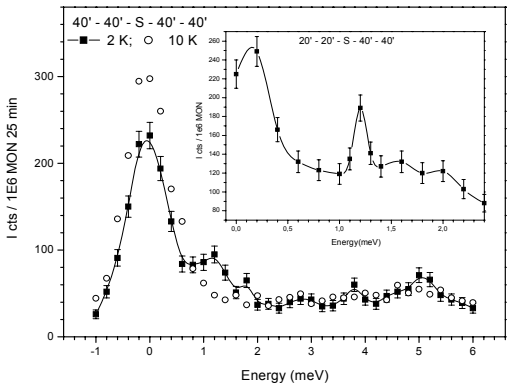

Fig. 1: The energy scan at Q= (1/2+4δ 1/2+4δ 1/2+4δ). The lines are guides to the eyes.

reflections can be indexed by (1/2±δ 1/2±δ 1/2±δ) with harmonics e.g. at (1/2±3δ 1/2±3δ 1/2±3δ), where δ= 0.035. Recently a strong diffuse scattering has been observed both below and above T_N which suggests that fcc symmetry reduces to simple cubic. The purpose of this experiment was to resolve the inelastic spectrum of the diffuse scattering. The experiment was performed on the E1-triple axis spectrometer. An isotopically enriched HoB_{12} single crystal was used. The crystal of cylindrical shape with 3 mm in diameter and 22 mm length was mounted with the (022) direction perpendicular to the spectrometer plane. Data were taken at a wavelength of 2.452 Å close to the Néel temperature, in the ordered state at 2K and at temperatures above T_N. The PG filter we used to reject high order contamination. Two basic configurations of the instrument have been used, one **a)** with collimation 40'-40'-S-40'-40' and one with a higher resolution **b)** 20'-20'-S-40'-40'. A set of scans at constant energy or constant wave vector were performed at reciprocal nodes (1/2±δ 1/2±δ 1/2±δ), (1/2+4δ 1/2+4δ 1/2+4δ) and (3/2+δ 3/2+δ 3/2+δ). The diffuse scattering close to reciprocal nodes (3/2 3/2 3/2), (1/2 1/2 1/2) has been reproduced at E= 0 at temperatures between 8 K and 60 K, for clarity we show only scans at 7.9 K and 59.7 K (Fig.1). The inelastic signal was weak and appeared only below T_N. Necessary counting times were around 25 min for each point, a fact that has limited systematic search possibilities. At low temperature around 2 K we find excitations at energy of 1.2 meV and 5 meV (Fig.2). As the excitations vanished at higher temperatures around 10 K one can conclude that they are magnetic in

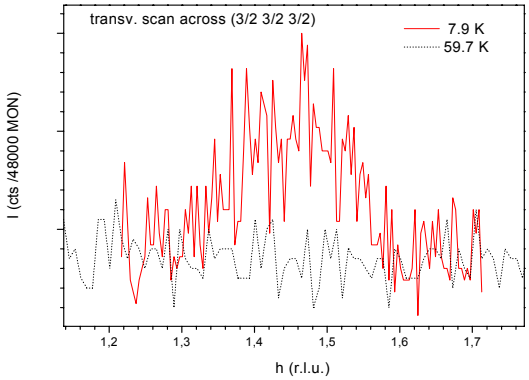

Fig. 2: Q-scans at (3/2+δ 3/2+δ 3/2+δ) at 7.9 K and 59.9 K.

origin. The inset of figure 2. shows an energy scan at (0.64 0.64 0.64) with higher energy resolution. Attempts to verify a possible q-dependence of the excitation at 1.2 meV have not been successful within (poor) statistical error and the range of scans. We believe that the typical q-dependence of a spin wave should have been seen, therefore the excitation should be mainly local. As they disappear above T_N, they cannot be attributed to crystal field excitations. The experiment shows that most of the diffuse signal - above and below T_N - is elastic, with E < 0.5meV. The data are not in conflict with a dimer model for diffuse scattering, however, they cannot yet provide evidence as well, mainly because the **q**- dependence could not well be determined.

Acknowledgements

S.M. acknowledges the support by INTAS 03-51-3036 and APVT-51-031704.

References

[1] A. Kohout, I. Bat'ko, A. Czopnik, K. Flachbart, S. Mat'as, M. Meissner, Y. Paderno, N. Shitsevalova and K. Siemensmeyer: Phys. Rev B **70**, 224416 (2004)

[2] S. Gabáni, I. Bat'ko, K. Flachbart, T. Herrmannsdörfer, R. König, Y. Paderno and N. Shitsevalova : J. Magn. Magn. Mater. **207**, 131 (1999)

	EXPERIMENTAL REPORT **Magnetic excitations in nanocrystalline Tb**	Proposal N° PHY-02-0447 Instrument **E1** Local Contact Jens Klenke
Principal Proposer: Experimental Team:	O. Moze - Physics Dept, Uni Modena, Italy O. Moze - Physics Dept, Uni Modena, Italy C. Vecchini - Physics Dept, Uni Modena, Italy J. Klenke - HMI Berlin	Date(s) of Experiment 13.09. - 26.09.2004

Date of Report: 10.10.2004

The magnetic microstructure of a nanocrystalline hard magnet, Tb has recently been investigated for the first time by SANS [1]. Two important parameters used in modelling the magnetic behaviour in this material, and indeed in understanding the nature of the large magnetic anisotropy in nanocrystalline Tb are the spin-wave stiffness constant D and the spin-wave gap Δ, which reflects dipolar and, most interestingly, anisotropy contributions.

We have recently re-attempted to measure the spin wave excitations in a sample of nano Tb (> 1 gm) with a grain size of 9 nm. Elastic scans were also performed above and below the ordering temperature of 225 K. The helical phase appears to be suppressed in nano Tb. An elastic scan at 50 K is displayed in Fig. 1 whilst in Fig. 2 the temperature dependence of the (101) peak is displayed (the nuclear contribution to this peak has been subtracted). An incident energy of 14.7 meV was used to perform constant - q scans (at q = 0.12, 0.08 and 0.06Å^{-1}) near the direction of the forward beam.

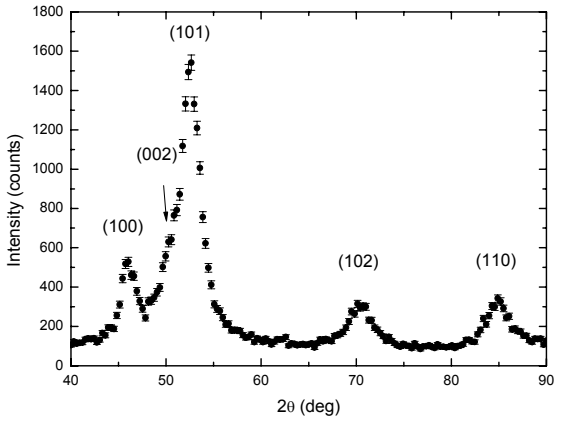

Fig. 1 Elastic scan for nano Tb at 50 K.

A constant q – scan at q = 0.08Å^{-1} at 175 and 250 K (above the ordering temperature) is displayed in Fig. 3 whilst the temperature dependence of the anisotropy gap for single crystal Tb is displayed in Fig 4. It is at the present moment speculative to argue that there is an inelastic peak at approx 0.55 meV. Further measurements with different incoming neutron energies are now needed. This will allow tracking of the inelastic signal over a wider temperature range.

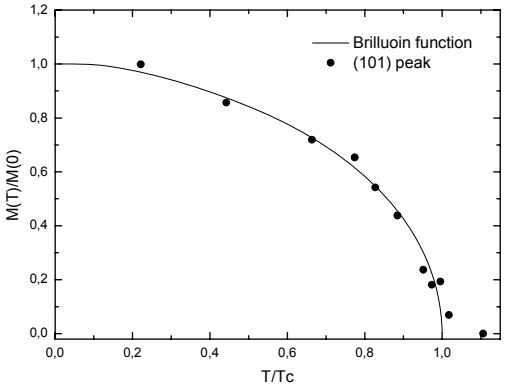

Fig. 2 Temperature dependence of the (101) reflection for nano Tb together with the Brillouin function dependence for J = 6.

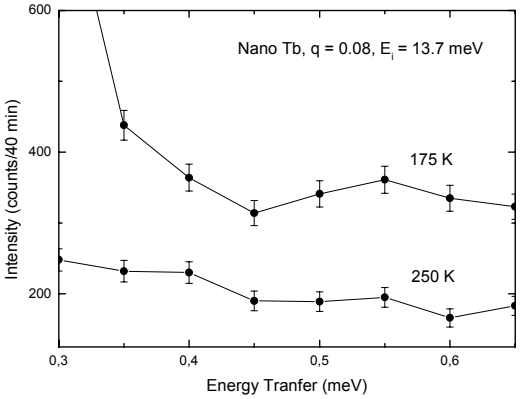

Fig. 3 Constant q scan for nano Tb at 175 and 250 K.

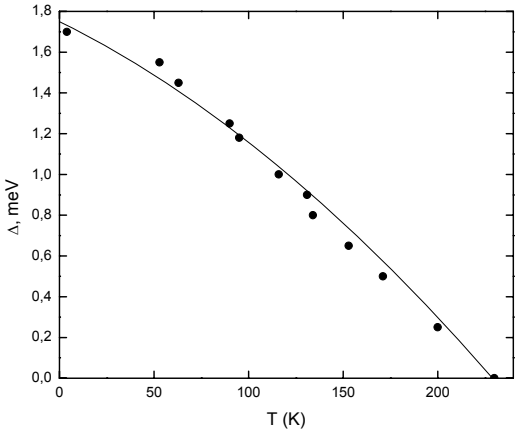

Fig. 4 Temperature dependence of Δ for Tb.

Reference

[1] Weissmüller et al, Phys. Rev. B **69**, 054402 [2004]

	EXPERIMENTAL REPORT **Magnetic excitations in nanocrystalline Tb**	Proposal N° PHY-02-0462 Instrument **E1** Local Contact Vadim Sikolenko
Principal Proposer: Experimental Team:	O. Moze - Physics Dept, Uni Modena, Italy O. Moze - Physics Dept, Uni Modena, Italy C. Vecchini - Physics Dept, Uni Modena, Italy V.V. Sikolenko - HMI Berlin	Date(s) of Experiment 05.04. - 14.04.2005

Date of Report: 10. May 2005

Crystalline Terbium has been widely studied in the past and most of its magnetic properties are known, but only recently has it been possible to study the magnetic microstructure of a nanocrystalline hard magnet. The first time a measurement were performed by SANS [1]. The two important parameters used in modelling the magnetic behaviour in this material are the spin-wave stiffness constant D and the spin-wave gap Δ, which reflects dipolar and, most interestingly, anisotropy contributions. We have recently re-attempted to measure the spin wave excitations in a sample of 1 gm of nano Tb with a grain size of 13 nm in order to investigate the nature of the large magnetic anisotropy in nanocrystalline Tb. Previous measurements were performed on E1 [2] on the same compound. Inelastic scans were performed at different temperatures in the ferromagnetic region (Tc=226K) and in the very low energy transfer regime because coarse Tb shows an anisotropy gap of less than 2 meV at very low temperature. Previously performed scans at Juelich Forshumzentrum on the Triple-Axis Spectrometer UNIDAS, gave evidence of the presence of an inelastic peak at about 8.8 meV at T = 150 K (Fig. 1) around the 101 rlp. The measurements on E1 were performed in the fixed initial energy mode (Ki=2.425 A-1) with energy transfer up to 9.5 meV. This position were chosen because of the high magnetic scattering intensity and much lower background and small angle scattering compared to the forward direction. Due to the low intensity of the inelastic magnetic signal, measurement times were very long. The purpose of this experiment was to trace the inelastic signal with changing temperature. Unfortunatly we were able to perform only a few measurements due to the low scattering intensity. In Fig. 2 we show the inelastic peak at T = 165 K that has subsequently moved to lower energies (8.5 meV) compared to the one observed at T = 150K. Due to technical problems associated with the reactor and the instrument we lost 2-3 days measuring time of a total of 10 days allocation time.

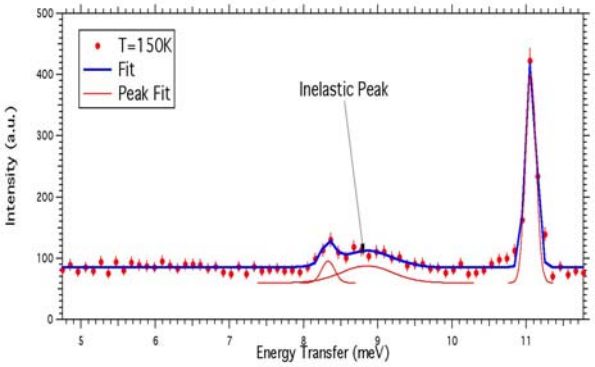

Fig. 1: Inelastic Scan at T = 150 K performed on the UNIDAS Triple axis Instrument. Two spurion Peaks are present at 8.2 meV and 11.0 meV. The inelastic broad peak is clearly visible at 8.8 meV.

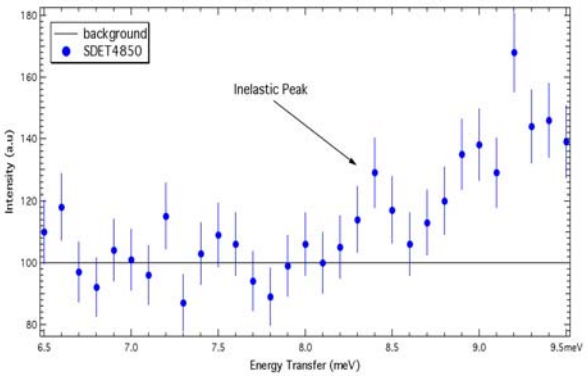

Fig. 2: Inelastic Scan at T = 165 K performed at E1. Inelastic Peak visible at 8.4 meV, while on the right end is visible the wing of a large spurion signal located at higher energies. The black line is the constant background.

References

[1] Weissmüller et al: Phys. Rev. B **69**, 054402 [2004]
[2] This Book - Report for Proposal N°: PHY-02-0447

	EXPERIMENTAL REPORT **Field dependence of magnetic excitations in $La_{7/8}Sr_{9/8}MnO_4$**	Proposal N° PHY-02-0466 Instrument **V2** Local Contact Klaus Habicht
Principal Proposer: Experimental Team:	D. Senff - II. Physikal. Inst., Univ. zu Köln M. Braden - II. Physikal. Inst., Univ. zu Köln	Date(s) of Experiment 20.06. - 30.06.2005

Date of Report: Dec. 2005

The magnetic excitation spectrum of single-layered $LaSrMnO_4$ is quite unusual: while the magnetic structure can be well described as a simple 2D-Ising-AFM with the ordered moment aligned along the tetragonal c-axis [1], inelastic neutron scattering unambiguously demonstrates, that the magnon spectrum consists of three well-separated branches [2]. One of the three branches shows a textbooklike dispersion nicely describable within linear spin-wave theory; in contrast the two additional modes are localized around **k** = 0 and do not show a significant **q**-dependence. The magnetic origin of these modes is clearly proven using polarized neutrons and by the application of an external field: a magnetic field of 13 T applied along the c-axis heavily affects the distribution of spectral weight among the three modes as intensity is transferred from the dispersive towards the localised modes.

Our aim of the experiment at the FLEX spectrometer was to study the field-dependence of the magnetic excitations in slightly doped $La_{7/8}Sr_{9/8}MnO_4$. Slight Sr-doping destabilizes the AFM-ordering as T_N is lowered from 127 K in undoped $LaSrMnO_4$ to 65 K in the doped compound. In addition, the results of a former quick TAS-experiments at the LLB in Saclay suggest a similar excitation-spectrum as in $LaSrMnO_4$, so that we expected to observe a similar or even stronger influence of the magnetic field on the spinwave-spectrum in $La_{7/8}Sr_{9/8}MnO_4$ [2].

For the experiment at the FLEX-spectrometer we used a single-crystal of volume ~ 0.25 cm grown using the floating-zone technique. The sample was aligned in the VM1-cryomagnet with the [100]- and the [010]-directions defining the scattering plane and thus the field applied along the vertical [001]-direction. With the energy of the scattered neutrons fixed to 4.97meV (k_f = 1.55 Å^{-1}) this geometry allowed a maximal energy-transfer of 10 meV at the AFM-zonecenter (0.5 0.5 0).

The main results of our experiment are demonstrated by the field-dependence of an energyscan at the AFM-zonecenter (0.5 0.5 0). The scan in zero field shows a clear, sizable signal only at large counting-times of ~ 50 min., which is equally well describable by either a single and rather broad gaussian centered at ~ 7 meV or three separated modes at 4.3 meV, 6.4 meV and 8.1 meV, which is in fair agreement with our previous experiment (see Fig. 1a). However, the impact of the magnetic field on the magnetic excitations is rather small and in contrast to our former results on $LaSrMnO_4$: With increasing magnetic field we observe a splitting and slight shift of spectral weight to lower energies (see Fig 1b.). But whether this shift can be interpreted in a picture similar to the unconventional behaviour of $LaSrMnO_4$ or whether it has to be regarded as the conventional splitting of the degenerate magnon branches in a magnetic field according to linear spin-wave theory can not be answered with the existing data.

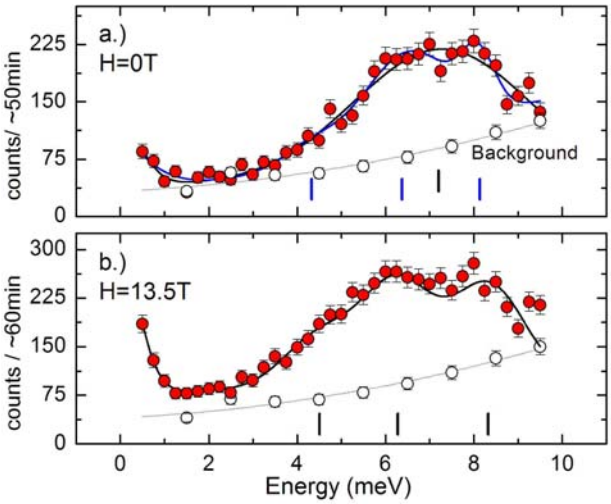

Fig. 1: Energy scan at the AFM-position (0.5 0.5 0)
(a.) at zero-field and
(b.) in an applied field of 13.5 T.
Solid lines represent fits with Gaussians and vertical bars the center of the assumed excitations.

References

[1] D. Senff et al.: Phys. Rev. B **71**, 024425 (2005)
[2] D. Senff, Diploma-Thesis, University of Cologne (2003)

BENSC	**EXPERIMENTAL REPORT** **Study of inelastic response to enhancement of the quasi-2D antiferromagnetic phase in superconducting ($Pr_{0.88}La)Ce_{0.12}CuO_4$ (T_c = 21K)**	Proposal N° PHY-02- 0471 Instrument **V2** Local Contact Klaus Habicht
Principal Proposer: Experimental Team:	S. Wilson - University of Tennessee P. Dai - University of Tennessee S. Li - University of Tennessee	Date(s) of Experiment 12.04. - 19.04.2005

Date of Report: 17.10.2005

The spin fluctuations within the high-T_c cuprates remain a subject of considerable importance. Several theories have suggested a possible spin fluctuation mediated pairing mechanism, yet the precise evolution of spin dynamics in these systems as they are doped into the superconducting phase remains unclear. Additionally, quantum critical (QC) fluctuations arising from the suppression of a magnetic ordered phase have been purported to strongly influence the electronic properties of these materials [1 - 4].

While the presence of such QC fluctuations has been demonstrated experimentally in hole-doped cuprates [5, 6], the precise nature of the competing phases within these systems remains unclear. Our previous work has unveiled a clear competition between an AF ordered magnetic phase and the superconducting phase within the electron-doped $Pr_{0.88}LaCe_{0.12}CuO_4$ PLCCO system [7].

In addition to the discovery of this competition in which the AF phase is suppressed to 0K at optimal superconductivity, we have identified QC excitations arising from this nearby QCP in the phase diagram within an underdoped T_c=21K sample [8]. While a distinct quantum critical scaling regime is evident within the low energy dynamics of this system, one important remaining question is: What is the response of these low energy QC excitations when a c-axis aligned magnetic field quenches the superconducting phase in the sample?

For electron-doped PLCCO (T_c=21K), the upper critical field is an experimentally accessible 8T. In our experiment we aligned a PLCCO T_c=21K sample in the HKO plane and mounted it within the 13T cryomagnet. Constant Q and constant E scans were performed about the (π, π) ordering wavevector where a quasi-2D SDW order arises in superconducting PLCCO concentrations [7].

Our results reveal an interesting result: the low energy fluctuations within the system are largely unaffected by the suppression of the superconducting phase within the sample (Fig1: a).

Additionally, it can be simultaneously seen that an enhancement of the quasi-2D static order at (π,π) emerges as T_c is suppressed in field. Also evident is the shift in onset temperature of this SDW order under 13T (Fig.1: c).

0.5 meV fluctuations are also plotted both in 13T and in 0T fields demonstrating the lack of any field effect in the low energy fluctuations of the system. One possible interpretation of this may be that the QC dynamics are not coupled directly to the superconducting phase in the system and that some other quantum-disordered phase arises near optimal superconductivity.

Further experiments on concentrations doped closer to the QCP in this system are necessary in order finalize the picture of how the QC dynamics in this system couple to the suppression of superconductivity within electron-doped PLCCO.

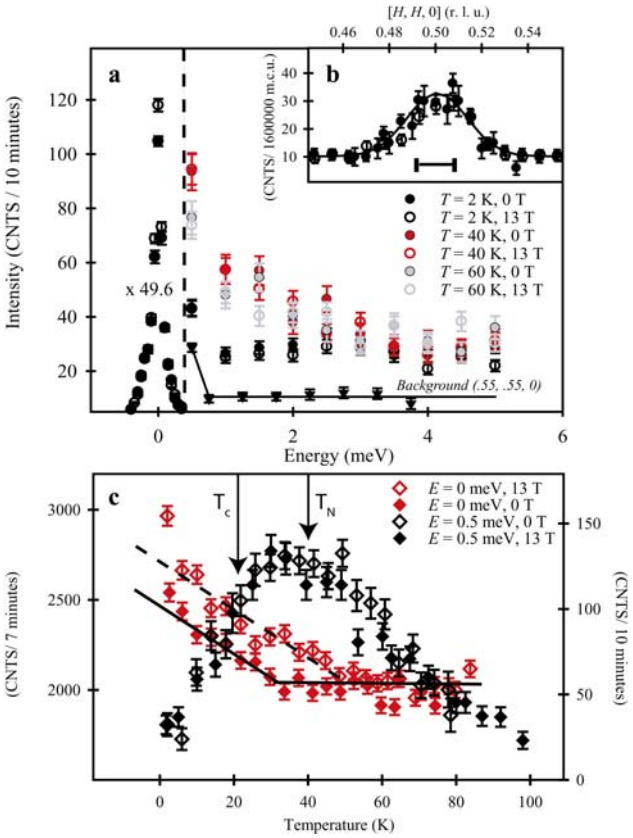

Fig. 1: a) Energy Scans at the (π,π) vector with nonmagnetic background shown in 0T and 13T. Scaled data at the elastic line is shown in left panel. **b)** Q scan at E=4meV in 13T and 0T showing no change.
c) T dependence of (π,π) at E=0 and E=0.5meV positions in 13T and 0T.

References:
[1] Chakravarty, S. et al.: *Phys. Rev. B.* **39**, 2344-2371 (1989)
[2] Varma, C. M. et al.: *Phys. Rev. Lett*. **83**, 3538-3541 (1999)
[3] Abanov, A. et al.: *Phys. Rev. Lett*. **84**, 5608 (2000)
[4] Sachdev, S. et al.: *Rev. Mod. Phys*. **75**, 913 (2003)
[5] Aeppli, G. et al.: *Science* **278**, 1432-1435 (1997)
[6] W. Bao et al.: Phys. Rev. Lett. **91**, 127005 (2003)
[7] H. Kang et al.: Phys. Rev. B **71**, 214512 (2005); 71, 100502 (2005)
[8] S. Wilson et al.: PRL (in review) (2005)

	EXPERIMENTAL REPORT **Quantum phase transitions in the organic quantum magnet $(C_5H_{12}N)_2CuBr_4$**	Proposal N° PHY-02-0495 Instrument **V2** Local Contact Klaus Habicht
Principal Proposer: Experimental Team:	Ch. Rüegg - LCN & UCL, London Ch. Rüegg - LCN & UCL, London B. Thielemann - LNS, ETH Zurich & PSI	Date(s) of Experiment 07.09. - 25.09.2005

Date of Report: 9 Jan 2006

The spin dynamics in the field-temperature phase diagram of gapped quantum magnets, like Haldane, ladder and dimer spin systems, has recently attracted considerable interest due to the presence of several novel quantum phases. Our search for a new model compound, where the complete phase diagram is accessible by INS, has been successful. The potential organic ladder compound $(C_5H_{12}N)_2CuBr_4$ [1], which should not be confused with the well-known frustrated spin-liquid $Cu_2(C_5H_{12}N_2)_2Cl_4$ [2], exhibits an optimal energy scale, see Fig. 1, to address the above for the first-time and has recently been grown in single crystalline form with sample mass (deuterated) suitable for a neutron scattering investigation.

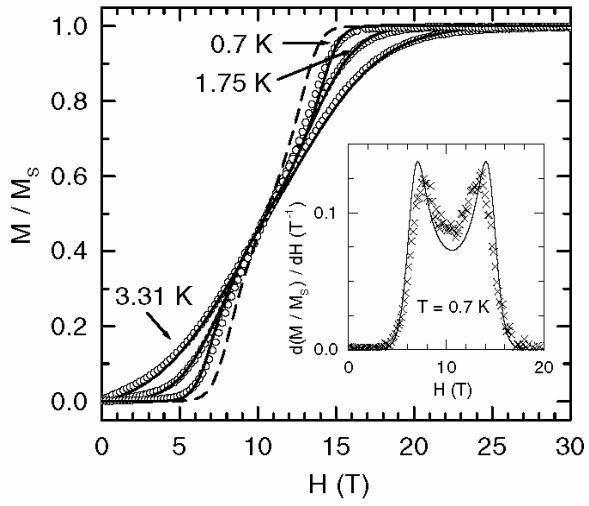

Fig. 1: Magnetisation of $(C_5H_{12}N)_2CuBr_4$ at different temperatures, from Ref. [1].

Following previous INS experiments on TASP (SINQ) and IN14 (ILL) at lower magnetic fields, on V2 (HMI) equipped with the 15 T vertical magnet and a dilution insert measurements were focussed on the spin wave dispersion in the saturated phase of the quantum spin ladder to additionally confirm the spin Hamiltonian determined in zero-field. We report excellent agreement between the two independent studies. Furthermore, by measuring the field-induced spin gap in the ferromagnetic phase especially at T=50 mK the saturation field of the compound was found to be approx. 1 T lower than previously determined [1] – an experimental finding which is fully consistent with the exchange parameters determined by INS. Specific heat measurements performed simultaneously at HMI down to 300 mK and up to magnetic saturation have further contributed to the characterisation of the compounds.

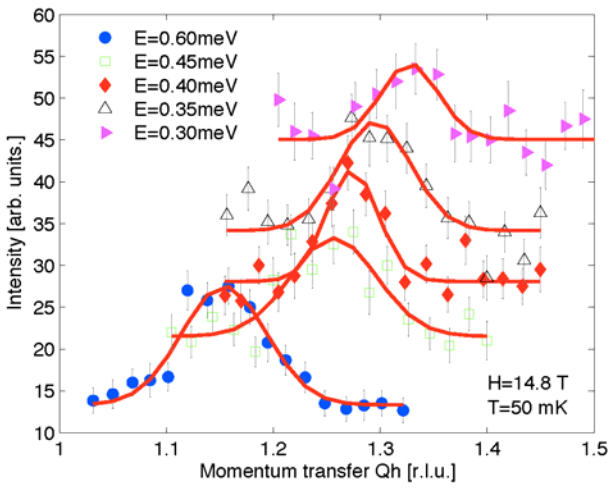

Fig 2: Q-scans at different energies as indicated in the saturated phase of the quantum spin ladder $(C_5H_{12}N)_2CuBr_4$.

In the future we plan to continue our study of the material along the lines of our investigations on the dimer compounds $TlCuCl_3$ and NH_4CuCl_3, but fortunately now in the quasi-1D limit for which exciting new effects are expected.

References

[1] B.C. Watson *et al.*: Phys. Rev. Lett. **86**, 5168 (2001)
[2] G. Chaboussant *et al.*: Eur. Phys. J. B **6**, 167 (1998)
[3] E. Dagotto *et al.*: Science **271**, 618 (1996)
[4] Ch. Rüegg *et al.*: Nature **423**, 62 (2003);
Phys. Rev. Lett. **93**, 037207 (2004);
Phys. Rev. Lett. **93**, 257201 (2004);
Phys. Rev. Lett. **95**, 267201 (2005)

BENSC	**EXPERIMENTAL REPORT** **Field dependence and quantum criticallity in the spin fluctuations of an electron-doped high-T_c cuprate, $Pr_{1-x}LaCe_xCuO_4$**	Proposal N° PHY-02-0501 Instrument **V2** Local Contact Klaus Habicht
Principal Proposer: Experimental Team:	S. Wilson - University of Tennessee P. Dai - University of Tennessee S. Li - University of Tennessee	Date(s) of Experiment 21.07. - 31.07.2005

Date of Report: 28.09.2005

The role of magnetism within the superconducting mechanism in the high-T_c cuprates remains an issue of considerable controversy. While spin fluctuations mediated electron-electron pairing mechanisms have been postulated in a number of scenarios, how magnetic fluctuations in these materials evolve with increasing doping is still not determined. On the other hand, quantum critical (QC) fluctuations arising from the suppression of a magnetic ordered phase to absolute zero through a second order phase transition have been thought to play a role in determining the electronic properties of these materials [1-4]. Whereas the presence of these QC fluctuations have been shown in various hole-doped cuprates [5,6], the nature of the competing phases and their relation to superconductivity remains unknown in electron-doped cuprates. Our previous studies have shown the presence of such quantum fluctuations within the electron-doped cuprate $Pr_{.88}LaCe_{.12}CuO_4$ T_c=21K [8]. In addition to the presence of these QC fluctuations, previous work has also identified how superconductivity is established in electron-doped materials [7]. In Kang's work, a quasi-2D spin density wave coexists with superconductivity and becomes weaker as optimal superconductivity is approached.

Our goal in this experiment was to probe spin fluctuations in a T_c=24K sample doped much closer to the QC point in the system than the previous T_c=21K sample. The evolution of the ω/T scaling regime and the possible presence of a spin gap in this nearly optimal doped sample were investigated. Additionally, we hoped to investigate whether the field can induce static AF order in this sample, which is known to have no static AF order at 0T. The field dependence of the spin fluctuations seen in the system was also investigated as superconductivity was suppressed in the sample.

Our results show a gapless spectrum in the spin fluctuations in the system (Fig. 1) that is unaffected by the application of a 13T field. There is a potentially intriguing effect at 0.5meV in which the field seems to suppress states below the superconducting transition temperature. Unfortunately, due to reactor difficulties in which approximately 5 days were lost, we were unable to finalize our measurements. This precludes our current data from addressing the modification to the quantum critical scaling regime in this nearly optimal doped sample. Additionally, we have observed a potential elastic field induced effect at the (0.5, 0.5, 0) SDW ordering wavevector (Fig. 2). Whereas no order can be seen down to 2K in 0T, there is an apparent enhancement at 2K under field at (0.5, 0.5, 0). Unfortunately, time did not permit a thorough investigation of the onset temperature of this field-induced order, but we know it is likely to be above 30K. Hopefully, if we may regain the 5 days lost from the original allotment of time, these remaining questions can be satisfactorily addressed.

References

[1] Chakravarty, S. et al.: *Phys. Rev. B.* **39**, 2344-2371 (1989)
[2] Varma, C. M. et al.: *Phys. Rev. Lett*. **83**, 3538-3541 (1999)
[3] Abanov, A. et al.: *Phys. Rev. Lett*. **84**, 5608 (2000)
[4] Sachdev, S. et al.: *Rev. Mod. Phys*. **75**, 913 (2003)
[5] Aeppli, G. et al.: *Science* **278**, 1432-1435 (1997)
[6] W. Bao et al.: *Phys. Rev. Lett.* **91**, 127005 (2003)
[7] H. Kang et. al.: *Phys. Rev. B* **71**, 214512 (2005); 71, 100502
[8] S. Wilson et al.: *PRL* (in review) (2005)

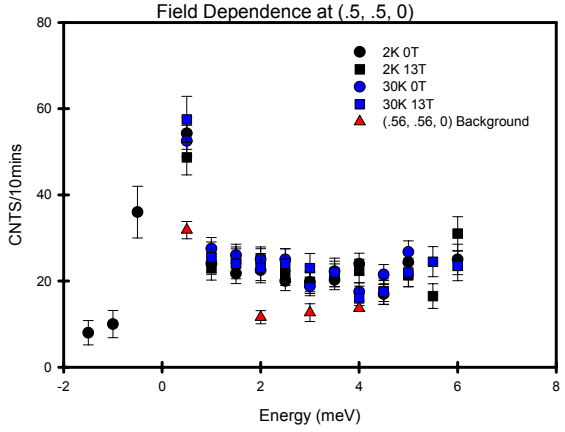

Fig. 1: Inelastic spectra at 2K along (0.5, 0.5, 0). Nonmagnetic background is shown in triangles.

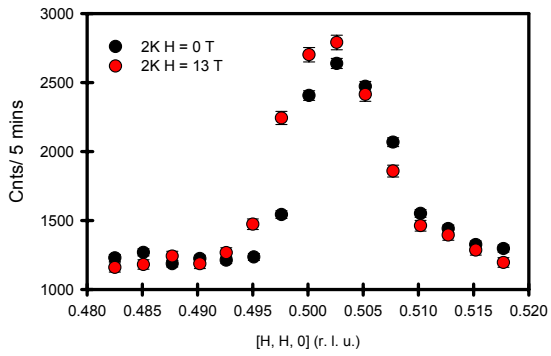

Fig. 2: Elastic Q scans at 2K through the (0.5, 0.5, 0) point showing an enhancement in 13T.

BENSC	**EXPERIMENTAL REPORT** **Investigation of antiferromagnetic spin fluctuations in $CePt_3Si$**	Proposal N° PHY-03-0380 Instrument **V3** Local Contact Margarita Russina
Principal Proposer: Experimental Team:	J.-G. Park - Sungkyunkwan University, KP J.-Y. So - Sungkyunkwan University, KP D.T. Adroja - RAL ISIS, UK E.A. Bauer - TU Wien, A	Date(s) of Experiment 07.02. - 11.02.2005

Date of Report: 04. Jan. 2006

Recently, we have discovered that tetragonal $CePt_3Si$ exhibits an antiferromagnetic ordering at $T_N = 2.2$ K and becomes a heavy fermion superconductor at $T_C = 0.75$ K without a center of inversion symmetry [1]. The tetragonal structure of $CePt_3Si$ can be derived by filling voids with Si in hypothetical $CePt_3$ of the cubic $AuCu_3$-structure. A distinct λ-type anomaly at 2.2 K in the heat capacity along with the peak in the susceptibility confirms the antiferromagnetic ordering of the Ce^{3+} moments in $CePt_3Si$. Interestingly the heat capacity ($C_p(T)/T$) exhibits logarithmic behaviour above 2.2 K that may be attributed to spin fluctuations associated with the magnetic order, thus causing a breakdown of the Fermi-liquid state. A small entropy gain at T_N is indicative of a magnetic ordering with a reduced size.

High energy inelastic neutron scattering experiment on $CePt_3Si$ was performed using HET of ISIS. From this HET experiment, we have found two inelastic magnetic peaks: one around 11 meV and another one at 1.4 meV. The higher energy peak was ascribed to a crystalline electric field excitation, but there is still a controversy over the origin of the lower energy peak. In order to clarify the origin of the lower energy peak, we investigated its temperature as well as momentum dependence using low energy neutrons.

We measured $CePt_3Si$ using the NEAT time-of-flight spectrometer. We chose incident energy of 4.5 meV with an estimated energy resolution of 0.25 meV. Chopper speed was kept at 10000 rpm except for the 4th chopper which ran at 3333 rpm. We also measured $LaPt_3Si$ as a phonon blank material. Using a He^3 dilution cryostat our experiments were carried out from 0.4 to 25 K.

In all our data, we observed a rather strong peak appearing at 0.5 meV and $\mathbf{Q} = 0.8$ A^{-1}. However, when we inspected our results taken with empty sample can as well as a standard vanadium sample we noticed a similar feature at more or less the same energy. (see Fig. 1) Furthermore, it does not satisfy the detailed balance factor nor have any clear temperature dependence at all. (see Fig. 2) All these experimental observations led us to conclude that the strong peak at E = 0.5 meV and $\mathbf{Q} = 0.8$ A^{-1} is most likely to be a spurious peak due to some multiple scattering. Unfortunately, the peak at 0.5 meV is so overwhelming that there is barely a sign of the expected peak around 1.4 meV in our data.

After discussing these results with our local contact, we concluded that we would need another experiment in near future in order to understand the origin of the 1.4 meV peak.

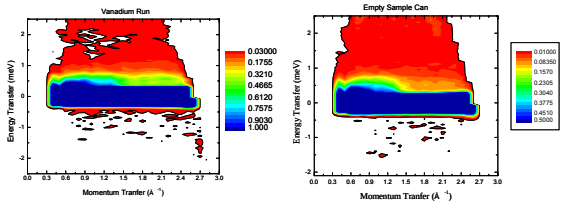

Fig. 1: E-Q plot of vanadium run (left) and empty can measurements (right).

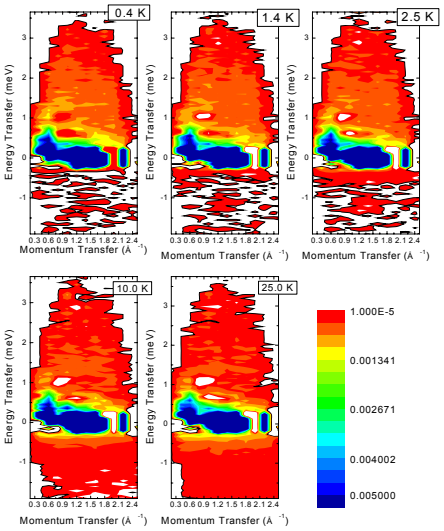

Fig. 2: E-Q plot of the magnetic excitations of $CePt_3Si$ given in absolute unit, mb/meV/sr/f.u. after phonon subtraction at 0.4, 1.4, 2.5, 10 and 25 K (clockwise from upper left).

Reference

[1] E. Bauer *et al.*: Phys. Rev. Lett. **92**, 027003 (2004)

	EXPERIMENTAL REPORT **The ground state of Pr^{3+} ion in PrB_6 : singlet or triplet?**	Proposal N° PHY-03-0407 Instrument **V3** Local Contact Konrad Siemensmeyer
Principal Proposer: Experimental Team:	N. Tiden - RRC "Kurchatov Institute", Moscow, RU E. Nefeodova - RRC "KI" K. Siemensmeyer - HMI Berlin A. Buchsteiner - HMI Berlin	Date(s) of Experiment 24.11. - 30.11.2005

Date of Report: 29.12.2005

Praseodymium hexaboride (PrB_6) is a metallic compound with a "non-Kramers" rare-earth ion, which exhibits two magnetic phase transitions at T~7K and 4.2K. The splitting scheme of the 4f shell ground multiplet in the crystalline electric field is the key point for understanding the peculiarities of the PrB_6 low temperature properties, in particular the magnetic properties. The only known inelastic neutron scattering experiment on PrB_6 defined the ground state as Γ_5, but in these measurements quasielastic scattering attributed to $\Gamma_5 \leftrightarrow \Gamma_5$ excitation has not been observed **[1]**.

In order to obtain information about the quasielastic scattering and its temperature dependence a detailed study of the magnetic response for $Pr^{11}B_{12}$ powder sample has been performed using the NEAT time of flight spectrometer. The sample was prepared with 99.52% ^{11}B isotopic enrichment in order to reduce absorption. The sample mass was about 6 g. The powder sample has been put into three rectangular containers from 0.05 mm aluminium foil which were fixed in a frame. The total dimension of sample was 30x55 mm^2. The incoming neutron energy E_i was selected as 12 meV and 9 meV which provide an elastic line resolution (FWHM for vanadium standard) of 1.4 meV and 0.5 meV respectively. Measurements were done at T=2K, 5K, 20K, 80K and 300K using an "Orange Cryostat". Measurements of a $La^{11}B_6$ reference sample and of the empty cell were performed (E_i=12 meV) to estimate the phonon and background contributions. For the absolute calibration of spectral data and detector efficiency a vanadium standard was measured. The experimentally defined transmission for all samples was about 80%.

The inelastic neutron scattering (INS) spectra obtained with high resolution at 2K, 80K and 300K for PrB_6 are displayed in **fig.1.** The INS spectra of PrB_6 with low resolution in comparison with LaB_6 are shown in the inset of

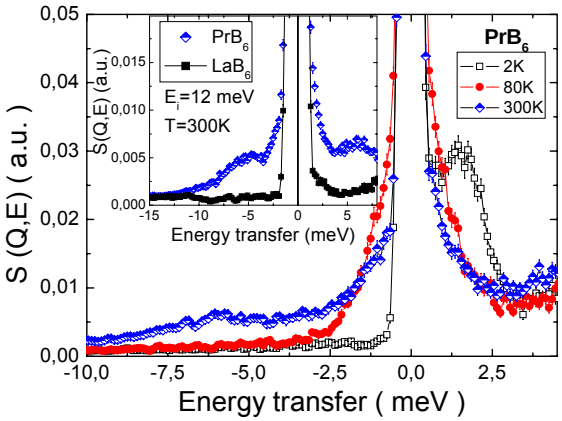

Fig.1: Inelastic neutron scattering spectra of PrB_6 at 2K, 80K and 300K for $<2\theta>=33^0$. Inset – comparison of PrB_6 and LaB_6 at 300K (poor resolution).

fig. 1. It is clearly seen from the inset that the nonmagnetic contribution even at 300K does not play a crucial role in the spectrum. From the INS spectra with high resolution (**fig.1.**) additional quasielastic scattering at 300K and 80K near the elastic line is clearly seen. At 2K (well below the two magnetic phase transitions) an inelastic peak with an energy of about 1.5 meV is observed. This peak could be from the Zeeman splitting of the degenerate paramagnetic phase ground state – Γ_5.

The preliminary estimate of the magnetic cross section corresponding to the quasielastic excitation gives a value of about 3 barn at 80K which is in good agreement with the calculation.

In summary, we have observed quasielastic scattering in PrB_6, for the first time that gives clear evidence of Γ_5 triplet to be the ground state in the paramagnetic phase.

Acknowlegments

This work was supported by INTAS Proj. # 03-51-3036 and RFBR grant 05-02-08079.

Reference

[1] Lowenhaupt and M. Prager, Z. Phys. B **62** (1986) 195

	EXPERIMENTAL REPORT **Shape crossover and time scaling of the critical dynamics of an Heisenberg ferromagnet**	Proposal N° PHY-03-0331 Instrument **V5** Local Contact Catherine Pappas
Principal Proposer: Experimental Team:	M. Alba - LLB, CNRS-CEA, Gif/Yvette, F C. Pappas - HMI Berlin	Date(s) of Experiment 26.05. - 06.06.2004

Date of Report: 15.03.2006

Summary :

We measured the $CdCr_2S_4$ sample (diluted at 95% of Chromium) at T_C (69.5 K) and above T_C , in the Q-range 0.06-0.16 $Å^{-1}$ above QD=0.05 $Å^{-1}$ where the relaxation time (4ps<t<60ps) enters the dynamic range of SPAN at λ = 4.5 Å and λ = 6.5 Å. The sample is made of isotopic ^{114}Cd and has a good transmission and scattering (more than 80 cps of magnetic scattering at T_C at the smallest Q).

Experiment schedule :

We have used two different setups , two standard NSE magnetic configurations without any π flipper, with λ = 4.5 Å and λ = 6.5 Å. We have spent three days for careful setup and resolution scans and two days at each temperature (six T values, nearly 36 H at T_C and more above). The resolution was measured in the very same configuration, simply by quenching the sample in the spin glass state below T = 5 K where its dynamics becomes completely static on the NSE timescales.

Half a day of beamtime was dedicated to a precise determination of the transition temperature and another half day of beamtime was dedicated to cryogenic duties (Helium and Nitrogen refill and temperature changes).

Results and data treatment :

We were therefore able to measure at T= 69.55, 70.5, 71, 73.5, 75.2, 77.6 K. We made a test at T=81 K but the signal becomes weaker and weaker as a function of the reduced temperature (T- T_C)/T .

The data reduction is complicated by some lack of statistics on the resolution scans at higher Q values and by a huge structural background at smaller Q values due to the powder state of the samples and the wide open geometry of the spectrometer. We made some test to shield the diffused beams and enhance the signal/noise ratio, especially at very low Q values with no success. However, the overall experiment is very successful in determining the correct spectrometer setups and locating the critical dynamics and the characteristic relaxation times.

In the future, we plan to kill the powder structural signals that scales like Q^{-4} by mixing the sample with glycerol-D3. It has the same neutron scattering length as $CdCr_2S_4$. It freezes at low temperature and will not crack and give rise to a small angle signal. It will also help in thermalizing the powdered sample.

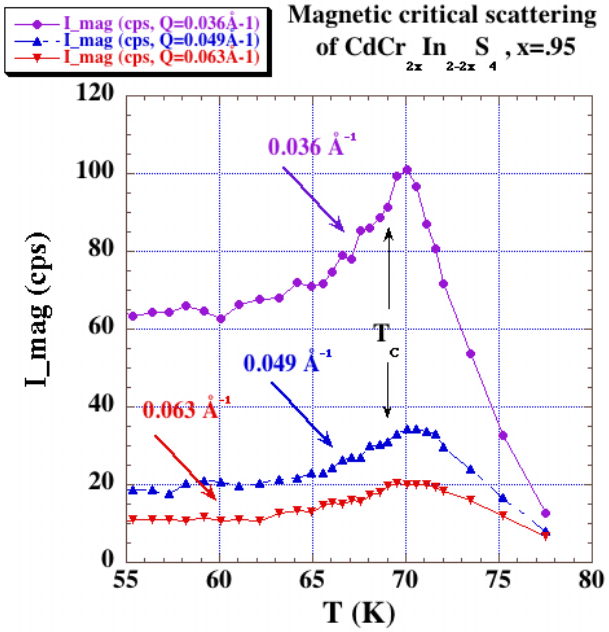

Fig. 1: Magnetic critical scattering of $CdCr_2S_4$ measured on SPAN with a 6.5 Å configuration. Temperature scans performed to determine the transition temperature.

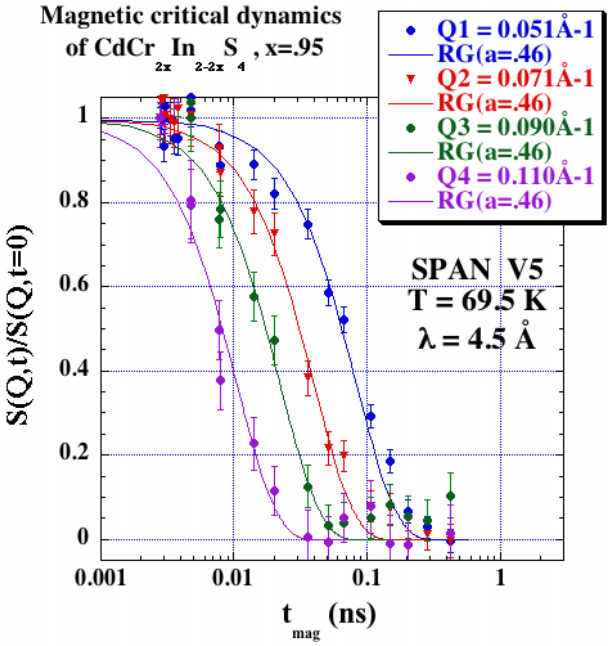

Fig. 2: Magnetic critical dynamics of $CdCr_2S_4$ measured at 69.5 K on SPAN with a 4.5 Å configuration. The magnetic relaxation is fitted by the RG theory predictions.

	EXPERIMENTAL REPORT **Diffuse scattering of cation-doped zirconia-oxynitrides**	Proposal N° CHE-01-1749 Instrument **E2** Local Contact Jens-Uwe Hoffmann
Principal Proposer: Experimental Team:	I. Kaiser-Bischoff - LMU München, Kristallogr. I. Kaiser-Bischoff - LMU München J.-U. Hoffmann - HMI Berlin, Uni Tübingen	Date(s) of Experiment 28.10. - 06.11.2005

Date of Report: 09.01.2006

Zirconia, ZrO_2 doped with cations and/or anions shows interesting order-disorder phenomena. The doping leads to oxygen vacancies, which is the basis of the high ionic conductivity. The short-range order originating from these vacancies can be identified by analyzing the diffuse scattering. Depending on the type and amount of dopants, different structures are formed. Like the doping with Yttrium, the doping with Magnesium stabilises the structures of pure ZrO_2 (m, t, and Fluorite). While an additional doping with Nitrogen does not lead to new structures for Y-doped samples, it causes rhombohedral superstructures for Mg-doped samples, which transform to the cubic structure at high temperatures.
From earlier investigations at E2 (CHE-01-1332, CHE-01-1440) we know that the cubic phases of doped ZrO_2 show a characteristic diffuse scattering. Diffuse maxima are parts of global features, such as diffuse bands perpendicular to <111>. Using the program TVtueb (written for E2) it was possible to refine a model for the defect structure, which is based on uncorrelated vacancies and radial relaxation of the surrounding ions. Ions lying on the same shell are displaced by the same amount ("shell cluster").

We investigated two single crystal samples of ZrO_2 doped with Mg, before and after a nitridation. The zeroth layers of the [1-10] (in cubic setting) zone have been measured with λ=0.91 Å from RT up to 1200°C. We used a closed cycle furnace (high vacuum) and high temperature glue.

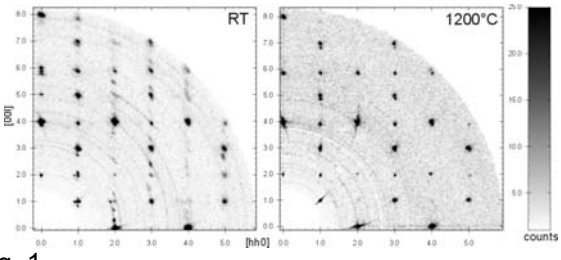

Fig. 1

Sample 1: The sample $Zr_{0.92}Mg_{0.08}O_{1.92}$ (ZrO_2+ 8mol% MgO) was measured at RT, 400, 1000 and 1200°C (Fig. 1). The RT phase seems to have a monoclinic structure, but we have to verify it with powder diffraction. At 1000°C it is changed to tetragonal structure and first weak diffuse scattering can be seen at (440) and (004). The transition to cubic structure could not be reached. The doubling of some reflections indicates a second individual.

Sample 2: The sample ZrO_2 + 8mol% MgO + N was measured at RT, 400 and 1200°C. At RT the samples shows a rhombohedral superstructure which could not be identified in this layer in cubic setting. But at 1200°C it is cubic and the characteristic diffuse scattering for cubic stabilized ZrO_2 is observed. It was possible to refine our defect model according to this data. The Zr-ions on the first shell are shifted away from the vacancy by 0.35 Å and the O-ions on the second shell towards the vacancy by 0.30 Å. Fig 2 shows the measured and simulated diffuse scattering.

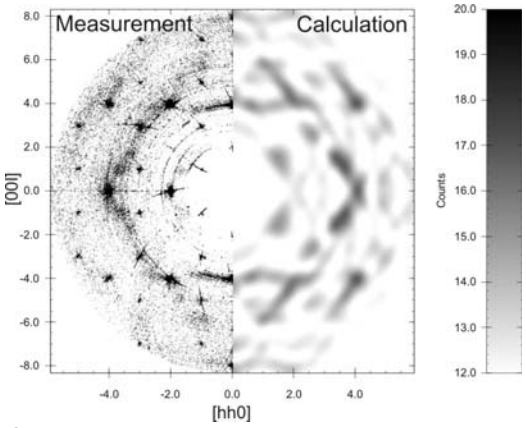

Fig. 2

Conclusion: The analyzing of these data is still going on. One result is that the doping with nitrogen reduces this transition temperature to cubic structure. The high temperature displacements of the cations on the first shell is smaller compared with a Zr-Y-O-N sample (0.37 Å), but the anion displacement is enlarged here (0.23 Å for Zr-Y-O-N).

Comparing these data with X-ray data (F1 at Hasylab/Hamburg), we see differences concerning the Bragg reflections for the sample Zr-Mg-O at RT: e.g. (332) can be observed with neutrons, but it is absent in the synchrotron measurement, which could not be explained until now.

Acknowledgement
This work is supported by DFG (Bo1199/2-2) within the SPP "Substitutionseffekte in ionischen Festkörpern".

BENSC	**EXPERIMENTAL REPORT** **Microstructural twinning characteristics in $YBa_2Cu_3O_{6+x}$ high-temperature superconductor at room temperature**	Proposal N° PHY-01-1683 Instrument **E2** Local Contact Jens-Uwe Hoffmann
Principal Proposer: Experimental Team:	D.K. Ross - University of Salford, UK L.F. Zhang - University of Salford, UK	Date(s) of Experiment 01.06. - 05.06.2005

Date of Report: August 2005

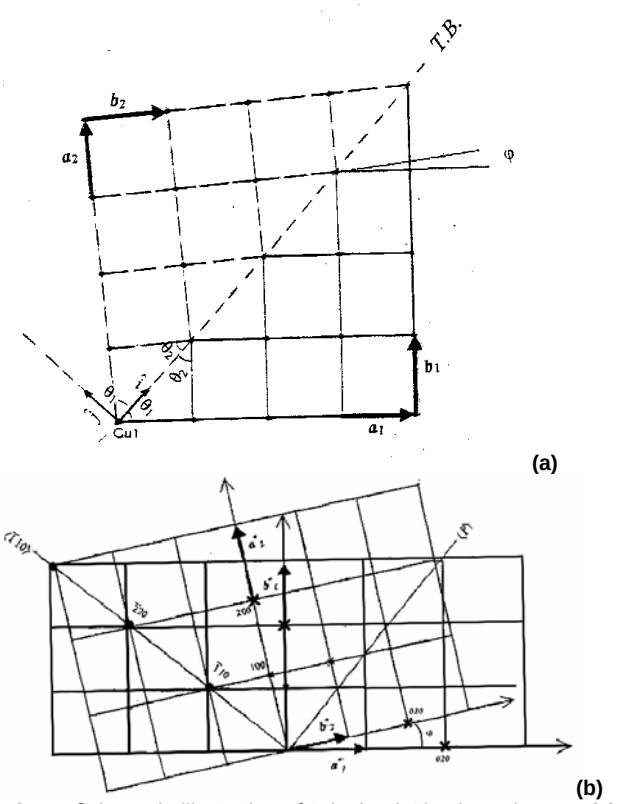

Fig. 1: Schematic illustration of twinning lattice in real space **(a)** and overlapping in reciprocal space **(b)**

In fig.1(a) we present the simple geometric model of adjoining twins adjacent in the basal plane of the orthorhombic phase. In this model the sites of the Cu atoms are sitting in the corners of the cells and the role of the oxygen atoms is just to lengthen the b parameter over a lattice parameter. Therefore the model can predict the main peculiarities of the diffraction pattern as seen later, such as (*h00*), and (*0k0*) reflections which we split into two peaks. The superposition of twin lattices having relative rotation around *C* by the angle of $\varphi = \tan^{-1}(a/b) - \tan^{-1}(b/a)$.

In fig.1(b) we present the twins in reciprocal space as the superposition of twin reciprocal lattices having relative rotation around C^* by the angle of $\varphi = \tan^{-1}(a/b) - \tan^{-1}(b/a)$. It is clear that (*-hh0*) reflections remains unsplit but other reflections are separated into two peaks, and the separation is larger when increasing the order of reflection.

We see fig.2(a) shows the distribution of diffraction patterns, which gives hints on the distribution of twin individuals. It is easy to see that there is no symmetry of intensity for these four diffraction patterns, since the twin gives rise to overlapping intensity.

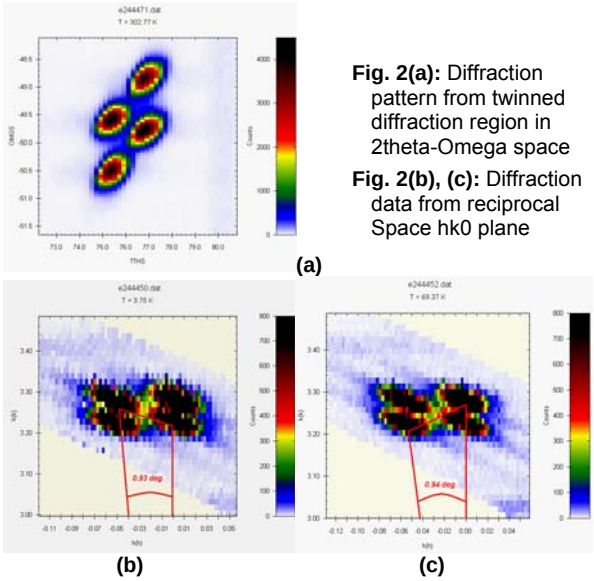

Fig. 2(a): Diffraction pattern from twinned diffraction region in 2theta-Omega space

Fig. 2(b), (c): Diffraction data from reciprocal Space hk0 plane

Finally, these two plots above fig.2(b), 2(c) show the twinning distribution in the crystal we have been measuring, the plot represent the region in reciprocal space where the twin patterns have been predicted by our previous calculation [Khoshnevisan, B 2002]. We calculated the angle between the overlapping lattice in fig.2(a), 2(b) diagonally, giving angle of φ ~ 0.93 deg, then we can estimate the ratio of lattice parameters a/b ~ 0.9680, from this ratio, we can retrieve a ~ 3.83 Å, b ~ 3.95 Å, which are consistent from the index of pattern, giving rise to a ~ 3.83 Å, b ~ 3.91 Å. These data however, are still being subject to careful examination to fully characterize the orientation of twinned crystal, and we expect to be able to observe structural transition from this orthorhombic phase to tetragonal phase by reducing the sample oxygen stoichiometry under high temperature (650°C) using thermal gravimetric method.

The objective of this proposal was to observe satellite peaks in $YBa_2Cu_3O_{6+x}$ single crystal, however we will hope repeat the measurements of high temperature to examine the transition to the tetragonal phase in situ.

Acknowledgement

We thank Berlin neutron scattering centre and financial infrastructure of European Union Access Scheme.

References

[1] Khoshnevisan, B., Ross, D.K., Broom, D.P. and Babaeipour, M.: "Observations of Twinning in YBa2cu3o6+X, 0 < X < 1, at High Temperatures" 2002, *Journal of Physics-Condensed Matter*, **14(41)** 9763-9778

[2] Mercer, M., Campbell, S. I., Bennington, S. M., Dreyer, J. W., Kemali, M., Shepherd, P. D. and Ross, D. K.: "A Study of the Tetragonal to Ortho 1 Phase Transition in YBa2cu3ox" 1997, *Physica B*, **234** 925-927

	EXPERIMENTAL REPORT **Neutron powder diffraction of Diindenoperylene**	Proposal N° PHY-01-1815-LT Instrument **E2** Local Contact Jens-Uwe Hoffmann
Principal Proposer: Experimental Team:	F. Schreiber - Uni Tübingen U. Amann - Uni Tübingen, HMI Berlin J.-U. Hoffmann - Uni Tübingen, HMI Berlin B. Maier - HMI Berlin	Date(s) of Experiment 16.07. - 19.07.2005 16.08. - 22.08.2005

Date of Report: 12.09.2005

Thin Films of the organic semiconductor diindeno-(1,2,3,-cd,1',2',3'-lm)perylene [$C_{32}H_{16}$ (DIP), Fig. 1] were recently studied for structural and physical properties. However, it is not much known about the bulk structure of DIP, which differs from the structure of DIP thin films.

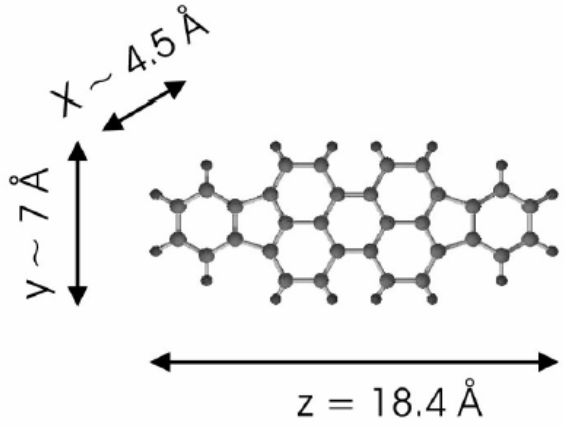

Figure 1: The DIP molecule

Research with X-Ray diffraction on DIP thin films - amongst other organic thin films - is well established in our group [1]. With complementary information of neutron data we expect to get deeper insight into the differences between structural details in DIP bulk material and in thin films.

The aim of our first neutron diffraction measurement on a DIP powder sample was to get accustomed to the general preparation, measurement and analysis techniques, as no comparable work was done before on this class of substance with neutron diffraction. In addition, with neutron diffraction data of a DIP powder sample [Fig. 2] we investigate the bulk structure of DIP.

Two different powder samples of DIP were used for the measurements: The first one purified by gradient sublimation, the second consists of raw synthesized material which was ground, as we learned from single crystal reflections obtained in the first measurement that the grain size in the powder was very large.

A triclinic bulk structure with four molecules per unit cell and P-1 symmetry was determined by Pflaum et al. by X-ray diffraction on DIP single crystals [2].

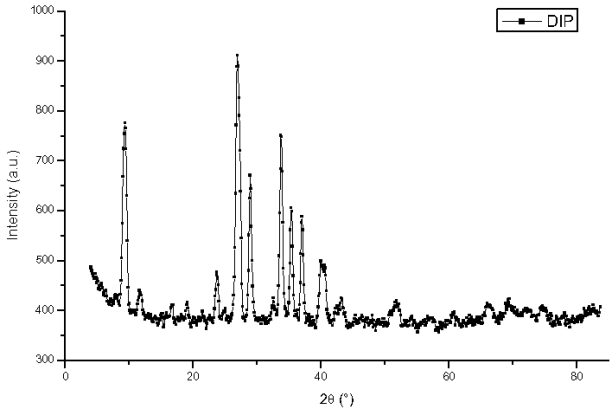

Figure 2: Diffraction pattern from DIP powder sample

In order to find an adequate structural model for fitting the measured data, further investigations will be carried out, in particular as a function of temperature, since this class of materials is known for a rather rich phase diagram.

References:

[1] F. Schreiber, Phys. Stat. Sol. 201 (2004), 1037;
A. C. Dürr et al., Phys. Rev. Lett. 90 (2003) 016104
[2] Pflaum et al.: in preparation

BENSC	**EXPERIMENTAL REPORT** **Neutron diffraction on birch wood for studying the space orientation of the crystalline areas of cellulose**	Proposal N° PHY-01-1723-EF Instrument **E5** Local Contact Manfred Reehuis
Principal Proposer: Experimental Team:	J. Peters - HMI Berlin J. Peters - HMI Berlin J.T. Bonarski - Inst. Metall. Mat. Sc., Krakow, PL W. Olek - Univ. of Poznan, Poland M. Reehuis - HMI Berlin	Date(s) of Experiment 07.02. - 15.02.2005

Date of Report: 10.05.2005

Wood being a natural biopolymer reveals a distinct preferred orientation of its crystalline part, i.e. cellulose. However, crystalline and amorphous parts of wood structure are not separated from each other. By means of X-ray diffraction, it is possible to distinguish Bragg peaks due to the crystalline structure from the surrounding amorphous part, which essentially contains water molecules, because X-rays interact only weakly with light atoms. This has been shown recently by different groups [1,2]. A typical X-ray diffraction pattern obtained for cellulose is shown in figure 1.

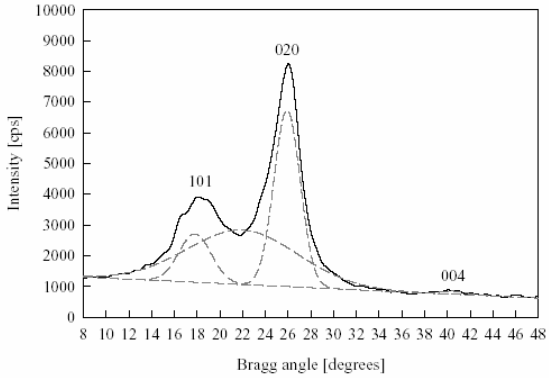

Fig. 1: *X-ray diffraction pattern with separates profiles of cellulose reflections and amorphous "hallo".*

The orientation distribution function (ODF) defines the continuous variation of the orientation and can be yielded from pole figures of the crystal direction measured by X-ray or neutron diffraction.

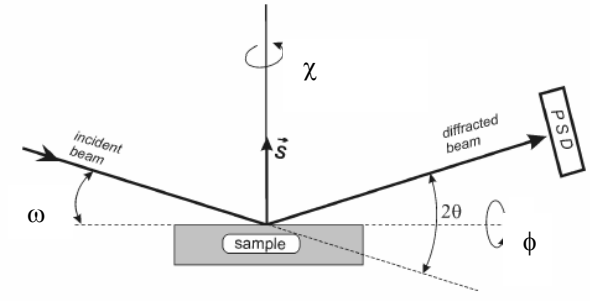

Fig. 2: *Experimental set-up at E5 and definition of sample angles 2θ, ω, χ and ϕ.*

We now performed a study of birch wood with neutron diffraction to see whether it is possible to distinguish Bragg peaks from the background and to yield pole figures by varying the 2θ- (11°- 69°), the ω- (θ ± 5 °), the ϕ- (45° corresponding to reflection and 138° to transmission geometry) and χ-scan (from 85° to 200°) angles by the means of the Eulerian cradle of E5 (see fig. 2).

Unfortunately, we failed in finding the Bragg peaks at the angles calculated for the neutron wavelength in use. Probably, this is due to the diffuse scattering of neutrons by hydrogen and the strong background resulting from this. We did amongst others an ω scan (10 – 28 °) with longer counting times around the supposed Bragg peak position in transmission configuration (χ = 180°, ϕ = 45 °). The figure 3 shows a contour plot at the maximum intensity position, as it was counted on the 2D detector.

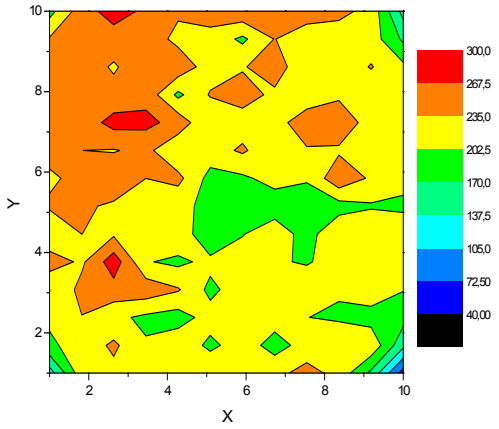

Fig. 3: *Contour plot of 4.5 x 4.5 cm² on the detector.*

Some regularities are evident and could be the subject of further investigations about the space organization of cellulose.

References

[1] J.T. Bonarski and W. Olek: Proc. of the "European Powder Diffraction Conference" (Prag, 2. - 5. Sep. 04), submitted for publication.

[2] J. Keckes, I. Burgert, K. Frühmann, M. Müller, K. Kölln, M. Hamilton, M. Burghammer S.V.Roth, S. Stanzl-Tschegg and P. Fratzl (2003): Nature Materials **2**, 811-814.

	EXPERIMENTAL REPORT **Crystal structure of $CaCu_2O_3$**	Proposal N° PHY-01-1838-EF Instrument **E5** Local Contact Manfred Reehuis
Principal Proposer: Experimental Team:	B. Lake - Oak Ridge National Laboratory, US M. Reehuis - MPI Stuttgart B. Lake - Oak Ridge National Laboratory, US D.A. Tennant - HMI Berlin H.J. Bleif - HMI Berlin	Date(s) of Experiment 04.04.-24.04.05 19.08.-28.08.05 07.09-18.09.05

Date of Report: 02.01.2006

Neutron diffraction experiments were carried out on the four-circle diffractometer E5 using a Cu-monochromator selecting the neutron wavelength λ = 0.8839 Å. Data sets of $CaCu_2O_3$ has been collected at room temperature from single crystals of two different sample charges: crystal 1 with a total of 1806 (456 unique) reflections and crystal 2 with a total of 2106 (438 unique) reflections. The refinement of the crystal structure was carried out with the program Xtal 3.4. The crystal structure of $CaCu_2O_3$ could be successfully refined in the space group *Pmmn*. The refinement of the overall scale factor, the positional and anisotropic thermal parameters resulted in the residuals R_F = 0.038 (R_w = 0.038) for crystal 1, and R_F = 0.051 (R_w = 0.035) for crystal 2, respectively. The results of the refinements presented in Table 1 are compared with those values published by Ruck et al. [1]. Here they found a full occupancy of Cu on the Wyckoff position 4*f* and an excess of Cu of about 13.5(2) % located near the Ca-site. In our study the refinements of the occupancies of both calcium and copper on the position 2*a* resulted in the values *occ*(Ca) = 1.015(21) and *occ*(Cu) = –0.015(21). This clearly suggests the absence of copper on the position 2*a*. It is further interesting to note that the value U_{33} of the Ca(Cu2) atom given by Ruck et al. is much smaller than the value determined in our work. Here it seems likely that strong correlations between the parameters U_{33}, *z* and *occ* of the Ca and Cu2 atoms occur in their structure refinements. On the other hand the values U_{11} and U_{22} show a good agreement, only with the tendency that our values are slightly smaller. In our last refinement we finally set *occ*(Cu2) = 0 and *occ*(Cu1) = 1. In Table 1 it can be seen that the refined occupancies of the O1 in 4*f* and O2 in 2*b* reach values very close to 1.

Both samples have been further investigated at the HMI with a Guinier focussing monochromator diffractometer using a Cu-anode (λ = 1.5406 Å). The Rietveld refinements showed that a powdered sample of crystal 1 contained 11 % of the ternary compound Ca_2CuO_3. A much higher content of 32 % of this material could be found for crystal 2. This crystal contained additionally the binary oxide CuO with a content of 13 %. Here it is interesting to see that despite of the presence of impurities the investigated compound $CaCu_2O_3$ does not form a disordered structure.

Table 1
Results of the single-crystal neutron diffraction study of $CaCu_2O_3$ at 295 K. The values obtained here are compared with x-ray single-crystal data of $CaCu_2O_3$ presented earlier in ref. [1]. The thermal parameters U_{ij} (given in 100 Å^2) are in the form $\exp[-2\pi^2(U_{11}\,h^2a^{*2} + \ldots 2U_{13}\,hla^*c^*)]$. For symmetry reasons all values U_{12} and U_{23} as well as the values U_{13} of the Ca- and O2-atoms are equal to zero in this structure. The shortest interatomic distances (in Á) between the Cu- and O-atoms as well as the Cu-O-Cu bond angle (in °) are also listed.

	$CaCu_2O_3$ crystal 1 †	$CaCu_2O_3$ crystal 2 †	$CaCu_2O_3$ ‡
a [Å]	9.9335(6)	9.9335(6)	9.946(1)
b [Å]	4.0718(2)	4.0718(2)	4.0789(3)
c [Å]	3.4573(3)	3.4573(3)	3.4600(3)
x (Cu1)	0.08252(4)	0.08249(6)	0.08258(1)
z (Cu1)	0.84254(13)	0.84171(16)	0.84150(4)
z (Cu2)	--	--	0.4204(4)
z (Ca)	0.3602(3)	0.3613(4)	0.3497(2)
x (O1)	0.08026(7)	0.08020(9)	0.08036(7)
z (O1)	0.8684(3)	0.8684(3)	0.8673(2)
z (O2)	0.5803(4)	0.5805(5)	0.5799(4)
U_{11} (Cu1)	1.10(2)	1.26(3)	1.323(4)
U_{22} (Cu1)	0.50(3)	0.40(4)	0.578(4)
U_{33} (Cu1)	1.44(2)	1.52(3)	1.632(3)
U_{13} (Cu1)	0.290(14)	0.266(15)	0.388(4)
U_{11}(Cu2/Ca)	1.01(3)	1.12(5)	1.311(8)
U_{22}(Cu2/Ca)	0.51(4)	0.41(6)	0.657(7)
U_{33}(Cu2/Ca)	1.66(5)	1.71(6)	0.99(2)
U_{11}(O1)	1.42(3)	1.60(4)	1.71(3)
U_{22}(O1)	0.64(3)	0.58(6)	0.64(2)
U_{33}(O1)	1.63(3)	1.74(4)	1.82(3)
U_{13}(O1)	0.39(2)	0.40(2)	0.53(2)
U_{11}(O2)	0.77(3)	0.95(4)	0.4(2)
U_{22}(O2)	1.16(4)	1.09(6)	0.7(3)
U_{33}(O2)	2.51(5)	2.52(6)	2.1(3)
occ(Cu1)	1.000	1.000	1.000
occ(Cu2)	0	0	0.135(2)
occ(Ca)	0.992(7)	0.996(13)	0.865(2)
occ(O1)	0.993(5)	1.008(10)	0.9775(3)
occ(O2)	0.987(6)	0.990(10)	0.9776(3)
d(Cu1-O2)	1.8946(8)	1.8932(9)	1.8953(6)
d(Cu1-O11)	1.8998(8)	1.9017(10)	1.9082(7)
d(Cu1-O12)	2.0381(1)	2.0381(1)	2.0415(2)
Cu-O2-Cu	122.82(7)	123.01(9)	122.94(7)

† present results; ‡ results of reference [1]

Reference

[1] K. Ruck, M. Wolf, M. Ruck, D. Eckert, G. Krabbes, K. H. Müller, Mat. Res. Bull. **36** (2001) 1995.

	EXPERIMENTAL REPORT X-ray and neutron diffraction study of $YTiO_3$	Proposal N° PHY-01-1724-LT Instrument **E5** Local Contact Manfred Reehuis
Principal Proposer: Experimental Team:	M. Reehuis, C. Ulrich, B. Keimer - MPI Stuttgart M. Reehuis - MPI Stuttgart H. J. Bleif - HMI Berlin	Date(s) of Experiment 27.05. - 05.06.2005 13.06. - 03.07.2005 15.07. - 29.07.2005

Date of Report: 02.01.2006

The magnetic structure of the Mott-Hubbard insulator $YTiO_3$ is complex, comprising substantial *G*-type and *A*-type antiferromagnetic components in addition to the predominant ferromagnetic component [1]. In the present work we investigated the crystal structure of $YTiO_3$ by x-ray and neutron diffraction, where samples with almost perfect stoichiometry were used.

A powder sample has been investigated with a Guinier diffractometer using a Cu-anode (λ = 1.5406 Å). The powder data have been collected between 10 and 300 K. The lattice parameters of $YTiO_3$ finally could be ob-tained from Rietveld refinements. Fig. 1 shows that the parameters *a* and *c* decrease with the temperature down to 100 K, whereas *b* increases. This is due to the fact that the TiO_6-octahedra are more strongly rotated around the *b*- and *c*-axes than along the *a*-axis at lower temperature. Further it can be seen that the parameter *c* and the cell volume reach a minimum at about 70 K. At the Curie temperature T_C = 27 K we could not see any anomaly. This is in contrast to the isotypic compound $LaTiO_3$, where the lattice parameter *a* showed a strong anomaly at the Néel temperature T_N = 145 K.

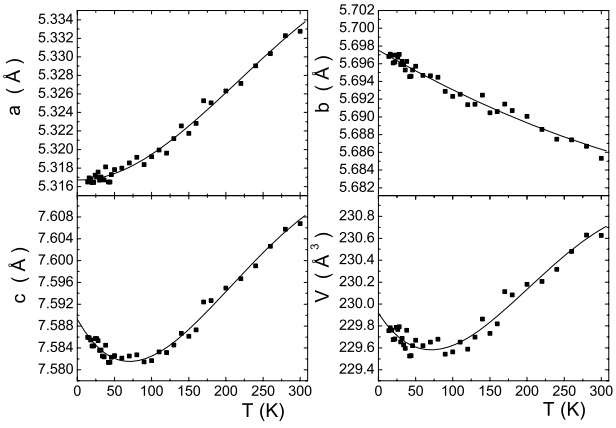

Fig. 1: Temperature dependence of the ortho-rhombic cell parameters of $YTiO_3$.

Single-crystal neutron diffraction data of $YTiO_3$ have been collected at 11 K, 33 K, 80 K and 300 K on the four-circle diffractometer E5. The used neutron wavelength was λ = 0.8839 Å (Cu-monochromator). For each temperature a total of about 1850 (662 unique) reflections was measured. The crystal structure of $YTiO_3$ could be successfully refined in the space group *Pbnm*. The refinement of the overall scale factor, the positional and anisotropic thermal parameters resulted in R_F-values between 0.033 and 0.037 for the different data sets. In Table 1 it can be seen that the Ti-O21-bond is strongly elongated. This can be ascribed to the influence of the Jahn-Teller-Effect. From 300 K down to 80 K the bond distances $d_{Ti\text{-}O11}$ and $d_{Ti\text{-}O22}$ only show a slight decrease and $d_{Ti\text{-}O21}$ a slight increase. From 80 K down to 33 K the bond distances do not shift significantly. But it is interesting to see that below T_C = 27 K the distances $d_{Ti\text{-}O11}$and $d_{Ti\text{-}O22}$ become exactly the same.

Table 1: Interatomic distances (Å) and angles (°) in the TiO_6-octahedron.

	$YTiO_3$ at 11 K	$YTiO_3$ at 33 K	$YTiO_3$ at 80 K	$YTiO_3$ at 300 K
Ti−O11	2.0199(3)	2.0192(3)	2.0188(3)	2.0221(3)
Ti−O21	2.0814(5)	2.0805(5)	2.0807(5)	2.0790(4)
Ti−O22	2.0199(5)	2.0206(5)	2.0206(5)	2.0244(5)
O11−O21	2.8097(6)	2.8097(6)	2.8105(6)	2.8176(6)
O11−O22	2.8453(8)	2.8455(8)	2.8450(8)	2.8470(8)
O11−O23	2.9883(8)	2.9862(7)	2.9851(8)	2.9806(7)
O11−O24	2.8678(6)	2.8677(6)	2.8674(7)	2.8756(6)
O21−O22	2.8821(7)	2.8824(7)	2.8835(7)	2.8901(7)
O21−O24	2.9185(7)	2.9181(6)	2.9170(6)	2.9134(6)
O11−Ti−O21	86.47(2)	86.51(2)	86.55(2)	86.78(2)
O11−Ti−O24	90.45(2)	90.44(2)	90.45(3)	90.57(2)
O21−Ti−O22	89.28(2)	89.29(2)	89.34(2)	89.54(2)
O22−O21−O24	88.28(2)	88.33(2)	88.32(2)	88.47(2)
O11−O21−O12	88.28(2)	88.28(2)	88.27(2)	88.41(2)
O11−O24−O12	90.00(2)	89.96(2)	89.95(2)	89.94(2)
O21−O22−O25	134.55(2)	134.54(2)	134.52(2)	134.61(2)
O13−O22−O26	154.83(2)	154.84(2)	154.85(2)	154.70(2)
O23−O22−O25	115.58(2)	115.53(2)	115.52(2)	115.51(2)
O12−O11−O12	139.73(2)	139.71(2)	139.75(3)	140.25(2)

References

[1] C. Ulrich, G. Khaliullin, S. Okamoto, M. Reehuis, A. Ivanov, H. He, Y. Taguchi, Y. Tokura, B. Keimer: Phys. Rev. Letters **89** (2002) 167202.

[2] M. Cwik, T. Lorenz, J. Baier, R. Müller, G. André, F. Bourée, F. Lichtenberg, A. Freimuth, E. Müller-Hartmann, M. Braden: Phys. Rev. B **68**, 060401 (2003).

BENSC	**EXPERIMENTAL REPORT** **High temperature crystal structure and phase transition of $CuCr_2O_4$**	Proposal N° EF Instrument **E9** Local Contact Michael Tovar
Principal Proposer: Experimental Team:	M. Tovar - HMI Berlin	Date(s) of Experiment 07.09. - 08.09.2005 23.09. - 25.09.2005

Date of Report: 15.4.2006

Oxide systems are well suitable systems for systematic studies of macroscopic and microscopic structure distortions due to the Jahn-Teller effect. The Jahn-Teller effect means an ion being in an energetic degenerated ground state (which holds for several transition metal ions) reduces its local symmetry to overcome the degeneration. The direction of the distortion can partially be predicted using orbital schematic considerations [1]. For example the introduction of Cu^{2+} ion (d^9-system) in a tetrahedral (oxygen) environment leads to a flattening of the tetrahedron, while the tetrahedron is elongated in case of Ni^{2+} (d^8-system) (fig. 1).

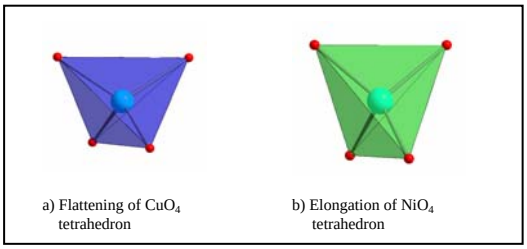

Fig. 1: Jahn-Teller effect on CuO_4 and NiO_4 tetrahedron

The investigated compound $CuCr_2O_4$ crystallizes at room temperature in a tetragonal distorted spinel structure, s.g. $I4_1/amd$, with axes ratio c/a<1 [2,3]. The distortion is caused by the Jahn-Teller ions Cu^{2+} which flatten the surrounding oxygen tetrahedra. On heating a phase transition to the cubic spinel structure occurs at about 850 K [3]. High temperature neutron powder diffraction measurements were carried out to investigate the phase transition and to determine the high temperature crystal structure.

Results: Temperature depending measurements between 820 K and 920 K revealed the phase transition tetragonal → cubic to start - according to literature – between 830 and 840 K and finish at 850 K. The phase transition is indicated by the merging of the tetragonally splitted reflections, visible when plotting special regions of the diffractograms as function of temperature (fig.2).

The high temperature crystal structure of $CuCr_2O_4$ could be refined in the ideal spinel space group *Fd3m*, structural data are listed in table 1.

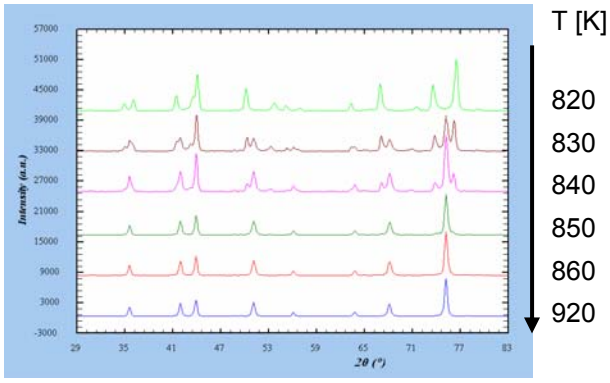

Fig. 2: High temperature neutron powder diffractograms of $CuCr_2O_4$ as function of temperature

Tab. 1: Structure data of $CuCr_2O_4$ in cubic phase, s.g. *Fd3m*

Atom	X	Y	Z	B [Å^2]
Cu	0.125	0.125	0.125	1.77 (6)
Cr	0.5	0.5	0.5	1.09 (5)
O	0.2612(3)	0.2612(3)	0.2612(3)	1.32 (5)

The resulting quality criteria are R_{Bragg}=4,66%, GoF=1.84. The Rietveld difference plot still shows some significant residuals (fig. 3). However, a further improvement of the refinement was not possible hence is aim of ongoing research.

Fig. 3: Rietveldplot of $CuCr_2O_4$ measured at 920 K

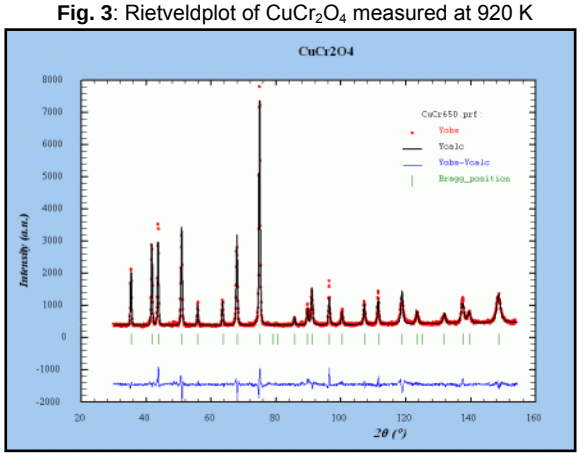

Refernces:

[1] Dunitz, J.D., Orgel, E.: Electronic properties of transition-metal oxides I., J. Phys. Chem. Solids 3 (1957), 20-29.

[2] Dollase, W.A., O´Neill, H.St.C.: The spinels $CuCr_2O_4$ and $CuRh_2O_4$. - Acta Cryst. C53 (1997), 657-659.

[3] Tovar, M. et al., Physica B 2006, accepted.

BENSC	**EXPERIMENTAL REPORT** **New nitrogen and hydrogen metal compounds**	Proposal N° CHE-01-1653 Instrument **E9** Local Contact Michael Tovar
Principal Proposer: Experimental Team:	G. Auffermann - MPI CPfS Dresden P. Höhn, A. Mehta - MPI CPfS Dresden G. Auffermann, R. Kniep - MPI CPfS Dresden M. Tovar - HMI Berlin	Date(s) of Experiment 08.04.-13.04.2005

Date of Report: 15.12.2005

The chemistry of ternary nitridometalates is a rapidly growing field in solid state chemistry [1]. This report is focused on ternary alkaline-earth nitridonickelates, which are characterized by low oxidation states of Ni.

$Ba_2[Ni_3N_2]$, the first mixed low-valency nitride-nickelate with a two-dimensional metal-nitrogen anionic network, was synthesized by the reaction of Ba_2N and Ni in nitrogen at 1173 K. Single crystal data refinements result in an displacement anomaly (cigar-shaped) for one nickel position, which was abolished using a split position [2]. To confirm the results of the X-ray diffraction investigations as well as to check whether the structure undergoes a phase transition to an ordered Ni arrangement at low temperature, neutron powder diffraction experiments were carried out at ambient temperature and 4 K. Supplementary to magnetic susceptibility measurements, neutron diffraction experiments should clarify if a 3-dimensionally long range antiferromagnetic ordering is visible.

Neutron diffraction experiments at room temperature confirmed the results determined by X-ray single crystal analysis in which one Ni is described with a split. The results at low temperature showed no indications for a phase transition to an ordered arrangement in a lower symmetry space group. Additionally, there is no evidence of magnetic ordering in the compound.

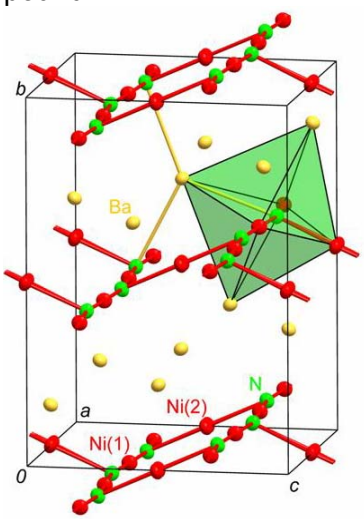

Fig. 1: Section of the crystal structure of $Ba_2[Ni_3N_2]$. Unit cell and coordination spheres of Ba, Ni and N are emphasized.

Table 1: Structural parameters of $Ba_2[Ni_3N_2]$ from neutron diffraction experiments using E9 (*Cmca*, 207 reflections).

		4 K	297 K
Lattice (Å)	*a*	7.1561(1)	7.1538(2)
	b	10.2692(2)	10.3111(2)
	c	7. 3816(1)	7.3903(2)
Ba in (8*f*)	*y*	0.1694(5)	0.1699(6)
	z	0.0903(5)	0.0916(6)
	B_{iso} (Å^2)	-0.2(2)	0.8(1)
Ni in (8e)	*Y*	0.4252(3)	0.4250(3)
	B_{iso} (Å^2)	0.46(5)	0.61(6)
Ni in (8*d*)*	*x*	0.5258(9)	0.520(2)
	B_{iso} (Å^2)	0.46(8)	1.1(1)
N in (8*f*)	*y*	0.4263(3)	0.4254(4)
	z	0.2313(4)	0.2293(4)
	B_{iso} (Å^2)	0.52(5)	0.81(6)
R_{Profil}/R_{Bragg}		0.050/0.059	0.049/0.079

* *pp* = 0.5

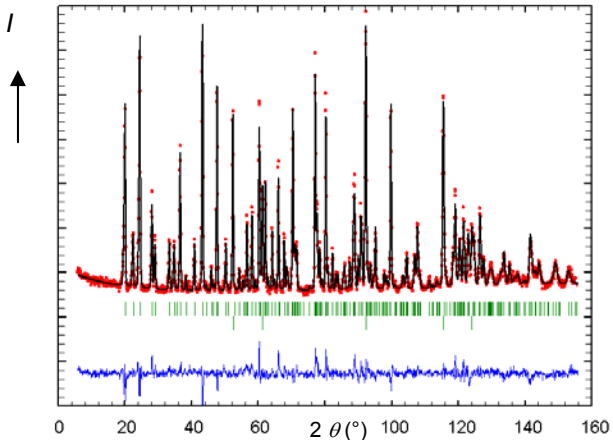

Fig. 2: Neutron powder diffraction pattern of $Ba_2[Ni_3N_2]$ at 297 K, exemplarily (observed (red), calculated (black) and difference (blue) profiles, green ticks mark the Bragg positions of the crystal structure of $Ba_2[Ni_3N_2]$ (upper row) and small impurities of nickel (lower row)).

References:

[1] R. Kniep, Pure Appl. Chem. 69 (1997) 185.

[2] A. Mehta, P. Höhn, W. Schnelle, V. Petzold, H. Rosner, U. Burkhardt, R. Kniep, Chem. Eur. J., in press.

	EXPERIMENTAL REPORT **Investigation of the crystal structure of deuterated Hydrocerussite**	Proposal N° CHE-01-1663 Instrument **E9** Local Contact Dimitri Argyriou
Principal Proposer: Experimental Team:	C. Christides - Univ. Patras, GR V. Psycharis - NCSR Demokritos, Athens, GR	Date(s) of Experiment 30.05. - 01.06.2005

Date of Report: Jan. 2006

Samples of single phase deuterated hydrocerussite are studied at three different temperatures (18K, 80K and 300K). One measurement at 300K was performed for the non-deuterated sample for comparative studies. Although hydrocerussite is frequently met in everyday life activities as a wathering by-product of lead containing materials (lead-acid battaries, potable water or bulding painting applications) its structure was unknown until recently [1]. According to this model, the hydrocerussite phase crystallizes in space group R-3m and the hexagonal unit cell has the lattice parameters a = 5.23 A and c =23.82 A. The hydrocerussite structure is formed by two types of layers that are normal to the hexagonal c-axis, one with $PbCO_3$ and the other with $Pb(OH)_2$ chemical synthesis. These type of layers are ordered along c-axis. Two successive $PbCO_3$ layers form the characteristic bilayer of the cerussite structure and the hydroxide layer is interleaved between two successive $PbCO_3$ bilayers. The main characteristic of the structure is that the layers with $Pb(OH)_2$ formula exhibit extensive positional disorder, i.e. the Pb and O atoms occupy statistically different sites.

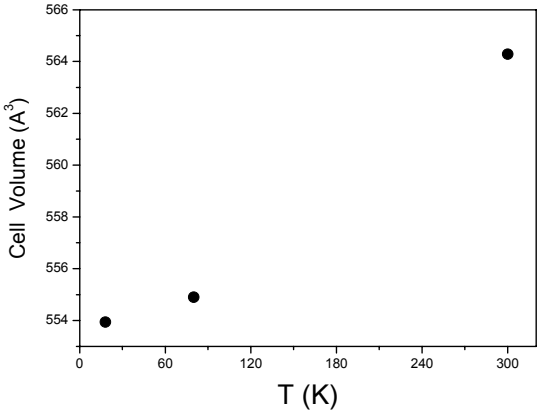

Fig.1

The increase of the unit cell volume for the deuterated sample is 1.9 % between 18 and 300K, whereas the *c*-axis expands by 1% relative to *a*-axis (0.44%).

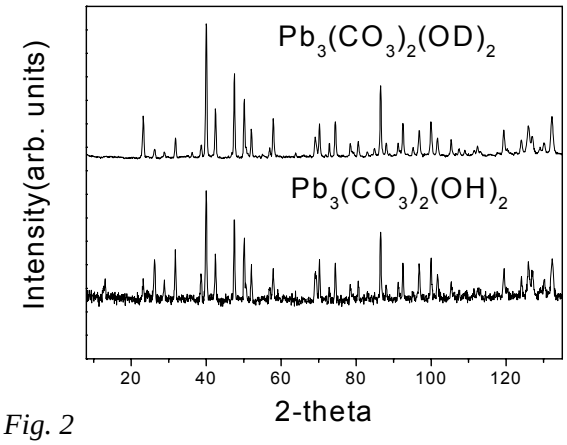

Fig. 2

The observed spectra of $[Pb_3(CO_3)_2(OD)_2]$ and $[Pb_3(CO_3)_2(OH)_2]$ at 300K (Fig.-2) exhibit marked differences in Bragg-peak intensities that arise from lattice planes occupied by $-(0H)_2$ and $-(OD)_2$.
Rietveld analysis of the diffraction spectra and traditional Fourier-map calculations were not adequate to resolve the disorder within the $Pb(OD)_2$ planes. Alternatively, the maximum-entropy method (MEM), based on the RIETAN-2000 and the PRIMA (VENUS programs), is employed to further elucidate the problem of disorder. Fig.3 shows the most successful Rietveld refinement (FULLPROF program) for the deuterated sample at 18 K.

Fig. 3

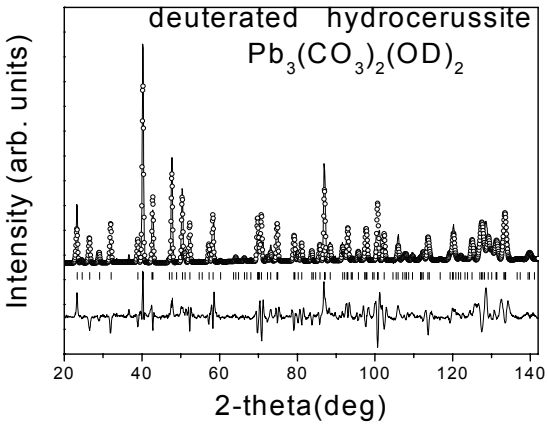

1) *P. Martinetto, et al. Acta Cryst. C58, (2002) i82*

BENSC	**EXPERIMENTAL REPORT** **Structural and magnetic studies of spinel oxides** **Part 3: Lithium ions distribution in the $Li_xMn_{3-x-y}Fe_yO_4$ system**	Proposal N° CHE-01-1664 Instrument **E9** Local Contact Michael Tovar
Principal Proposer: Experimental Team:	E. Wolska - AMU Poznań, Poland J. Darul, W. Nowicki - AMU Poznań, Poland M. Tovar - HMI Berlin	Date(s) of Experiment 24.05. - 31.05.2005

Date of Report: 07.07.2005

The cubic spinel phase system $LiMn_2O_4$-$Li_{0.5}Fe_{2.5}O_4$ forms a continuous series of solid solutions. Our previous investigations of lithium-iron-manganese oxides evidenced changes in the distribution of Li^+ ions over the spinel cationic sublattices, caused by Fe^{3+} substitution into the $LiMn_2O_4$ structure.

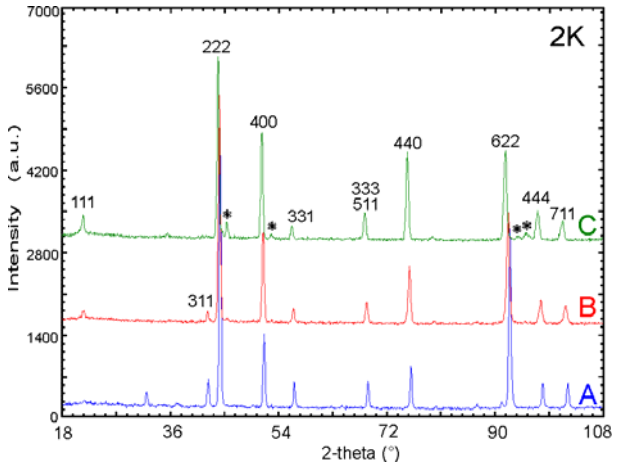

Fig.1. Neutron powder diffraction patterns recorded at the temperature of 2K, for samples: $Li_{0.95}Fe_{0.205}Mn_{1.845}O_4$ (A), $Li_{0.9}Fe_{0.42}Mn_{1.68}O_4$ (B), and $Li_{0.85}Fe_{0.645}Mn_{1.505}O_4$ (C); (- Li_2MnO_3).*

The preference of Li^+ to occupy the octahedral sites increases with the increasing Fe^{3+} content, resulting in the inverse spinel phase of $Li_{0.5}Fe_{2.5}O_4$ [1, 2]. The location of cations using X-ray diffraction was difficult because of low electron density of Li and of similarity of the Fe and Mn form factors. In the present neutron diffraction experiments it was possible to ascertain differences in the peak intensities indicating changes in cation distribution.

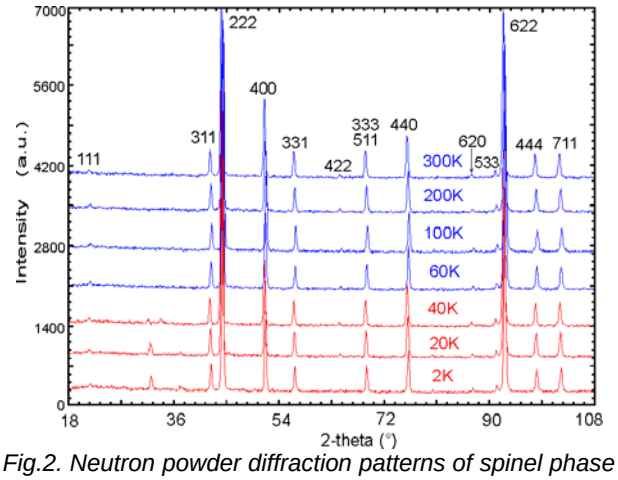

Fig.2. Neutron powder diffraction patterns of spinel phase $Li_{0.95}Fe_{0.205}Mn_{1.845}O_4$, in the temperature range 2K-300K.

Patterns in Fig.1 have been recorded for samples with the *Fe:(Fe+Mn)* molar ratio of 0.1 (A), 0.2 (B) and 0.3 (C). Variations of the intensity of (111), (311) and (440) reflections evidence the occupancy of tetrahedral sites with Fe^{3+} and octahedral with Li^+. More detailed quantitative evaluation would be possible after measurements of full $Li_xMn_{3-x-y}Fe_yO_4$ series. Moreover, presence of traces of Li_2MnO_3, undetectable with X-ray, was shown in sample C.
On the neutron diffraction pattern of sample A, at the temperature of 2K, a new reflections in the low angular range can be visible, pointing to a different magnetic ordering [3]. The set of patterns in Fig.2 reveals the temperature dependence of this peak: it disappears at 60K. Explanation of such effect requires further neutron powder diffraction experiments.

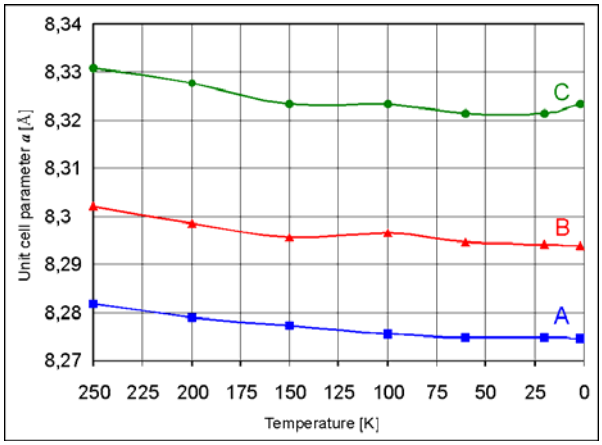

Fig.3. Unit-cell parameter, "a", of the spinel series $Li_xMn_{3-x-y}Fe_yO_4$, plotted as a function of temperature (A, B, C - notation as in Fig.1.)

The precise determination of lattice constants of the cubic unit cell of the $LiMn_2O_4$/$Li_{0.5}Fe_{2.5}O_4$ solid solution series reveals that the replacement of Mn^{3+} with Fe^{3+}, having equal ionic radii, causes the increase of the spinel unit-cell volume. Changes of the lattice parameters with the temperature are presented in Fig.3.

References:

[1] E. Wolska, K. Stempin, O. Krasnowska-Hobbs: Solid State Ionics 101-103 (1997) 527.
[2] S.M. Woodley, C.R.A. Catlow, P. Piszora, K. Stempin, E. Wolska: J. Solid State Chem. 153 (2000) 310.
[3] E. Wolska, M. Tovar, B. Andrzejewski, W. Nowicki, J. Darul, P. Piszora: Solid State Sciences (in press).

	EXPERIMENTAL REPORT New nitrogen and hydrogen metal compounds	Proposal N° CHE-01-1757 Instrument **E9** Local Contact Dimitri Argyriou
Principal Proposer: Experimental Team:	G, Auffermann - MPI CPfS Dresden P. Höhn, R. Niewa - MPI CPfS Dresden G. Auffermann, R. Kniep - MPI CPfS Dresden D. Argyriou - HMI Berlin	Date(s) of Experiment 27.10.- 31.10.2005

Date of Report: 20.12.2005

In the ternary system EA-In-N (EA = alkaline earth metal) numerous compounds were characterized in the past 20 years.
Recently, single phase products of the compounds $Ca_7N_4[In_x]$ and $(Ca_{19}N_7)[In_4]_2$ were successfully prepared [1, 2]. The complete structure determinations succeeded by using a combination of X-ray and neutron powder diffraction experiments. The neutron powder diffraction patterns were taken with E9. The refinements of the Ca and N sites showed no indication for a significant occupation below unity for both compounds, whereas the occupancy for the In positions in the channels in the crystal structure of $Ca_7N_4[In_x]$ led to $x = 1.04$. The In arrangements contain either infinite chains (s. Fig. 1) or isolated tetrahedra (s. Fig. 2).

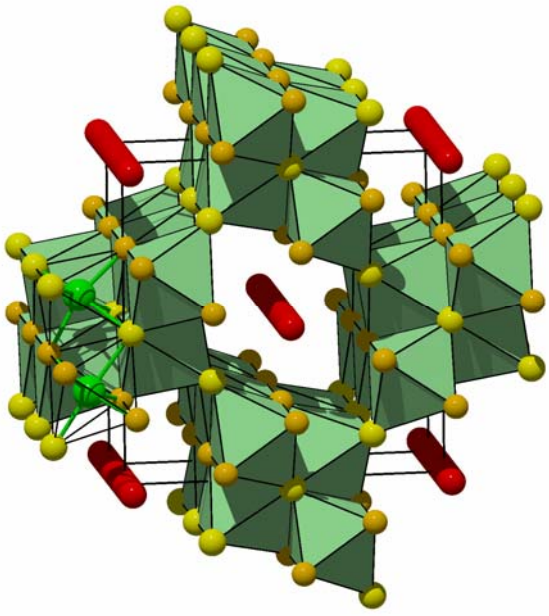

Fig. 1: Crystal structure of $Ca_7N_4[In_x]$ ($x = 1.04$): The Ca/N partial structure is formed by compact one-dimensional blocks of edge and corner sharing Ca_6N octahedra (green) which are connected via common apices to a three dimensional structure. The large channels within the Ca/N structure are occupied by infinite In chains (red) [1].

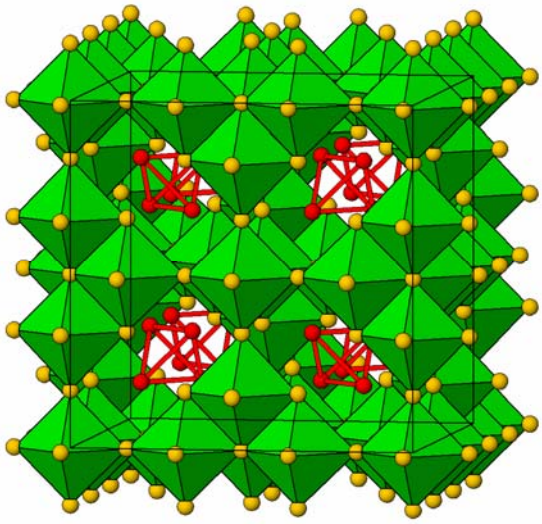

Fig. 2: Crystal structure of $(Ca_{19}N_7)[In_4]_2$: Isolated tetrahedra $[In_4]$ (red) embedded in a framework of edge- and corner-sharing (Ca_6N) octahedra (green) [2].

Yet another neutron diffraction experiment was carried out on the compound $(Ba_3N_x)Sn$ at the E9 powder diffractometer. The joint Rietveld refinement of this neutron powder diffraction pattern and the corresponding X-ray powder diffraction pattern result in a nitrogen site occupancy of $x = 0.64(1)$, which is consistent with the composition derived by chemical analysis. The phase crystallizes in a cubic anti-perovskite type arrangement [3].

References:

[1] P. Höhn, R. Ramlau, H. Rosner, W. Schnelle, R. Kniep:
a) Z. Anorg. Allg. Chem. **630** (2004) 1704;
b) Scientific Report, MPI-CPfS, Dresden 2006, in preparation.

[2] M. Kirchner, W. Schnelle, F.R. Wagner, R. Kniep, R. Niewa:
Z. Anorg. Allg. Chem. **631** (2005) 1477.

[3] F. Gäbler, M. Kirchner, W. Schnelle, M. Schmitt, H. Rosner, R. Niewa:
Z. Anorg. Allg. Chem. **631** (2005) 397.

	EXPERIMENTAL REPORT **Determination of structural stabilising O-H species in cubic $Ba_2Mg_3F_{10}$**	Proposal N° CHE-01-1765 Instrument **E9** Local Contact Michael Tovar
Principal Proposer: Experimental Team:	F. Werner - Technische Universität Wien F. Werner - Technische Universität Wien M. Tovar - HMI Berlin	Date(s) of Experiment 25.10. - 27.10.2005

Date of Report: 30.12.2005

The newly found cubic Ba-Mg-fluoride phase with the idealised formula Ba2Mg3F10 shows a small discrete mass loss in a temperature range typic for the release of water from inorganic fluorides. To detect whether the hydrogens are present as fluoride substituting OH--ions and/or incorporated water molecules, samples were obtained as colourless powders by dissolving Ba-acetate and Mg-nitrate in D2O and precipitating the title compound with various fluorides (NaF, KF and NH4F). These reactions are sensitive to concentration effects, i.e. at higher molarities phase mixtures of cubic Ba2Mg3F10 and BaMgF4 [1] are obtained. Thus diluted solutions of the educts were used. As it was necessary to purify the precipitates to remove the water soluble by-products, the reaction mixtures were centrifuged and washed with H2O. Since all the heavy water that was at disposal went into the synthesis to prepare diluted solutions, it was not possible unfortunately to use this solvent for the washing procedure. Keeping this in mind one had to be aware of a possible deuteriumhydrogen exchange.

The high background, typical for hydrogen containing phases, in the neutron powder diffraction pattern confirmed the latter (Fig. 1).

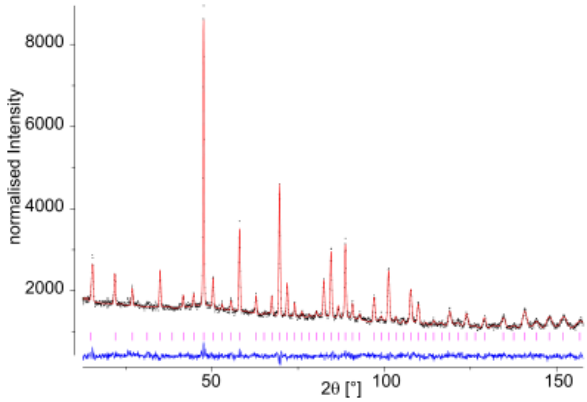

Fig. 1: Structure refinement [2] of the neutron powder pattern (λ=1.79740Å) of cubic $Ba_2Mg_3F_{10}$ (observed (black), calculated (red), vertical bars (reflection positions), difference (blue))

From the qualitative appearance of Fig. 1 it was clear that some OH-species were incorporated into the structure. When the atomic parameters, previously obtained by single crystal X-ray diffraction, were applied to the Rietveld refinement the calculated pattern was in close match to the observed one. After refining the positional parameters a satisfactory result was obtained (Fig. 1). Due to the bad parameter/reflection ratio release of the thermal parameters resulted in divergence and thus were taken from the single crystal measurement. Then it was tried to locate hydrogen of fluoride replacing OH--ions and/or O/H from incorporated water molecules from a difference Fourier map. But neither positive (O) nor negative (H) peaks were found. Although hydrogen is harder to detect than deuterium, in case of an ordered arrangement it is possible to locate H, even when it is present at a low mole fraction.[3]

From this information one can draw the conclusion that no H2O-molecules are present in the tittle phase and the OH--groups are disordered on all four crystallographic positions of fluoride, substituting it to a certain extent.
The study will be completed by vibrational spectroscopy and thermal analysis of the samples measured at the BENSC.

Acknowledgement

This research project has been supported by the European Commission under the 6th Framework Programme through the Key Action: Strengthening the European Research Infrastructures. Contract n°: RII-CT-2003-505925 (NMI 3).

References

[1] F. Gingl, Z. Anorg. Allg. Chem. **623** (1997), pp. 705 - 709
[2] GSAS. A.C. Larson, R.B. Von Dreele: Los Alamos National Laboratory Report LAUR 86 - 748, 2000
[3] M. Bostrom, M. Gemmi, W. Schnelle, L. Eriksson, J. Solid State Chem. **177** (2004), pp. 1738-1745

BENSC	**EXPERIMENTAL REPORT** **Structural and magnetic studies of spinel oxides** **Part 4: Ferrimagnetic spinel phase in the $Li_xMn_{3-x-y}Fe_yO_4$ system**	Proposal N° CHE-01-1773 Instrument **E9** Local Contact Michael Tovar
Principal Proposer: Experimental Team:	E. Wolska - AMU Poznań, Poland W. Nowicki, J. Darul, E. Wolska - AMU Poznań, Poland O. Prokhnenko, M. Tovar - HMI Berlin	Date(s) of Experiment 02.12.- 07.12.2005

Date of Report: 31.12.2005

Determination of the magnetic structure of $Li_xMn_{3-x-y}Fe_yO4$ spinel solid solutions appears to be essential, because the samples reveal different magnetic properties, from spin-glass behaviour of $LiMn_2O_4$ at low temperature [1], through the antiferromagnetic ordering found for $0<n_{Fe}<0.3$, where n_{Fe}= Fe/(Fe+Mn) [2, 3], to the distinct ferrimagnetic exchange occurring between the A and B sublattices in AB_2O_4, with increasing Fe^{3+} ions content [4].
We report new results obtained for the single phase spinel solid solution, with Fe/(Fe+Mn) =0.4, of a composition $Li_{0.63}Mn_{1.422}Fe_{0.948}O_4$. The experiment was performed at HMI, on the high-resolution neutron powder diffractometer E9 (FIREPOD), using Ge monochromator, plane (511). The incident neutron wavelength was 1.79740Å, and the standard orange cryostat has been used to measurements in the temperature range from 2K to 500K. About 3g of sample were encapsulated into vanadium container.

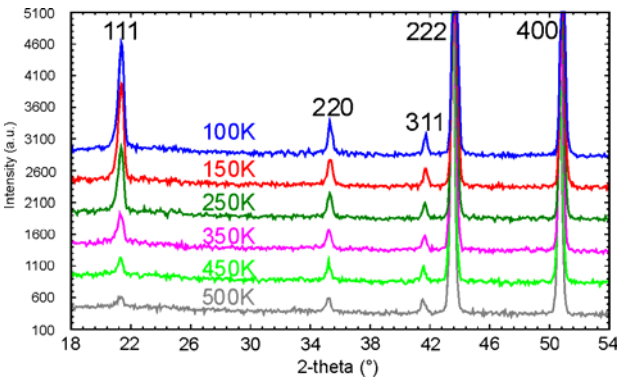

Fig. 1. Neutron powder diffraction patterns of the $Li_{0.63}Mn_{1.422}Fe_{0.948}O_4$ spinel solid solution, recorded in the temperature range of 100K – 500K.

Fig.1. shows the sections of diffraction patterns indicating the presence of Fe^{3+} ions in the tetrahedral 8a spinel sites (increasing intensity of 220 reflection) [5], and the A-B ferrimagnetic order below room temperature (high intensity of the predominantly magnetic reflection 111). Thermal evolution of this peak enables to fix the Curie temperature at about 450K, and separate the nuclear and magnetic scattering effect. It has to be stressed that the calculation of cation distribution over the tetrahedral and octahedral sublattices, and the spinel structure refinement, could be performed on the basis of neutron powder diffraction patterns recorded at the temperature above Curie point.

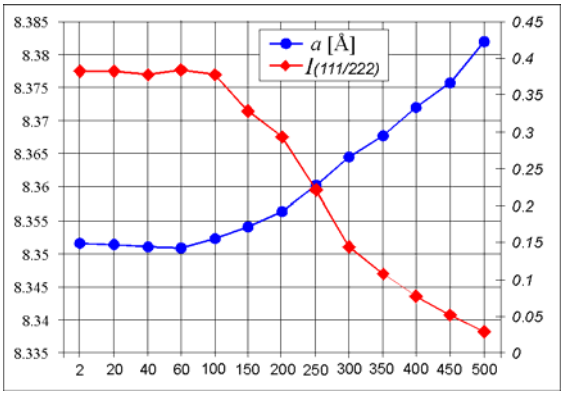

Fig. 2. Unit cell constant, a, and integrated intensity ratio, $I_{(111/222)}$, of the $Li_{0.63}Mn_{1.422}Fe_{0.948}O_4$, plotted as a function of temperature.

The gradual decrease of intensity of the (111) reflection, presented as the (111)/(311) ratio, illustrates Fig.2, comprising additionally the temperature plot of the unit cell constants. The relatively high values of lattice parameter indicate indirectly the transformation from the normal spinel to inversed spinel structure.
The relationship between structural phase transitions, magnetic ordering and charge ordering, caused by the Fe for Mn substitution in the $Li_xMn_{3-x-y}Fe_yO_4$ system, would be the main question to undertake in further studies.

References:

[1] J.E. Greedan, C.R. Wiebe, A.S. Wills, J.R. Stuart, Phys. Rev.B65 (2002) 184424.
[2] E. Wolska, M. Tovar, B. Andrzejewski, W. Nowicki, J. Darul, P. Piszora, Solid State Sciences 8 (2006) 31.
[3] Experimental Report: CHE-01-1664 (2005/I)
[4] E. Wolska, K. Stempin, O. Krasnowska-Hobbs, Solid State Ionics 101-103 (1997) 527.
[5] S.M. Woodley, C.R.A. Catlow, P. Piszora, K. Stempin, E. Wolska, J. Solid State Chem. 153 (2000) 310.

	EXPERIMENTAL REPORT **Structural study of $(LaSr)_{n+1}Fe_nO_{3n+1}$ and $La_2Ni_{1-x}Cu_xO_4$ solid solutions**	Proposal N° MAT-01-1767 Instrument **E9** Local Contact Oleksandr Prokhnenko
Principal Proposer: Experimental Team:	S. Neov - Inst.Nucl.Res.& Energy, Sofia-1784 O. Prokhnenko - HMI Berlin N. Velinov - UCTM, Sofia-1756 V. Kozhukharov - UCTM, Sofia-1756	Date(s) of Experiment 25.11 - 29.11.2005

Date of Report: Jan. 2006

The Ruddlesden-Popper (R-P) phases have general formula $A_{n+1}B_nO_{3n+1}$, where A is alkali metal, alkaline earth or lanthanide, B is octahedrally coordinated cation, *n* determines the thickness of perovskite slab and gives the number of BO_6 octahedra corner sharing the *c* axis. The layered R-P perovskites are suitable for application in electro-chemical devices due to their mixed ionic-electronic conductivity easily modified by substitution of A- or/and B-cations. The absolute value of conductivity and its temperature dependence **σ(T)** are the most important characteristics of R-P perovskites as cathode material in solid oxide fuel cells, operating at elevated temperatures. The knowledge of structure parameters is the key for understanding the observed **σ(T)** behaviour and improvement of material's parameters. The goal of neutron diffraction experiments was to study the structure of R-P perovskites at temperature below and above the regions of **σ(T)** anomalies. Synthesis of samples, Table 1, was carried out by nitrate-citrate method using high purity starting materials: Ni_2O_3, La_2O_3, Cu_2O and $Fe(NO_3)_3.9H_2O$. All samples were tested by X-ray diffraction, scanning electron microscopy and ESR.

Table 1.
Sample composition and unit cell parameters at room temperature.

Composition	**S.G.**	***a* (Å)**	***b* (Å)**	***c* (Å)**
La_2NiO_4	*I4/mmm*	3.860	3.860	12.67
$La_2Ni_{0.6}Cu_{0.4}O_4$	*I4/mmm*	3.849		12.90
$La_2Ni_{0.2}Cu_{0.8}O_4$	*Abma/*	5.404	5.388	13.05
ND	*Pbcm*	5.398	5.389	13.06
La_2CuO_4	*Abma*	5.397	5.356	13.13
ND	*Pbcm*	5.403	5.354	13.14
$LaSrFeO_4$	*I4/mmm*	3.869	3.869	12.72
$LaSr_3Fe_3O_{10}$	*I4/mmm*	3.870	3.870	28.06

To detect small changes of atomic arrangement and oxygen content of RP-oxides, neutron diffraction (ND) experiments were carried out: the sensitivity of ND to the location of oxygen nuclei is about 33 times greather in relation to X-rays. Neutron scattering experiments were realized on E9 diffractometer. Six samples, Table 1, were measured in the temperature interval 25-650^{0}C, Fig.1.

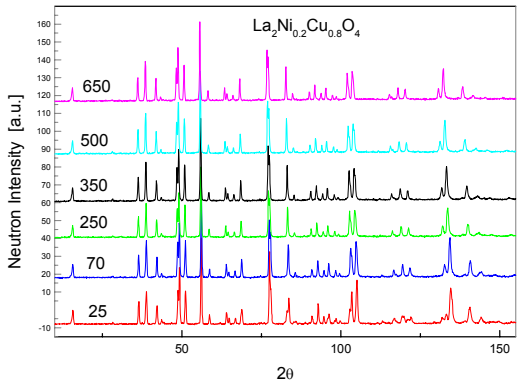

Fig. 1. ND spectra of $La_2Ni_{0.2}Cu_{0.8}O_4$, T=25-650^{0}C.

The crystal structure was refined by Rietveld analysis of ND data using FullProf program, [J.Rodriguez-Carvajal, FullProf Version 3.5d Oct.1998, LLB (CEA-CNRS)]. Preliminary results indicate that in the studied temperature interval the Ni substitution for Cu stimulates the transition from orthorhombic (*Pbcm*) to tetragonal (*I4/mmm*) symmetry. While *a* and *b*-axes change linearly, tetragonal *c*-axis shows non-linear trend with temperature increase, Fig.2, which correlates within some limits with **σ(T)**.

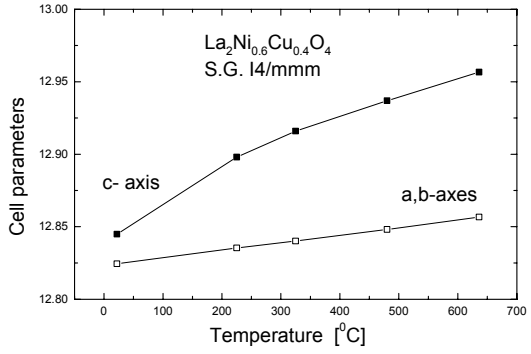

Fig. 2. Temperature dependence of cell constants of $La_2Ni_{0.6}Cu_{0.4}O_4$.

	EXPERIMENTAL REPORT **Structural phase transitions in $CaTaOAlO_4$**	Proposal N° OTH-01-1655 Instrument **E9** Local Contact Michael Tovar
Principal Proposer: Experimental Team:	T. Malcherek - Mineralogisch-Petrogr. Institut, Universität Hamburg T. Malcherek - Uni Hamburg M. Tovar - HMI Berlin	Date(s) of Experiment 30.06. - 02.07.2005

Date of Report: 31.01.2006

The structure of $CaTaOAlO_4$ (CTAO) is known to be of the titanite aristotype only at elevated temperatures [1,2]. Below T = 320K at least one structural phase transition occurs, giving rise to a structure with distorted AlO_4-tetrahedra, as evidenced by ^{27}Al-NMR spectroscopy [2]. Crystal structure determination of the low temperature phases by X-ray diffraction methods is encumbered by the lack of available single crystals and by the domination of the X-ray scattering power by the Ta-atoms. Using X-ray powder diffraction it has therefore only been possible to determine the occurence of spontaneous strain and of a split Ca-position, while the C2/c space group symmetry of the aristotype structure appears to remain intact in the distorted phase(s). However, a possible candidate for the ground state structure has been predicted by first principle computational methods to exhibit space group symmetry $P2_1/n$ [2]. As the small displacements giving rise to this distorted structure would mainly involve the O-atoms, a neutron diffraction study provides the appropriate means to verify the low temperature structure of CTAO.

Neutron powder diffraction data of CTAO have been collected at 5 temperatures between 80K and 350K, using a wavelength of 1.79743 Å. Preliminary analysis of the data collected for T=80K shows that the neutron diffraction data exhibit no significant deviation from SG symmetry C2/c at the available resolution. Using the thermal parameters estimated by Rietveld refinement in this higher symmetry setting, it is possible to compare the predicted $P2_1/n$-structure to the data measured at T=80K (Fig. 1), using the structural parameters given in Ref. [2]. The refined lattice parameters at this temperature are a=6.6113(3) Å, b=8.9510(4) Å, c=7.3517(4) Å and β=113.666(4)°.

Judging by the fact that even the strongest predicted diffraction maxima unique to $P2_1/n$ symmetry, e.g. 1 0 -1 or 1 2 –4, do not appear to have intensity values significantly above background level, the $P2_1/n$ structure model cannot be confirmed at this temperature. This might indicate that either the ground state structure is only attained at T < 80K or that the actual atomic displacements are smaller than predicted. However, at the given intensity level, Rietveld refinement in SG $P2_1/n$ does not converge to a satisfactory solution.

Fig. 1: Neutron diffraction data at T=80K: The calculated profile (red) corresponds to the $P2_1/n$-structure with atomic positions given in Ref. [2].

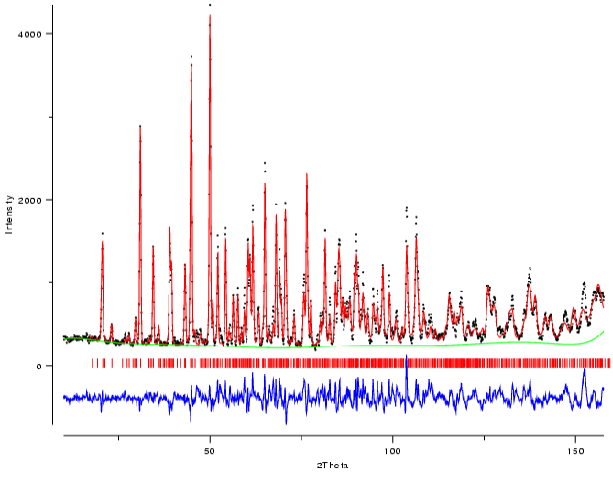

References

[1] M. Sales, G. Eguia, P. Quintana, L.M. Torres-Martinez and A.R. West: J. Solid State Chem. **143** (1999) 62.
[2] T. Malcherek, M. Borowski, A. Bosenick: J. Appl. Cryst. **37** (2004) 117.

BENSC	**EXPERIMENTAL REPORT** **Investigation of lattice deformation in segregations in $(2ZnSe)_x(CuInSe_2)_{1-x}$**	Proposal N° PHY-01-1657 Instrument **E9** Local Contact Michael Tovar
Principal Proposer: Experimental Team:	S. Schorr - University Leipzig S. Schorr - University Leipzig M. Tovar - HMI Berlin	Date(s) of Experiment 02.06. - 05.06.2005

Date of Report: 10.01.2006

The solid solution series $(2ZnSe)_x(CuInSe_2)_{1-x}$ and $(2ZnTe)_x(CuInTe_2)_{1-x,}$ both potential photovoltaic materials, were intensively studied concerning structure and phase relations in the past year [1, 2].

The series are formed by alloying the binary wide band gap semiconductor ZnSe in the ternary semiconductor $CuInSe_2$ and thereby substitute 2Zn $\leftrightarrow$ (Cu,In). Both structures are closely related, the binary end member crystallizes in the zinc-blende type structure (sg. $F\bar{4}3m$), the ternary end member belongs to the chalcopyrite compound family and crystallizes in the tetragonal chalcopyrite-type structure (sg. $I\bar{4}2d$).

Within the $(2ZnX)_x(CuInX_2)_{1-x}$ (X=S, Se, Te) alloys a structural phase transition tetragonal – cubic occurs in dependence of the chemical composition. The transition goes along with a phase separation by chemical disorder, characterized by a broad miscibility gap, the 2-phase field, in the range $0.1 < x < 0.40$ (X=S) [3, 4], 0.35 (X=Se) [1] and 0.32 (X=Te) [2]. In this region two phases occuring as tetragonal domains (x~0.1) and cubic matrix (x~0.40, 0.35 and 0.32 resp.), coexist. For the first system of the homologeous series, $(2ZnS)_x(CuInS_2)_{1-x}$, it was revealed that the lattice parameters, i. a. the cubic lattice constant a of the matrix and the tetragonal lattice constant a and c of the domains, influence each other [4]. The result is a matching of a_{cubic} with $a_{tetragonal}$ in the **a**-**b** plane giving rise to an increase of the tetragonal lattice parameter c and herewith a distinct increase of the tetragonal deformation $\eta(=c/2a)$.

Neutron diffraction experiments on $(2ZnSe)_x(CuInSe_2)_{1-x}$ and $(2ZnTe)_x(CuInTe_2)_{1-x}$ powder samples should give a deeper insight into the phase relations of the 2-phase region in these soild solution series. The measurements were performed at the high resolution powder diffractometer E9 using a wavelength of 1.7974 Å.

The diffraction data show clearly the existence of 2 phases, the tetragonal domains and cubic matrix (see figure 1). But the tetragonal line splitting (for instance the distance between the 008 and 400 reflexes) is much smaller in the $(2ZnSe)_x(CuInSe_2)_{1-x}$ than in the $(2ZnS)_x(CuInS_2)_{1-x}$ series.

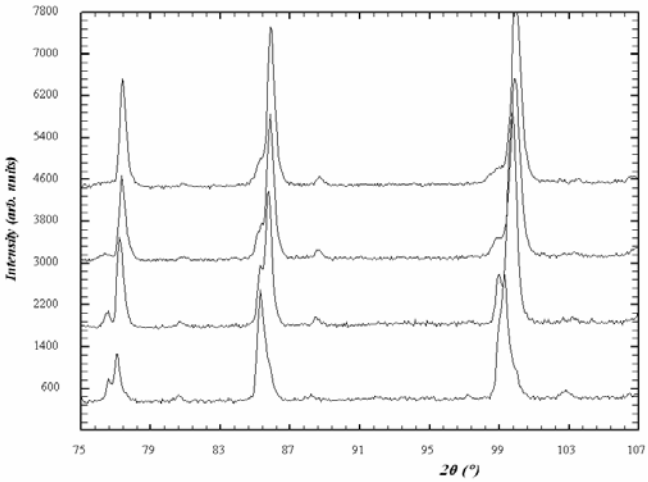

Figure 1: Part of the neutron powder diffraction pattern of $(2ZnSe)_x(CuInSe_2)_{1-x}$ alloys with x=0.15; 0.25; 0.30 and 0.33 (from down to up). The first both shown reflexes are 008 and 400 of the chalcopyrite type structure.

These splitting is determined by the difference of the tetragonal lattic parameters, i. e. c/2a. The determination of the lattice parameter of the domains and matrix becomes more an more difficult as the line splitting becomes smaller.

Because within the homolegous series the tetragonal deformation decreases
c/2a(X=S) > c/2a(X=Se) > c/2a(X=Te),
the Rietveld analysis of diffraction data of 2-phase samples is more difficult within the both systems investigated in the experiment and the data treatement is ongoing.

References

[1] G. Wagner, S. Lehmann, S. Schorr, J. Sol. State Chem. 178 (2005) 3631.
[2] L. Roussak, G. Wagner, S. Schorr, K. Bente, J. Sol. State Chem. 178 (2005) 3476.
[3] G. Wagner, F. Fleischer, S. Schorr, J. Cryst. Growth 283 (2005) 356.
[4] S. Schorr, G. Wagner, J. Alloys Comp. 396 (2005) 202.

	EXPERIMENTAL REPORT **Structural disorder study on UPt_2Si_2**	Proposal N° PHY-01-1755 Instrument **E9** Local Contact Michael Tovar
Principal Proposer: Experimental Team:	S. Süllow, IPKM - TU Braunschweig O. Prokhnenko - HMI Berlin M Tovar - HMI Berlin	Date(s) of Experiment 19.09. - 21.09.2005

Date of Report: 05.01.2006

Recently, we presented evidence for the presence of crystallographic disorder in a single crystalline, stoichiometric correlated electron material, UPt_2Si_2 [1]. From a detailed single crystal structural study on a specimen UPt_2Si_2 we find the system to crystallize in the $CaBe_2Ge_2$-structure, with anomalously large thermal displacement parameters U_{11}/U_{22} for Pt and Si on the Pt(2) and Si(2) sites of the $CaBe_2Ge_2$-structure [2]. This we take as evidence for frozen-in strain disorder on the Pt(2) and Si(2) sites. In order to directly verify that the values of the displacement parameters are not thermally induced, we now carried out powder neutron diffraction experiments on UPt_2Si_2 as function of temperature, using the E9 spectrometer with a neutron wavelength λ = 1.797429Å.

In Fig. 1 we plot the neutron diffraction spectrum of UPt_2Si_2 measured at 50K. We include the result of a Rietveld refinement of the data, using a fully ordered $CaBe_2Ge_2$ lattice. With this structure we reproduce all peak positions observed experimentally, using lattice parameters of a = 4.19615(5) and c = 9.65632(14), in good agreement with previous reports. Moreover, as for the single crystal measurements we find for the Pt(2) and Si(2) sites very much enhanced values β_{11}/β_{22} = 0.026(2) (Pt) and 0.033(4) (Si), as compared to β_{33} or the corresponding values for U, Pt(1) and Si(1) (β_{11}/β_{22} = 0.001). Further, as temperature is increased from 50 K to 200 K, the values of the anisotropic displacement parameters decrease. At 200 K we obtain a best fit with anisotropic thermal displacements factors for Pt(2) [Si(2)] of β_{11}/β_{22} = 0.018(2) [0.027(3)] (R_{Bragg} = 5.9%).

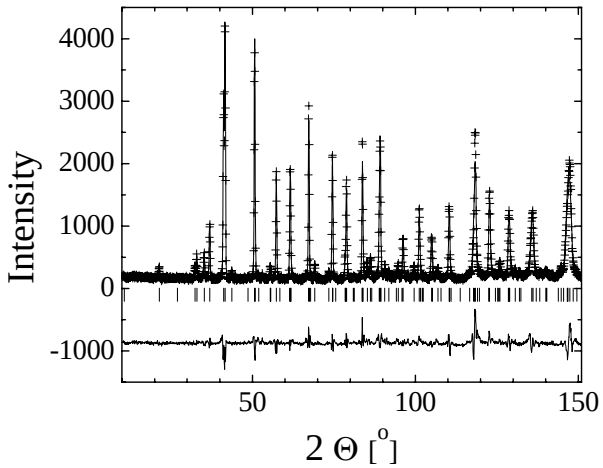

Fig. 1: Neutron powder diffraction spectrum taken on UPt_2Si_2 at 50K: (+) experimental data, solid line and tics indicate the result of a Rietveld refinement of the data, the lower panel displays the difference between fit and data; for details see text.

In Table 1 we summarize the temperature dependence of the lattice parameters. Remarkably, there is a minimum in the T dependence of the *a* axis value. As yet, it is not understood what leads to this minimum.

Clearly, our data prove the notion that the anomalous displacement parameters are not thermally induced. Hence, they do reflect frozen-strain disorder on the Pt(2) and Si(2) sites of the $CaBe_2Ge_2$-lattice. Therefore, the presence of crystallographic disorder in UPt_2Si_2 has unambiguously been established.

T (K)	*a* (Å)	*c* (Å)	R_{Bragg} (%)
50	4.19615(5)	9.65632(14)	7.9
100	4.19598(5)	9.66160(14)	7.1
150	4.19615(4)	9.66869(13)	6.9
200	4.19648(4)	9.67702(12)	5.9

Table 1: Lattice parameters and refinement values from the Rietveld analysis of the neutron powder diffraction data of UPt_2Si_2 measured as function of temperature .

References:

[1] A. Otop et al.: J. Appl. Phys. **95** (2004) 6702; S. Süllow, J. Appl. Phys., in print (2006).
[2] S. Süllow, A. Loose, and R. Feyerherm: BENSC Experimental Report **2004** (2005)

	EXPERIMENTAL REPORT **Analysis of hydrogen forms on nanocrystalline $LiBFeH_x$**	Proposal N° OTH-03-0378 Instrument **V3** Local Contact Margarita Russina
Principal Proposer: Experimental Team:	P.J. Hall - University of Strathclyde, UK J. Gil Posada - University of Strathclyde, UK	Date(s) of Experiment 14.02. - 21.02.2005

Date of Report: 26. Jan. 2006

The measured inelastic neutron scattering spectra of metallic samples consists of two parts. Firstly a broad band due to scattering from translationally bound hydrogen molecules, experimenting rotational transitions and a series of bands originated from crystalline active modes and/or high order rotational states. The second part consists in a broad band related to the metallic (intermetallic) hydride transitions.

As can be seen from Figure 1, the inelastic neutron scattering spectra of the samples in general exhibits one main peak centred at around 14.5meV, this peak is attributed mainly to a possible electronic transition, coming from the different hydrogen species (ortho and para) from its ground state ${}^1\sum_g^+$ to the first exited state ${}^1\sum_u^+$. The second peak centred at 66meV could be a magnesium hydride non-Raman active mode, in this case B_{1u} and/or the E_u.

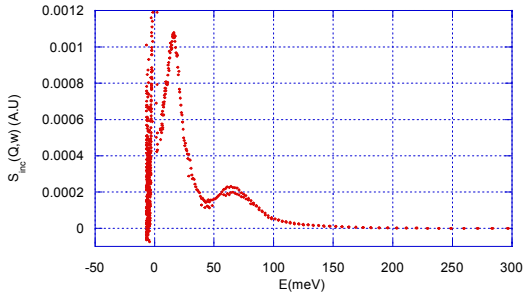

Figure 1. INS spectra at room temperature of Mg+0.22%Cd+0.5%Ca derived sample.
Foaming temperature T = 720°C.
Hydrogenation conditions: 300°C and 100 Bar for 24 h

It is important to note that the second peak was not always present, which means that maybe it does not originate from the H_2 molecule, certainly it can't be a high order rotational state because it is not close to 44 or 88 meV.

Each one of the two main peaks were de-convoluted by expressing them as a linear combination of Lorentzian functions. An objective function, based on the least squares method was used until the resulting $S_{inc}(\vec{Q},\omega)$ predicted by the model approximated to the experimental values, or in other words the quantity Ξ given by Equation 1 was minimised.

$$\Xi = \sum_{i=1}^{i=n}\left[\left\langle S_{inc}(\vec{Q},\omega)\right\rangle_{Exp} - \left\langle S_{inc}(\vec{Q},\omega)\right\rangle_{Mod}\right]^2 \quad (1)$$

The subscripts Exp and Mod refers respectively to the experimental measured and the predicted by the model values of the incoherent inelastic structure factor. Figure 2 shows the measured incoherent inelastic structure factor for single-walled carbon nanotubes expressed as a combination of four Lorentzian functions.

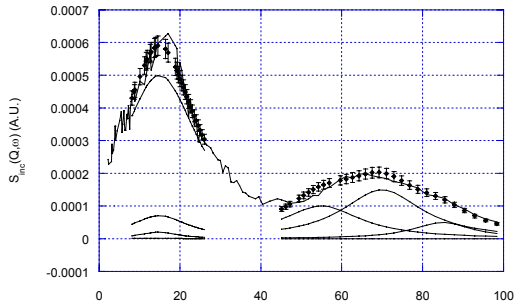

Figure 2. Deconvolution of the INS spectra of Mg+0.22%Fe+0.1%Cs derived sample by using a four Lorentzian model.
Foaming temperature T = 750°C.
The diamonds represent the experimental data.

	EXPERIMENTAL REPORT **Small-angle neutron scattering investigation of the disproportionation process in silicon sub-oxides**	Proposal N° CHE-04-1093 Instrument **V4** Local Contact Uwe Keiderling
Principal Proposer: Experimental Team:	A. Hohl - Darmstadt University of Technology A. Hohl - TU Darmstadt U. Keiderling - HMI Berlin	Date(s) of Experiment 08.02. - 09.02.2005

Date of Report: 09.01.2006

On the way to detailed structural models for silicon sub-oxides (SiO_x) we study the phase separation (disproportionation) process and the intermediate length scale (range of cluster sizes) within completely amorphous and within partly crystallized SiO_x modifications (differently prepared samples) by means of small-angle neutron scattering (SANS).

We had one day for SANS experiments at the instrument V4 at BENSC on powder samples of bulk silicon monoxide (SiO), which had been prepared at 600 °C [1] and additionally thermally treated to get different degree of disproportionation (increased sizes of clusters of Si and of SiO_2) by different annealing at temperatures between 850 °C and 1150 °C.

Fig. 1(a)-(g) shows the scattering curves of the samples between $q = 0.226\ nm^{-1}$ and $q = 6.79\ nm^{-1}$. With increasing annealing temperature the peak position q_{peak} shifts to smaller q values. This peak shift covers the whole measured q range. A first estimation of the cluster sizes can be made assuming a strong correlation between the mean cluster sizes and the mean cluster distances in the disproportionated structure. We consider the volume ratio $3\rho_0(Si)/\rho_0(SiO_2) \approx 2.3$ (calculated from the number densities for overall 1:1 stoichiometry and an abrupt interface between Si and SiO_2 [1]) and resulting diameter ratio of about 1.3 of SiO_2 clusters and Si clusters. The mean distance d of the clusters calculated from $d = 2\pi/q_{peak}$ increases from 1.9 nm to 12.1 nm (Fig. 1(h)). These values should be multiplied by 1/2.3 and 1.3/2.3 to obtain mean cluster sizes for Si and SiO_2, respectively.

From Fig. 1(h) it can be seen that cluster growth may be enhanced in the temperature range between 900 °C and 1000 °C where Si crystallization begins and between 1050 °C and 1150 °C where SiO_2 starts to change its structure.

A more detailed evaluation using a morphological model will follow, as the development of such a model with reasonable propability is in progress.

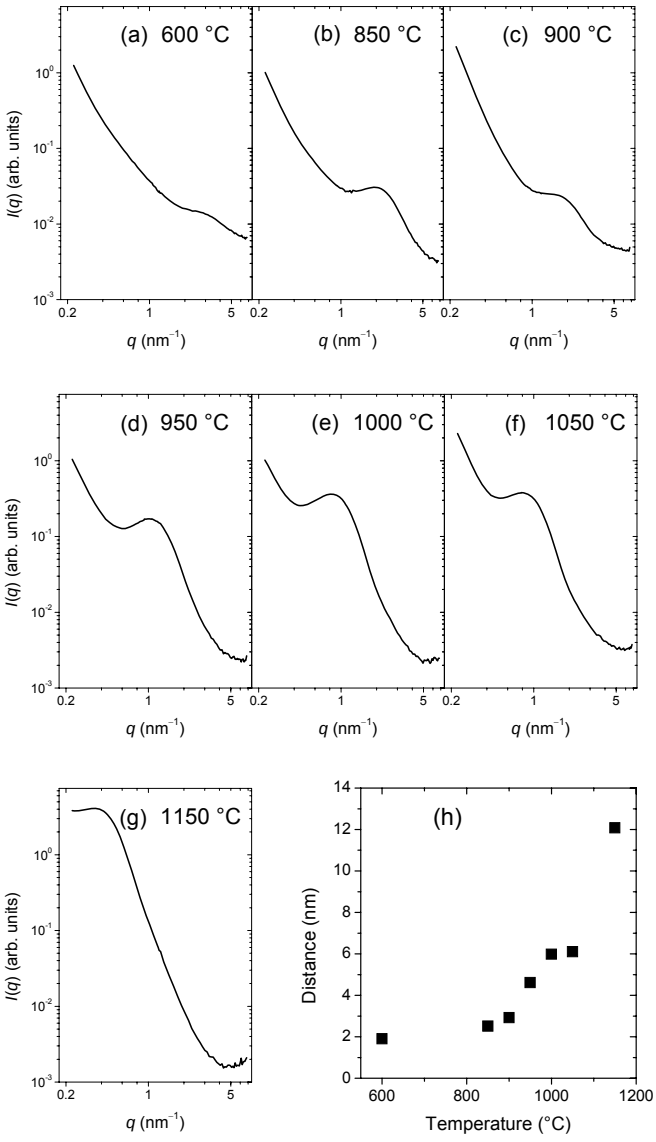

Fig. 1: Plots of the SANS curves for SiO samples with different production **(a)** and thermal annealing **(b)-(g)** temperature and a plot **(h)** of the estimated mean cluster distances (corresponding to one diameter of an Si cluster plus one diameter of an SiO_2 cluster).

Reference

[1] A. Hohl, T. Wieder, P.A. van Aken, T.E. Weirich, G. Denninger, M. Vidal, S. Oswald, C. Deneke, J. Mayer, H. Fuess: J. Non-Cryst. Solids **320** (2003) 255.

	EXPERIMENTAL REPORT **Defect induced phase transition in doped GaAs**	Proposal N° PHY-02-0448 Instrument **E1** Local Contact Vadim Sikolenko
Principal Proposer: Experimental Team:	A. Naberezhnov - PTI S-Petersburg, Russia V.V. Sikolenko - HMI Berlin S. Borisov - PTI S-Petersburg, Russia	Date(s) of Experiment 14.06. - 28.06.2005

Date of Report: 14.09.2005

It is known that the physical properties of strongly doped A^3B^5 semiconductors are essentially modified. For example in GaAs doped by Te and Se it was observed the anomalies of sound velocity, specific heat and IR absorption near the room temperature [1.2]. The theoretical consideration confirms the possibility of appearance of specific ferroelectric/ferroelastic phase transition (PT) in these compounds [1], but the lattice dynamics of similar crystal did not practically investigated . We have carried out the study of evolution of Δ_{TA} resonance lineshape at 103, 293, 308, 320, 335, 350, 369 and 417 K (i.e. in a vicinity of expected phase transition) using GaAs single crystal doped by Te (with carriers concentration $N_e \approx 2\times10^{18} cm^{-3}$). Above room temperature at small reduced wave vector q in a vicinity of (220) lattice point we have observed a broad phonon resonance but at q>0.15 the width of this resonance decreased sharply (Fig.1) and was practically equal to experimental resolution at large q.

These results are in a good agreement with our preliminary data obtained earlier [3]. We believe that observed broadening of Δ_{TA} resonance could be attributed to mode coupling with specific local mode originating from doping of crystal by Te. The temperature dependences of integrated intensity of phonon resonance at different reduced wave vectors are presented on Fig.2. It is easy to see that at small q these curves demonstrate a peculiarity near 300 K, as it is expected in a case of possible phase transition. In a vicinity of (222) lattice point there the Δ_{TA} resonance strongly depresses due to small inelastic structure factor we have observed the traces of unexpected intensive diffuse scattering, but because of lack of experimental time we cannot study the distribution of this scattering in detail.

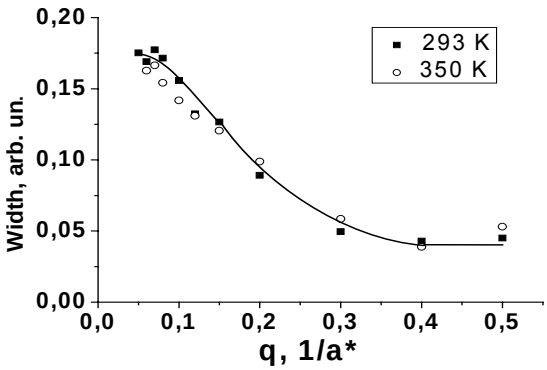

Fig. 1

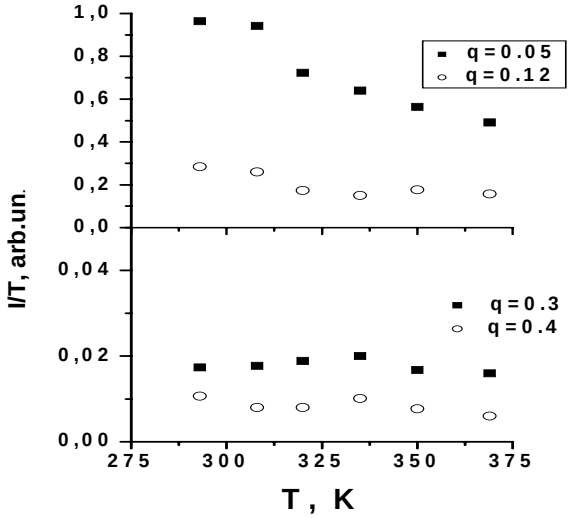

Fig. 2

References

[1] Prudnikov, V.V., Prudnikova, I.A.: *Kristallographija*, **37**, 1992, 1093 (in Russian)

[2] Balagurova, E.A., Grekov, Yu.B., Kravchenko, A.F., Prudnikov, V.V., Prudnikova, I.A., Semikolenova, N.A.: *Physics and Technics of Semiconductors*, **19**, 1985, 1566 (in Russian)

[3] S.A. Borisov, S.B.Vakhrushev, A.A. Naberezhnov, N.M. Okuneva: Phys. of the Solid State 47(6), 2005, 1060

	EXPERIMENTAL REPORT **Anisotropic Debye Waller factors of $La_{0.7}Sr_{0.3}MnO_3$ from powder diffraction**	Proposal N° PHY-01-1759 Instrument **E9** Local Contact Oleksandr Prokhnenko
Principal Proposer: Experimental Team:	D. Reznik - Forschungszentrum Karlsruhe F. Weber - Forschungszentrum Karlsruhe O. Prokhnenko - HMI Berlin D. Argyriou - HMI Berlin	Date(s) of Experiment 18.08. – 23.08.2005

Date of Report: December 2005

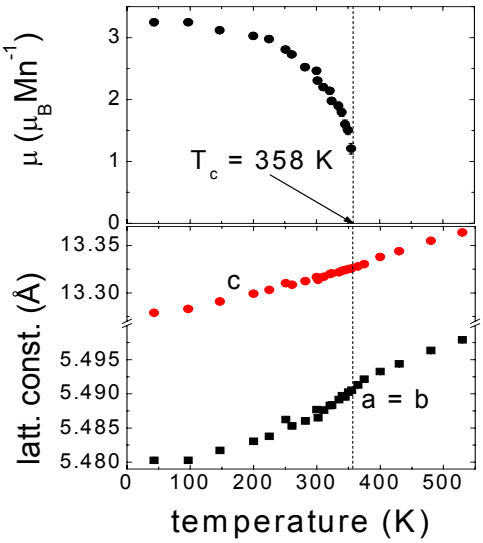

Fig. 1 Temperature dependence of magnetic moment per Mn site and lattice constants of $La_{0.7}Sr_{0.3}MnO_3$. The low temperature value of the moment is 3.24 $\mu_B Mn^{-1}$. As the c lattice constant is not affected by the FM transition, there is a kink at T_c in the a/b lattice constants.

Many perovskite manganites exhibit, a ferromagnetic – paramagnetic (FM) transition, which is accompanied by large magnetoresistance (MR). For $La_{0.7}Ca_{0.3}MnO_3$, known for the colossal magneto resistance effect (CMR), the polaronic picture with short range charge order is widely accepted but the smaller MR in $La_{0.7}Sr_{0.3}MnO_3$ is thought to be due to double exchange alone [1,2]. However, our earlier measurements have shown that phonons in $La_{0.7}Sr_{0.3}MnO_3$ and $La_{0,8}Sr_{0.2}MnO_3$ show a strong renormalization of certain bond stretching modes near T_c, but no effect in the bond bending modes near the FM transition [3].
The powder experiment was carried out to look for the anisotropic Debye-Waller (DW) factors of the oxygen atoms in $La_{0.7}Sr_{0.3}MnO_3$ (space group R-3C, #int. tables 167). In this compound all oxygen atom positions are equivalent. However, the vertical axis of the MnO_6 octahedra is tilted out of the a-b plane by roughly 34° along the (1,-1,0) direction.

The refined magnetic moment is 3.24 μ_B at T = 43 K and agrees well with T_c = 358 K as transition temperature (Fig. 1). From the above mentioned phonon measurements we suggested that there should be difference between the main directions of the MnO_6 octahedra. This effect is clearly seen in Fig. 2. The refined anisotropic displacement U of the oxygen atoms is shown for the two directions perpendicular (green) and parallel (red) to the MnO_6 octahedral plane. The temperature effect across the FM transition is roughly 50% of the low temperature value for both directions. However, the large difference between the absolute values of U (factor of 2) shows an anisotropic dynamic distortion of the MnO_6 octahedra.
The main question to answer is, whether dynamic distortions of the MnO_6-octahedra occur also in the Sr doped manganite. To compare our data to results for the CMR manganite $La_{0.75}Ca_{0.25}MnO_3$ [4], where a sharp kink for the anisotropic displacement U is seen at $T_c \approx 250$ K, more data points at temperatures above 400 K are needed.

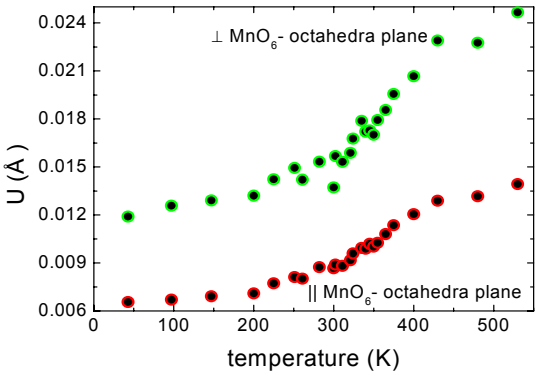

Fig. 2 Mean square displacement U of oxygen atoms refined from neutron powder diffraction patterns. Data shown for direction perpendicular to the MnO_6 octahedral plane (green) and parallel to Mn-O bond in the MnO_6 octahedral plane (red)

References

[1] C. P. Adams et al., Phys. Rev: Lett. **85**, 3954 (2000)
[2] A. Urushibara et al., Phys. Rev. B **51**, 14103 (1995)
[3] D. Reznik et al., cond-mat/0312368
[4] P. G. Radaelli, Phys, Rev. B **54**, 8992 (1996)

	EXPERIMENTAL REPORT **Phonon anomalies in the martensitic phase of Ni_2MnGa**	Proposal N° EF Instrument **V2** Local Contact Klaus Habicht
Principal Proposer: Experimental Team:	P. Vorderwisch - HMI Berlin S.M. Shapiro - Brookhaven Nat. Lab P. Vorderwisch - HMI Berlin K. Habicht - HMI Berlin	Date(s) of Experiment 18.-26. October 2005

Date of Report: 14.03.2006

The ferromagnetic shape-memory alloy Ni_2MnGa undergoes (for stoichiometric composition at $T_M \approx 220$ K) a thermally induced martensitic transformation from a cubic austenite phase ($L2_1$ Heusler structure) to a tetragonally distorted ($c_t/a_t = 0.94$) martensite phase. The transformation is preceded by an intermediate ('pre-martensitic') phase which exists in the temperature range $T_M \leq T \leq 260$ K. This phase is characterised by a commensurate modulation with wave vector $\mathbf{q} = (2\pi/a_c)$ (⅓ ⅓ 0). The low-temperature martensite phase is also modulated, however with an incommensurate wave vector $\mathbf{q} = (2\pi/a_t)$ (0.425 0.425 0).

Phonon dispersion measurements in the austenite phase [1] and in the martensite phase [2] reveal a phonon anomaly in the [110] transverse acoustic branch TA_2 (with polarisation in [1 -1 0] direction) at the modulation wave vector of the corresponding phase. This anomaly is identified as a Kohn anomaly through examination of Fermi-surface nesting and electron-phonon coupling [3].

In a recent experiment [4] with a thermal triple-axis-spectrometer in the martensite phase (using the same crystal as in Refs. [1,2]), an indication of an additional low-lying mode has been found. This additional mode emerges from the incommensurate modulation wave vector $\mathbf{q} = (2\pi/a_t)$ (0.425 0.425 0) of the martensite phase.

This low-lying mode was now re-measured on FLEX with better resolution. A typical const.-Q phonon scan for the two temperatures T = 100 K and T = 200 K is shown in Figs. 1 and 2, respectively. The higher-energy phonon (at $\Delta E = 3.1$ meV and $\Delta E = 2.85$ meV, respectively) is T-dependent and corresponds to the known transverse acoustic phonon branch emerging from the Brillouin zone center [2]. The new lower-energy excitation (at $\Delta E = 2.05$ meV), emerging from the incommensurate q-vector, is found to be T-independent. The complete dispersion for both branches (at 200 K) is inserted into the intensity contour plot on the title page of this report.

The new mode shows the characteristics of a **phason** in an incommensurate displacively modulated crystal: it is only observed in the neighbourhood of the satellite reflection, it is acoustic-like (with a slope different from that of the TA_2 phonon), and its frequency is temperature-independent. This result is exciting insofar as inelastic neutron scattering has rarely succeeded in unambiguously revealing the existence of phasons.

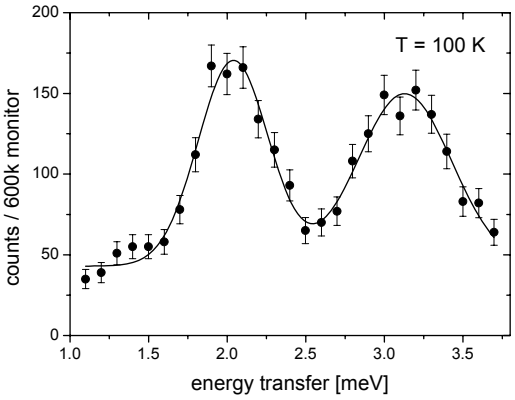

Fig.1: Const.-Q scan at Q = (2.32, 1.68 0) and at a sample temperature T = 100 K

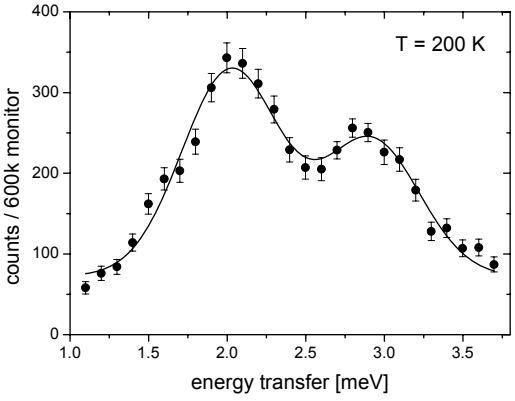

Fig.2: The same const.-Q scan as in Fig.1, now at a sample temperature T = 200 K

References:

[1] A. Zheludev *et al.*: Phys. Rev. B **54** (1996) 15045
[2] P. Vorderwisch, S.M. Shapiro: Mat. Sci. Eng. A (accepted)
[3] C. Bungaro *et al.*: Phys. Rev B **68** (2003) 134104
[4] P. Vorderwisch *et al.*: FRM-II proposal 117, performed with the thermal TAS PUMA in 08/2005

	EXPERIMENTAL REPORT NRSE investigation of phonon life times in the conventional superconductor Nb	Proposal N° PHY-02-484-LT Instrument **V2** Local Contact Klaus Habicht
Principal Proposer: Experimental Team:	K. Habicht - HMI Berlin + TU-Darmstadt F. Mezei - HMI Berlin T. Keller - MPI f. FKF, Stuttgart, FRM-II, Garching B. Keimer - MPI f. FKF, Stuttgart	Date(s) of Experiment 26.05.-02.06.2005

Date of Report: 10.01.2006

The most direct microscopic evidence of superconductivity is obtained by a study of the line width or life time of those excitations which strongly interact with the charge carriers. Changes in the line width are observed upon pairing of the charge carriers at the characteristic temperature T* when the relaxation channel due to interaction with the electrons (or holes) is forbidden. In the conventional elemental superconductors the dominant interaction mechanism of the electrons is with phonons [1]. Our investigation of phonon line widths in the BCS superconductor Nb is part of an extended research programme with challenges with respect to the high energy resolution.

The neutron resonance spin-echo technique (NRSE) is well suited to overcome the resolution limits of the standard spectroscopic techniques, since it can resolve energy transfers within the resolution ellipsoid of a background three-axis spectrometer. Phonons relevant for the electron-phonon interaction are usually dispersive, so the spin-echo focusing technique with tilt able fields is appropriate.

In previous experiments using the NRSE technique on the cold three-axis instrument V2 a large change in line width ($\Delta 2\Gamma \simeq 60$ μeV) for the acoustic T_1 phonon has been observed upon cooling an Nb sample below the superconducting transition temperature T_C. The aim of this experiment was to extend the dataset in the temperature range below T_C to confirm this large change.

The TAS was operated in a configuration with scattering senses (SM=-1, SS=-1, SA=+1) in order to minimize the effects of the curvature of the dispersion surface. The transverse Q-resolution was about 0.015 $^{-1}$ FWHM at fixed incident $k_i = 2.0$ $^{-1}$. Second-order contamination is substantially suppressed by the curved neutron guide. No additional collimators were used besides the bender polarizers after the PG monochromator and after the PG analyzer.
The required tilt angles of the RF-flippers were calculated from Born-von-Kàrmàn fits to data taken in previous experiments. For the [0.025 0.025 0] T_1 phonon investigated, tilt angles are θ_1= -31.3° and θ_2= 27.4°. We have used a large high-quality Nb-crystal produced by the MPI für Metallforschung, Stuttgart, with a crystal mosaicity of 8.9 min as confirmed by gamma diffraction experiments. The crystal was mounted with the [100] axis perpendicular to the scattering plane and T_1 phonons were measured along (1-ζ 1+ ζ 0) to satisfy the phonon focussing conditions and match the slope of the dispersion.

Fig. 1 displays the temperature dependence of the phonon line width as obtained from the raw data normalized to the polarization measured in the direct beam. No correction for sample mosaicity or dispersion curvature has been applied. From complementary TAS data in the low-q range we can rule out artificial effects due to energy shifts of the dispersion. The new data is still consistent with a rather large change of line width.

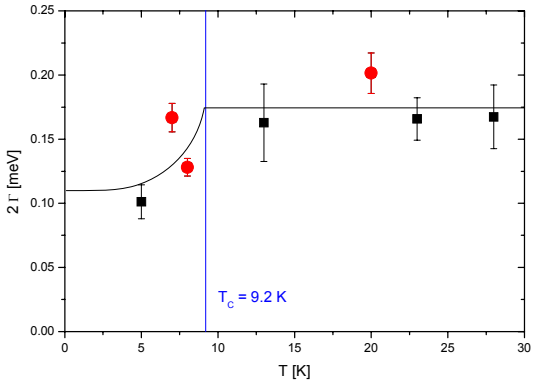

Fig. 1: Line width of the [0.025 0.025 0] T1 phonon as a function of temperature. New NRSE data (full circles, red) in comparison to data previously collected on V2. Below T_C the line through the NRSE data represents the temperature dependence of the line width as given by Bobetic [2]; above T_C the line width is assumed to be constant.

References

[1] J.D. Axe, G. Shirane: Phys. Rev. Lett. **30**, 6, 214 (1973)
[2] V.M. Bobetic: Phys Rev., **136**, A 1535 (1964)

	EXPERIMENTAL REPORT **Temperature dependence of the phonon-dispersion in Nb at low q**	Proposal N° PHY-02-485-LT Instrument **V2** Local Contact Klaus Habicht
Principal Proposer: Experimental Team:	K. Habicht - HMI Berlin K. Habicht - HMI Berlin	Date(s) of Experiment 18.03.-23.03.2005

Date of Report: 10.01.2006

The present experimental investigation is part of an ongoing research program focused on high-resolution studies of phonon line widths in BCS superconductors with strong electron-phonon coupling. We have measured the temperature dependence of the dispersion along the T_1 acoustic phonon branch in the (110) direction at low wave vectors. Phonons in this wave vector range have been previously investigated by our NRSE experiments revealing a large change in phonon line width ($\Delta 2\Gamma \simeq 60$ μeV) upon cooling the crystal below the superconducting transition temperature T_C. The main objective of the experiment was to determine whether the dispersion stiffness changes with temperature which is a potential source of instrumental misalignment in a high-resolution NRSE experiment since the coil tilt angles are chosen according to the slope of the dispersion.

The instrument was operated with scattering senses SM=-1, SS=-1, SA=+1 with collimations 20'-20'-20' at fixed k_F= 1.57 Å^{-1}. A cooled Be-filter was used to suppress second order contamination. In this configuration the experimentally determined elastic energy resolution was found to be 66 μeV at the 110 Bragg peak (84 μeV vanadium width).

We have used a large high-quality Nb-crystal produced by the MPI für Metallforschung, Stuttgart, with a crystal mosaicity of 8.9 min as confirmed by gamma diffraction experiments. The crystal was mounted with the [100] axis perpendicular to the scattering plane and T_1 phonons were measured along (1+ζ 1-ζ 0).

The dispersion is well in agreement with earlier data by Shapiro *et al.* [1]. No energy shift of the dispersion is observed with a temperature change between 5 K and 15 K. From the data we extract a constant slope of the dispersion $d\hbar\omega/dq$ = 16.53(4) meV Å. The inelastic resolution was approximately 270 μeV FWHM fitting the data to Gaussian profiles. Changes in the phonon line width with decreasing temperature could only be found for ζ = 0.06 r.l.u. where the Gaussian FWHM decreased from 280(15) μeV to 208(12) μeV (see Fig. 2). However the statistical quality of the data is insufficient to extract definite information on the phonon life times.

We have also collected data in off-symmetry directions close to the [110] direction which is not available in the literature. This gives valuable information on the curvature of the dispersion, which is important for data correction to extract intrinsic line widths from our NRSE data.

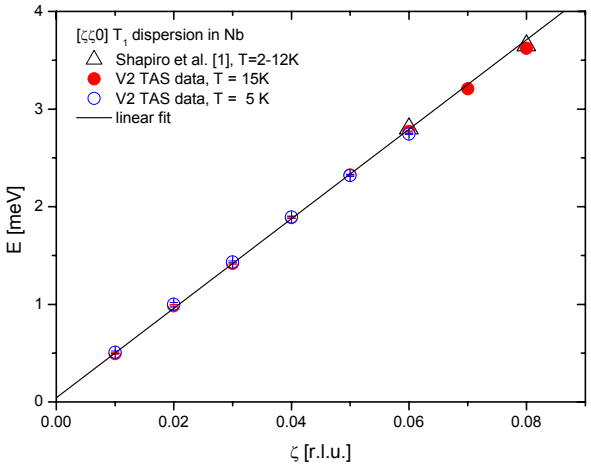

Fig. 1: T_1 phonon dispersion for two temperatures T = 15 K and T = 5 K compared to literature data [1]. Error bars are smaller than the symbol size.

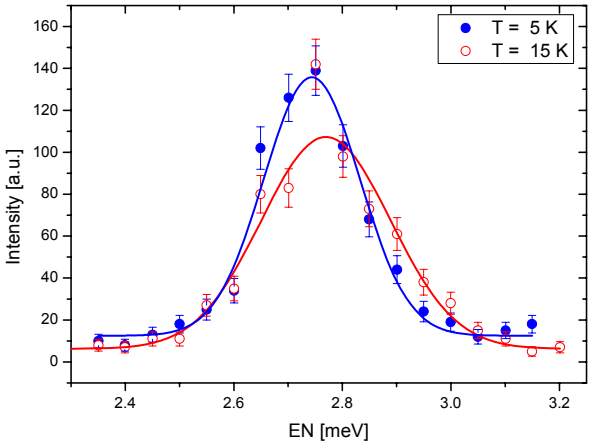

Fig. 2: Constant-Q-Scans for ζ = 0.06 r.l.u. at temperatures T = 15 K and T = 5 K.

Reference

[1] S.M. Shapiro *et al.*:
Phys. Rev. B **12**, 11, 4899 (1975)

	EXPERIMENTAL REPORT **Influence of polaron localization on G(ε) in intercalation compounds M_xTiSe_2**	Proposal N° PHY-03-0388-EF Instrument **V3** Local Contact: Jörg Pieper
Principal Proposer: Experimental Team:	O. Sobolev - HMI Berlin S. Titova - Inst. of Metallurgy, Ekaterinburg, RU A.N. Skomorokhov - IPPE, Obninsk, RU J. Pieper - HMI Berlin	Date(s) of Experiment 10.04. - 15.04.2005

Date of Report: 07. Dec. 2005

The materials with polaron charge carriers attracts significant attention due to their unusual properties such as superconductivity, colossal magnetoresistence etc. Theoretical approach for adiabatic single-particle approximation predicts an absence of influence of polaron charge carriers on crystal lattice [1]. However, in dense polaron system as intercalation compounds based on $TiSe_2$, localization of polarons causes a growth of the density of states at the Fermi level and affects the elastic constants. Earlier we have shown an influence of polaron formation on phonon density of states for $Fe_{0.25}TiSe_2$ [2]. The composition 0.25 is chosen, because it is upper boundary of the concentration range when the polarons may be considered as non-interacting [3]. The aim of the current work was to compare such an influence for different metal intercalated. The M_xTiSe_2 with M=Fe, Ni and Cr were studied at DIN-2PI spectrometer, JUNR, while $Ag_{0.25}TiSe_2$ was studied at V3 (NEAT) spectrometer, BENSC. Measurement with V3 spectrometer was done with initial neutron wavelength 3.3 Å at *T* = 150 and 250 K. After applying typical correction experimental data collected at a large angular range (15 – 135°) were transformed to the dynamic structure factor $S(Q,\varepsilon)$. The neutron-weighed phonon density of states G(ε) was obtained in incoherent approximation after appropriate *Q* averaging. Data were analyzed in G(ε) terms.

Fig. 1 shows the origin of the difference – potential of ionization of intercalated transition metal determines the value of a decrease of the free energy of electrons during polaron formation ΔE. For the first time we are able to observe the clear correlation between ΔE and phonon density of states G(ε) at small value of the energy transfer: G(ε) shifts to higher frequencies with increasing ΔE (and back). This result shows that the increase of the ΔE value is accompanied by lattice hardening. It means that lattice elasticity restricts the degree of localization of polarons.

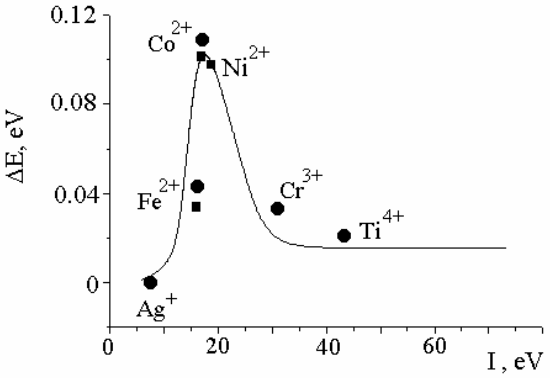

Fig. 1: The polaron shift vs potential of ionization of metal intercalated in $TiSe_2$.

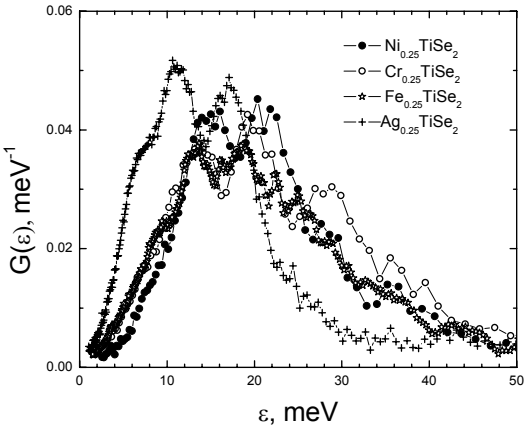

Fig. 2: Phonon density of states for $M_{0.25}TiSe_2$; M=Ag, Cr, Fe, Ni.

References

[1] A.S.Alexandrov, N.Mott: *Polarons and Bipolarons* World Scientific Publ. Singapore (1995).

[2] A.N. Titov, S.G. Titova, A.N. Skomorokhov, V. Rajevac, V.A. Semenov: *Proc. Of 7th International Symp. "Phase Transitions in Solid Solutions and Alloys OMA–2003", 6-10 Sept.* 2004, Sochi, P. 287.

[3] A.N. Titov, Yu.M. Yarmoshenko, M. Neumann, B.G. Pleschev, S.G. Titova: *Fizika tverdogo tela (rus)* 2004, v. 46, p. 1628.

	EXPERIMENTAL REPORT **Guest molecules dynamics in iodomethane hydrate**	Proposal N° CHE-03-0400 Instrument **V3** Local Contact Margarita Russina
Principal Proposer: Experimental Team:	F. Mançois - LPCM, Univ. Bordeaux 1 A.Desmedt - LPCM, CNRS-Univ. Bordeaux 1 M. Prager - Forschungszentrum, Jülich	Date(s) of Experiment 19.07. - 26.07.2005

Date of Report: 08.09.2005

In clathrate hydrates, a host structure comprises a hydrogen bonded arrangement of water molecules and contains inclusion cavities within which a large number of guest molecules can be located. The research undertaken on clathrate hydrates are particularly worthwhile in view of the economical and environmental importance that systems such as methane hydrates represent [1]. In addition, these materials are interesting in view of their specific fundamental properties such as the "glass-like" heat transport properties involving the lattice dynamics of the water matrix [2] or their proton conduction properties involving protons delocalisation in the host substructure when acidic or basic molecules are included [3]. The host-guest interactions play a key role in the stability of clathrate hydrates and in their specific properties [4]. Many groups have undertaken detailed studies on (molecular and lattice) dynamics properties in methane hydrate, which represents a prototypical system of a non-polar guest molecule. In contrary, very little is known about hydrates of polar guest molecules. Such model system might be represented by the iodomethane hydrate.

From 1.7 K to 270 K, the structure of CH_3I-$17H_2O$ is of type II, i.e. cubic unit cell (*a* ~ 17 Å) made of two types of water cages [5]. The guest molecules are located within the largest cages. The aim of the experiment was to study the iodomethane dynamics by means of incoherent Quasi-Elastic Neutron Scattering (QENS).

On this issue, the QENS experiments have been performed on the selectively deuterated sample, $(CH_3)I$ - $17D_2O$ with the time-of-flight spectrometer NEAT. Two energy resolutions (noted ΔE) have been used: (a) $\Delta E \approx 100\mu eV$, $\lambda_o = 5.1$ Å (270 K, 230 K, 190 K, 150 K), (b) $\Delta E \approx 50$ µeV, $\lambda_o = 7.0$ Å (270 K, 150 K). On the spectra, two main features are observed:

- At about 1meV (see figure), one observes a mode (weak intensity), that is probably associated to the rattling motions of the guest molecules within the cages.

- Quasi-Elastic broadening has been observed for all temperatures and resolutions. As seen on the figure, the elastic intensity is very large. This contribution is mainly due to the host aqueous substructure (~ 95% deuterated), which scatters elastically and represents about 50% of the total incoherent scattering. For the 100 µeV resolution (a), the width of the QENS component is about 900 µeV at 150 K. According to previous results [5], this component may be associated to the rotation of the methyl group about the C_3 axis of the iodomethane molecule. With the configuration (b), it was difficult to observe any additional narrower QENS component.

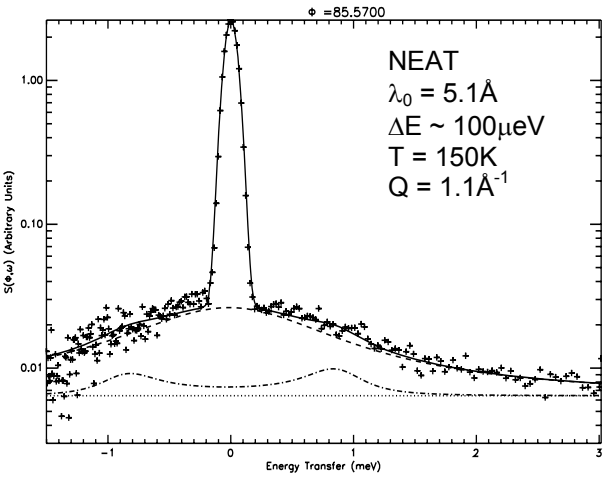

In order to develop a complete model describing the iodomethane molecules dynamics, we have undertaken a study combining Molecular Dynamics (MD) simulations and the QENS measurements and further investigations with a backscattering spectrometer might be necessary.

References

[1] - C.A. Koh: *Chem. Soc. Rev*. **31**, 157 (2002)
[2] - J. Baumert *et al*.: *Phys. Rev. B* **68,** 174301(2003)
[3] - A. Desmedt *et al*.: *J. Chem. Phys.* **121,** 11916 (2004)
[4] - H. Schober *et al*.: *Eur. Phys. J. E* **12,** 41 (2003)
[5] - M Prager *et al*.: *J. Phys. Condens. Matter* **16,** 7045 (2004).

	EXPERIMENTAL REPORT **Determination of diffusion mechanism and position of nitrogen in quaternary oxide Hexaluminate at temperatures up to 1200K**	Proposal N° MAT-03-0397 Instrument **V3** Local Contact Alexandra Buchsteiner
Principal Proposer: Experimental Team:	B. Saruhan-Brings - DLR Köln M. Stranzenbach - DLR Köln C.G. Mondragon Rodriguez - DLR Köln	Date(s) of Experiment 07.09. - 13.09.2005

Date of Report: 29. Sept. 2005

In the experimentation with time of Flight (TOF) on neutrons source the objective was to determine the diffusion processes of NO molecules adsorbed on the surfaces of hexaaluminate and perovskite base materials. Since Oxygen has no scattering intensity, the experiments were worked out only on the scattering intensity of Nitrogen. Three different samples were analyzed by neutron scattering experiments at the high temperature furnace (equipment V3) in which initially different scattering conditions were tested (150, 70 and 35 µeV resolution) in order to find out the best conditions for the diffusion detection.
The tested specimens were repaired by an acid sol-gel route and calcined up to 1100°C for 3 hours. After heat treatment the as-received powders were exposed to Ar and heated up to 800°C in order to clean the surface. During the cooling phase (10 hours) to room-temperature the samples were exposed to NO (1000ppm). In order to get a better scattering intensity, 5 g of each powder was press to a plate of 1mm thickness yielding a density of about 1,7 g/cm^3.

The obtained results principally confirmed the potential of Time of Flight (TOF) in the measurement of diffusion processes of NO species over ceramic oxide based materials. As it is shown in the below graphic, the statistic in the results obtained in this measurement period were not satisfactory. The resolution of the measurements was 5,5 Å / 75 µeV at temperatures between 275 K and 973 K, with measuring steps every 50 K / 100 K. Therefore, it is not possible to make a detailed discussion of the diffusion process at the different temperatures. This graph presents the raw data summarising over all possible angles, without the correction for vanadium and for the empty cell. A very small quasi-elastic contribution which decreases with the increase of temperature (295 K – 673 K) can be observed, however, it is difficult to quantify precisely this effect due to the very low scattering intensity of the diffused nitrogen. The application of a higher resolution (5,1 Å / 32 µeV) which is applied to provide a better qualification of the quasi-elastic scattering part, and thus, the diffusion process, resulted in an extremely low statistic. The application of a lower resolution (8 Å / 270 µeV) results in a better statistic, but seems to have a very low time constant for the diffusion process. As it can be seen from the graphic below, the quasi-elastic contribution is already observable at room temperature, which indicates the starting point of diffusion at lower temperatures at the given conditions.

In order to overcome these difficulties and to get reasonable results, it is necessary to repeat the experiments in a new measurement period by extending the measurement times significantly to receive a better statistic. This means that a thorough investigation of one single substance (material) should be taken into consideration. Moreover, in order to increase nitrogen concentration (and therefore scattering intensity), the preparation of the specimens should be optimized (e.g. longer gas exposure, higher pressure). Moreover, the comparison of samples with and without NO-exposure could help to interpret the detected processes. The high temperature furnace attached to the V3 is capable of function under vacuum, thus, it is likely that the diffusion process occurs at a higher rate under the selected measurement conditions. In order to overcome this, it may be necessary to employ a kyro-furnace with less or no vacuum and use smaller temperature intervals (e.g. 30°C) and lower temperature gradients (e.g. – 100° to 100°C) with yielding special attention of applying maximum moderate temperatures such as 300° - 350°C.

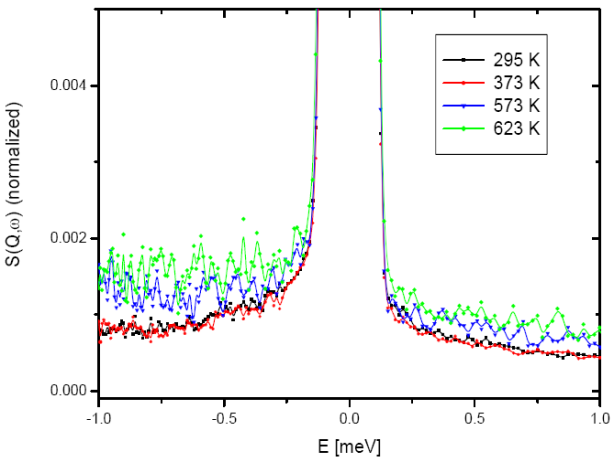

	EXPERIMENTAL REPORT **Molecular dynamics in Tryglicine Sulphate (TGS) using TOF neutron spectroscopy**	Proposal N° PHY-03-0376 Instrument **V3** Local Contact Jörg Pieper
Principal Proposer: Experimental Team:	V. Tripadus - NIPNE Bucharest A. Buchsteiner - HMI Berlin A. Radulescu - ISSR Juelich D. Aranghel, M.Gugiu, M. Statescu - NIPNE	Date(s) of Experiment 13.06. - 20.06.2005

Date of Report: Jan. 2006

In our previous measurements at BENSC-NEAT TOF neutron spectrometer we established the main dynamical parameters that describe the ferroelectric - paraelectric phase transition in TGS. From this work the following conclusions were drawn:

- The main motion that governs the phase transition it is given by the dynamics of the GI glycine molecule
- The flip motion of the amino group takes place at a time scale of 0.85÷1.05 10-11 s
- Two lorentzians fitting was used for quasielastic scattering law spectra from which we have obtained the energy levels of the hindered rotations of the NH3 group around the main axis of thetraedron . A ratio of 4 was obtained for the widths of the two lorentzians, the first one having a value around 0.5meV.

In the present experiment we have carried out TOF measurements on partially deuterated TGS intending to confirm the conclusions of the previous experiment. By deuteration we have replaced the protons from the amino group from the glycine molecules. The hydrogen atoms from CH2 still remained. We are not sure if the protons from H-bond between GI and GII were removed or not. Using an energy window of 93 μeV, which is the same like in the previous measurements for non deuterated sample we have obtained the dynamical parameters of the sample and we have compared with the previous ones.

In *fig.1* we present a quasielastic scattering law pattern fitted with one lorentzian. As the fitting procedure gave better results using only one lorentzian we concluded that the first energy level of the rotational motion assigned to amino group is still present in the quasielastic line. The mean energy value connected with this motion is about 0.57 meV. Although the quasielastic line is less dominated by the incoherent scattering, this lorentzian assigned to amino rotational motion remained. As concern the motion of CH2 group this belongs to the whole flipping motion and cannot be putted in evidence in this energy window.

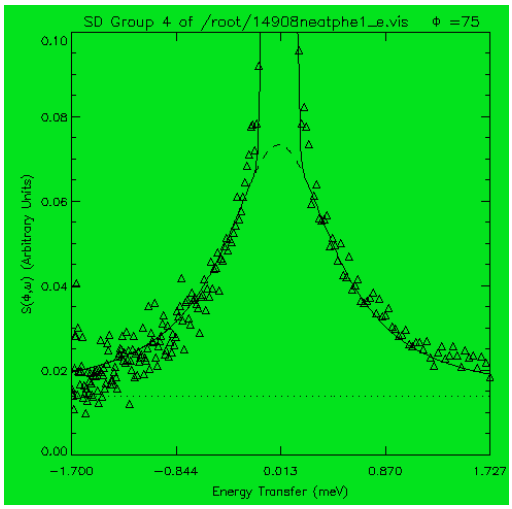

Fig.1: An example of fitted QENS spectrum of partially deuterated TGS at a scattering angle of 93º.

The measurements were carried out at various temperatures, both under the critical point and above it. The elastic incoherent structure factors - EISF reflects the immobility of the protons under the critical point. The value of the EISF is around 0.97. Above critical point the behavior of EISF as a function of impulse transfer Q shows a descending behavior attending a value of 0.92 at the greatest value of Q.

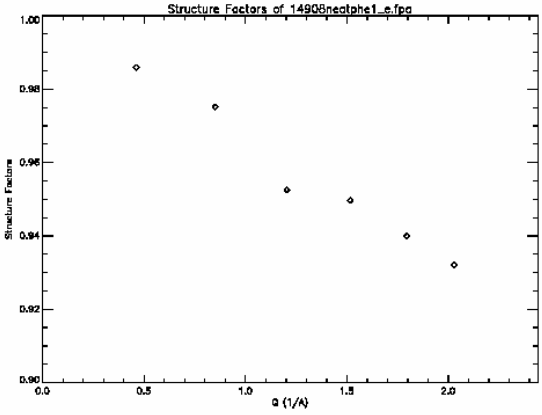

Fig.2: EISF as a function of impulse transfer Q

	EXPERIMENTAL REPORT **Dynamic study on superionic phosphate glasses $(AgI)_x(AgPO_3)_{1-x}$ x=0.0, 0.3, 0.5**	Proposal N° PHY-03-0379 Instrument **V3** Local Contact Margarita Russina
Principal Proposer: Experimental Team:	E. Kartini - R&D Centre for Materials Science and Technology, BATAN, Indonesia F. Mezei - HMI Berlin M. Arai - KEK and JAEA, Japan M. Nakamura - JAEA, Japan	Date(s) of Experiment 17.05. - 04.06.2005

Date of Report: 08. Jan. 2006

Introduction

AgI-doped fast ion conducting glasses have been paid considerable attention for the last few years due to their potential applications as solid state batteries, sensors, fuel-cell, etc. Among superionic glasses, the AgI-$AgPO_3$ system has been extensively studied by different methods, because of its high conductivity up to 10^{-2} S.cm^{-1} at ambient temperature. The conductivity of the insulator glass $AgPO_3$ is ~ 10^{-7} S.cm^{-1}. Its conductivity increases with increasing amount of dopant salts (AgI), and the glass transition decreases [1].

The neutron diffraction and the inelastic neutron scattering methods have been widely used to investigate the structure of the AgI-$AgPO_3$ glasses [2]. So far, there have been only few dynamic studies such as quasi-elastic and inelastic neutron scattering performed on superionic phosphate glasses. In order to have more understanding on the structure and dynamic of the silver phosphate glasses, we performed series of neutron diffraction and the inelastic scattering experiments on series of $(AgI)_x(AgPO_3)_{1-x}$ (x=0.0, 0.3 and 0.5) glasses.

Experimental Procedures

The silver phosphate glasses $(AgI)_x(AgPO_3)_{1-x}$ with x=0.0, 0.3 and 0.5 or AIX00, AIX03 and AIX05) have been prepared by melt quenching method as described elsewhere [3]. The later is a highly conducting glass. The neutron inelastic experiment was performed on V3-NEAT spectrometer at BENSC, HMI, Germany. A selected elastic energy resolution was 187 μeV with an incident wavelength of 4 Å. The 141 detectors were grouped into 27 groups in order to improve the statistic with the momentum transfer Q was from 0.38 to 2.90 Å $^{-1}$. The spectra were converted from time of flight to the scattering function S(Q,ω), where the intensity was normalized to a vanadium standard. Corrections were made from absorption, shelf –shielding, and empty Al can.

Results and Discussions

Fig.1(a) shows the comparison between the static structure factor S(Q) and the elastic structure factor S(Q,ω=0) from $AgPO_3$ and AIX05 glasses. In general, both spectra show similar behaviour. A prepeak at low Q~0.7Å^{-1} appears in AIX05 , but not in $AgPO_3$ glass. The origin of the prepeak is related to the distance between the phosphate chains. The distance increases with the introduction of large I ions into the interchain interstices [2,3]. Figure 1(b) shows the elastic structure factor from AIX05 at temperatures 20 K and 300 K. The main elastic peak intensity decreases with temperature, while the prepeak intensity is temperature resistant. This shows an increase of the long-time (> 10 ps) correlations at the IRO. The prepeak indicatives of some form of intermediate range order with a characteristic length d = 2π/Q ~ 10 Å.

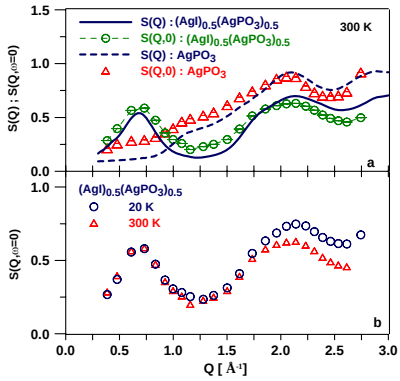

Fig.1:(a) S(Q) and S(Q,ω=0) from $AgPO_3$ and $(AgI)_{0.5}(AgPO_3)_{0.5}$; **(b)** S(Q, ω=0) from $(AgI)_{0.5}(AgPO_3)_{0.5}$ at 20 K and 300 K

Figure 2 shows the dynamic structure factor S(Q,ω) at fixed Q~2.5 Å^{-1} from $AgPO_3$, AIX03 and AIX05 glasses. It is clear that there is an excess vibration at energies around 2-3 meV in all glasses. This called a Boson peak and normally observed in neutron and Raman spectra of glasses. The amplitude of Boson peak correlates with the degree of fragility of the system. The amplitude is high for strong glasses like SiO_2 or B_2O_3 and very weak for fragile systems like CK. Our result suggested the $AgPO_3$ glass that made from glass former P_2O_5 and glass modifier Ag_2O is in the category of a strong glass. The nature of the excess vibrations, the origin, and how the doping salt AgI changes the peak properties are currently subjects of intensive discussion.

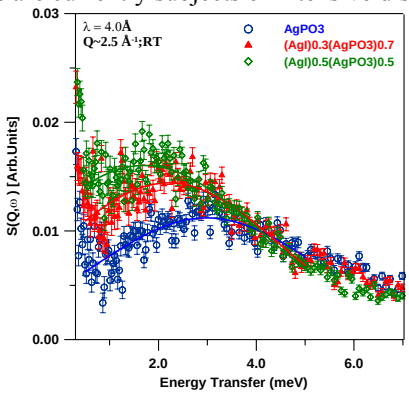

Fig.2: S(Q,ω) from $AgPO_3$ $(AgI)_{0.3}(AgPO_3)_{0.7}$ and $(AgI)_{0.5}(AgPO_3)_{0.5}$ near the Boson-peak (Solid line – Gaussian fit to the Boson peak)

References

[1] M.F. Collins and E.Kartini: Recent Research Developments in Solid State Ionics, **1** (2003) 157

[2] J.D.Wicks, L.Borjesson, G. Bushnell-Wye, W.S. Howells, and R.L. McGreevy: Physical Review Letters **74** (1995) 726

[3] E. Kartini, S. J. Kennedy, K. Itoh, T. Kamiyama, M. F. Collins, S.Suminta: Solid State Ionics **167** (2004) 65

	EXPERIMENTAL REPORT **Low energy dynamics of superionic conductor AgI-Ag_2S-$AgPO_3$ glass**	Proposal N° PHY-03-0381 Instrument **V3** Local Contact Margarita Russina
Principal Proposer: Experimental Team:	M. Arai - JAEA Japan M. Nakamura - JAEA Japan E. Kartini - BATAN Indonesia M. Russina - HMI Berlin	Date(s) of Experiment 17.05. - 27.05.2005

Date of Report: 09.01.2006

One of the most famous unsolved questions in condensed matter science is as follows; "*Why do the disordered structures such as superionic conducting glasses show high ionic conductivity?"* Superionic conducting glasses are also technologically important materials, because they can play a prominent role in many solid electrolyte applications including batteries, sensors, and displays[1].

In this experiment, the phonon dynamics in low energy region for superionic conducting glass was investigated by inelastic neutron scattering measurements using the NEAT spectrometer (V3). We have prepared two samples $(AgI)_{0.33}(Ag_2S)_{0.33}(AgPO_3)_{0.34}$ and $(AgI)_{0.5}(AgPO_3)_{0.5}$ as superionic conducting glasses (σ~10^{-7} S/cm at RT). The insulator glass $AgPO_3$ (σ~10^{-2} S/cm at RT) was also prepared in order to elucidate the characteristic properties of superionic conducting glass. A selected elastic energy resolution was 187μeV by an incident wavelength of 4 Å. The 141 detectors were grouped into 17 groups in order to improve the statistics of data.

We have observed the low-energy excitations of both superionic conducting glass and insulator glass as shown Fig.1. These data were measured at room temperature. It is clear that the superionic glasses have an excess of low-energy intensity compared with insulator glass. The Q dependences of low-energy region between 1 meV and 3 meV for both superionic conducting glass and insulator glass are compared in Fig.2, which clearly indicate that an excess intensity of the superionic conducting glass is caused by unique dynamics in the range beyond 1.8 $Å^{-1}$. We can also observe the peak profile at around Q = 2.2 $Å^{-1}$ only in the superionic conducting glasses. We consider that these unique dynamics in low-energy region should be universal phenomena in silver-salt superionic conducting glasses. A peak at around Q = 2.2 $Å^{-1}$ should be related to a distance in real space by $2\pi/Q$ = 2.8 Å, which can be assigned to Ag-Ag bond length[2]. It seems reasonable to conclude that the silver-salt superionic conducting glasses intrinsically realize the coherent correlation between neighboring silver ions.

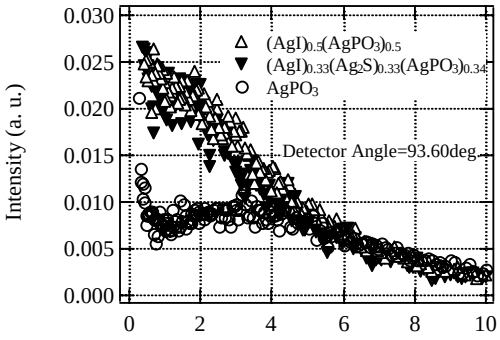

Fig1: The E-dependences of dynamical structure factor are plotted for two types of superionic conducting glasses and one insulator glass.

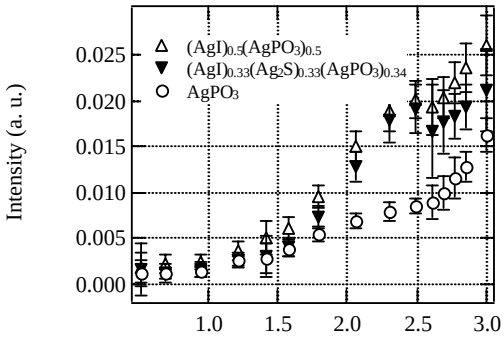

Fig2: The Q-dependences of dynamical structure factor integrated from 1meV to 3meV are plotted for two types of superionic conducting glasses and one insulator glass.

References:

[1] M. Balkanski: Physics World **3** (1990) 29
[2] J.D. Wicks *et al*.: Phys. Rev. Lett. **74** (1995) 726

	EXPERIMENTAL REPORT **Interaction of Dicynthaurin with lipid model membranes**	Proposal N° BIO-01-1689 Instrument **V1** Local Contact Thomas Haußß
Principal Proposer: Experimental Team:	F. Bringezu - University of Leipzig M. Majerowicz - University of Leipzig T. Haußß, S. Dante - HMI Berlin	Date(s) of Experiment 17.05.-02.06.2005

Date of Report: Sept. 2005

In recent work we have applied small angle neutron diffraction to gain insights in the peptide membrane interaction of antimicrobial peptides using supported lipid bilayers as model system. Our study was focused on Cynthaurin – an antimicrobial peptide from hemocytes of a tunicate, *halocynthia aurantium*. Lipid peptide interactions are of high significance for the recognition of the target membrane. They are responsible for the mode of action of the bacteria membrane perturbation of that finally leads to cell death because of leakage. The structure of active peptides, however, is diverse thus different mechanisms of membrane perturbation are discussed.

To get an insight in the structural details of the interaction of Cynthaurin with bacterial membrane lipids, measurements were performed on lipid bilayers composed of a POPC/POPG (3/1 mol/mol) mixture (**1**) and subsequent mixtures with the peptide dimer CAD (**2:** 0.5 mol%, **3**: 1 mol%) and partially deuterated dimer samples synthesized using per-deuterated alanine.

Oriented samples were obtained by slightly dropping the aqueous dispersions on quartz slides (65 x 15 x 3 mm), removing the solvent in vacuum (12 h) and final rehydration for 24 h at room temperature at 98 % humidity maintained by K_2SO_4 solution. Contrast variation was achieved by adjusting the atmosphere in the sample chamber at three different H_2O/D_2O compositions (50 %, 20 % and 8 % D_2O). The diffraction intensities were measured up the 5'th order of the lamellar spacing at 20 °C. The sample quality was proofed by measuring the mosaicity using rocking scans. Sample **1** shows a mosaicity of ~ 0.25 ° indicating the excellent sample quality. With increasing peptide concentration in samples **2** and **3** the mosaicity increases suggesting a strong disturbance of the long range order between adjacent layers.

Fig. 1 compares the diffraction patterns obtained for **1**, **2** and **3**, respectively. The pure lipid, sample **1,** shows five orders of the lamellar spacings. From the peak positions a d-value of 55 Å can be calculated. Samples **2** and **3** show slightly changed diffraction patterns, exhibiting lower intensities with increasing peptide concentration. Consequently, only the first three orders can be observed. In addition intensities at small angle below the first order reflection occur, that are more pronounced at larger peptide concentration (Samples **2** and **3** , *middle* and *bottom*).

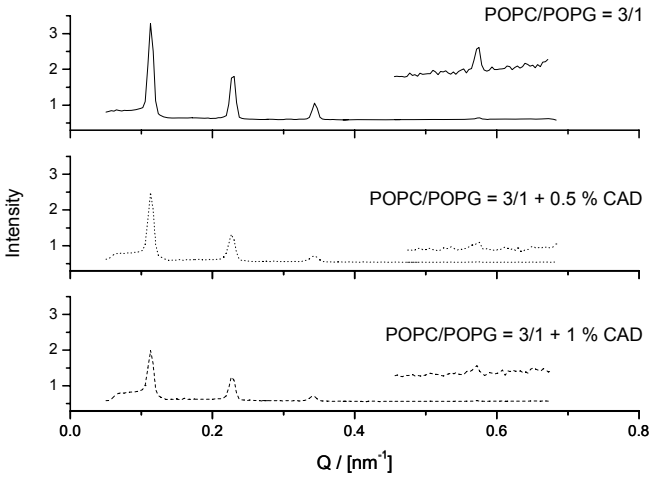

Fig. 1

Such findings suggest that the peptide interacts with the model membrane by forming lipid membrane complexes of a larger dimension compared to the lipid bilayer. However, these intensities are only observed below the first order reflection and do not show up at higher orders, suggesting a lack of long range order. Further analysis based on isomorphous replacement yielded the phased structure factors as plotted in **Fig. 2**

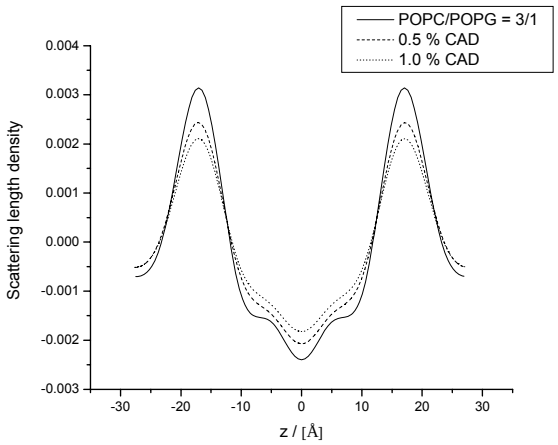

For the lipid, the typical membrane profile was obtained. Upon addition of peptide, this profile becomes much less pronounced which can by associated with the disturbance of the lipid bilayers caused by the antimicrobial peptide. Further analysis will be performed with the data on the deuterated samples to get more details on the peptide orientation upon binding.

BENSC	**EXPERIMENTAL REPORT** **Investigation of deuterium labeled model stratum corneum lipid membranes**	Proposal N° BIO-01-1690 Instrument **V1** Local Contact Thomas Hauß
Principal Proposer: Experimental Team:	M. Kiselev – FLNP, JINR, Dubna, Russia. D. Otto, B. Dobner, R. Neubert - MLU, Halle N. Ryabova - FLNP, JINR S. Dante, T. Hauß - HMI Berlin	Date(s) of Experiment 5.04-19.04.2005

Date of Report: 29.04.2005

Mixed quaternary systems composed of ceramide 2/ cholesterol/ palmitic acid/ cholesterol sulfate with component ratio about 55/25/15/5 (w/w) were characterized by neutron diffraction with protonated and deuterated cholesterol (cholesterol D6 and cholesterol D7). Ceramide 2 has been synthesized at Martin Luther University (Halle). Samples were prepared as oriented multilamellar film of lipids on the quartz substrate. Diffraction pattern was collected as rocking curves measured at appropriate scattering angles 2θ. Samples were equilibrated at 60% humidity of water with 8%, 20%, and 50% D_2O. Diffraction pattern in Fig. 1 demonstrates two lamellar phases: cholesterol poor (La, d=58.2 Å) and cholesterol rich (Lb, d=41 Å) phases and reflection 010 from pure cholesterol crystals. It was shown by neutron diffraction that percentage of cholesterol crystallites depends on the type of the ceramide. Cholesterol is less soluble in the ceramide 2 based membranes relative to that of ceramide 6.

Diffraction patterns from binary DPPC/ceramide 6 system with protonated DPPC and deuterated DPPC_d75 were recorded at molar ratio of the ceramide 6: 0, 0.32, 0.5. Fig. 2 presents five diffraction orders recorded from DPPC/ceramide 6 film. Obtained results will be used for the Fourier synthesis of the neutron scattering length density profile and in-depth analysis of bilayer structure. Preliminary neutron diffraction and small-angle scattering results shows that ceramide 6 increases intermembrane attractive forces. The water spacing decrease on the value of 4 Å at 32% of ceramide 6, relative to that of pure DPPC. More systematic study of ceramide 6 induced increasing of the intermembrane attractive forces planes to carry out at second part 2005 (proposal BIO_01_1800).

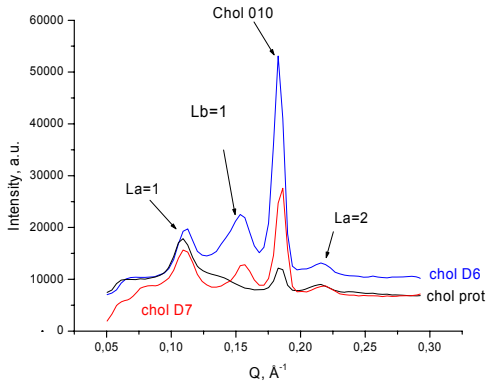

Fig. 1. Rocking curves of quaternary systems with protonated (black) and deuterated (blue and red) cholesterol. Humidity 60%, 20% D_2O, T=20 ^oC.

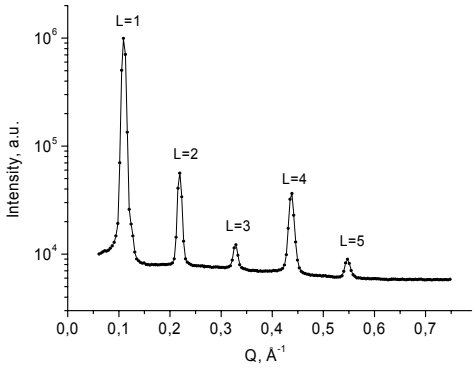

Fig. 2. Diffraction pattern from mixed DPPC/ ceramide 6 multilamellar film at 32% of molar ceramide 6 concentration. Humidity 60%, 50% D_2O, T=20^{o}C. Repeat distance d=57.5 Å.

References:

1. B.H.S. Shien, L. G. Hoard, C.E. Nordman. The structure of cholesterol. Acta Cryst. B37 (1981) 1538-1543.
2. M.A. Kiselev, V. Haramus, R. Neubert. Structural investigation of mixed DPPC /ceramide 6 vesicles. GKSS experimental report 2004.

	EXPERIMENTAL REPORT **Effect of cholesterol on the penetration of Alzheimer's peptide Aβ(25-35) into lipid membranes**	Proposal N°BIO-01-1727-LT BIO-01-1841-LT Instrument **V1** Local Contact Silvia Dante Thomas Hauß
Principal Proposer: Experimental Team:	S. Dante - HMI Berlin S. Dante - HMI Berlin T. Hauß - TU-Darmstadt, HMI Berlin N. Dencher - TU-Darmstadt	Date(s) of Experiment 07.03. - 24.03.2005 07.09. - 25.09.2005

Date of Report: 26.01.2006

The physiological relationship between brain cholesterol content and the action of amyloid β (Aβ) peptide in Alzheimer's disease (AD) is a highly controversially discussed topic. Evidences for modulations of the Aβ/membrane interaction induced by plasma membrane cholesterol have been already observed. We have recently reported that Aβ(25-35) is capable to insert in lipid membranes, either negatively charged or zwitterionic, and to perturb their structure. Applying neutron diffraction and selective deuteration, we have now investigated the the capability of Aβ(25-35) to penetrate into lipid bilayers in the presence of cholesterol.

Lipid multilayers containing POPC and POPS in a relative ratio of 92:8 and cholesterol in different amount were investigated; in particular, samples containing cholesterol in a ratio of 1, 5, 20 and 40% molar with respect to the total lipid amount were prepared. Some of the samples had already been investigated previously and have been repeated to check the reproducibility of procedure for the sample preparation and of the results. The peptide, either not-deuterated (H-Leu34-Aβ(25-35)) or selectively deuterated (^{2}H-Leu34-Aβ(25-35)) was added to the dissolved lipids in a P/L molar ratio of 1:33. The lipid-peptide mixtures (20 mg) were sprayed with an artist airbrush onto quartz slides (65 mm x 15 mm x 1 mm). Samples consisting of POPC/POPS and POPC/POPS/cholesterol were prepared as well, as references. The samples were dried under vacuum for 12 hours and re-hydrated in a chamber at a relative humidity of 98% maintained by an aqueous saturated solution of K_2SO_4. Samples prepared in this way consisted of about 2000 membrane layers and after hydration had a thickness of 1 μm.

The samples were placed vertically in an aluminum container at controlled temperature (T = 25.0 ± 0.1 ^{o}C) and relative humidity (r.h. 98%). After reaching the thermodynamic equilibrium condition, the diffraction patterns of POPC/POPS/cholesterol bilayers, and of POPC/POPS/cholesterol bilayers containing either 3% (mol) (^{2}H-Leu34)-Aβ(25-35) or 3% (mol) (H-Leu34)-Aβ(25-35) were measured by rocking the samples around the expected Bragg position θ by θ ± 2^o. Up to 5 lamellar orders for each sample were measured. After background subtraction, the experimental Bragg reflections were fitted to Gaussians to obtain the integrated intensities. Scaled intensities, corrected with absorption and Lorentz factors, were square-rooted to produce the structure factor amplitudes F(h). The Fourier synthesis of the structure factors allowed reconstructing the scattering length density profiles ρ(z). The structure factor phase assignment was obtained with the isomorphous replacement methods, using the D_2O/H_2O exchange at three different ratios (8:92; 20:80; 50:50).

The scattering length density profiles of the membranes containing deuterated and protonated Aβ(25-35) in the presence of different amount of cholesterol were calculated and, from their difference, the deuterated label was localized. It was found that, depending on its concentration, cholesterol inhibits the penetration of Aβ(25-35) in the lipid bilayers. For molar concentration of cholesterol as low as 1%, the peptide was found in the same position as in the POPC/POPS membrane not doped with cholesterol, i.e. in the hydrocarbon region of the bilayer. At cholesterol concentration equal or higher than 5% molar, Aβ(25-35) does not penetrate the lipid membrane.

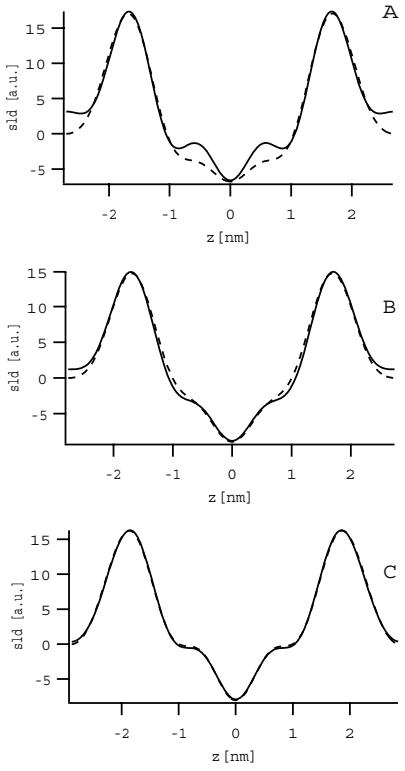

Fig.1: Scattering length density profiles (sld) of lipid membranes in the presence of H-Leu34-Aβ(25-35) (dashed line) and of ^{2}H-Leu34-Aβ(25-35) (solid line) at 1% (A), 5% (B) and 20% (C) cholesterol molar.

	EXPERIMENTAL REPORT **Lamellar diffraction of spin-labelled membrane protein Colicin A**	Proposal N° BIO-01-1731-DT Instrument **V1** Local Contact Thomas Hauß
Principal Proposer: Experimental Team:	K. Lieutenant - ILL, France E. Bordignon - Universität Osnabrück L. Pulagam - Universität Osnabrück	Date(s) of Experiment 19.-22.04.2005

Date of Report: 09.01.2006

During the experiment we found that the sample preparation had not worked. The membranes did not form parallel layers, thus the method used to determine the structure of membrane proteins from V1 measurements could not be applied.

Additionally, the measurements were stopped before the planned end of the beam-time by a shutdown of the reactor on 22. April 2005.

Therefore the experiment did not yield any result concerning the protein structure, i.e. there is nothing that could be published.

The sample preparation procedure is going to be improved. But maybe it is advantageous to use reflectometry instead of diffraction for this investigation in the future.

	EXPERIMENTAL REPORT **Membrane-binding of the N-terminus of annexin A1**	Proposal N° BIO-01-1797 Instrument **V1** Local Contact Thomas Haußß
Principal Proposer: Experimental Team:	J.P. Bradshaw - University of Edinburgh A. Hofmann - University of Edinburgh N.-J. Hu - University of Edinburgh T. Haußß - HMI Berlin	Date(s) of Experiment 16.10.05 – 01.11.05

Date of Report: 16.12.05

Annexins are a large family of membrane-binding proteins. As part of an on-going study of annexin structure and interactions, we have carried out neutron diffraction measurements of the membrane-interaction of a peptide representing the N-terminus of annexin A1 (AnxA1).
These studies are contributing to an understanding of the molecular details of the protein-phospholipid interaction and of the role that membrane-binding plays in the function of this protein.

The huge family of annexin proteins shares a characteristic topology, calcium-binding sites, flexible loops and the overall shape which is constituted by the slightly curved core and the amino-terminal tail on the concave side of the molecule (for a recent review see Hofmann & Huber, 2003). These well-defined properties are contrasted by an enormous variety of possible functions and involvements in physiological pathways. Annexins share the characteristics of peripheral membrane-binding proteins. Their characterising feature is the binding to the surface of membranes containing acidic phospholipids. This process is calcium-mediated in the case of vertebrate members of this protein family.

Evidence collected over the last 25 years suggests that this is also the place where annexin carry out their functions. Despite being cytosolic proteins, annexins seem to fulfil their physiological functions in membrane-bound states or by the timed attachment to or desorption from membranes. In order to understand AnxA1 function in inflammatory diseases as well as normal cellular processes, it is necessary to clarify the molecular mechanisms of membrane-bound AnxA1. Several crystal structures of AnxA1 have been solved, revealing that (i) the N-terminal can adopt α-helical structure and (ii) the protein can adopt a “closed” and “open” conformation, where the N-terminal domain is either fold back into the core or exposed on the concave side (for a review see: Rosengarth & Lücke, 2003). Two different structural models of the membrane aggregation activity of AnxA1 can be proposed (see figure).
With the aim of structural characterisation of AnxA1 aggregation and fusion properties, we have embarked on a series of neutron diffraction measurements. Important variables will be the length of the peptide (which will relate to crucial residues for membrane interaction), the phosphorylation state and the bilayer composition.

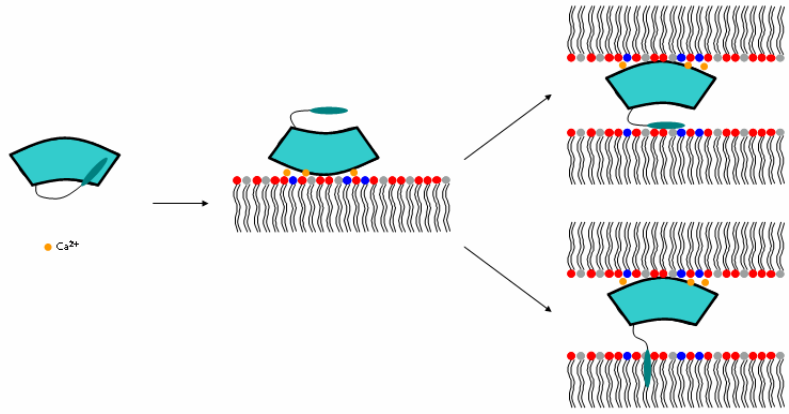

Figure: Calcium-dependent membrane binding of AnxA1 leads to a conformational change from the “closed” to the “open” state. Interactions with an adjacent membrane surface might be achieved either by annealing or insertion of the N-terminal helix.

Using the V1 instrument, lamellar neutron diffraction data were collected from a peptide representing the N-terminus of AnxA1, in stacked phospholipid bilayers at 1% peptide. The lipids, DMPC and DMPS in a 3:1 molar ratio, were also run in the absence of peptide, to act as a control. Four different relative humidity/D2O concentration combinations were used and each sample was replicated using deuterated DMPC in the lipid mixture. These data are currently under analysis.

References

Hofmann, A. & Huber, R. (2003) In: *Annexins: Biological importance and annexin-related pathologies*.
Rosengarth, A. & Lücke, H. (2003) In *Annexins: Biological importance and annexin-related pathologies*

	EXPERIMENTAL REPORT **Orientation dependence of the structural flexibility of granal thylakoid sample: thylakoid membranes (isolated from plant leaves)**	Proposal N° BIO-01-1798 BIO-01-1799 Instrument **V1** Local Contact Silvia Dante
Principal Proposer: Experimental Team:	G. Garab - HAS BRC Szeged, H G. Garab - HAS BRC Szeged, H S. Krumova - HAS BRC Szeged, H S. Dante - HMI Berlin, TU Darmstadt	Date(s) of Experiment 25.07. – 27.07.2005 31.10. – 06.11.2005

Date of Report: Jan. 2006

The major aim of the experiment was to measure the mosaicity of isolated membranes, which were oriented in a magnetic field and dried under controlled degree of humidity. The mosaicity data are to be used for interpreting the quasi elastic neutron scattering experiments at V3.

Isolated chloroplast thylakoid membranes were loaded in thin layers on Aluminum plates, and inserted into the magnet (VM5 superconducting magnet, AS Scientifi products Ltd). The vertical field of 2.0 T oriented the membranes. During drying, for about 16 hours, this orientation state could be trapped.

The humidity of the samples was adjusted by placing the samples into an exsiccator containing a saturated salt solution – different relative humidity values could be obtained by using different salts. In order to obtain better contrast, the solutions were made in D_2O.

The experiments revealed that: (i) for thylakoid membranes, the relative humidity of 75-90 %, cannot be applied because the samples, especially in vertical position (for QUENS), lose their orientation and often slide from the plate; (ii) for intact thylakoid membranes, the maximum relative humidity was 60 % - this was probably related to the high water content of the lumen; (iii) isolated membranes enriched in photosystem II (BBY subchloroplasts particles) could be orineted and dried in a similar way as intact thylakoid membranes; (iv) BBY membranes, obtained from grana, due to clevage of the margin by detergent, and membrane fusion, lose their lumen; hence, a much higher relative humidity can be obtained in the oriented membranes; (v) rocking curve experiments revelaed that BBY samples oriented and dried in a chamber, placed to 2T, with a relative humidity between 57 and 75 % exhibited a sufficiently high mosaicity for QUENS experiments.

	EXPERIMENTAL REPORT **The interaction of the antibiotic peptide KLA1 with neutral model membranes**	Proposal N° PHY-01-1599 Instrument **V1** Local Contact Thomas Haußß
Principal Proposer: Experimental Team:	B. Klösgen - Univ. Odense, DK B. Klösgen - Univ. Odense, DK M. Dathe - FI Mol. Pharm. Buch T. Haußß - HMI Berlin, TU DA	Date(s) of Experiment 20.06. - 03.07.2005

Date of Report: Feb. 2006

KLA1 is an amphiphilic artificial peptide of 18 residues that resembles the natural toxin magainin in its physico-chemical properties and its antibiotic efficiency for gram-negative bacteria. Its working mechanism is probably an increased membrane permeability induced to the lipid bilayer as the peptide spontaneously precipitates into the membrane from its aqueous solution.

The permeability increase had been confirmed by micromechanical experiments that as well exhibited an extreme weakness of the peptidized bilayer upon expansion to the extent that no related modules could be measured, even down to an aqueous peptide concentration of the nM range. In dynamic expansion studies the membranes showed a pronounced decrease of the failure tension as compared to control membranes free of KLA1.

Diffraction experiment performed at HMI gave evidence of the general structural stability of the bilayer conformation: there was no indication of a transition into another lipid phase up to mM peptide concentration in the bilayer!

Therefore, new studies were performed in spring (at D16, ILL, Grenoble, France) and summer 2005 (at V1, HMI, Berlin, Germany) to acquire information on the average position that the peptide resumes as it inserts into the lipid phase.

Specifically deuterated KLA1 varieties (L2, L8, L17) were synthesized at MDC (Berlin-Buch) and embedded to test membranes composed of pure POPC and of a mixture of lipids as of 5% POPG in POPC (mol/mol). The slight surface charge of 5% was chosen different from the initial plans in order to provide a more biomimetic interface for the cationic peptide. The intended peptide concentration in the membrane was set to 3mol%, and diffraction experiments were performed at different D_2O/H_2O compositions, namely at 0%, 8%, 20%, 30%, and 50% (all mol/mol).

At ILL, a vapour equilibration chamber was used to set the relative humidity to 98%, at HMI a thin chamber for liquid equilibration could be used. Both institutions allowed to gather diffraction data over five orders of magnitude.

Results from both experimental series are being combined to yield the phase information and then deduct the scattering profile shift that is due to the insertion of the peptide into the membrane. Detailed results will be reported in a related paper.

BENSC	**EXPERIMENTAL REPORT** **Negative solubility coefficient and dynamics of hydrophobic interactions in aqueous solutions of native and methylated Cyclodextrins**	Proposal N° BIO-03-0370 Instrument **V3** Local Contact Alexandra Buchsteiner
Principal Proposer: Experimental Team:	R.E. Lechner - Int. Graduate School FU Berlin T. Aree - Univ. Bern, CH + FU Berlin A. Kouzmine - FU Berlin, Inst. für Krist. W. Saenger - FU Berlin, Inst. für Krist.	Date(s) of Experiment 05.04. - 10.04.2005

Date of Report: 04.01.2006

The α-, β- and γ-cyclodextrins (CDs) are a family of cycloamyloses composed of 6, 7 and 8 α(1-4) linked D-glucoses, respectively [1]. If the glucoses of the CDs are per-dimethylated at all their O2 and O6 (Fig. 1) or per-trimethylated at all their O2, O3, O6, the solubility coefficients of the methylated CDs (mCDs) for water become negative, i.e. they are better soluble in cold than in hot water, where they finally crystallize and precipitate. Unmethylated CDs show the usual positive solubility coefficient in water. We assume that at low temperatures, the mCDs feature well-ordered hydration shells and are therefore so soluble. At higher temperature, water molecules become more mobile and the ordered hydration breaks down so that the hydrophobic mCD molecules start to aggregate.

Fig. 1 β-CD DIMEB

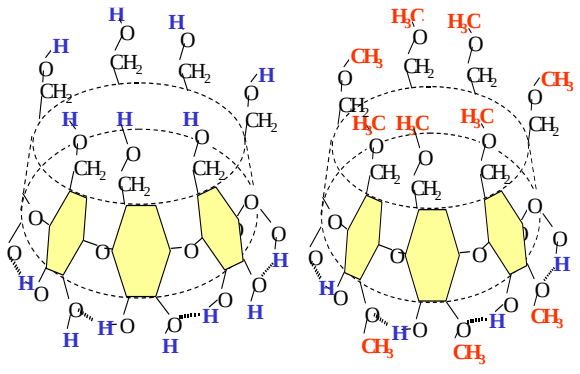

In the course of the NEAT experiment we recorded QENS spectra of heavy water and of solutions of β-CD and DIMEB in D_2O (9.0 and 53.0 mg/ml, respectively) in the temperature range 280 – 316 K. Incident neutron wavelength: 5.1 Å; Q – range: 0.3 - 2.3 $Å^{-1}$; energy resolution (FWHM) ≈ 90 μev; the corresponding observation time is about 10 ps, so that the translational motion of water molecules can be studied directly. Fig.2 illustrates the presence of effects due to hydration water. For Q > 1 A^{-1}, the β-CD spectrum at 280 K only slightly differs from the corresponding D_2O spectrum. At 316 K the difference in the spectra is more pronounced – the difference in the low-energy dynamics of bulk and hydration water increases. The same can be seen in the case of DIMEB. To extract information on hydration water, a subtraction of the bulk water contribution from the measured spectra is required.

Fig. 2

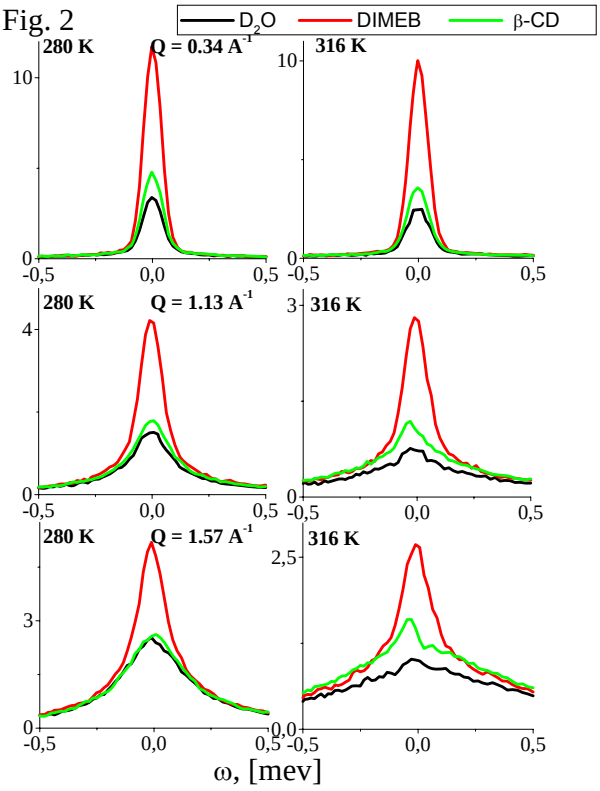

In order to achieve this with an appropriate, theoretically sound weighting, a detailed anylysis is under way, taking into account explicitly the translational and rotational dynamics of the bulk water solvent, hydration water and cyclodextrin solute molecules.

Reference

[1] W. Saenger, J. Jacob, K. Gessler, T. Steiner, D. Hoffmann, H. Sanbe, K. Koizumi, S. M. Smith, T. Takaha: Chem. Rev. **98**, (1998), 1787-1802

	EXPERIMENTAL REPORT **Protein dynamics in the light-harvesting complex II of green plants**	Proposal N° BIO-03-0371 Instrument **V3** Local Contact Jörg Pieper
Principal Proposer: Experimental Team:	K.-D. Irrgang - Max-Vollmer-Institut, TU Berlin J. Pieper - HMI Berlin K.-D. Irrgang - Max-Vollmer-Institut, TU Berlin	Date(s) of Experiment 21.02. - 26.02.2005

Date of Report: 09. Jan. 2006

The photosynthetic Chlorophyll (Chl) a-, Chlorophyll b-, carotenoid-binding protein complex LHC II is the major antenna complex of plant thylakoid membranes. Its main function is to absorb light in a broad spectral range as well as to efficiently transfer excitation energy to the photochemical reaction center, where charge separation takes place and electron transfer is initiated.

While Chl b → Chl a excitation energy transfer in LHC II is only weakly temperature-dependent [1], pigment-protein interactions seem to strongly affect the electronic energy level structure of this antenna complex [2]. Briefly, an unexpected red-shift of LHC II fluorescence above 120 K suggests that conformational changes and the onset of diffusive protein motions may affect both, the pigment-protein interactions as well as excitonic coupling between the pigments. Thus the present experiment was aimed at studying the nature of the protein dynamics of LHC II in the relevant temperature range.

For QENS experiments, a special large scale preparation protocol was developed based on our standard method [3] for ensuring that trimeric LHC II is completely solubilized in a D_2O containing buffer and reducing the solvent scattering significantly. Solubilized LHC II and the buffer solution were separately investigated in order to subtract the solvent contribution as reported in [4].

QENS spectra of solubilized LHC II were measured at temperatures between 5 and 300 K. The experiments were carried out using an incident neutron wavelength of 5.1 Å and an elastic resolution of 93 µeV on NEAT. Corresponding SANS measurements were employed at four representative temperatures using the multidetector of NEAT to characterize the gyration radius of trimeric LHC II.

The mean square displacement for LHC II clearly increases with increasing temperature as was calculated from the elastic scattering intensity. This linear increase for T < 120 K is characteristic for vibrational motions (range A) while there is a stronger increase for T > 120 (range B) and 240 K (range C) due to the onset of large amplitude motions. The observed transition temperatures correlate well with the above-mentioned fluorescence behavior.

Acknowlegdement

Financial funding by the DFG (SFB 429, project A3) is gratefully acknowledged.

References

[1] Bittner, T.; Wiederrecht, G. P.; Irrgang, K.-D.; Renger, G.; Wasilewski, M. R.: Chem. Phys. **194**, (1995), 311

[2] Pieper, J.; Schodel, R.; Irrgang, K.-D.; Voigt, J.; Renger, G.: J. Phys. Chem. B. **105**, (2001), 7115

[3] Irrgang, K.-D.; Boekema, E. J.; Vater, J.; Renger, G.: Eur. J. Biochem. **178**, (1988), 209.

[4] Pieper, J.; Irrgang, K.-D.; Renger, G., Lechner, R. E.: J. Phys. Chem. B. **108**, (2004), 10556.

	EXPERIMENTAL REPORT **Thermo-optical rearrangements in the thylakoid membrane of green plants**	Proposal N° BIO-03-0372 Instrument **V3** Local Contact: Jörg Pieper
Principal Proposer: Experimental Team:	G. Garab - BRC Szeged G. Garab - S. Krumova - BRC Szeged K.-D. Irrgang - Max-Volmer-Institut, TU Berlin J. Pieper - HMI Berlin	Date(s) of Experiment 18.03. – 24.03.2005

Date of Report: 29.03.2005

Structural flexibility of the thylakoid membrane is essential in the temperature and light adaptation mechanisms of plants. There are light-induced structural reorganizations within the thylakoid membrane leading to a monomerization of the trimeric light harvesting complex of photosystem II (LHC II) [1,2]. These reorganizations are approximately linearly proportional to the light intensity above the saturation of photosynthesis. Therefore, this process is most probably an important mechanism in photoprotection of plants. To gain further evidence for a correlation between structural changes in the lipid phase [3] and the monomerization of LHC II, we have investigated the dynamics of intact thylakoid membranes in solution and trimeric LHC II in the temperature range of 200 – 335 K and upon *in-situ* light illumination.

QENS spectra of isolated (trimeric) LHC II obtained with an incident neutron wavelength of 5.1 Å (~3.2 meV) and an elastic energy resolution of 93 µeV indicate an increased flexibility upon temperature increase and, especially, upon *in-situ* illumination with laser light at 532 nm at constant temperature (see Fig. 1). These effects may indicate monomerization as shown by a separate study of monomeric and trimeric LHC II (BIO-03-371). In addition, analysis of specific inelastic features and complementary SANS data obtained simultaneously with the NEAT multidetector will provide more information on the extend of LHC II monomerization.

Initial QENS measurements on thylakoids showed a contribution from non-exchanged H_2O (see line A in Fig. 2). Therefore, the samples were re-treated following a protocoll adapted from ref.[4]. The resulting angle spectrum (line B in Fig.2) reveals a significant improvement of the sample quality, i.e. a total incoherent scattering consistent with the thylakoid content and a clear coherent contribution from D_2O. Unfortunately, the necessary preparative effort led to a shortage of beam time, so that it was only possible to carry out experiments for a control and a temperature treated sample. Thus, we would like to re-apply to complete our measurements on improved thylakoid samples.

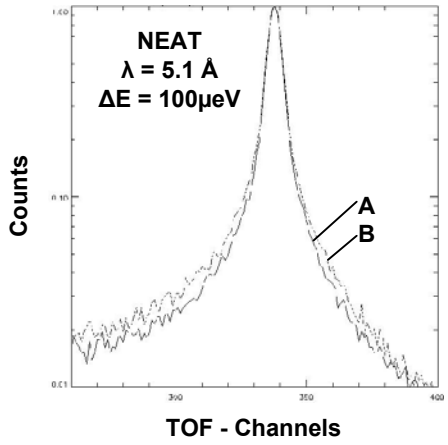

Figure 1
QENS spectra of trimeric LHC II at 293 K obtained in the dark (A, lower line) and with in-situ illumination at 532 nm (B, upper line).

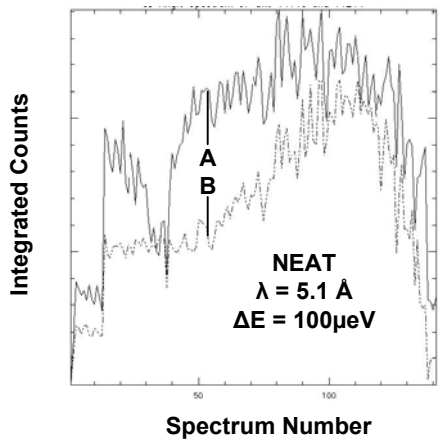

Figure 2
Angle spectra (integrated counts) of thylakoid membranes in buffer solution before (A) and after (B) treatment according to ref. [4].

References:

[1] Garab et al.: 1988, Biochemistry 27, 2430
[2] Dobrikova et al.: 2003, Biochemistry 42, 11272
[3] S. Krumova, C. Dijkema, G. Garab, H. van Amerongen: submitted
[4] Pieper, J.; Irrgang, K.-D.; Renger, G.; Lechner, R.E.: J. Phys. Chem. B (2004), 108,10556

	EXPERIMENTAL REPORT **Directional dynamics in DMPC membranes containing gangliosides**	Proposal N° BIO-03-0403 Instrument **V3** Local Contact Jörg Pieper
Principal Proposer: Experimental Team:	L. Cantu - University of Milano, I F. Natali - CNR, c/o ILL, Grenoble, F A. Deriu - University of Parma, I	Date(s) of Experiment 01.11. - 06.11.2005

Date of Report: 22.12.2005

A particular class of biological sugar containing molecules is that of gangliosides, glycolipids abundant in neuronal plasma membranes. They are
suggested to play a key role in process like protein binding, cell recognition and signal transduction, while being embedded in membrane microdomains. The experiment at BENSC was conceived within a long-term study concerning the effect induced by small amounts of gangliosides molecules on the dynamics of oriented membranes of DMPC. The investigation is intended to clarify the hypothesis, drawn on the basis of previous experimental results with a multi-technique approach, that they are able to establish an extended network of interactions, and then that gangliosides play a central role in the coordination of the structure and dynamics of their environment.
Previous incoherent elastic neutron scattering experiments, recently performed on the high-resolution backscattering spectrometer IN13 at ILL (Grenoble/France), have revealed interesting features concerning the dynamics of low-hydration lamellar systems containing gangliosides. The IN13 elastic experiments were performed over a wide temperature range, form the harmonic regime, typically found at low temperature, up to the gel-liquid lipid phase transition, occurring (for low-hydration DMPC) at ~ 320 K and more. Our results indicate that while no anisotropy and GM1-dependence is observed in the low T region, an abrupt increase of the mean square displacement, as calculated from the Q dependence of the elastic intensity at low Q, observed for T > 320 K, accounts not only for a much higher lipid dynamics in the liquid phase, which is normally expected, but also for a strong anisotropic effect. Both features are present in the naked and in the mixed systems. Nevertheless, the extent and characteristics of the transition depend on the presence of GM1. The choice of proposing an experiment on the NEAT/V3 instrument was justified by the experimental observation of the pronounced dynamics in the IN13 time domain, which suggested that a quasi-elastic component should be clearly observed even at lower energy resolution.
Both naked DMPC and mixed DMPC+GM1 systems were investigated. The recently increased flux available on NEAT allowed to perform quasi-elastic scans, with an incident 6A beam, at 3 different temperatures, namely 290 K, ~310 K e 340 K, with a counting time of 8 hours per scan. The choice of the three temperatures is intended to investigate the effect induced by the presence of gangliosides molecules on membrane dynamics across the gel-liquid membrane phase transition. The experiment was done at 2 different orientations of the sample with respect to the incoming beam to evidence the appearing of anisotropic motions. As far as the actual V3 results are concerned, data reduction has been already performed and the analysis is now under progress.
The expected results will provide unique complementary information on the results previously observed in a slower time scale (~100 ps).
Indeed, the previous incoherent elastic neutron scattering experiments performed on IN13 at ILL have shown that the presence of gangliosides induces a clear increase in anisotropy, dampening the mean square displacement in out-of-plane direction, and in a kink mainly affecting the in-plane curve at temperatures slightly lower than 300 K, as if a double process is taking place. The presence of domains enriched in gangliosides could provide the clue for a reasonable interpretation of these results.

	EXPERIMENTAL REPORT **Hydrophobic interactions: Aggregation behaviour of native and methylated Cyclodextrins in aqueous solutions**	Proposal N° BIO-04-1090 Instrument **V4** Local Contact Martin Kammel
Principal Proposer: Experimental Team:	R.E. Lechner - Int. Graduate School FU Berlin T. Aree - FU Berlin, Inst. für Krist. A. Kouzmine - FU Berlin, Inst. für Krist. W. Saenger - FU Berlin, Inst. für Krist.	Date(s) of Experiment 21. 01. - 25. 01. 2005

Date of Report: 30.01.2006

The α-, β- and γ-cyclodextrins (CDs) are a family of cycloamyloses composed of 6, 7 and 8 α(1-4) linked D-glucoses, respectively [1]. If the glucoses of the CDs are per-dimethylated at all their O2 and O6 (Fig. 1) or per-trimethylated at all their O2, O3, O6, the solubility coefficients of the methylated CDs (mCDs) for water become negative, i.e. they are better soluble in cold than in hot water, where they finally crystallize and precipitate. Unmethylated CDs show the usual positive solubility coefficient in water. We assume that at low temperatures, the mCDs feature well-ordered hydration shells and are therefore so soluble. At higher temperature, water molecules become more mobile and the ordered hydration breaks down so that the hydrophobic mCD molecules start to aggregate. Aggregation of CD and mCD has been studied by DSC [2] and light scattering [3], but these methods are not sensitive to the possible changes in hydration shell.

Fig. 1: β-CD DIMEB

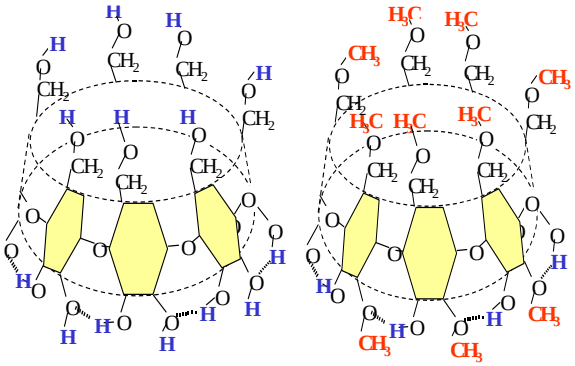

In the course of the experiment we recorded SANS spectra of solutions of β-CD and DIMEB in D_2O (9.0 and 45.2 mg/ml, respectively) in the temperature range 293 – 333 K at the sample – detector distances of 1, 4 and 16 m. The small angle scattering from β-CD solution had low intensity, due to low concentration and weak contrast. Scattering of DIMEB at 1 and 4 m detector distance (Q range 0.15-3.5 nm^{-1}) was recorded with good statistics. Upon heating the sample, the SANS intensity first rises. But then, between 45° and 50°, it starts to drop again (T=23.5-60°C, with 5° steps, see Fig. 2):

Fig. 2 SANS of DIMEB in D_2O

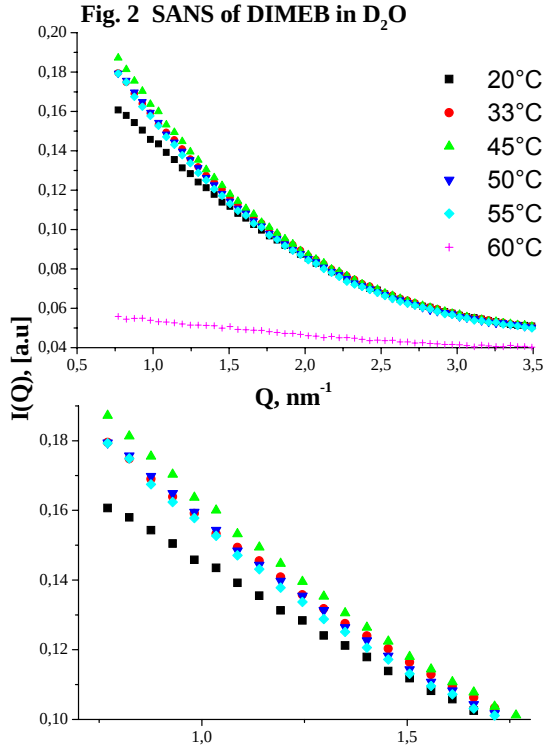

Crystallization occurs above 55°C. We repeated the measurement with 1° T-steps from 39° to 50 °C, and found reproducibility.

Changes in the intensity can be either due to the modification of the hydration pattern or due to the appearance of di-, tri-, etc. oligomers. A detailed analysis combining SANS and QENS data (from NEAT) is under way.

References

[1] W. Saenger, J. Jacob, K. Gessler, T. Steiner, D. Hoffmann, H. Sanbe, K. Koizumi, S. M. Smith, T. Takaha: Chem. Rev. **98**, (1998), 1787-1802

[2] J. Frank, J. F. Holzwarth and W. Saenger: Langmuir **18**, (2002), 5974-5976

[3] P.Umbach, Y. Georgalis and W. Saenger: JACS **118**, (1996),9314-9319

	EXPERIMENTAL REPORT **Neutron imaging of water uptake in plants**	Proposal N° BIO-04-1170 Instrument **V7** Local Contact Nikolay Kardjilov
Principal Proposer: Experimental Team:	U. Matsushima - Iwate University, JP N. Kardjilov - HMI Berlin W. Herppich, - ATB Potsdam A. Hilger - HMI Berlin	Date(s) of Experiment 20.09. - 23.09.2005

Date of Report: 09.01.2006

Background

A novel application was used to measure water flow in tomato seedlings. We employed D_2O, which has a smaller mass absorption coefficient than H_2O, as a tracer.

Materials and Methods

Tomato seeds (Var. Harzfeuer) were sown on sand. After they had 2 or 3 true leaves, each seedling was transplanted to a soda glass beads medium in a quartz glass tube. At about one month, seedlings were employed as samples. Cold neutron radiography (CNR) was conducted at V7, HMI. Teflon lids were fitted to both ends of the glass tube. A lid for top had a soda glass tube to observe water uptake by the sample. The other lid had vinyl tube connected to the D_2O and H_2O bottles (Figure 1). D_2O and H_2O were added from the bottles to the sample one after the other. During the experiments, CNR images were taken every 15 seconds with an exposure time was 10 seconds.

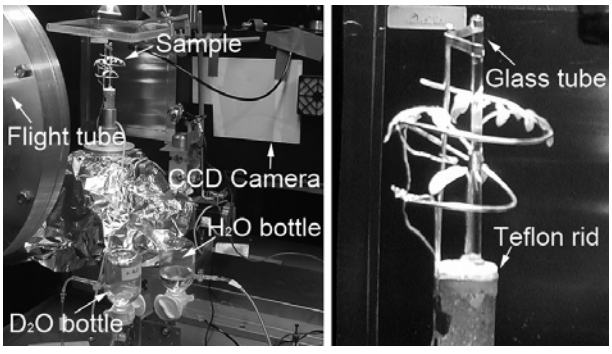

Figure 1 Experimental setting.
Left: Full view Right: Sample

Results and Discussion

After up-take by the sample, the D_2O created positive contrast in the roots and the stem. Water flow in the sample was clearly observed from the movement and the increase of transmission in CNR images (Figure 2).

Flow velocity was estimated from the CNR images. Figure 3 shows the rate of change in transmission along the streamline in the stem at selected time intervals. The region of interest in the streamline is shown in Figure 2 (*). The direction of the streamline is from left to right along the x-axis. The higher rate demonstrates an increase in transmission after D_2O supply. Figure 3 shows the location and amount of D_2O at different timelines. The horizontal dotted line represents a rate of change in transmission of 1.4. Vertical dotted lines indicate the intersections of each line and the horizontal dotted line. Thus those intersections had the same amount of D_2O at different timelines. Arrows show the respective positions. The average flow velocity calculated from the set of positions and the timeline was about 2.6 cm h^{-1}. The amount of D_2O up take should be considered when judging the reliability of that calculated velocity.

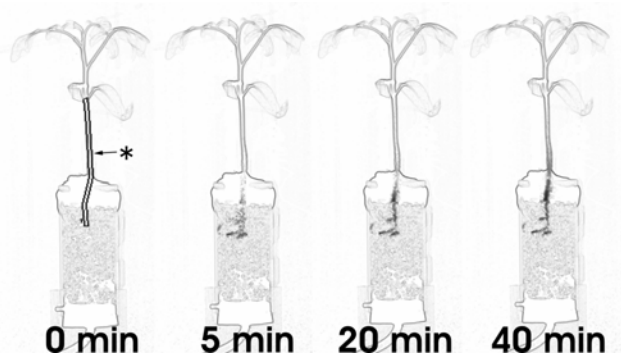

Figure 2 Increase in transmission by uptake of D_2O in series of CNR images.
Increase by transmission is represented by the black shadow. * : A ROI for Figure 3.

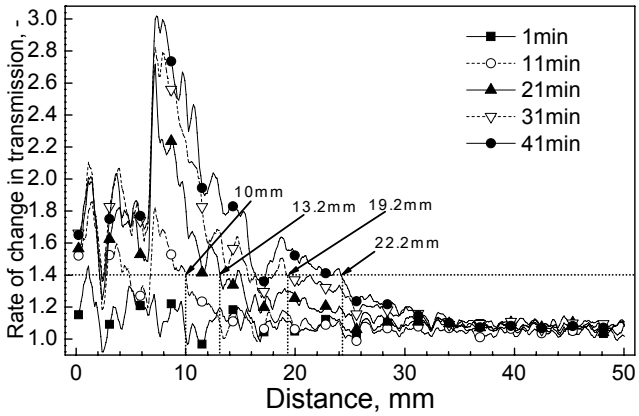

Figure 3 Rate of change in transmission along the streamline at selected time intervals.

	EXPERIMENTAL REPORT **Characterisation of composite microporous bone substitutes**	Proposal N° BIO-04-1119 Instrument **V12a** Local Contact Markus Strobl
Principal Proposer: Experimental Team:	C. Panayiotou - Aristotle Univ. Thessaloniki Ch. Ritzoulis - Aristotle Univ. Thessaloniki M. Strobl - HMI Berlin & TFH Berlin	Date(s) of Experiment 22.08. - 29.08.2005

Date of Report: Dec. 2005

Replacement of bone lost due to injury or disease like cancer or osteo arthritis produces a growing demand for osteoconductive and biodegradable substitutes. Hence there is the challenge to develop such kinds of artificial materials with sufficient mechanical and biological properties, similar to those of natural bone. This is not just of outstanding interest to the biomedical industry but also to a significant percentage of the population concerning the enhancement of their quality of life.

The main bone material with 70% of the bone weight is hydroxyapatite ($Ca_{10}(PO_4)_6(OH)_2$). It is a brittle ceramic that needs mechanical reinforcement in order to cope with the stress related to the normal function of bone [1]. In natural bone this reinforcement is provided by a sophisticated network of proteins. A promising and direct approach for reinforcing hydroxyapatite-based bone substitutes is to produce composite hydroxyapatite-protein materials [2]. Hence hydroxyapatite-protein composite samples have been prepared using sodium caseinate. Sodium caseinate is a commercially available and inexpensive milk protein with a high affinity to calcium due to its high phosphoserine content.

Microporosity, a parameter crucial for the development of bone after implantation of the artificial bone, has been achieved by means of emulsion templating [3,4]. Microporous Hydoxyapatite-Caseinate (HAP-Cas) samples have been studied by ultra small angle scattering (USANS) using the V12a double crystal diffractometer (DCD) at the Hahn-Meitner Institute in Berlin [5]. Samples of monomodal and bimodal size distribution have been prepared by means of altering the dimensions of the template droplets. Systems of bimodal pore size distributions are of special interest in the biomedical sector, as different pore sizes are needed with respect to hosting osteoblasts (bone-cell builders) on one hand and enhance their attachment by smaller pores on the other hand.

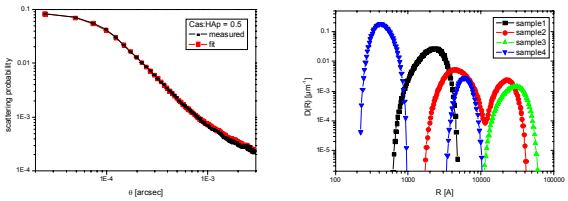

Fig. 1: ***left:*** example for measured curve and fit; ***right:*** four examples of monomodal and bimodal pore size distributions calculated from fitted USANS curves

Pore sizes and size distributions for diameters between 0.1 µm and 6.5 µm could be identified and calculated from fitting the measurements with corresponding model functions. One of the main conclusions was that the actual pore sizes are smaller than the template droplets and hence smaller than expected. For example a sample rendered porous through templating with emulsion droplet sizes of 1 µm could be measured to have mean pore sizes of only about 0.5 µm (Fig.1: sample 1). Further measurement series are to come in order to find a reliable correlation between the templates and the pore size distribution. The production of bimodal pore size distributions turned out to be successful (e.g. samples 2 & 4 in Fig.1). Additional X-ray tomographies are to be taken especially for pore sizes beyond USANS resolution i.e. >50 µm.

References

[1] W. Suchanek et al.: *J. Mat. Res.* 13 (1998) 94
[2] I. Ono et al.: *J. Bone Miner. Metab.* 16 (1998) 81
[3] C. Ritzoulis et al.: *J. Biom. Mat. R. A* 71A (2004) 675
[4] C. Ritzoulis et al.: *Food Hydrocol.* 19 (2004) 575
[5] M. Strobl et al.: Phys. B *(accepted f. publ .in 03.2006)*

	EXPERIMENTAL REPORT **Local dynamics of polyethylene and its oligomers**	Proposal N° CHE-03-0377 Instrument **V3** Local Contact Alexandra Buchsteiner
Principal Proposer: Experimental Team:	V. Arrighi - Heriot-Watt University V. Arrighi - Heriot-Watt University J. Tanchawanich - Heriot-Watt University A. Buchsteiner - HMI Berlin	Date(s) of Experiment 20.04. - 24.04.2005

Date of Report: 4. Jan. 2005

In this experiment carried out on NEAT, we performed measurements on short alkanes. Our aim was to obtain experimental data that could support predictions from molecular dynamics (MD) simulations of polyethylene (PE). In particular, we intended to test MD results from the I(Q,t) data obtained from the MD trajectories [1,2]. It has been shown that the shape of the distribution of relaxation times (DRT) derived from I(Q,t) using a CONTIN analysis changes with temperature and Q but it never resembles the asymmetric distribution associated with a KWW function, the empirical model extensively used to describe local chain dynamics. Thus, the relaxation of PE at high temperature (> 450 K) was shown to proceed via a single process, interpreted as a resulting from the combination of torsional oscillations and conformational relaxation. Only at lower temperature, close to 350 K, these two dynamics processes distinctly appear in DRT.

In order to access experimentally the low temperature range, QENS measurements were carried out on $C_{30}H_{62}$, chemically similar to PE but with low melting temperature.

The intermediate scattering function was computed from the NEAT spectra and good overlap was obtained with data from OSIRIS. The data shown in Figure 1 cover a wide time range, as a result of using two different configurations on NEAT and the backscattering spectrometer OSIRIS. This has made it possible to extract the DRT and show that the I(Q,t) data can be described by single a log-Gaussian distribution of exponentials (continuous line in Figure 1).

An apparent activation energy, E_a, for the relaxation process was obtained from data collected at different temperatures, using the Arrhenius equation. The E_a decreases with increasing Q (Figure 2). At low Q, E_a values are comparable to those obtained from rheological measurements [3], while lower values are obtained at high Q. Although, there is no evidence for two separate processes in our experimental data, even at 350 K (at least for $C_{30}H_{62}$), the data analysis gives some support to the MD predictions. In fact the observed Q dependent E_a values could be due to two overlapping elementary processes, e.g. torsion-vibration and conformational relaxation, with different Q dependent amplitudes.

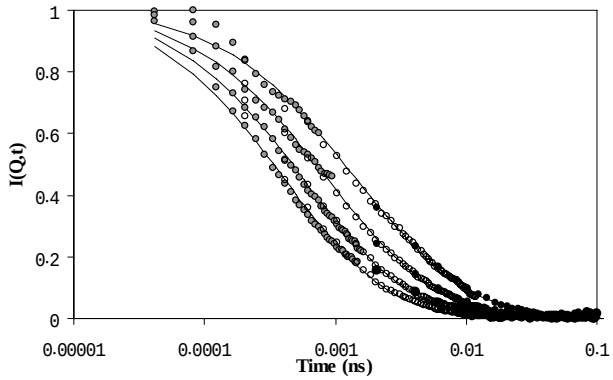

Figure 1 – I(Q,t)data of $C_{30}H_{62}$ from NEAT (energy resolution = 1.4 meV and 93 μeV) and OSIRIS (energy resolution = 24.5 μeV) at 350 K and Q = 1.25, 1.50, 1.75 and 2.00 $Å^{-1}$ (from top to bottom).

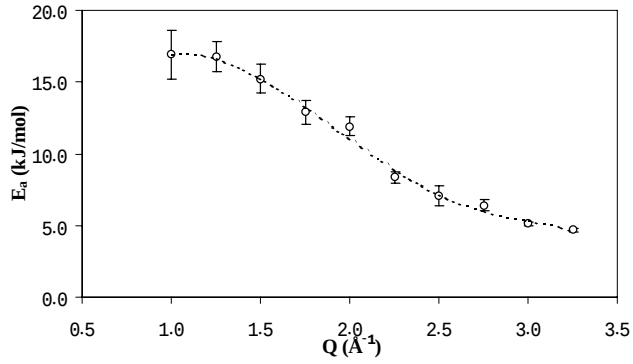

Figure 2 – Q dependence of E_a values for $C_{30}H_{62}$ as determined from fitting I(Q,t) data in the temperature range 350 K to 450 K.

References

[1] G. Arialdi et al.: Chem Phys **292**, (2003), 371
[2] G. Arialdi et al.: Macromolecules, **36**, (2003), 8864
[3] D.S. Pearson et al.: Macromolecules, **20**, (1987), 1133

	EXPERIMENTAL REPORT IQENS on monohydric alcohols/CCl_4 mixtures	Proposal N° PHY-03-0358 Instrument **V3** Local Contact Alexandra Buchsteiner
Principal Proposer: Experimental Team:	F. Aliotta - IPCF-CNR-Messina, I C. Vasi - IPCF-CNR-Messina, I F. Saija - IPCF-CNR-Messina, I	Date(s) of Experiment 18.07.-23.07.2004

Date of Report: 26. Jan. 2006

The intent of the experiment was of investigating the diffusive dynamics in CCl_4/monohydric alcohols mixtures. In particular the interest was devoted to the study of the concentration dependence of rotation and diffusion due to some hypothesized electrostatic interaction between carbon tetrachloride and alcohol.
In the proposal we asked for a higher resolution than that actually used. (ΔE=140μeV). This choice has been made at the time of the experiment in order to try to overcome some difficulties originated by the geometry of our home made scattering cell. This cell was built in stainless steel (aluminium was not allowed since it is reactive with our samples) and it was a cylindrical one with an external radius of 39mm). This large radius caused that the elastic peak (from vanadium) appeared to be separated in two lines at some scattering angles (due to the large different in the position on the beam of the scattering volumes on the opposite side of the cell.

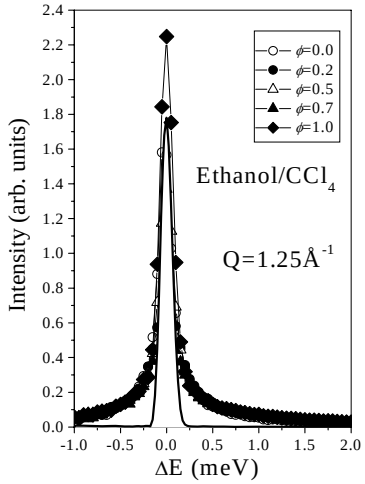

FIG.1

The adopted resolution turned out able to solve this problem but, unfortunately it was not able to resolve the scattering contributions in which we ere interested.
Each collected spectrum, in fact, result just in a resolution enlarged line (whose intensity is probably concentration dependent) plus a broad contribution that appears to be independent of the exchanged wave vector and of the concentration. In the figs. 1 and 2 the normalized spectra from different alcohols are reported to illustrate the situation
The same difficulty is observed when solutions of the same alcohol at different concentration are compared (see fig.3)..

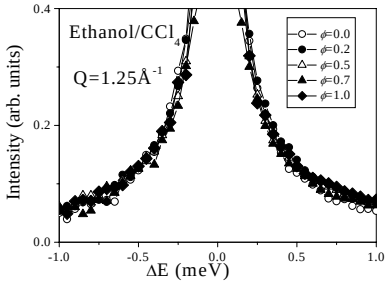

FIG. 2

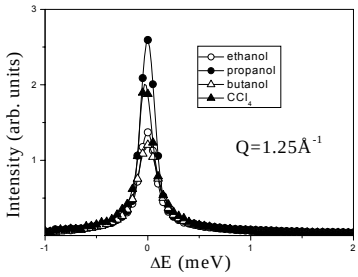

FIG.3

Probably due to the same reasons we have experienced a number of difficulties in obtaining a safe normalization of the different run. The situation is depicted in fig. 4 where we show the result obtained at enough large Q-values after subtraction of the celle contribution.
Our conclusion are that the experiment should be repeated with a better resolution after the adoption of a different geometry.

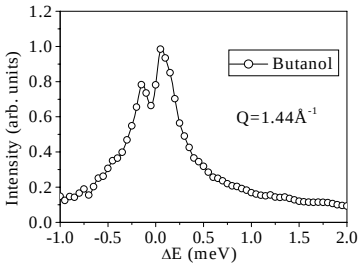

FIG.4

We think that, if a very good resolution is required a slab cell should be the better choice.

	EXPERIMENTAL REPORT **Microscopic dynamics of a glass-forming liquid in soft confinement**	Proposal N° PHY-03-0396 Instrument **V3** Local Contact Margarita Russina
Principal Proposer: Experimental Team:	R. Zorn - Forschungzentrum Jülich M. Mayorova - Forschungzentrum Jülich	Date(s) of Experiment 18.10 - 25.10.2005

Date of Report: 06. Jan. 2006

The influence of spatial confinement is of high interest for the physics of glass formation. Any correlation length or cooperativity range should be limited by a restriction of the spatial dimensions. Unfortunately wall interactions play a crucial role. Microemulsions as PG/AOT/decalin are as close as one can experimentally get to 'free' surface conditions. Confinement by microemulsions offers the investigation of soft confinement, where the confining material is more fluid than the confined material. At the same time, these nanodroplets have much better defined geometries than the typical porous glasses, and the confined droplet remains in thermodynamic equilibrium with its surrounding.

The purpose of this experiment was to complete existing data from the neutron backscattering spectrometer IN16 in the short time range. An incident wavelength of 5.5 Å was selected yielding a resolution FWHM of 117 µeV at high angles. 8 – 10 hours registration time was spent on each sample / temperature to obtain good statistics.

Spectra were taken from bulk PG and microemulsions containing d-PG and h-PG with the other components deuterated. By subtracting the two isotopic variants of the microemulsion the incoherent scattering from the confined PG was extracted.

Fig. 1 shows the spectra converted to S(Q,E). By comparing spectra at same temperatures one recognises that the effect of confinement is not just a shift of the time scale but a change of the shape of the quasielastic scattering.

This becomes clearer in the Fourier transforms shown in Fig. 2. Constant-Q interpolated spectra at 230 K and 270 K were Fourier transformed and divided by their respective resolution from the 2 K spectra.

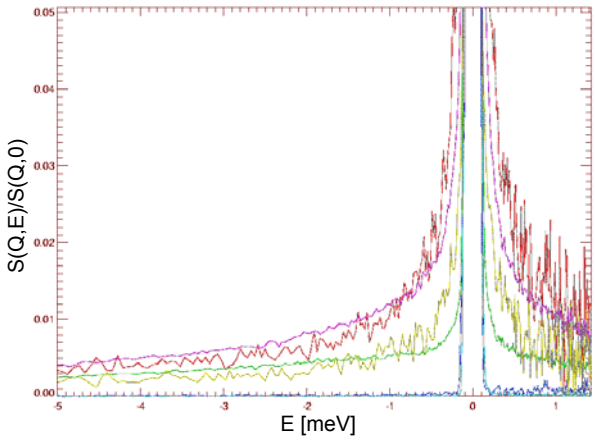

Fig. 1: TOF spectra at $2\theta = 105°$ ($Q_0 = 1.8$ Å^{-1}). Bulk: 2 K (cyan), 230 K (green), 270 K (magenta); confined: 2 K (blue), 230 K (yellow), 270 K (red).

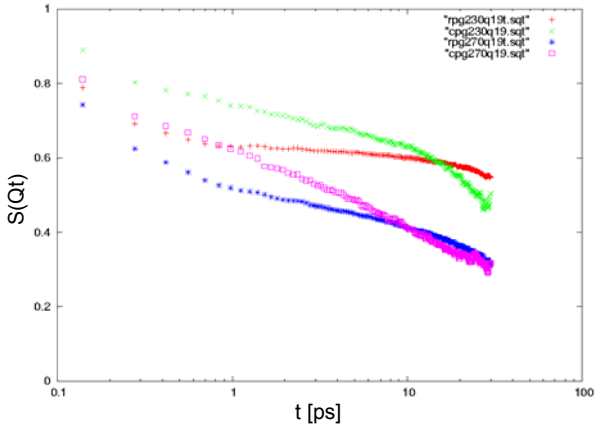

Fig. 2: Fourier transformed TOF spectra at Q = 1.88 Å^{-1}. Bulk: 230 K (red), 270 K (blue); confined: 230 K (green), 270 K (magenta).

It can be seen that the confinement causes a completely different dynamical behaviour. For bulk PG the decay of the fast motion to the non-ergodicity plateau is clearly visible around 1 ps. For the confined PG there is a smooth transition between the fast motion and the α relaxation. In addition the α relaxation seems to be faster.

In order to clarify this the data obtained here will be combined with Fourier transformed backscattering data yielding a dynamical range up to 2 ns.

BENSC	**EXPERIMENTAL REPORT** **Quasielastic measurements on liquid n-tetracosane in oriented, tubular silicon mesopores**	Proposal N° PHY-03-0399 Instrument **V3** Local Contact Margarita Russina
Principal Proposer: Experimental Team:	P. Huber - Universität Saarland R. Zorn, M. Mayorova - FZ Jülich M. Russina - HMI Berlin D. Wallacher, T. Hofmann, P. Kumar - Universität Saarland	Date(s) of Experiment 24.10. - 01.11.2005

Date of Report: 09. Jan. 2006

We carried out quasielastic neutron scattering experiments on liquid n-tetracosane (n-$C_{24}H_{50}$) confined to tubular, parallel aligned mesopores of porous silicon.

Porous, crystalline silicon <100> wafers were electrochemically etched and the pore properties characterized by nitrogen sorption isotherms at 77K: porosity of the porous epilayer 60%, mean pore diameter 5nm. In total three samples (the bulk, the empty pores, the completely filled pores) were investigated at different temperatures, T=2.5K, 340K, 350K and 400K.

A comparison of the quasielastic scattering of the bulk sample and the pore confined tetracosane indicates a significantly slower diffusion of confined tetracosane or at least of one component of the pore condensed molecules - see the different widths of the energy scans of bulk and confined n-alkane in Fig. 1.

In addition to the comparison of bulk and spatial confined diffusion behaviour, we were interested in a possible anisotropy of the molecules' dynamics imposed by the strongly anisotropic spatial confinement (pore diameter 5nm =><= pore length 250 um). Therefore, we performed measurements with scattering vector transfers, q, parallel and perpendicular to the pore axes. However, as can be seen in the reasonably well overlapping spectra for such two different orientations (see Fig. 2), we found no hints for an anisotropy in the diffusion dynamics.

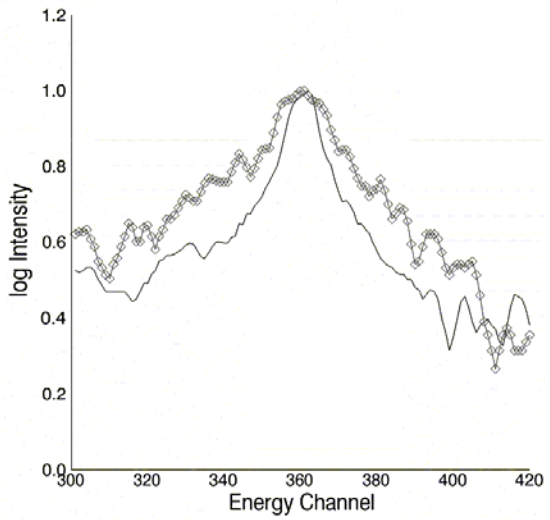

Fig. 1: Comparison of quasielastic scattering of bulk (diamonds) and pore condensed n-C24H50 (solid line) at T=350K.

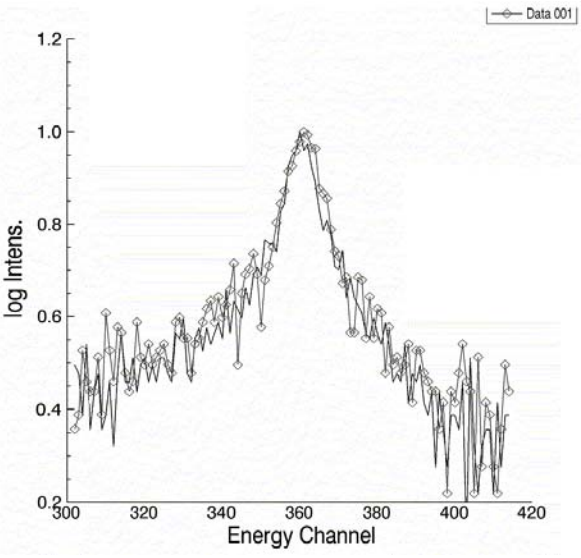

Fig 2: Comparison of the quasielastic scattering intensity for two pore orientations: q parallel (solid line) and perpendicular (diamonds) to the long pore axes, resp. (T=350K).

	EXPERIMENTAL REPORT **Heterogeneous polymer micelles and their interactions with proteins**	Proposal N° BIO-04-1104 Instrument **V4** Local Contact Elvira Garcia-Matres
Principal Proposer: Experimental Team:	H. Bianco-Peled - Technion Haifa, IL K. Shamai - Technion Haifa, IL E. Garcia-Matres - HMI Berlin	Date(s) of Experiment 21.02. - 24.02.2005

Date of Report: 28. Dec. 2005

Background

Our research deals with heterogeneous polymer brush (HPB) and their interactions with proteins. Our HPB are prepared via selfassembly of mixture of neutral (polystyrene-bpolyethylene glycol) (PS34-PEG377) and charged (polystyrene-b-polyacrylic acid) (PS32-PAA277) diblock copolymers.

Since PS-PAA is not soluble in aqueous media, the block copolymers were first dissolved in Tetrahydrofuran (THF) which is a common solvent for PS and both hydrophilic blocks (PEG,PAA). Then, addition of H2O, a selective precipitant of PS, induces micelles formation.

During the preparation of the samples we have noticed large differences in the turbidity between samples in which the water were added gradually (equilibrium) and samples that were quenched from THF in to aqueous solution. These findings led us to believe that a controllable production of mixed micelles could not be achieved without understanding the self assembly kinetics and the resulted morphology of each copolymer separately. In order to do so we measured 3 sets of samples in D_2O: S1-S2) 1mg/ml PS-PAA that were self assembled in equilibrium [E] or quenched [Q] respectivelly, S3-S4) 1mg/ml PS-PEG in equilibrium or quenched, and S5-S6) 3mg/ml PS-PAA, in equilibrium or quenched.

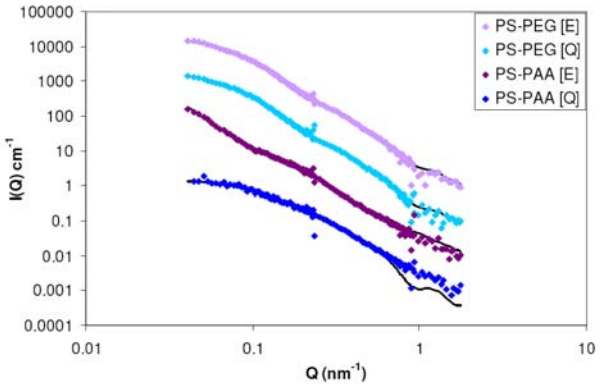

Fig. 1: Scattering curves for
- ♦) 1mg/ml PS-PEG [E] micelles in equilibrium
- ♦) 1mg/ml PS-PEG [Q] micelles quenched
- ♦) 1mg/ml PS-PAA [E] micelles in equilibrium
- ♦) 1mg/ml PS-PAA [Q] micelles quenched

The solid lines represent the curves fit to the theoretical model [1].

Results

The scattering curves from samples S1-S4 are summarized in Fig 1. All samples have the same background but for the sake of clarity each curve has been translated vertically by one decade. The scattering curves were fitted to a theoretical model of micelles with a spherical core (R) a Gaussian polymer chain (Rg) attached to the surface, where Nc is the number of chains in each micelle [1].

A comparison between the quenched and the equilibrium sample revealed morphology difference only for the 1mg/ml PS-PAA sample. At the PS-PEG and the 3 mg/ml PSPAA there was no change in the morphology.

From these changes it might be concluded that PS32-PAA277 micelles freeze at a specific concentration of water. This critical water concentration decreases as the concentration of the polymer increase. At 3mg/ml the micelles freeze immediately and the morphology does not depend on the preparation method. Since the PS34-PEG377 is completely soluble in water the micelles are not frozen and blocks can move freely in the solution.

Acknowledgement

This research has been supported by the European commission under the 6th framework program through the key action: strengthening the European research infrastructures.
Contract no: RII-CT-2003-505925 (NMI3)

1mg/ml	R (nm)	Rg (nm)	N_c
PS-PAA [E]	8.6	53.8	53
PS-PAA [Q]	4.7	9.7	21
PS-PEG [E]	4.6	14.9	51
PS-PEG [Q]	4.5	15.3	63

Reference

[1] Pedersen, Jan Skov; Gerstenberg, Michael C.: *Scattering Form Factor of Block Copolymer Micelles* Macromolecules (1996), **29**(4), 1363-5.

	EXPERIMENTAL REPORT **Nucleic acid inclusion in water in oil microemulsions formed by phosphatidylnucleosides**	Proposal N° BIO-04-1107 Instrument **V4** Local Contact Astrid Brandt
Principal Proposer: Experimental Team:	D. Berti - CSGI and University of Florence, I F. Betti - CSGI and University of Florence, I	Date(s) of Experiment 25.06. - 29.06.2005

Date of Report: 03. Jan. 2006

The investigation proposed concerns the ternary systems cyclohexane/POPN/TRIS buffered solution, where POPN is a palmitoyloleoyl-phosphatidyl-nucleoside, with N= adenosine, uridine or a 1:1 mixture of the two complementary bases. The O/W microemulsions obtained from the analogous derivatives DLPN have been studied by our group in the past. In particular SANS experiments have shown that the introduction of oil in the hydrophobic core of the micelles induces a structural transition from cylindrical aggregates to globular microemulsions: also the molecular recognition pattern is affected from the structural change, demonstrating that we can monitor it aging on the system composition.

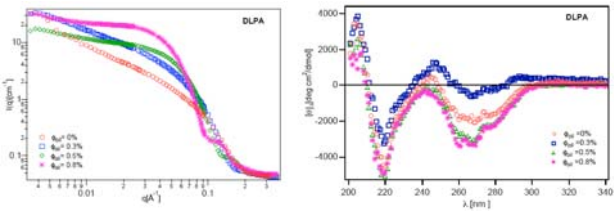

The interest in the reverse ternary systems of POPNs is the use of supramolecular aggregates with a negative curvature to control and modulate the base-base affinities changing the extent of water pool, and the possibility to use these aqueous pools as nanocompartments for the solubilization of biological macromolecules (i.e. nucleic acids). In order to characterize the overall microstructure of the aggregates small angle neutron scattering experiments were performed as a function of surfactant volume fraction and as a function of the amount of W0=[water]/[POPN]. Different water contents were measured for each ternary system to investigate the whole phase diagram. A parallel SAXS investigation on the same samples has showed that for both surfactant concentrations (5x10-2M and 7.5x10-2M) the addition of a water solution promotes a structural change from ellipsoidal micelles to discoidal aggregates.

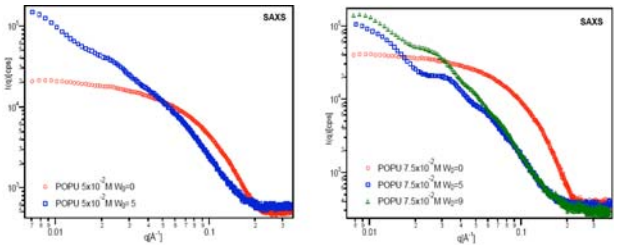

SANS measurements had been carefully planned to get a self-consistent picture, but some problems with the instrument setup have prevented us to measure all the samples. Globally a quarter of the complete set of samples has been lost and therefore it has not been possible to fulfill the experiment highlighted in the title of this proposal. However some interesting findings emerge even in the absence of nucleic acid inclsuion Independently of the surfactant volume fraction and of the nature of the polar head, the three binary systems show the same self-assembling behaviour; an increase of the surfactant volume fraction induces in fact, a transition from ellipsoidal to more globular aggregates. The structural change is more evident if we consider the quaternary system cyclohexane/POPN (75%wt)/lecithine(25%)/TRIS buffered solution (Figure 3).

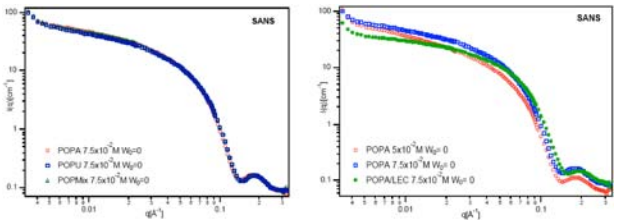

The effect of water addition is pronounced: a qualitative analysis of the data with W0>0 shows that local disc-shape or possibly tubular structures are formed. This behaviour differs from the one observed for the W/O lecithin microemulsions for which water addition promotes a monodimensional growth from spherical aggregates to cylindrical ones. Even if the full set of data will be necessary to draw some conclusive remarks, the interplay between selfassembly and base-base interaction is clear and worth further investigations.

	EXPERIMENTAL REPORT **Mechanism of cryoprotection of lipid bilayers by simple sugars.**	Proposal N° BIO-04-1116 Instrument **V4** Local Contact Uwe Keiderling
Principal Proposer: Experimental Team:	C.J. Garvey - ANSTO, Australia T. Lenné - RMIT University, Australia G. Bryant - RMIT University, Australia U. Keiderling - HMI Berlin	Date(s) of Experiment 29.06. - 01.07.2005

Date of Report: 29.08.2005

The experiments conducted during this project were preliminary in nature, and were aimed at determining if contrast variation SANS could be used to answer the following questions:

(1) are low hydration membrane/solute/water systems homogeneous? That is, do they consist of membranes separated by a homogeneous water/solute mixture, or, does the presence of the solutes induce a phase separation into a membrane/solute/water phase and an excluded solute/water phase at a (potentially) different concentration?

(2) if there are two phases, can the concentrations of the solutes in the two phase be determined?

In the beamtime available (reduced as to reactor went down for several hours), we were able to determine the optimal sample conditions, and to determine the contrast match points for samples at one water content. Figure 1 shows the scans for DPPC (top) and DPPC:glucose 2:1 at several D_2O H_2O ratios.

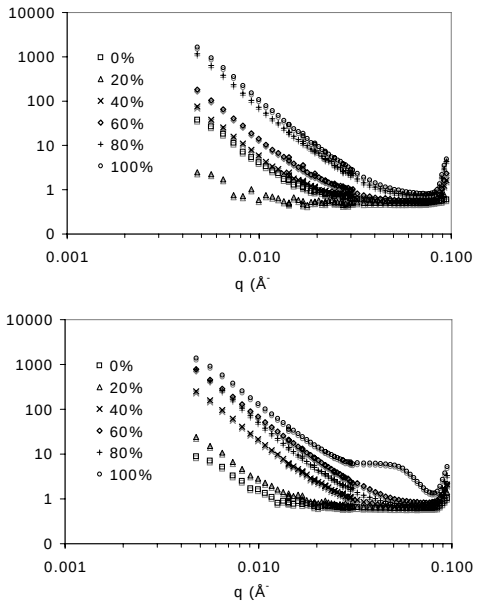

Figure 1

The contrast match points are determiend from the low q results, as shown in figure 2. The contrast match points are clearly different. This information was used to determine the concentration of the glucose in the two phases – for these experiments, we found that the glucose in the excluded phase has about twice the concentration of the glucose between the membranes, for this hydration.

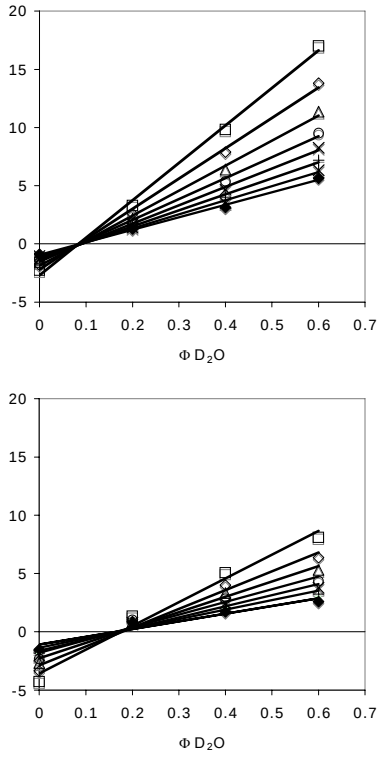

Figure 2

These results have been submitted for presentation at the Internation Conference on Neutron Scattering in Sydney in November 2005, and the proceedings will be published in Physics B: Lenné, Bryant, Garvey, Keiderling and Koster, “Location of sugars in multilamellar membranes at low hydration.” (submitted).

BENSC	**EXPERIMENTAL REPORT** **Self-aggregation and solubilisation properties of a novel type of amphiphilic terblock copolymers in aqueous solution**	Proposal N° CHE-04-1010 Instrument **V4** Local Contact André Heinemann
Principal Proposer: Experimental Team:	M. Gradzielski - TU Berlin, Stranski-Lab. A. Boschetti de Fierro, D. Fierro, P. Simon, V. Abetz - GKSS-Forschungszentrum Geesthacht A. Heinemann - HMI Berlin	Date(s) of Experiment 27.01. - 30.01.2005.

Date of Report: 07.01.2006

The self-assembly of amphiphilic copolymers in aqueous solution is being intensively studied [1-4]. One potential application generating such interest is the use of aggregates as selective carriers for the delivery of active agents, a topic of high relevance for drug-delivery, cosmetics etc.

We have recently synthesized a novel type of water-soluble triblock terpolymer of polybutadiene-*b*-polystyrene-*b*-poly(ethylene oxide, PB-PS-PEO). Such terpolymers can become dispersed in aqueous solution by different techniques, e. g. by vigorous shaking, ultrasonification or aqueous dilution of a concentrated solution dissolved in dioxane or THF [5]. The generated micellar aggregates have a hydrophobic core which could be sub-divided into 2 chemically different regions determined by the two hydrophobic blocks.

The samples used in our experiments were PB-PS-PEO triblock terpolymers with different compositions, as well as one PS-PB-PEO for a comparison. The triblock terpolymers are referred to as $A_xB_yC_z^m$, where the subscript stands for the mass fraction in wt% and the superscript indicates the overall number-averaged molecular weight M_n in kg/mol.

In order to study the potential of the formed micelles as carriers, experiments were performed on micelles containing a solubilisate. Toluene (a good solvent for PS) was added into the polymer solution in dioxane (equal mass as the PS+PB block). Afterwards, two different dispersion methods were employed. Either D_2O was added slowly and drop-wise to the polymer solution under stirring (Method 1), or the polymer solution was added to the D_2O under vigorous stirring (Method 2). The dioxane to D_2O ratio was 1:49, the final polymer concentration in the dispersion was kept at 0.1 wt-%. As solubilisates both toluene and d_8-toluene were used, in order to deduce the toluene location from the different contrast condition. The scattering curves for the $B_{19}S_{34}EO_{47}^{142}$ terpolymer are given in Figure 1.

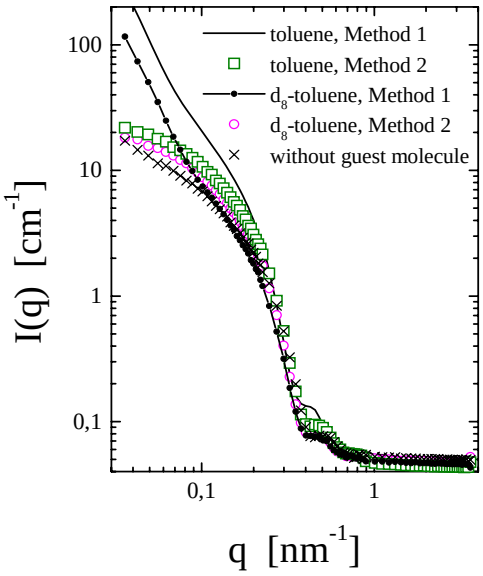

Fig. 1: Neutron scattering of $B_{19}S_{34}EO_{47}^{142}$ triblock terpolymer in dioxane: D_2O with toluene as solubilisate and different preparation methods.

Evidently smaller and more monodisperse aggregates are obtained by method 2. Toluene becomes incorporated (as seen by the increasing intensity) and it appears to be preferentially located in a shell around the core as seen from fitting a core-shell model to the data.

References

[1] V. Balsamo, G. Gil, C. Urbina de Navarro, I.W. Hamley, F. von Gyldenfeldt, V. Abetz, E. Canizales: Macromolecules **36**, 4515 (2003)

[2] D.E. Discher, A. Eisenberg: Science **297**, 967 (2002)

[3] S. Förster, V. Abetz, A.H.E. Müller: Adv. Polym. Sci. **166**, 173, (2004)

[4] D.V. Pergushov, E.V. Remizova, M. Gradzielski, P. Lindner, J. Feldthusen, A.B. Zezin, A.H.E. Müller, V.A. Kabanov: Polymer **45**, 367 (2004)

[5] A. Boschetti, V. Abetz, M. Drechsler, M. Drechsel, M. Gradzielski: in preparation.

	EXPERIMENTAL REPORT **Internal composition of polyelectrolyte-protein complexes**	Proposal N° CHE-04-1103 Instrument **V4** Local Contact Daniel Clemens
Principal Proposer: Experimental Team:	J. Gummel - LLB CEA Saclay J. Gummel - LLB CEA Saclay F. Cousin - LLB CEA Saclay F. Boué - LLB CEA Saclay	Date(s) of Experiment 12.07. - 22.07.2005

Date of Report: 06.01.2006

This experiment follows the one done in 2004 on V4 as well (exprep OTH-04-0942). The system used is sodium (poly)-styrenesulfonate (PSSNa), a negatively charged polyelectrolyte with a size of 50 monomers, and lysozyme, a globular protein positively charged at low pH. We study the formation of complexes made with those two components in solution. The two species being of an opposite charge, we use here the charge ratio [-]/[+] introduced in solution instead of concentrations. We made vary two different parameters independently: first the charge ratio [-]/[+] introduced and then the concentration of the species at a given the charge ratio [-]/[+] introduced. We did a model to fit the SANS spectra based on a dense sphere model. This fit can be done on the two contrasts and then it enables us to get the size and the density of the complexes in the point of view of each component. Finally we can get the global structure and the inner charge ratio of the complexes.

A first part of the study has consisted in making complexes in a buffer at pH 3. In Fig.1 is given an example of the typical curve shape observed for the two contrasts with the corresponding fits.

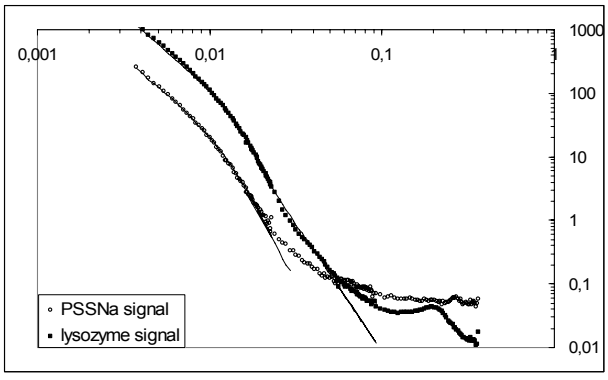

Fig. 1: experimental curves and fits for pH = 3, [-]/[+] = 2 and for the two contrasts

The complexes made at pH 3 are strictly the same than the ones at ph 4.7 (made in previous studies) for a given [-]/[+] introduced. The structure is a globular primary complex very dense with a size between 100 and 200 Å which can be surrounded by a polymeric shell when negative charges are in excess. Those complexes are then distributed in a fractal way. The excess of protein stays in solution and the excess of PSSNa is either in solution or the shell.

The structure is seen to be stoechiometric in the point of view of the charges in the core of the complexes. In Fig.2 is given the [-]/[+] inner as a function of the [-]/[+] introduced. One can see that it stays close to one for any [-]/[+] introduced.

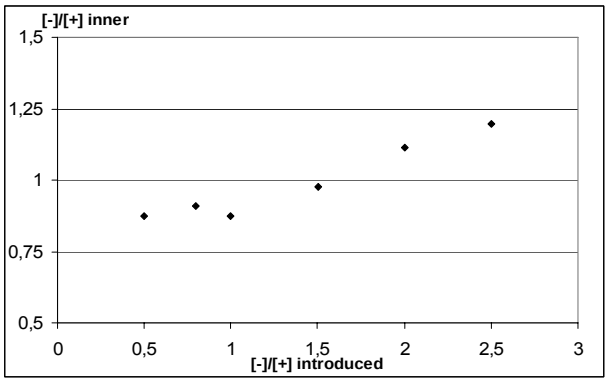

Fig. 2: [-]/[+] inner as a function of [-]/[+] introduced

A second part has consisted in varying the concentrations of each component at a given charge ratio. We found that the structure obtained is the same; the only difference is the size of the primary complexes that increases with the concentration. R increases like c^(1/3). It shows thus than the number of complexes is independent from the concentration of species introduced. In Fig. 3 is given the average radius of the primary complexes as a function of the concentration introduced (normalized at 1 for the lowest).

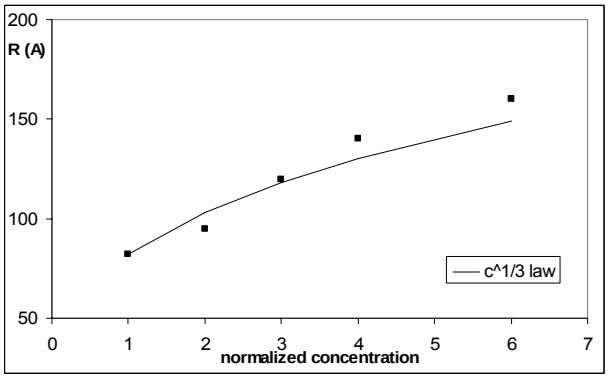

Fig. 3: average radius of the primary complexes

	EXPERIMENTAL REPORT **Structural study of new contrast agents for Magnetic Resonance Imaging**	Proposal N° CHE-04-1108 Instrument **V4** Local Contact Astrid Brandt
Principal Proposer: Experimental Team:	L. Paduano - Univ. Naples "Federico II", I G. Mangiapia - Univ. Naples "Federico II", I A. Brandt - HMI Institut	Date(s) of Experiment 10.02. - 13.02.2005

Date of Report: 09. Jan. 2006

The aim of this research project has been to develop and characterize new high-relaxivity Magnetic Resonance Imaging (MRI) contrast agent, having high specificity for particular tumor pathologies. New mixed micelles and vesicular aggregates, having potential application in γ-scintigraphy and Magnetic Resonance Imaging (MRI), have been designed and synthetized: these are formed by two alkylic chains derivatived with DTPAGlu, a claw molecule for Gd (III) ions, and CCK8, a polypeptide sequence able to bind to the cellular cholecystokinin receptors. A structural study of these aggregates, performed by small angle neutron scattering measurements, has allowed understanding how to enhance their potential properties in the medical diagnostics. Binary and ternary aqueous solutions containing DTPAGlu (or DTPAGluGd) and CCK8 at different ratios of them and at various pH values have been analyzed. Scattering spectra of solutions containing DTPAGlu at low pH values (~3) show a power law dependence $d\sigma/d\Omega \propto q^{-2}$, typical of presence of sheets. Actually, on the q scale of the SANS measurements performed, vesicles that should be present in samples (as revealed by cryo-tem images), may in first approximation be regarded as randomly oriented infinite planar sheets, justifying the power law found. An increasing of the pH (from ~ 3 to ~ 4.5) results in a destruction of vesicular structures, leading to a formation of smaller aggregates; the power law found in SANS spectra, $d\sigma/d\Omega \propto q^{-1}$, is characteristic of cylindrical objects. The presence of such transition can probably be ascribed to the repulsion occurring among the polar heads of DTPAGlu units (each of which has five negative charges): when pH is increased carboxylic groups of DTPAGlu heads are deprotonated and the repulsions increase. This seems also be confirmed by SANS measurements executed on DTPAGluGd binary solutions: such measurements have shown the presence of vesicles at pH ~3 that still exist if pH is increased. DTPAGluGd units have a smaller charge (-2); as result of that, the repulsions among polar heads are smaller if compared to those of DTPGlu units. Results obtained for binary solutions are substantially similar for ternary systems containing CCK8 molecules. Effect of ionic strength has also been analyzed: an increasing of this parameter, attained by adding NaCl to the systems, produces the same effects caused by operating at low pH values: the presence of salt should partially shield repulsions among polar heads. Indeed aqueous ternary solutions of DTPAGluGd/CCK8 show vesicular aggregates even at physiological pH values (7.4).

In the following figure some selected SANS spectra are shown with the legend.

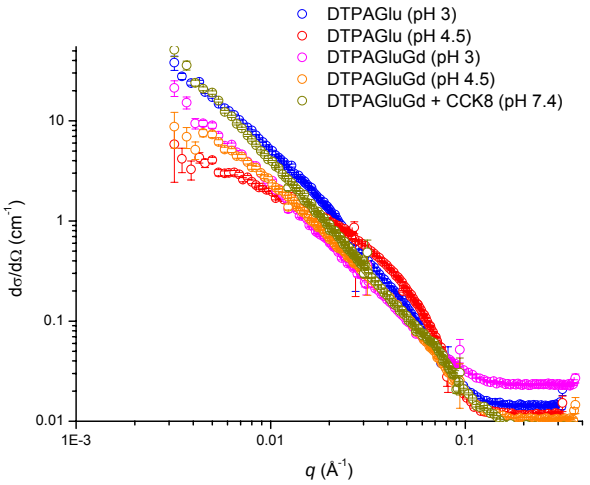

Acknowledgement

This work has been supported by the European Commission under the 6th framework Programme through the Key Action: Strenghtening the European Research Infrastructures.
Contract n°: RII-CT-2003-505925 (NMI3)

	EXPERIMENTAL REPORT **Pluronic micelles swollen with homopolymer**	Proposal N° CHE-04-1112 Instrument **V4** Local Contact Daniel Clemens
Principal Proposer: Experimental Team:	T. Cosgrove - University of Bristol, UK M. Sharp - University of Bristol, UK A. Woodward - University of Bristol, UK D. Clemens - HMI Berlin	Date(s) of Experiment 14.02. - 17.02.2005

Date of Report: 18. Dec. 2005

The pharmaceutical industry are interested in developing new systems for the controlled release of drugs. The drugs must be encapsulated, in order to protect them until they reach the desired release site. There is a considerable interest in the use of block copolymers for the purpose of encapsulation, due to similarities between polymeric micelles and natural carriers, and it is possible for the micelles to mimic aspects of the biological transport system [1].

Our system is a model system, comprising of block copolymer (Pluronic) micelles with a homopolymer (poly(propylene glycol)) of the same chemical structure as the core of the micelle. As far as we have been able to ascertain, this is a novel idea. By swelling the micelles, we hope to increase the capacity of the drug delivery vehicle. We wish to obtain the detailed structure of these swollen micelles (internal size, degree of penetration of the block copolymer into the swollen core and to the bulk solvent). Small-angle neutron scattering is probably the only way of obtaining this information directly.

Pluronics are block copolymers, consisting of propylene oxide (PO) and ethylene oxide (EO), of the form $(EO)_n(PO)_m(EO)_n$. Four Pluronic block copolymers were studied. These were Pluronics P85, F127, P105 and F88. The Pluronic micelles were swollen by incorporation of homopolymer poly(propylene glycol) of molecular weight 700, 1000 and 2000. Three concentrations of homopolymer were used. The measurements were carried out at three temperatures 25°C, 30°C and 37°C, in order to study the temperature range of interest for possible pharmaceutical applications.

The neutron wavelength selected was 7Å, and two sample-detector distances were used, 1m and 4m. This gave a Q-range of approximately 0.1 to 3.2 nm^{-1} $Å^{-1}$.

The results for Pluronic P85 swollen with homopolymer of molecular weight 700 is shown below. As can be seen, the statistics at low Q-values are very poor. This unfortunately means the data cannot be model fitted successfully. However, it appears that as homopolymer is added, the scattering intensity rises and the slope becomes steeper, which indicates the presence of larger aggregates.

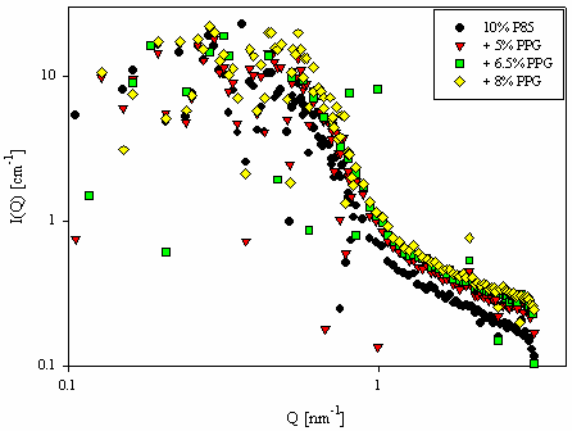

Acknowledgement
This Research project has been supported by the European Commission under the 6th Framework Programme through the Key Action: Strengthening the European Research Infrastructures.
Contract n°: RII-CT-2003-505925 (NMI3).

Reference

[1] Lavasanifar, A.; Samuel, J.; Kwon, G.S.: *Advanced Drug Delivery Reviews* (2002), ***54***, 169

	EXPERIMENTAL REPORT **Micelles in room temperature ionic liquids**	Proposal N° PHY-04-1149 Instrument **V4** Local Contact Uwe Keiderling
Principal Proposer: Experimental Team:	A. Triolo - IPCF-CNR, Messina, I A. Triolo - IPCF-CNR, Messina, I O. Russina - HMI Berlin U. Keiderling - HMI Berlin	Date(s) of Experiment 13.08. - 14.08.2005

Date of Report: 14.09.2005

The proposed experiment dealt with the study of both homopolymers and block copolymers solutions in room temperature ionic liquids (RTILs). We asked for four days beam time to accomplish this study, but two days were awarded proposing to focus on one of the two issues. We decided to mainly focus on the morphology of homopolymers dissolved in RTILS.

The latter are organic ionic substances built up by a bulky cation and an inorganic (fluorine containing) anion, such as 1-methyl-3-butyl imidazolium tetrafluoroboride ([bmim][BF_4]).

These salts are typically liquid at room conditions and tend to crystallise only much below 0°C. They are presently attracting a great attention as environmentally responsible replacements for the noxious organic volatile solvents, such as toluene, CCl_4 etc for the possibility of running bio-catalytic, electro-chemical and inorganic reactions in these neoteric solvents.

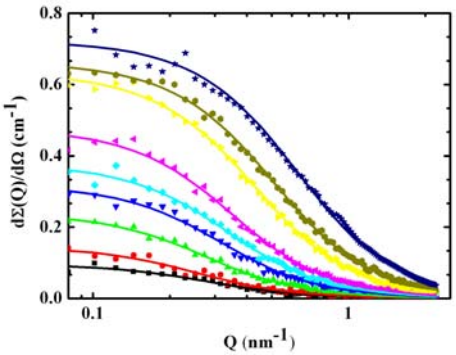

Fig. 1: Background subtracted SANS pattern from solutions of d-PEO (MW=25,000) in [bmim][BF_4] for different concentrations (0.01-6 %wt.) at 25 °C. The continuous lines correspond to a modelling of the experimental data in terms of random coils.

We are presently active in the characterization of many chemical- physical features of these materials and among the rest, we are investigating the possibility of dissolving block-polymers in RTILs, thus building up nano-pools which might lead to the formation of microemulsions in these green solvents.

As a first step in this long-term project we explored the morphology of homopolymers in RTILs. In particular, we used the SANS technique to study the structure of deuterated polyethylene oxide (-(CD_2-CD_2-O)$_n$-) when dissolved in a selection of RTILs.

In Figure 1, we report selected SANS patterns from solutions of d-PEO in [bmim][BF_4], for different homopolymer concentrations at room temperature.

In the explored concentration range (0.01-6 % wt.), the SANS patterns can be described in terms of the Debye model for non interacting random coils; the continuous lines in Figure 1 correspond to a fit of the experimental data in terms of such a model. To investigate the effect of the solvent on the polymer morphology, other RTILs were used as solvents, namely [bmim][PF_6] and [bmim] [$(CF_3SO_2)_2N$]. In Figure 2, a comparison of the solvent effect on the SANS pattern form d-PEO solutions at the same composition is shown.

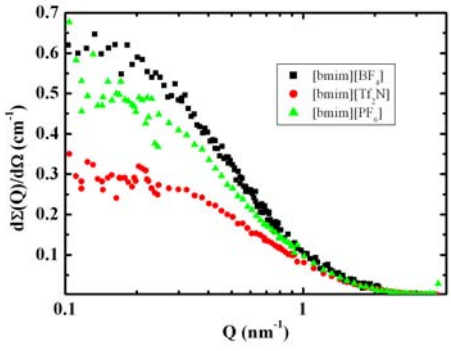

Fig. 2: Comparison of SANS patterns from 3% wt. solutions of d-PEO in three different RTILs at 25 °C.

	EXPERIMENTAL REPORT **Aggregate structure of cationic surfactants in the pores of SBA-15 silica**	Proposal N° CHE-04-1091 Instrument **V4** Local Contact Astrid Brandt
Principal Proposer: Experimental Team:	G.H. Findenegg - TU Berlin G.H. Findenegg - TU Berlin T. Shin - TU Berlin	Date(s) of Experiment 17.02. - 21.02.2005

Date of Report: 15. April 2005

We are studying the structure of surfactant aggregates in the pores of SBA-15, a periodic mesoporous silica with two-dimensional (2D) hexagonal arrangement of cylindrical pores of uniform size (pore radius 4.5 nm). As an extension of our earlier study of nonionic surfactants [1,2], we have now investigated ionic surfactants, in order to assess the influence of (i) surfactant-surface interactions via electrostatic forces and (ii) the effective head-group size of ionic surfactants, which strongly depends on the concentration of added electrolyte due to the screening of the electrostatic head-group interactions. Two cationic surfactants of different chain length, dodecylpyridinium chloride (DPC) and hexadecylpyridinium chloride (CPC), were studied at two salt concentrations (10^{-3} M and 10^{-1} M KCl) and three scattering length densities (SLD) of water (pure D_2O [SLD = 6.34×10^{10}cm^{-2}], H_2O/D_2O of SLD = 5.0×10^{10}cm^{-2} and contrast matching H_2O/D_2O of SLD = 3.7×10^{10}cm^{-2}). Samples were prepared by contacting the SBA-15 silica powder with a mixture of the surfactant and the aqueous electrolyte and adjusting the pH to pH 9. The SANS measurements were made in aluminium cells specially developed for such studies. The measurements were made over a q range from 0.04 to 5 nm^{-1}.

Scattering curves exhibit Bragg peaks from the 2D-hexagonal lattice of the matrix (q_{10} = 0.678 nm^{-1} for the present SBA-15 sample). Porod scattering from the outer surface of the SBA-15 particles is dominating at q < 0.2 nm^{-1} (Fig. 1). The intensities of the prominent Bragg peaks (*10*, *11*, *20*, and *21*) are strongly affected by the adsorption of the surfactant into the pores and have been studied as a function of the experimental parameters

(a) surfactant type (DPC or CPC)
(b) SLD of water (3.7, 5.0, or 6.34)
(c) salt concentration (10^{-3} M or 10^{-1} M KCl)
(d) sample preparation (mix =mixing type, wash = washing type).

In the absence of surfactant the intensity of the (*10*) Bragg peak I_{10} is much higher than that of the (*11*) peak (I_{10}/I_{11} > 5 in D_2O) and the (20) and (21) peaks appear as a shoulders higher q. No Bragg peaks are detectable in contrast-matching H_2O/D_2O. In the presence of surfactant the Bragg peaks reappear but their intensities vary greatly with the experimental conditions. Specifically, in contrast-matching water the (10) peak can be strongly reduced or even completely absent in the case of DPC (Fig. 1), but not for CPC (Fig. 2). For each of the two surfactants the relative intensities of the first and second Bragg peaks also depend strongly on the salt concentration and sample preparation, indicating that the surfactant self-assembly in the pores is affected by these parameters. A further important finding is that the relative intensities of the first and second Bragg peaks are strongly dependent on the chosen contrast (Fig. 3).

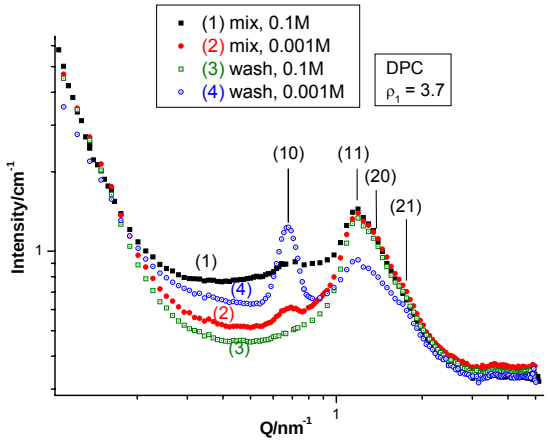

Fig. 1: Experimental scattering curves for DPC in SBA-15 in contrast-matching H_2O/D_2O at two salt concentrations (mixing and washing type samples)

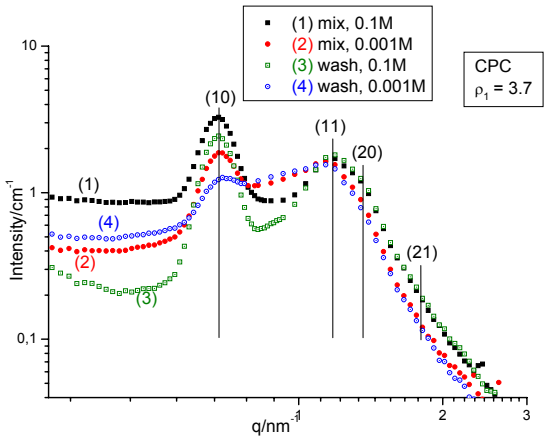

Fig. 2: Scattering curves for CPC after subtraction of incoherent background, but otherwise as in Fig.1

→

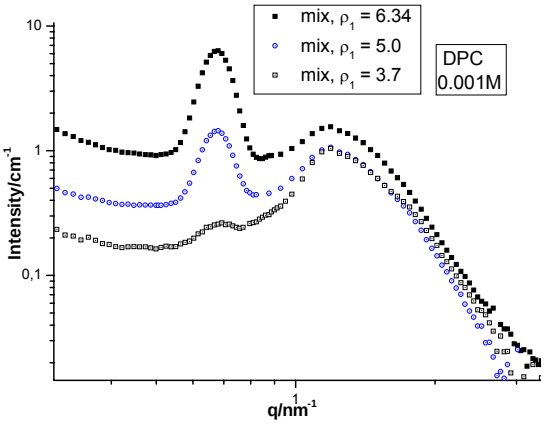

Fig. 3: Influence of water contrast on the scattering curves for DPC in SBA-15 (low salt concentration)

We are analysing the SANS spectra in terms of a model which combines the structure factor S(q) of a 2D hexagonal lattice with the form factor F(q) of cylindrical pores (radius R) without or with an adsorbed surfactant film of uniform thickness d, which is modelled by a core-shell cylinder with three SLD levels for the core liquid (ρ_1), adsorbed film (ρ_2 =1.65x10^{10}cm^{-2}) and matrix (ρ_3 =3.7x10^{10}cm^{-2}).

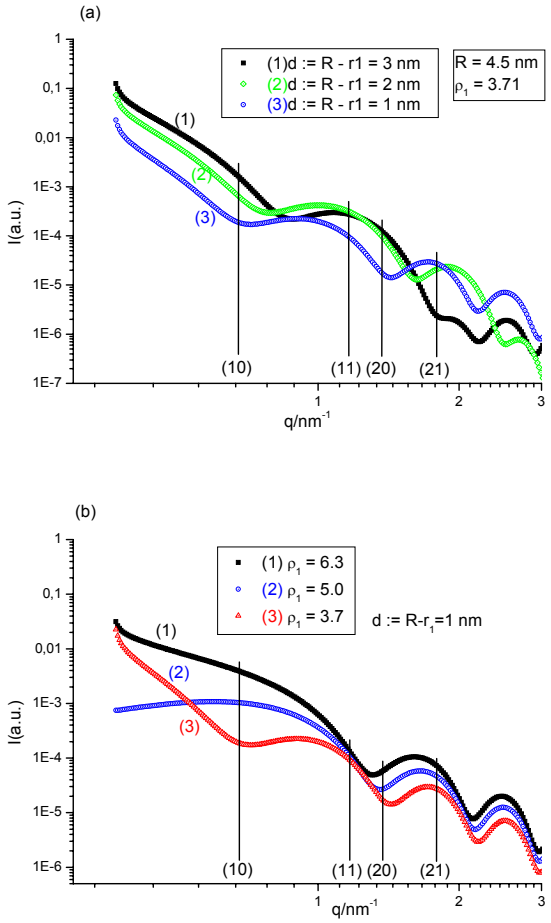

Fig. 4: Form factor $F(q)^2$ of core-shell cylinder illustrating the influence of (a) the shell thickness d and (b) the scattering length density of the core ρ_1. The positions of the prominent Bragg peaks (*hk*) of the SBA-15 sample are marked by vertical lines.

As shown in Fig. 4, the quantity $F(q)^2$ exhibits pronounced minima at q values which are strongly dependent on the film thickness d and the density ρ_1, which explains that these parameters will directly affect the intensity of the Bragg peaks. Specifically, for the contrast-matching core liquid (ρ_1 = 3.7x10^{10}cm^{-2}) the value of $F(q)^2$ at the position of the (*10*) Bragg peak increases by one order of magnitude as the film thickness increases from 1 nm to 3 nm, which offers an explanation for the sensitivity of this Bragg peak to the adsorbate.

For the quantitative analysis of the SANS data it is necessary to account for the scattering background of the samples. A combination of a Porod term I_P/q^4 and a Debye term $I_D/(1+\xi^2q^2)^2$ was found to give a fair representation but further studies are in progress. A fit of the data for a sample with CPC in contrast-matching water is shown in Fig. 5.

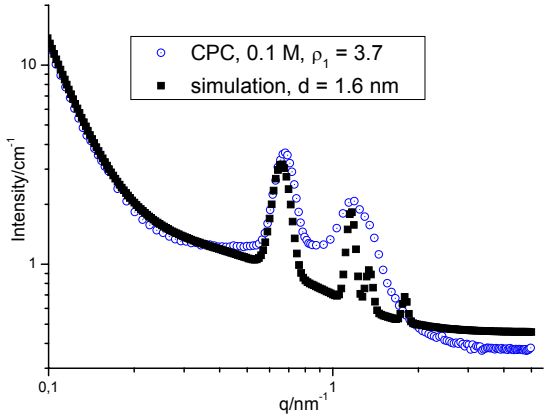

Fig. 5: Fit of a scattering curve for CPC in contrast-matching water by the present model (see text)

References

[1] BENSC EXPERIMENTAL REPORTS **2004**, p.84, CHE-04-0935

[2] BENSC EXPERIMENTAL REPORTS **2004**, p.85, CHE-04-1011

	EXPERIMENTAL REPORT **Effect of PEI as a first layer and treatment of PAH/PSS films on their structure**	Proposal N° EF Instrument **V6 / X-ray** Local Contact Rumen Krastev
Principal Proposer: Experimental Team:	M.Kolasińska - ICSC PAS, Cracow, Poland M.Kolasińska - ICSC PAS, Cracow, Poland R.Krastev - MPI, Golm P.Warszyński - ICSC PAS, Cracow, Poland	Date(s) of Experiment 23.02. - 28.02.2005

Date of Report: 02.03.2005

The sequential adsorption of oppositely charged polyelectrolytes from their solutions (layer-by-layer deposition technique [1]) is a powerful method for obtaining materials with controlled surface properties [2]. Therefore, such self - assembled PE films have a great application potential [3]. They can be used as supporting layers in biomaterials or for chemical and biochemical sensing as well as separation membranes for gases or dissolved species.

In our research we studied PAH/PSS films consisting of 13 and 14 layers, terminated with PAH and PSS, respectively. Films were deposited on silicon wafers. Such multilayers were compared with analogous –having PEI as the first (anchoring) layer. We focused also on the effect of post-treatment by 48-hours conditioning in HCl and NaOH solutions having the same ionic strength (10^{-3}M) and pH value: 3 and 11, respectively.

The properties of given multilayers were studied by X-ray reflectometry. The experiments were performed in Θ/2Θ geometry. The solid/air and solid/ water vapour experimental set-ups were employed.

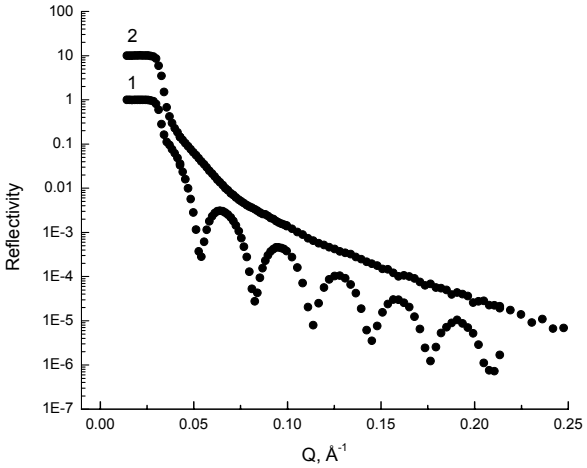

Fig. 1: Reflectivity curves of PEI/$(PSS/PAH)_6$ (1) and $(PAH/PSS)_6$PAH (2) multilayers measured in water vapour atmosphere

There is a tremendous difference between two films containing PEI and analogous without PEI layer (see fig. 1) One can observed well pronounced fringes in case of PEI/(PSS/PAH) films, while PAH/PSS films seem to be very rough or heterogenous.

		PAH/PSS		PEI(PSS/PAH)	
		thickness /A	**roughness /A**	**thickness /A**	**roughness/ A**
13	Untreated	126.33	34.63	152.52	6.842
	pH = 3	135.90	15.62	163.31	6.116
	pH = 11	126.26	12.52	152.31	6.063
14	Untreated	129.06	19.76	156.19	4.29
	pH = 3	134.03	19.71	154.68	9.19
	pH = 11	128.75	24.28	148.63	10.60

Tab. 1: Results for measurements carried out in air atmosphere

		PAH/PSS		PEI(PSS/PAH)	
		thickness /A	**roughness /A**	**thickness /A**	**roughness/ A**
13	Untreated	165.77	5.802	198.54	6.636
	pH = 3	-	-	160.128	11.252
	pH = 11	161.01	6.122	191.44	6.854
14	Untreated	187.42	6.046	211.18	5.906
	pH = 3	-	-	162.71	10.783
	pH = 11	189.63	6.641	211.57	6.751

Tab. 2: Results for measurements carried out in water vapour cell

Results collected in Tab.1,2 show that presence of PEI makes films thicker and more ordered. Treatment doesn't influence the thickness of given films.

References

[1] G.Decher: Science **277** (1997) 1232

[2] P.T. Hammond: Current Opinion in Colloid and Interface Science, **4** (2000) 430-442

[3] P.Bertrand, A.Jonas, A.Laschewsky, R.Legras: Macromol. Rapid Commun. **21** (2000) 319

	EXPERIMENTAL REPORT **Neutron diffraction measurements on micro- and nano-sized precipitates embedded in a Ni-base superalloy and after their extraction from the alloy**	Proposal N° MAT-01-1763 Instrument **E9** Local Contact Michael Tovar
Principal Proposer: Experimental Team:	R. Gilles - TU München R. Gilles - TUM FRMII M. Hölzel - TUM FRM II + TU DA D. Mukherji - ETH Zürich, CH P. Strunz - ASCR NPI Rez, CZ M. Tovar - HMI Berlin	Date(s) of Experiment 12.09. - 19.09.2005

Date of Report: 09.01.2006

Neutron and X-ray diffraction are eminently suitable techniques to determine lattice misfit in nickel-base superalloys. Due to the different measuring techniques and sensitivities of the probes, sometimes one method is preferable to the other one. Lattice parameter misfit value between coherent precipitate and the matrix in Ni-base superalloys plays a significant role in controlling the precipitate morphology in the alloy. Modern single crystal superalloys contain relatively large γ' precipitates (450 nm cuboidal Ni_3Al with $L1_2$ crystal structure) but recently, it was demonstrated that intermetallic phase nano-particles (10 – 100 nm size) can also be extracted from such Ni-base superalloys [1, 2]. The misfit value in the superalloys is generally controlled to a low value as it affects the structural instability at high temperatures. Obviously it is necessary to use high resolution mode to distinguish the reflections from the two phases of precipitate and matrix. It is however, not indispensable to have split reflections but only necessary to have enough information to fit a second peak in the reflection. Because of mosaicity and slight variations in chemical composition inside the bulk material, the different peaks are broadened which decrease the resolution for misfit measurements. This fact makes perfect alignment for a Bragg peak over a representative sample volume in the order of mm^3 or bigger more difficult. Statistical occupation of the Ni_3Al structure by heavy elements like W, Ta, Cr, Mo present in superalloys for strengthening the precipitates could also lead to very small shifts of the d-values for the different lattice planes hkl. It means, alignment of a single reflection (h_1,k_1,l_1) do not automatically provide other (h,k,l) positions with high accuracy. In the present measurements each (hkl) reflection in the oriented superalloy sample was optimised with a ω-tilting procedure [3].

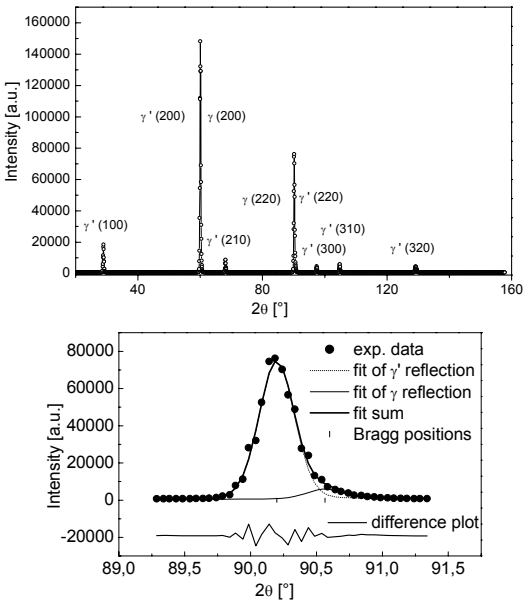

Fig. 1: Top: Neutron diffraction pattern of extracted micro-particles (λ = 1.795 Å).
Bottom: A fit of the (220) reflection including the two phases γ and γ'.

Summary of measurements: Lattice constants [nm] in micro-particles/nano-particles: a) extracted γ' particles 0.358502(60)/ 0.35843(10); b) γ' in γ/γ' bulk samples 0.35848(70)/ 0.35853(100) and c) γ in γ/γ' bulk samples 0.3573(10) /0.3576(20) with resulting misfit
δ (%) + 0.33/+ 0.27.

References

[1] D. Mukherji, R. Müller, R. Gilles, P. Strunz, J. Rösler and G. Kostorz, Nanotech. (2004), 15, 648.
[2] J. Rösler, D. Mukherji. Advance Engg. Mater. (2003), 5, 916.
[3] R. Gilles, D. Mukherji, M. Hoelzel, P. Strunz, D.M. Toebbens and B. Barbier, Acta Materialia (2006), in print.

	EXPERIMENTAL REPORT **Evolution of pore microstructure in thermal barrier coatings**	Proposal N° MAT-04-1127-EF Instrument **V4** Local Contact Jörg Haug
Principal Proposer: Experimental Team:	A. Wiedenmann - HMI Berlin B. Saruhan-Brings - DLR Köln J. Haug - HMI Berlin	Date(s) of Experiment 01.06. 05.06.2005

Date of Report: 09. Jan. 2006

Thermal barrier coatings (TBCs) protect turbine blades and other hot-structure components of gas turbines and engines. A TBC system consists of a Ni-based superalloy substrate, a metallic bond coat and a ceramic top coat based on partially Yttria stabilized Zirconia (PYSZ). As-coated EB-PVD PYSZ layers consist of individual columns which are weakly interconnected and display intercolumnar open porosity leading to high thermal shock resistance. Additionally, most of the open porosity at the column edges is due to the nanosized secondary columns, so called feather-arms which are built by secondary shadowing and depend on the rotation speed and the angle between the substrate and the vapour during evaporation. Furthermore, due to the interruption of deposition by rotation, finer elongated channellike pores are formed within the primary columns (i.e. intra-columnar voids).

SANS is sensitive to pores in the nanometer scale and therefore intracolumnar voids and feather-arms of the EB-PVD TBCs can be investigated with this method. In this experiment we investigated the morphology changes of anisotropic pores in two EB-PVD TBCs with different sample morphologies during heat treatment.

SANS measurements perpendicular to the substrate show highly anisotropic 2-D pattern which vary for the different morphologies (Fig. 1). Fig. 2 shows the apparent Porod constants for the samples with standard and fine morphology [1,2]. The as-coated samples show anisotropy which can be described by elliptical voids. After heat treatment at 1100°C the values for the apparent Porod constants decrease drastically indicating a reduction in the apparent surfaces. This indicate that the elliptical voids in the as deposited state reduce there surface very fast at heating up to 1100°C leading to more spherical but still anisotropic surfaces.

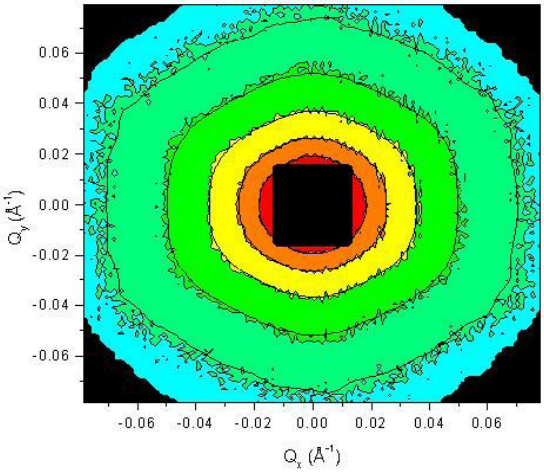

Fig. 1: Measured and fitted (solid lines) 2D scattering curve of the sample with fine morphology.

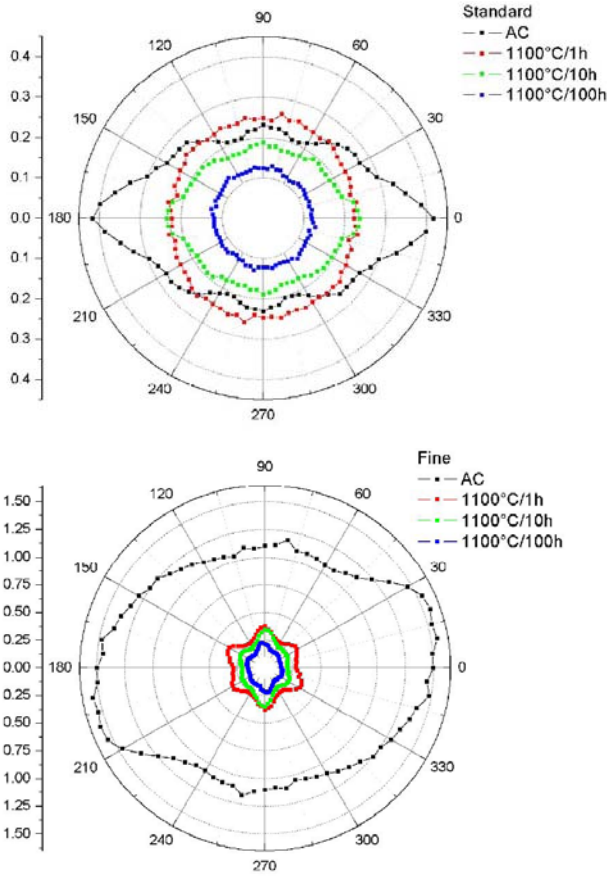

Fig. 2: Anisotropic apparent Porod constants as a function of the azimuthal angle around the incident beam for samples with standard (top) and fine (bottom) morphology.

References

[1] J. Haug, A. Wiedenmann, A. Flores, B. Saruhan-Brings, P. Strunz: *Evolution of pore microstructure in Thermal Barrier Coatings studied by SANS*, Physica B, submitted

[2] A. Flores Renteria, B. Saruhan, U. Schulz, H.-J. Raetzer-Scheibe, J. Haug, A. Wiedenmann: *Effect of Morphology on Thermal Conductivity of EB-PVD PYSZ TBCs*, Surface and Coatings Technology, submitted

	EXPERIMENTAL REPORT **Contrast variation method to reduce the open porosity in thermal barrier coatings**	Proposal N° MAT-04-1180-EF Instrument **V4** Local Contact Jörg Haug
Principal Proposer: Experimental Team:	A. Wiedenmann - HMI Berlin B. Saruhan-Brings - DLR Köln J. Haug - HMI Berlin	Date(s) of Experiment 09.08. - 11.08.2005

Date of Report: 09. Jan. 2006

Partially yttria stabilized zirconia (PYSZ) based thermal barrier coatings (TBC) manufactured by electron beam – physical vapour deposition (EB-PVD) process is a crucial part of a system which protects the blades working under severe service conditions at the high pressure sector of aero engines and stationary turbines. These materials show a high strain tolerance relying on their unique coating morphology which is comprised by weakly bonded columns. Growth of these columns occurs in a preferred crystallographic orientation producing inter-columnar gaps in between them. Furthermore, the open porosity is enhanced by the presence of voids between feather-like sub-columns which are surrounding the primary column surfaces inclined toward their growing axis. Finally, rotation of the specimens during the vapour deposition process produces additional intra columnar closed pores formed inside the primary columns.

SANS is sensitive to pores in the nanometer scale and therefore closed as well as open porosity can be investigated. To reduce the scattering from the inter-columnar gaps and feather arms, SANS contrast variation technique was applied. Contrast matching involves identification of a solvent having the same neutron scattering length density as the porous TBCs. Pores are filled with different mixtures of H_2O/D_2O in the range of the theoreticaly scattering length density (ideal mixture: $10\%H_2O/90\%D_2O$). To check the wetting of the surface, also deut. Toluol was used.

Fig. 1 shows the SANS curves for the dry sample and in immersion liquid. In all liquids the scattered intensity is decreased in the low Q range.

In fig. 2 the apparent Porod constants are plotted. With immersion a decrease in the scattering interface can be seen in all directions.

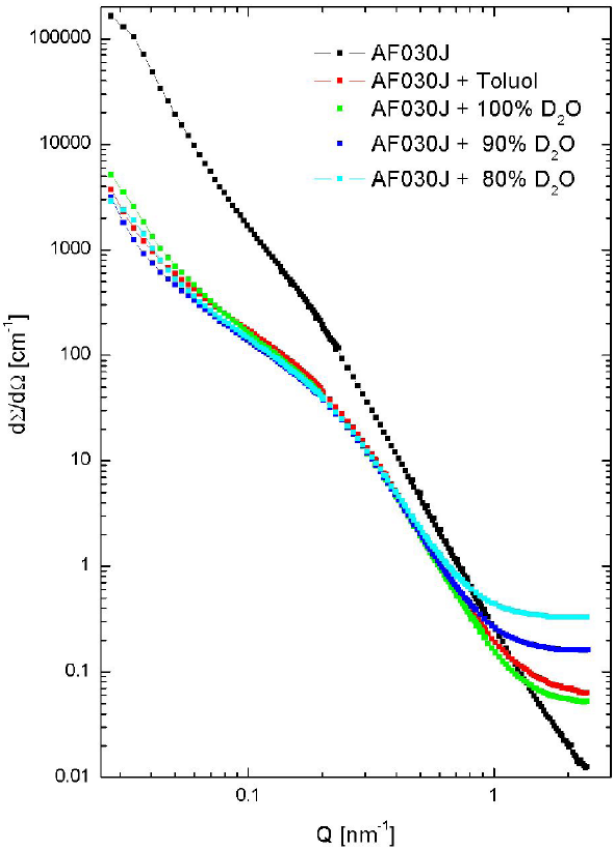

Fig. 1: SANS curves from dry sample and samples in deut. Toluol and H2O/D2O mixtures

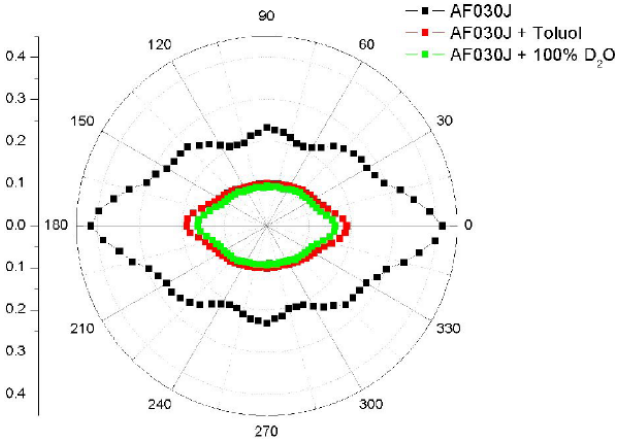

Fig. 2: Anisotropic apparent Porod constants as a function of the azimuthal angle around the incident beam for dry sample and samples with deut. Toluol and D2O

	EXPERIMENTAL REPORT **Solution treatment optimization in SX-CM186LC superalloy using in-situ SANS**	Proposal N° MAT-04-1111 Instrument **V4** Local Contact Jörg Haug
Principal Proposer: Experimental Team:	J. Zrník - TU Košice, Slovakia P. Strunz - NPI Řež near Prague J. Zrník - TU Košice J. Haug - HMI Berlin	Date(s) of Experiment 24.05 - 28. 5.2005

Date of Report: 09.01.2005

An important way to improve properties of materials for power generation is to optimize their microstructure through heat treatment. The primary purpose of the proposed experiment is to investigate in situ the solution treatment process of SX-CM186LC superalloy [1]. SX-CM186LC contains increased amount of grain boundary strengthening elements what can result in a significant decrease of its incipient melting temperature and so affect the complete dissolution of γ' phase. The solutioning process have to care about proper dissolving of MC complex carbide as well. In-situ high-temperature SANS method [2] was primarily used for this task.

In Fig. 1, a rough evaluation of the SANS data for two measured samples is plotted. The displayed parameter, i.e. the maximum intensity of the measured data at Q=0 (for SDD=16m and λ=19.6 Å) in dependence on time and temperature, is an inverse quantity to the scattering probability. With decreasing volume fraction of precipitates and/or their scattering contrast, this quantity should increase, reaching an absolute maximum when all the precipitates are dissolved.

The performed SANS experiment revealed, that a large majority of the γ' phase in SX-CM186LC is dissolved already at 1200°C. The remaining large γ' precipitates, γ/γ' eutectics and/or carbides, however, remain in the material still at least up to 1325°C. Homogenization of the γ matrix (between dendritic and interdendritic regions) can be observed within this range, causing an increase of the scattering contrast between the matrix and the remaining particles (and consequently the decrease of the maximum intensity - Fig. 1, sample 2).

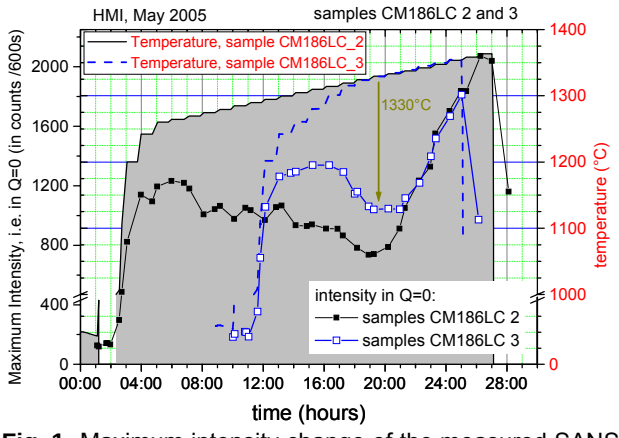

Fig. 1: Maximum intensity change of the measured SANS data at Q=0 for the two measured CM186LC samples.

At around 1330°C, the dissolution of remaining large precipitates starts. When increasing the temperature gradually (linear increase with time) up to 1365°C (i.e. the highest applied temperature, where the sample is already partially melted), a gradual dissolution can be observed without any sharp step-like dependence. It indicates, that the dissolution proceeded depending on the particular size of the precipitates and carbides within their size distribution (smaller precipitates dissolved first). Even at 1365°C, there was no full dissolution of the remaining inhomogeneities. It means that a complete dissolution of inhomogeneities cannot be reached for SX-CM186LC. On the other hand, elemental homogenization of the γ matrix itself can be most probably obtained when heating up to approximatelly 1330°C.

The second performed in-situ measurement (sample No. 3, see Fig. 1) was intended to compare influence of the initial heating rate on the dissolution of precipitates. Starting at 1325°C, the thermal history followed the thermal history of the sample No.2 (except of the highest reached temperature – see Fig.1). The scattering intensity of the sample No. 3 at high temperatures fits that one of the slowly heated-up sample No.2. It indicates that the elemental homogenization, which occurred during the slow temperature increase in sample No.2, occurs equivalently well at higher temperatures (1315-1340°C) and in shorter time period for sample No.3. The longer heat treatment thus has seemingly no advantage over the shorter one.

Transmission measurement, which was also performed during temporarily stops in the temperature increase, indicated reduction of the sample thickness during the exposure above 1200°C. From the slope of the transmission increase, it can be deduced that rather elements with higher absorbtion cross section (B, Co, Hf, W, Ni) content were reduced during that exposure.

The usable measuring time was unfortunately significantly shortened due to the damage of both thermocouples in the sample stick. Only a limited number of the measurements was thus performed.

References

[1] Harris, K. and Wahl, J.B.: in Parsons 2000, Advanced Materials for 21st Century Turbines and Power Plant, Proceedings of the 4th International Charles Parsons Turbine Conference, A. Strang et al (eds.) (2000), pp. 832-846.

[2] P. Strunz, D. Mukherji, R. Gilles, J. Rösler and A. Wiedenmann: Materials Science Forum 426-432 (2003) 821-826

	EXPERIMENTAL REPORT **Reordering dynamics in Co-ferrofluids studied by stroboscopic SANS**	Proposal N° MAT-04-1125-EF Instrument **V4** Local Contact Albrecht Wiedenmann
Principal Proposer: Experimental Team:	A. Wiedenmann - HMI Berlin R. Gähler - ILL Grenoble, F A. Wiedenmann, U. Keiderling, K. Habicht - HMI Berlin	Date(s) of Experiment 01.11. - 06.11.2005

Date of Report: 09. Jan. 2006

Real-time investigations of nanosized inhomogeneities by means of SANS usually are limited to slow processes where during data acquisition time the system remains in a quasi-steady state. For oscillating processes stroboscopic SANS measurements are possible in short time slices when data collection can be synchronized with the periodic process [1-3].

The aim of this proposal was to investigate the dynamics of the ordering process which occurs in concentrated Co-ferrofluids when a magnetic field is applied. Here we compare the classical stroboscopic technique with the result of a TISANE experiment [4]. A solenoid was built which provided a periodic sine-wave modulation of the vertical external magnetic field up to amplitudes of 25 mT and frequencies up to 3 kHz. The same concentrated Co-ferrofluid sample (MFT3) has been used as in the TISANE experiment. List-mode data acquisition was performed in the 2 D-detector of the SANS instrument V4 at HMI. Using a trigger signal from the ac-field SANS intensities of corresponding time slices were accumulated. The reversibility of the reordering process has been confirmed by comparing the SANS results obtained with the oscillating magnetic field with those at fixed magnetic field provided by a dc- current in the solenoid.

At low frequencies of the applied magnetic field we observe again a periodic response of the 2D-scattering patterns. The scattering intensity is isotropic for the time channels which correspond to the zero value of the magnetic field while for maximum and minimum amplitude of H strongly anisotropic behaviour is observed. This is characteristic for the alignment of the magnetic moments of the nanoparticles along the external field. The time variation of the sum intensity is shown in fig. 1 for different frequencies of the ac-field. Oscillations of the intensities were detected with decreasing amplitudes only up to about $\nu_s = 600$ Hz, while in TISANE the threshold frequency of about 1300 Hz was observed. In fact, in the conventional stroboscopic technique the limit of time resolution results from the different velocities of neutrons present in the incident beam. In fig. 2 we present the scattering intensities which result from a sine-wave oscillation of the magnetic field with frequencies ν_s calculated for the detector distance of 4 m and smeared out by a triangular wavelength-distribution of $\Delta\lambda/\lambda = 0.1$ with an average wavelength of $\lambda = 0.6$ nm. Under the experimental conditions it is evident that already at $\nu_s = 600$ Hz the intensity modulation produced by the oscillating magnetic field will be mostly smeared out.

The limitation of the conventional technique is clearly seen by comparing with the results obtained by TISANE [4]. While the scattering intensities were much higher and the Q resolution was better in the conventional stroboscopic SANS technique a clear superiority of TISANE occurs concerning the time-resolution. In the present case of reordering dynamic in ferrofluids the threshold of 1300 Hz observed by TISANE is a real physical quantity since this value is still far below the time resolution. In the conventional technique the time resolution limit can be further increased by reducing $\Delta\lambda/\lambda$ of the velocity selector or by the use of an additional chopper.

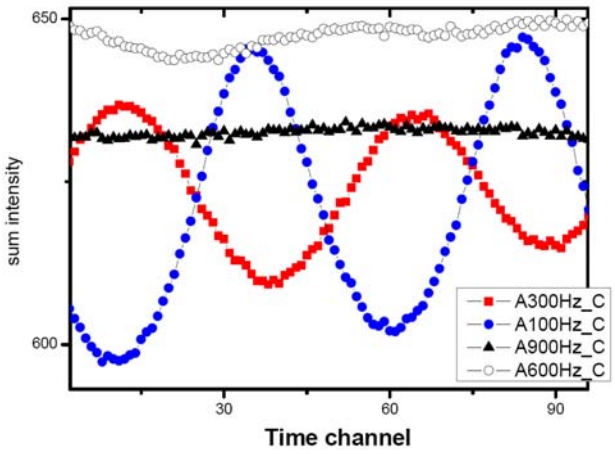

Fig. 1: Time dependence of integrated SANS intensity for oscillating magnetic fields with frequencies 100, 300, 600 and 900 Hz and a maximum amplitude of 200 Gs.

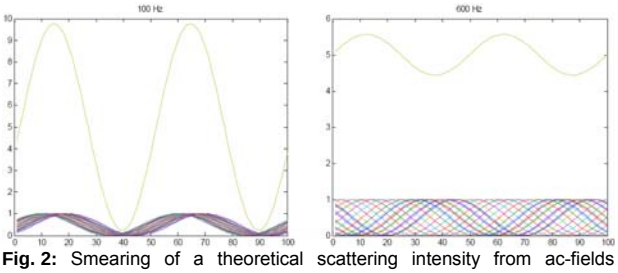

Fig. 2: Smearing of a theoretical scattering intensity from ac-fields oscillating with frequencies of 100 Hz (lhs) and 600 Hz (rhs) by wavelength spread of 10 % at a detector distance of 4m.

Acknowledgement
The project was supported by DFG Project Wi 1151/2

References

[1] A. Wiedenmann, A. Hoell, M. Kammel, P. Boesecke: Phys Rev. E 68 (2003) 031203, 1-10
[2] A. Wiedenmann, U. Keiderling R. May, C. Dewhurst: Physica B(2006)
[3] U. Keiderling, A. Wiedenmann: Physica B(2006)
[4] A. Wiedenmann, U. Keiderling, K. Habicht, M. Russina, R. Gähler: BENSC report (2005)

BENSC	**EXPERIMENTAL REPORT** **Field-dependent relaxation behaviour of Co-ferrofluid investigated with stroboscopic time-resolved SANS and SANSPOL**	Proposal N° MAT-04-1130-EF Instrument **V4** Local Contact Uwe Keiderling
Principal Proposer: Experimental Team:	A. Wiedenmann - HMI Berlin U. Keiderling - HMI Berlin A. Wiedenmann - HMI Berlin	Date(s) of Experiment 18.09. - 20.09.2005

Date of Report: 09. Jan. 2006

In a different report of this volume, we described the first application of the new time-resolved stroboscopic SANS technique established at the V4 SANS instrument. Using listmode data acquisition and a comfortable software solution allowing fully flexible control over the spacial and time resolution of the results after the experiments, we investigated the decay process of inter-particle order in a Co-ferrofluid. The present work now continues and expands this first attempt, refining the experiments and interpretation, and aiming to gain new results on the correlation between the strength of the magnetic field and the decay time constant.

In these new experiments, the same concentrated Co-ferrofluid [1] contained in a Hellma quartz cell of 1 mm thickness was placed in the homogeneous field of a standard electromagnet, at a fixed sample-detector distance of 4 m. Polarized neutron in-situ SANS measurements (SANSPOL) were now performed with various magnetic fields between 0.005 T and 1 T. For each field, the scattering intensities were measured subsequently with incident neutron beam polarization parallel (I-) and antiparallel (I+) to the magnetic field. For each of these polarizations, listmode data were acquired with the field cycling between the two values "field on" (0.005 T ... 1 T, depending on the particular experiment) and "field off" (remanence < 0.005 T). Approximately 200 to 1200 of these "on"/"off" cycles were stroboscopically superimposed by the software to obtain sufficient statistics for data evaluation with a time resolution of 100 ms. Subtraction of the SANSPOL intensities (I-)-(I+) yielded solely the nuclear-magnetic contribution which is affected by the interparticle correlation , leading to an anisotropic structure factor [2].

The "on" phase with a duration of 3 to 5 s created the magnetic ordering in the sample. The ordering process turned out to take place significantly faster than the realizable up-ramp of the standard electromagnet used (e.g. ≈ 0.18 s ramp for 0 T → 0.005 T, ≈ 3 s ramp for 0 T → 1 T). We found that the ordering already starts at very small fields, and then continuously develops with increasing field strength, as shown in fig.1. The kinetics of ordering has been investigated separately with the TISANE method [3], and has been described in a different report of this volume.

Evaluation and interpretation of the data is now in progress, and results will be published in [4].

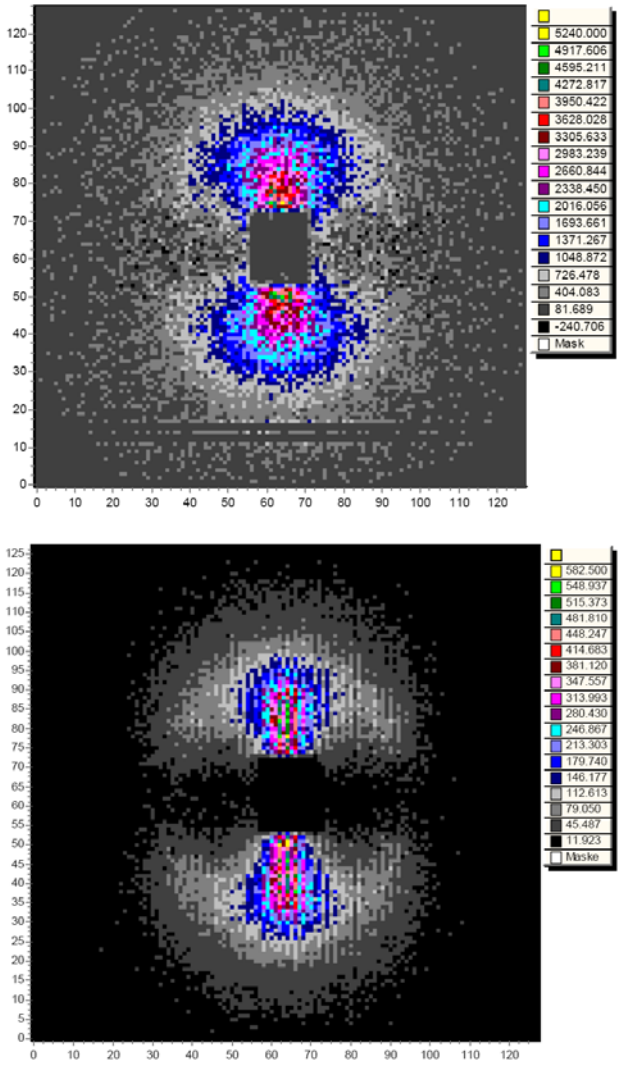

Fig. 1: SANSPOL intensity difference pattern during "field on", at H = 0.005 T (top) and H = 1 T (bottom). The display colors were normalized to the individual data ranges.

References

[1] A. Wiedenmann, A.Heinemann: JMMM **289** (2005) 58-61

[2] A.Wiedenmann: Physica B **256** (2005) 246-253

[3] R. Gähler, R. Golub: ILL Scientific council April (1999) SC99-1, 73

[4] U. Keiderling, A. Wiedenmann: to be presented at SAS2006 Kyoto

	EXPERIMENTAL REPORT $Nd_{60}Fe_{20}Co_{10}Al_{10}$ alloys measured by SANSPOL at high magnetic field	Proposal N° MAT-04-1177-EF Instrument **V4** Local Contact Olivier Perroud
Principal Proposer: Experimental Team:	A. Wiedenmann - HMI Berlin O. Perroud - HMI Berlin A. Wiedenmann - HMI Berlin	Date(s) of Experiment 13.06. - 17.06.2005

Date of Report: 06. Jan. 2006

Bulk amorphous $Nd_{60}Fe_{20}Co_{10}Al_{10}$ rods show hard magnetic behaviour at room temperature. The alloy is composed of a Nd-rich and a Fe-rich phase. The preparation of such alloys have a strong influence of the magnetic properties. For the present alloy, a rod of 3mm was used for which the magnetization curves [1] show two Curie temperatures at T_{c1} = 50 K and T_{c2} = 495 K attributed to some Nd-rich nanoparticles and a metastable U-phase [2].

Small angle neutron scattering with polarised neutrons were carried out at the V4 instrument. The experiment was equipped with the VM1 vertical cryomagnet which reaches a magnetic field up to 15 T. Due to the magnetic environment around the instrument, only 10 T measurements were allowed. A relatively high background was encountered, probably due to the Al-alloy of the cryomagnet windows in the beam. The sample have been studied by Small Angle Scattering using polarized neutrons (SANSPOL). This technique is very sensitive of magnetic components in the alloys and allows us to separate accurately nuclear and magnetic scattering contributions. Despite the high background, this technique allows to obtain reliable data by subtracting the intensities of the two polarisation states I^- and I^+, respectively.
Previous experiments performed one the same alloys at 6 T have shown an increase of the scattering intensity at Q > 0.2 nm^{-1} with respect to H = 1 T [3,4]. In the present experiment at 10 T, an additional increase of the SANSPOL difference intensity was observed in the same Q range. A comparison of the two experiment is shown in fig. 1 which confirms fully our previous hypothesis: Nanosized Nd-rich particles are embedded in the Fe-rich matrix. At 150 K the matrix is ferromagnetic while the Nd-particles are non-magnetic. However, the ferromagnetic matrix is not fully magnetized even in strong external fields: Even at 10 T magnetic domains are partly pinned at the nonmagnetic nanoparticles. The use of the VM1 cryomagnet is not optimal but many progress were made to improve this sample environment. The experiments were performed at 5 K and 150 K with an applied magnetic field of 1 T and 10 T.

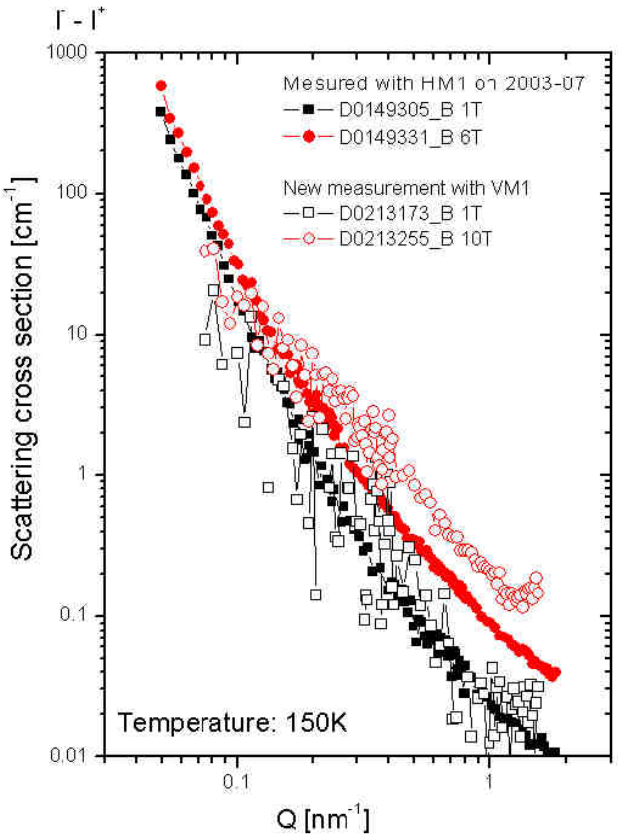

Fig. 1: shows the one-dimensional pattern of $Nd_{60}Fe_{20}Co_{10}Al_{10}$ measure at 150 K with different sample environment at 1 T, 6 T, 10 T.

Acknowledgement
This work is supported by DFG-project Wi 1151/3-2

References

[1] A. Inoue et al.: Mat. Transactions JIM **V37**-2(1996)99-108
[2] G. Kumar et al.: J. of Alloys and Compounds **248** (2003) 309.
[3] E. García-Matres et al.: BENSC EXP. REPORTS **2004**, p.60
[4] E. García-Matres et al.: Physica. B **350** e315-e318 (2004)

	EXPERIMENTAL REPORT **Reordering in magnetic colloids induced by variation of magnetic fields**	Proposal N° MAT-04-1178-EF Instrument **V4** Local Contact Albrecht Wiedenmann
Principal Proposer: Experimental Team:	A. Wiedenmann - HMI Berlin A. Heinemann - HMI Berlin M. Kammel - HMI Berlin A. Wiedenmann - HMI Berlin	Date(s) of Experiment 21.03. - 24.03.2005

Date of Report: 17. Jan. 2006

Small-angle neutron scattering with polarized neutrons (SANSPOL) has been proved as an excellent tool to get insights into the inherent and magnetic field induced nano-structure of magnetic liquids [1]. Information obtained so far turned out to be essential for the understanding of structure formation as well as the fluid response under magnetic field and shear-forces [2, 5]. Many experiments were performed on a wide range of fluids and signatures from different structures have been observed [2, 3, 4]. To cancel out some ambiguities in this experiments we carried out more sophisticated SANSPOL experiments with a Co-based magnetic liquids on the V4 instrument. A horizontal cryo-magnet was installed on a turntable to vary the angle between the incoming neutron and the external field **H** both spanning a plane perpendicular to the detector. By turning the cryo-magnet both the field and the sample change there orientations in respect to the neutron beam. Additionally the sample could be rotated independently. We performed three combinations of these rotational degrees of freedom and analyzed the 2-D scattering pattern with a newly developed fit procedure taking into account all influences of the varying orientation between **Q**-vector and **H**. Furthermore the use of polarized neutrons enables us to obtain also quantitative values for the form and structure factor parameters. All results are consistent with the picture of a local hexagonal ordering of the nanoparticles induced by the external magnetic field. The results show unambiguously that the magnetic moments are aligned along the external magnetic field. This re-orientation of the particle moments must give rise to a rearrangement of the local hexagonal structure in respect to the new field direction to explain the observed scattering signatures.

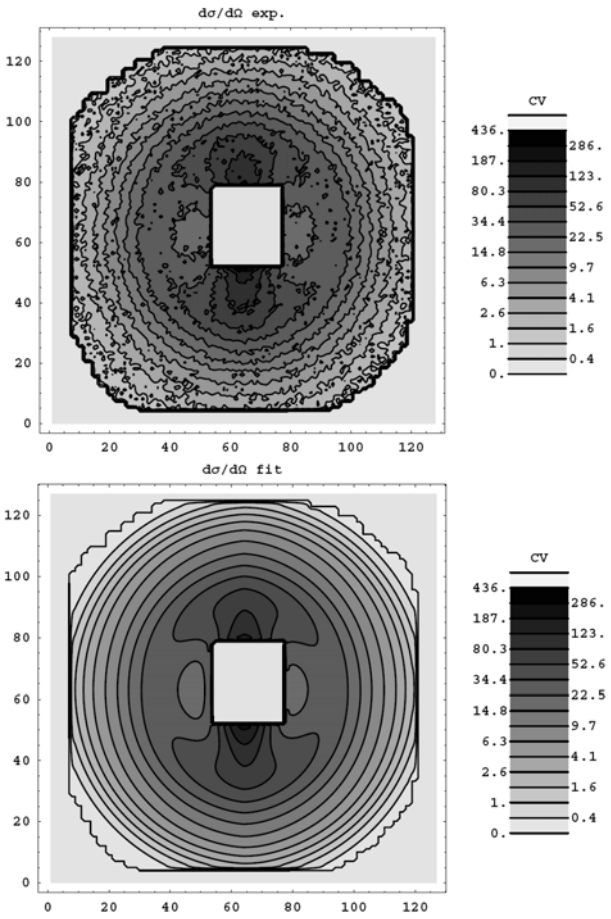

Fig. 1: Experimental data (top) and fit results (bottom) for the horizontal (1 T) magnetic field case, using a hexagonal structure factor and core-shell form factors.

Acknowledgement
Work supported by DFG priority program SPP1104.

References

[1] A. Heinemann and A. Wiedenmann, J. Appl. Cryst. **36** (2003) 845-849.

[2] A. Wiedenmann, A. Hoell, M. Kammel and P. Boesecke, Phys. Rev E **68** (2003) 031203.

[3] A. Heinemann and A. Wiedenmann, JMMM **289** (2005) 149-151.

[4] A. Wiedenmann and A. Heinemann, JMMM **289** (2005) 58-61.

[5] L. Pop et al., JMMM **289** (2005) 303-306.

	EXPERIMENTAL REPORT The nanostructure of encapsulated magnetite nanoparticles - a SANSPOL study	Proposal N° MAT-04-1179-EF Instrument **V4** Local Contact Albrecht Wiedenmann
Principal Proposer: Experimental Team:	A. Wiedenmann - HMI Berlin M. Kammel - HMI Berlin A. Wiedenmann - HMI Berlin A. Heinemann - HMI Berlin	Date(s) of Experiment 15.04. - 23.04.2005

Date of Report: Jan. 2006

Polystyrene nanoparticles can be produced by the miniemulsion process which gives access to a broad range of possible particle sizes with a small size distribution [2]. The surface of such particles can be modified to bind biological active agents (e.g. antibodies) on them. Additionally, the miniemulsion process can encapsulate magnetic nanoparticles to the polystyrene nanoparticles which allows to influence the particles by external magnetic fields. In order to evaluate the unknown structure of the polystyrene particles, as well as the magnetic structure of the encapsulated magnetic nanoparticles Small Angle Neutron Scattering with polarized neutrons (SANSPOL) [1] was performed.

The samples were prepared with Magnetite nanoparticles (Fe_3O_4) with deuterated and non-deuterated solvents (water) and polystyrene. Additionally, we investigated the pure Magnetite nanoparticles dispersed on octane to get detailed information about the nanoparticles before the preparation step of the miniemulsion. The measurements have been performed at the instrument V4, using polarized neutrons with a wavelength $\lambda = 0.6$ nm, covering a range of momentum transfer Q between 0.04 nm^{-1} and 4 nm^{-1}. A magnetic field up to 1T was applied to the samples.

The SANSPOL intensities for two polarisation states $I^+(Q\perp H)$ and $I^-(Q\perp H)$ are presented on fig. 1 for non encapsulated Magnetite nanoparticles in octane and for deuterated styrene in water. The intensity of the nonencapsulated particles strongly depends on the polarization direction of the neutrons. The analysis results in a logarithmic normal distribution of magnetic particles with a mean size of 2.7 nm.

On the other hand the intensity of the encapsulated particles shows no significant change by changing the polarization direction of the neutrons. The intensity is dominated by the scattering of the polystyrene nanoparticles.

The data analysis is in progress.

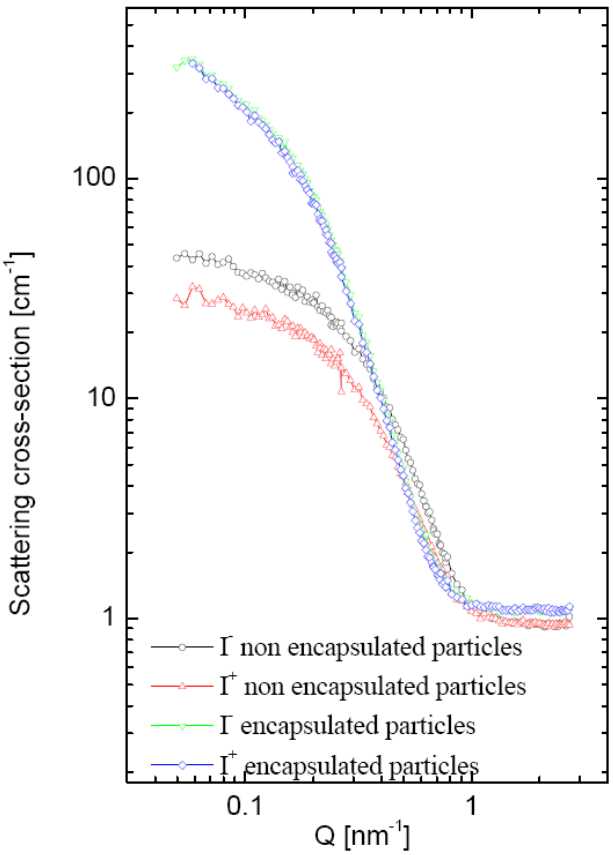

Fig. 1: SANSPOL intensities I^- and I^+ of encapsulated and non-encapsulated magnetite nanoparticles.

Acknowledgement

Work supported by DFG project Wi 1151/2-2 in the frame of priority program SPP1104.

References:

[1] A. Wiedenmann: Mat. Science Forum, **312-314** (1999) 315-324.

[2] K. Landfester, L.P. Ramírez: J Phys. Condensed Matter **15** (2003) 1345-1361.

	EXPERIMENTAL REPORT SANSPOL investigation of magnetic particles for medical applications	Proposal N° CHE-04-1106 Instrument **V4** Local Contact Albrecht Wiedenmann
Principal Proposer: Experimental Team:	P. Baglioni - University of Florence, I M. Bonini - University of Florence, I A. Wiedenmann - HMI Berlin	Date(s) of Experiment 24.06. - 26.06.2005

Date of Report: 05.01.2006

During recent years, there has been an increasing interest in the use of magnetic fluids and magneto-liposomes for biotechnology and biomedical applications[1]. Super-paramagnetic iron oxide nanoparticles show higher molar relaxivities than paramagnetic ions and, when used as blood pool and tissue-specific agents, they offer advantages at low concentrations. In the same way, the use of magnetic particles for the delivery of chemotherapeutic agents has recently attracted the attention of many research groups.

Liposomes, i.e. artificial, single or multilamellar vesicles made from lipids, are commonly used for the delivery of a variety of biological molecules or molecular complexes to cells. By combining their ability to include lipophilic molecules in the bilayer and the possibility to retain the magnetic particles in specific parts of the body depending on the placement of an external magnet results in the guided drug-delivery to specific targets. So called *magneto-liposomes* have been used in the hyperthermia approach to cancer therapy since the hysteresis loss of a magnetic particle in an alternate magnetic field enables effective thermotherapy.

In this experiment we have investigated two biocompatible magnetic systems suitable for biomedical applications.

The first one is constituted by magnetic particles surrounded by a tunable silica shell and dispersed in water through the use of tetramethylammonium hydroxide. We have previously shown that magnetic particles as small as about 5 nm in radius with a well defined silica coating can be obtained by means of a convenient synthetic route [2,3]. Being constituted by an inert material, the outer shell of silica makes these particles biocompatible.

The second system we have investigated is constituted by magnetic particles coated with a silica shell surrounded by another layer that acts at the same time as dispersant for the nanoparticles and as carrier for molecules to be selectively delivered. In particular, the silica layer is monoatomic, while the surrounding layer consists of a short aliphatic chain (C8 or C12). Owing to the hydrophobic nature of the coating, these nanoparticles present a marked affinity for lipophilic domains, such as apolar organic solvents or the bilayer of liposomes.

Small Angle Scattering of Polarized Neutrons (SANSPOL) by means of the V4 instrument at the Hahn-Meitner Institute provided very useful information: in fact, it has been possible to accurately evaluate the size and the polydispersity of the magnetic cores, as well as the thickness of the shell for both the silica and the organic coating. These results will be of great help in the design of new systems to be employed in biomedical applications.

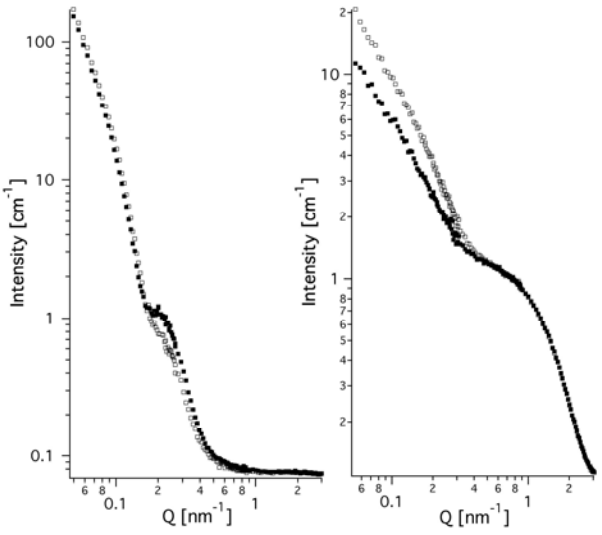

Figure 1: SANSPOL Intensities perpendicular to the applied field for magnetic cores coated by a silica shell (on the left) and by an organic layer (on the right).

References

[1] Shinkai, M: Journal of Biosciences and Bioengineering, 94 (2002) 606-613.

[2] Bonini, M.; Wiedenmann, A.; Baglioni, P. *Journal of Physical Chemistry B*, 108 (2004) 14901-14906.

[3] Bonini, M.; Wiedenmann, A.; Baglioni, P. *Physica A: Statistical Mechanics and its Applications*, 339 (2004) 86-91.

	EXPERIMENTAL REPORT **Investigation of the microstructure of ferrofluids using Small Angle Neutron Scattering**	Proposal N° MAT-04-1092 Instrument **V4** Local Contact Albrecht Wiedenmann
Principal Proposer: Experimental Team:	S. Odenbach - TU Dresden L.M. Pop - TU Dresden T. Gerdes - ZARM University of Bremen M. Kammel - HMI Berlin	Date(s) of Experiment 18.05. - 23.05.2005

Date of Report: 15.01.2006

Ferrofluids are stable suspensions of nanometer size particles in appropriate carrier liquids. Due to their normal liquid behaviour, coupled with superparamagnetic properties they are useful for a wide area of applications, bringing solution to a lot of highly demanding scientifical and technological problems.
In the presence of magnetic fields, ferrofluids show an increase of their viscosity of several hundred percent compared to the viscosity without magnetic field, the so called magnetoviscous effect.
The experimentally observed field induced changes of the viscosity of ferrofluids under shear flow can be theoretically explained using a model based on chain-like structure formation in the fluids. To correlate the rheological behaviour of ferrofluids to their microstructure, small angle neutron scattering experiments were carried out using a specially designed rheometer, adapted for the use in the V4 setup. For the SANS experiments two configurations, with magnetic field oriented parallel to the neutron beam and with 10 degree between magnetic field direction and neutron beam have been used. Both, rheological and SANS investigations have been carried out for magnetic fields varied between 0 and 160 kA/m, applied perpendicular to the vorticity of the flow. The shear rates have been varied within the range from 0 up to 200 s^{-1}.
It has been observed that, in the absence of a magnetic field, the obtained scattering patterns, are isotropic, indicating a statistical distribution of the magnetic moments of the particles. Applying a magnetic field to the ferrofluid samples, formation of chain-like structures is expected. In the static case the chains are aligned parallel to the magnetic field direction (see fig. 1). A shear flow applied to the fluid sample causes a deviation of the chains from their initial direction while a further increase of the shear rate leads to the disruption of the chains.

Previous investigations have shown that the anisotropy of the scattering patterns obtained in the presence of a magnetic field for the sheared case, as well as without shear but with 10 degree between magnetic field and neutron beam, could be related to the presence of chain-like structures in the ferrofluid samples [1]. A question which arose concerns the orientation of the local magnetisation of the sample in a shear flow relative to the direction of the chains.

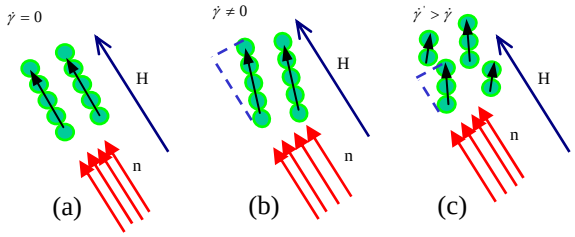

Fig. 1: *Chain-like structure formation in ferrofluids, aligned with the magnetic field (a). An applied shear diverts the chains from the initial direction (b). Breakage of the chains with increasing shear rate (c).*

The 2-D fitting procedure of the scattering intensity [2] for the sheared and non sheared samples could not distinguish between scattering due to orientated cylinder-like structures in the fluid sample and the magnetic scattering due to the orientation of the magnetic moments of the particles along a common direction. Thus, SANS investigations of a representative cobalt-based ferrofluid sample, Co87_03, have been performed, by using polarised neutrons. Data evaluation concerning the length and deviation of the chains as well as concerning the orientation of the local magnetisation of the sample is in progress.

References

[1] L.M. Pop et al.: JMMM **289** (2005) 303-306

[2] A. Heinemann, A. Hoell, A. Wiedenmann, L.M. Pop: Physica B (2006), in press.

	EXPERIMENTAL REPORT **Nanoclusters in oxide-dispersion-strenghened steel**	Proposal N° MAT-04-1159 Instrument **V4** Local Contact Uwe Keiderling
Principal Proposer: Experimental Team:	X.-L. Wang - ORNL-Spallation Neutron Source, US A.D. Stoica - ORNL-Spallation Neutron Source, US C.-T. Liu - ORNL-Metals and Ceramics Division, US U. Keiderling - HMI Berlin	Date(s) of Experiment 21.08. - 25.08.2005

Date of Report: 09. Jan. 2006

Oxide-dispersion-strengthened (ODS) steel, a Cr-based steel alloyed with a minor composition of W, Ti and Y, exhibits excellent mechanical properties at high-temperature. For example, at temperatures between 650 and 900 °C, the creep rate of Fe-14Cr-3W+0.25Y+0.4Ti (wt %) ODS steel is six orders of magnitude lower as compared to the parent material. This level of improvement represents a major breakthrough in the use of ferritic alloys for high temperature structural applications.

It has been suggested that the unusually low creep rate in ODS steel is related to the nanoclusters formed as a result of the alloying. Indeed, microscopy and atom probe tomography studies on several ODS alloys confirmed the presence of high-density nanoclusters, which are distinctly enriched with Ti, O, and Y atoms and have a diameter of 2-5nm. Surprisingly, these nanoclusters are highly stable as no significant coarsening was observed even after heat treatments up to 1300°C.

We have conducted an in-situ small angle neutron scattering experiment using V4 to identify the nanoclusters in ODS steel and to study their thermal stability. While detailed data analysis is being carried out, surprising results are already noted. Significant scattering intensity are seen over the range of 0.01-0.3 A-1. Two log-normal size distributions were needed to fit the data. The fitted particle size distribution is shown in Fig. 1. The maximum corresponds to particles of diameters of 2 and 12 nm, respectively.

Both types of nanoclusters were also observed in TEM studies. In-situ measurements further reveal that the 12-nm clusters are stable and grows only slightly even at 1400 °C. The number of 2-nm clusters, on the other hand, decreased appreciably. More detailed analysis will be forthcoming.

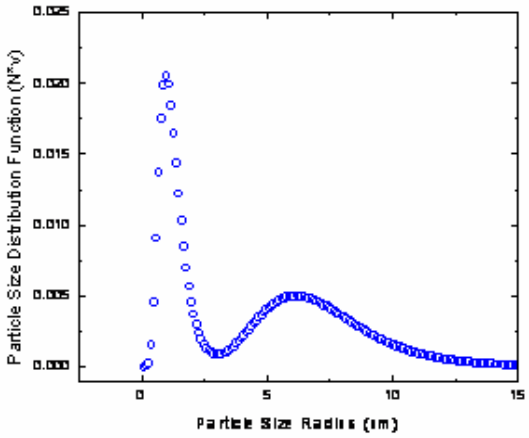

Fig. 1: Particle size distributions obtained from fitting SANS data at 1000 C

	EXPERIMENTAL REPORT SANS experiment on self-ordered arrays of electrodeposited FeNi nanowires	Proposal N° PHY-04-1019 Instrument **V4** Local Contact Elvira Garcia-Matres
Principal Proposer: Experimental Team:	V. De La Prida, Universidad Oviedo, E J. Blanco, Universidad Oviedo, E J. Campo, ICM Aragon, E	Date(s) of Experiment 12.03. - 15.03.2005

Date of Report: 15.03.2005

Highly self-ordered periodic arrays of magnetic nanowires, with diameter dimensions smaller than 100 nm and several microns in length show outstanding magnetic behaviour and can be considered as one of the families of advanced materials displaying special geometrical features and excellent magnetic properties of great interest for research in technological applications.

In particular, nanowires are interesting systems in which carriers are confined in the radial dimension, even though transport is possible along the axial dimension of the nanowire. These patterned magnetic media are now with increasing interest of applications, because can act as information storage systems, where each single-domain nanowire represents one bit, depending on its magnetization state, in which data are stored in a large area (over 70 cm^2 or larger) periodic arrays of single-domain magnetic nanowires, which could enable data recording densities exceeding 150 Gbit cm^{-2}. Furthermore, in some magnetoelectronic devices, the information is transmitted along ferromagnetic wires of submicrometre width by domain wall (DW) motion, being the device speed linked to the DW velocity.

Motivated by the relevance this phenomenon plays in some magnetic devices used for information transmission along sub-micron size ferromagnetic wires by domain wall motion, we planned to study by small angle neutron scattering (SANS) technique these arrays of magnetic nanowires embedded into the self-ordered nanoporous alumina, in order to extract their local magnetic structure and correlations over a range of length scales.

In this experiment, we have performed a polarized neutrons SANS experience in the instrument V4, at BENSC in HMI, on arrays of ferromagnetic nanowires fabricated in our laboratory, with nominal compositions of Ni and Co, with d = 35-40 nm in diameter, L = 5 microns in length and D = 105 nm of hexagonal lattice parameter. 2D SANSPOL diffraction patterns were collected at room temperature and at 70 K for the Ni sample, for detector distances of 12, 4 and 1 m, using the neutron wavelength of 6.07 Å, in the Q range 10-3 $Å^{-1}$ < Q < 2 $Å^{-1}$, and in the following configurations: without applied magnetic field, at the saturating applied magnetic field of 1 Tesla, at zero applied field again for the remanence state, and finally, at the coercive field value of –0.02 T, so describing the different magnetic states of the hysteresis loop for this sample. The arrays of the ferromagnetic nanowires were perpendicularly aligned to the horizontally applied static magnetic field H in each case, in order to allow the separation of nuclear and magnetic scattering, as can be seen in the preliminar data treatment shown in the figure 1. Unfortunately, due to the necessary long time spend for data collection (e.g. about 4 h at 12 m distance detector) at the several applied magnetic field and temperature values, we could not complete all our temperature and magnetic field analysis for the Co samples, neither start it for the case of the $Fe_xNi_{(1-x)}$ samples. We hope, in the next future, complete this polarized SANS experience for the rest of the different compositions of the nanowire arrays.

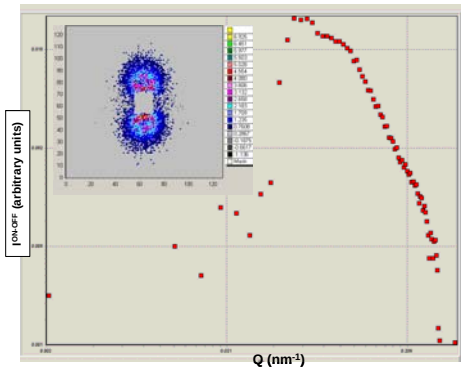

Fig. 1: I^{ON-OFF} as a function of Q, at RT and 1 Tesla, for an array of Ni nanowires

	EXPERIMENTAL REPORT **Small angle neutron scattering studies on FeCo ferrofluids**	Proposal N° PHY-04-1094 Instrument **V4** Local Contact André Heinemann
Principal Proposer: Experimental Team:	W. Kleemann - Uni Duisburg-Essen S. Bedanta, O. Petracic - Uni Duisburg-Essen A. Hütten - Uni Bielefeld M. Kammel - HMI Berlin	Date(s) of Experiment 09.03. - 12.03.2005

Date of Report: 09. Jan. 2006

Frozen ferrofluids are model systems to study the effects of dipolar interaction. The cooperative behavior in a frozen ferrofluid depends on the magnetic particle concentration. Ferrofluids containing FeCo nanoparticles with organic surfactant coating in hexane with volume ratios 1:1 and 1:5 were studied by polarized small angle neutron scattering.

The magnetic properties of the frozen ferrofluid [$Fe_{55}Co_{45}$ / hexane] (1:1) have been measured with SQUID magnetometry and susceptometry. The magnetic moments **m** of the dense frozen ferrofluid induced at low field under zero field cooled (ZFC) and field cooled (FC) conditions exhibit irreversibility at temperatures below the blocking temperature $T_b \approx 30$ K. FC in $\mu_0 H \leq 5$ T gives rise to shifted minor loops below T_b. At $T_c \approx 10$ K sharp peaks of m^{ZFC} and the ac-susceptibility χ', a kink of the thermoremanent magnetic moment m^{TRM} and a sizeable reduction of the coercive field H_c, and the appearance of a spontaneous moment m^{SFM} indicate a phase transition with near mean-field critical behavior of both m^{SFM} and χ'. These features are explained within a core-shell model of nanoparticles, whose strongly disordered shells become gradually blocked below T_b, while their soft ferromagnetic cores couple dipolarly and become superferromagnetic (SFM) below T_c [1]. To estimate the correlations length as a function of the temperature in particular in the vicinity of T_c, SANSPOL measurements were performed on the ferrofluids. More detailed information on the magnetic contrast between particles and their environment and on the magnetic core-shell structure of single particles respectively were desired to be available from polarized SANS.

Measurements were performed on the instrument V4, using the polarization option, SANSPOL.

The SANSPOL intensity vs. scattering vector Q measured at 5 K in a magnetic field of 0.03 T on the (1:1) ferrofluid is shown in fig. 1.

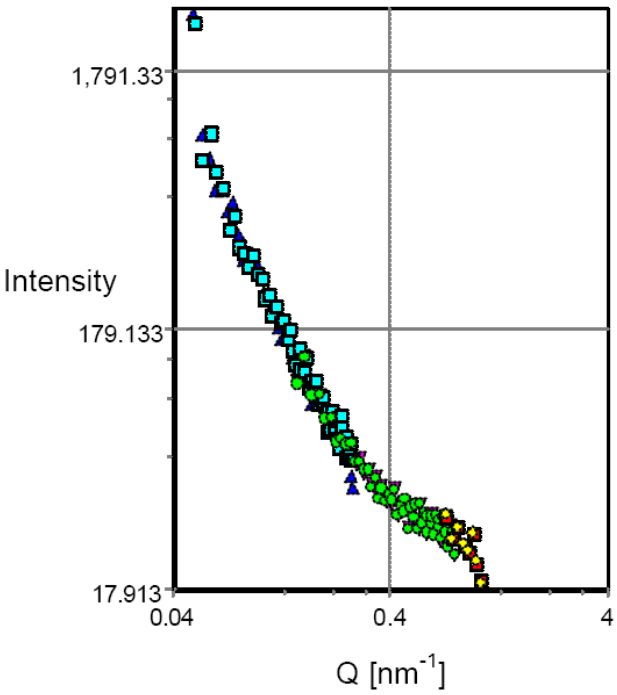

Fig. 1: SANSPOL intensities of the [$Fe_{55}Co_{45}$ / hexane] (1:1) ferrofluid measured at 5 K with $\mu_0 H$ = 0.03 T.

Unfortunately both samples lost ferrofluid material due to a crack in the glue of the sample container while cooling down. The data on the (1:5) sample is, hence, not reliable, since the sample lost material continuously during the measurement. However the data on the (1:1) sample (fig. 1) is still reliable, because the ferrofluid was quickly frozen in.

The data analysis is in progress.

Reference:

[1] S. Bedanta et al.: Phase Transitions **78**, 121 (2005).

	EXPERIMENTAL REPORT **Nanostructures in colloidal dispersions of nearly monodisperse Magnetite**	Proposal N° PHY-04-1154 Instrument **V4** Local Contact Albrecht Wiedenmann
Principal Proposer: Experimental Team:	B. Erne - Univ. Utrecht, NL B. Erne - Univ. Utrecht, NL M. Klokkenburg - Univ. Utrecht, NL A. Wiedenmann - HMI Berlin	Date(s) of Experiment 07.09. - 16.09.2005

Date of Report: 5. Jan. 2006

Using SANSPOL, we aimed to study the effect of particle size on the interactions (magnetic, steric, Van der Waals) and nanostructure formation in liquid dispersions of nearly monodisperse magnetite (Fe_3O_4) nanoparticles.

We measured SANSPOL on three systems, relatively concentrated colloidal dispersions of nearly monodisperse magnetite nanoparticles of three different diameters: 21 nm, 16 nm, and 12 nm.

Hexagonal structures similar to those reported for cobalt ferrofluids were discovered in applied field (fig. 1) only for dispersions containing the 21 nm particles. The scattering data of the dispersion with 16 nm particles exhibits strong anisotropy but not yet hexagonal patterns. Using a cryomagnet, we performed a systematic investigation of the effects of temperature (fig. 2) and magnetic field on the hexagonal structures (21 nm).

Fig. 2 shows the gradual development of the hexagonal scattering patterns with decreasing temperature. Field variation resulted in less well-defined hexagons. Currently, we are studying the possible colloidal crystal structures that correspond to the observed scattering patterns.

Fig. 3 shows the SANS POL results for the 21 nm system, reflecting the additional magnetic contribution in the 90 degrees direction, and confirming the hexagonal arangement of the particles.

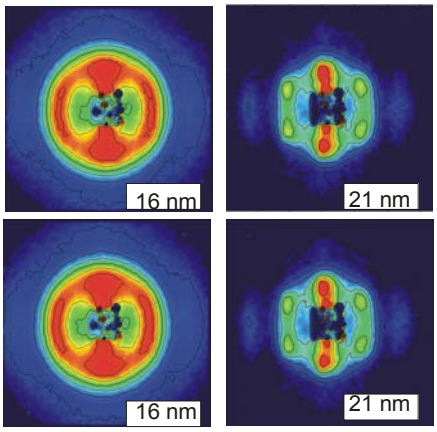

Fig. 1: 2D SANS intensity patterns of Fe_3O_4 dispersions with a mean diameter of either 16 or 21 nm. The field (1T) was applied perpendicular to the incoming neutrons.

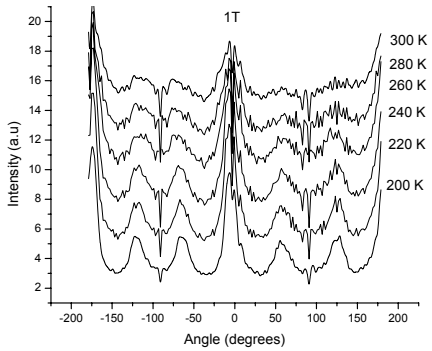

Fig. 2: The development of the hexagonal scattering patterns for the 21 nm dispersions as a function of temperature in 1T.

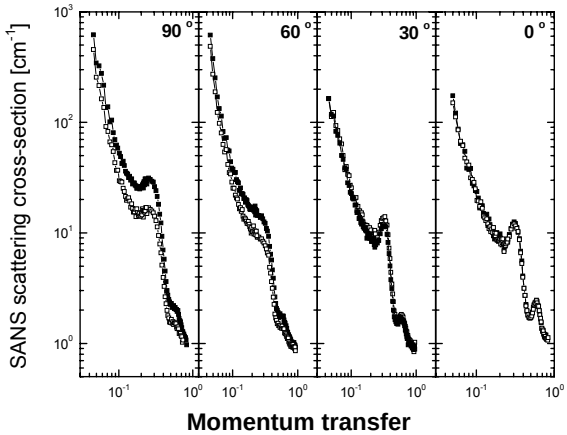

Fig. 3: SANS-POL intensities I^+ (solid) and I^- (open) for different azimuth angles of 10^0 measured at 100 K and 1T.

Acknowledgement
This research has been supported by the European Commision under the 6th Framework through the Key Action: Strengthening the European Research Infrastructures. Contact-n°: RII-CT-2003-505925

BENSC	**EXPERIMENTAL REPORT** **Correlation of defect distribution and twinning stress in Ni_2MnGa MSMAs**	Proposal N° MAT-01-1750 Instrument **E2/E2a** Local Contact Jens-Uwe Hoffmann
Principal Proposer: Experimental Team:	H. Schmidt - Robert Bosch GmbH M. Köhl - Universtität Tübingen J. Ihringer - Universität Tübingen R. Schneider - HMI Berlin	Date(s) of Experiment 16.09. - 25.09.2005

Date of Report: 13.12.2005

Introduction

A correlation between the macroscopic properties of Ni_2MnGa Magnetic Shape Memory (MSM) crystals and their microscopic properties is sought. Two macroscopic properties are considered, viz. the temperature evolution of twinning stress and maximum field-induced strain (MFIS). The microscopic struture and its temperature dependence are studied by neutron scattering.

Twinning Stress

Magnetomechnic measurements (e.g. twinning stress and MFIS vs. temperature) have been performed at Robert Bosch GmbH. From such experiments, two sets of crystals were identified from different ingots that show signficantly different active properties, as reported in Fig. 1 showing the twinning stress vs. temperature (red and blue line are a hard and a soft sample used in the present study, respectively, green line is data taken from literature [1]). For maximum MSM effect soft crystals are desireable, so the soft sample, marked blue, is considered the best sample in this study.

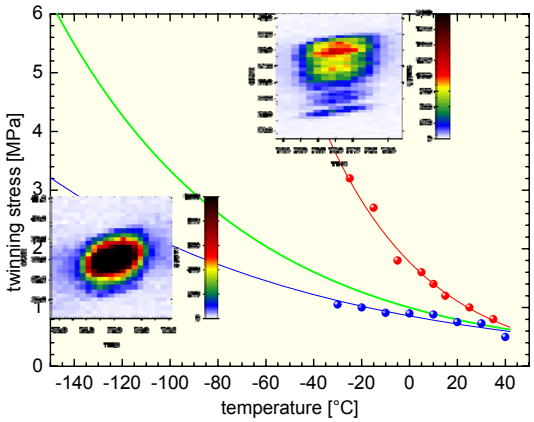

Fig. 1: Twinning stress vs. temperature

Maximum Field-Induced Strain

From temperature dependent neutron scattering experiments at BENSC, the temperature dependence of tetragonality was determined (an example of data taken on a hard sample is shown in the inset of Fig. 2, 440 reflex upon heating). The resulting tetragonality in soft samples is found to closely correlate to the MFIS (main panel of Fig. 2), while in hard samples, the MFIS abruptly disappears when a lower limiting temperature of the MSM effect is reached (not shown).

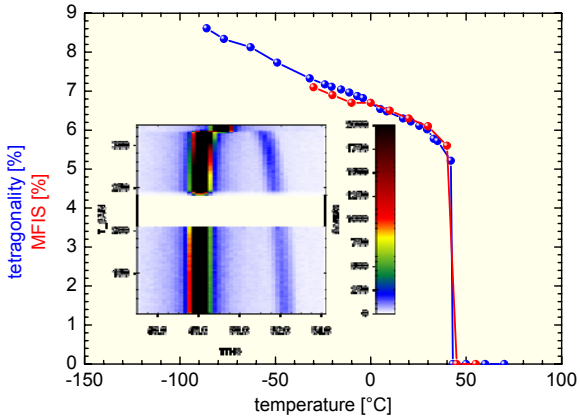

Fig. 2: MFIS and tetragonality vs. temperature

Single Crystal Quality

In order to assess the single crystal quality of the two sets of crystals, the shape of the diffraction peaks was studied, and it is found that the soft sample shows sharp, single peaks (left inset to Fig. 1), while the hard sample shows multiple (four) peaks of different intensity (right inset to Fig. 1), indicative of multiple crystallites that are slightly misaligned. Such misalignment of crystallites may be perceived to hamper the free movement of twin boundaries, resulting in an increase of macroscopic twinning stress. The magnetomechanic properties are thus found to be in qualitative agreement with the microscopic structure of the studied crystals.

Reference

[1] O. Heczko and L. Straka: Temperature Dependence and Temperature Limits of Magnetic Shape Memory Effect, J. Appl. Phys. **94** (2003) 7139

	EXPERIMENTAL REPORT **Cladding stresses by sin2 psi method**	Proposal N° MAT-01-1607 Instrument **E3** Local Contact Poeste / Wimpory
Principal Proposer: Experimental Team:	C. Ohms - EC-JRC-IE Petten, NL T. Poeste - HMI Berlin R. Wimpory - HMI Berlin	Date(s) of Experiment Aug/September 2005

Date of Report: March 2006

Welded austenitic claddings are often applied when large engineering components made of ferritic steel need to be protected against corrosion (e.g. reactor pressure vessels) [1]. The application of a welded austenitic steel cladding on a ferritic substrate introduces residual stresses. Non-destructive measurement of such stresses is challenging because of the existence of a "hidden" interface and because such components generally have a considerable thickness. The specimen investigated here was a rectangular block of ferritic steel (130x128x40 mm^3) clad with a 5 mm welded austenitic layer.

The experiment was carried out on the hkl 310 in the ferritic phase of the cladding. This provided a 2theta scattering angle of 98.8 degrees which consequently allowed a greater range of omega angles. One would normally measure on the hkl 211, at an angle of 2θ = 72.6 degrees (the current neutron wavelength on E3 being 1.37 Å).

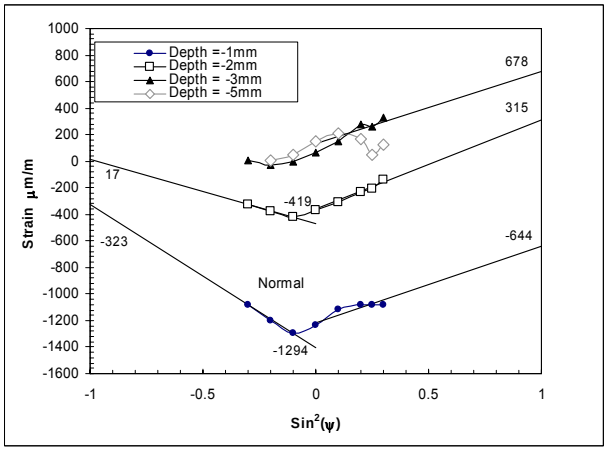

Figure 1. Strain values in out of plane (normal $sin^2\psi$ =0) and in plane directions ($sin^2\psi$ =1)

Figure 1 shows the strain calculated from the gradients of the $sin^2\psi$ method. $Sin^2\psi$ =0 is the normal direction and $sin^2\psi$ =1 is the in-plane 'Longitudinal' direction. The Typical error in strain was +/- 150 um/m. The strain results are depicted in figure 2 as a function of position.

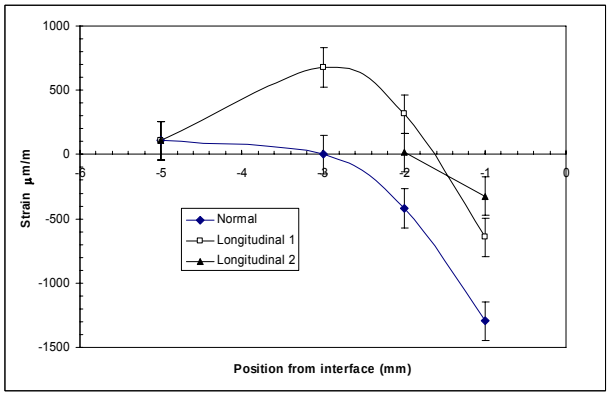

Figure 2. Strain as a function of position from the cladding interface.

Using other methods (such as Finite element modelling and Deep Hole drilling [1]) show a high tensile stress in the cladding (austenitic) layer). This is clearly the case, as the ferritic phase is strongly in compression balancing the strain/stress in the cladding layer. Further work is needed however to optimise the technique and to compare the reliability with other techniques. Neutron diffraction is the technique of choice when destruction of the test piece is not an option. The biggest problem for neutron diffraction is that neutrons cannot penetrate the substantial thicknesses involved in for example large claddings. The indirect measurement of strain using the $sin^2\psi$ method is one method to help overcome this problem as long as the overall neutron path length does not exceed 40mm.

Reference

[1] H. Hein, B. Brown, D. Lawrjaniec, C. Ohms, R.C. Wimpory and C. Truman:
"ENPOWER – Repair Welds and Residual Stresses in Clad Plates"
in: Proceedings of 2005 ASME Pressure Vessels and Piping Conference, Denver, July 17-21, CD published by ASME, ISBN: 0-7918-3763-7, 2005

	EXPERIMENTAL REPORT **Influence of residual stress on fatigue crack propagation in Al 6056 laser-welded specimens**	Proposal N° MAT-01-1805 Instrument **E3** Local Contact Robert Wimpory
Principal Proposer: Experimental Team:	F. Fiori - UPM Ancona, I A. Manescu - UPM Ancona, I V. Calbucci - UPM Ancona, I	Date(s) of Experiment 16.11. - 26.11.2005

Date of Report: 09.01.2006

The experiment was carried out in the framework of a research aiming to the modelling of the influence of the laser welding process on the propagation of fatigue cracks in Al 6056 components.
In particular, the goal is the experimental determination of the residual stress field induced by the combined action of welding and fatigue, to be used for the validation of a numerical model which is being developed in parallel.

The first step was the analysis of the stresses in a welded plates with no notch - as-welded condition. Two different plates were measured: one with the welding in the middle of the specimen (Sample A) – see Fig.1 below, and another one (Sample B) where the welding was at 12 mm from the centre of the specimens. The dimensions of the samples were: 50 x 50 x 5mm^3. The thickness of the welding was about 3mm.

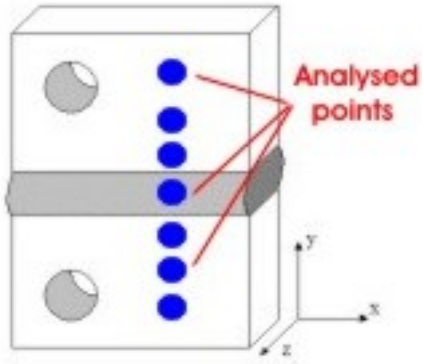

Fig. 1 - As welded specimen

The measurements were performed at Hahn-Meitner-Institut, BENSC, on the E3 diffractometer. We used a wavelength of 1.37 angstrom. The intial slit of 2mm x 2mm together with a secondary slit having an aperture of 2mm defined the analysed gauge volume.
Several points on a line crossing the welding (y direction) were analysed : a scan from the welding area, passing through the heat affected zone and finally towards the margins of the specimens was performed, in order to see the stresses induced by the welding and their behaviour at different distances from the welding.
The measurements were done in the three orthogonal directions indicated in Fig.1.

Assuming a biaxial stress field (due to the sample geometry), the strain/stress state was determined in the longitudinal and transversal directions, with respect to the weld seam (x and y in fig.1, respectively). The unstrained interplanar distanced d_0 was obtained by imposing the stresses in the z direction to be zero:

$$d_0 = \frac{(1-\nu)d_z + \nu(d_x + d_y)}{(1+\nu)}$$

In the Fig. 2 below one can see the evolution of the stresses across the welding – a previous tension state seems to be present in Sample A while in both samples can be noticed the parabolic behaviour of the stresses, specific to weldings.

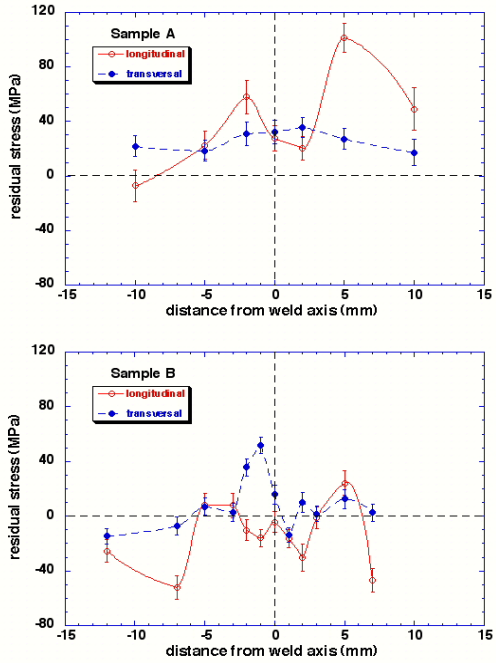

Fig. 2 – Residual stresses in the two analysed specimens

	EXPERIMENTAL REPORT **Structural studies of the magnetic shape memory compound Ni-Mn-Ga**	Proposal N° MAT-01-1671 Instrument **E4** Local Contact Karel Prokes
Principal Proposer: Experimental Team:	O. Heczko - HUT (TKK), Finland O. Heczko - HUT (TKK), Finland K. Prokes - HMI Berlin	Date(s) of Experiment 23.5. – 5.6. 2005

Date of Report: 09.01.2006

Single crystal measurements of the typical example of magnetic shape memory (MSM) alloy $Ni_{49.7}Mn_{29.3}Ga_{21}$ was carried out. The lattice constants of 5M martensite exhibiting MSM effect are $a_M = b_M = 0.595$ nm, $c_M = 0.561$ nm at room temperature with easy axis magnetization along the short (c-) axis. Due to tetragonality there are three twin-related martensite variants with different orientation with nearly perpendicular c-axes. The redistribution of these variant in the magnetic field is the origin of the MSM effect [1].

The quality and inhomogeneity of the single crystal and martensite variant distribution was studied using ω scan and 2D position sensitive detector. The example of the ω scan taken at 110 K is shown in Fig. 1 after cooling in magnetic field 5T from 330 K through martensite transformation finished at 301 K. The measurement shows that the material is not in a single variant martensite phase as is often assumed and residual variant with easy axis perpendicular to magnetic field also occurs during transformation in the field. The neutron studies reveal unexpected split of the 020 reflection of major martensite variant (inset in Fig. 1) and structural inhomogeneities (weak spot in Fig 1 C, next to principal martensite reflection). These observations need additional studies.

Using measurement in reciprocal space we recorded a set of reflections that appear due to structural modulation (5M) of the martensite phase (Fig. 2), however the set seems to be incomplete with missing or very weak reflections of second order compared with X-ray diffraction. The line of the magnetic reflection arising from the supposed antiferromagnetic ordering of the excess Mn atoms [2] is very weak and it is difficult to discern it from the background. The results are inconclusive and more detailed measurements are needed.

The large changes of the martensitic structure during transformation and induced reorientation, which results in the large position changes of the reflections, justify the using of PSD. This allows direct observation of the structure evolution without position readjustment of the detector.

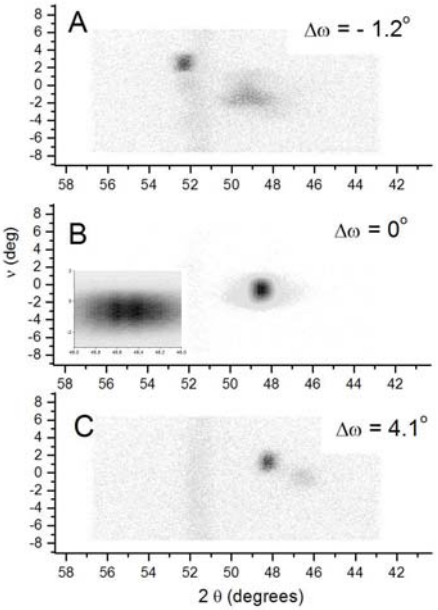

Fig. 1. 2D figure of 020 and 002 reflections for different ω angles at 110 K. The maximum intensity of the reflection in A (minor variant) and C is about 30 counts per channel, in B (major variant) about 500 counts per channel. Fig. 1C shows weak reflection at 46.5 deg not belonging to the martensite variant. Line running vertically is the reflection due to cryostat and holder. Inset in B shows the splitting of the reflection of the major variant.

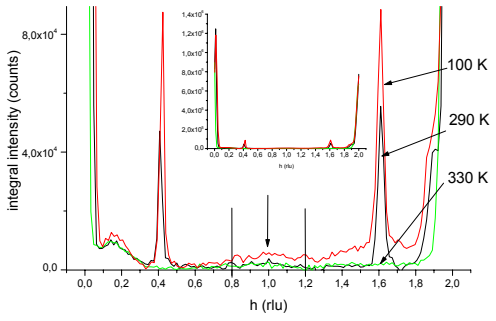

Fig. 2. *q* scan along h-k0 between the –200 to 020 reflection at different temperatures showing the temperature evolution of the modulation superstructure reflections. The theoretical positions of the second lines are marked in figure. The expected peak of antiferro-magnetic of ordering of the excess Mn atoms is marked in figure by arrow. The inset shows the q-scan in full.

References

[1] O. Heczko, A. Sozinov and K. Ullakko: IEEE Trans. Mag., Vol. 36 No.5 (2000).

[2] J. Enkovaara, O. Heczko, A. Ayuela, R.M. Nieminen: Phys. Rev. B, 67, 212405, (2003).

	EXPERIMENTAL REPORT **Study of crystalline phases (microlites) in natural obsidian**	Proposal N° GEO-01-1656-DT Instrument **E9** Local Contact Michael Tovar
Principal Proposer: Experimental Team:	G. Kloess - University Leipzig S. Schorr - University Leipzig G. Kloess - University Leipzig M. Tovar - HMI Berlin	Date(s) of Experiment 26.02. - 27.02. 2005

Date of Report: 30.01.2006

Obsidian is a natural volcanic glass, which contains between 0.1 and 1 vol% micro- and nanocrystals. Microcrystals with size>0.6 µm are called microlites, whereas nanocrystals with size<0.6 µm are called nanolites [1]. The structure and composition of the crystalline phases in obsidians are the primary source of information concerning the pressure and temperature of crystallisation as well as the kinetics of crystallisation and therefore the thermal history. The flow of obsidian lava leads to crystal alignments that reflects both the accumulated strain and the type of flow across the surface. Furthermore obsidians are also used for provenance studies for reconstructing of ancient exchange networks [2]. Chemical and physical properties as well as microlite populations are peculiar of the specific occurrence and allow their discrimination.

Obsidian is coloured from black over red-brown to ocher. The colouring phenomena of obsidian is a complex unsolved problem and also subject of our studies. Quantity and size of micro- and nanolites, especially the iron-rich phases, determine the colour of the obsidian. Surprisingly even obsidians with the same chemical composition show an extreme variation of colour from black to red.

The neutron diffraction experiments were carried out at the E9 beamline using counting times of 12 hours per sample. For the experiment we used 1 powder sample and 2 obsidian rods of different flow orientation. Thus the non-homogeneous stereometry of the micro- and nanolites could be proved. That cannot be done using X-ray powder diffractometry. The minerals hematite, magnetite, biotite, and albite-like feldspar could be found.

Comparing diffraction patterns of the obsidian rods of different orientation texture effects appear significantly. In particular it can be seen regarding the following reflection intensities: plagioclase (040), (204), (004), hematite (104), (116), and the strongest biotite peak (136). Detailed and further interpretation should be done using TEM images reflecting the morphology of the crystals.

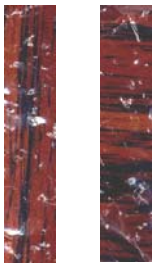

Fig. 1: Obsidian from Büyük Yayla, Eastern Pontides, 25 km SSE of Rize, Turkey, with vertical and horizontal stripes like in the measured rods (width: 8 mm).

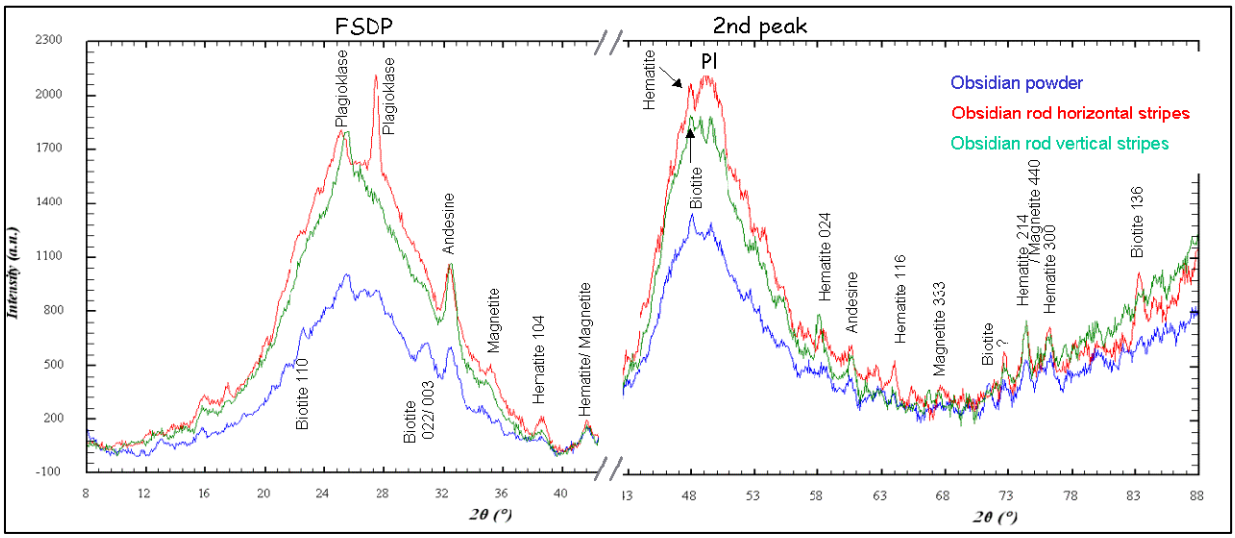

Fig. 2: Diffraction pattern of 3 obsidian samples.

References:

[1] Sharp, T.G. et al.: Bull. Volcanol. **57** (1996) 631

[2] Oddone M. et al.: J. Radioanal. Nucl. Chem. **243** (2000) 673

BENSC	**EXPERIMENTAL REPORT** **Structures and textures of martensitic phases in deformed polycrystalline shape memory alloys**	Proposal N° MAT-01-1660 Instrument **E9** Local Contact Michael Tovar
Principal Proposer: Experimental Team:	P. Sittner - ASCR IP Prague, CZ V. Novak - ASCR IP Prague, CZ P. Molnar - ASCR IP Prague, CZ M. Tovar – HMI Berlin	Date(s) of Experiment 16.03. - 21.03.2005

Date of Report: 30.05.2005

The unique properties of shape memory alloys (SMA) are based on martensitic transformations. Depending on chemical composition, texture and stress-strain-temperature history of the material, different phase compositions and structures appear.

Important characteristics for the modelling of shape memory alloys are lattice parameters of austenite phase and martensite phases. Another important characteristic is the preferred crystal orientation after the deformation of SMA. Neutron diffraction is a unique technique, which allows us to obtain this information.

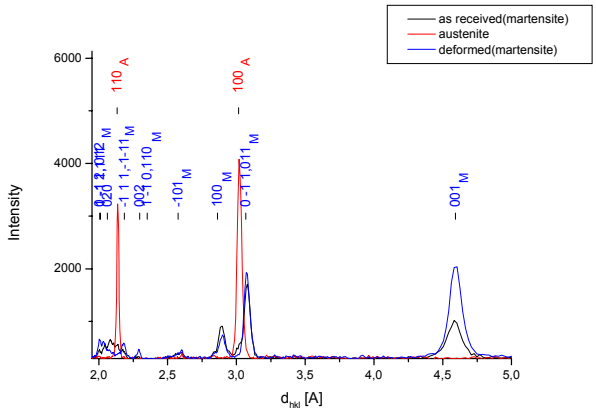

Figure 1: Part of the neutron diffraction spectrum from NiTiCu sample in austenitic state (red curve) and martensitic state after cooling (black) and deformed (blue)**.**

In the present experiment three NiTiCu samples were studied with neutron powder diffractometer E9. First sample was in austenite state with cubic B2 structure. The second sample was in martensite after cooling and the third one was deformed in martensite state (Fig.1.). Further analysis of measured data is necessary as two types of martensite (monoclinic and orthorhombic) are expected.

The texture measurement under variable omega conditions was carried out on the NiTi-L sample cooled under compression stress applied (Fig.2). The orientation of diffracting lattice planes with respect to load (bar) axis (angle δ) is defined by angles Θ and Ω. The variation of integral intensities of individual reflections is due to the very strong martensite texture partially inherited from that of the parent austenite but additionally affected by the preferential martensite variant formation under applied stress. The integral intensity variations of individual martensite reflections with the angle omega were analyzed.

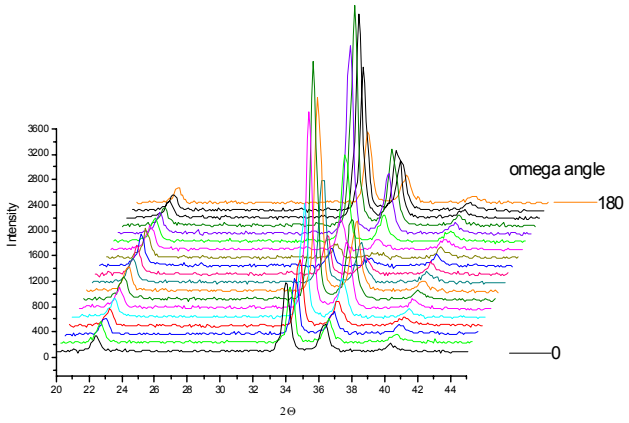

Figure 2: Neutron powder diffraction data of NiTi bar specimens in the martensite phase induced under compression stress – variation with angle omega.

The measured data will be compared with computer simulation of stress induced martensite texture and its omega dependence.

Additional samples from CuAlNi and CuAlMn shape memory alloys were prepared as a powder. In these alloys two types of martensite are expected (monoclinic 18R and orthorhombic 2H). These powder samples were measured at different temperatures in order to obtain the lattice parameters of individual martensite structures and the austenite.

	EXPERIMENTAL REPORT **In situ study of the phase composition in the Na_3AlF_6-Al_2O_3 within 930°C - 1350°C**	Proposal N° MAT-01-1666 Instrument **E9** Local Contact Michael Tovar
Principal Proposer: Experimental Team:	L. Smrcok - SAS Bratislava, SK L. Smrcok, O. Pritula, M. Kucharik - Inst. Inorg. Chemistry., SAS Bratislava, SK M. Tovar - HMI Berlin	Date(s) of Experiment 17.05. – 20.05.2005

Date of Report: 27.05.2005

Industrial production of primary aluminium is nowadays carried out only by the Hall-Héroult process. In this process alumina (Al_2O_3) is dissolved in electrolyte consisting mainly of liquid cryolite, Na_3AlF_6. The Hall-Héroult process belongs among the most energy demanding industrial productions and has considerable influence on environment. The aim of the project is to find out the phase composition of crystalline matter in the Na_3AlF_6–Al_2O_3 system at the temperatures within 930-1300°C in situ. We suggested using high temperature neutron diffraction for determination of the presence of oxofluoroaluminate compound in solid state. A mixture of 50 mol % cryolite and 50 mol.% of alumina was homogenized and filled to a closed carbon holder designed for this experiment. Carbon was chosen mostly for safety reasons - the mixture under study is extremely corrosive at the selected temperatures. Neutron diffraction patterns were proposed to be collected at four temperatures. Unfortunately, due to problems with detector's power supply the start of our experiment was postponed for ~18 hours and the total time for all measurements was thus shorter. Because we preferred to scan the patterns at all temperatures of interest, patterns collection times were shorter and the patterns noisy. The patterns were collected at i) 1374°C where the sample was assumed to be molten, ii) 1255°C, where a part of the sample should crystallize, iii) 1152°C leading to large amount of crystalline phase(s) and iv) 1005°C where ~90% of the sample was expected to be crystalline. Measured patterns were dominated by diffractions of the carbon holder, whose wall proved to be too thick. Such a design could be however explained by extreme corrosivity of the sample and the fact that no such in situ measurements have been previously reported.

In Fig.1 the parts of the patterns uninfluenced by diffraction from the holder are shown. The explanation of phase composition is due to low counts a little bit complicated, but we propose the following. It is probable the holder's cup was not completely tight and under the vacuum and increased temperatures the sample decomposed and part of it evaporated. As a consequence the intensities of solid phase(s) upon cooling did not increase as expected.

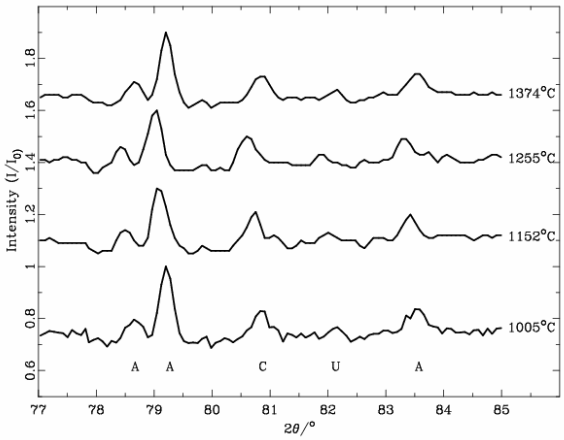

Fig.1: Wavelet denoised [1] parts of diffraction patterns taken at four temperatures. λ=1.7974Å. A-alumina, C-cryolite, U-unknown phase.

The process can be described by the following scheme: Na_3AlF_6 (l) = 2 NaF (l) + $NaAlF_4$ (g)
In such a case, the system is enriched in NaF and according to the phase diagram of the system NaF–AlF_3–Al_2O_3 [2], the excess of α–alumina transforms into β-alumina, a solid solution with approximate composition $NaAl_{11}O_{17}$. This process can be expressed by the reaction 2 NaF (l) + (3x+1)/3 Al_2O_3 (s, alpha) = $Na_2O{\cdot}xAl_2O_3$ (s) + 2/3 AlF_3 (l), where x = 11. [3,4]

After cooling the powder which remained in the holder was analysed by high resolution X-ray diffraction In the mixture beta-alumina and corrundum were unambiguosly identified by Rietveld method. This is confirmed above proposed reaction scheme.

Acknowledgement
This research project has been supported by the European Commission under the 6th Framework Programme through the Key Action : Strengthening the European Research Area, Research Infrastructures. Contract no : RII3-CT-2003-505925 (NMI3)'.

References

[1] Smrčok, Ľ. , Ďurík, M. & Jorik, V. *Powder Diffraction*, 1999, **14,** 300
[2] Foster, P. A. Jr. *J. Am. Ceram. Soc*. **1975**, *58,* 288
[3] Sterten, A., Hamberg, K., Maeland, I., *Acta Chem. Scand*., **1982**, 36A, 329
[4] Kucharik, M., Boca, M., Bessada, C., Fuess, H., *Eur. J. Inorg.Chem*.,**2005(9)**, 1781

	EXPERIMENTAL REPORT **Neutron diffraction studies of the relaxor PLZT 8/65/35 powder irradiated by high-current pulsed electron beam**	Proposal N° PHY-01-1659 Instrument **E9** Local Contact Vadim Sikolenko
Principal Proposer: Experimental Team:	K. Iakoubovskii - KU Leuven, Belgium A. Sternberg - ISSP, Latvia A. Kuzmin - ISSP, Latvia V. Efimov - JINR, Russia	Date(s) of Experiment 17.02 – 23.02.2005

Date of Report: 14.03.2005

$(Pb_{1-x}La_x)(Zr_{0.65}Ti_{0.35})O_3$ (PLZT X/65/35) ceramics is ferroelectric perovskite, and the latter exhibits relaxor-type behavior with X = 7 ÷11 % [1]. PLZT 8/65/35 is characterized by excellent optical, dielectric, electrooptical and piezoelectric properties [1]. The study of single radiation damage processes, their correlation with structural changes and above-mentioned physical properties in transparent ferroelectric PLZT 8/65/35 ceramics, seem to represent an interesting aspect of materials science.

In present work we studied the effect of single irradiation (one pulse = $5 \cdot 10^{14}$ electrons/cm^2) by high-current pulsed electron beam with energy E = 800 keV, beam current I = 200 A, pulse duration τ = 200 ns and annealing at 200, 400 and 650 ^{0}C after irradiation on structure transformation of the PLZT 8/65/35 powder at the E9 spectrometer with incident neutron wavelength λ = 1.7973 Å.

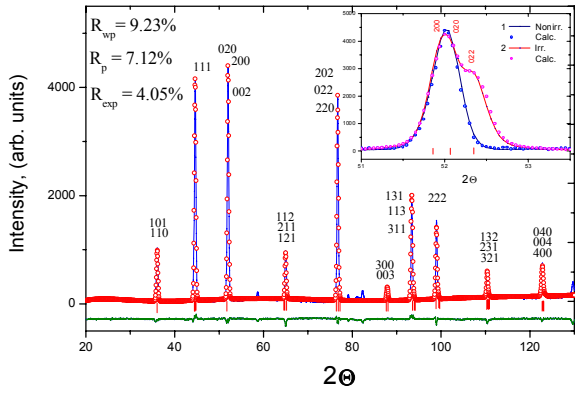

Fig. 1. Rietveld refinement plot for irradiated PLZT 8/65/35. The observed and calculated patterns are shown by solid line and dots, respectively. The vertical marks show the positions of calculated reflections. The trace in bottom is a plot of the differences between the observed and calculated intensities.

Figure 1 shows representative experimental and calculated profiles for the irradiated PLZT 8/65/35 powder. Neutron powder diffraction study of PLZT 8/65/35 ceramics irradiated by one pulse shown the transformation of the cubic structure (sp. gr. Pm-3m (Z = 1)) into orthorhombic Pmmm (Z = 1) with decreased lattice volume (see table 1) like in [2, 3]. The inset in figure the pronounced split of (200) reflection into an asymmetric doublet for irradiated PLZT 8/65/35 sample is observed. It is known [4] that similar splitting of this peak is responsible for orthorhombic distortion of cubic perovskite structure. An annealing at 200 ^{0}C of the single irradiated sample leads to the partial restore of the single irradiated structure (see table 1). However the significant decrease of the orthorhombic splitting of all peaks was observed after an annealing at 400 ^{0}C. The final restoration from orthorhombic Pmmm in cubic Pm-3m perovskite structure is taken place only after an annealing at 650 ^{0}C (table 1). It should be noted that above mentioned structural changes correlate well with a significant increase in their intensity and appearance of two additional bands and a shift of O-Zr-O band and especially of Zr-O band to the short wave infrared region in Raman spectroscopy measurements [3]. These changes also related with a lowering of lattice symmetry from Pm-3m to Pmmm.

Table 1. Structural parameters for unirradiated PLZT 8/65/35 sample, single irradiated and then annealed at 200, 400 and 650 ^{0}C.

		Unirr.	Irr.		200 ^{0}C	400 ^{0}C	650 ^{0}C
Sp. gr.		**Pm-3m**	**Pmmm**		**Pmmm**	**Pm-3m**	**Pm-3m**
a (Å)		4.085(2)	4.090(2)		4.088(2)	4.086(2)	4.085(2)
b (Å)		4.085(2)	4.086(2)		4.086(2)	4.086(2)	4.085(2)
c (Å)		4.085(2)	4.071(2)		4.073(2)	4.081(2)	4.084(2)
α (deg)		90.00	90.00		90.00	90.00	90.00
V (Å^3)		**68.167**	**68.033**		**68.034**	**68.134**	**68.150**
Pb / La	x	0.0000	0.0000		0.0000	0.0000	0.0000
	y	0.0000	0.0000		0.0000	0.0000	0.0000
	z	0.0000	0.0000		0.0000	0.0000	0.0000
Zr / Ti	x	0.507(1)	0.502(2)		0.503(2)	0.505(2)	0.508(2)
	y	0.507(1)	0.502(2)		0.503(2)	0.505(2)	0.508(2)
	z	0.507(1)	0.502(2)		0.501(2)	0.505(3)	0.508(2)
O	X	0.546(2)	0.506	0.507	0.013	0.555(2)	0.552(3)	0.549(2)
	Y	0.546(2)	0.511	0.014	0.510	0.556(2)	0.553(3)	0.551(2)
	Z	0.013(1)	0.021	0.508	0.511	0.012(2)	0.012(1)	0.012(2)
R_{wp}(%)		8.22	9.23		9.05	8.72	8.47

References

[1] A.Sternberg, et.al.: *Ferroelectrics*, **131**, 275, (1992).
[2] V.Efimov, et.al.: Phys.stat.sol.(C) **2**, №1, p.449, (2005).
[3] V.Efimov, A.Sternberg, V.Sikolenko et. al.: *Ferroelectrics*, **302**, 327, (2004).
[4] E.T. Keve and K.L. Bye: J. Appl. Phys. **46**, 810 (1975).

	EXPERIMENTAL REPORT **Hybrid organic/inorganic silica aerogel: Control of mechanical behaviour**	Proposal N° MAT-04-1098 Instrument **V4** Local Contact Uwe Keiderling
Principal Proposer: Experimental Team:	V. Morales-Flórez - Univ. de Cádiz, España N. de la Rosa-Fox - Univ. de Cádiz, España U. Keiderling - HMI Berlin	Date(s) of Experiment 01.07. - 03.07.2005

Date of Report: 03.Oct. 2005

TEOS a silicon alkoxide, easily polycondenses to form a 3D entangled network of silica clusters. We have used organic modified silicates (ORMOSIL) [1] to modify the network of the inorganic silica clusters using PDMS (polydimethylsiloxane) a hydroxyl terminated polymer. Reactions are assisted by high power ultrasounds (0.6 kJ/cm^3). After the corresponding polycondensation these gels can be processed by supercritical drying of the corresponding alcogel in ethanol, giving a monolithic solid known as aerogel. We have used several polymer contents ranging from 10 to 50 wt.% of the total silica content.

From a mechanical point of view these materials can be tuned from brittleness to rubbery as a function of the organic polymer content [2]. Their structure must be depicted by the organic chain crosslinking bonded to the porous inorganic silica clusters. Textural characterization by gas physisorption and electronic microscopy confirm the above premises indicating their nanostructured nature.

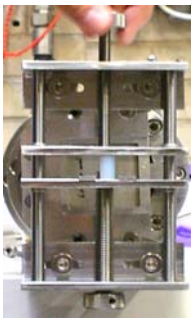

We have designed a specific sample-holder to measure "in situ" the uniaxial compression of the aerogel. In this way the sample, as a cylinder of 16 mm long and 8 mm diameter, is placed between two horizontal plates and by means a step screw (1 mm by turn) permits to control the load on the sample knowing previously its deformation from the experimental stress-strain curves.

By using a neutron wavelength of 0.605 nm and the available sample-detector distances and collimator the q-range covered in the experiment was 0.02 to 3.7 nm^{-1}. Each sample was measured first without compression and then under several loads determined by its deformation controlled by the step screw.

Fig. 1 shows the scattered intensities from the aerogels without compression as a function of the polymer content. A wide Guinier region indicates a homogeneous particle size distribution. The increases of the incoherent contribution in the high q-region, produced by the methyl radicals of the PDMS, run parallel with the polymer content. In this way, the use of deuterated PDMS organic polymer should be an improvement for the future.

Fig. 1

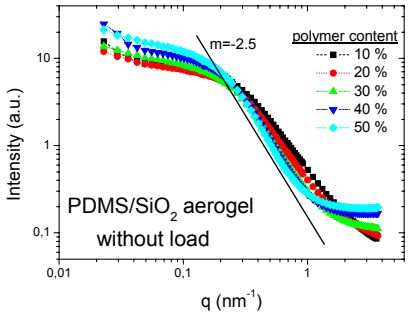

On the other hand the Fig. 2 shows the intensities from an aerogel of 40wt.% under compression for the marked loads. The spectra were significantly anisotropic in the perpendicular direction of the uniaxial load. The average angular anisotropic spectra were taken ±20º from the horizontal direction.

Fig. 2

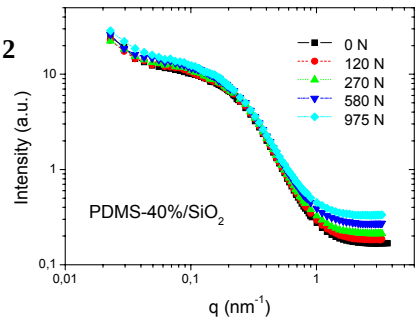

The upward shift of the curves are mainly due to the increase of the material density submitted to the compression.

Some improvement in the sample-holder could be necessary to obtain better results in the future, in order to avoid unwished effects and inconveniences.

References

[1] C. Sanchez and B. Lebeau: MRS Bulletin (May 2001) p. 377.

[2] O. Foussaier, M. Menetrier, J.-J. Videau and E. Duguet: Mater. Lett. **42**, 305 (2000).

	EXPERIMENTAL REPORT **In-situ SANS- isothermal ageing measurements of EB – PVD thermal barrier coatings**	Proposal N° MAT-04-1143 Instrument **V4** Local Contact Jörg Haug
Principal Proposer: Experimental Team:	B. Saruhan-Brings - DLR Köln A. Flores Renteria - DLR Köln J. Haug - HMI Berlin A. Wiedenmann - HMI Berlin	Date(s) of Experiment 16.08. - 20.08.2005

Date of Report: 09. Jan. 2006

Metallic blades localized at the high temperature sector of aircraft and stationary turbines are protected against the heat by thermal barrier coatings. The Electron Beam - Physical Vapour Deposition (EB-PVD) coating process enhances the creation of a columnar microstructure, which compiles satisfactory thermo-mechanical properties required for these severe service conditions. The microstructure of these coatings encloses open porosity in form of inter-columnar gaps between primary columns grown perpendicular to the substrate's plane, and gaps between feather-arms grown outwards from inside the columns and located at their periphery in an oblique angle; and closed porosity in form of intra-columnar porosity inside of the primary columns. The attained physical properties of these coatings are influenced by the spatial and geometrical characteristics of all these pores, which are known to be anisotropic. Thus, these properties alter due to sintering of the porosity after an ageing process. Since small-angle neutron scattering (SANS) is capable to measure the open and closed porosity, it is an appropriated method for the analysis of thermal induced changes of the pores within EB-PVD TBCs.

Four microstructures produced at different process parameters conditions were in-situ aged in vacuum (1000°C)/measured at the small-angle neutron instrument – BENSC (V4), using the incident beam along the plane perpendicular to the substrate (parallel to the columns axis). The obtained raw information was converted into Porod Constant, P_c values of the pores (proportional to its Apparent Porod Surface Area) as function of the azimuthal angle by converting the 2-D data to 1-D scattering profiles averaged over 5° (see Fig. 1).

The polar shapes of the Porod Constants in Fig. 1 clearly show the anisotropic character of the pores surface area distribution at each of the analysed microstructures. Differences in the polar distribution and values of the Porod Constant between the microstructures are related to the geometrical and spatial characteristics of their porosity, which are govern by the differences in the parameters conditions during the EB-PVD coating process. Annealing of the specimens at 1000°C in vacuum activates atomic diffusion processes. This contributes the porosity to change into shapes with the lowest surface energy (lower surface area for the same volume, e.g. spheres), which is the activations energy for the sintering process.

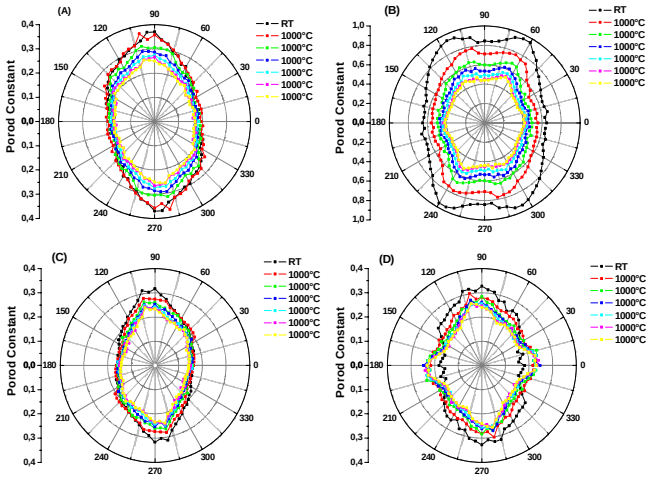

Fig. 1: Polar distribution of the surface area (proportional to the Porod constant) of the porosity enclosed within the analysed EB-PVD TBCs.

	EXPERIMENTAL REPORT **Solution treatment of the single-crystal Ni-base superalloy CMSX4: a detail view**	Proposal N° MAT-04-1144 Instrument **V4** Local Contact Jörg Haug
Principal Proposer: Experimental Team:	P. Strunz - NPI Řež near Prague, CZ P. Strunz - NPI Řež, CZ D. Mukherji - ETH J. Rösler - TU Braunschweig Zuerich, CH R. Gilles - TU München J. Haug - HMI Berlin	Date(s) of Experiment 20.09. - 25.9.2005

Date of Report: 09.01.2005

The evaluation of the previous experiment (2004, MAT-04-1018) on CMSX4 brought open questions in solution-treatment proccess and the intention of the present in-situ SANS experiment was to help to solve them. First, the influence of the hold at around 10K below the solidus temperature of this Re-containing commercial superalloy on solutionizing process was studied. Second, the effect of hold on elemental homogenization at temperatures between 1200-1300°C wass assessed. A certain complication during the experiment was cooling of the velocity selector as well as of the furnace and, mainly, uncertainty in the temperature as the displayed values of the two used thermocouples differed significantly (clarified after the beam time). These items hindered the full exploitation of the beam time.

In Fig. 1a and b, a rough evaluation of the SANS data for two newly measured samples and their comparison with the previous measurement is plotted (a detailed evaluation is currently being carried out). The displayed parameter, i.e. the maximum intensity of the measured data at Q=0 (for SDD=16m and λ=19.6 Å) in dependence on time and temperature, is an inverse quantity to the scattering probability. With decreasing volume fraction of precipitates and/or their scattering contrast, this quantity should increase, reaching an absolute maximum when all the precipitates are dissolved.

Previous in-situ performed solution treatments on CMSX4 samples including the hold at either 1210 or 1280°C prior the standard solution treatment resulted in the full dissolution on further temperature increase to 1341°C. Preliminary data evaluation of the new results shows that standard solution treatment (i.e. 1277-1280-1296-1304-1313-1316-1318°C), even though followed by an increase of the temperature up to 1341°C (Fig. 1a) does not cause the full dissolution of the largest precipitates or γ/γ' eutectics in the interdendritic regions of CMSX4 superalloy. That means that the hold at either 1210 or 1280°C prior the standard solution treatment is extremely important for a proper solution treatment of CMSX4.

The second part of the experiment was focused on the possibility to reach full dissolution and elemental homogenization by holding at 1332°C, without a need to increase the temperature up to 1341°C. The results (Fig. 1b) show that the hold for 4 hours (remaining beam time did not allow a longer measurement) is not sufficient to achieve the full solutioning. Nevertheless, when extrapolating the observed tendency, a 12 hours hold at 1332°C could have the same effect as the temperature increase up to 1341°C.

The experiments also showed that a fine-structure patterns of the volume fraction times contrast evolution with temperature in the range 1305-1330°C which were observed in the previous experiment are not visible in the new samples (see Fig. 1b). As the measurement was done with samples originating from a different bar than in 2004, this difference can be ascribed most probably to the small variations between the bars itself and/or to the small differences in the temperature or to the holding time variations for the individual samples.

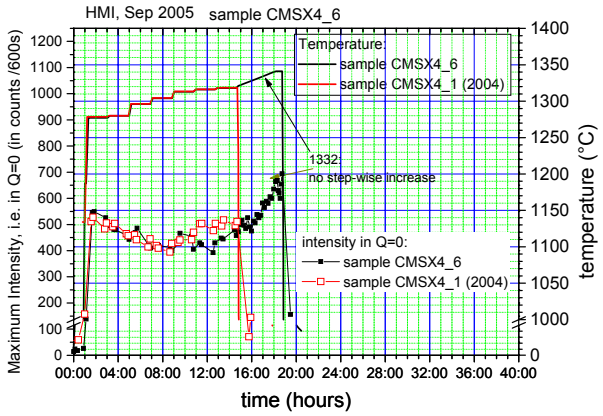

Fig. 1a: Intensity in maximum (Q=0) evolution for the treatments without any long hold.

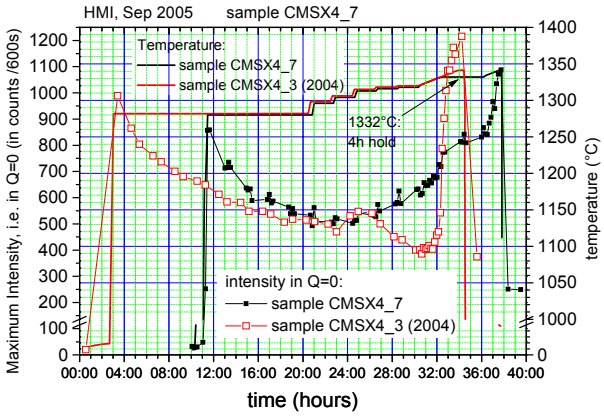

Fig. 1b: Intensity in maximum (Q=0) change for the treatments including hold at 1282°C.

	EXPERIMENTAL REPORT **Isothermal development of the microstructure in molten AlSi alloys**	Proposal N° PHY-04-1101 Instrument **V4** Local Contact Jörg Haug
Principal Proposer: Experimental Team:	U. Dahlborg - LSG2M, Ecole des Mines, Nancy, F U. Dahlborg - LSG2M J. Haug - HMI Berlin	Date(s) of Experiment 28.05.-01.06.2005

Date of Report: 20. Jan. 2006

The microstructure of hypereutectic AlSi alloys consists of primary silicon and the Al-Si eutectic under normal cast conditions. It has been found that some coarse primary silicon is detrimental to the mechanical properties and limits the application of the alloy. Generally it can be concluded from this kind of studies that a control of the type and the distribution of the intermetallics are of importance in commercial applications. Recent investigations have shown that the primary silicon can be refined by a proper melt overheating treatment. Furthermore, at increased solidification rates that are facilitated by high undercooling ability other opportunities to control the microstructure has become available. In eutectic Al-based systems, i.e. Al-Si, this makes it possible to alter the primary phase and to produce unique nanoscale microstructures with outstanding mechanical properties. A key issue in the synthesis of nanocrystalline Al microstructures is the capability to control the nucleation density that is linked to the presence of quenched-in pre-existing clusters in the melt and their time dependence. The purpose of the project is to obtain the necessary information on these two phenomena on the structure and microstructure of an Al-Si melt at different temperatures and Si concentrations.

Molten $Al_{1-x}Si_x$ alloys of different compositions have been studied on V4 during different heating conditions. Thus the microstructural development of the melt has been studied both during stepwise heating and during isothermal conditions. The investigations were performed on alloys with x=0.07, 0.126 and 0.2. Earlier similar studies have been performad at ILL and the two sets of measurements show similar and unexpected. results.

Fig. 1 shows how the total intensity of the SANS pattern develops after that the melt with the eutectic composition $Al_{0.874}Si_{0.126}$ has been rapidly heated to 800C. This temperature is about 240 degrees above the melting temperature. Immediately after melting the signal decreases. However, after a few minutes it increases to decrease again after a few minutes. The same effect was seen in the earlier measurements and it is thus reproducible.

When the sample undergoes continuous heating from the melting point up to 800C the signal changes in a completeley different way as can be seen in fig.2. Following an initial decrease after that the melting is completed the signal increases and a broad maximum can be seen. This is a strong indication that clusters are formed in the melt during heating the step-wise heating. Similar phenomena are seen in alloys of other compositions and the results are presently under further analysis.

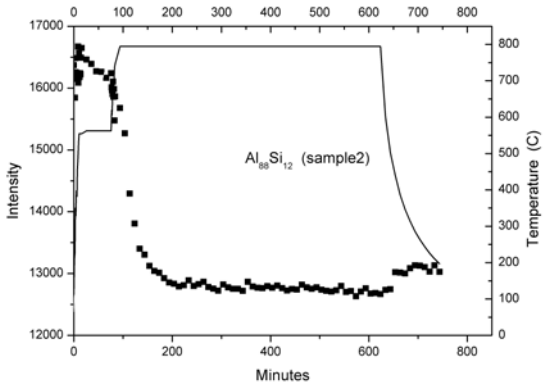

Fig. 1: The development of the SANS signal after that the $Al_{0.874}Si_{0.126}$ melt is rapidly heated as given by the full line and right vertical axis.

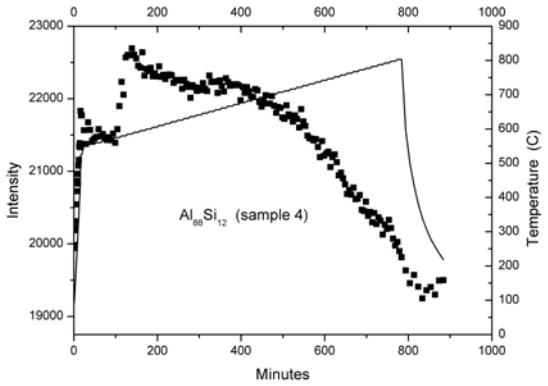

Fig. 2: The development of the SANS signal during heating of the $Al_{0.874}Si_{0.126}$ melt as given by the full line and right vertical axis.

	EXPERIMENTAL REPORT **Formation of liquid water and carbon dioxide in fuel cells**	Proposal N° MAT-04-1172-DT Instrument **V7** Local Contact Ingo Manke
Principal Proposer: Experimental Team:	C. Hartnig - ZSW Ulm M. Grünerbel, J. Kaczerowski, C. Hartnig - ZSW Ulm I. Manke, A. Hilger, N. Kardjilov - HMI Berlin	Date(s) of Experiment 12.09. - 16.09.2005

Date of Report: 08. Jan. 2006

Introduction

Polymer Electrolyte Membrane Fuel Cells (PEMFCs) are developed for a wide range of mobile, portable and stationary applications. Considering the developments from the very first beginning to state-of-the-art fuel cells a lot of improvements have been reached with regard on, e.g., durability, cost reduction, overall increase of power density. Furthermore, the geometrical setup (for example thickness of gas diffusion layers, geometry of flow fields) has been optimized by computer-aided design. One of the main problems that still remain unsolved is the optimization of the water management in the fuel cell. By means of neutron radiography investigations the formation of liquid water in the flow fields can be identified and possible failure mechanisms can be detected.

For another type of low temperature fuel cells which are fed with an aqueous methanol solution instead of gaseous hydrogen (Direct Methanol Fuel Cells, DMFCs), the formation of gas bubbles stemming from the fuel cell reaction $CH_3OH + 3/2\ O_2 \rightarrow CO_2 + 2\ H_2O$ is an important topic with respect to blocking of the active sites. First experiments anticipating this issue were installed.

Experimental procedure

Two different single cells were prepared, the first one with the DMFC setup and the second one with the standard PEMFC setup. Materials like steel and plastics were excluded in order to avoid excessive absorption. The PEMFC was operated at normal and so-called 'wet' operating conditions; the latter ones are characterized by excessive formation of liquid water.

Results and discussion

a) DMFC

The time evolution of the formation of carbon dioxide bubbles was monitored on the neutron radiographic images.

By repeated purging and restarting of the reaction the most active spots could be identified and influences effecting the formation of carbon dioxide were investigated.

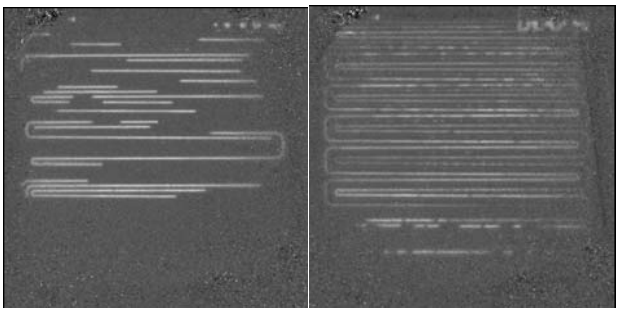

Fig. 1: Time evolution of carbon dioxide formation (bright areas) in a Direct Methanol Fuel Cell (DMFC)

b) PEMFC

In fig. 2 the formation of liquid water is monitored. The temporal evolution and the following migration of the droplet are clearly visible. With the newly developped flowfield design excess water formation can be controlled and liquid water can be transported out of the cell.

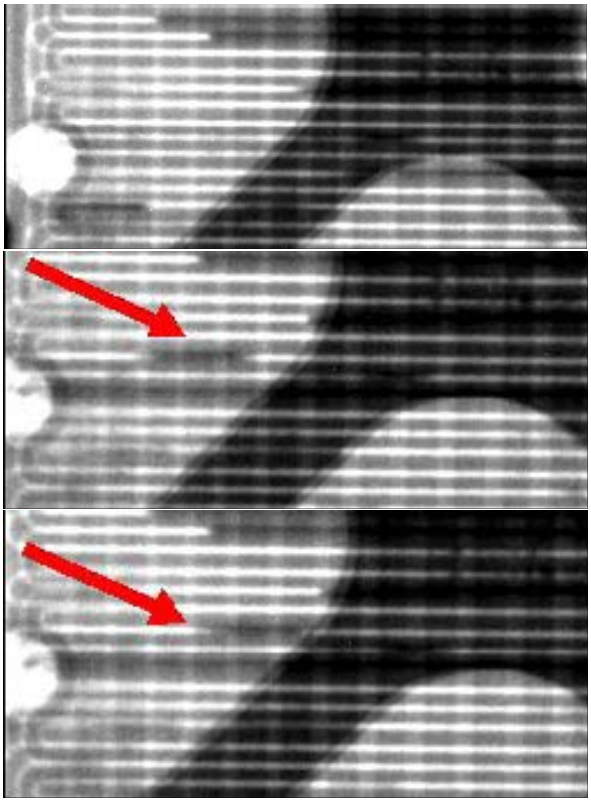

Fig. 2: Formation and migration of water droplets (indicated by arrow) in flowfields

BENSC	**EXPERIMENTAL REPORT** **Neutron pre-examination of "Portrait – Amedeo Modigliani" attributed to Amedeo Modigliani, 55 x 46 cm²**	Proposal N° ART-05-0010 Instrument **B8** Local Contact Birgit Schröder-Smeibidl
Principal Proposer: Experimental Team:	B. Schröder-Smeibidl - HMI Berlin C. Laurenze-Landsberg - Gemäldegalerie Berlin C. Schmidt - Gemäldegalerie Berlin L.A. Mertens - HMI Berlin	Date(s) of Experiment 25.08.2004 / 01.07.2005

Date of Report: 13.03.2006

Introduction

When investigating paintings, the information provided by research methods using photon radiation at both extreme positions of the electromagnetic spectrum is limited. X-radiography principally indicates the distribution of the pigment lead white, whilst infrared reflectography is used to reveal black, carbon-based media which have been applied on a light ground. In contrast, neutron autoradiography (NAR) is capable of revealing different paint layers superimposed during the creation of a painting. In many cases, the individual brushstroke applied by the artist is made visible as well as changes made during the painting process.

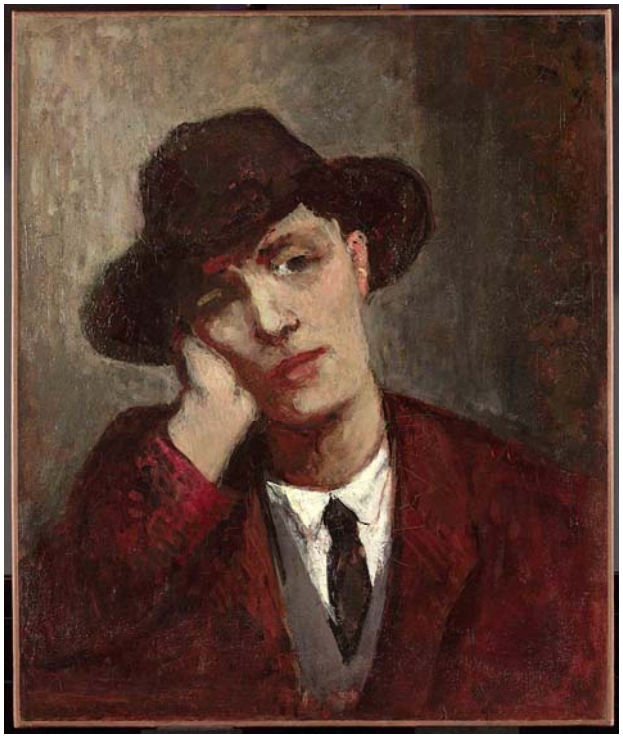

Fig. 1: Portrait of Amedeo Modigliani, oil on canvas 55 x 46 cm², private property

The present painting (fig. 1) was supposed to be an original self-portrait of Amedeo Modigliani created in the early 20th century. A. Modigliani (1884-1920), an Italian painter and sculptor, developed while living in Paris his own unique style. Today graceful portraits and lush nudes spread over famous museums such as the Metropolitan Museum of Modern Art in New York remind the art interested community of the artist Modigliani and his brief career. This painting which has been investigated in the collaboration of HMI and the Berlin Picture Gallery was very interesting because it has been the first painting of the 20th century to be examined with neutrons at BENSC. Therefore for the first time in this joint research project, this experiment offered the possibility to learn more about pigments which were applied in (almost) modern paintings. The second reason for this experiment was to provide an informative basis to the open question whether this painting was originally painted by Modigliani himself, e.g. by finding a signature. The earlier taken X-ray record revealed a further interesting fact, a female portrait lying under the visible male portrait.

Results

Unfortunately, already during the short pre-irradiation – usually done to clarify the content of ^{59}Co in the painting and finally to avoid the generation of the long-lived ^{60}Co – an unexplained high gamma dose rate was observed (more than a factor of 5 higher than in previous experiments). To clarify this high rate we performed on the one hand additional short irradiations detecting simultaneously the gamma peaks revealing the isotopes by their specific energy and on the other hand PIXE (proton induced x-ray emission) measurements at the Ion Beam Lab at the HMI. The following elements were analysed: Fe, Pb, Cd, Ba, Zn, Cr, Se, Sr, Co. No signature could be observed neither with neutrons nor with other methods such as infrared or ultraviolet examinations applied at the Gallery. All of the observed pigments, especially lead white and zinc white, were known and used in the era of Modigliani. Therefore there is no contradiction with an authorship of Modigliani. But, the found data do not provide enough evidence to allow attribution to him. The high Cd concentration in the painting was suspected to be responsible for the high gamma dose during the irradiation. But despite of all examinations, it was not possible to clarify the origin of the high gamma dose rate with ultimate reliability and, thus, an adverse effect for the painting could finally not be excluded. Therefore the decision was made to pass on the main irradiation. After all, the investigation confirmed that several parts of the visible painting were taken over from the underlying female portrait. For instance, the arm which supports the head is part of both pictures.

Conclusion

The question what happens at modern paintings and the issue of authorship of the present painting attributed to Modigliani still remain unsolved. Especially, works of the 20th century have to be investigated to clarify the composition of modern pigments and their impact on neutron activation analysis.

We gratefully acknowledge Andrea Denker (HMI), who has performed the PIXE measurements.

	EXPERIMENTAL REPORT **Neutron autoradiographs of "Ceres, Sitting on the Rim of a Fountain" by Sebastiano del Piombo, 74,5 x 45,5 cm²**	Proposal N° ART-05-0011 Instrument **B8** Local Contact Birgit Schröder-Smeibidl
Principal Proposer: Experimental Team:	C. Laurenze-Landsberg - Gemäldegalerie Berlin C. Laurenze-Landsberg, C. Schmidt - GMB L.A. Mertens, B. Schröder-Smeibidl - HMI Berlin	Date(s) of Experiment 15.03.2005

Date of Report: 28.02.2006

Introduction

Neutron autoradiography (NAR) is used to analyse materials and techniques of paintings. X-ray-radiography indicates the distribution of heavy elements. In contrast, NAR is capable of revealing different paint layers superimposed during the creation of the painting. In many cases the individual brushstrokes applied by the artist are made visible, as well as, changes made during the painting process. When investigating paintings that have been reliably authenticated, it is possible to identify the particular style of an artist.

The investigation of the painting "Ceres, Sitting on the Rim of a Fountain" by Sebastiano del Piombo (fig. 1) belonging to the Berlin Picture Gallery (Cat. No 56.1) has to be discussed in the context of the NAR investigation of the painting "Picture of a Young Roman Lady" also created by Piombo. The picture "Ceres" is only attributed to Piombo, whereas the painting "The Young Roman Lady" is accepted as being a certain work of Piombo. To clarify the issue of authorship of "Ceres" by comparing painting techniques a NAR investigation was performed.

Fig. 1: "Ceres, Sitting on the Rim of a Fountain" by Sebastiano del Piombo, Berlin Picture Gallery

S. del Piombo (1485-1547) was a representative of the Italian Renaissance mannerist.

Results

The NAR yielded success. The painting technique and the composition of pigments in the picture "Ceres" are in accordance to the result of the painting "Picture of a Young Roman Lady". As shown in fig. 2 a lot of pentimenti could be observed in the NAR record.

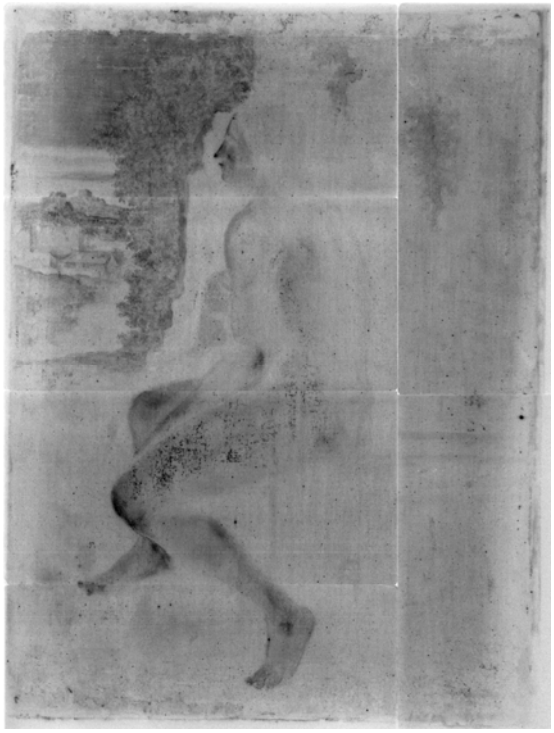

Fig. 2: "Ceres, Sitting on the Rim of a Fountain" by Sebastiano del Piombo, 4th neutron autoradiography

The arm now holding the cloth and the wheat originally supported the body. The first version presented at the 3rd autoradiography did not show any attribute which could be associated with the goddess Ceres. The observed pentimenti contradict the suggestion that this painting might be a copy. In addition, the shape of the face and body fit in the Venetian ideal of beauty of the early 16th century.

Conclusion

The brushstroke, the composition of colours containing azurite and smalt revealed in the ceiling and the enhancement of the contour of the face by vermilion (containing Hg) allow for a precise attribution of this painting to S. del Piombo.

BENSC	**EXPERIMENTAL REPORT** **Neutron autoradiographs of "The Repudiation of Hagar" by Govert Flinck, 110 x 138,7 cm^2**	Proposal N° ART-05-0012 Instrument **B8** Local Contact Birgit Schröder-Smeibidl
Principal Proposer: Experimental Team:	C. Laurenze-Landsberg - Gemäldegalerie Berlin C. Schmidt - Gemäldegalerie Berlin L.A. Mertens - HMI Berlin B. Schröder-Smeibidl - HMI Berlin	Date(s) of Experiment 31.05. / 20.09.2005

Date of Report: 28.02.2006

Introduction

Neutron autoradiography (NAR) has turned out to be a suitable non-destructive method to investigate paintings. The main advantages of neutrons in comparison to X-rays are the high penetration depth and the fact that the activation cross section (n,β) depends on the isotope. Therefore different pigments due to different nuclides with different half-life periods can be depicted on separated films yielding a contrast variation. In the present experiment this method is used to analyse the painting techniques in order to learn more about the special individual technique and brushstroke of the artist.

A few years ago the painting "Susanna and the Elders", an art work which is only attributed to G. Flinck, was investigated by NAR at the BER II and a characteristic handwriting applied by the artist was observed. In 2004 a neutron investigation of the painting "The Hermit", a work of an unknown artist, was performed which was suspected of being created by

Fig. 1. *The Repudiation of Hagar* by Govert Flinck, canvas 110,7 x 138,7 cm^2, Gemäldegalerie Berlin Cat. No 815

H. Rembrandt. But, by neutron autoradiography we found characteristic features which could be identified with the handwriting of G. Flinck, because there was a remarkable accordance to the NAR results of the painting "Susanna and the Elders". It was the aim of the present study of the painting "The Repudiation of Hagar" (Die Verstoßung der Hagar), a painting which is signed by Govert Flinck and insofar accepted as being an original of Flinck, to learn more about Flinck's original handwriting, to compare the results with the earlier experiments and to possibly enlighten the issue of authorship of "The Hermit".

Govert Flinck (1615-1660) apprenticed by Rembrandt and known as one of his best pupils, was a Dutch painter of the Baroque era famous for his portraits and historical scenes. Among others, he worked also for the Great Elector, Friedrich Wilhelm of Brandenburg. The topic of the present painting is the scriptural story of Abraham, Sara and Hagar. As Sara had finally born Isaac, Hagar and Ishmael, the son of Abraham and the maid Hagar, were banished by Abraham into the desert.

Results

Because of the size of the painting, the neutron irradiation had to be carried out in two steps. Afterwards the neutron autoradiographs were assembled (see Fig. 2). In the neutron autoradiographs, revealing the elements Hg and Cu contained in the pigments vermilion and malachite, several pentimenti could be observed. Obviously in the background on the right side the figure

Fig. 2: 3rd autoradiograph of *The Repudiation of Hagar* by Govert Flinck

of Sara wearing a cape was painted in an earlier version. This additional figure was already anticipated by an Infrared record done complementary at the Berlin Picture Gallery. Unfortunately a clear individual brushstroke or characteristic feature of G. Flinck could not be observed and documented in this work. Therefore, this up to now sole examination of a certain and accepted work of Flinck did neither foster the thesis that the unknown work "The Hermit" might be attributed to Flinck nor confirm that the special brushstroke observed in the painting "Susanna and the Elders" could be definitely linked with Flinck. These questions still remain unsolved. Additional works of G. Flinck have to be investigated to verify this issue and to clearly identify the individual style and brushstroke of G. Flinck.

BENSC	**EXPERIMENTAL REPORT** **Neutron autoradiographs of "Picture of a Young Roman Lady" (~1512/13) by Sebastiano del Piombo, 78 x 61 cm²**	Proposal N° ART-05-0013 Instrument **B8** Local Contact Birgit Schröder-Smeibidl
Principal Proposer: Experimental Team:	C. Laurenze-Landsberg - Gemäldegalerie Berlin C. Laurenze-Landsberg, C. Schmidt - GMB L.A. Mertens, B. Schröder-Smeibidl - HMI Berlin	Date(s) of Experiment 12.04.2005

Date of Report: 28.02.2006

Introduction

Neutron autoradiography (NAR) is a very effective, non-destructive, but rather exceptional method applied in the examination and analysis of materials and techniques used in painting. It allows for visualization of structures and layers under the visible surface and, in addition, enables one to identify in detail the elements contained in the pigments. In many cases, the individual brushstroke applied by the artist is made visible as well as changes and corrections introduced during the painting process. By using paintings that have been reliably authenticated, one can identify the unique style or "hand" of a particular artist.

The painting "Picture of a Young Roman Lady" (fig. 1) by Sebastiano del Piombo created 1512/13 belongs to the Berlin Picture Gallery (Cat. No 259B) and is accepted as being an original work of Piombo. The aim of the investigation of this painting by NAR was to identify the characteristic brushstroke of Piombo in order to compare the result with other works of Piombo which are only attributed to him.

Fig. 1: "Picture of a Young Roman Lady", by S. del Piombo ~ 1512/13, Berlin Picture Gallery

Sebastiano del Piombo (born 1485 in Venice, died 1547 in Rome, originally Sebastiano Luciani) was a Venetian renaissance mannerist. He was a pupil of Bellini and afterwards of Giorgione and in Rome a friend of Michelangelo. Piombo was famous for the combination of the colours of the Venetian school and the monumental forms of the Roman school.

Results

In the 2nd NAR record (fig. 2) revealing the pigments smalt and azurite several changes and pentimentis are observed made by the artist himself. Originally the head of the lady was surrounded by green leaves containing a Cu pigment. In addition, the basket, the hands and arms were located a little bit higher. The fur collar was added later to cover the pentimentis in the pink dress.

Fig. 2: "Picture of a Young Roman Lady", 2nd neutron autoradiography

Conclusion

In the NAR the typical pigments used by Piombo and his individual brushstroke is observed. Comparisons with other works of Piombo could be drawn.

BENSC	**EXPERIMENTAL REPORT** **Neutron autoradiographs of "The Fair at Bezons" (1733) by Jean-Baptiste Pater, 91,5 x 130 cm^2**	Proposal N° ART-05-0014 Instrument **B8** Local Contact Birgit Schröder-Smeibidl
Principal Proposer: Experimental Team:	J. Bartoll - Stift. Preuss. Schlösser und Gärten (SPSG) B. Jackisch - SPSG Berlin-Brandenburg C. Laurenze-Landsberg - GMB L.A. Mertens, A. Niemann, B. Schröder-Smeibidl - HMI	Date(s) of Experiment 18.06. / 13.09.2005

Date of Report: 28.02.2006

Introduction

The painting "The Fair at Bezons" (1733) or more exactly "A Fair in Wide Landscape with Italian Architecture" by Jean-Baptiste Pater (1695-1736) is owned by the Foundation *Preußische Schlösser und Gärten Berlin-Brandenburg*. It is exhibited at Sanssouci, in Potsdam, in the gallery of Frederick the Great of Prussia, who collected more than forty pictures of Pater. "The Fair at Bezons" (fig. 1) is the first painting which has been investigated in the collaboration of HMI and the Prussian Palaces and Gardens Foundation Berlin-Brandenburg and, in addition, this painting has been the first painting of the 18th century to be examined with neutrons at BENSC.

Fig. 1: "A Fair at Bezons", Jean-Baptiste Pater 1733, Prussian Palaces and Gardens Foundation Berlin-Brandenburg

Pater, a French painter of the Rococo era, was born in Valenciennes in 1695 where he first studied with a local painter and his sculptor father before moving to Paris to do an apprenticeship under Jean-Antoine Watteau. Dismissed by the latter he later worked for some of Watteaus clients. Pater was also influenced by Flemish art and, in his lifetime, he became as famous as Watteau.

Most of Pater's pictures have not yet been investigated using scientific methods or even with neutrons. Pater is one of the 3 French painters of the early 18th century – Pater, Watteau and Lancret – that we are interested in. When comparing the neutron autoradiographs of these paintings we expect to find special features e.g. brushstrokes, characteristics of the French painting of that time. Observing special individual techniques or the used pigments of these 3 French masters could support the clarification of authorship of paintings in case of unclear attribution and to distinguish among each other. The picture "The Fair at Bezons" illustrates the fair, annually held on the first Sunday in September in a village near Versailles. As an additional goal of the present examination, we intend to compare the Potsdam painting with a second larger version belonging to the New York Metropolitan Museum of Art.

Results

Unlike most of the paintings investigated so far, the autoradiographs of Pater's painting (fig. 2) did not show any pentimenti. One can assume that Pater knew exactly what he wanted to demonstrate. In addition, pigments containing the element Cu could surprisingly not be observed. This is an astonishing feature, because all until now investigated artists of the 16th and 17th centuries used to use Azurite and Malachite pigments - both of them contain copper.

Fig. 2: 3rd neutron autoradiography of "A Fair at Bezons" by Jean -Baptiste Pater

In the autoradiographs the structures due to the blackening by the pigment Naples-Yellow containing Sb could be clearly observed. Pater frequently used this pigment in the whole picture. A special handwriting of Pater could be interpreted in the way he pictured the foliage. But, to be sure about his special brushstroke other paintings of Pater's accepted work have to be investigated. Frome the absence of pentimentis one might conclude that the Potsdam painting is a duplicate of the version exhibited in New York.

	EXPERIMENTAL REPORT Texture and morphology of ancient wooden artcraft	Proposal N° CHE-04-1153 Instrument **V4** Local Contact Uwe Keiderling
Principal Proposer: Experimental Team:	R. Triolo - Univ. Palermo, I R. Triolo - Univ. Palermo, I U. Keiderling - HMI Berlin	Date(s) of Experiment 11.08. - 19.08.2005

Date of Report: Jan. 2006

Introduction

The wooden handcrafts of historical and/or artistical interest are frequently deteriorated. The wood decays through the combined effects of biodegradation and of environmental factors (pH, moisture, finding site). In the past, different materials and methods have been used in relationship to the dimensions, to the wooden taxon and the state of maintenance of the artefacts. Today a great deal of research is performed to explore the possibility of preserving important artistic handcraft by treatments with strengthening chemicals.

Experiment

In recent years a research program aimed at the conservation and the treatment of degraded waterlogged woods started in the Department of Physical Chemistry at the University of Palermo. Samples have been provided by Archaeologists and Heads of Museums. Samples coming from wreckages of known origin and from lake-dwelling with different taxa and state of degrade, have been impregnated with selected mixtures characterized by suitable physical-chemical parameters. Besides more traditional treatments, thanks to the efforts of prof. D.I. Donato, a new tecnique able to syntetize polymers inside the treated wood has been developed in ours laboratories; woods are treated with “easy to flow” solutions of ethilmetacrylate, metacrylate and a polymerization initiator. The “in situ” polymerization produces a polymeric compound, similar to Paraloid B72, but without the “flow problems” experienced earlier. This polymer is a strenghtening, preservative and antifungi agent.

Results and discussion

We have investigate the structure of a limited number of samples before and after treatment, in order to learn about the distribution of the preserving polymer inside the pieces and the stability of the treatment. SANS measurements have been performed and data analysis is in progress.

An example of undeteriorated sample equilibrated with a preserving solution is shown in figure 1, while figure 2 shows the effect of different solutions on a deteriorated sample. Also USANS and Neutron Tomography measurements have been performed and will be subject of separate reports. The main goal of the study is to show the spatial distribution of the impregnating solution in the wood matrix and to extract a quantitative information about the volume fraction of the solution.

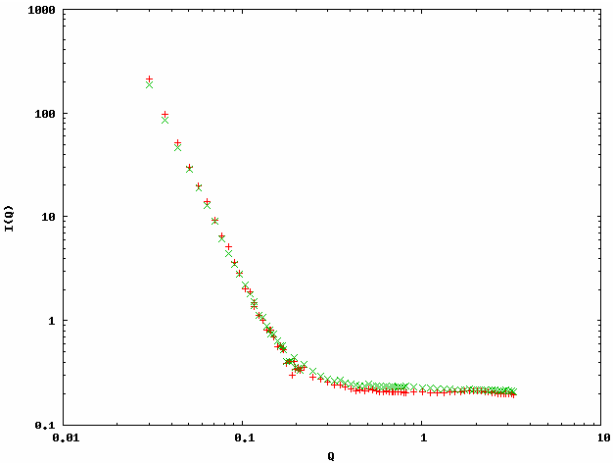

Fig. 1: SANS data on a sample of undeteriorated samples before and after impregnation. Little difference can be found.

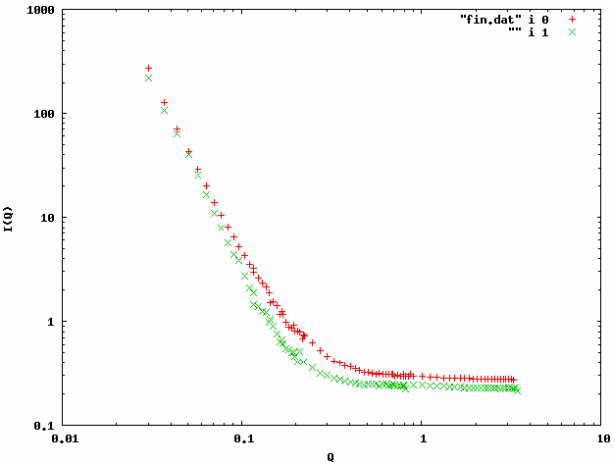

Fig. 2: SANS data on a sample of deteriorated samples using different impregnation solutions. Substantial difference is found, showing high selectivity in one case.

Acknowledgement

This research project has been supported by the European Commission under the 6th Framework Programme through the Key Action: Strengthening the European Research Area, Research Infrastructures.
Contract n°: RII3-CT-2003-505925 (NMI3).

BENSC	**EXPERIMENTAL REPORT** **SANS investigation of Cu/Zn alloys for applications to technology for the restoration of ancient European organs**	Proposal N° MAT-04-1148 Instrument **V4** Local Contact Martin Kammel
Principal Proposer: Experimental Team:	A. Manescu - UPM Ancona, I V. Calbucci - UPM Ancona, I M. Kammel - HMI Berlin	Date(s) of Experiment 26.07. – 01.08.2005

Date of Report Jan. 2006

With the aim to investigate the microstructure and the presence of inhomogeneities, such as precipitates, grain (nanostructure), pores, cavities and defects, we have carried out SANS measurements on V4 instrument on eight copper-zinc alloy samples, seven of these historical organ reed pipes coming from different organs across Europe, and the last one a new brass reference sample.

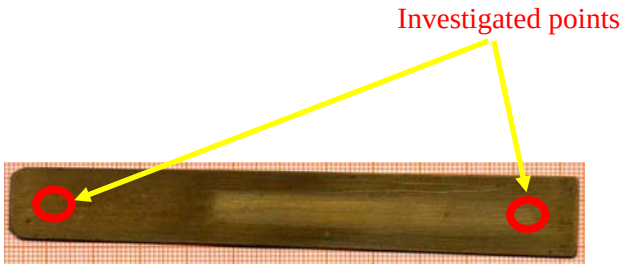

Fig. 1: Geometry of a tongue and measuring areas. Överselö church (Sweden), 1754 – 8Cs sample

Fig. 2: Reference Sample. New Brass, product in Sweden (1999) – New sample

All the measurements have been performed selecting the beam wavelength at 6Å and every sample was been measured with a sample-detector distance of 1*m*, 4*m*,12*m* and 16*m*, as the collimation distance. On five of the eight samples the measurements have been performed in two points, in the vibrating and in the fixed part of reed pipe. The dimensions of the circular slits in front the samples varied from 4.5*mm* of diameter for the smaller sample to 13*mm* of diameter for the larger ones.
The following experimental SANS curve has been obtained for two of the analyzed samples: new brass (reference sample) and one of the historical samples (the sample in the figure 1). For this two samples we have used the same slit, with 13*mm* of diameter.

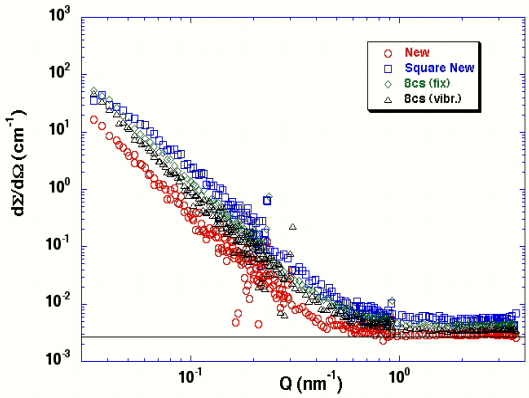

Fig. 3: Comparison between New Brass SANS curve and vibrating and fixed part SANS curve of the historical sample shown in fig.1

The different incoherent background for various specimens indicates a different alloy compostion.
An analysis in the low range of Q (Guinier region) was done for the various specimens – see Fig.4, which allowed an evaluation of the radius of gyration for different specimens.

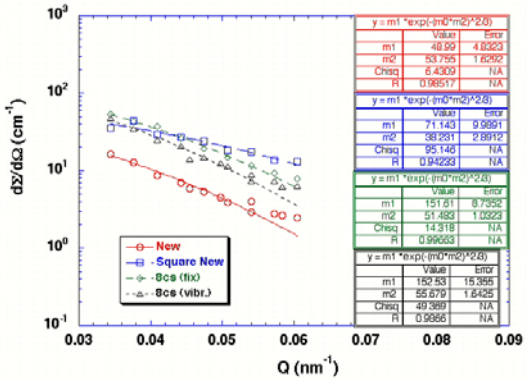

Fig. 4: Comparison between the 8Cs and New samples for the Guinier region

The gyration radius observed are in the range of 30-60 nm, slightly higher for the historical samples.There is also a difference in the density of the inhomogeneities between different historical samples – due to different manufacturing processes.

	EXPERIMENTAL REPORT **Texture and morphology of ancient wooden artcraft**	Proposal N° CHE-04-1169 Instrument **V7** Local Contact Nikolay Kardjilov
Principal Proposer: Experimental Team:	R. Triolo - Univ. Palermo, I D.I. Donato - Univ. Palermo, I N. Kardjilov - HMI Berlin A. Hilger - HMI Berlin	Date(s) of Experiment 11.08. - 19.08.2005

Date of Report: Jan. 2006

Introduction

Important application of neutron tomography is the non-destructive inspection of the results of a preservation treatment of a wood by means of impregnation with aqueous polymer solution. The high sensibility of neutrons to hydrogen allows good visualisation of the polymer distribution inside the sample.

Experiment

The experiments were performed at the neutron tomography instrument V7 (CONRAD). Wood samples after preservation treatment with different aqueous solutions were investigated.

The tomography experiments were performed with L/D ratio of 250 which gives a spatial resolution of approximately 200 µm. 300 projections were taken of the sample on an angular range of 180 degree. The beam size was 10x10 cm^2.

Results and discussion

The main goal of the study was to show the spatial distribution of the impregnation solution in the wood matrix and to extract a quantitative information about the volume fraction of the solution.

Such an example can be seen in Fig. 1 where a piece of wood PG+ was preserved by impregnation solution. The tomography reconstruction shows high contrast between the wood and the solution due to the different attenuation coefficients of the two materials for neutrons (see Fig. 1).

The data were quantified by using of the three-dimensional rendering software Volume Graphics Studio. The software allows to extract the histogram of the attenuation coefficients in the sample (see Fig. 2) and to calculate the volume fraction of a defined material (see Fig. 3).

Nine wood samples treated with different impregnation solutions were investigated using the features shown above. The data were systemized in tables and graphs.

Acknowledgement

This research project has been supported by the European Commission under the 6th Framework Programme through the Key Action: Strengthening the European Research Area, Research Infrastructures. Contract n°: RII3-CT-2003-505925 (NMI3).

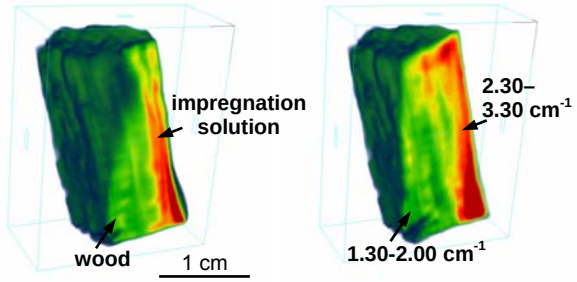

Fig. 1: Tomographic slices of impregnated wood. The attenuation coefficients for the solution (dark) and the wood (bright) are shown in the left hand side image.

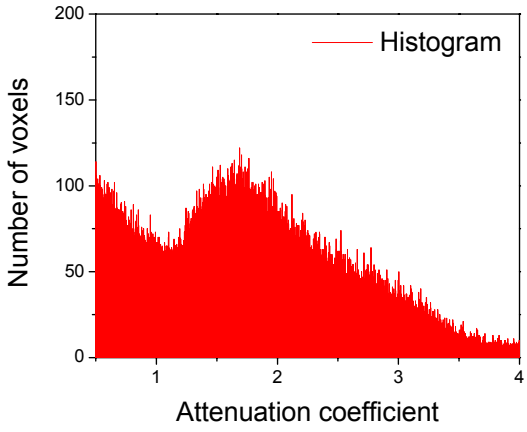

Fig. 2: Histogram of the attenuation coefficients represented in the sample. The main maximum at 1.70cm^{-1} corresponds to the wood matrix and the tail 2.30cm^{-1} - 3.30cm^{-1} is assigned to the impregnation solution.

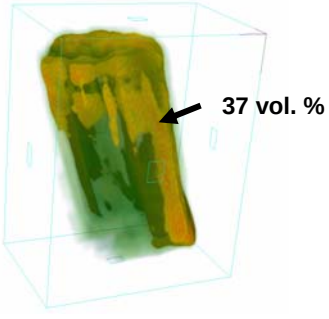

Fig. 3: The volume fraction of the impregnation solution in the wood sample was calculated to be 37vol.%.

	EXPERIMENTAL REPORT **Texture and morphology of marble artefacts from Villa Adriana (Tivoli, Rome)**	Proposal N° OTH-04-1168 Instrument **V7** Local Contact Nikolay Kardjilov
Principal Proposer: Experimental Team:	F. Lo Celso - Università di Palermo, I F. Lo Celso - Università di Palermo, I R. Triolo - Università di Palermo, I	Date(s) of Experiment 08.08. - 10.08.2005

Date of Report: 30. Aug. 2005

The present Neutron Tomography experiment have made possible to collect data to look for inhomogeneities and therefore texture identification in white and polychromic marbles from Villa Adriana. Villa Adriana (Tivoli, Roma, Italy), inscribed in the World Heritage List by Unesco, is an exceptional complex of classical buildings which was created in the 2nd century AD by the Roman Emperor Hadrian.
Undoubtely it represents one of the most complex and significant examples of the building genius of the Romans.
A quite large number of samples have been examined and we report here only a couple of representative results for two different kind of coloured marble with clear inhomogeneous patterns.

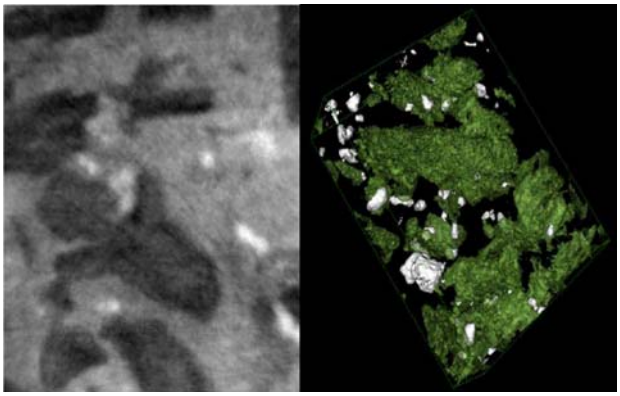

Fig. 1: 16-bit gray scale NT slice of a polychromic marble (left) and 3D rendered image of a solid region 12x20x8mm(right)

In fig. 1 it is shown a sample with two different components (white and dark gray region embedded in a light gray matrix) together with a 3D reconstruction where the original matrix has been filtered out. It is evident that the two components have different volume fractions and particle size distribution. A preliminary quantitative analisys has been performed on another ploychromic sample. In fig. 2 it is reported the histogram of gray population in the entire solid samples (Stack Histogram).
The black area represents the linear scale while the gray area is referred to a semilog scale (y axis). From this figure it is possible to distinguish two contribution where one component represents the major one. From a preliminary voxel counting procedure (based on a 8 bit gray scale), the volume fraction of the second component, which represents the minor one, is around 4.4 %.

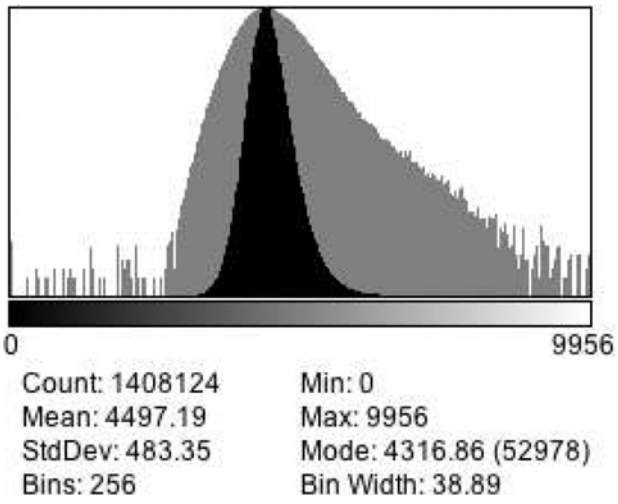

Fig. 2: 16-bit gray scale histogram of a polychromic marble (see fig. 3)

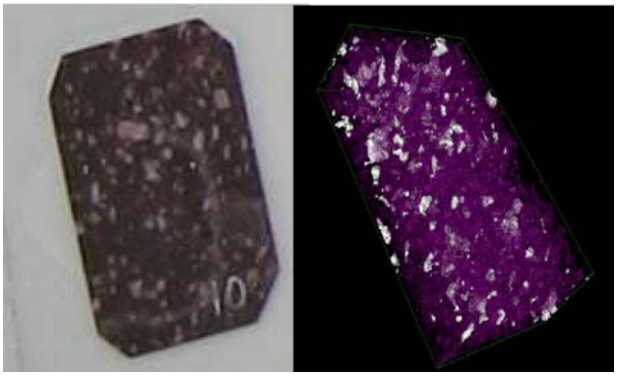

Fig. 3: Original slice of polychromic marble (left) and 3D rendered image of a solid region (right)

In fig. 3 the original sample is shown together with the 3D NT reconstruction (the major component is slightly transparent).
The investigation on these samples will be integrated by using other different techniques, including neutron diffraction, scattering and spectroscopy, X-rays etc., addressing the archeometric issue in a multidisciplinary context.

	EXPERIMENTAL REPORT **Texture and morphology of ancient wooden artcraft**	Proposal N° CHE-04-1164 Instrument **V12a** Local Contact Markus Strobl
Principal Proposer: Experimental Team:	R. Triolo - Univ. Palermo, I R. Triolo - Univ. Palermo, I I. Ruffo - Univ. Palermo, I M. Strobl - HMI Berlin	Date(s) of Experiment 12.08. - 22.08.2005

Date of Report: Jan. 2006

Introduction

The wooden handcrafts of historical and/or artistical interest are frequently deteriorated. The wood decays through the combined effects of biodegradation and of environmental factors (pH, moisture, finding site). The principal objective of a conservative intervention is to preserve and to consolidate the degraded components, having care to maintain the dimensions, the aesthetical characteristics and the practical qualities of the native handcraft. The knowledge and the diagnostics of an artefact are preliminary phases of work, and are essential when planning a protective intervention.

Experiment

In the past the waterlogged woods have been consolidated with aqueous solutions of PEGs. Some recent studies have shown that the wood anatomical structure (omoxile or eteroxile) plays a fundamental role, but the penetration of the impregnating agents is related to the ability to flow within the lumen both of the tracheids and of the cellular rays. Parameters such as stringiness, surface tension, contact angle with the substratum and diameter of the lumens, strongly influence the flow of the impregnating material. For this reason samples coming from wreckages of known origin and from lake-dwelling with different taxa and state of degrade, have been impregnated with selected mixtures (Paraloid B72) characterized by suitable physical-chemical parameters. Besides more traditional treatments, thanks to the efforts of prof. D.I. Donato, a new tecnique able to syntetize polymers inside the treated wood has been developed in ours laboratories at the University of Palermo; woods are treated in such a way to produce a polymeric compound, similar to Paraloid B72, but without the “flow problems” experienced earlier (“in situ” polymerization). Samples cut from the original piece were exposed to the neutron beam and measured at the double crystal camera at BENSC.

Results and discussion

We have investigate the structure of a limited number of samples before and after treatment, in order to learn about the distribution of the preserving polymer inside the pieces and the stability of the treatment. USANS data on undeteriorated samples have been also performed, in order to use them as reference materials. Data analysis is underway, especially as desmearing programs are being written. Also SANS and Neutron Tomography measurements have been performed and will be subject of separate reports. SANS and USANS data will be combined in order to assess the efficiency of the impregnation procedure. The main goal of the study is to show the distribution of the impregnating solution in the wood matrix at different space resolution and to compare results obtained with “macroscopic” techniques with those based on the use of neutrons as probe.

Acknowledgement

This research project has been supported by the European Commission under the 6th Framework Programme through the Key Action: Strengthening the European Research Area, Research Infrastructures.
Contract n°: RII3-CT-2003-505925 (NMI3).

	EXPERIMENTAL REPORT SANS investigation of brass reed tongues taken from historical and modern organs	Proposal N° MAT-04-1162 Instrument **V12a** Local Contact Markus Strobl
Principal Proposer: Experimental Team:	A. Manescu - UPM Ancona, I A. Manescu - UPM Ancona, I M. Strobl - HMI Berlin	Date(s) of Experiment 23.05-30.05.2005

Date of Report: 07.06.2005

The investigated samples were historic organ brass tongues. The tongues come from different organs across Europe and we wanted to investigate the microstructure (porosity, precipitates) for each of them and also the differences between them. Also the difference between historical and modern organ tongues was intended to be analysed.
The tongues have a vibrating part and a fixed part; we analysed both parts for each sample, using a slit of 10 mm x 3 mm – see Figure 1 below:

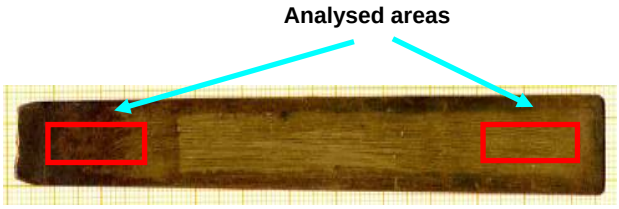

Figure 1: Geometry of a tongue and measuring areas

Experiments were performed on the V12a double-crystal diffractometer at the HMI-BENSC, Berlin. The incident neutron wavelenght was $\lambda = 4.76$ Å, the bending of the analyser crystal was 125 micrometers.

A corection file for the efficiency of the channels was collected and also an empty beam file, in which the direct beam was measured.
Correction and normalisation was performed next for all the files corresponding to the different samples and in the end the scattered intensity was obtained.

In the Figures 2 one can see the scattered intensity in function of Q(nm^{-1}) for one of the analysed samples – fixed and vibrating part (VEf, VEv), and also a comparison with a modern brass tongue (NEW).

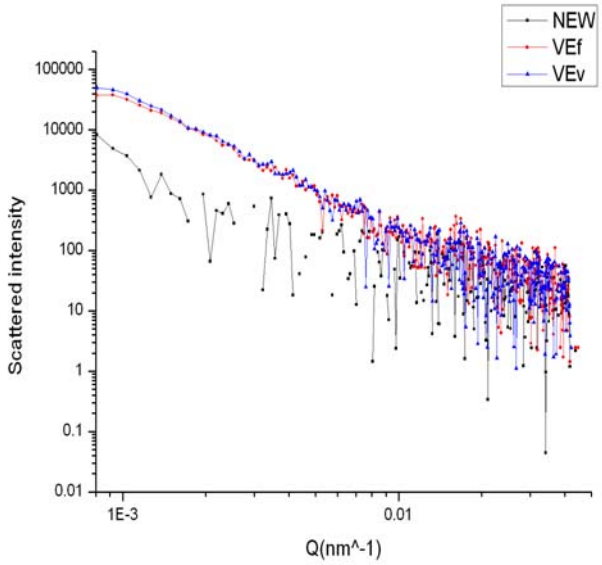

Figure 2: Scattered intensity for VE and NEW samples

The scattering in the analysed samples in mainly due to the presence of lead precipitates. The lead concentration varies from sample to sample; there is anyway a direct proportion between the scattering intensity and the quantity of lead present in the samples.
In the historical samples, the lead concentration is much higher than in modern organ tongues – a stronger scattering effect was observed in the historical tongues.

Then, we also calculated the radius of gyration of the lead particles; there are differences between various specimens probably due to the manufacturing process; anyway, in the historical tongues the radius of gyration is slightly higher than for the modern tongues.

	EXPERIMENTAL REPORT **Texture and morphology of marble artefacts from Villa Adriana (Tivoli, Rome)**	Proposal N° OTH-04-1163 Instrument **V12a** Local Contact Markus Strobl
Principal Proposer: Experimental Team:	F. Lo Celso - Università di Palermo, I F. Lo Celso - Università di Palermo, I R. Triolo - Università di Palermo, I M. Strobl - HMI Berlin	Date(s) of Experiment 08.08. - 12.08.2005

Date of Report: 30. Jan. 2006

Villa Adriana (Tivoli, Roma, Italy), is an exceptional complex of classical buildings which was created in the 2nd century AD by the Roman Emperor Hadrian. It encompasses the best elements of the material cultures of Egypt, Greece, and Rome in the form of an "ideal city." The analytical investigation on the monumental complexes of the Roman Empire Age complements the studies carried out on architectural and building engineering in order to achieve unitary views on this historical period. The present experiment (USANS) is thought to be part of a series of experiments that includes and Small Angle Neutron Scattering (USANS-SANS) and Neutron Tomography in order to obtain information on the structural parameters, inhomogeneities and therefore texture identification in white and polychromic marbles from the above cited site.

Marble is one of the most common stones used for monuments, statues and other objects of archaeological interest in the Villa.

In this context the provenance and, to a lesser extent considering the texture identification, the state of conservation of stone objects are of key importance.

A series of USANS experiments has been performed on 16 samples of white and polychromic marbles. In Figure 1 three smeared scattering curves are reported for different samples. All the experimental curved need to be desmeared, in other words the experimental curve should refer to a pin-point geometry to be inposed on the SANS scattering curve. The basic idea is to obtain a scattering profile on a length scale that goes from microns to angstroems. The total scattering profile usualy resembles a multi slope curve in a double logarithmic scale typical of fractal structures. In particular, for what concerns marbles, they are strictly considered as multi-phase systems but can be treated as two phase ones since most of the scattering originates from the contrast between the inorganic components (the largely prevailing carbonate grains) and the voids.

Very recently we have carried out the analysis of the combined USANS-SANS scattering data on a polychromic marble sample from the Villa using a hierarchical structure model which takes into account the existence of a network of fractal aggregates formed by monodispersed solid primary particles, giving evidences of a structure at two different length scales.

Further analysis are in progress.

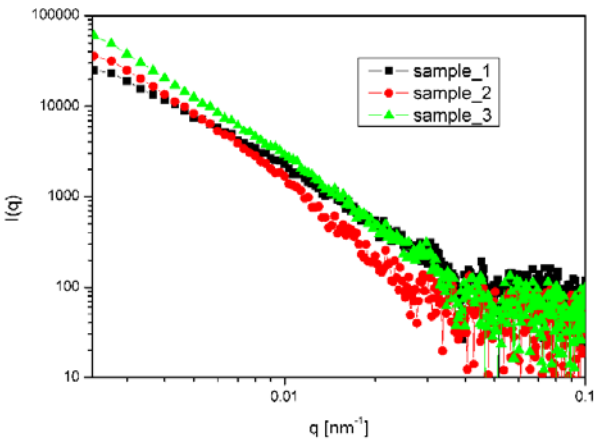

Fig. 1: USANS smeared scattering curves for three polychromic marbles.

	EXPERIMENTAL REPORT **Neutron deflection by a single crystal prism**	Proposal N° PHY-04-1165 Instrument **V12b** Local Contact Wolfgang Treimer
Principal Proposer: Experimental Team:	A.G. Wagh - BARC, IN S. Abbas - BARC, IN M. Strobl - HMI Berlin W. Treimer - HMI Berlin	Date(s) of Experiment 21.10. - 03.11.2005

Date of Report: 09. Jan. 2006

For neutron incidence near a Bragg reflection of a single crystal prism, the deflection of the transmitted neutron beam differs from its off-reflection value δ_{am}, the difference increasing monotonically in magnitude [1,2] as the Bragg reflection is approached from either side. The prism deflection attains extrema at either extreme of the total reflectivity range.

With channel-cut monochromator and analyser crystals, each performing 7 {111} Ewald reflections and a deflection by a Si wedge after 3 reflections, a 2 arcsec wide rocking curve [3] was attained for 5.24 Å neutrons. Between the monochromator and analyser, a single crystal silicon prism of apex angle A, was installed on a precision goniometer. Neutrons were incident at the prism face cut at an angle θ_S to the {111} planes. A part of the neutron beam passed directly to the analyser to serve as a reference for the prism deflection measurement. Using an additional detector to record neutrons Bragg reflected from the prism, the few arcsec wide Bragg reflection of the prism was located and optimised by varying the prism tilt angle. The analyser rocking curves were recorded for several angles of incidence at the prism covering a span of about 40 arcsec centred at the total reflectivity domain. The direct and deflected neutron peaks were simultaneously recorded in each analyser scan. beams The prism reflection was continuously monitored to confirm the stability of its Bragg reflection.

The observed neutron deflections and transmittivities for 3 different prisms are depicted in the adjoining figure. The data agree well with theory.

A single crystal prism thus provides a smooth control over the neutron deflection. The rocking curve of the V12b instrument can hence be made narrower without a significant intensity loss by exploring neutron incidence near the Bragg reflection of each Si wedge.

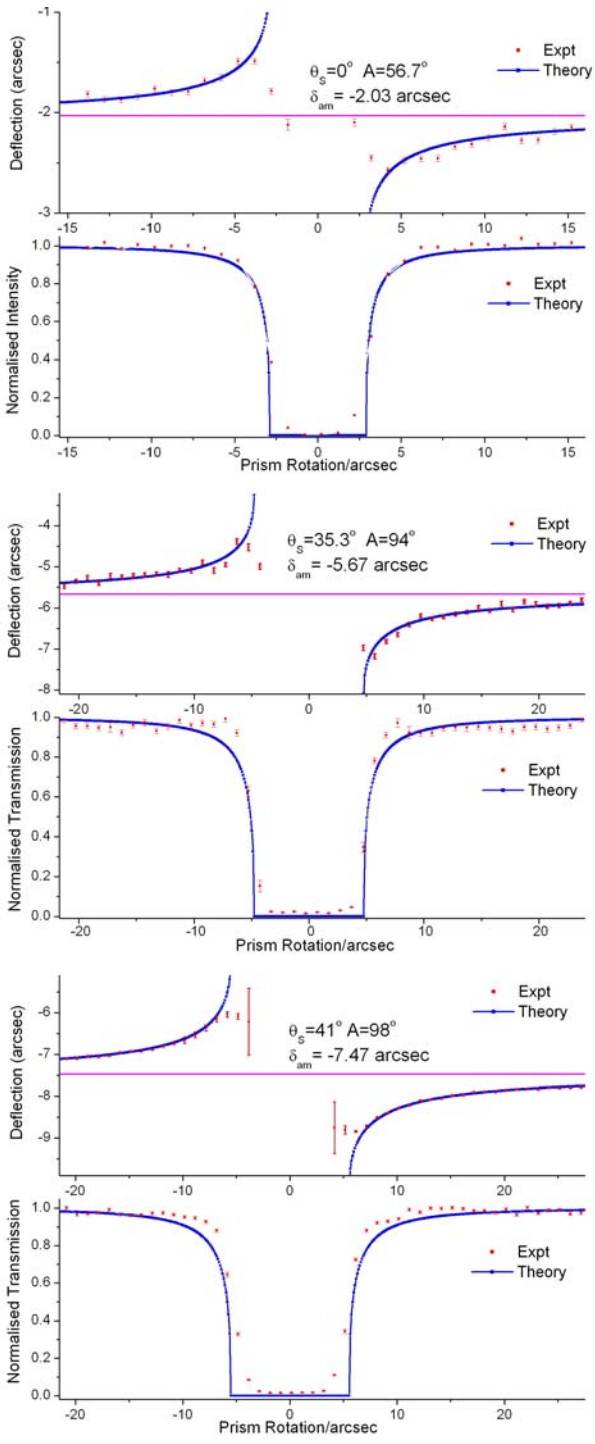

References

[1] A.G. Wagh: Phys. Lett. A **121**, 45 (1987); **123**, 499 (1987)

[2] S. Abbas, A.G. Wagh: Sol. St. Phys. (India) **50**, 317 (2005)

[3] W. Treimer, M. Strobl, A. Hilger: Appl. Phys. A **74** (Suppl.), S191 (2002)

	EXPERIMENTAL REPORT **Evaluation of the scission neutron fraction in U-235 fission**	Proposal N° PHY-05-0009 PHY-05-0015 Instrument **V13** Local Contact Margarita Russina, Thomas Wilpert
Principal Proposer: Experimental Team:	G.V. Danilyan - RF SSC ITEP Moscow, RU V.S. Pavlov, P. Shatalov, - RF SSC ITEP Moscow E.V. Brakhman, V.A. Krakhotin, A.S. Danilyan - RF SSC ITEP Moscow, RU T. Wilpert, M. Russina - HMI Berlin	Date(s) of Experiment Feb. - Dec. 2005

Date of Report: 14.12.2005

The main goal of the project was to search for the scission neutrons (ScN) using new method – P-odd asymmetry measurements of the prompt fission neutron (PFN) emission.

In 1998 large left-right asymmetry of α-particle emission was found in ternary fission experiment at ILL.

The origin of the asymmetry is not understood yet. The proposed experimental study was aimed to search for the T-odd triple correlation in neutral component of ternary fission. If the same asymmetry will be found in scission neutron emission it will mean that strong interaction is responsible for the effect. Otherwise, the electromagnetic interaction simulates such T-odd correlation.

To achieve the project's goals we developed and built the new 10 channels time-of-flight fast neutron spectrometer at ITEP (Moscow). The spectrometer has been successfully tested and installed on the polarized cold neutron beam (instrument V-13) of the BER-II reactor. Using the spectrometer we have been able to collect time-of-flight spectra for the particles detected at different angles (35^o, 55^o, 90^o, 125^o, 145^o, 215^o, 235^o, 270^o, 305^o and 325^o) relative to the fission axis measured. Unfortunately we could not improve the accuracy of the measured asymmetry during the second half of 2005. During the first half we've found that P-odd asymmetry measured at the angle 90^o relative to the fission axis is equal to $A(90^o) = (2.2 \pm 0.6)\cdot 10^{-5}$. Nevertheless we've used new installation to obtain an additional result. We investigated the angular distributions of the detected particles. The results are very encouraging. Fig. 1 shows TOF spectra for 3 angles: 35^o, 55^o and 90^o. Using the collected data we've been able to evaluate for the first time the angular distributions of prompt fission neutrons (PFN) for 3 energy intervals of PFN (Fig. 2). We found that behaviors of the angular distributions for prompt fission gamma-rays (PFG) and neutrons (PFN**)** *are opposite* **(**which confirms the theory) – the maximum of the gamma-rays emission is directed to right angle relative to fission axis; at the same time the faster the prompt fission neutron the larger is the elongation along the fission axis. It's necessary to emphasize, that fissile nuclei polarization, which arise due to the capture of cold polarized neutrons, was also orthogonal to the fission axis.

Comparing the above asymmetry coefficient with the same for light fragments emission ($8.8\cdot 10^{-5}$) we can make the conclusion that the relative part of scission neutrons in PFN is about (25 ± 8)%. This amount of scission neutrons is enough to undertake an experiment to search for the T-odd triple correlation in emission of PFN.

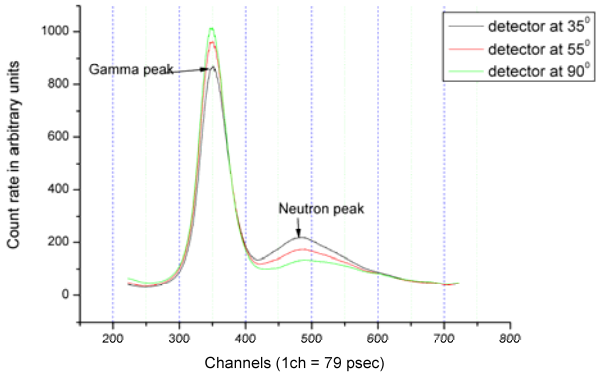

Fig. 1 Time-of-flight spectra for different detectors

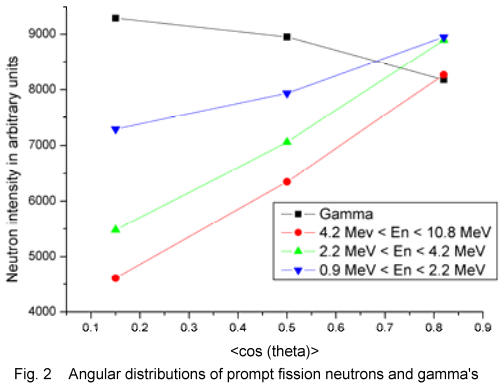

Fig. 2 Angular distributions of prompt fission neutrons and gamma's

	EXPERIMENTAL REPORT Larmor-phase corrections for NRSE	Proposal N° PHY-02-457-LT Instrument **V2** Local Contact Klaus Habicht
Principal Proposer: Experimental Team:	K.Habicht - HMI Berlin, TU-Darmstadt K.Habicht - HMI Berlin, TU-Darmstadt	Date(s) of Experiment 20.05. - 24.05.2005

Date of Report: 10.01.2006

Theoretical analysis and experimental evidence have identified sample properties, e.g. curvature of the dispersion surface, to be crucial to resolution in single-crystal spectroscopy using the NRSE technique on TAS instruments [1]. The standard setup with mechanically tilt able coils allows matching planes of constant Larmor phase with the slope of the dispersion. However curvature of the dispersion within the resolution ellipsoid of the TAS might over shade intrinsic line widths to some extent. The overall goal of this work is to experimentally eliminate this effect by a set of correction elements which provide additional Larmor precession such that surfaces of constant Larmor phase distinct from the planar geometry could be realized.

Two simple experimental configurations have been investigated:

(1) A symmetrical setup of two current sheets (with constant current density) and a single flat, rectangular coil operated as a π-flipper at their centre. These components were situated between the two bootstrap coils of the first NRSE arm. The current sheets were operated with a current vertically perpendicular to the neutron beam, thus providing a magnetic field oriented horizontally perpendicular to the neutron beam. The NRSE was operated in non-bootstrap mode at effective frequencies f_{eff} = 200 kHz and echo amplitudes have been measured in a direct beam geometry to probe depolarization effects ($k_I = k_F = 1.7$ Å^{-1}).

(2) A symmetrical setup of 4 current sheets with three flat rectangular coils operated as π-flippers between the sheets. All components were situated in between the two bootstrap coils of the first NRSE arm. With this setup different neutron trajectories of the incident neutron beam accumulate a different Larmor phase depending linearly on the divergence angle, i.e. the setup provides an effective tilt. To detect this effective tilt, the echo amplitude was measured as a function of the rotation angle of the bootstrap coils in the second spectrometer arm.

Using setup (1) it could be shown that either a single or a set of two current sheets acts on the spin fan after the first NRSE coil to depolarize the echo signal very quickly. However operating the π-flipper leaves the echo amplitude practically unchanged over the experimentally reachable range 0-10 A (see Fig. 1). Using setup (2) it could be shown that indeed an effective tilt could be provided (see Fig. 2). However at higher sheet currents ~6A significant depolarization of the maximum echo amplitude by a factor ~1.5 was observed. Most likely this is due to the horizontal field component at the position of the flat coil π-flippers.

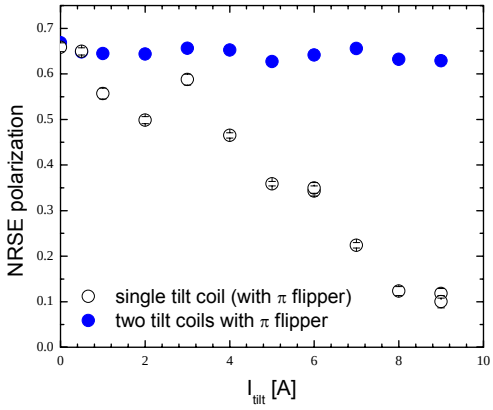

Fig.1: Echo polarization as a function of the current in the current sheets.

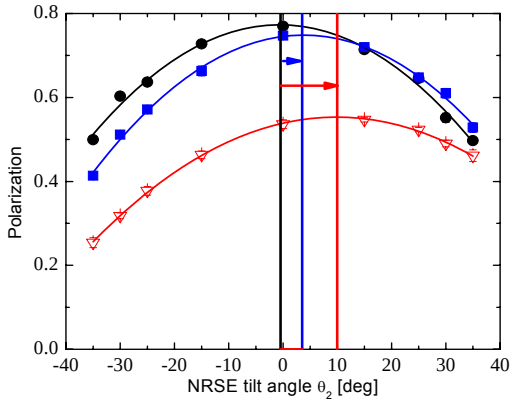

Fig.2: Echo polarization as a function of the tilt angle in the second spectrometer arm. Black circles: I_{sheets}=0A, Black circles: I_{sheets}=3A, Black circles: I_{sheets}=6A.

Acknowledgement

This research project has been supported by the European Commission under the 6th Framework Programme through the Key Action: Strengthening the European Research Area, Research Infrastructures. Contract n°: RII3-CT-2003-505925.

Reference

[1] K.Habicht *et al.*, J.Appl.Cryst. **36**, 1307 (2003)

	EXPERIMENTAL REPORT **Time-resolved SANS studies (TISANE) of field induced ordering in Ferrofluids**	Proposal N° PHY-03-0413-EF Instrument **V3** Local Contact Margarita Russina
Principal Proposer: Experimental Team:	A. Wiedenmann - HMI Berlin R. Gähler, N. Thillosen - ILL, Grenoble, F A. Wiedenmann, U. Keiderling - HMI Berlin K. Habicht, M. Russina - HMI Berlin	Date(s) of Experiment 21.09. - 25.09.2005

Date of Report: 09. Jan. 2006

Here we report on a first application of the new time-resolved technique, TISANE, proposed by Gähler [1] which allows to extend the time resolution to sub-ms range. This is achieved by using a chopper (at a distance L_1 from the sample) of frequency ν_e which is synchronized with the oscillation frequency ν_s of the sample state and the data acquisition of the detector at frequency of ν_d, when the condition

$$\nu_d = \nu_s - \nu_e \text{ for } \nu_e * L_1 = (\nu_s - \nu_e) * L_2 \quad \textbf{(1)}$$

is full-filled (L_2: distance between sample and detector).

Previous Polarised Small Angle Neutron Scattering studies (SANSPOL) have shown that in concentrated Co-Ferrofluids inter-particle interactions are induced by an external magnetic field that gives rise to pseudo-crystalline ordering of the nanosized magnetic particles [2]. When the magnetic field was switched off we found an exponential decay of the magnetic correlations between the nanoparticles with a characteristic time of the order of 1 - 5 s [3].

The onset of the local ordering, however, was too fast to be observed by this direct mode. Instead we built a special solenoid which provided a periodic sine-wave modulation of the external magnetic field up to amplitudes of 26 mT and frequencies up to 3 kHz. The TISANE principle has been set-up on the NEAT instrument of HMI by using a single fast chopper with variable frequencies up to ν_e = 666 Hz at L_1 = 13 m. The data acquisition in the 2-D SANS-detector placed at L_2 = 4 m was triggered by a high precision frequency generator where ν_d was adjusted to the frequency of the oscillating magnetic field ν_s and to ν_e according to eqn. (1). A maximum frequency of the ac-field of ν_s = 2800 Hz could be applied. A considerable intensity gain and gain in resolution were achieved by the TISANE technique where a large frame overlap and high repetition rates could be achieved.

Using this setup we were able to study the ordering and re-ordering kinetics forced by the alternating magnetic field. As long as the magnetic moments followed the applied field the scattering patterns changed as a function of time from fully isotropic at time t_0 (fig. 1 top) when the field was zero to strongly anisotropic (fig. 1 bottom) at $t_{H\text{-max}}$ and $t_{H\text{-min}}$ where the amplitude of H was maximum and minimum, respectively. Oscillating scattering patterns were observed up to about 1300 Hz (fig. 2) which was still far below the resolution limit of the TISANE technique. The observed threshold frequency must therefore result from the characteristic time needed for re-orientation of the magnetic particle moments.

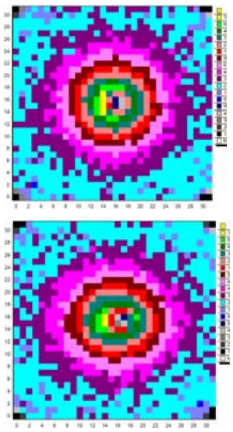

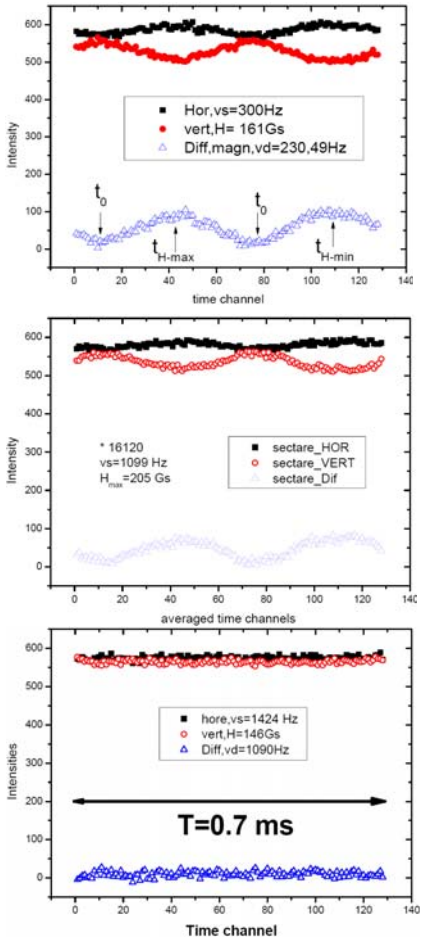

Fig. 1: Time-resolved SANS patterns of Co-FF in TISANE: isotropic at t_0 (H = 0) (top) and anisotropic at $t_{H\text{-max}}$ (Vertical field H = 25 mT) (bottom).

Fig. 2: Time variation of vertical and horizontal sector intensities and the difference for ν_s = 300 Hz, 1099 Hz and 1424 Hz

The dynamical range obtained by the TISANE experiment corresponds to that of X-ray photon-correlation spectroscopy which could never be exploited with neutrons up to now.

Acknowledgement
The project was supported by DFG Project Wi 1151/2

References

[1] R. Gähler, R. Golub: ILL SC (1999) **99-1**, page 73

[2] A. Wiedenmann, A. Hoell, M. Kammel, P. Boesecke: Phys. Rev. E **68** (2003) 031203, 1-10.

[3] A. Wiedenmann, U. Keiderling R. May, C. Dewhurst: Physica B(2006)

	EXPERIMENTAL REPORT **Test of the polarised ^{3}He refilling device in combination with a sample magnet**	Proposal N° MAT-04-1126-EF Instrument **V4** Local Contact Uwe Keiderling
Principal Proposer: Experimental Team:	A. Wiedenmann - Hahn-Meitner-Institut, Berlin A. Rupp, U. Keiderling - HMI Berlin W. Heil, J. Klenke - Universität, Mainz	Date(s) of Experiment 05.04 - 08.04.2005

Date of Report: 12.05.2005

^{3}He based spin filter cells to polarise neutrons with their acceptance for neutron divergence and spread of wavelength fit perfectly in a small angle neutron scattering (SANS) instrument as an analyser. The disadvantage of permanent decay of the ^{3}He polarisation in the analyser cell can be overcome by refilling this cell during an experiment from an outside reservoir with new polarised ^{3}He gas in periods of typically 5-10 hours. For this purpose an "easy to use" device has been constructed which consists of two units, an outside Helmholtz coil system (0.8 mT) which provides the magnetic guiding field for the reservoir cell with approx. 3 bar*l of polarised ^{3}He and an analyser cell in between the pole shoes of the electro-magnet of V4. The refilling is done via pneumatic valves, operated by a pressure controlled switch circuit which is secured against maloperation. The analyser cell placed inside the sample magnet of V4 is immersed to a magnetic field of $B_{MAX} \sim 1$ T (most of the measurements had been done at a field of 0.6 T). To avoid the decay of the ^{3}He polarisation due to small relative magnetic field gradients, the sample magnet was equipped with new pole-shoes to get an almost homogeneous field within the volume of the analyser cell ($(\partial B_r / \partial r)/B_0 \approx 10^{-4}$ / cm). The stray fields of the sample magnet and the stray fields of the Helmholtz coils overlap properly to transfer the gas from the reservoir to the analyser cell via small plastic tubes without loss of polarisation. Two types of analyser cells were tested. The first type is a cylindrical cell ($\varnothing$ = 5 cm, l = 5 cm) completely made out from GE180 glass (aluminosilicate glass). For the second type of cell which has similar size Duran glass is used for the body with entrance and exit windows made of discs of silicon single crystal. Finally this cell is coated with a Cs-layer to increase the wall relaxation time while the first one is a bare glass cell.

The inlet for both types of cells can be opened and closed by a glass valve and terminates in a clamp flange. The glass valve should be open during the measurement while the gas exchange is controlled by a pneumatic valve which is situated on the yoke of the magnet directly beneath the pole shoes and to which the cell is mounted. Prior to the test-experiment, the characteristic T_1 relaxation time of the ^{3}He polarisation had been measured under ideal conditions at the Universität Mainz being approx. 40 h in both cases. Contrary to that during the experiment all cells had showed a surprisingly fast relaxation time of only 15 min during the test-experiment. The relaxation time could be increased by closing the glass valve after filling the analyser cell. This measure cut that part of the cell's volume which reached into an area of bigger field gradients, i.e. the area close to the edges of the pole shoes. Nevertheless, the observed relaxation time of 2 h still was a factor of 20 less than the expected relaxation time under ideal field conditions. Perhaps the magnetic field gradients within the pole shoes are not optimal yet. A complete mapping of the magnetic field was done to get exact values for the relative field gradients. Having localized field gradient relaxivity as main source of the observed relaxation, one has to upgrade the field homogeneity of the electro-magnet by an appropriate shimming.

The pressure controlled switch circuit and the pneumatic valves worked as expected. Also the homogeneity of the Helmholtz coils is within the expected range.

	EXPERIMENTAL REPORT **Stroboscopic time-resolved SANS technique for dynamical studies of Co-ferrofluid relaxation with SANSPOL**	Proposal N° MAT-04-1182-EF Instrument **V4** Local Contact Uwe Keiderling
Principal Proposer: Experimental Team:	A. Wiedenmann - HMI Berlin U. Keiderling - HMI Berlin A. Wiedenmann - HMI Berlin	Date(s) of Experiment 18.05. - 24.05.2005

Date of Report: 09. Jan. 2006

The new electronics installed on the 2D detector of the SANS instrument V4 produces listmode data, containing full spatial and time information for each neutron. Based on the listmode data acquisition we developed a time-resolved stroboscopic SANS technique allowing the investigation of reversible dynamical processes. Their characteristic time constant of several 100 ms is by far too slow to be measured by quasi-elastic or spin-echo neutron scattering techniques ($<10^{-8}$ s) but too fast for conventional SANS. We successfully applied this technique to study the sluggish kinetics of relaxation in a concentrated Co-ferrofluid induced by an external magnetic field [1], in conjunction with polarized SANS (SANSPOL).

The sample was placed in a homogeneous magnetic field permanently cycling between "field on" (1 T, applied for 5 s), and "field off" (remanence, applied for 15 s), as shown in fig. 1. Both phases were linked by an up-ramp and a down-ramp of 3 s each, caused by the maximum slope provided by the magnet power supply. Scattering intensities were measured subsequently with incident neutron beam polarization parallel (I-) and antiparallel (I+) to the magnetic field. For each polarization, listmode data were recorded during cycling, with a trigger signal related to the periods merged in the data.

We implemented handling of the listmode data to our "BerSANS-PC" data reduction software [2], which enables fully flexible control over the spatial and time resolution of the results after the experiments. Using the trigger information, the data were regrouped to superimpose all cycles, yielding a time-resolved recording of the formation and decay process of the inter-particle order with a time resolution of 100 ms and very good statistics.

The points in fig. 1 display the total detector intensity for the difference (I-)-(I+), representing the nuclear-magnetic interference term of the magnetic particles [3]. Each point has been calculated from one time frame with a width of 100 ms, after accumulation of approx. 700 cycles.

The ordering after switching on the field occurred so fast that the limiting factor for the observed ordering kinetics appeared to be the slope of the field up-ramp, rather than the native sample dynamics. We therefore only investigated the relaxation after switching off the field, which turned out to be about 2 orders of magnitude slower than the ordering.

It is known that this ferrofluid reveals coexistence of a pseudo-crystalline hexagonal ordering of core-shell nanoparticles, and segments of dipolar chains aligned along the magnetic field [3]. We separated the scattering contributions from these two components by analysing decay curves similar to fig. 1, but limited to certain detector zones containing only the interference peaks from one particular component, as shown in fig. 2. Detailed results are given in [4].

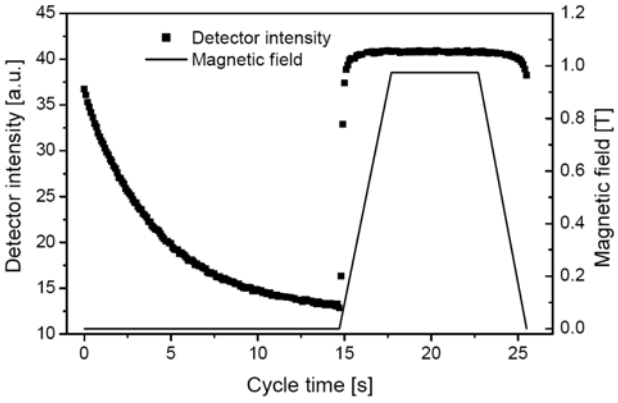

Fig.1: Magnetic field and total detector intensity during the cycles

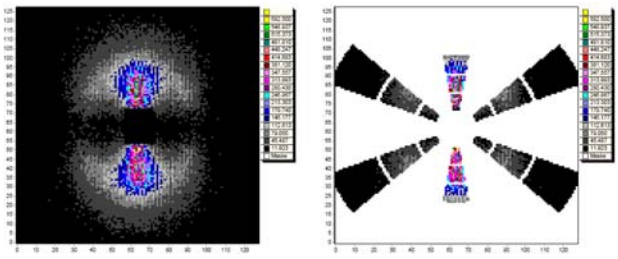

Fig.2: Scattering pattern (I-)-(I+) at 1T (left) and area zones used to analyze individual peaks (right)

References

[1] A. Wiedenmann, A.Heinemann: JMMM **289** (2005) 58-61
[2] U. Keiderling: BENSC Experimental Reports **2003** & BENSC Experimental Reports **2004**
[3] A.Wiedenmann, U.Keiderling, R.P.May, C.Dewhurst: accepted for Physica B (2006)
[4] U.Keiderling, A.Wiedenmann, J.Haug: accepted for Physica B (2006)

	EXPERIMENTAL REPORT The new neutron tomography instrument CONRAD	Proposal N° EF Instrument **V7** Local Contact Nikolay Kardjilov
Principal Proposer: Experimental Team:	N. Kardjilov - HMI Berlin N. Kardjilov - HMI Berlin A. Hilger - HMI Berlin	Date(s) of Experiment 2005

Date of Report: Jan. 2006

Introduction

The new cold neutron radiography instrument CONRAD is a multifunctional facility for radiography and tomography with cold neutrons at Hahn-Meitner-Institut Berlin. It is located at the end of a curved neutron guide, which faces the cold neutron source of the BER-II research reactor. The geometry provides a cold neutron beam with wavelengths between 2 Å and 12 Å. Two measuring positions are available for radiography and tomography investigations (see fig. 1). The first one is placed at the end of the guide and it is optimized for in-situ experiments in which a high neutron flux is required. The available flux at this position is app. 10^9 $cm^{-2}s^{-1}$. The second measuring position uses a pin-hole geometry which allows better beam collimation (L/D up to 1000) and higher image resolution in the range of 200 µm in the CCD based detector system (10 x 10 cm^2). The use of cold neutrons for radiography purposes increases the image contrast and improves the sensibility for e.g. the detection of small amounts of water and hydrogen containing materials in metal matrixes. On the other hand the cold neutron beam can be modified easily by using diffraction and neutron optical techniques.

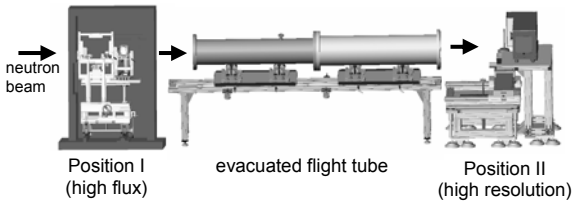

Fig. 1: Drawings of the CONRAD instrument set-up

Results

a) high-flux position

The flux density at the first measuring position is approximately 1 x 10^9 n/cm^2s which is sufficient to perform unique real-time experiments [1] or high-speed tomography. The beam size on the other hand is limited to the cross section of the guide which is 3 x 12 cm^2.

The resolution can be given with 500 µm at a distance of 5 cm between object and detector screen.

b) high-resolution position

To optimize the beam for the second position an additional collimation system, consisting of a flight tube of 5 m length and a set of diaphragms, is installed (see fig. 1). This way the spatial resolution improves to up to 100 µm. A pinhole exchanger, placed at Position I, with 3 circular apertures (1 cm, 2 cm and 3 cm of diameter) allows choosing the optimal collimation ratio and flux for corresponding measurements. The maximum spatial resolution was measured by using the line spread function at the edge of a Gd-foil placed at a distance of 5 cm from the detector. The obtained value was 238 µm. The used detector system is based on a 16-bit cooled CCD camera (Andor DW436N-BV) with 2048 by 2048 pixels. The beam size at the second position is approximately 10 x 10 cm^2.

A comparison between radiography images obtained at the two described measuring positions is given in Fig. 2.

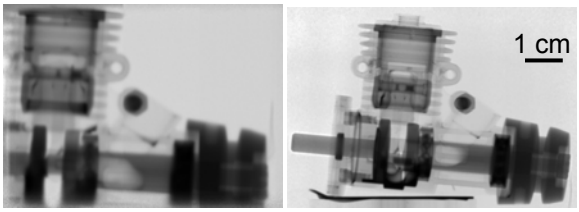

Fig. 2: Model air-craft engine measured at Position I (L/D of 70; exposure time: 0.5 s) and at Position II (L/D of 500; exposure time: 25 s).

An example of high-resolution neutron tomography at position II is the fossil sample (ammonite) presented in fig. 3. For this experiments 300 projections were taken from the sample on an angular range of 180 degree. The exposure time for a projection was 25 s resulting in a total measuring time for the whole tomography experiment of 2.5 hours.

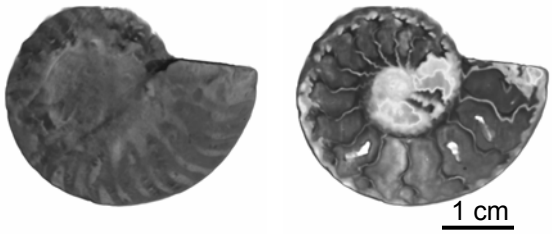

Fig. 3: High resolution neutron tomography of a fossil sample (ammonite). General view (left) and tomography slice (right). The grey scale represents attenuation values from low (black) to high (white).

Reference

[1] N. Kardjilov, BENSC EXP. REP. **2004**, p. 184, MAT-04-1079-EF

	EXPERIMENTAL REPORT A double-monochromator device for CONRAD	Proposal N° EF Instrument **V7** Local Contact Nikolay Kardjilov
Principal Proposer: Experimental Team:	M. Strobl - TFH Berlin & HMI Berlin M. Strobl, A. Hilger, M. Rimke , W. Treimer - TFH Berlin & HMI Berlin N. Kardjilov - HMI Berlin	Date(s) of Experiment Sep. - Oct. 2005

Date of Report: Jan. 2006

CONRAD the new cold neutron radiography and tomography instrument at the Hahn Meitner Institute in Berlin recently started operation as a part of the Berlin Neutron Scattering Centre (BENSC) [1]. CONRAD exploits the advantages of an intense cold neutron beam for imaging. However an additional feature was developed and implemented in order to use a monochromatic beam at any wavelength selectable from the provided spectrum. Using different wavelengths enables monochromatic imaging avoiding beam hardening [2], energy selective imaging [3] and by scanning the spectrum even stress and strain measurements (which is described in another report of this issue). CONRAD includes two measurement positions [1] of which the first one which is located directly at the end of the NL1b neutron guide was used to install a flexible double monochromator device as an additionally available insert (fig. 1).

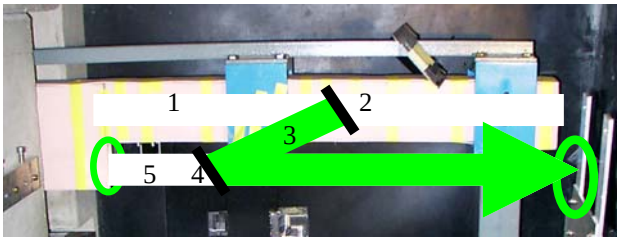

Fig. 1: Schematic image of the double monochromator insert;

(1) upper beam (to V14),
(2) first PCG monochromator,
(3) monochromatic beam (green),
(4) second monochromator,
(5) original CONRAD beam path (blocked)

While the CONRAD instrument uses in standard operation the full cold spectrum of the lower part of the guide a first PCG[002] monochromator (2) with a mosaic spread of app. 1° is placed in the upper beam part (1) deflecting neutrons downwards (3). The initial lower beam part (5) is blocked by a shutter and on a linear manipulation table behind it the second corresponding graphite crystal (4) is installed. Hence, while both crystals can be rotated to chosen Bragg angles, the second one can be positioned along the original beam direction in order to reflect the monochromatic beam coming from the first crystal into the initial beam path of the CONRAD instrument. This construction enables to choose a monochromatic beam with wavelengths between 0.25 nm and 0.65 nm (including Bragg edges of important materials like brass, Cu, Fe etc.) for high resolution imaging at the second measurement position of CONRAD app. 5 m downstream. A number of test measurements have been recorded. First the intensity was measured at different monochromator positions scanning the spectrum (fig. 2a) the second peak in the spectrum can be explained by higher order reflections. Tomographies and radiographies involving different materials have been recorded and measured attenuation spectra have been compared to tabulated values (fig. 2b). As mentioned above applications are ranging from energy selective radiography to stress mapping.

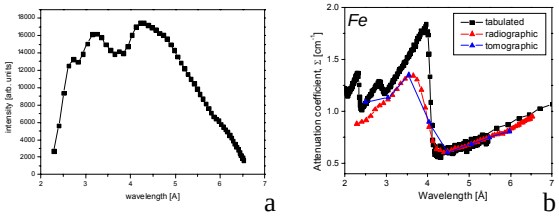

Fig. 2: (a) scanned spectrum, (b) attenuation spectrum of steel measured radiographical and tomographical compared to tabulated Fe values

References

[1] N. Kardjilov et al.: NIMA **542** (2005), 16-21

[2] M. Strobl: BENSC EXP. REP. **2004**, p.172, PHY-04-1074-LT

[3] N. Kardjilov et al.: NIMA **501** (2003), pp 536

	EXPERIMENTAL REPORT **Bragg-edge radiography using the monochromatic option at CONRAD**	Proposal N° EF Instrument **V7** Local Contact Nikolay Kardjilov
Principal Proposer: Experimental Team:	N. Kardjilov - HMI Berlin N. Kardjilov - HMI Berlin A. Hilger - HMI Berlin M. Strobl - HMI Berlin	Date(s) of Experiment November 2005

Date of Report: Jan. 2006

Introduction

The neutron attenuation coefficient for polycrystalline materials decreases suddenly for well-defined neutron wavelengths – the so-known Bragg edges. The position of these edges is defined by the symmetry and the parameters of the crystal lattice. At wavelengths greater than this critical value, no scattering by particular {h k l} lattice spacing can occur because the corresponding Bragg reflection angle reaches its maximum of 2θ=180°. Therefore a sharp increase in the transmitted intensity occurs.

Using energy-selective neutron imaging the position, magnitude and the shape of defined Bragg edge can be determined with two dimensional resolution of the sample for a corresponding material. These parameters content information about the stress state, texture and phases presented in the material.

Results

The experiments were performed at the neutron tomography station CONRAD (V7) using the new set up monochromatic option described elsewhere in this issue. The neutron spectrum was scanned in the interval from 2.5 Å up to 6.5 Å with steps of 0.1 Å. For each wavelength two radiographic images were recorded – with and without the sample in the beam. Dividing the two images at a corresponding wavelength, the neutron transmission for each point of the sample was determined. The transmission curves as a function of the wavelength for three positions of a bended steel plate with a thickness of 10 mm is shown in fig. 1. The bended areas are indicated as areas 2 (slight bending) and 3 (strong bending) and the first straight part as 1 (see fig. 2).

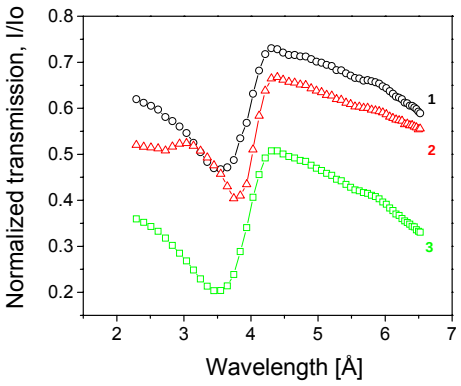

Fig. 1: Transmission curves from different areas of bended steel plate.

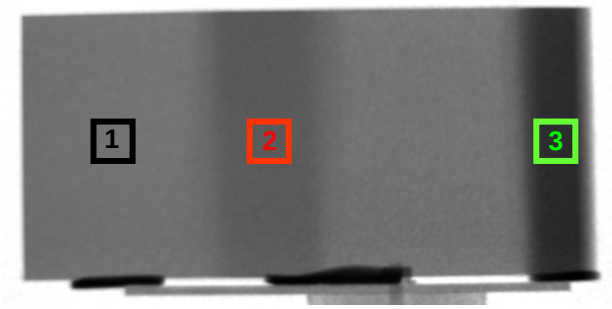

Fig. 2: Radiographic image of a bended steel plate

For each pixel of the sample the transmission curve was composed and the first derivation was taken. Gaussian functions were used to fit the obtained derivation curves. The parameters of the Gaussian fits were calculated for each pixel separately. For example the position of the maximum and the amplitude of the curve are shown in fig. 3. These parameters can be related to the position and the steepness of the Bragg edge correspondingly.

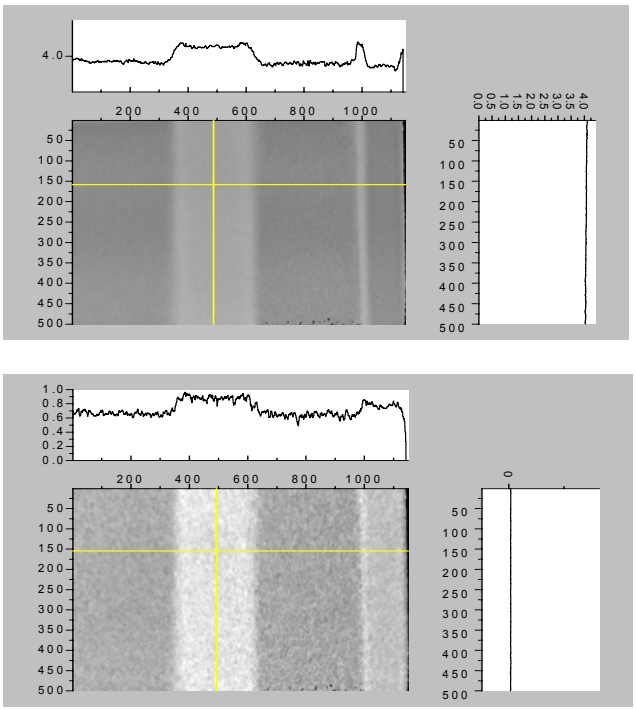

Fig. 3: The position (top) and the steepness (bottom) of the Bragg edge for the steel material.

This information can be used for mapping of residual stresses and textures in steel samples.

BENSC	**EXPERIMENTAL REPORT** **Neutron scattering effects in cold neutron radiography**	Proposal N° OTH-04-1171-LT Instrument **V7** Local Contact Nikolay Kardjilov
Principal Proposer: Experimental Team:	F. de Beer - Necsa, Pretoria, South Africa N. Kardjilov - HMI Berlin A. Hilger - HMI Berlin	Date(s) of Experiment 13.07. - 18.07.2005

Date of Report: 05. Jan. 2006

Aim: Scattered neutrons cause distortions, blurring and is the cause of wrong answers in quantitative analysis in neutron radiography images taken at small distances between the investigated object and detector. This phenomenon is well known in thermal neutron radiography when the object is made of strong neutron scattering material. The aim of this study is to experimentally determine the contribution of the scattering effect of neutrons in cold neutron radiography investigations from highly attenuating materials such as a STST and Cu and to compare it to a low scattering material such as Al. The results are compared and correlated with the correction for the high scattering metal samples done by Necsa with thermal neutrons.

Experimental set-up: Cube Al and Stainless Steel (STST) samples of various thicknesses (1-10mm) were positioned at different distances (5 – 50mm) from the CCD detector in the CONRAD facility. 2D radiographs of the samples were taken.

Results:

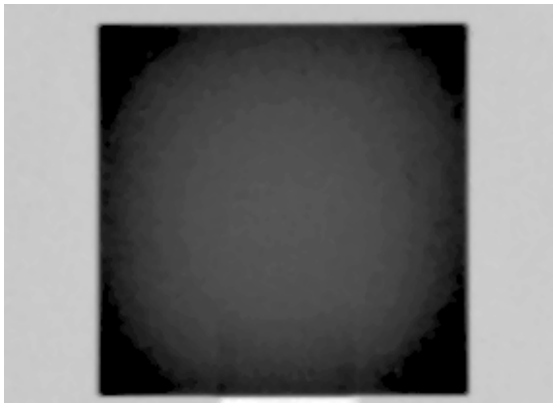

Fig-1: Multiple neutron scattering effect in a STST slab of 10mm thickness and 5mm from the CCD detector. (Image enhanced)

A line profile in a horizontal plane in the center the sample reveals the following**:**

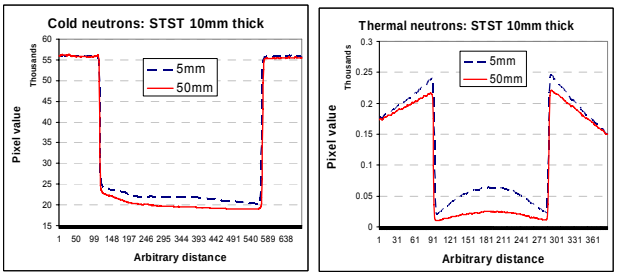

Fig-2: Intensity line profiles for Cold and Thermal neutron radiography

Less neutron scattering effect is observed in the cold neutron results compared to the thermal neutron imaging result.

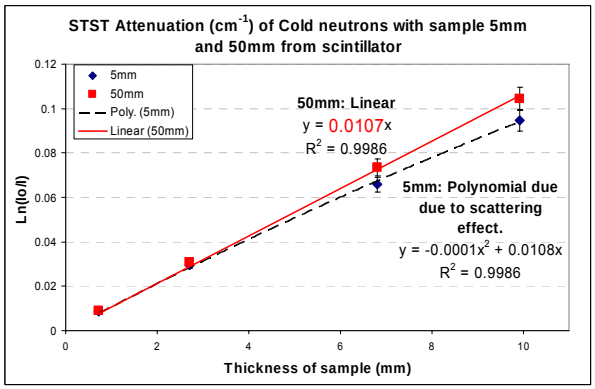

Fig-3: The effect of multiple scattering on the Cold neutron attenuation of a STST sample 5mm and 50mm from the detector.

Conclusion: These experiments show that for cold neutrons, scattering has an effect on the accuracy of the quantitative neutron radiography investigations of highly scattering materials but not as much as in thermal neutron radiography.

Future work:
A correction procedure for cold neutrons based on analytically described point scattered functions will be developed and tested.

	EXPERIMENTAL REPORT New V12a set-up	Proposal N° BIO-04-1134-LT Instrument **V12a** Local Contact M. Strobl, W. Treimer
Principal Proposer: Experimental Team:	M. Strobl - HMI Berlin & TFH Berlin M. Strobl - HMI Berlin & TFH Berlin W. Treimer - HMI Berlin & TFH Berlin	Date(s) of Experiment 2005

Date of Report: 05.01.2006

The complete V12 instrument (V12a and b) had to be deconstructed for the construction works connected with the new guide hall. This provided the possibility to redesign and improve the whole set-up. The new V12 instrument is a multiple set-up combining several techniques to investigate the internal structure of bulk samples. Again it consists of two double crystal diffractometers (DCDs) (V12a and b) and additionally an attenuation tomography device operating with monochromatic neutrons (i.e. V12b II, replacing the shut down E8 instrument). As before the instrument is mainly divided in two parts V12a and V12b using different monochromators (Fig.1). The position of the V12a monochromator has moved app. 1.5 m upstream the neutron beam of the NL3b. Contrary to the former set-up no pre-monochromator is used and the perfect Si monochromator of the DCD has been installed in the neutron guide.

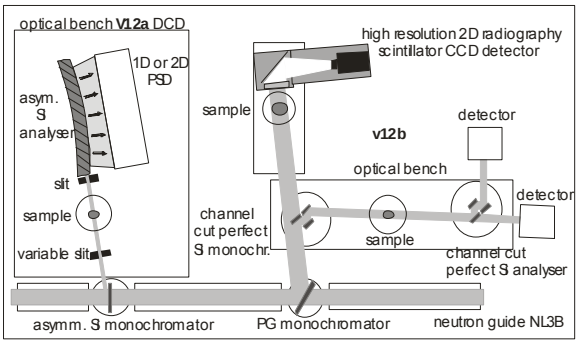

Fig. 1: V12 set-up; schematic drawing

The new V12a monochromator is an asymmetric (α = 41°) cut perfect Si single crystal (111) that selects λ = 0.476(2) nm neutrons by Bragg diffraction and compresses the beam cross section form 3 x 5 cm^2 of the guide to 0.5 x 5 cm^2 on the sample and analyzer side. With this monochromator the ratio between intensity gain and resolution loss is 4/2 and superior compared to the one of the bendable symmetric monochromator used in the old V12a set-up with 1/1 , 2/3 and 3.5/5.5 (Fig.2). The flux density at the sample position can be given with app. 3 x 10^3 $cm^{-2}s^{-1}$. The analyzer crystal did not change and is a completely asymmetric cut bent perfect Si single crystal (111) with an entrance window of 0.3 x 2 cm^2 at its small front side. Depending on their wave vector neutrons get diffracted at different positions of the analyzer and leave it through the long side towards the position sensitive detector (PSD). Using different analyzer bending the q-range which is registered in 512 channels on 20 cm in the position sensitive detector can be tuned up to q_{max} = 10^{-1} nm^{-1} in order to overlap and extend the range of SANS machines by about 2 orders of magnitude. The full width at half maximum of the resolution function is 7.7 x 10^{-4} nm^{-1} with a peak to background ratio of nearly 10^4. The 1-dim. PSD (ORDELA 1250N, ^{3}He) is going to be exchanged by a 2-dim. PSD (DENEX-200TN, ^{3}He) in order to enable spatial resolution of the scattering patterns in vertical direction and hence 3D tomographic reconstruction from tomographic scans [1].

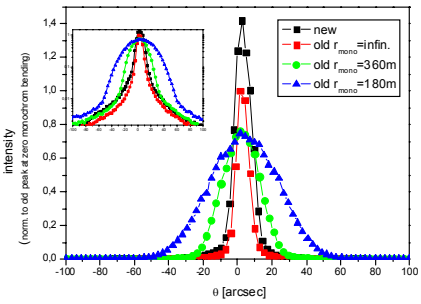

Fig. 2: Comparing the new V12a resolution function to the ones of the old V12a set-up with different monochromator curvatures

Acknowledgement
Supported by BMBF Proj**.** 03TR6TFH

Reference

[1] M. Strobl, W. Treimer, A. Hilger: NIM B **222**, 3-4 (2004) 653

	EXPERIMENTAL REPORT **Towards quantitative refraction contrast tomography**	Proposal N° BIO-04-1134-LT Instrument **V12a** Local Contact Markus Strobl
Principal Proposer: Experimental Team:	M. Strobl - HMI Berlin & TFH Berlin M. Strobl - HMI Berlin & TFH Berlin W. Treimer - HMI Berlin & TFH Berlin K. Staack - TFH Berlin	Date(s) of Experiment Oct. - Nov. 2005

Date of Report: Jan. 2006

After the development of refraction contrast tomography and the successful application of this technique using double crystal diffractometers (DCD) for 3 dimensional tomographic imaging the challenge arises to derive quantitative information rather than the qualitative one represented by reconstructed images of inner structures. In the DCD the deviation of the beam caused by refraction at and in the sample can be measured very accurate (i.e. µrad). From a set of such refraction angles in a radiographic scan phase retrieval is possible and from a number of projection scans a tomographic image representing the refractive index distribution in the sample can be reconstructed [1-5]. Of course such reconstructions have been made, but up to now never with respect to achieve quantitative refraction index values rather than qualitative contrast between areas of different refraction index. Earlier radiographical tests [6] have shown that the accuracy of measuements the refraction angles compared to calculations can be sufficient but time consuming (Fig.1). In a first attempt for tomography a sample was used, which was used for quantitative attenuation contrast tomography before, like described in another report in this issue. It is a cylindrical Al matrix containing pieces of different well known materials (e.g. brass, steel, Al). Measurements have been performed already and first reconstructions of the refraction contrast signal are available (Fig.2). However, no quantitative information has been achieved yet, as a lot of corrections and data treatment is necessary and programs for the huge amount of data is in progress. Detector effeciencies and instrumental instabilities have to be taken into account as well as the influence of spatial resolution onto the calculations and reconstruction. The results will be compared with theoretical calculations of the correspondimg refraction indices (based on tabulated measured bound scattering lengths b_c) and straight forward measurements of the refraction indices in the DCD.

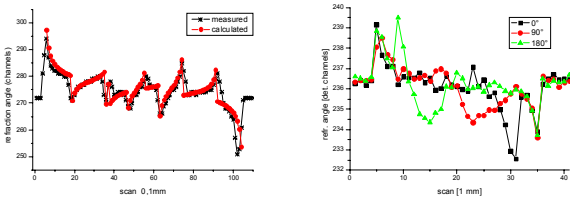

Fig. 1: Comparison of an old refraction projection pattern [6] with theoretic calculations (left side) and recent patterns at different projection angles taken with worse statistics corresponding to exposure times of tomographic scan measurements

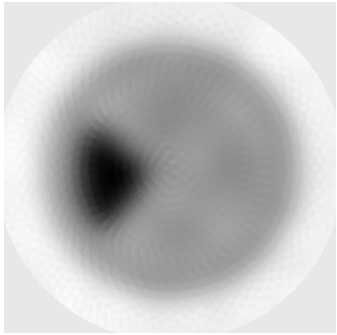

Fig. 2: Recent qualitative reconstruction of the Al matrix (diameter 3 cm) containing only Al and one piece of brass (dark)

Acknowledgement
Supported by BMBF Proj**.** 03TR6TFH

References

[1] M. Strobl et al.: Appl. Phys. Let. **85**, 3 (2004) 488
[2] M. Strobl: Dissertation, TU-Wien (2003)
[3] M. Strobl et al.: Phys. B **350**, 1-3 (2004) 155
[4] M. Strobl et al.: NIM A **542** (2005) 383
[5] W. Treimer et al.: App. Phys. Let. **83**, 2 (2003) 398
[6] W. Treimer et al.: BENSC EXP. REP. **2000**, p.254

	EXPERIMENTAL REPORT **The V12b monochromatic neutron tomography set-up and applications**	Proposal N° PHY-04-1135-LT Instrument **V12b** Local Contact Wolfgang Treimer
Principal Proposer: Experimental Team:	M. Strobl - HMI Berlin & TFH Berlin I. Manke - HMI Berlin & TU Berlin M. Strobl - HMI Berlin & TFH Berlin O. Neumann - TFH Berlin	Date(s) of Experiment Apr. - Jul. 2005

Date of Report: Jan. 2006

In the course of redesigning and reconstruction of the V12 instrument a radiography and tomography device (V12b II) operated with a high monochromatic flux could be installed on the V12b side (Fig. 1). A pyrolythic graphite (PG) (002), provides a broad wavelength band (λ = 0.52(1) nm) and hence a high flux density (app. 5 x 10^5 $cm^{-2}s^{-1}$) for this position (compare old set up of E8 [1,2]). The perfect Si DCD monochromator installed in the beam deflected by the PG does not affect the quality of the radiography beam. The radiography and tomography position consists of an automatic sample manipulation table and a state of the art 2D scintillator CCD detector system (BC-704, ANDOR DV434). The beam cross section at the sample position is 5 x 5 cm^2 and a spatial resolution of 300 µm can be achieved in radiographic and tomographic images. The monochromatic beam provides higher sensitivity to small differences in the attenuation coefficient than broader spectra which are commonly used [2,3].

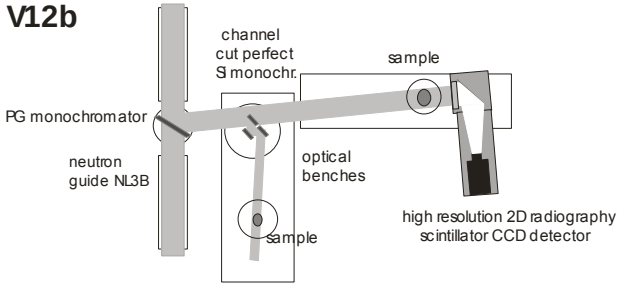

Fig. 1: Schematic set-up of V12b II tomography instrument

Although the set-up is not yet completed and the beam path for the radiography set-up is to be elongated in order to improve the resolution some preliminary results achieved in applications of the new device can be given. The first example is an alkali manganese battery which was imaged tomographically two times (Fig. 2) in order to watch the compositional and structural changes between the charged and discharged state.

Another example are diesel particulate filters in which the distribution of the sedimentation of the soot particles is of high technical interest for the development of these devices (Fig. 3). Both tomograms consist of 200 projection images recorded with exposure times of 60 seconds.

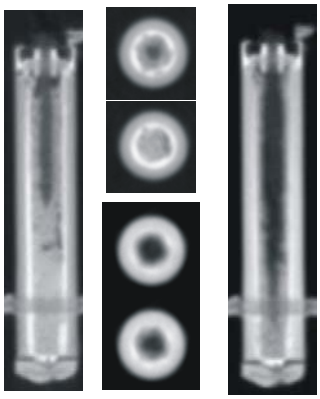

Fig. 2: vertical and horizontal cuts of the 3 dim. reconstructions of an Aalkali-Mn battery (d = 0.8 cm); left and upper middle: charged; right and lower middle: discharged

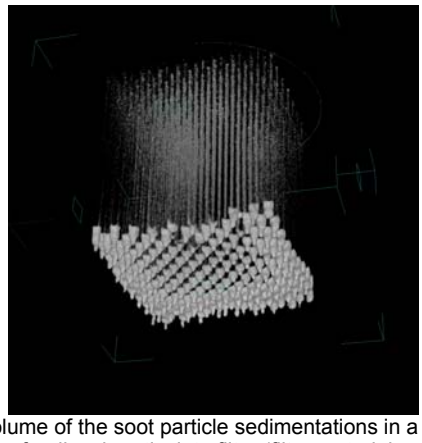

Fig. 3: volume of the soot particle sedimentations in a 5 x 5 x 5 cm^3 piece of a diesel particulate filter (filter material set invisible)

Acknowledgement

Supported by BMBF Proj**.** 03TR6TFH

References

[1] M. Strobl: BENSC EXPERIMENTAL REPORTS **2004**, p.185, PHY-04-1078-LT
[2] C. Lewis: BENSC EXPERIMENTAL REPORTS **2004**, p.171, PHY-04-1074-LT
[3] M. Strobl: BENSC EXPERIMENTAL REPORTS **2004**, p.172, PHY-04-1074-LT

	EXPERIMENTAL REPORT Quantitative tomography with monochromatic neutrons	Proposal N° PHY-04-1135-LT Instrument **V12b** Local Contact Markus Strobl
Principal Proposer: Experimental Team:	M. Strobl - HMI Berlin & TFH Berlin W. Treimer - HMI Berlin & TFH Berlin M. Strobl - HMI Berlin & TFH Berlin O. Neumann - TFH Berlin	Date(s) of Experiment Aug. - Sept. 2005

Date of Report: Jan. 2006

One advantage of using monochromatic neutrons for radiography and tomography is that no spectral effects like beam hardening take place [1,2]. Therefore a higher sensitivity and reliability (no beam hardening artifacts) can be achieved for radiography and tomographic reconstruction. That opens the possibility of improved quantitative analyses concerning accurate determination of thicknesses of layers measured radiographically, but also the analyses of attenuation coefficients and identification of materials in tomographic reconstructions. In order to examine the accuracy of such quantitative tomography at the new V12b II radiography and tomography set-up a cylindrical Al sample matrix (diameter 2.5 cm) was used. The matrix was loaded with quarter cake shaped pieces of different materials like brass, copper, two types of steel and Al. The composition of the materials is well known as well as the wavelength of the monochromatic beam that has been measured with a Ge[111] crystal to be 0.52(1) nm. The attenuation coefficients of the given materials have been calculated [3] on one hand and measured at the V12b II radiographically (Fig. 1) (piece by piece) and tomographically (Fig. 2) on the other hand. A tomography consisted of 200 projection images on a range of 180° with exposure times of 60 seconds. From the radiographic images the attenuation coefficients were calculated after necessary corrections (e.g. dark field) straight-forward using the exponential attenuation law. The tomographic reconstruction based on the attenuation law and the filtered back projection (FBP) algorithm provides directly the attenuation per voxel dimension (i.e. pixel resolution) and hence only correct unit scaling was necessary to achieve comparable attenuation coefficients. For comparison with the calculated values, mean values of area (radiography) respectively volume (tomography) were used, while their fluctuations are taken into account for the error estimations. Values at the borders (within the limit of geometrical resolution) of the material pieces are neglected as geometrical blur strongly affects their reliability. In Tab. 1 the achieved values are listed for comparison and the matching is within deviations of less than 5% and hence promising for a lot of applications.

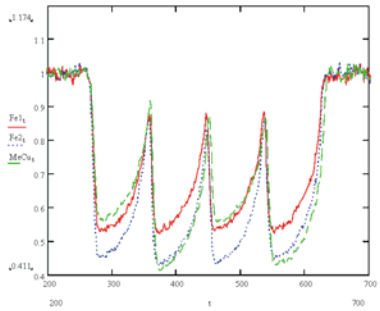

Fig. 1: Line profiles of radiography of metal cake pieces; red: steel 1, blue: steel 2, green: two brass (lower contrast) and two Cu pieces

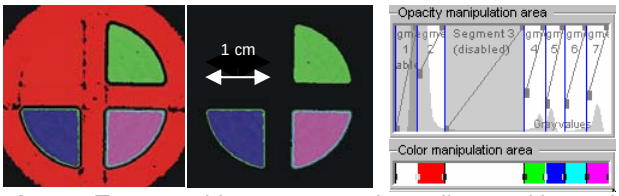

Fig. 2: Tomographic reconstruction slices with and without Al matrix; histogram with colour table

Mean values [cm-1]	radiogr.	tomo	calc.
brass	0.64(2)	0.64(3)	0.67(3)
steel1 (105WCR6)	0.72(2)	0.72(3)	0.74(3)
steel2 (X5CrNi18-9)	0.94(2)	0.93(3)	0.92(3)

Tab. 1: in radiography and tomography measured values compared to calculations

Acknowledgement

Supported by BMBF Proj**.** 03TR6TFH

References

[1] C. Lewis: BENSC EXPERIMENTAL REPORTS **2004**, p.171, PHY-04-1074-LT

[2] M. Strobl: BENSC EXPERIMENTAL REPORTS **2004**, p.172, PHY-04-1074-LT

[3] NIST: http://www.ncnr.nist.gov/resources/sldcalc.html

	EXPERIMENTAL REPORT The new V12b double crystal diffractometer	Proposal N° PHY-04-1135-LT Instrument **V12b** Local Contact Wolfgang Treimer
Principal Proposer: Experimental Team:	M. Strobl - HMI Berlin & TFH Berlin W. Treimer - HMI Berlin & TFH Berlin M. Strobl - HMI Berlin & TFH Berlin	Date(s) of Experiment 2005

Date of Report: Jan. 2006

The second part of the reconstructed V12 instrument (see report before) is now subdivided into the V12b DCD and a monochromatic radiography and tomography facility (V12b II). A second crystal in the NL3b for the new V12 set-up, a pyrolythic graphite (PG) (002), provides a broad wavelength band (λ = 0.52(1) nm) and hence a high flux density (app. 5 x 10^5 $cm^{-2}s^{-1}$) for the radiography and tomography position. The V12b DCD takes out an extremely well defined wavelength (λ = 0.524(1) nm) by a perfect Si channel cut single crystal (5 x 10^2 $cm^{-2}s^{-1}$) (Fig.1) located in this beam.

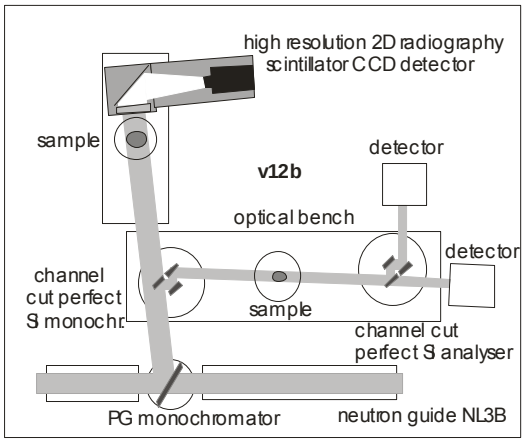

Fig. 1: Schematic drawing of the V12b instrument including the DCD and radiography/tomography (V12b II) positions

The V12b DCD can be equipped with different channel cut perfect crystals for special applications and developments [1,2,3]. The first one, the monochromator deflects the beam out of the radiography beam like mentioned above and a second one with the same design acts as an analyzer. The highest achievable resolution could be tuned to 7 x 10^{-5} nm^{-1} [4] or a peak to background ratio of 10^5 could be realized with the old set-up.

Contrary to the former V12b DCD set-up only one pre-monochromator provides the beam for the DCD perfect Si monochromator and the beam path is reduced significantly. That resulted in an intensity gain by a factor of close to 4 (Fig. 2) using the same DCD crystals and hence resolution than in comparable measurements with the old set-up. The peak to background ratio on the other hand still needs improvement as the shielding is not yet optimized. First measurements with both instrument parts i.e. the tomography set-up and the V12b DCD installed showed that the tomography set-up is not handicapped by the installation of the DCD perfect Si monochromator. Further details on the tomography set-up and first results achieved by application are given in other reports as well as a first user experiment on the V12b DCD.

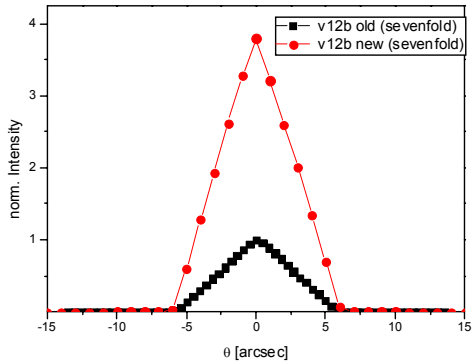

Fig. 2: Comparison of the rocking curve using sevenfold perfect Si crystals in the old and new V12b set-up

Acknowledgement

Supported by BMBF Proj**.** 03TR6TFH

References

[1] W. Treimer, M. Strobl, A. Hilger: J. Appl. Phys. A **74** [Suppl.] (2002) 191

[2] A. Wagh, V.C. Rakhecha, W. Treimer: Phys. Rev. Let. **87** (2001) 125504, 1-4

[3] A. Wagh, V.C. Rakhecha, M. Strobl, W. Treimer: PRAMANA J. Phys. **63**, 2 (2004) 369

[4] W. Treimer, M. Strobl, A. Hilger: Phys. Let. A **289**, 3 (2001) 151

	EXPERIMENTAL REPORT **Test of multi-pinhole grids for VSANS**	Proposal N° EF Instrument **V13** Local Contact Margarita Russina
Principal Proposer: Experimental Team:	D. Clemens - HMI Berlin L. Mokrani - HMI Berlin F. Mezei - HMI Berlin	Date(s) of Experiment 22.-24.10.2005

Date of Report: 15.03.2006

Neutron trajectories can be defined by a system of multi-pinhole absorber grids that is designed to collimate the beam to a divergence adequate for the experiment. This technique has been proposed to fulfill the needs for high resolution neutron scattering at very small angles. A prototype consisting of 20 precisely manufactured cadmium pinhole grids, each separately adjustable in the beam has been realized at BENSC. Under the influence of gravity the trajectories can be directed to a focal point, e.g. in the plane of a detector. The new instrument for very small angle neutron scattering VSANS in the second neutron guide hall, recently inaugurated at BENSC, will take advantage of this new focussing system in order to achieve momentum transfers of 10^{-3} nm^{-1}.

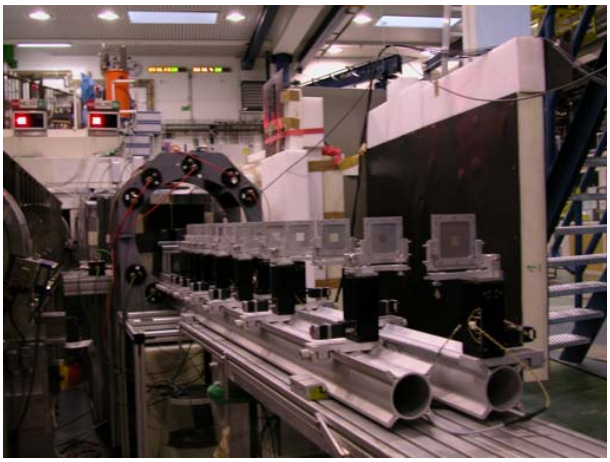

Fig.1: Multi-pinhole grid collimator aligned on a twinned optical bench at the V13 beam position

20 grids were aligned on a twinned optical bench over a distance of 2 m. Each had pinholes that decreased in size and covered area from the first to the last grid. In this way 144 flight channels were defined. They were arranged in a way that no switch from one to another channel should be geometrically allowed.

The images taken in the detector plane itself and in front of it were recorded using a commercial 2D fluorescence detector with a sensitive area of ~50 mm in diameter. Production errors of the grids and imaging errors due to the inappropriate optical bench as well as air scattering effects led to unwanted trajectories on which neutrons still could reach the detector off the focal point. The focus, additionally dithered by air scattering, had a size of 4 mm.

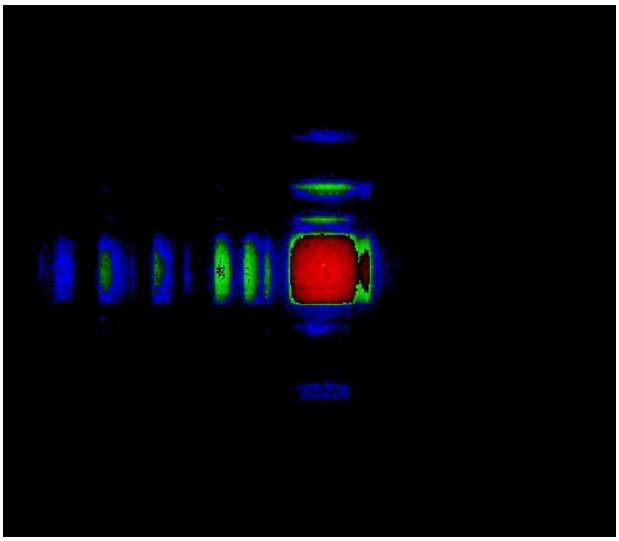

Fig.2: Logarhythmic intensity distribution in focal plane.

The tests were important to direct the activities in the further persuation of this project.

	EXPERIMENTAL REPORT **Focusing lens and polarising supermirror**	Proposal N° EF Instrument **V14** Local Contact Thomas Krist
Principal Proposer: Experimental Team:	T. Krist - HMI Berlin N. Behr - HMI Berlin J.-E. Hoffmann - HMI Berlin T. Krist - HMI Berlin	Date(s) of Experiment 2005

Date of Report: 21.01.2006

A solid state lens was designed, built and tested at BENSC, realizing for the first time a proposal of Mildner [1].

It consists of silicon wafers with the dimensions of 20 mm high, 140 mm long and 0.15 mm thick. They were coated in cooperation with the group at BNC, Budapest on one side with Ni-Ti supermirrors with m=2, where m denotes the ratio of the critical angle of the supermirror to the critical angle of natural nickel. 100 of these wafers were put into a holder which bends the wafer stack to the desired bending radius.

Experiments were performed at the BENSC reflectometer V14 with a neutron beam with a wavelength of 4.72 Å, a width of 0.4 mm, and a divergence of 0.035°. A ^{3}He detector with a slit of 0.4mm width was placed different distances behind the lens. The background was $5 * 10^{-4}$ of the direct beam.

Fig. 1 shows as the broad curve the profile of the direct beam perpendicular to the flight direction. The other curves show the beam profile with the lens inserted into the beam at different distances behind the lens. The highest curve is measured at 36mm behind the end of the lens, the two other curves at 44mm and 88mm respectively. Compared to the direct beam the curve with the well focused beam displays a peak intensity which is 3 time larger than the direct beam.

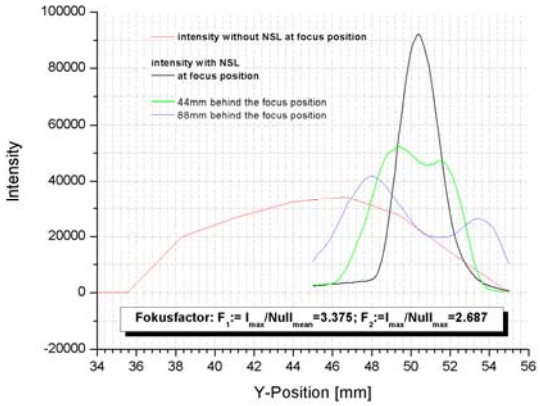

Fig. 1: Neutron intensity transmitted through the leans described in the text, showing in the peak 3 times the intensity of the beam without the lens.

At BENSC polarising Fe-Si supermirrors are steadily improved. Recently we succeeded to increase the number of layers up to 1000. Tests of this mirror were performed at V 14 which has a polarisation of the incoming beam of 96.6%.

Fig. 2 shows the reflection from this supermirror which was deposited on a float glass substrate for both spin components together with polarization and flip ratio. The data are corrected for the incoming polarization. The reflectivity at m=3.3 is above 80% and the average flip ratio is above 60.

Fig.3 shows the transmission through this supermirror for both spin components together with polarization and flip ratio. The flip ratio is above 40 up to m=2.5 and above 20 up to m=3.

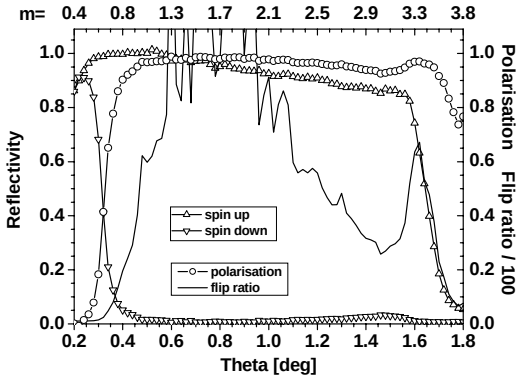

Fig. 2: Neutron intensity reflected from Fe-Si supermirror with 1000 layers for both spin components together with polarization and flip ratio.

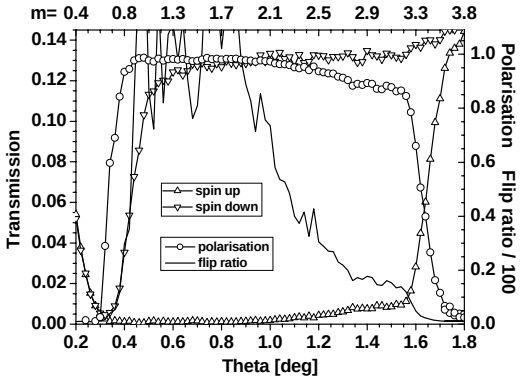

Fig. 3: Neutron intensity transmitted through a Fe-Si supermirror with 1000 layers for both spin components together with polarization and flip ratio.

Reference

[1] Mildner: Nucl. Instrum. & Meth. A**299**(1990)416

BENSC	**EXPERIMENTAL REPORT** **Mass-filtered cobalt clusters on non-magnetic surfaces**	Proposal N° BESSY Instrument (UE46-PGM) **S1** Local Contact Paolo Imperia
Principal Proposer: Experimental Team:	J. Bansmann - Uni Rostock P. Imperia - HMI Berlin A. Kleibert, K.H. Meiwes-Broer - Uni Rostock F. Bulut, M. Getzlaff - Uni Düsseldorf C. Boeglin, A. Barla - IPCMS Strasbourg, F	Date(s) of Experiment 2005

Date of Report: Jan. 2006

It is well-known that small clusters deposited on surfaces exhibit magnetic properties that strongly differ from those for thin films and bulk systems [1,2]. Analogously, even large clusters with about several thousands of atoms have enhanced orbital moments although only the outer two layers of the clusters are influenced [3-5]. Moreover, the electronic structure of the interface also has an influence on the magnetic properties of the clusters that cannot be neglected. Large mass-filtered Fe and Co clusters deposited on Ni(111) films show different magnetic properties when compared to depositions on iron and cobalt films [6].

Hybridization effects of the electronic states between clusters and underlying substrate / film can modify these cluster-specific properties significantly. Up to now we have deposited Fe and Co clusters on ferromagnetic films in order to magnetize the clusters remanently by exchange interaction with magnetic film. For the investigations presented here, we have chosen an Au(111) single crystal as a substrate. Cobalt films on Au(111) show spin-reorientation transitions both as a function of size and temperature [7,8]. Mass-filtered cobalt clusters with a size of about 9nm have been deposited in-situ onto the clean surface and afterwards investigated with XMCD using the superconducting magnet systems of the Strasbourg group. For this purpose the small and transportable arc cluster ion source (briefly described in [9]) has been adapted to the preparation chamber of the magnet system. The source was developed for producing mass-filtered metal clusters in the size range from 5 nm to 15 nm that can be deposited in-situ on surfaces without fragmentation. The mass filtering process is carried out in an electrostatic quadrupole deflector, cf. fig. 1.

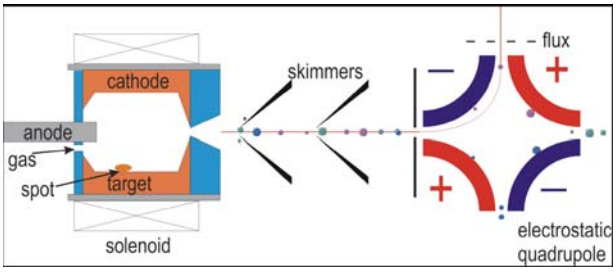

Fig. 1: *Schematic drawing of the arc cluster ion source ACIS and the mass-filtering unit*

The measurements have been carried out at the UE46-beamline at different temperatures (40 K and 300 K). An external magnetic field of 4 T has always been applied along the direction of the incoming photon beam. For the individual measurements, the photon polarisation has been reversed. The XMCD data taken in total electron yield clearly show the typical absorption features at the Co 2p edge with different intensities in the two peaks when switching the circular polarisation from σ^+ to σ^-, cf. fig. 2.

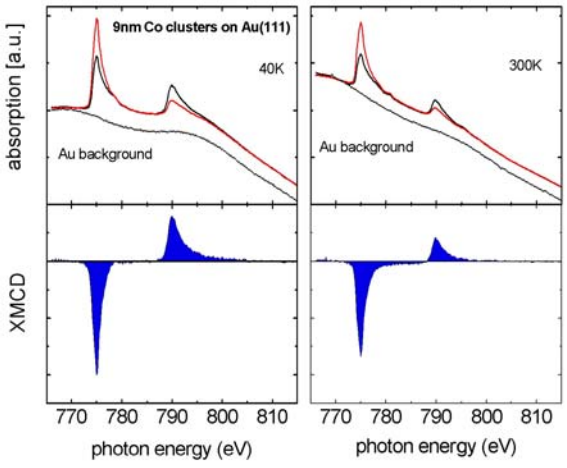

Fig. 2: *Photoabsorption (upper part) and XMCD spectra (lower part) from an 9nm clusters Co deposited on clean Au(111)*

→

The upper panels show the spectra recorded at 40 K (left) and 300 K (right) at an angle of 40 taken for opposite photon helicities together with the background from the clean Au(111) sample. Please note the strong feature in the clean gold spectrum at low temperature which is located directly at the Co 2p absorption edge. The lower panels display the corresponding XMCD intensity difference. Clearly, the area of the Co $2p_{½}$ peak is smaller at 300 K indicating a reduced spin moment when compared to 40 K. By integrating the XMCD curve, one has access to the ratio of orbital to spin moment which is being discussed in the following.

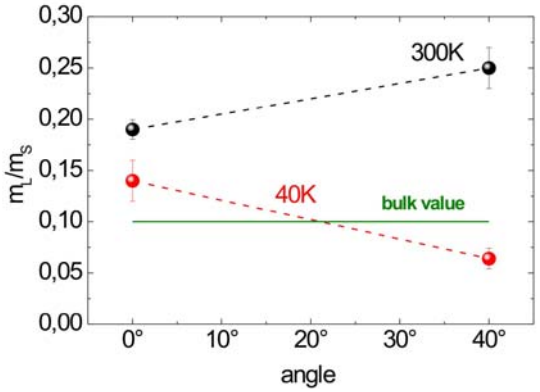

Fig. 3: *Ratio of orbital (m_L) to spin moment (m_S) for 9nm Co nanoparticles on Au(111) at 300K and 40K for different angles of the magnetization direction with respect to the surface normal. The solid green line denotes the hcp bulk cobalt value*

The ratio of orbital (m_L) to spin moment (m_S) presented in fig. 3 significantly depends on the angle of incidence (and thus the magnetization direction), the values are different in normal emission and 40° off-normal. The lower data set (40 K) indicates a preferential magnetization orientation in perpendicular magnetization direction whereas the increasing value for 300 K is a clear hint for an in-plane magnetization direction.

The spin moment of the cobalt clusters, however, is independent of the direction of magnetization after correcting for the dipole term. Thus, it does alter this ratio. Of course, the spin moments are dependent on the temperatures, they vary from $m_S \approx 1.65\ \mu_B$ at 40 K to $1.4\ \mu_B$ at 300 K. The easy magnetization direction is usually oriented along the maximum value of the orbital moment. These results clearly underline the importance of the electronic structure of the substrate on the magnetic properties of deposited clusters. It is not only the size of the clusters that determines the spin and orbital moments, one has also to take into account the interaction with the surface. Further investigations on different surfaces are planned in order to get a better understanding of the interaction between deposited the clusters and the surface of the substrate.

Acknowledgement
This work was supported by DFG via BA 1612/3-1 (in the DFG priority call 1153)

References:

[1] K.W. Edmonds et al.: JMMM **220**, (2000)
[2] J.T. Lau et al.: Phys. Rev. Lett. **89**, 057201 (2002)
[3] J. Bansmann and A. Kleibert: Appl. Phys. A **80**, in press (2005)
[4] J. Bansmann et al.: Surface Science Reports **56**, 189 (2005)
[5] A. Kleibert, Disseration, Univ. Rostock (2006)
[6] J. Bansmann et al.: Appl. Phys. A **82**, 73 (2006)
[7] R. Sellmann et al.: Phys. Rev. B **64**, 054418 (2001)
[8] Weller et al.: Phys. Rev. Lett. **75**, 3752 (1995)
[9] R.P. Methling et al.: Europ. Phys. J. D **16**, 173 (2001)

	EXPERIMENTAL REPORT **Reading magnetism of one layer of Single Molecule Magnets**	Proposal N° BESSY Instrument (UE46-PGM) **S1** Local Contact Paolo Imperia
Principal Proposer: Experimental Team:	D. Gatteschi - Univ. Florence, I M. Mannini, R. Sessoli - Univ. Florence, I A. Cornia, L. Zobbi - Univ. Modena, I C. Cartier dit Moulin - LCIMM-UPMC Paris, F P. Sainctavit - LMC-UPMC Paris, F	Date(s) of Experiment 2005

Date of Report: Jan. 2006

Nowadays chemists are able to produce molecules having, individually, properties of bulk materials or even capable to execute a function. Thus molecules can constitute the building blocks for the growing little world of nanotechnologies.
Magnetic materials make no exception. Actually since the early nineties of the last century a new kind of molecules has been investigated that individually behaves like a magnet and for this reason they have been called Single Molecule Magnets (SMMs).[1] They show a magnetic hysteresis that, contrarily to traditional materials is not a cooperative effect but rather a feature of the molecule on its own. SMMs are in fact polynuclear metal complexes comprising paramagnetic transition metal centres that, thanks to exchange interactions inside the molecule, originate a high spin ground state. When a large spin in the ground state is associated with a strong easy axis magnetic anisotropy the magnetization freezes at low temperature as its reversal requires the overcome of an energy barrier. Due to their reduced dimensions quantum effects are important and in principle SMMs could be exploitable in quantum devices.[2]

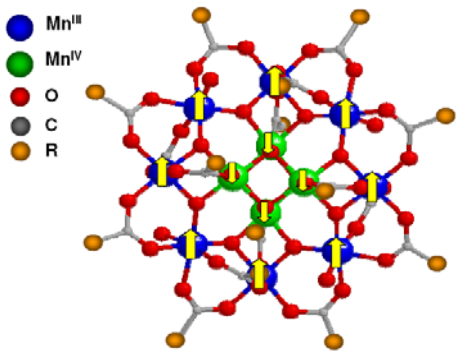

Fig. 1: *Schematic view of the structure of the Mn12 cluster*

The first and most investigated SMM is a cluster constituted by twelve Mn atoms (called Mn12, fig. 1) organized in an internal tetrahedron of four Mn^{IV} and an external ring of eight Mn^{III} atoms; all Mn atoms are in an octahedral coordination, connected by oxygen atoms creating a sort of mixed valence manganese oxide in which the growth is systematically blocked by an external organic shell (16 carboxylic acids) creating a perfectly monodisperse set of magnetic particles. Each Mn^{IV} owns a magnetic moment antiparallel to those of the Mn^{III} atoms, resulting in a ferromagnetic structure that determines a ground state characterized by a total spin S = 10.

The interesting potentiality of this kind of materials resides in the magnetic memory of the individual molecule, but, up to now, single molecule properties have been extrapolated from the those of bulk samples (single crystal, powder, and diluted solution). The simplest strategy to reach individual addressing of the clusters is to organize SMMs on surfaces and use techniques such as Scanning Probe Microscopy (SPM) that indeed have the high spatial resolution required for single–molecule addressing.

Recently different methods of depositing Mn12 derivatives on a surface have been reported.[3] For instance we have suggested some chemical modifications of the original external organic shell to graft the clusters on a gold surface. A crucial step is to evidence that during the deposition procedure the complex molecule still retains its structure and, above all, its peculiar magnetic behaviour. Traditional techniques for magnetic characterization lacks the necessary sensitivity while the x-ray absorption spectroscopy (XAS), through the x-ray magnetic circular dichroism (XMCD) method, has shown to be able to detect the magnetism of a submonolayer of magnetic atoms.[4] Moreover, by recording the magnetic dichroic signal at the manganese $L_{2,3}$ edges in Mn12 clusters, one has immediate access to the magnetic structure of the cluster, because the contribution from Mn^{III} is easily distinguished from that of the antiparallel aligned Mn^{IV} ions, as shown for the simplest derivative of Mn12.[5]

We have used XMCD technique to characterize the bulk properties of Mn12TE = ($[Mn_{12}O_{12}(OOCPhSCH_3)_{16}(H_2O)_4]$), a more complex Mn12 derivative (fig. 2) that is able to bind gold surfaces through sulphur atoms; XAS and XMCD characterizations, obtained recording signals in total electron yield at 4 K and using a field of 4 T evidence the persistence of the characteristic ferrimagnetic spin structure.

→

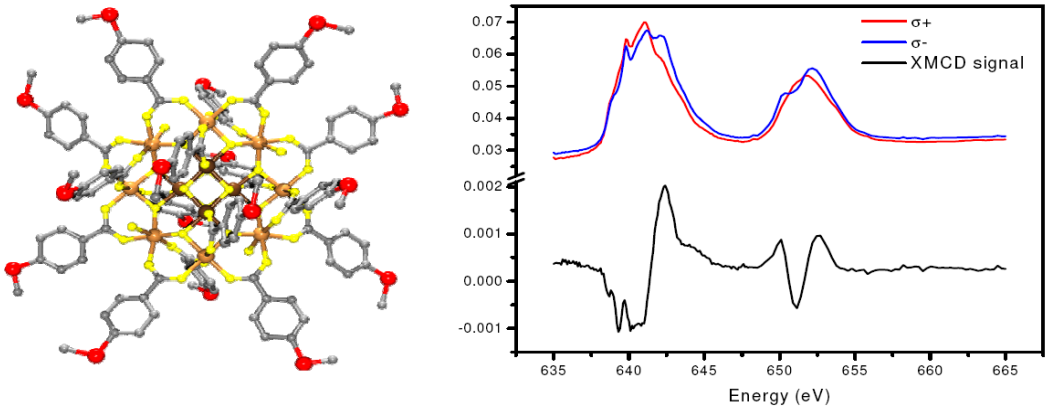

Fig. 2: *Structure of the Mn12TE cluster (left) and bulk XAS and XMCD spectra (right)*

When transferring this kind of characterizations to the analysis of a single layer of molecule problems related to photo-reduction can be easily encountered due to the high energy of third generation synchrotron radiations. The necessity of a lower flux appears as counter-intuitive but indeed position and energy stability play a key role in our experiment. For this reason BESSY, and in particular UE46 - PGM beamline, represents the ideal facility for this kind of characterizations. In fact, playing with various parameters we reduced the number of photons by a factor of 500 and an extra factor of 400 concerning the photon density was obtained thanks to the UE46 parallel beam mirror system.

In this way we have been able to characterize samples prepared ex situ starting from a solution o f Mn12TE that is adsorbed on a gold (111) surface. The Mn12TE clusters form a submonolayer in which each molecule is isolated from the others, as shown in fig. 3, leaving a wide clean gold surface in which each molecule is well identifiable and addressable.[6]

This kind of sample was inserted inside the liquid He cryostat of the XMCD setup and during one day of measurements no evidences of significant photo-reduction have been noticed.

Preliminary results (see fig. 3) evidence that XAS spectra strongly resemble those of the bulk sample with a slight increase of a signal due to spurious Mn^{II} contributions. Surprisingly the dichroic signal is substantially modified after the deposition on the Au surface.

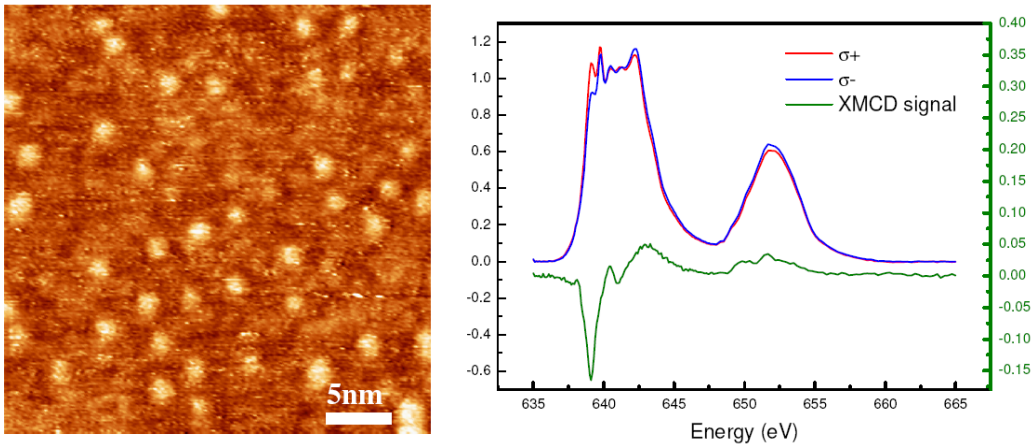

Fig. 3: *Constant–current STM image of Mn12TE assembled on the Au(111) surface (left) and XAS and XMCD spectra (right) of this submonolayer*

A qualitative analysis, to be confirmed by a series of detail calculations now in progress, suggests that in addition to Mn^{III} and Mn^{IV} also a Mn^{II} component is present. Moreover the typical fingerprint of antiparallel alignment of Mn^{III} and Mn^{IV} is not detected from the monolayer. Interactions with the gold substrate, as well as a reduction during the grafting reaction, might be at the origin of this observation. This intriguing result does not however reduce the interest in this kind of innovative materials but suggests us to continue this investigation by playing on the deposition conditions and by exploiting different substrates.

Acknowledgments

The authors are grateful to the BESSY staff, for support before and during measurement time.

Financial support from the EC through BESSY IA-SFS Access Programme Contract N° R II 33-CT-2004-506008, "Magmanet" NMP3-CT-2005-515767, and "QuEMolNa" MRTN-CT-2003-504880 projects is gratefully acknowledged.

References

[1] D. Gatteschi et al.: Molecular Nanomagnets, Oxford University Press, Oxford 2006
[2] H. Park et al.: Nature **407**, 57 (2000)
[3] A.Cornia et al.: Structure & Bonding, (2006) in press
[4] P. Gambardella et al.: Nature **416**, 301 (2002)
[5] R. Moroni et al.: Phys. Rev. B **68**, 064407 (2003)
[6] L. Zobbi et al.: Chem. Comm. **12**, 1640 (2005)

	EXPERIMENTAL REPORT **Magnetic anisotropy of triangular shaped, hexagonally arranged Co nanostructures**	Proposal N° BESSY Instrument (UE46-PGM) **S1** Local Contact Paolo Imperia
Principal Proposer: Experimental Team:	P. Imperia - HMI Berlin W. Kandulski, A. Kosiorek - CAESAR Bonn H. Głaczyńska, M. Giersig - CAESAR Bonn D. Schmitz, H. Maletta - HMI Berlin	Date(s) of Experiment 2005

Date of Report: Jan. 2006

The quest for new materials and technical solutions able to match the requirements of modern performances for data storage devices produced in the last few years a large number of studies about the magnetic properties of nanostructured materials. The control of the magnetic properties by means of the shape could be decisive in improving the performances of newly designed devices [1, 2]. The ways devised to induce the shape anisotropy have especially tampered with adjustments of the substrate topology or have deployed the power of electron beam lithography. Here we report on the in plane magnetic anisotropy observed in nanostructured Co thin films prepared by nanosphere lithography [3]. This relatively young technique allows the simple and economical preparation of thin films of magnetic metals laterally structured in a number of different topologies [4].
Polystyrene (PS) latex particles of 1710 nm diameter were deposited from a water surface on the polished surface of a chemically cleaned Si substrate by a methodology related to the preparation of Langmuir-Blodget films [4]. Then, a Co layer of 32 nm thickness was deposited by electron beam evaporation on top of the PS mask in high vacuum (HV) conditions. After the chemical removal of the nanosphere mask the final result is a matrix of polycrystalline triangular elements arranged in a highly ordered hexagonal symmetry. Atomic force microscopy (AFM) has been used to investigate the samples homogeneity and to determine the orientation of the evaporated triangular nanostructures with respect to the substrate (fig. 1).

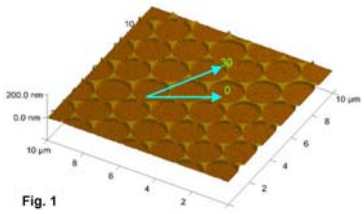

Fig. 1

The magnetic properties were studied by means of x-ray magnetic circular dichroism (XMCD) at the beam line UE46 - PGM at BESSY, Berlin. The experimental technique allows to determine separately the orbital and spin moment.

The relative simplicity of the substrate preparation constitutes the main advantage of the sample preparation technique. However, the necessity to chemically remove the mask ex situ produces Co structures covered with a natural thin layer of CoO, thus the X-ray absorption spectra (XAS) show the typical splitting of the Co L_3 edge. A way designed to remove the CoO layer is H^+ ion sputtering. This method has been already successfully used to remove the oxide shell of chemically synthesised Co nanoparticles [5].

The samples were etched for 210 minutes at a relatively low sputtering energy (700 eV, H^+ pressure of 2.4×10^{-5} mbar). The sputtering parameters were carefully adjusted to allow an effective removal of the CoO layer without destroying the sample's regular pattern. Longer sputtering time at lower energy as well as shorter sputtering time at higher energies destroy partially or completely it. The sputtering energy and the time necessary to remove the CoO layer depend on the sample thickness and on the diameter of the PS lattex spheres. Each combination of Co thickness and triangles lateral dimension has a different sputtering time. Fig. 1 shows a typical AFM picture of our samples, the triangular structures are well defined with a very low density of defects, the shape and dimension of the Co pattern are given by the curvature of the latex spheres. The AFM scan shows that the samples retain their well-ordered geometry after the correct H^+ sputtering procedure. Small debris, resulting from the cleaning action of the H^+ ions and having a diameter between 2 and 10 nm, are present on the Si surface in between the metal triangular structures.

The XMCD measurements were done in remanent magnetisation at room temperature (RT). A pulsed field of 800 Oe was applied alternating its direction planar to the sample surface at each energy scan point. After each scan the sample was rotated around its axis. The arrows imposed on the AFM picture of fig. 1 show the geometry of the experiment. The angle φ defines the direction along the triangle pattern; the angle $\varphi = 0°$ is the direction along the spherical voids, while $\varphi = 30°$ defines the direction along the triangles edges. The geometry of the experiment was carefully planned to make sure the position of the centre of the samples remained unaltered after changing the azimuthal angle, the correct position of the sample with respect to the incident synchrotron light beam was checked at each measurement step. The XAS spectra were recorded in total electron yield, collecting the sample drain current. The spectral curves were normalised toward the incident incoming light by means of the last mirror current. The measurements were performed in grazing incidence, the angle of the sample surface with respect the incoming circularly polarised light was $\theta = 20°$. In the data analysis no self absorption effects were taken into account.

→

The upper panel of fig. 2 shows the typical line shape of the absorption spectra after sputtering. Three lines are drawn: the sum of the positive and negative magnetised spectra (black), the step function representing the $L_{2,3}$ absorption edge jump (blue), and the isotropic spectrum resulting from the subtraction of the previous two (black). During the data analysis the orbital and spin moments, μ_l and μ_s respectively, were calculated assuming the 3d electron occupation number as for bulk hcp Co $\mathbf{n}_{3d}$ = 7.5. The shoulders at the lower and higher energies of the main peak at the Co L_3 edge (fig. 2) reveal that despite the H^+ etching procedure a small amount of oxide is still present. The separation of the metallic and non metallic contributions to the magnetic properties of the Co crystal cannot be easily achieved; the presence of a small amount of CoO on the surface of the samples has an impact on the results obtained by the surface sensitive XAS technique. It leads primarily to a reduced remanent magnetisation of the samples. The calculated values of the orbital and spin moment are lowered by an unknown factor with respect to a perfectly oxide free surface. The lower panel of fig. 2 shows the dichroic signal as a result of the subtraction of the positive and negative magnetised XAS spectra, the XMCD signal (black line), together with its integral value (red line).

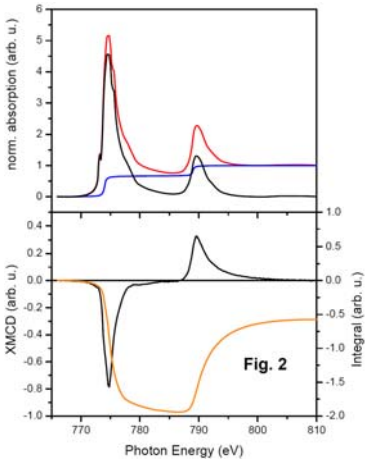

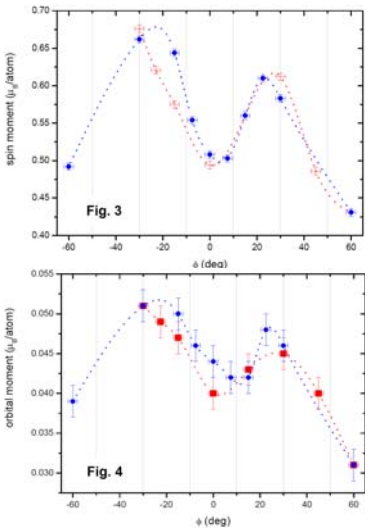

Fig. 3 shows the spin moment, μ_s versus the azimuth angle φ, while fig. 4 shows the orbital moment, μ_l. Clearly, the patterned samples have an angular dependency with a period of $\varphi = 60°$. Two sets of data are shown in the graph. The black line represents the first run from $\varphi = -30°$ to $\varphi = 60°$ while the red line the way back from $\varphi = 60°$ to $\varphi = -60°$. The μ_s and μ_l maxima were both found at azimuth angles of $\varphi = -30°$ and $\varphi = 30°$ while the minima at $\varphi = -60°$, $\varphi = 0°$ and $\varphi = 60°$, respectively. According to the geometry of the experiment this means that the magnetization easy axis lies along the edge to edge direction of the triangle pattern, while the hard magnetization axis lies along the sphere to sphere center direction.

The orbital and spin moment variation is about 15 % for both values. The maximum value calculated for the spin moment is $\mu_s = 0.68\ \mu_B$/atom while the minimum value is $\mu_s = 0.43\ \mu_B$/atom. The maximum and minimum value for the orbital moment are $\mu_l = 0.051\ \mu_B$/atom and $\mu_l = 0.031\ \mu_B$/atom.

The absolute values of μ_l and μ_s calculated by means of the sum rules are lower with respect to the calculated or measured values of the orbital and spin moments for hcp bulk Co. Several factors play a role in such a result. Probably the applied pulsed field of 800 Oe leads to an incomplete magnetisation of the samples measured in remanence. Static magnetization loops show that the saturation for non H^+ sputtered samples is achieved at about 2 kOe and the cycle becomes reversible at about 800 Oe. However, for samples having their oxidised surface removed the magnetic hysteresis cycles are different and 800 Oe should be enough to nearly fully saturate them. Turning back the angle φ the minima/maxima get shifted of about 10° like if an energetic barrier must be overcome in order to rotate the magnetic ordering of the triangles. Theoretical calculation have been planned to explain such behaviour. The dipolar interaction probably plays a role in the magnetic alignment of the triangular elements and the geometrical arrangement of the patterned elements should play a significant role in the observed anisotropic effect. The sixfold magnetic anisotropy shown by the Co patterned samples is consequence of the pattern shape. The effect probably can be ascribed to configurational anisotropy [6]; a deviation from the uniform magnetization driven by the shape of the pattern. With respect to previous studies on triangular nanostructures in the present case the sixfold anisotropy cannot be ascribed only to the shape of a single triangular element, but is consequence of the symmetry of the whole Co pattern. The variation of the magnetic moment as a function of the azimuthal angle obtained by XMCD was also independently confirmed by the angular dependence of the coercive field obtained from magnetic hysteresis loops using a vibrating sample magnetometre.

Acknowledgement

We thank S. Rudorff for the technical support during measurements at BESSY, Dr. H. Rossner, Dr. E. Holub-Krappe and Prof. A. Tennant for useful scientific discussion and continuos encouragement.

References

[1] C. Chappert et al.: Science **280**, 1919 (1998).

[2] A. Ney et al.: Nature **425**, 485 (2003).

[3] J. Rybczynski et al.: Colloids Surf. A: Physicochem. Eng. Aspects **219**, 1 (2003).

[4] A. Kosiorek et al.: Nano Lett. **4**, 1359 (2004).

[5] P.Imperia et al.: Phys Rev. B **72**, 014448 (2004)

[6] R. P. Cowburn et al.: Phys. Rev. Lett. **83**, 1042 (1999).

BENSC	**EXPERIMENTAL REPORT** **Exchange bias and the role of uncompensated Fe spins in epitaxially grown fcc Fe_xMn_{1-x} at the interface to Co**	Proposal N° BESSY Instrument (UE46-PGM) **S1** Local Contact Detlef Schmitz
Principal Proposer: D. Schmitz - HMI Berlin Experimental Team: H. Maletta - HMI Berlin M. Gruyters, H. Winter - HU Berlin		Date(s) of Experiment 2005, KW 32/33

Date of Report: Feb. 2006

Exchange bias occurs in systems where a ferromagnetic and an antiferromagnetic material are in contact [1]. During the last year we studied epitaxially grown ferromagnetic Co (5 ML thick) on antiferromagnetic Fe_xMn_{1-x} (12 ML thick) on Cu(001) in order to elucidate the role of uncompensated Fe moments at the interface to Co. Epitaxially grown systems have the advantage to exhibit a much better defined interface as compared with polycrystalline systems prepared by sputtering. Per definition, Fe moments of one antiferromagnetic sublattice are called "uncompensated" if Fe moments of the other antiferromagnetic sublattice, oriented into the opposite direction and therefore usually compensating the moment from the first sublattice, are missing. If the magnetization direction of the Co is reversed, one part of the uncompensated Fe moments follows because the coupling to the ferromagnet dominates. Another part of the uncompensated Fe moments does not reverse with the Co because the coupling to the antiferromagnet dominates. This is the so-called "pinned fraction" of uncompensated Fe moments which has been supposed to be responsible for exchange bias [2].

Since the uncompensated Fe spins are ferromagnetically ordered, they can be detected and quantified by XMCD. This had already been used by the group of J. Kirschner as magnetic contrast mechanism in a fascinating Photoelectron Emission Microscopy study concentrating on the FeMn thickness dependence [3]. In order to study the uncompensated Fe spins for different Fe concentrations, we performed XMCD measurements by reversing the helicity of the synchrotron radiation in successive magnetization states of the samples, i.e., magnetized after deposition, field cooled, reversed magnetization and reversed magnetization again. Magnetizing after deposition creates a well defined state of the Co magnetization, field cooling activates the exchange bias, reversing the magnetization reverses most uncompensated spins whereas the pinned fraction keeps the old magnetization, and reversing the magnetization a second time serves to test whether the first reversal is reversible.

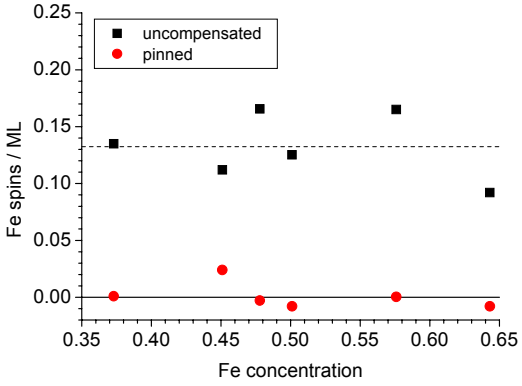

Fig. 1: Uncompensated (black squares) and pinned (red circles) Fe spins in atomic layers vs. Fe concentration

Fig. 2: Ratio of Co asymmetries after field cooling to before field cooling vs. Fe concentration. The ratio is larger (smaller) than one for antiferro-magnetic (paramagnetic) FeMn films

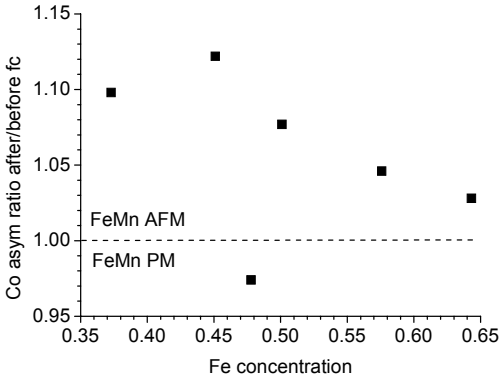

After two beamtimes for this project the following new conclusions can be drawn. In all magnetization states the absolute value of the Fe L_3 asymmetry is small, *i.e.*, a few percent. The Fe and Co XMCD spectra have been evaluated and the corresponding magnetic moments have been determined. The moment analysis reveals that about 0.13(3) ML Fe spins at the interface to Co are ferromagnetically ordered (see fig.1). These values do not change with Fe concentration between 0.37 and 0.64, *i.e.*, within the range for which the structure of Fe_xMn_{1-x} is known to be fcc [4]. The amount of pinned Fe spins is below the detection limit, *i.e.*, it is at most 0.01 ML.

Nevertheless, the ratio of Co asymmetries after field cooling to before field cooling, which is a measure for the exchange bias field, decreases systematically with Fe concentration above x = 0.5 (see fig.2). This behavior cannot exclusively be explained by the concentration dependence of the antiferromagnetic ordering temperature in thin FeMn films which was determined in Ref. [4]. Otherwise the Co asymmetry ratio would further increase with decreasing Fe concentration below x = 0.5. In order to verify that this Co asymmetry ratio is connected with the antiferromagnetic ordering of the FeMn a sample with a reduced FeMn thickness of 8 ML and an Fe concentration of 0.48 has been prepared. For this reduced FeMn thickness the antiferromagnetic ordering temperature is reduced to room temperature [4], therefore the FeMn is paramagnetic and consequently the Co asymmetry ratio is reduced (see fig.2).

In contrast to the Fe spin moment, the Fe orbital moment in the biased state depends on the Fe concentration and changes with the magnetization state. This finding and the corresponding characteristic changes in the asymmetry spectrum are our starting point for further work and a deeper understanding of exchange bias in Co/FeMn.

References

[1] W.H. Meiklejohn et al.: Phys. Rev. **102** (1956) 1413, Phys.Rev. **105** (1957) 904
[2] H. Ohldag et al.: Phys. Rev. Lett. **91** (2003) 017203
[3] F. Offi et al.: Phys. Rev. B **67** (2003) 094419
[4] F. Offi et al.: Phys. Rev. B **66** (2002) 064419

BENSC	**EXPERIMENTAL REPORT** **Determination of magnetization depth profiles of V/Fe/V(110) with X-Ray Resonant Magnetic Reflectometry**	Proposal N° BESSY Instrument (UE46-PGM) **S1** Local Contact Detlef Schmitz
Principal Proposer: Experimental Team:	D. Schmitz - HMI Berlin P. Imperia, H. Maletta, D.A. Tennant - HMI Berlin U. Grüner, M. Harlander, S. Macke, E. Goering - MPI MF Stuttgart	Date(s) of Experiment 2005

Date of Report: Feb. 2006

The magnetic part of the x-ray scattering amplitude is resonantly enhanced by orders of magnitude if the photon energy is tuned to an absorption threshold [1]. This has been utilized to determine the element-specific magnetization depth profiles of ultrathin Fe films deposited *in-situ* onto a V(110) single crystal and covered with V. For this purpose X-Ray Magnetic Circular Dichroism (XMCD) measurements in absorption, X-Ray Resonant Magnetic Reflectance (XRMR) measurements and a reflectance simulation program have been combined [2]. The XMCD was measured as a function of photon energy across the $L_{2,3}$ absorption edges at fixed angle of incidence in order to determine the optical constants which were later used to simulate the reflectances. The specular reflectances were measured as a function of the angle of incidence reversing the helicity of the incoming elliptically polarized radiation. For all measurements the samples were magnetized to remanence.

Tuning the photon energy to an absorption threshold has important consequences for the optical constants. They depend on the chemical environment and the magnetic state of the element under consideration, experimental conditions like energy resolution, and especially the magnetic part is resonantly enhanced. Therefore a careful experimental determination of the optical constants has been performed. The imaginary part of the scattering amplitude f_2 and the corresponding magnetic part m_2 were measured in absorption, and the corresponding real parts f_1 and m_1 were determined by Kramers-Kronig transformation. The resulting scattering amplitudes are shown in fig.1 for Fe (upper row) and V (lower row), respectively.

In order to determine a magnetization depth profile the measured reflectance asymmetry has to be fitted with a simulated reflectance asymmetry. This was performed with a computer program which is based on the Parratt algorithm. The program takes into account the non-magnetic and magnetic contributions to the scattering amplitude and the polarization of the incident radiation. Moreover, it is possible to simulate the magnetization at interfaces by magnetic Gaussian depth profiles. The chemical profile was determined from the non magnetic average reflectance and kept constant during the determination of the magnetic profile.

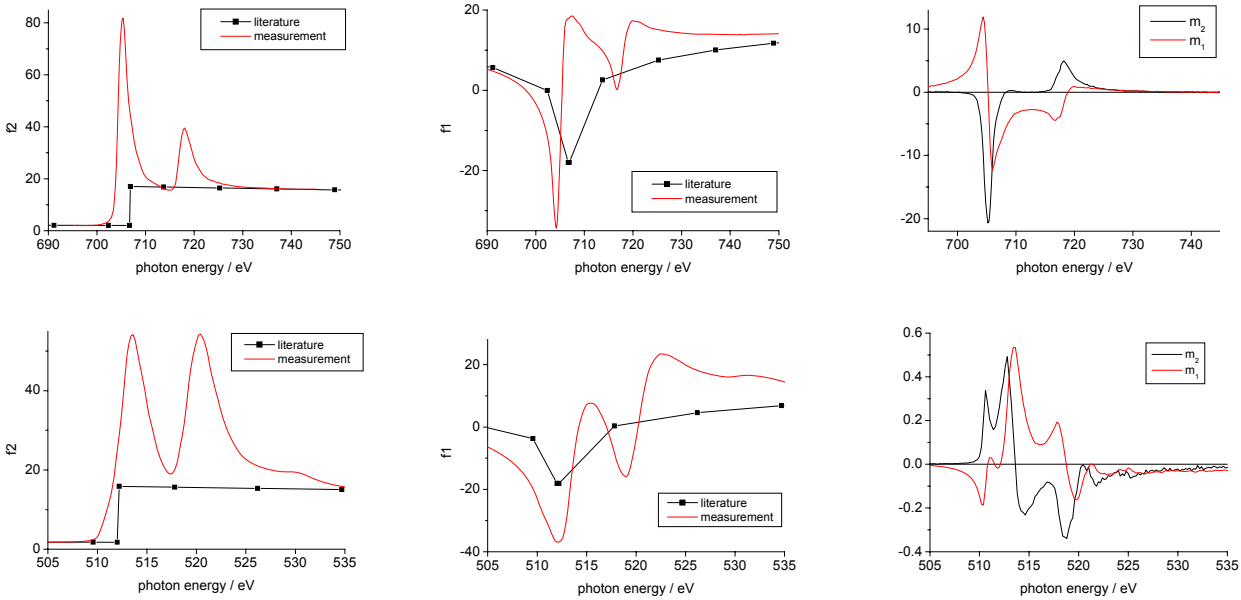

Fig. 1: Scattering amplitudes of Fe (upper row) and V (lower row). The imaginary parts f_2 and m_2 were measured in absorption and with XMCD, and the corresponding real parts f_1 and m_1 were determined by Kramers-Kronig transformation.

→

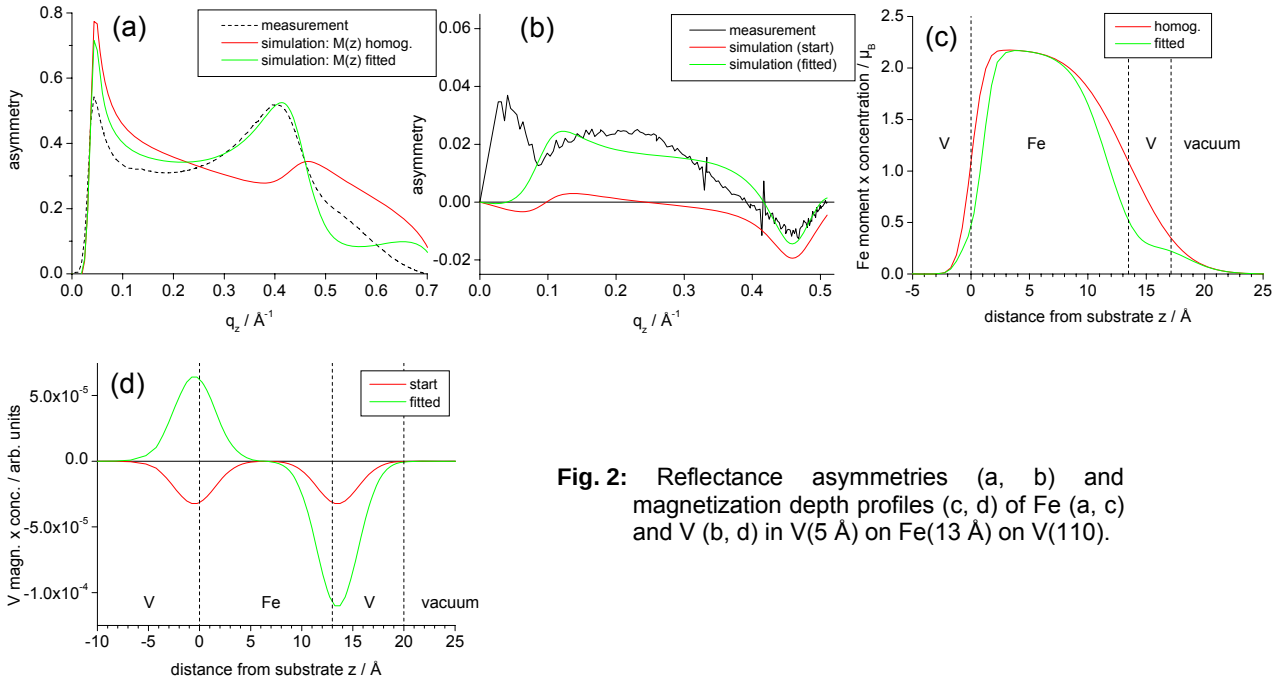

Fig. 2: Reflectance asymmetries (a, b) and magnetization depth profiles (c, d) of Fe (a, c) and V (b, d) in V(5 Å) on Fe(13 Å) on V(110).

In fig.2 the reflectance asymmetries (a, b) and resulting magnetization depth profiles (c, d) of V(5 Å) on Fe(13 Å) on V(110) are shown. The measured asymmetries (black line) were taken with resonant excitation, *i.e.*, with photon energies tuned to the Fe L_3 (704.25 eV, fig.2a) and V L_3 (511.6 eV, fig.2b) absorption edge. The grazing incidence angle range was from 0° to 80° which corresponds to a momentum transfer range along the sample surface normal from 0 Å^{-1} to 0.7 Å^{-1} for 704.25 eV and to 0.5 Å^{-1} for 511.6 eV. For each element two simulated asymmetries are shown for comparison: one for a reasonable starting configuration (red line) and one for the best fit (green line).

For Fe a homogeneous magnetization (red line, fig.2c) results in a simulated asymmetry (red line, fig.2a) which agrees already quite well with the measured asymmetry, except that the peak at 0.5 Å^{-1} is slightly too high in momentum transfer and too small in intensity. If the Fe magnetization is reduced at both interfaces to V the agreement between measurement and simulation (green line) becomes very good. Please note that the problem of the wrong sign of the simulated asymmetry below 0.05 Å^{-1} as described for Fe in the former annual report [3] has been solved. It was due to a systematic error in the determination of $m_1(Fe)$.

The reduction of the Fe magnetization at the interfaces to V is theoretically expected because of the Fe*3d*-V*3d* hybridization [4] and has been measured with XMCD comparing Fe/V(001) superlattices with different layer thicknesses [5] and Fe/V/Fe(110) trilayers with different deposition temperatures [6]. The fact that our XRMR results are in accordance with these earlier findings clearly proofs that our realization of this new method including the simulation program works.

The reasonable starting configuration for the V magnetization profile is shown as a red line in fig.2d. There it has been assumed that V at the interface to Fe is ferromagnetic with *antiparallel* coupling to the Fe magnetization and with values for the magnetic part of the optical constants as determined with XMCD (fig.1). The overall shape of the corresponding simulated asymmetry (red line, fig.2b) is quite similar to the measured asymmetry, but the relative amplitudes differ. The agreement becomes better (green line) if it is assumed that the V magnetization at the lower interface is *parallel* to the Fe magnetization and that the absolute value of the V magnetization at the upper interface is larger as the one at the lower interface (green line, fig.2d).

The V asymmetry is more than one order of magnitude smaller than the Fe asymmetry, because the V magnetization is induced only at the interface to Fe. On the one hand the statistical quality of the measured V asymmetry is still good, indicating that the sensitivity of the measurement is sufficient. On the other hand we have not yet found a V magnetization profile for the capped samples which is consistent with both, the measured asymmetries in reflection and in absorption. Therefore the question arises whether our realization of the new method is accurate enough to determine the profile of the tiny V magnetization.

Further analysis is under way to answer this question.

Acknowledgement
We would like to thank S. Rudorff and S. Miemietz for technical support.

References

[1] M. Blume et al.: Phys. Rev. Lett. **61**, 1241 (1988); E.D. Isaacs et al.: Phys. Rev. Lett. **62**, 1672 (1989)

[2] J. Geissler et al.: Phys. Rev. B **65**, 020405(R) (2001)

[3] D. Schmitz et al.: BESSY Annual Report, **242** (2004)

[4] J. Izquierdo et al.: Phys. Rev. B **64**, 060404 (2001)

[5] A. Scherz et al.: Phys. Rev. B **64**, 180407 (2001)

[6] A. Scherz et al.: Phys. Rev. B **68**, 140401(R) (2003)

	EXPERIMENTAL REPORT **Depth resolved X-ray residual stress analysis in CVD multi-layer hard coatings on WC-substrates**	Proposal N° BESSY Instrument (MagS) **S2** Local Contact Esther Dudzik
Experimental Team:	E. Dudzik - HMI Berlin M. Klaus - HMI Berlin	Date(s) of Experiment 1. Halbj. 2005

Date of Report: Feb. 2006

Objectives

The aim of our first beamtime (BESSY.05.I. No 50) was the diffraction residual stress analysis of buried sublayers in CVD multilayer hard coatings on WC-substrates. These multilayer systems usually consist of stacks of sublayers, which are different with respect to structure and thickness. If the lattice parameters of adjacent sublayers are similar, like in the case of TiN and TiCN, a separation of the diffraction lines becomes difficult (or even impossible if using conventional lab X-ray tubes) and the obtained information on the strain state cannot assigned doubtless to the one or the other sublayer.

We therefore carried out special measurements with the objective to analyse the residual stress state in buried and adjacent TiN- and TiCN-sublayers of a CVD multilayer system. The basic idea of these investigations was to perform diffraction experiments below and above the TiKbeta absorption edge (4.9 keV). In this case, the information depth tau is mainly restricted to the upper sublayer for energies above the edge (5.5 keV), but tau is much larger for energies below the edge (4.8 keV). That way it becomes possible to separate the information coming from adjacent sublayers which are of slightly different chemical composition (Fig. 1).

Achievements

We performed diffraction experiments with monochromatic radiation at both sides of the TiKbeta absorption edge (4.9 keV). For an energy of 4.8 keV, which is below the edge, the penetration depth is considerably larger than for 5.5 keV and consequently, the signal detected in the first case includes information on both neighbouring sublayers of interest, whereas the information mainly comes from the upper sublayer in the latter case. That way we were able to achieve a separation of both sublayers with respect to the diffracted signal.

For residual stress analysis we applied the sin psi method. We used the PSI-mode of diffraction, where the diffraction spectra are recorded after stepwise sample tilt around the CHI-axis of the diffractometer. Further, we used a secondary monochromator attachment in the diffracted beam to suppress fluorescence and to minimize geometrically caused diffraction line shifts due to sample misalignment.

In both cases, i. e. for 4.8 keV- and for 5.5 keV-radiation, we yielded diffractograms which contain diffraction lines of both adjacent sublayers being of particular interest. But in contrast to the measurements performed in our lab using a conventional X-ray tube, the separation of the individual diffraction lines is much more clearly in the present case (Fig. 1). However, Fig. 1 also demonstrates, that it was not possible under the chosen experimental conditions to suppress the contribution of the adjacent bottom sublayers more or less completely.

For the measurements performed with both radiation energies, 4.8 keV and 5.5keV, residual stress analysis was possible for both sublayers of interest. Thus, the separation of the residual stress state of two neighbouring sublayers having very similar lattice parameters was possible for the first time. If we take into consideration the results obtained using synchrotron radiation and the measurements in our lab using a conventional X-ray tube (CoKa radiation, 7 keV) and analyzing different reflections hkl, we get a first idea of the residual stress depth profile concerning the upper sublayers of the multilayer system (Fig. 2).

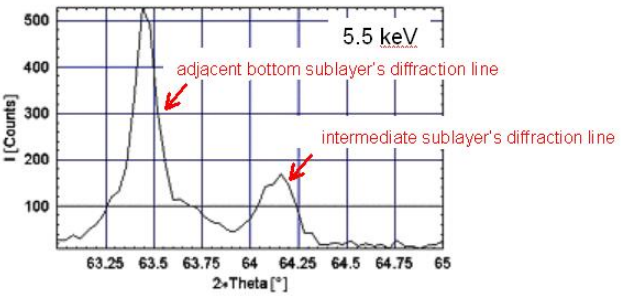

Figure 1

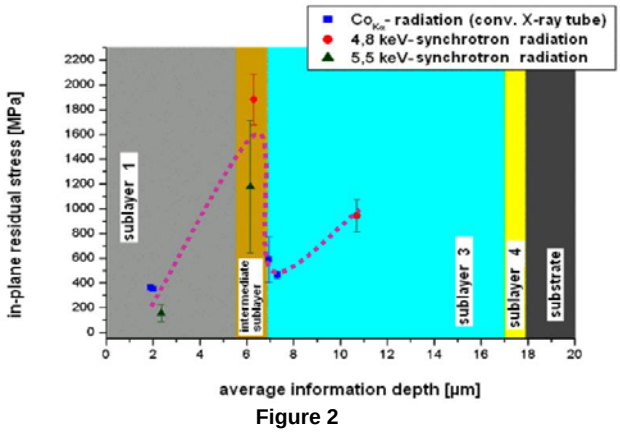

Figure 2

	EXPERIMENTAL REPORT **Depth resolved X-ray residual stress analysis in CVD multi-layer hard coatings on WC-substrates**	Proposal N° BESSY Instrument (MagS) **S2** Local Contact Esther Dudzik
Experimental Team:	E. Dudzik - HMI Berlin M. Klaus - HMI Berlin	Date(s) of Experiment 2. Halbj. 2005

Date of Report: Feb. 2006

Objectives

In a recent beamtime (first semester 2005) we concentrated on near-surface buried sublayers in a CVD multilayer stack of hard coatings which are of slightly different chemical composition. The aim of this beamtime was to investigate the residual stress state of the WC-substrates which pose as basis material for the hard coating systems.
The residual stress analysis is performed by applying the sin2psi-method which is based on a sample tilt around the Chi-axis of the diffractometer.

The use of rather hard monochromatic X-rays up to 30keV enables the access to the near interface region of the substrates. In order to get an idea of the residual stress depth distribution, we used different energies which means a discontinuous variation of the penetration depth of X-rays, whereas the stepwise variation of the angle psi between the scattering vector and the surface normal corresponds to a quasi-continuous depth profiling.

Achievements

We investigated the WC-substrates of two CVD multilayer hard coating systems. Both multilayer systems exhibit the same thicknesses and arrangement of sublayers (TiN, TiCN, Al2O3 in alternating sequence) and the same microstructure, but one system is in its as-grown state, whereas the other one was shot-peened after the deposition. Shot-peening is well-known to influence the residual stress state considerably by introducing steep compressive stress gradients. Since the total thickness of the investigated multilayer-systems was about 20µm, we were not able to get diffracted information from the WC-substrates with our low energy laboratory X-ray source [E(CoKalpha) ~ 7keV]. Hence, in our synchrotron experiments we used hard monochromatic X-rays of 20keV and 30keV, respectively. We decided to apply these two energies in order to vary the average penetration depth realised in a sin2psi-experiment, which is given by tau = [tau(psimax)+tau(psimin)]/2. Thus, first hints according to the residual stress depth distribution in the WC-substrates become available.
The results of the residual stress analysis on the WC-substrates according to both, the as-grown sample and the shot-peened sample, are represented in Fig. 1. The analysis was performed at the 101-diffraction line of WC. Although the residual stress analysis based on the sin2psi-method yields integrated information over the total irradiated volume, the information depth depends on the particular diffraction geometry and is given by the fundamental relation in residual stress/strain depth profiling [1]. In order to analyse multilayer systems, we extended this relation to a more general case, which includes the special assembly of diffracting and non-diffracting sublayers within the investigated multilayer stacks [2]. Using this extended expression the determined residual stresses can be assigned to an average information depth in the substrate (Fig. 1).
The results clearly show that despite the multilayer stack thickness of about 20µm lying on top, the shot-peening process even influences the residual stress state of the WC-substrate. In case of the as-grown sample, the tensile stresses in the layer system are balanced by rather small compressive residual stresses in the near-interface region of the WC-substrate. Shot-peening obviously leads to a significant increase of the compressive stresses. Furthermore, in both cases the stresses decrease with increasing distance from the interface.

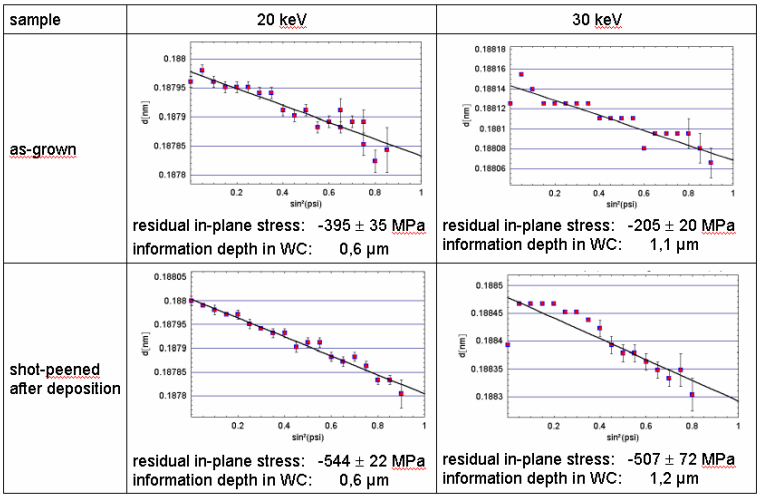

Fig. 1 *Lattice spacing d vs. sin2psi-distributions for the WC-substrate of the as-grown (top) and the shot-peened (bottom) sample measured at 20keV (left) and 30keV (right). The determined in-plane residual stresses and the respective information depths are denoted.*

References

[1] Ch. Genzel, Mat. Sci. Technol. 21 (2005), 10 - 18.
[2] M. Klaus, I. Denks, Ch. Genzel, submitted to the ECRS-7, Berlin, 13.-15.09.2006

	EXPERIMENTAL REPORT **Lock-in transition of sodium ordering in single crystal $Na_{0.48}CoO_2$**	Proposal N° BESSY Instrument (MAGS) **S2** Local Contact Ralf Feyerherm
Principal Proposer: Experimental Team:	R. Feyerherm - HMI Berlin E. Dudzik - HMI Berlin Samples: D. Argyriou, N. Aliouane - HMI Berlin	Date(s) of Experiment August 2005

Date of Report: 30.01.2006

The system Na_xCoO_2 currently arises considerable interest after it has been demonstrated that intercalation of water into samples with x = 0.35 leads to super-conductivity with a T_C of up to 5 K [1]. The aim of the present x-ray diffraction study was to investigate in detail the temperature dependence of the Na ordering in a single crystal Na_xCoO_2 with an x value close to 0.5 and to look for indications of possible charge-ordering coinciding with the magnetic ordering transitions at 52 and 87 K reported in [2].

A single crystal Na_xCoO_2 with average composition x = 0.48 was grown at HMI, and was studied by x-ray diffraction on the beamline MAGS at the 7 Tesla wiggler in the temperature range 10-550 K. A number of weak superstructure reflections were identified and studied as a function of temperature. In order to enhance possible Co^{3+}/Co^{4+} charge ordering effects, resonant scattering at the Co K-edge was involved. Our sample is a piece of a batch used simultaneously for neutron diffraction studies of the magnetic ordering.

The first central result is that there are no indications in our data for any significant structural changes around the magnetic ordering temperatures. In contrast, we unexpectedly found that $Na_{0.48}CoO_2$ exhibits a reversible transition around 225 K from a commensurate superstructure, stable below that temperature, to an incommensurate superstructure existing between 225 and 430 K (see fig. 1). The commensurate phase is consistent with the orthorhombic superstructure reported previously for polycrystalline $Na_{0.5}CoO_2$ [3], related to the original hexagonal cell by $a' = \sqrt{3}a$, $b' = 2a$, $c' = c$, i.e., a doubling of the unit cell along both basal plane axes. The incommensurate phase is a modulation of this orthorhombic cell with a modulation wave vector $\boldsymbol{q} = (0, \delta, 0)'$. The value of δ exhibits a temperature dependent variation between 0.055 and 0.11, showing a broad plateau at the latter value between 260 and 360 K. Above 430 K, the sodium ordering breaks down.

An incommensurate phase has been observed recently in electron diffraction studies after long irradiation of a $Na_{0.5}CoO_2$ sample and was discussed in terms of a regular arrangement of extra sheets of voids introduced to the Na_xCoO_2 system for $x < 0.5$ [4]. In this model, the observed plateau value of δ is consistent with x = 0.47, in close agreement with x = 0.48 measured on our sample by neutron activation analysis.

We argue that there are two possible explanations for the in-commensurate-to-commensurate phase transition observed in this phase. Below 225 K, either a phase separation into two volume fractions with x = 0.5 and x<<0.5 takes place, or the extra sheets of voids loose their regular arrangement and distribute in a random fashion in the commensurate phase. The former model would point to a surprisingly high long-range mobility of Na ions at 225 K. The latter model would imply an even more interesting transition from a disordered low-T to an ordered high-T phase, hence a structural analogue to re-entrant spin glass behaviour.

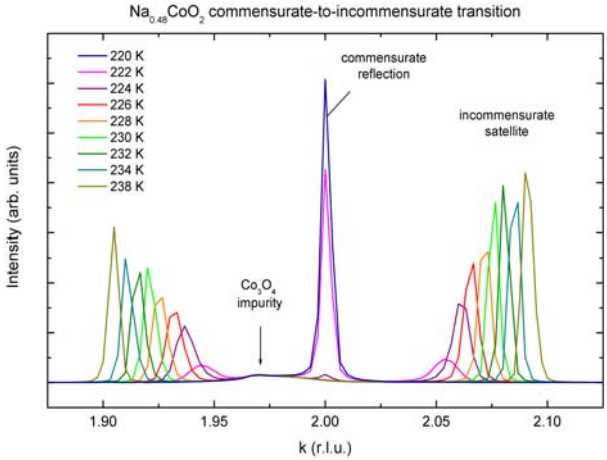

Fig. 1: Longitudinal scans along (0k0)' at various temperatures. The (020)' splits off in two satellites around 220 K marking the commensurate-to-incommensurate transition. The broad bump at k = 1.97 stems from the (220) reflection of a highly textured Co_3O_4 impurity.

References

[1] Takada *et al.*: Nature **422** (2003) 53

[2] P. Mendels *et al.*: PRL **94** (2005) 136403

[3] Huang, *et al.*, J. Phys.: Condens. Matter **16** (2004) 5803

[4] Zandbergen, *et al.*: PRB **70** (2004) 024101

	EXPERIMENTAL REPORT **Structural distortion induced by magnetic ordering in $TbMnO_3$ and $DyMnO_3$**	Proposal N° BESSY Instrument (MAGS) **S2** Local Contact Esther Dudzik
Principal Proposer: Experimental Team:	R. Feyerherm - HMI Berlin E. Dudzik - HMI Berlin Samples: D. Argyriou, N. Aliouane - HMI Berlin	Date(s) of Experiment January/July 2005

Date of Report: 31.01.2006

In orthorhombic $TbMnO_3$ the Mn spins order in an incommensurate magnetic structure below T_{Mn} = 42 K and the corresponding incommensurate magnetic propagation vector q_{Mn} = (0,0.28,0) locks below T_{lock} = 27 K . This lock-in transition is associated with a jump of the electric polarization [1]. The Tb spins also order antiferromagnetically below 7 K with a different q_{Tb} = (0,0.42,0). Similar behaviour is observed for $DyMnO_3$ for which, however, the Dy ordering is unknown yet. Here, T_{Mn} ~ 40 K and T_{lock} ~ 20 K. The goal of the present experiments was to study the lattice distortions induced by the incommensurate ordering of the Mn magnetic moments through the magnetic and the successive lock-in transition.

We have performed high-resolution diffraction experiments on single crystals of $TbMnO_3$ and $DyMnO_3$ using the beamline MAGS at x-ray energies between 8 and 14 keV. These crystals were produced and characterized at HMI. For both crystals we observed *crystallographic* superstructure reflections of type (0 2+*q*' L) with integer L. The intensity of these reflections were less than 10^{-6} of that of the neighbouring (0 2 3) standard reflection, showing that the corresponding superstructure can be hardly studied with a laboratory x-ray instrument or neutron diffraction.

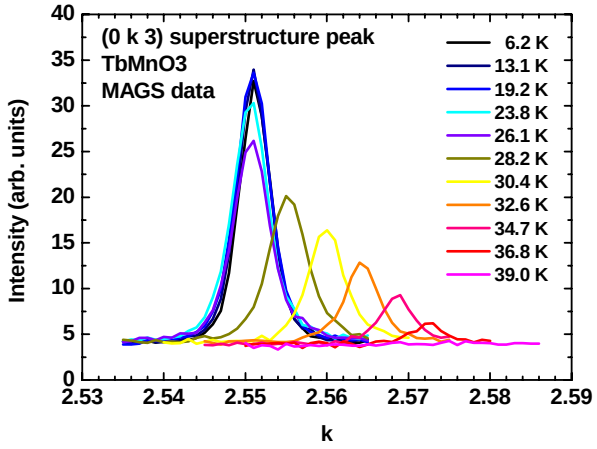

Fig. 1: *(0, 2+q', 3) superstructure reflection measured at various temperatures.*

Fig. 1 shows the (0 2 + *q*' 3) Bragg reflection observed in $TbMnO_3$ at different temperatures. Our data confirm previously published data by a Japanese group [2] but are of better resolution.

Fig. 2 shows the temperature dependence of the value of *2+q'* compared to the corresponding data for the magnetic superstructure measured by neutron diffraction at HMI. We observe the relation *q' = 2q*, which is expected if the crystallographic distortions at the magnetic ordering are due to exchange striction effects. Our experiments are the first to verify this relation in $TbMnO_3$ by two experiments *on the same crystal*. In addition, we observed that below T_{lock} the *T*-dependence of the intensity of the crystallographic superstructure reflection varies from that of the magnetic order parameter in showing a decrease below about 20 K. The origin of this behavior is unclear.

Similar measurements were carried out on $DyMnO_3$, for which no neutron diffraction results are available yet because Dy is a strong neutron absorber. Here, we observe an incommensurate value of *q*' = 0.76 below the lock-in transition temperature, consistent with previously reported results. For the first time, however, we observed a pronounced hysteresis of the lock-in transition. Comparison with the results on $TbMnO_3$ suggest that the unusual non-monotonous temperature dependence of the intensity does not directly reflect the behaviour of the magnetic ordering parameter.

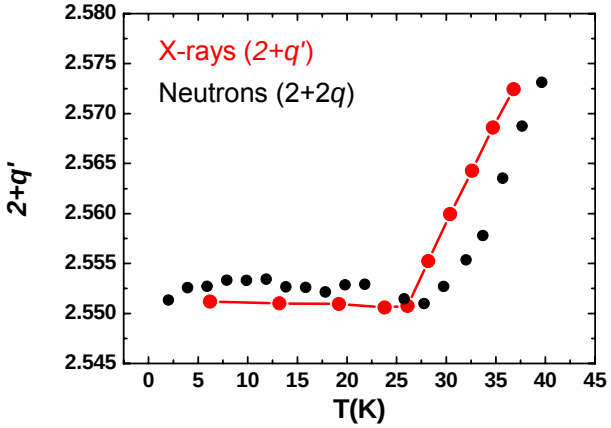

Fig. 2: *Temperature dependence of the position of the crystallographic and the magnetic superstructure reflections measured by x-ray and neutron diffraction.*

References

[1] T. Kimura *et al.*, Nature **426** (2003) 55
[2] T. Kimura *et al.*, Phys. Rev. B **68** (2003) 060403

	EXPERIMENTAL REPORT **ASAXS investigation of gold nanoparticles in glass**	Proposal N° BESSY Instrument (ASAXS) **S3** Local Contact Armin Hoell
Principal Proposer: Experimental Team:	A. Hoell - HMI Berlin I. Zizak, S. Haas, J. Banhart - HMI Berlin D. Tatchev - BAS IPC Sofia, BG M. Eichelbaum, K. Rademann - HU Berlin	Date(s) of Experiment 2005

Date of Report: Feb. 2006

Colorless glasses doped with very few Au atoms become characteristically ruby-colored after annealing because of the formation of gold colloids. The absorption of light is caused by an exitation of collective oscillations of gold valence electrons, called surface Plasmon resonance. The wavelength of the Plasmon depends on size, shape, topology and the dielectric environment of the metal clusters [1, 2]. Some years ago the nonlinear optical properties of gold nanoparticles became accessible. Therefore it is a challenge to control locally the size, and shape of gold clusters in glasses. The nucleation process of gold clusters can be activated by using synchrotron radiation [3].

Nanosized gold clusters were obtained in glasses of composition $70SiO_2$-$20Na_2O$-10CaO (mol %) which contains 0.01 mol % of dispersed Au. The gold nanoparticles were grown during annealing at 550°C up to 30 min in regions previously irradiated by 32 keV X-rays. These glasses exhibit interesting nonlinear optical properties that depend on the size and the size distribution of the nanoparticles. Therefore, the aim is to estimate the particle size distributions and their homogeneity by ASAXS.

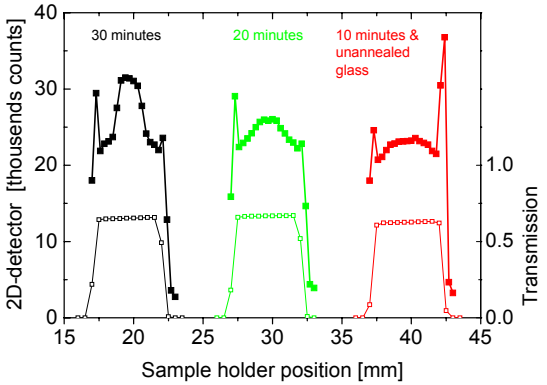

Fig. 1: After annealing for 30 min the irradiated area scatters significantly stronger than the non-irradiated and also stronger than the shorter annealed samples. In comparison the transmissions in the graphs below show no effect.

In fig. 1 the integral detector intensities of three different annealed samples are shown as the function of the sample positions. Do to the small amount of gold the transmissions of the irradiated and non irradiated regions are the same showing that the compositions are unchanged. The differences of the intensities from the irradiated and non irradiated area collected by the 2D detector suggest that the growth behavior of gold nanoparticles is faster in irradiated regions.

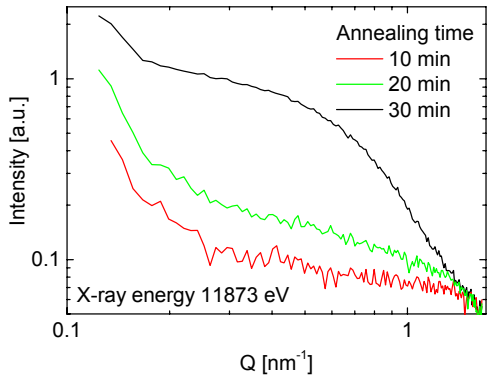

Fig. 2a: Scattering curves for samples annealed for different time periods at 550°C, measured in the pre-irradiated regions.

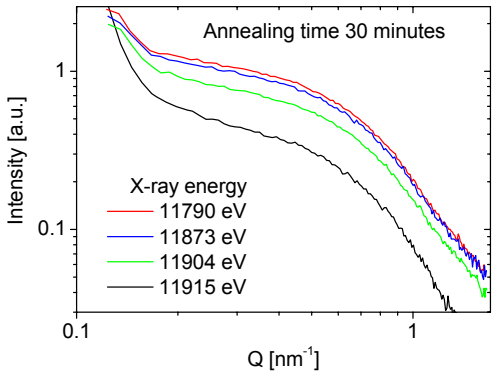

Fig. 2b: The scattering curves measured at different energies show very clear anomalous scattering effect. Ek(L_{III}) = 11919 eV

As shown in fig. 2a the intensity of the scattering at small angles increases with the annealing time, from 10 to 30 min, due to the process of nucleation and growth of gold nanoparticles.

The strong anomalous effect near the Au absorption edge, L_{III}, is presented in fig. 2b.

→

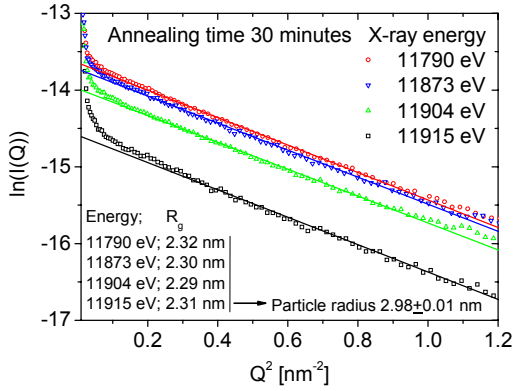

Fig. 3: The Guinier radius is independent on the x-ray energy. This means that the particles are homogeneous.

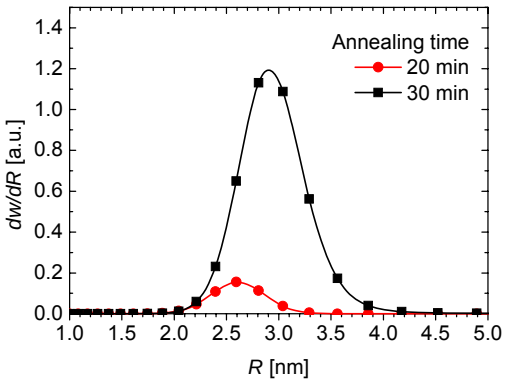

Fig. 4: Differential volume fraction size distributions obtained from the scattering curves by the maximum entropy method.

A nice outcome is depicted in fig. 3. The Guinier radius of the particles is independent of the x-ray energy. This proves that the particles are homogeneous.
After background subtraction, the scattering curves were fit with spherical particle model by the maximum entropy method.

These results represent the first anomalous small angle x-ray scattering experiment performed with the new ASAXS device installed on the 7T-WLS beamline at BESSY.

Fig. 4 shows the differential volume fraction size distributions for two annealing times. It is seen that the particle size and volume fraction grow with the annealing time.

References

[1] U. Kreibig et al.: Optical properties of Metal Clusters, Springer, Berlin, 1995, p.13
[2] R.H. Doremus et al.: J. Mat. Science **11** (1976) 903-907
[3] M. Eichelbaum et al.: Angew. Chem. Int. Ed. **44** (2005) 7905.

	EXPERIMENTAL REPORT **Energy-dispersive diffraction analysis of non-uniform near surface residual stress fields induced by mechanical surface processing - I. Evaluation of the Laplace stress profiles sigma_ij(tau)**	Proposal N° BESSY Instrument (EDDI) **S4** Local Contact Christoph Genzel
Experimental Team:	C. Genzel - HMI Berlin I. Denks - HMI Berlin	Date(s) of Experiment 1. Halbj. 2005

Date of Report: Feb. 2006

Objectives

The main goal of the beamtime was to test several measuring techniques for residual stress analysis, which have been applied so far predominantly in the angle-dispersive diffraction mode, with respect to their applicability to the energy-dispersive case of diffraction. In preliminary investigations done in our lab using a high energy tungsten X-ray tube as well as from experiments performed at HASYLAB we were able to gather first experiences in white beam residual stress analysis. However, concerning our lab investigations the photon flux and therefore, the quality of our data was rather poor. At HASYLAB, on the other hand, the beamline where we performed our measurements was not equipped with adequate slit systems necessary for collimating the diffracted beam in an appropriate way.

Therefore, the beamtime was dedicated to the following special objectives:

1. Evaluation of the optimum configuration for our secondary slit systems for sin psi-based residual stress gradient analysis.

2. Verification of results obtained previously at specially prepared test samples (shot-peened inconel and titanium alloys).

3. Enhancement of our software package EDDI for energy dispersive diffraction analysis on the basis of the collected data.

Achievements

We started the beamtime with a systematic investigation of the influence of our secondary beam optic devices on the results of a sin psi stress analysis. We were especially interested in quantifying the shifts delta_E(hkl) of diffraction lines as a function of the secondary slit aperture. From these investigations we obtained the following results:

1. A soller slit, which limits the equatorial divergence of the diffracted beam to 0.1° (which corresponds to the uncertainty of the Bragg angle theta of 0.05°), is not sufficient to limit the diffraction line shifts to an amount below about 20...30 eV, which would correspond to an uncertainty in residual stress evaluation of about 50 MPa (steel, diffraction line at 50 keV). Instead we observed line shifts up to 500 eV, which are unacceptable for residual stress measurements.

2. Using a double slit system consisting of two slits with an equatorial aperture of 100 µm and a distance from each other of 350 mm, on the other hand, we obtained much better results. In this case the total divergence reduces to about 0.03° (which means a delta_theta of 0.015°). The maximum line shifts at 100 keV we found were about 100 eV. The E(hkl) vs. sin psi-plots in all cases have a characteristic run, which we could show to be directly related to the sphere of confusion of the CHI-circle of our diffractometer.

Although the use of the narrow slits mean a considerable improvement of the geometrically caused line shifts delta_E(hkl), the result is not sufficient for residual stress analysis of an absolute scale. A reduction of the slit aperture to 50 µm led to some further improvement of the situation but at the expense of the time necessary for collecting evaluable diffraction spectra. For this reason we prepared an additional module in our MATHEMATICA program system EDDI for pre- and postprocessing of energy dispersive diffraction experiments, by means of which any stress measurement can be calibrated against corresponding measurements performed at stress-free reference samples. We tested the module by a series of measurements performed at plates prepared with W- and Au-powder and a normalized ferritic standard plate. We applied the sin psi- as well as the scattering vector method, and in both cases we obtained excellent results: The corrected "residual stress depth profiles" of the reference samples showed only very small dispersion of +/- 30 MPa about the expected value of zero.

We then used the remaining beamtime to investigate two shot-peened samples (IN 718 and Ti6242) with respect to their near surface residual stress state. The goal of these measurements was to verify the results of former investigations achieved at the beamline F1 / HASYLAB. Therefore, we chose the same geometrical diffraction conditions (2theta, step width delta_psi, psi angles for scattering vector scans) as in Hamburg. In all cases we obtained residual stress depth profiles, which agree with those evaluated in Hamburg within a scatter band of +/- 100 MPa.

	EXPERIMENTAL REPORT **Energy-dispersive diffraction analysis of non-uniform near surface residual stress fields induced by mechanical surface processing - II. Evaluation of the real space stress profiles σ_{ij} (z)**	Proposal N° BESSY Instrument (EDDI) **S4** Local Contact Christoph Genzel
Experimental Team:	C. Genzel - HMI Berlin I. Denks - HMI Berlin	Date(s) of Experiment 1. Halbj. 2005

Date of Report: Feb. 2006

Objectives

The beam time at the first semester 2005 was for testing a new method for residual stress analysis in real space. On the one hand the experimental setup had to be tried out and optimized; on the other hand, first experimental data had to be taken in order to show the new method's potential.

Besides the diffractometer itself, the main part of the experimental setup consisted of a combined sample and slit holder which allowed scanning a defined gauge volume through a bulk material.

Since a gauge volume of just a few microns is aimed, and a spatial resolution of a fraction of that, high demands are set on the slit quality and the mechanical reliability of the experimental setup, which had to be tested.

Furthermore, a main objective was to work out an adjusting procedure and a way of defining the gauge size precisely as it determines the methods high resolution.

First measurements under $\psi = 0$ were aimed to be carried out on a stress free standard material in order to verify the new method under ideal condition. Different experimental setups (as inclination angle and slit widths) had to be tested to get best results in deep sample regions (200 µm in steel).

Achievements

An adjustment procedure had been established allowing the alignment of the first and second gauge volume slits with the sample surface. Due to divergence problems a secondary guard slit had been introduced.

Total reflection had been found as one of the main problems as it spreads the gauge volume significantly leading to minor spatial resolution and causing peak position shifts. Adjustment of the primary gauge volume slits parallel to the incident beam in the range of 1°/1000 and reduction of the guard slit width was leading to significant decline of the total reflection effect.

Volume gauge sizes down to 7 µm could be created by using Kapton foil as spacer between the slits. The best way of defining the volume gauge had been worked out by scanning glass carrier with a 90 nm Au sputter layer through the volume gauge. In order to reveal total reflection effects, first experiments have been done in energy dispersive determination of the volume gauge by scanning a flat Kapton foil and differing the monitored energy ranges.

First measurements on a standard steel sample under $\psi = 0$ show that diffraction information down to 200 µm can be obtained in sufficient quality with a 13 µm depth resolution. First rotation of the sample and gauge volume has been carried out. Though it had been shown that the rotation of all optical components is possible in sufficient precision, no satisfying results could be obtained due to lack of time.

Work had been done on the effects of the peak position shifts when scanning a thin foil. This is important as it simulates a single layer in a multi layer system. It has been found that suppression of the total reflection effect can lead to the method's application on layer systems.

	EXPERIMENTAL REPORT **Locally resolved residual stress analysis in individual sublayers of CVD multilayer systems by means of energy dispersive diffraction**	Proposal N° BESSY Instrument (EDDI) **S4** Local Contact Christoph Genzel
Experimental Team:	C. Genzel - HMI Berlin I. Denks - HMI Berlin	Date(s) of Experiment 2. Halbj. 2005

Date of Report: Feb. 2006

Objectives

The aim of this beamtime was to gain access to the residual stress state within individual sublayers of CVD hard coating multilayer systems on WC-substrates. The results are needed to assess complementary investigations performed by means of the so-called Laplace space methods, which first of all yield integral information on the upper sublayers the stack consists of [1]. Therefore, we applied a new depth scanning method based on energy dispersive diffraction which is still in its development phase [2]. Its fundamental idea relies on a well-defined volume gauge. Since the individual hard coating sublayers exhibit thicknesses in the range of some microns or less, a rather narrow volume gauge has to be defined by a new sophisticated slit system which is provided at the EDDI beamline at BESSY [2].

Achievements

We investigated a hard coating system consisting of TiN-, TiCN- and Al_2O_3-sublayers in alternating sequence, each of them having a thickness between about 0.7 and 8 µm. The depth scanning was performed at a scattering angle 2 theta = 6 deg. The volume gauge was defined by narrow slits with an aperture of about 13 µm in the primary and the diffracted beam. The gauge is of rhombohedral shape with a large aspect ratio of 13 µm in height and 200 µm in width and therefore, fulfils the condition that its height does not exceed the thickness of the examined sublayer plus the total thickness of the two adjacent sublayers which are of different crystallographic structure.

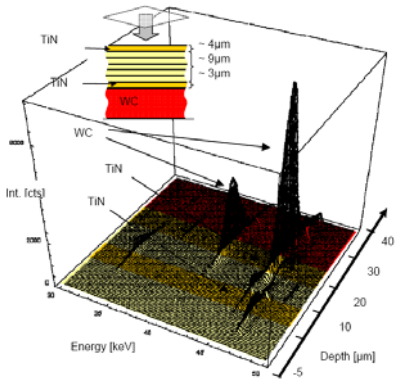

Fig. 1: *Stack plot diagram visualising the depth scan through the multilayer hard coating system including the near interface zone of the WC-substrate. The energy dispersive spectra in the range between 30 and 50 keV are shown with respect to the depth below the sample surface.*

The result of the depth scanning procedure, which was performed in very fine steps of $\Delta z = 0.5$ µm is shown in Fig. 1. The stack plot diagram clearly evidences that the experimental arrangement used for the investigations is well suited to get separate information from the individual sublayers. Thus, the depth scan mirrors the microstructure of the multilayer system.

In particular, we analysed in more detail two TiN-sublayers of the multilayer system (one at the top and one near the interface between the layer system and the substrate). They exhibit the same crystallographic structure and chemical composition, but they are separated by other sublayers of different structure and composition. Thus, the two considered sublayers contribute to the same diffraction lines, but the information coming from each of them is separated by distance between the layers, i. e. the respective diffraction lines appear at different positions z of the volume gauge.

The quantitative evaluation of the diffraction line positions allows to estimate the difference of the layer inherent residual stresses (Fig. 2). Because the height of the volume gauge is similar to the total thickness of the multilayer stack, the information stemming from the two considered TiN sublayers overlaps, but can be separated easily (upper diagram in Fig. 2). From the lower diagram in Fig. 2 it can be seen, that the diffraction line positions within one sublayer remain nearly constant, but a clear shift of about 40 eV is observed between the two layers. This difference ΔE corresponds to a lattice strain in the layer normal direction of about 0.0005 which means a difference in the in-plane residual stress of about 500 MPa.

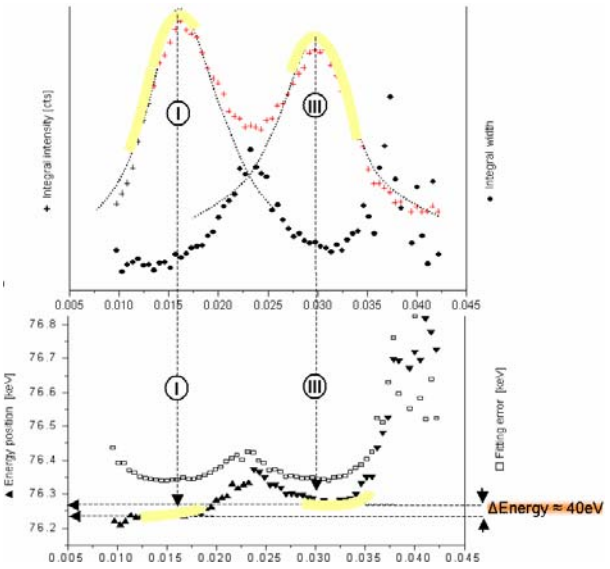

Fig. 2: *Analysis of the 220-TiN diffraction line of both, the top sublayer and the sublayer near the interface to the WC-substrate. The analysis includes the assessment of the position of the diffraction lines, their integral intensity and integral width.*

References

[1] M. Klaus, I. Denks, Ch. Genzel, submitted to the ECRS-7, Berlin, 13.-15.09.2006

[2] I. Denks, M. Klaus, Ch. Genzel, submitted to the ECRS-7, Berlin, 13.-15.09.2006

BENSC	**EXPERIMENTAL REPORT** **Improvement on stem cell cultivation in 3D artificial bone structures by pore size optimization using synchrotron tomography**	Proposal N° BESSY Instrument (Tomography) **S5** Local Contact Astrid Haibel
Principal Proposer: Experimental Team:	A. Haibel - HMI Berlin H. Freidank, J. Banhart - HMI Berlin A. Berthold, H. Schubert - TU Berlin	Date(s) of Experiment 2005

Date of Report: Feb. 2006

Stem cells are located in the umbilical cord and the bone marrow. They are responsible for the regeneration of blood and the refreshment of the body's immune system. One of the main objectives of our research in external cultured stem cells is the optimization of their ex vivo cultivation. Successful results of this project would allow for improved treatment in cancer therapies.

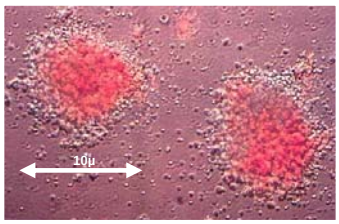

Fig. 1: Light microscopic image of bone marrow stem cells.

Aggressive chemo therapy kills not only tumour cells but also weakens the immune system at the same time. The regeneration of the immune system is only possible by the insertion of stem cells. As a result, there has been an increasing interest towards to extract stem cells of a patient before a chemo therapy, to cultivate them ex vivo and give them back in a sufficient quantity after the therapy. But the ex vivo cultivation of stem cells is difficult, because successful stem cell growth relies heavily on the cultivation environment.

The basis for a successful ex vivo cultivation of the stem cells is to find an appropriate culture medium. Ceramic foams have a similar structure than human bones. Therefore an obvious idea is to use such foams as 3D matrix for the cultivation of stem cells. The 3D porous structure of the ceramic foams would provide for a better cultivation environment than flat cell cultivation dishes [1,2]. To guarantee an adequate supply of the cells with nutrients a good penetrable, large-pored foam structure is required. For this reason, special attention is needed on the size of the pores and their interconnection.

In this project, ceramic foams are made using ceramic powder Al_2O_3 (AKP 50, Sumitomo Chemicals Co., Japan) with a purity of 99.99% and particle size between 0.1 and 0.3 µm. A chemical modified protein (bovine serum albumin) is used as foaming agent. (From the food chemistry it is known that an acetylation or a glycation of proteins with sugar yields to enhanced foaming and emulsifying properties, i.e. to an increase of the foaming ability.)
A dispersing agent (Dispex A40, Ciba Speciality Chemicals, Basel) and demineralised water are also used [3,4,5].

All components are mixed and foamed by a ball mill. The ceramic foam precursor material is then processed in a microwave or in a drying chamber alternatively. The ceramic foams are sintered in a high-temperature furnace at T = 1600°C as the last step.

Fig. 2: Ceramic foam production route. a) ball mill, b) drying chamber, c) microwave, d) high-temperature furnace

The three-dimensional investigation of the foamed ceramic samples were carried out using high-resolution synchrotron radiation tomography at the synchrotron BESSY in Berlin. Absorption tomography is based on the detection of radiation attenuated by the samples for many different angular positions (see fig. 3). After passing through the samples, the monochromatic X-rays (E = 25 keV) were converted to visible light using a Gd2O2S scintillator. The optically magnified images (image voxel size 3.6 µm) were then captured by a 2048 2048 pixel CCD camera. Depending on the required spatial resolution, up to 2400 radiographic images are needed. This results in a set of projections which are used for reconstructing a complete 3D image representing the local X-ray attenuation coefficients in the sample [6].

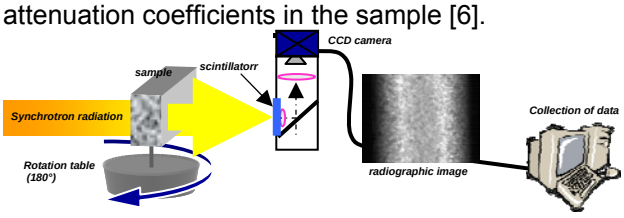

Fig. 3: Sketch of the tomographic setup.

Resulting images are displayed in fig. 4. The foams illustrated in fig 4 were prepared in four different ways. Only the original components were used in foam (a). The precursor material was processed by micro wave radiation before sintering. Here the mean pore size and the interconnections are much smaller compared to the other foams. For the foam in fig. 4(b), a dispersing agent was added →

in the precursor material. The effect is a broader pore size distribution, but the interconnections are still small. By using a glycated protein for foaming (see fig. 4c), the mean pore size is larger as in the case of foam (a) and (b) and the interconnections of the pores are increased. The foam displayed in fig. 4(d) was also prepared with glycated protein but additionally processed in a drying chamber instead of a micro wave. In that case, the mean pore size is increased too and the pore interconnections are very large.

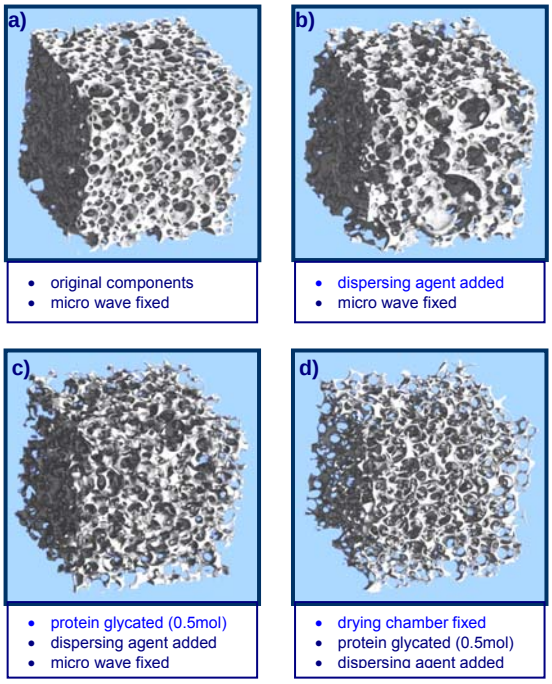

Fig. 4: Ceramic foam structure after the sintering process for four different prepared samples, edge-length: 1.44 mm
a) Only the original components were used.
b) A dispersing agent was added to the original components.
c) Furthermore the protein was modified by glycation with sugars.
d) The foam precursor material was processed in a drying chamber.

For a quantitative 3D image analysis of the tomographic images the pores were identified and separated into Boolean images by using appropriate grey scale thresholds. Two transformations (Euclidean distance transformation and Watershed transformation) in an image analysis software were used to process the image. The interconnected pores were separated (see fig. 5) and the pore size distributions and pore shapes were analysed.

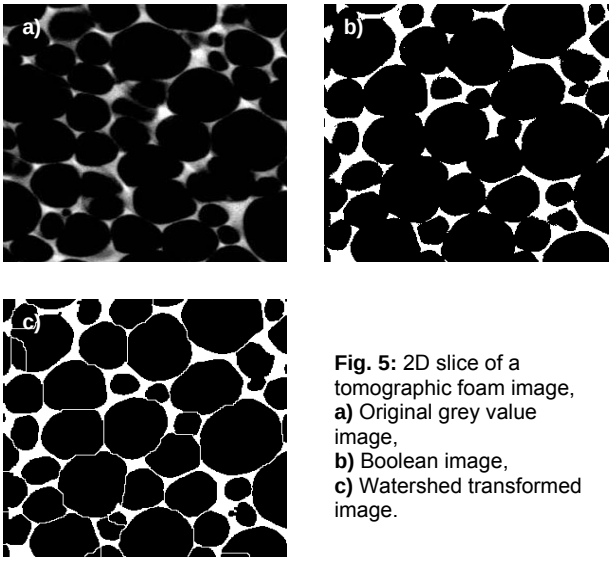

Fig. 5: 2D slice of a tomographic foam image,
a) Original grey value image,
b) Boolean image,
c) Watershed transformed image.

The quantitative pore size analysis is plotted in fig. 6. The qualitative results of fig. 4 are confirmed. By preparing the samples using a dispersing agent and chemical modified proteins as well as by sample processing in the drying chamber the mean pore size, the pore size distribution and the porosity increase whereas the number of pores decreases.

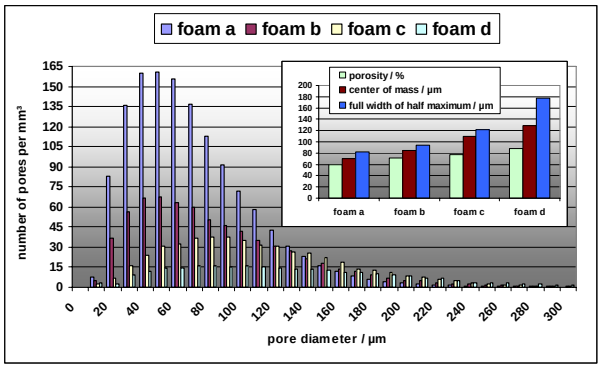

Fig. 6: Pore size distribution of the four ceramic foams in fig. 4. In the cut-out the porosity, the center of mass and the full width of half maximum for the four foams are plotted.

Based on these results, we will be able now, to adapt the ceramic foam shape and pore size individually at the requirements of each specific stem cell line by varying the processing parameter (microwave or drying chamber), by modifying the protein and/or by using dispersing agents [7]. The appropriateness of the new tailored substrate material will be proofed in cultivation experiments, now.

References:

[1] N. Banu et al.: Cytokine, **13** (2001), 349

[2] J. Bagely et al.: Exp. Hematol., **27** (1999), 496

[3] I. Garrn et al.: J. Eur. Ceram. Soc. **24** (2004), 579

[4] K.L. Franzen et al.: J. Agric. Food Chem. **24** (1976), 788

[5] A. Baniel et al.: J. Agric. Food Chem. **40** (1992), 200

[6] A.C. Kak et al.: Principals of Computerized Tomographic Imaging, IEEE Press, New York, 1987

[7] A. Berthold et al.: J. Mat. Sci.: Mat. Med., submitted

	EXPERIMENTAL REPORT **High-resolution tomography investigations of micro-cracks in hard rocks**	Proposal N° BESSY Instrument (Tomography) **S5** Local Contact Astrid Haibel
Principal Proposer: Experimental Team:	K. Thermann - TU Berlin B. Kremmin - TU Berlin S. Zabler - HMI Berlin I. Manke, J. Tiedemann - TU Berlin	Date(s) of Experiment 2005

Date of Report: Feb. 2006

To investigate fracture propagation in hard rocks in response to applied loads it is essential to know the existence and orientation of pre-existent microcracks. Because nucleation, growth and interaction of microcracks are considered to be the dominant, controlling mechanisms of macroscopic failure. Nevertheless, grain boundaries, low-aspect ratio cavities or interfaces of two different minerals can also function as stress concentrators and be responsible for crack initiation. In former publications, transparent materials (resin, glass, PMMA) or rock type materials (gypsum, cements, mortar) that simulate brittle failure of rock were investigated to study the different influences and their interaction [2, 3, 4, 5, 6]. Synchrotron tomography at BESSY provides the possibility to investigate microscopic features of natural rock samples.

Two different types of sedimentary rocks were investigated. A Carboniferous greywacke as a clastic sedimentary rock and a Triassic limestone as a chemical sedimentary rock. Whereas limestone is composed mainly of the mineral calcite ($CaCO_3$) a greywacke consists of angular grains of quartz, feldspar, and small rock fragments (e.g. quartzite, slate, various schists, or gneiss) set in a compact, clay-fine matrix. Because of the large sample height of 10 mm three vertical sections were measured. After the reconstruction the sections were merged to a complete tomogram of the sample on which the analysis was finally done. Rock samples loaded to different stress stages were investigated. A noticeable crack initiation was not observed until the loading stage at approximately 90 % of the uniaxial compressive strength of the particular material.

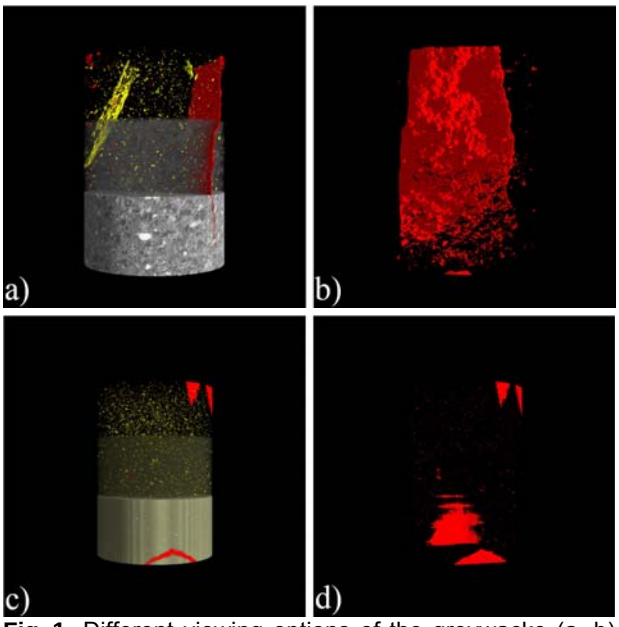

Fig. 1: Different viewing options of the greywacke (a, b) and the limestone sample (c,d)

In fig. 1 voids (pores, cavities, cracks) are coloured red whereas high absorbing particles have a yellow colour. In the greywacke tomogram (fig. 1a) a quartzite healed fracture (yellow) can be seen. The new propagated crack has nearly the same orientation as the healed crack. The high absorbing phase in the limestone sample (fig. 1c) is pyrite (FeS_2). As a result of limiting resolution these cubic minerals appear spherical in the tomogram. In fig. 1(b) the fracture process zone in front of the crack tip can be seen.

According to the site of origin microcracks can be subdivided into grain boundary cracks, intragranular cracks and inter- or transgranular cracks but often an unambiguous classification is not possible. Hence, crack type labels also depend to some extent on the resolution of the observation [6]. Concerning crack tip displacement three basic modes exist: mode I - tensile, mode II - in-plane shear and mode III - anti-plane shear [1].

→

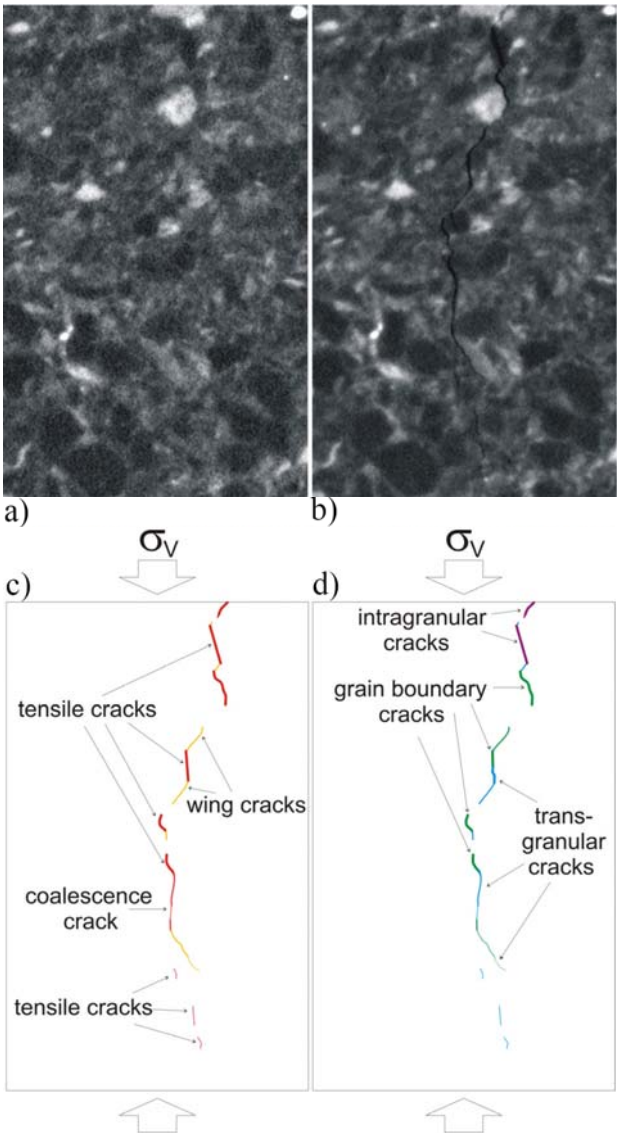

Fig. 2: Section of the unloaded (a) and loaded (b) sample and sketches of the propagated cracks (c and d)

In fig. 2 a section of the unloaded (a) and loaded sample (b) is shown. In fig. 2(c) the cracks were characterized according to their type of mode whereas in fig. 2(d) the location was analyzed. As is shown in fig. 2, first tensile or mode I cracks at grain boundaries are generated. In the upper part of fig. 2(b) can be seen that intragranular crack initiation is possible, too.

The tensile cracks are oriented sub-parallel to the loading direction. At the tips of these cracks were wing cracks initiated. These wing cracks start at the tips of the pre-existing cracks and propagate in a curvilinear path as the load is increased. According to [2] wing cracks grow in a stable manner since an increase in load is necessary to lengthen the cracks, and align with the direction of the most compressive load. In fig. 2 can also be observed that crack coalescence occurred when cracks (grain boundary, intragranular or transgranular) were sufficiently close to each other.

In a next step the crack in the greywacke sample (fig. 1b) was precisely analyzed. At first the crack was separated from the sample and the geometrical parameters were determined. A plane was fitted to the crack to investigate the orientation (dip direction, dip angle) of the crack. The distance of each crack voxel to the plane can be calculated and so information about the crack surface roughness can be gained.

Further investigations on a larger number of samples are needed to specify the results and to accomplish a statistical assessment.

References

[1] Atkinson, B.K.: *Fracture mechanics of rock* Academic Press, London, (1987)

[2] Bobet, A. et al.: Int. J. Rock Mech. Min. Sci. **35**, 7, 863-888, (1998)

[3] Dyskin, A.V. et al.: Engineering Fracture Mechanics **70**, 2115-2136, (2003)

[3] Hoek, E. et al.: Int. J. Fract. Mech. **1**, 137-155, (1965)

[5] Horii, H. et al.: Journal of Geophysical Research **90**, B4, 3105-3125, (1985)

[6] Kranz, R.K.: Tectonophysics **100**, 449-480, (1983)

[7] Landis, E.N. et al.: Engineering Fracture Mechanics **70**, 911-925, (2003)

Part II

LIST OF PUBLICATIONS

Theses	196
Papers	197
Conference Contributions, Seminar Talks and Posters	207
Contributions to the BENSC Users' Meeting 2005	220

Theses 2005
Examina

PhD-theses

2004 (supplement)

Gilles, R.: **Das neue Strukturpulverdiffraktometer SPODI an der Neutronenquelle des FRM-II sowie Untersuchungen an Nickel-Basis Superlegierungen mit den Methoden der Neutronen-, der Röntgen-, der Synchrotronstreuung und der Elektronenmikroskopie** Habilitationsschrift (2004) 1 - 228	E9

2005

Christensen, N.B.: **Neutron scattering studies of two-dimensional antiferromagnetic spin fluctuations in insulating and superconducting S = ½ systems (PhD thesis)** University of Copenhagen, 2005	V2 IHP I: 232 IHP I: 233 IHP I: 317
Gäbler, F.: **Die quaternären Systeme Ba-Sr-E-N(O) mit E = Bi, Sb: Zur Strukturvielfalt von inversen Perowskit-Varianten (diploma)** TU Dresden, 2005	E6 / E9
Glavatskyy I.: **Temperature dependence and time stability of the magnetic field induced strains in Ni-Mn-Ga alloys** Ph.D. Theses (2005) 1 - 131	E1 / E2
Loosvelt, H.: Dr. (PhD thesis) K.U. Leuven, 2005	V6 IHP II: 499 IHP II: 546 NMI3: 1005
Rüegg, Ch.: **Neutron Scattering Investigation of Quantum Phase Transitions in the Dimer Spin Systems $TlCuCl_3$ and NH_4CuCl_3 (PhD thesis)** ETH Zurich, 2005	V2 IHP II: 543 NMI3: 1006
Thielemann, B.: **Spin Dynamics of (C5H12N)2CuBr4 (diploma)** ETH Zurich, 2005	V2 NMI3: 1127
Vaccaro, M.: **COLLOIDAL PARTICLES AS DIAGNOSTIC TOOLS IN MRI** (diploma) Università di Napoli "Federico II", 2005	V4 NMI3: 1107
Wawrzynska E.: **Magnetic structures of $R_3T_4X_4$ compounds (PhD thesis)** Jagiellonian University, 2005	E6 IHP II: 466 IHP II: 519 IHP II: 578 NMI3: 1027

Publications 2005
BENSC Experiments and BENSC Authors

2001 (supplement)	
Weissmüller, J.; Michels, A.; Barker, J.G.; Wiedenmann, A.; Erb, U.; Shull, R.D.: **Analysis of the small-angle neutron scattering of nanocrystalline ferromagnets using a micromagnetics model** Physical Review B: Condensed Matter **63** (2001), 214414	V4
2003 (supplement)	
Recko, K.; Dobrzynski, L.; Szymanski, K.; Satula, D.; Perzynska, K.; Biernacka, M.; Waliszewski, J.; Zaleski, P.; Suski, W.; Wochowski, K.; Hofmann, M.; Hohlwein, D.: **Magnetic properties of $ThFe_xAl_{12-x}$ alloys** phys.stat.sol.(a) **196**, No. 1, 344–347 (2003)	
2004 (supplement)	
Carriere, D.; Krastev, R.; Schönhoff, M.: **Oscillations in Solvent Fraction of Polyelectrolyte Multilayers Driven by the Charge of the Terminating Layer** Langmuir **20** (2004), 11465-11472	V6
Genzel, C.; Stock, C.; Reimers, W.: **Application of energy-dispersive diffraction to the analysis of multiaxial residual stress fields in the intermediate zone between surface and volume** Materials Science and Engineering A **372** (2004), 28-43	ETA
Genzel, C.: **Diffraction Stress Analysis in Thin Films and Coatings - Problems, Methods and Perspectives** Journal of Neutron Research **12** (2004), 233-241	ETA
Gilles, R.; Mukherji, D.; Hoelzel, M.; Strunz, P.; Barbier, B.; Toebbens, D.M.: **Scattering methods to investigate nano-sized precipitates extracted from Ni-base** Proceedings of the 7th International Conference on Nanostructured Materials (2004), 208f	E9
Glinel, K.; Prevot, M.; Krustev, R.; Sukhorukov, G.; Jonas, A.; Möhwald, H.: **Control of the Water Permeability of Polyelectrolyte Multilayers by Deposition of Charged Paraffin Particles** Langmuir **20** (2004), 4898-4902	V6
Gupta, M.; Gutberlet, T.; Stahn, J.; Keller, P.; Clemens, D.: **AMOR - the time-of-flight neutron refelctometer at SINQ/PSI** PRAMANA - journal of physics **63** (2004), 57-63	
Kardjilov, N.; Lee, S. W.; Lehmann, E.; Lim, I. C.; Steichele, E.; Sim, C. M.; Vontobel, P: **Applied phase-contrast radiography with polychromatic thermal neutrons** Key Engineering Materials **270-273** (2004), 1330-1336	
Kavecansky, V.; Matas, S.; Mihalik, M.; Mitroova, Z.; Lukacova, M.: **Neutron diffraction study of crystal and magnetic structure of $Dy[Fe(CN)_6].4D_2O$** Czechoslovak Journal of Physics **54** (2004) D571 – D574	E6 IHP II 468 E9

Publications 2005
BENSC Experiments and BENSC Authors

Ono, T.; Tanaka, H.; Kolomiyets, O.; Mitamura, H.; Goto, T.; Nakajimy, K.; Oosawa, A.; Koike, Y.; Kakurai, K.; Klenke, J.; Smeibidl, P.; Meißner, M.: **Magnetization plateaux of the S = ½ two-dimensional frustrated antiferromegnet Cs_2CuBr_4** Journal of Physics: Condensed Matter **16** (2004), S773-S778	E1
Simonsen, A.C.; Hansen, P.L.; Klösgen, B.: **Nanobubbles give evidence of incomplete wetting at a hydrophobic interface** Journal of Colloid and Interface Science **273** (2004), 291-299	V6

2005

Abbas, S.; Wagh, A.G.: **Neutron Deflection by a Perfect Crystal Prism** Sol. St. Phys. (India) **50** (2005), 317-318	V12b
Aliouane, N.; Argyriou, D.N.; Strempfer, J.; Zegkinoglou, I.; Landsgesell, S.; Zimmermann, M.v.: **Field induced linear magneto-elastic coupling in multiferroic $TbMnO_3$** Physical Review B: Condensed Matter **73** (2005), 020102-1-020102-4	V2
Appavou, M.-S.; Gibrat, G.; Bellissent-Funel, M.-C.; Plazanet, M.; Pieper, J.; Buchsteiner, A.; Annighöfer, B.: **The influence of a medium pressure on the structure and dynamics of a bovine pancreatic trypsin inhibitor protein** Journal of Physics: Condensed Matter **17** (2005), S3093-S3099	V3 NMI3 1013
Argyriou, D.N.; Radaelli, P.G.; Milne, C.J.; Aliouane, N.; Chapon, L.C.; Chemseddine, A.; Veira, J.; Cox, S.; Mathur, N.D.; Midgley, P.A.: **Crystal structure of the superconducting layered cobaltate $Na_xCoO_2*yD_2O$** Journal of Physics: Condensed Matter **17** (2005), 3293-3304	E9
Auffermann, G.; Bronger, W.; Müller, P.; Roth, G.; Schilder, H.; Sommer, T.: **Cs_3OsH_9; Synthese, Struktur und magnetische Eigenschaften** Zeitschrift für Anorganische Allgemeine Chemie **631** (2005) 1060 - 1064	E6 E9
Baran, S.; Gondek, L.; Hernandez-Velasco, J.; Kaczorowski, D.; Szytula, A.: **Magnetic ordering in $HoFe_{0.33}Ge_2$** Journal of Magnetism and Magnetic Materials **285** (2005), 188 - 192	E6 NMI3 1026
Bastürk, M.; Arztmann, J.; Jerlich, W.; Kardjilov, N.; Lehmann, E.; Zawisky, M.: **Analysis of neutron attenuation in boron-alloyed stainless steel with neutron radiography and JEN-3 gauge** Journal of Nuclear Materials **341** (2005), 189-200	
Bastürk, M.; Kardjilov, N.; Lehmann, E.; Zawisky, M.: **Monte Carlo simulation of neutron transmission of boron-alloyed steel** IEEE Transactions on Nuclear Science **52** (2005), 394-399	
Bastürk, M.; Kardjilov, N.; Rauch, H.; Vontobel, P.: **Neutron imaging of fiber-reinforced materials** Nuclear Instruments and Methods in Physics Research Section A **542** (2005), 106-115	
Beutier, G.; van der Laan, G.; Chesnel, K.; Marty, A.; Belakhovsky, M.; Collins, S.P.; Dudzik, E.; Toussaint, J.-C.; Gilles, B.: **Characterization of FePd bilayers and trilayers using soft x-ray resonant magnetic scattering and micromagnetic modeling** Physical Review B: Condensed Matter **71** (2005), 184436/1-12	
Bowers, J.; Zarbakhsh, A.; Christenson, H.K.; McLure, I.A.; Webster, J.R.P.; Steitz, R.: **Neutron reflectivity studies of critical adsorption: behaviour of the surface scaling function** Physical Review E **72** (2005), 041606/1-7	V6 NMI3 1036

Publications 2005
BENSC Experiments and BENSC Authors

Bucherl, T.; Kardjilov, N.; von Gostomski, C.L.; Calzada, E.: **Performance studies of a mobile neutron source based on the SbBe reaction** IEEE Transactions on Nuclear Science **52** (2005), 342-345	
Carelli, C.; Jones, R.A.L.; Young, R.N.; Cubitt, R.; Krastev, R.; Gutberlet, T.; Dalgliesh, R.; Schmid F.; Sferrazza, M.: **The effects of long-ranged and short-ranged forces in confined near-critical polymeric liquids** Europhysics Letters **71** (2005), 763-769	V6 IHP II 524
Chemnitzer, R.; Auffermann, G.; Többens, D.M.; Kniep, R.: **$(Sr_2N)H$: Untersuchungen zur Redox-Intercalation von Wasserstoff in Sr_2N** Zeitschrift für Anorganische Allgemeine Chemie **631** (2005) 1813 – 1817	E9
Christianson, A.D.; Llobet, A.; Bao, W.; Gardner, J.S.; Swainson, I.P.; Lynn, J.W.; Mignot, J.-M.; Prokes, K.; Pagliuso, P.G.; Moreno, N.O.; Sarrao, J.L.; Thompson, J.D.; Lacerda, A.H.: **Novel Coexistence of Superconductivity with Two Distinct Magnetic Orders** Physical Review Letters **95** (2005), 217002	E4
Cousin, F.; Gummel, J.; Ung, D.; Boué, F.: **Polyelectrolyte-Protein Complexes: Structure and Conformation of Each Specie Revealed by SANS** Langmuir **21**, (2005) 9675-9688	V4 NMI3 1018
Delajon, C.; Gutberlet, T.; Steitz, R.; Möhwald, H.; Krastev, R.: **Formation of Polyelectrolyte Multilayer Architectures with Embedded DMPC Studied in Situ by Neutron Reflectometry** Langmuir **21** (2005) 8509 - 8514	V6 NMI3 1020
Dennison, S.R.; Dante, S.; Hauß, T.; Brandenburg, K.; Harris, F.; Phoenix, D.A.: **Investigation into the Membrane Interaction of m-Calpain Domain V** Biophysical Journal **88** (2005), 3008-3017	V1
Eschricht, N.; Hoinkis, E.; Mädler, F.; Schubert-Bischoff, P.; Röhl-Kuhn, B.: **Knowledge-based reconstruction of random porous media** Journal of Colloid and Interface Science **291** (2005) 201-213	V4
Faulhaber, E.; Stockert, O.; Jeevan, H.S.; Prokes, K.; Deppe, M.; Geibel, C.; Steglich F.; Loewenhaupt, M.: **Magnetic field dependence of the magnetic order in A-type $CeCu_2Si_2$** Physica B - condensed matter **359-361** (2005), 357-359	E4
Frey, F.; Boysen, H.; Kaiser-Bischoff, I.: **Diffuse scattering and disorder in zirconia** Z. Kristallogr. **220** (2005) 1017–1026	
Gäbler, F.; Kirchner, M.; Schnelle, W.; Schmitt, M.; Rosner, H.; Niewa, R.: **$(Sr_3N_x)E$ and $(Ba_3N_x)E$ (E = Sn, Pb): Preparation, Crystal Structures, Physical Properties and Electronic Structures** Zeitschrift für Anorganische Allgemeine Chemie **631** (2005) 397 – 402	E9
Genzel, C.: **X-ray residual stress analysis in thin films under grazing incidence - basic aspects and applications** Materials Science and Technology **21** (2005), 10-18	ETA
Genzel, C.; Klaus, M.; Denks, I.; Wulz, H.G.: **Residual stress fields in surface-treated silicon carbide for space industry--comparison of biaxial and triaxial analysis using different X-ray methods** Materials Science and Engineering A **390** (2005), 376-384	ETA
Gil, A.; Penc, B.; Hernández-Velasco, J.; Wawrzynska, E.; Szytula, A.: **Low temperature neutron diffraction data for $CeCo_{0.86}Ge_2$** Journal of Alloys and Compounds **387** (2005), L8 - L10	E6 NMI3 1027 IHP II 466 IHP II 519

Publications 2005
BENSC Experiments and BENSC Authors

Gilles, R.: **Neutrons scattering , a powerful tool in material science exemplary on superalloys** Zeitschrift für Metallkunde **96** (2005), 325-334	E9
Gjoka, M.; Mergia, K.; Niarchos, D.: **Neutron diffraction study of the rare earth-Fe-Co-V intermetallic compounds** Proceedings of the XXI Greek Conference on Solid State Physics and Material Science (2005), 100	E9 NMI3 1054
Gondek, L.; Baran, S.; Szytula, A.; Kaczorowski, D.; Hernández-Velasco, J.: **Crystal and Magnetic structures of RPdIn (R = Nd, Ho, Er) compounds** Journal of Magnetism and Magnetic Materials **285** (2005), 272 - 278	E6 NMI3: 1026
Gopinadhan, M.; Ahrens, H.; Günther, J.-U.; Steitz, R.; Helm C.A.: **Approaching the precipitation temperature of the deposition solution and the effects on the internal order of polyelectrolyte multilayers** Macromolecules **38** (2005) 5228 - 5235	V6
Graubner, V.-M.; Clemens, D.; Gutberlet, T.; Kötz, R.; Lippert, T.; Nuyken, O.; Schnyder, B.; Wokaun, A.: **Neutron reflectometry and spectroscopic ellipsometry studies of cross-linked poly(dimethylsiloxane) after irradiation at 172 nm** Langmuir **21** (2005), 8940-8946	
Hagiwara, M.; Regnault, L.P.; Zheludev, A.; Stunault, A.; Metoki, N.; Suzuki, T.; Suga, S.; Kakurai, K.; Koike, Y.; Vorderwisch, P.; Chung, J.-H.: **Spin excitations in an anisotropic bond-alternating quantum S=1 chain in a magnetic field: contrast to Haldane spin chains** Physical Review Letters **94** (2005), 177202/1-4	V2
Handstein, A.; Rößler, U.K.; Idzikowski, B.; Kozlova, N.; Nenkov, K.; Müller, K.-H.; Kreyssig, A.; Loewenhaupt, M.; Heinemann, A.; Hoell, A.; Stüßer, N.: **Change of magnetoresistivity and magnetic structure of $MnAu_2$ by iron substitution** Journal of Magnetism and Magnetic Materials **290-291** (2005), 1093-1096	E6 V4
Hauß, T.; Dante, S.; Haines, T.H.; Dencher N.A.: **Localization of coenzyme Q_{10} in the center of a deuterated lipid membrane by neutron diffraction** Biochimica et Biophysica Acta: Bioenergetics **1710** (2005), 57-62	V1
Heinemann, A.; A. Wiedenmann: **Insight into the formation of partially ordered structures in Co-Ferrofluids** Journal of Magnetism and Magnetic Materials **289** (2005), 149-151	V4
Hoell, A.; Haibel, A.; Goerigk, G.: **Early stages of metal foam formation studied by ASAXS** HASYLAB Annual Report 2004 (2005), 199-200	S3
Hoell, A.; Kranold, R.; Goerigk, G.; Komatsu, T.; Müller, R.: **Nanocrystallization of $25K_2O$-$25Nb_2O_5$-$50GeO_2$ glass studied by SAXS/ASAXS** HASYLAB Annual Report 2004 (2005), 309-310	S3
Hoinkis, E.; Röhl-Kuhn, B.: **Application of Percolation Theory to the Drainage of Liquid Nitrogen from Mesoporous Silica Xerogel Gelsil 50** Langmuir **21**, (2005) 7366-7372	V4
Hutanu, V.; Rupp, A.: **Research on 3He spin filter cells made of quartz glass** Physica B **356** (2005) 91 - 95	E1
Imperia, P.; Schmitz, D.; Maletta, H.; Sobal, N.S.; Giersig M.: **Effect of Ar^+ and H^+ etching on the magnetic properties of Co/CoO core-shell nanoparticles** Physical Review B: Condensed Matter **72** (2005), 014448/1-7	S1
Jackler, G.; Czeslik, C.; Steitz, R.; Royer, C. A.: **Spatial distribution of protein molecules adsorbed at a polyelectrolyte multilayer** Physical Review E **71** (2005) 041912	V6

Publications 2005
BENSC Experiments and BENSC Authors

Jauch, W.; Reehuis, M.: **Electron-density distribution in cubic $SrTiO_3$: a comparative gamma-ray diffraction study** Acta Crystallographica Section A: Foundations of Crystallography **61** (2005), 411-417	
Kaiser-Bischoff, I.; Boysen, H.; Frey, F.; Hoffmann, J.-U.; Hohlwein, D.; Lerch, M.: **The defect Structure of Y- and N-doped zirconia** Journal of Applied Crystallography **38** (2005) 139 - 146	E2
Kamarad, J.; Prokhnenko, O.; Prokes, K.; Arnold, Z.: **Magnetization and neutron diffraction studies of Lu_2Fe_{17} under high pressure** Journal of Physics: Condensed Matter **17** (2005) S3069 - S3075	E4 IHP II 447 IHP II 549 NMI3 1085
Kang, AH.J.; PengchengDai; Mook, H.A.; Argyriou, D.N.; Sikolenko, V.; Lynn, J.W.; Kurita, Y.; Komiya, S.; Ando, Y.: **Electronically competing phases and their magnetic field dependence in electron-doped nonsuperconducting and superconducting $Pr_{0.88}LaCe_{0.12}CuO_4$** Physical Review B: Condensed Matter **71** (2005) 214512-1 - 214512-17	E4 E1
Kardjilov, N.; Böni, P.; Hilger, A.; Strobl, M.; Treimer, W.: **Characterization of a focusing parabolic guide using neutron radiography method** Nuclear Instruments and Methods in Physics Research Section A **542** (2005), 248-252	V12b
Kardjilov, N.; de Beer, F.; Hassanein, R.; Lehmann, E.; Vontobel, P.: **Scattering corrections in neutron radiography using point scattered functions** Nuclear Instruments and Methods in Physics Research Section A **542** (2005), 336-341	
Kardjilov, N.; Hilger, A.; Manke, I.; Strobl, M.; Treimer, W.; Banhart, J.: **Industrial applications at the new cold neutron radiography and tomography facility of the HMI** Nuclear Instruments and Methods in Physics Research Section A **542** (2005), 16-21	V7
Kardjilov, N.; Lee, S.W.; Lehmann, E.; Lim, I.C.; Sim, C.M.; Vontobel, P.: **Improving the image contrast and resolution in the phase-contrast neutron radiography** Nuclear Instruments and Methods in Physics Research Section A **542** (2005), 100-105	V7
Karpinsky, D. V.; Troyanchuk, I. O.; Barner, K.; Szymczak, H.; Tovar, M.: **Crystal structure and magnetic ordering of the $LaCo_{1-x}Fe_xO_3$ system** Journal of Physics: Condensed Matter **17** (2005) 7219 - 7226	E9 NMI3 1110
Khaykovich, B.; Wakimoto, S.; Birgeneau, R.J.; Kastner, M.A.; Lee, Y.S.; Smeibidl, P.; Vorderwisch, P.; Yamada, K.: **Field-induced transition between magnetically disordered and ordered phases in underdoped $La_{2-x}Sr_xCuO_4$** Physical Review B: Condensed Matter **71** (2005), 220508/1-4	V2
Kirchner, M.; Schnelle, W.; Wagner, F.R.; Kniep, R.; Niewa, R.: **$(A_{19}N_7)[In_4]_2$ (A = Ca, Sr) and $(Ca_4N)[In_2]$: Synthesis, Crystal Structures, Physical Properties and Chemical Bonding** Zeitschrift für Anorganische Allgemeine Chemie **631** (2005) 1477	E9
Kiselev, M.A.; Zbytovska, J.; Matveev, D.; Wartewig, S.; Gapienko, I.V.; Perez, J.; Lesieur, P.; Hoell, A.; Neubert, R.: **Influence of trehalose on the structure of unilamellar DMPC vesicles** Colloids and Surfaces A: Physicochemical and Engineering Aspects **256** (2005), 1-7	V4
Kiselev, M.A.; Gutberlet, T.; Lesieur, P.; Hauß, T.; Ollivon, M.; Neubert, R.H.H.: **Properties of ternary phospholipid/dimethyl sulfoxide/water systems at low temperatures** Chemistry and Physics of Lipids **133** (2005) 181 - 193	V1
Kiselev, M.A.; Ryabova N.Y.; Balagurov, A.M.; Dante, S.; Hauß, T.; Zbytovska, J.; Wartewig, S.; Neubert, R.H.: **New insights into the structure and hydration of a stratum corneum lipid model membrane by neutron diffraction** European BiophysicsJournal **34** (2005), 1030-1040	V1

Publications 2005
BENSC Experiments and BENSC Authors

Köbler, U.; Hoser, A.; Bos, J.; Schäfer, W.; Pohlmann, L.: **Weak ferromagnets with integer and half-integer spin quantum numbers** Physica B **355** (2005), 90 - 99	E6
Köbler, U.; Hoser, A.: **Stable magnetic universality classes for T-> 0** Physica B - condensed matter **362** (2005), 295-305	E1
Koteski, V.; Haas, H.; Holub-Krappe, E.; Ivanovic, N.; Mahnke, H.-E.: **Lattice relaxation around arsenic and selenium in CdTe** Physica Scripta **T115** (2005), 369-371	
Kreitlow, J.; Menzel, D.; Wolter, A.U.B.; Schoenes, J.; Süllow, S.; Feyerherm, R.; Doll, K.: **Pressure dependence of $C_4N_2H_4$-mediated superexchange in $XCl_2(C_4N_2H_4)_2$ (X = Fe, Co, Ni)** Physical Review B: Condensed Matter **72** (2005), 134418/1-6	
Kreitlow, J.; Mathoniére, C.; Feyerherm, R.; Süllow, S.: **Pressure response of the bimetallic chain compound $MnNi(NO_2)_4(en)_2$; en = ethylenediamine** Polyhedron **24** (2005) 2413-2416	E6
Krist, T.; Peters, J.; Shimizu, H.M.; Suzuki, J.; Oku, T.: **Transmission bender for polarizing neutrons** Physica B - condensed matter **356** (2005), 197-200	V14
Kühn, P.; Pieper, J.; Kaminskaya, O.; Eckert, H.-J.; Lechner, R.E.; Shuvalov, V.; Renger, G.: **Reaction pattern of photosystem II: Oxidative Water Cleavage and Protein Flexibility** Photosynthesis Research **84** (2005), 317-323	V3
Lake, B.; Tennant, D.A.; Frost, C.D.; Nagler, S.E.: **Quantum criticality and universal scaling of a quantum antiferromagnet** Nature Materials **4** (2005), 329-334	
Lake, B.; Lefmann, K.; Christensen, N. B.; Aeppli, G.; McMorrow, D. F.; Ronnow, H. M.; Vorderwisch, P.; Smeibidl, P.; Mangkorntong, N.; Sasagawa, T.; Nohara, N.; Takagi H.: **Three dimensionality of field-induced magnetism in a high-temperature superconductor** Nature Materials **4** (2005), 658-662	V2 IHP I 317 IHP II 478 IHP II 525
Lee, S.; Podlesnyak, A.A.; Prokes, K.; Sikolenko, V.; Ermolenko, A.S.; Gerasomov, E.G.; Dorofeev, Yu.A.; Vokhmyanin, A.P.; Park, J.G.; Pirogov, A.N.: **Magnetic phase transititons in $TbNi_5$ single crystal: bulk properties and neutron diffraction studies** JETP Letters **82** (2005) 36 – 40	E4
Lieutenant, K.: **Optimization of neutron scattering instruments using different optimization routines** Journal of Physics: Condensed Matter **17** (2005), S167-S174	
Lieutenant, K.; Gutberlet, T.; Wiedenmann, A.; Mezei, F.: **Monte-Carlo simulations of small angle neutron scattering instruments at European spallation source** Nuclear Instruments and Methods in Physics Research Section A **553** (2005), 592-603	
Löffler, J.F.; Braun, H.B.; Wagner, W.; Kostorz, G.; Wiedenmann, A.: **Magnetization processes in nanostructured metals and small-angle neutron scattering** Physical Review B: Condensed Matter **71** (2005), 134410-1-134410-15	V4
Manke, I.; Haibel, A.; Rack, A.; Zabler, S.; Banhart, J.: **Hochauflösende Tomographie mit Synchrotronstrahlung an Papier** PTS-MS **529** (2005), 11.1-11.18	S5
Manke, I.; Kardjilov, N.; Haibel, A.; Hartnig, C.; Strobl, M.; Rack, A.; Hilger, A.; Scholta, J.; Lehnert, W.; Treimer, W.; Zabler, S.; Banhart, J.: **Untersuchung der Wasserverteilung in Brennstoffzellen** DGZfP-Berichtsband **94** (2005)	E8 S5

Publications 2005
BENSC Experiments and BENSC Authors

Manke, I.; Kardjilov, N.; Haibel, A.; Rack, A.; Hilger, A.; Stroble, M.; Treimer, W.; Zabler, S.; Banhart, J.: **Untersuchung industrieller Bauteile mit bildgebenden Verfahren** DGZfP-Berichstband **94** (2005), 39, 1-11	S5 V7
Matsushima, U. ; Kawabata, Y. ; Kardjilov, N. ; Herppich, W.B.: **The potential of neutron and X-ray imaging to observe water transport in plants** Proc. COST-924-Workshop Non-destructive methods for detecting health-promoting compounds, Potsdam, 07. - 08.12.2005 (2005), 87-89	V7
Mezei, F.: **Polarized neutron scattering research: the beginning** Physica B - condensed matter **356** (2005), 64-70	
Monkenbusch, M.; Ohl, M.; Richter, D.; Pappas, C.; Zsigmond, G.; Lieutenant, K.; Mezei, F.: **Aspects of Neutron Spin-echo Spectrometer Operation on a Pulsed Source** Journal of Neutron Research **13** (2005), 36-66	
Ono, T.; Tanaka, H; Kolomiyets, O; Mitamura, H.; Ishikawa, F.; Goto, T.; Nakajima, K.; Oosawa, A.; Koike, Y.; Kakurai, K.; Klenke, J.; Smeibidl, P.; Meissner, M.; Coldea, R.; Tennant, D.A.; Ollivier, J.: **Field-induced phase transitions driven by quantum fluctuation in S=1/2 anisotropic triangular antiferromagnet Cs_2CuBr_4** Progress of Theoretical Physics Supplement **159** (2005), 217-221	E1
Pappas, C.; Mezei, F.; Triolo, A.; Zorn, R.: **Going to the limits of the NSE** Physica B - condensed matter **356** (2005), 206-212	V5
Peters, J.: **Neutron transmission probability through a revolving slit for a continuous source and a divergent neutron beam** Nuclear Instruments and Methods in Physics Research Section A **540** (2005), 419-429	V15
Pissas, M.; Margiolaki, I.; Papavassiliou, G.; Stamopoulos, D.; Argyriou, D.: **Crystal and magnetic structure of the $La_{1-x}Ca_xMnO_3$ compound (0.11<or=x<or=0.175)** Physical Review B: Condensed Matter **72** (2005), 064425/1-15	E6 NMI3 1011
Pop, L.M.; Odenbach, S.; Wiedenmann, A.; Matoussevitchc, N.; Bönnemann, H.: **Microstructure and rheology of ferrofluids** Journal of Magnetism and Magnetic Materials **289** (2005) 303–306	V4
Popova, E.; Loosvelt, H.; Gierlings, M.; Leunissen, L.H.A.; Jonckheere, R.; Van Haesendonck, C.; Temst, K.: **Magnetization reversal in exchange biased Co/CoO patterns** European Physical Journal B **44** (2005) 491 – 500	V6 NMI3 1005 IHP II 546
Prokes, K.; Bewley, R.; Eccleston, R.; Brück, E.; Syshchenko, O.; Sechovsky, V.: **Magnetic response function in URhGe** Physica B - condensed matter **359-361** (2005), 1123-1125	
Prokes, K.; Muñoz Sandoval; E., Chinchure; A.D., Mydosh, J.A.: **Uncompensated antiferromagnetic structure of Ho_2Ni_2Pb** European Physical Journal B **43** (2005), 163-174	E6
Prokhnenko, O.; Kamarad, J.; Prokes, K.; Arnold, Z.; Andreev, A.V.: **Helimagnetism of Fe: High Pressure Study of an Y_2Fe_{17} Single Crystal** Physical Review Letters **94** (2005) 107201-1 - 107201-4	E4 NMI3: 1047
Rocha, S; Krastev, R.; Thünemann, A.F.; Carmo Pereira, M.; Möhwald, H.; Brezesinski, G.: **Adsorption of Amyloid b-Peptide at Polymer Surfaces: A Neutron Reflectivity Study** ChemPhysChem **6** (2005), 2527-2534	V6
Romer, R.L.; Heinrich, W.; Schröder-Schmeibidl, B.; Meixner, A.; Fischer, C.-O.; Schulz, C.: **Elemental dispersion and stable isotope fractionation during reactive fluid-flow and fluid immiscibility in the Bufa del Diente aureole, NE-Mexico: evidence from radiographies and Li, B, Sr, Nd, and Pb isotope systematics** Contributions to Mineralogy and Petrology (2005) **149**, 400 - 429	B8

Publications 2005
BENSC Experiments and BENSC Authors

Rossner, H.H. ; Holub-Krappe, E. ; Fieber-Erdmann, M. ; Krappe, H.J.: **Lattice dynamics information obtained from EXAFS measurements on Ta** Physica Scripta **T115** (2005), 45-48	
Sahoo, K.L.; Wollgarten, M.; Haug, J.; Banhart, J.: **Effect of La on the crystallization behaviour of amorphous $Al_{94-x}Ni_6La_x$ (x = 4-7) alloys** Acta Materialia **53** (2005), 3861-3870	
Sazonov, A.P.; Troyanchuk, I.O.; Sikolenko, V.V.; Chobot, G.M.; Szymczak, H.: **Crystal structure, magnetic and electrical properties of the $Nd_{1-x}Ba_xCoO_3$ system** Journal of Physics: Condensed Matter **17** (2005) 4181 – 4195	E9
Schorr, S.; Tovar, M.; Sheptyakov, D.; Keller, L.; Geandier, G.: **Crystal structure and cation distribution in the solid solution series 2(ZnX)-$CuInX_2$) (X=S, Se, Te)** Journal of Physics and Chemistry of Solids **66** (2005) 1961 – 1965	E9
Sechovsky, V.; Honda, F.; Prokes, K.; Griveau, J.C.; Andreev, A.V.; Arnold, Z.; Kamarad, J.; Oomi, G.: **Pressure effects on magnetism in U intermetallics: the UPtAl case** Journal of Magnetism and Magnetic Materials **290–291** (2005) 629–632	
Sechovsky, V.; Vejpravova, J.; Andreev, A.V.; Honda, F.; Prokes, K.; Santava, E.: **Specific heat and magnetism of a UIrGe single crystal** Physica B **359–361** (2005) 1126–1128	
Smarsly, B.; Thommes, M.; Ravikovitch, P.I.; Neimark, A.V.: **Characterization of Worm-Like Micro- and Mesoporous Silicas by Small-Angle Scattering and High-Resolution Adsorption Porosimetry** Adsorption **11** (2005) 653 – 655	V4
Sobolev, O.; Vorderwisch, P.; Desmedt, A.: **Free NH_3 quantum rotations in Hofman clathrates: structure factors and line widths studied by inelastic neutron scattering** Chemical Physics **308** (2005), 147-157	V2 V3
Steitz, R.; Schemmel, S.; Shi, H.; Findenegg, G.H.: **Boundary layers of aqueous surfactant and block copolymer solutions against hydrophobic and hydrophilic solid surfaces** Journal of Physics: Condensed Matter **17** (2005), S665-S683	V6
Stock, C.; Wakimoto, S.; Birgeneau, R.J.; Danilkin, S.; Klenke, J.; Smeibidl, P.; Vorderwisch, P.: **Enhancement of magnetic order in the incommensurate phase of Mg-doped $CuGeO_3$** Journal of the Physical Society of Japan **74** (2005), 746-752	V2 E1
Strobl, M.; Treimer, W.; Kardjilov, N.; Hilger, A.: **Application of refraction contrast tomography** Nuclear Instruments and Methods in Physics Research Section A **542** (2005), 383-386	V12a
Strunz, P.; Mukherji, D.; Schumacher, G.; Vassen, R.; Gilles, R.; Rösler, J.; Wiedenmann, A.: **Microstructure Investigation of Superalloys and Ceramic Coatings Using Small-Angle Neutron Scattering** Freiberger Forschungshefte **B331** – Werkstoffwissenschaf (proc.of BHT2005, colloquium “Microstructure Analysis in the Materials Science”, Freiberg, 15–17.6.2005), ed. D.Rafaja, S.Unterricker, R.Kleeberg (2005) 39 - 41	V4 NMI3 1007
Stüßer, N.; Hoser, A.; Meißner, M.: **The magnetic spiral in the frustrated antiferromagnet $RbCuCl_3$ studied by means of neutron diffraction** Journal of Physics: Condensed Matter **17** (2005), 1335-1340	E1
Szytula, A.; Penc, B.; Wawrzynska, E.; Hernández-Velasco, J.: **Magnetic structure of the $TbCu_2In$ compound** Journal of Alloys and Compounds **388** (2005), L4 - L7	E6 IHP II 465
Tatchev, D.; Hoell, A.; Kranold, R.; Armyanov, S.: **Size distribution and composition of magnetic precipitates in amorphous Ni-P alloy** Physica B - condensed matter **369** (2005), 8-19	V4 IHP I 234

Publications 2005
BENSC Experiments and BENSC Authors

Ter-Avetisyan, S.; Schnürer, M.; Hilscher, D.; Jahnke, U.; Busch, S.; Nickles, P.V.; Sandner, W.: **Fusion neutron yield from a laser-irradiated heavy-water spray** Physics of Plasmas **12** (2005), 012702/1-5	
Tishchenko, V.; Herbach, C.-M.; Hilscher, D.; Jahnke, U.; Galin, J.; Goldenbaum, F.; Letourneau, A.; Schröder, W.-U.: **Fast decision in favor of the slow fission process** Physical Review Letters **95** (2005), 162701/1-4	
Toca-Herrera, J.-L.; Krastev, R.; Bosio, V.; Küpcü, S.; Pum, D.; Fery, A.; Sára, M.; Sleytr, U.B.: **Recrystallization of Bacterial S-Layers on Flat Polyelectrolyte Surfaces and Hollow Polyelectrolyte Capsules** SMALL **1** (2005), 339-348	V6 NMI3 1003
Treimer, W. ; Hilger, A. ; Kardjilov, N. ; Strobl, M.: **Review about old and new imaging signals for neutron computerized tomography** Nuclear Instruments and Methods in Physics Research Section A **542** (2005), 367-375	V12a V12b
Treimer, W.; Kardjilov, N.; Feye-Treimer, U.; Hilger, A.; Manke, V.; Strobl, M.: **Absorption- and phase-based imaging signals for neutron tomography** Advances in Solid State Physics **45** (2005), 407-420	V12a V12b
Treimer, W.; Strobl, M.; Hilger, A.; Peschke, H.J.; Seifert, C.: **Neuton tomographic imaging using refraction data** IEEE Transactions on nuclear science **52** (2005), 386-388	V12a
Triolo, R.; LoCelso, F.; Benfante, V.; Triolo, A.; Wiedenmann, A.; Bernstorff, S.: **Small angle scattering of poly(methylmethacrylate)-block-poly(ethylene oxide) block co-polymer in aqueous solution** Progress in Colloid and Polymer Science **130** (2005), 1-6	V4
Ulbricht, A.; Böhmert, J.; Uhlemann, M.; Müller, G.: **Small-angle neutron scattering study on the effect of hydrogen in irradiated reactor pressure vessel steels** Journal of Nuclear Materials **336** (2005), 90 - 96	V4
Wagh, A.G.; Rakhecha, V.C.; Strobl, M.; Treimer, W.: **SUSANS With Polarised Neutrons** Journal of Research of NIST **110** (2005) 231 - 235	V12b
Wawrzynska, E.; Balanda, M.; Baran, S.; Leciejewicz, J.; Penc, B.; Stuesser, N.; Szytula, A.: **Commensurate-incommensurate magnetic phase transitions in $PrCu_2Ge_2$ and $NdFe_2Ge_2$** Journal of Physics: Condensed Matter **17** (2005) 1037 – 1047	E6 NMI3 1027
Wawrzynska, E.; Hernández-Velasco, J.; Penc, B.; Rams, M.; Szytula, A.: **Magnetic structures of $R_3Pd_4Ge_4$ (R = Tb and Er)** Journal of Magnetism and Magnetic Materials **288** (2005) 111 - 120	E6 IHP II 578
Wiedenmann, A.: **Polarized SANS for probing magnetic nanostructures** Physica B - condensed matter **356** (2005), 246-253	V4
Wiedenmann, A.; Heinemann, A.: **Field-induced ordering phenomena in ferrofluids observed by small-angle neutron scattering** Journal of Magnetism and Magnetic Materials **289** (2005), 58-61	V4
Wilmer, D.; Feldmann, H.; Lechner, R.E.; Combet, J.: **Sodium Ion Conduction in Plastic Phases: Dynamic Coupling of Cations and Anions in the Picosecond Range** Journal of Materials Research **20** (2005), 1973-1978	V3
Wilmer, D.; Feldmann, H.; Lechner, R.E.; Combet, J.: **Sodium Ion Conduction in Plastic Phases: Dynamic Coupling of Cations and Anions in the Picosecond Range** Material Research Society Symposium Proceedings **835** (2005) K1.2.1 - K1.2.6	V3

Publications 2005
BENSC Experiments and BENSC Authors

Wollgarten, M.; Hiller, S.; Vierke, J.; Haibel, A.; Schubert-Bischoff, P.; Sahoo, K.L.; Banhart, J.: **Study of the microstructure of rapidly solidified Al-Ni-La-Zr alloys by synchrotron tomography and transmission electron microscopy** Proceedings / Microscopy conference 2005 ; 6. Dreiländertagung : August 28 - September 2, 2005, Davos	
Wolter, A.U.B.; Wzietek, P.; Süllow, S.; Litterst, F.J.; Honecker, A.; Brenig, W.; Feyerherm, R.; Klauss, H.-H.: **Giant spin canting in the S = ½ antiferromagnetic chain $[CuPM(NO_3)_2(H_2O)_2]_n$ observed by ^{13}C-NMR** Physical Review Letters **94** (2005), 057204/1-4	
Wolter, A.U.B.; Wzietek, P.; Jerome, D.; Süllow, S.; Litterst, F.J.; Feyerherm, R.; Klauss, H.-H.: **Observation of solitons in the S = ½ antiferromagnetic chain $[CuPM(NO_3)_2(H_2O)_2]_n$ by ^{13}C-NMR** Journal of Magnetism and Magnetic Materials **290–291** (2005) 302–305	
Zhang, L.; Moze, O.; Prokes, K.; Tegus, O.; Brück, E.: **Neutron diffraction study of history dependence in $MnFeP_{0.6}Si_{0.4}$** Journal of Magnetism and Magnetic Materials **290-291** (2005), 679-681	E6 IHP II 572
Zvyagin, S.A.; Kolezhuk, A.K.; Krzystek, J.; Feyerherm, R.: **Electron spin resonance in sine-Gordon spin chains in the perturbative spinon regime** Physical Review Letters **95** (2005), 017207/1--4	

Seminars and Conference Contributions 2005

Invited Talks

2004 (supplement)

Gradzielski, M.: **Vesicle gels - phase behaviour and process of formation** Workshop Short Range Interactions in Soft Condensed Matter - From Solutions to Materials and Biological Systems, Regensburg, 26.02. - 28.02.2004	V4
Gradzielski, M.: **Aggregatbildung in amphiphilen Systemen: Von Vesikelgelen und Organogelen bis zu selbstaggregierenden Blockcopolymeren** Kolloquium des Sfb448, Berlin, 08.06.2004	V4
Gradzielski, M.: **Vesikel und Vesikelgele** BASF Kolloquium, Ludwigshafen, 30.08.2004	V4

2005

Clemens, D.: **Information from the Deep - Analysis of Stratified Media using Polarized Neutron Reflectometry** 3rd Central European Training School on Neutron Scattering and COST Training School on Neutron Optics, Budapest, Ungarn, 18.04. - 23.04.2005	
Feyerherm, R.: **Quantum sine-Gordon behaviour in cooper pyrimidine dinitrate** Symposium, Königstein (Taunus), 17.10. - 19.10.2005	
Gradzielski, M.: **Structure and Dynamics of Interpolyelectrolyte Complexes of Charged Block Copolymer Micelles** 42. Kolloidtagung, Aachen, 26.09. - 28.09.2005	V4
Haibel, A.; Zabler, S.; Rueda, A.; Freidank, H.; Grupp, R.; Henkel, F.; Boin, M.; Banhart, J.; Weidemann, G.; Riesemeier, H.; Goebbel, J.: **Synchrotron-Tomographie: Prinzip und Anwendungen in der Materialforschung** Sommerschule an der Humboldt-Uni, Berlin, Germany, 02.08.2005	S5
Haug, J.; Hoell, A.; Heinemann, A.; Kammel, M.; Keiderling, U.; Wiedenmann, A.: **Small angle scattering facilities at HMI, Berlin** Industrietag des HMI, HMI Berlin, 01.06.2005	V4
Herbach, C.-M.; Hilscher, D.; Jahnke, U.; Tishchenko, V.G.; Galin, J.; Letourneau, A.; Peghaire, A.; Filges, D.; Goldenbaum, F.; Pienkowski, L.; Schröder, W.U.; Töke, J.: **Systematic investigation of 1.2-GeV proton-induced spallation reactions on targets between Al and U** International Conference on Accelerator Applications 2005, Venice, Italy, 29.08. - 01.09.2005	
Hoell, A.: **The new SAXS instrument at Bessy 7T-Wiggler** Benchmarking zur Kleinwinkelstreuung, Berlin, Germany, 20.09.2005	S3
Kammel, M.; Wiedenmann, A.; Heinemann, A.; Bönnemann, H.: **Evidence for oxide coating in air stable Co-ferrofluids** Ferrofluid workshop, Saarbrücken, Germany, 21.07.2005	V4
Krist, T.: **Neutron optics from HMI Berlin** Hanaro 2005 Int. Symp. on Reactor Research and Neutron Science, Daejeon, KR, 11.04. - 13.04.2005	V14

Seminars and Conference Contributions 2005

Krist, T.: **Neutron optics from HMI Berlin** ORNL / SNS Seminarvortrag 31. Mai 2005, Oak Ridge, TN, USA, 31.05.2005	V14
Krist, T.: **Neutron optics from HMI Berlin** ANL Seminarvortrag 6. Juni 2005, Argonne, USA, 06.06.2005	V14
Krist, T.: **Neutron optics from HMI Berlin** Seminarvortrag, ISIS, France, 29.09.2005	V14
Krist, T.: **Neutron optics from HMI Berlin** Seminarvortrag, JAERI, Japan, 15.11.2005	V14
Krist, T.: **Neutron optical devices** Seminarvortrag, ANSTO, Sydney, Australia, 24.11.2005	V14
Lake, B.; Lefmann, K.; Christensen, N. B.; Aeppli, G.; McMorrow, D. F.; Ronnow, H. M.; Vorderwisch, P.; Smeibidl, P.; Mangkorntong, N.; Sasagawa, T.; Nohara, N.; Takagi H.: **High Magnetic Fields for Neutron Scattering** Probing Matter At High Magnetic Fields with X-Rays and Neutrons, Tallahassee, FL, U.S.A., 10.05. - 12.05.2005	V2 IHP I: 317 IHP II: 478 IHP II: 525 IHP II: 584
Lake, B.; Lefmann, K.; Christensen, N. B.; Aeppli, G.; McMorrow, D. F.; Ronnow, H. M.; Vorderwisch, P.; Smeibidl, P.; Mangkorntong, N.; Sasagawa, T.; Nohara, N.; Takagi H.: **Superconductivity and Magnetism in the Cuprate** Physical Phenomena at High Magnetic Fields, Tallahassee, FL, U.S.A., 05.08. - 09.08.2005	V2 IHP I: 317 IHP II: 478 IHP II: 525 IHP II: 584
Manke, I.; Haibel, A.; Rack, A.; Zabler, S.; Banhart, J.: **Hochauflösende Tomographie mit Synchrotronstrahlung an Papier** Workshop Moderne Oberflächenanalytik und bildgebende Verfahren, PTS, 10.05. - 11.05.2005	S5
Pappas, C.; Cywinski, R.; Hillier, A.; Manuel, P.; Bentley, P.; Alba, M.; Mezei, F.; Campbell, I.A.; Zimmermann, U.: **Relaxation in Glassy Magnets** NSE 2005, ILL - Grenoble Frankreich, 08.09. - 10.09.2005	V5
Perroud, O.; Wiedenmann, A.; Garcia-Matres, E.: **Small Angle Neutron Scattering Investigations in Nd-based alloys** DFG- Kolliquium SPP1120, Bad Honef, 19.05.2005	V4
Perroud, O.; Wiedenmann, A.; Garcia-Matres, E.: **Small Angle Neutron Scattering Investigations in Nd-based alloys** Int. Conf. on Rapidly quentched materials RQ12, Korea, 25.08.2005	
Pieper, J.; Irrgang, K.-D.; Renger, G.; Lechner, R.E.: **Light-induced Protein Dynamics in the Light-Harvesting Complex II of Green Plants** Workshop "Dynamique et cinétique des biopolymères", Synchrotron Soleil, St. Aubin (Frankreic, 16.06. - 17.06.2005	V3
Pop, L.P.; Odenbach, S.; Wiedenmann, A.: **The Microscopic mechanisms of the magnetoviscous effect in ferrofluids investigated by SANS** Int. Conf. on Fundamental and Applied Magnetohydrodynamics, 15. PAMIR, Riga, 28.06.2005	V4
Pop, L.P.; Odenbach, S.; Wiedenmann, A.: **Microstructure and rheological characterisation of ferrofluids** International Conference on Neutron Scattering 2005, Sydney, Australia, 27.11. - 02.12.2005	V4
Rack, A.: **Analyse von Synchrotronaufnahmen moderner Werkstoffe und komplexer Materialsysteme** Analyse von Volumenbildern der Mikrostruktur von Werkstoffen, Kaiserslautern, 17.02.2005	S5

Seminars and Conference Contributions 2005

Rack, A.: **Characterization of complex materials with synchrotron-tomography and 3d image analysis** Arbeitstreffen ESRF (Arbeitsgruppenseminar ID19), Grenoble, Frankreich, 23.05. - 27.05.2005	S5
Rüegg, C.: **Condensate ground-states in dimer spin-liquids** International Conference on Physical Phenomena in High Magnetic Fields PPHMF-V, Tallahassee, 2005	V2 IHP II: 543 NMI3: 1006
Rüegg, C.: **Field- and pressure-induced quantum phase transitions in gapped spin systems** International Conference on Strongly Correlated Electron Systems SCES'05, Vienna, 2005	V2 IHP II: 543 NMI3: 1006
Rüegg, C.: **From magnetization plateaus to BEC of magnons – quantum phase transitions in magnetic insulators** General ILL Seminar organized by College IV, Grenoble, 2005	V2 IHP II: 543 NMI3: 1006
Rüegg, C.: **From magnetization plateaus to BEC of magnons – quantum phase transitions in magnetic insulators** Seminar Geballe Laboratory for Advanced Materials, Stanford University, 2005	V2 IHP II: 543 NMI3: 1006
Rüegg, C.: **Magnetic field- and pressure-induced quantum phase transitions in the spin-liquid $TlCuCl_3$** International Conference on Low-Temperature Physics LT24, Orlando, 2005	V2 IHP II: 543 NMI3: 1006
Rüegg, C.: **Pressure- and field-induced quantum phase transitions in dimer spin-liquids** International Workshop on Collective Quantum Sttes in Low-Dimensional Transition Metal Oxides, Dresden, Germany, 22.02. - 25.02.2005	V2 IHP II: 543 NMI3: 1006
Rüegg, C.: **Quantum phase transitions in magnetic insulators – novel ground states at "T = 0 K"** Berliner Tieftemperatur-Kolloquium, Berlin, 2005	V2 IHP II: 543 NMI3: 1006
Rupp, A.: **A filling station for polarised 3He** Seminar talk at Institut für Festkörperforschung, FZ Jülich, Jülich (Germany), 2005	
Rupp, A.; Hutanu, V.; Klenke, J.; Drescher, L.; Mueller, R.; Sander-Thömmes, T.; Kilian, W.: **Compressor, filling station and "magnetised" filter cells** NMI3 General Meeting, Rutherford Appleton Laboratory, Chilton, Didcot, UK, 26.09. - 29.09.2005	
Schorr, S.; Tovar, M; Stuesser, N.; Sheptyakov, D.; Koza, M.; Geandier, G.: **The structural phase transitions in $CuBX_2$ (B=Al, Ga, In, X=S, Se, Te): A combined use of neutrons and synchrotron radiation** 12th International Seminar on Neutron Scattering Investigations in Condensed Matter, Poznan, Polen, 05.05. - 07.05.2005	E6
Steitz, R.: **Reflectometry studies of structured interfaces and thin films** Moderne Materialanalytik mit Neutronen, Ionen und Synchrotronstrahlung, Berlin, 01.06.2005	V6
Steitz, R.: **Untersuchung dünner Schichten mit Neutronenreflektometrie** Moderne Materialanalytik mit Neutronen, Ionen und Synchrotronstrahlung, Berlin, 01.06.2005	V6
Steitz, R.: **Neutron reflectivity and soft condensed matter** Abteilungsseminar SE2, Hahn-Meitner-Institut, 21.06.2005	V6
Steitz, R.: **How to investigate ultrathin films on liquid surfaces - a neutron reflectivity approach** Earthscience and nanoscience with neutrons at IBR-2/IBR-2M (JINR Dubna), GFZ Potsdam, 05.09. - 06.09.2005	V6

Seminars and Conference Contributions 2005

Steitz, R.; **Boundary Layers of Water at Polymer-Liquid Interfaces** Struktur und Dynamik kondensierter Materie, TUM München, 21.10.2005	V6
Steitz, R.: **Neutron reflectivity of ultrathin films and their relevance to bioscience** Physikalisches Kolloquium, Universität des Saarlandes, Saarbrücken, 01.12.2005	V6
Steitz, R., Findenegg, G.H., v. Klitzing, R.: **Swelling and structural changes of polyelectrolyte multilayers in contact with aqueous solution studied by neutron and X-ray reflectometry** 344. WE-Heraeus-Seminar, Bad Honnef, 04.04. - 06.04.2005	V6
Steitz, R.; Czeslik, C.; Haas, H.; Riccio, P.: **Soft Interfaces on the Nanometer Scale - How Neutrons Contribute to a Deeper Understanding on the Supramolecular Level** AVS 52nd International Symposium & Exhibition, Hynes Convention Center, Boston, MA, 30.10. - 04.11.2005	V6
Strunz, P.; Del Genovese, D.; Zrník, J.; Mukherji, D.; Rösler, J.; Seliga, T.; Penkalla, H.J.: **In-situ SANS investigation of high-temperature precipitate morphology in polycrystalline Ni-base superalloys** 7th SINQ Users' Meeting, PSI Villigen, Switzerland, 27.01.2005	V4 NMI3: 1076
Tennant, D.A.: **Probing Quantum Criticality with Neutron Scattering** Colloquium to Physics Department, Technische Universität, Dresden, 08.11.2005	
Tennant, D.A.: **Advances in studying molecular magnets with neutrons** Osnabrück workshop on nanomagnets (invited talk), University of Osnabrück, 17.11. - 19.11.2005	
Tennant, D.A.: **Neutrons, Magnetic fields, and Quantum States** FOM December Days (Plenary), Veldhoven, NL, 13.12 - 14.12.2005	
Tennant, D.A.; Roger, M.; Morris J.; Goff J.P.; Gutmann, M.J.; Lake, B.; Prabhakaran, D.: **Sodium ordering in Na_xCoO_2** Invited Talk at Theoretical and Experimental Magnetism Workshop 2005, Coseners House, Abingdon, UK, 02.08. - 03.08.2005	
Vakhrushev, S.; Golosovsky, I.; Kumzerov, Yu.; Naberezhnov, A.; Smirnov, O.; Shnaidshtein, I.; Hansen, T.; Tovar, M.; Zalar, B.; Lebar, A.; Blinc, R.: **Structure and properties of ferroelectrics in a restricted geometry** XVII Russian Conference on Ferroelectricity, Penza, Russia, 25.06. - 01.07.2005	E9
Vorderwisch, P.: **The Cold Neutron Triple-Axis-Spectrometer FLEX at BENSC** Taiwan-Australia Workshop on Neutron Scattering Science, National Central University, Chung-Li, Taiwan, 27.10.2005	V2
Vorderwisch, P.: **Selected Experiments Using Cold Neutron Spectroscopy at BENSC (Berlin Neutron Scattering Center)** Satellite Meeting on Neutron Scattering, Eleventh Users' Meeting & Workshops, National Synchrotron Radiation Research Center (NSRRC), Hsinchu, Taiwan, 25.10.2005	V2
Vorderwisch, P.; Shapiro, S.M.; Stuhr, U.: **Phonon dispersion and lattice instabilities in the ferromagnetic shape-memory alloy Ni_2MnGa studied by neutron spectroscopy** Workshop on Magnetic Shape Memory Alloys, Ascona, Switzerland, 11.09. - 16.09.2005	V2
Wiedenmann, A.: **SANS facility at BENSC** Workshop on benchmarking for small-angle scattering, Berlin, Germany, 20.09.2005	V4

Seminars and Conference Contributions 2005

Wiedenmann, A.: **Introduction to SANS** HMI Tutorial BENSC, Berlin, 21.09.2005	V4
Wiedenmann, A.: **Magnetic Nanostructures as Probed by Polarized Small Angle Neutron Scattering** NIM3-School "Polarized Neutrons for Material and Life Sciences", Anglet, France, 07.06.2005	V4
Wiedenmann, A.: **Polarized Small Angle Neutron Scattering: A nano-analytical technique for magnetic systems** Van't Hoff Laboratory, University of Utrecht, The Netherlands, 08.11.2005	V4
Wiedenmann, A.; Kammel, M; Heinemann, A.: **Magnetic Nanostructures Studied by Polarized Small Angle Neutron Scattering** International Symposium on Research Reactor and Neutron Science, HANARO -Daejeon, Korea, 13.04.2005	V4
Wiedenmann, A.; May, R.P.; Dewhurst, C.; Haug, J.; Heinemann, A.; Kammel, M.; Keiderling, U.: **Time dependence of field induced ordering processes in Ferrofluids studied by Small Angle Neutron Scattering** Ferrofluid workshop, Saarbrücken, 20.07.2005 -	V4
Wiedenmann, A.; May, R.P.; Dewhurst, C.; Haug, J.; Heinemann, A.; Kammel, M.; Keiderling, U.: **SANS Study of Time Dependent Ordering Processes in Concentrated Ferrofluids Induced by External Magnetic Fields** 6th Ferrofluid workshop Saarbrücken, Saarbrücken, Germany, 20.07.2005	V4
Wiedenmann, A.; May, R.P.; Heinemann, A.; Kammel, M.; Keiderling, U.: **SANS study of time dependent ordering processes in concentrated Ferrofluids induced by external magnetic fields** 15. Int. Conf. of Fundamental and Apllied Magnetohydrodynamics, PAMIR, Riga, 27.06.2005	V4

Talks

2002 (supplement)

Eschricht, N.; Hoinkis, E.; Mädler, F.: **Reconstruction of mesoporous silica glasses from SANS-data** 6th Int. Sympos. on the characterization of Porous Solids (COPS-VI), Alicante, Spain, 08.05. - 11.05.2002	V4

2003 (supplement)

Keiderling, U., Sieger,H., Winterer, M.; Hahn,H.: **Impact of ultrasonic agitation on dispersions of ultrafine silica powders, analyzed with time-resolved SANS** 3rd ECNS 2003, Montpellier, France, 03.09. - 06.09.2003	V4

2004 (supplement)

Almeida, F., L'abbé, C., Gierlings, M., Maletta, H., Meersschaut, J.: **Spin configuration in Fe/Cr(100) multilayers studied with polarized neutron reflectometry** General meeting of the Belgian Physical Society, 10.05. - 17.05.2004	V6

Seminars and Conference Contributions 2005

Almeida, F., L'abbé, C., Gierlings, M., Maletta, H., Meersschaut, J.: **Transverse moments in Fe/Cr(100) superlattices studied with polarized neutron reflectometry** Workshop on Synchrotron Radiation for the study of Magnetic Nanosystems, Leuven (Belgien), 01.11. - 06.11.2004	V6
Nickles, P.V.; Schnürer, M.; Ter-Avetisyan, S.; Busch, S.; Kemp, A.; Hilscher, D.; Jahnke, U.; Sandner, W.: **Particle acceleration from laser-created relativistic plasmas** 20th General Conference of the Condensed Matter Division of the European Physical Society, Prague, 19.07.2004	
Peters, J.; Lieutenant, K.; Clemens, D.; Mezei, F.: **EXED : the new Extreme Environment Diffractometer at the Hahn-Meitner-Institut Berlin** IX. European Powder Diffraction Conference, Prague, 02.09.2004	V15
Wiedenmann, A.; Heinemann, A.; Kammel, M.: **Project Wi 1151: Field-Induced Ordering Phenomena In Ferrofluids Observed by Small Angle Scattering** 5th Colloquim DFG-Priority Program "Kolloidale magnetische Flüssigkeiten: Grundlagen, Entwicklung und Anwendung neuartiger Ferrofluide", Benediktbeuern, 27.09.2004	V4

2005

Bentley P.M.; Pappas C.; Habicht H.; Lelievre-Berna E.: **Evolutionary Programming Neutron Instrument Optimisation** International Conference on Neutron Scattering 2005, Sydney, Australia, 27.11. - 02.12.2005	
Bentley, P.M.; Lelièvre-Berna, E.; Pappas, C.: **Optimisation of Neutron Spin Echo Instrumentation for Implementing Spherical Polarimetry** NSE2005, Grenoble, 07.09. - 10.09.2005	V5
Clemens, D.; Mezei, F.: **Neutron trajectory definition by multi-pinhole grids** International Conference of Neutron Scattering 2005, Sydney, Australien, 27.11. - 02.12.2005	
Feyerherm, R.; Zvyagin, S.A.; Wolter, A.U.B.: **Quantum sine-Gordon behaviour in copper pyrimidine dinitrate** DPG Frühjahrstagung, Berlin, 04.03. - 09.03.2005	
Glavatskyy, I.; Glavatska, N.; Urubkov, I.; Hoffman, J.-U.; Bourdarot, F.: **Magnetic structure evolution with temperature in Ni-Mn-Ga magnetic shape memory martensite** International Conference of Functional Materials, Ukraine, Crimea, Partenit, 2005	E2
Habicht, K.: **Larmor phase corrections in neutron resonance spin-echo: curved dispersion surfaces** NMI3 General Meeting, Rutherford, 26.09. - 29.09.2005	V2
Haibel, A.; Zabler, S.; Banhart, J.: **Structural and Chemical Material Characterization by Means of Synchrotron Tomography** EUROMAT 2005, Prag, 05.09. - 08.09.2005	S5
Hassanein, R.; de Beer, Frikkie; Kardjilov, N.; Lehmann, E.: **Scattering Correction Algorithm for Neutron Radiography and Tomography Tested at Facilities with Different Beam Characteristics** International Conference of Neutron Scattering 2005, Sydney, Australien, 27.11. - 02.12.2005	V7
Haug, J.; Wiedenmann, A.; Flores, A.; Saruhan-Brings, B.; Strunz, P.: **Evolution of pore microstructure in Thermal Barrier Coatings studied by SANS** International Coference of Neutron Scattering 2005, Sydney, Australia, 27.11. - 02.12.2005	V4
Heinemann, A.; Kammel, M.; Wiedenmann, A.: **Small-angle scattering of orientated magnetic structures and applications to magnetic colloids** International Coference of Neutron Scattering 2005, Sydney, Australien, 28.11. - 02.12.2005	V4

Seminars and Conference Contributions 2005

Heinemann, A.; Wiedenmann, A.; Kammel, M.; Buske, N.: **SANS investigation of inter-particle correlations in concentrated Fe3O4 ferrofluids** Ferrofluid workshop, Saarbrücken, Germany, 20.07. - 22.07.2005	V4
Heinemann, A.;Hoell, A., Wiedenmann, A.; Popp, L.: **Small-angle scattering of orientated magnetic structures and applications to magnetic colloids** International Conference on Neutron Scattering 2005, Sydney, Australia, 27.11. - 02.12.2005	V4
Hoell, A.: **Untersuchung von Nanostrukturen mit Synchrotron-Kleinwinkelstreuung** HMI-Industrietag, Berlin, Germany, 01.06.2005	S3
Hoell, A.; Heinemann, A.; Kammel, M.; Wiedenmann, A.: **Nanostructure and ordering in magnetic liquids probed by SAXS and SANS** International Union of Crystallography, Florenz, Italy, 23.08. - 31.08.2005	S3 / V4
Holub-Krappe, E.; Andersson,C.; Konishi, T.; Karis, O.; Maletta, H.-J.; Arvanitis, D.: **Spin Reorientation in Thin Au/Co/Au Films: in-situ XMCD and EXAFS Study** XX Conference of the Int. Union of Crystallograpy, IUCr2005, Florence, Italy, 22.07. - 01.09.2005	
Imperia, P., Sobal, N., Schmitz, D., Giersig, M., Maletta, H.: **Effect of Ar^+ and H^+ etching on the magnetic properties of Co/CoO core-shell nanoparticles** **Nanomagnetism: New Insights with Synchrotron Radiation** WE-Heraeus-Seminar im Physikzentrum in Bad Honnef, Bad Honnef (Germany), 05.01. - 07.01.2005	S1
Kaiser-Bischoff, I., Frey, F., Boysen, H.: **X-ray and neutron scsttering by cation and anion deficient zirconia** XX Congress of the International Union of Crystallography, Florenz, 23.08. - 31.08.2005	E2
Kardjilov, N.; Hilger, A.; Manke, I.; Strobl, M.; Treimer, W.; Banhart, J.: **The new cold neutron radiography and tomography instrument CONRAD at HMI Berlin** International Workshop of Neutron Imaging Using Cold Neutrons, Paul Scherrer Institute, Schweiz, 13.10.2005 - 14.10.2005	V7
Karpinsky, D.V.; Troyanchuk, I.O.; Dobryansky, V.M.; Fedotova, Yu.A.; Kondratchik, R.B.: **Magnetic and structural investigations of the $LaCo_{1-x}Fe_xO_3$ system** Actual Problems of the Solid State Physics, Minsk, Belarus, 26.10. - 28.10.2005	V4
Keiderling, U.; Wiedenmann, A.; Haug, J.: **Stroboscopic time-resolved SANS technique for dynamical studies of slow relaxation processes** International Conference on Neutron Scattering 2005, Sydney, Australia, 27.11. - 02.12.2005	V4
Krist, T.: **Solid state devices** 3rd General NMI3 Meeting, RAL, Didcot, GB, 26.09. - 29.09.2005	V14
Kumzerov, Yu.; Naberezhnov, A.; Vakhrushev, S.; Hansen, T.; Tovar, M.; Kutnjak, Z.; Vodopivec, B.; Zalar, B.; Lebar, A.; Blinc, R.: **Phase Transitions in a Confined Sodium Nitrite** Dynamical Properties of Solids - XXX, Czekh Republic, 27.09. - 01.10.2005	E9
Lee, S.W.; Kardjilov, N.; Cho, S.J.; Sim, C.M.: **Conceptual Design of the Cold Neutron Radiography Facility at HANARO** IEEE Nuclear Science Symposium and Medical Imaging Conference, Puerto Rico, 24.10. - 29.10.2005	
Manke, I.: **Untersuchung industrieller Bauteile mit bildgebenden Verfahren am Hahn-Meitner-Institut** DGZfP-Jahrestagung 2005, Rostock, 02.05. - 04.05.2005	V7 / S5 / V12
Manke, I.; Stobl, M.; Kardjilov, N.; Hilger, A.; Scholta, J.; Lehnert, W.; Treimer, W.; Banhart, J.: **Neutron radiography on fuel cells** 69. Jahrestagung der Deutschen Physikalischen Gesellschaft, Berlin, Germany, 04.03. - 09.03.2005	V7 / S5 / V12
Matsushima, U.; Kawabata, Y.; Kardjilov, N.; Herppich, W.B.: **The Potential of Neutron and X-ray Imaging to Observe Water Transport in Plants** Non-Destructive Methods for Detecting Health Promotion CompoundsWorking Group Meeting; Leibniz-Institute of Agricultural Engineering, Potsdam-Bornim, 07.12.2005 - 08.12.2005	V7

Seminars and Conference Contributions 2005

Paduano, L.: **Supramolecular Aggregates as Tumor Specific Contrast Agents in MRI** Annual Meeting of the Italian Center for Colloid and Surface Science, Colle val d'Elsa (SI), Italy, 17.06. - 19.06.2005	V4 NMI3: 1107
Perroud, O.; Garcia-Matres, E.; Kumar, G.; Eckert, J.; Wiedenmann, A.: **Small Angle Neutron Scattering studies of hard magnetic $Nd_{60}Fe_{\{30-x\}}Co_xAl_{10}$ bulk amorphous alloys** RQ 12, Jeju, Korea, 21.08. - 26.08.2005	V4
Perroud, O.; Wiedenmann, A.; Holland-Moritz, M.; Herlach, G.: **SANS an unterkühlten Schmelzen** DPG Frühjahrtstagung, Berlin, Germany, 04.03. - 09.03.2005	V4
Peters, J.; Mezei, F.: **General time-of-flight technique for high resolution diffraction on continuous and pulsed sources** ICANS-XVII, Santa Fe, New Mexico, USA, 25.04. - 29.04.2005	
Pop, L.P.; Odenbach, S.; Wiedenmann, A.: **Magnetoviscous effect in Co based ferrofluids analysed by SANS** Ferrofluid Workshop, Saarbrücken, Germany, 20.07. - 22.07.2005	V4
Rossner, H.H.: **Bayes-Turchin Analysis of x-ray absorption data above the Fe-Ledges** Seminar at Institute of Physics, Polish Academy of Science, Warsaw, Warsaw, 01.12. - 01.12.2005	
Rupp, A.; Hutanu, V.; Klenke, J.; Drescher, L.; Mueller, R.; Thömmes-Sander, T.; Kilian, W.: **Compressor, filling station and „magnetised" filter cells** (PNT & NSF)-JRA Joint Meeting at 3rd general meeting of the NMI3 project, Chilton, Didcot, UK, 26.09. - 29.09.2005	
Rupp, A.; Hutanu, V.; Klenke, J.; Thömmes-Sander, T.; Kilian, W.: **Rebuilding of the filling station and „magnetisation" of filter cells** 3rd NSF-JRA Meeting, Garching (Germany), 2005	
Sazonov, A.P.; Troyanchuk, I.O.; Sikolenko, V.V.; Dobrjansky, V.M.: **Neutron diffraction study of the Nd_2CoMnO_6+delta** Actual problem of the solid state physics, Minsk, Belarus, 26.10. - 28.10.2005	E9
Sazonov, A.P.;Troyanchuk, I.O.; Stefanopoulos, K.L.; Gamari-Seale, H.; Sikolenko, V.: **Magnetic behavior and magnetic structure of the perovskite $TbCo_{0.47}Mn_{0.53}O_3$** XXI Hellenic Solid State Physics and Materials Science Conference, Nicosia, Cyprus, 28.08. - 31.08.2005	E9 NMI3: 1097
Schorr, S.; Kloess, G.; Wagner, G.; Tovar, M.; Geandier, G.: **Nano-hematite in obsidian: a study using TEM, neutron and synchrotron X-ray diffraction** 83rd Annual Meeting of the German Mineralogical Society, Aachen, 09.09. - 12.09.2005	E9
Shin, T; Findenegg, G.H.: **Structural study of surfactant aggregates in the pores of SBA-15 using SANS** Doktorandenkolloquium of Sonderforschungsbereich 448 "Mesoskopisch strukturierte Verbundsysteme", Rostock, Germany, 28.04. - 30.04.2005	V4
Sikolenko, V.; Efimov, V.V.; Efimova, E.A.; Sazonov, A.P.;Krivencov, V.V.; Kochubej, D.I.: **Neutron Diffraction and SR (EXAFS, XANES) studies of La-based cobaltites** V. Russian National Conference on Application of Neutrons, Synchrotron Radiation and Electron in Nanosystems Studies (RSNE NANO-2005), Moscow, 14.11. - 19.11.2005	
Steitz, R.; Schemmel, S.; Findenegg, G.H.: **Boundary Layers of Water at Polymer-Liquid Interfaces** 104. Hauptversammlung der Deutschen Bunsen-Gesellschaft für Physikalische Chemie e.V., Frankfurt/Main, 05.05. - 07.05.2005	V6
Stiller, M.; Rack, A.; Zabler, S.; Weidemann, G.; Riesemeier, H.; Goebbels, J.; Knabe, C.: **Histologie und Synchrotron-CT zur Beurteilung humaner Biopsien nach dem Sinuslift mit Beta-TCP** ZMK-Jahrestagung, Berlin, Germany, 26.10. - 30.10.2005	S5

Seminars and Conference Contributions 2005

Strobl, M.; Treimer, W.; Hilger, A.: **Phase retrieval and tomographic reconstruction of the refractive index distribution from DEI** Int. Workshop on phase retrieval and coherent scattering, porquerolles, 15.06. - 17.06.2005	V12a
Strobl, M.; Treimer, W.; Hilger, A.: **Scattering related contrast signals in neutron computerized tomography and the new V12 instrument at HMI Berlin** International Conference on Neutron Scattering 2005, Sydney, Australia, 27.11. - 02.12.2005	V12a
Treimer, W.: **Neutron and Synchrotron Radiography and tomography and applications in material engeneering sciences** Autumn School, Ammersbach, 10.10. - 14.10.2005	V7 V12a S5
Treimer, W.; Strobl, M.; Hilger, A.: **USAS vs refraction - a phase based problem** Int. Workshop on phase retrieval and coherent scattering, porquerolles, 15.06. - 17.06.2005	V12a
Treimer, W.: **Advances in neutron tomography** Uni Melbourne Seminar, Melbourne, 14.12.2005	V12a
Treimer, W.; Strobl, M.; Hilger A.: **Slit and phase grating diffraction with a DCD** International Conference on Neutron Scattering 2005, Sydney, Australia, 27.11. - 02.12.2005	V12a
Treimer; W.: **Absorption and phase based imaging signals for neutron tomography** DPG Tagung, TU-Berlin, 07.03. - 11.03.2005	V12a
Vorderwisch, P.; Shapiro, S.M.; Stuhr, U.: **Phonon dispersion in the ferromagnetic shape-memory alloy Ni_2MnGa studied by neutron spectroscopy** International Conference on Martensitic Transformations / ICOMAT'05, Shanghai, China, 14.06. - 17.06.2005	V2
Wollgarten, M.; Sahoo, K. L.; Haug, J.; Banhart, J.: **Der Einfluß von La auf das Kristallisationsverhalten von amorphen $Al_{\{94-x\}}Ni_6La_x$ (x = 4 - 7) Legierungen** Frühjahrstagung der DPG, Arbeitskreis Festkörperphysik,, Berlin, 04.03. - 09.03.2005	V4
Wollgarten, M.; Sahoo, K.L.; Haug, J.; Banhart, J.: **Influence of La on the crystallisation behaviour of amorphous $Al_{\{94-x\}}Ni_6La_x$ (x = 4 - 7) alloys** RQ 12, Jeju, Korea, 21.08. - 26.08.2005	V4

Poster

2004 (supplement)

Gilles, R.; Mukherji, D.; Hoelzel, M.; Strunz, P.; Barbier, B.; Toebbens, D.M.: **Scattering methods to investigate nano-sized precipitates extracted from Ni-base superalloys** 7th International Conference on Nanostructured Materials, Wiesbaden, 20.06. - 24.06.2004	E9
Kavecansky, V.; Mihalik, M.; Matas, S.; Mitroova, Z.; Lukacova, Z.: **Crystal structure and magnetism of $Pr[Fe(CN)_6].4D_2O$** IX.European Powder Diffraction Conference - EPDIC, Prague, 2004	E9 IHP II: 468

Seminars and Conference Contributions 2005

2005

Andersson, C.; Konishi, T.; Holub Krappe, E.; Karis, O.; Maletta, H.; Arvanitis, D.: **Magnetization reorientation in Au/Co: in-situ prepared ultra-thin films** 50th Magnetism and Magnetic Materials Conference, MMM 2005, San Hose, California, USA, 29.10. - 04.11.2005	
Boin, M.; Haibel, A.; Rack, A.; Zabler, S.: **Kompensation von Artefakten in Tomogrammen** BESSY User Meeting 2005, Berlin / Adlershof, 01.12. - 02.12.2005	S5
Dudzik, E.;Feyerherm, R.;Argyriou, D.;Aliouane, N.;Tennant, A.: **A synchrotron x-ray diffraction study of $Na_{0.48}CoO_2$** Orbital 2005 - 4th Workshop on Orbital Physics and Novel Phenomena in Transition Metal Oxides, Hamburg, 05.10. - 06.10.2005	S2
Fiori, F.; Giunta, G.; Hilger, A.; Kardjilov, N.; Rustichelli, F.: **Nondestructive characterization of archaeological glasses by neutron tomography** International Conference on Neutron Scattering 2005, Sydney, Australien, 27.11. - 02.12.2005	V7
Freidank, H.; Haibel, A.; Berthold, A.; Riesemeier, H. **Synchrotron-Tomographie an proteinbasierten keramischen Schäumen** BESSY User Meeting 2005, Berlin / Adlershof, 01.12. - 02.12.2005	S5
Gräber, H.; Apel, C.; Rack, A.; Haibel, A.; Manke, I.; Riesemeier, H.; Weidemann, G.; Goebbels, J.; Banhart, J.: **High resolution synchrotron-tomography on human tooth tissue** 69. Jahrestagung der Deutschen Physikalischen Gesellschaft (DPG), Berlin, 04.03. - 09.03.2005	S5
Gräber, H.G.; Apel, C.; Rack, A.; Haibel, A.; Manke, I.; Riesemeier, H.; Weidemann, G.; Goebbels, J.; Banhart, J.: **Hochauflösende Synchrotron-Tomographie zur Darstellung kariöser Prozesse** BESSY User Meeting 2005, Berlin / Adlershof, 01.12. - 02.12.2005	S5
Gräber, H.G.; Apel, C; Rack, A.; Haibel, A.; Manke, I.; Riesemeier, H.; Weidemann, G.; Goebbels, J.; Banhart, J.: **Hochauflösende Synchrotron-Tomographie zur Darstellung kariöser Prozesse** ZMK 2005, Berlin, Germany, 26.10. - 30.10.2005	S5
Haibel, A.; Rack, A.; Manke, I.; Riesemeier, H.; Goebbels, J.; Weidemann, G.; Banhart, J.: **Synchrotron-Tomographie am BESSY** Werkstoffwoche 2004, München, 21.09. - 23.09.2005	S5
Hilger, A.; Kardjilov, N.; Strobl, M.; Treimer, W.; Banhart, J.: **The new cold neutron radiography and tomography instrument CONRAD at HMI Berlin** International Conference of Neutron Scattering 2005, Sydney, Australien, 28.11. - 02.12.2005	V7
Hoell, A.; Kranold,R.; Goerigk, G.; Haas, S.; Müller, M.: **ASAXS studies on silverfree photochromic glasses** HASYLAB User Meeting, DESY in Hamburg, 27.01. - 28.01.2005	S3
Hoell, A.; Zizak, I.; Bieder, H.; Winter, W.; Banhart, J.: **The new SAXS instrument at the BESSY 7T Wiggler** HASYLAB User Meeting, DESY in Hamburg, 27.01. - 28.01.2005	S3
Hoell, A.; Zizak, I.; Haas, S.; Tatchev, D.; Bieder, H.; Banhart, J.: **The new SAXS instrument at BESSY - (7T-WLS-SAXS)** BESSY User Meeting 2005, Berlin / Adlershof, 01.12. - 02.12.2005	S3
Hoell, A.; Zizak, I.; Haas, S.; Tatchev, D.; Klobes, B.; Banhart, J.: **The new SAXS instrument at Bessy - first measurements** BESSY User Meeting 2005, Berlin / Adlershof, 01.12. - 02.12.2005	S3

Seminars and Conference Contributions 2005

Jauch, W.; Reehuis, M.: **Electron Density in Cubic $SrTiO_3$ from Gamma-ray Diffraction** XX Congress of the International Union of Crystallography, Florenz (Italien), 23.08. - 31.08.2005	gamma
Kamarad, J.; Prokhnenko, O.; Prokes, K.; Arnold, Z.: **Pressure induced non-collinear magnetic structures in Fe-based intermetallics** Joint 20th AIRAPT and 43rd EHPRG Conference, Karlsruhe, 26.06. - 01.07.2005	E4 IHP II: 447 IHP II: 549 NMI3: 1047 NMI3: 1085
Kammel, M.; Wiedenmann, A.; Heinemann, A.; Bönnemann, H.; Matoussevitch, N.: **Oxide coating of Co-Ferrofluids studied by polarized SANS** International Conference on Neutron Scattering 2005, Sydney, Australia, 27.11. - 02.12.2005	V4
Kammel, M.; Wiedenmann, A.; Heinemann, A.; Matoussevitch, N.; Bönnemann, H.: **Evidence for oxide coating in air stable Co-ferrofluids** 6. Ferrofluid-Workshop, Universität des Saarlandes, Saarbrücken, 20.07. - 22.07.2005	V4
Kardjilov, N.; Celso, F. L.; Hilger, A.; Triolo, R.: **Applied Neutron Tomography in Modern Archaeology** RICH Meeting, Triest, Italy, 12.12. - 13.12.2005	V7
Krist, T.: **Test of a two dimensional neutron spin analyzer** International Conference on Neutron Scattering 2005, Sydney, Australia, 27.11. - 02.12.2005	V14
Krist, T.: **Neutron optics from HMI Berlin** International Conference on Neutron Scattering 2005, Sydney, Australia, 27.11. - 02.12.2005	V14
Krist, T.: **Neutron optics state of the art in polarisation and collimation** International Workshop on Reflectometry, Off-specular scattering and GISANS, Villigen PSI, 23.10. - 26.10.2005	V14
Manke, I.; Haibel, A.; Kardjilov, N.; Strobl, M.; Rack, A.; Hilger, A.; Scholta, J.; Hartnig, C.; Banhart, J.: **Investigation of Fuel Cells by Means of In-situ Neutron Radiography and Synchrotron Tomography** European Congress on Advanced Materials and Processes 2005, Prague, Czech Republic, 05.09. - 08.09.2005	V7 S5 V12
Manke, I.; Haibel, A.; Kardjilov, N.; Strobl, M.; Rack, A.; Hilger, A.; Scholta, J.; Hartnig, C.; Zabler, S.; Banhart, J.: **Investigation of Fuel Cells by means of Synchrotron Tomography and In-Situ Neutron Radiography** BESSY User Meeting 2005, Berlin / Adlershof, 01.12. - 02.12.2005	V7 S5 V12
Manke, I.; Haibel, A.; Rack, A.; Kardjilov, N.; Hilger, A.; Melzer, A.; Banhart, J.: **Untersuchung von Alkaline-Batterien mit bildgebenden Verfahren** DGZfP Jahrestagung 2005, Rostock, Germany, 02.05. - 04.05.2005	S5 V7
Manke, I.; Kardjilov, N.; Haibel, A.; Hartnig, C.; Strobl, M.; Rack, A.; Hilger, A.; Scholta, J.; Lehnert, W.; Treimer, W.; Zabler, S.; Banhart, J.: **Untersuchung der Wasserverteilung in Brennstoffzellen** DGZfP Jahrestagung 2005, Rostock, Germany, 02.05. - 04.05.2005	V7 V12 S5
Nakamura, M.; Arai, M.; Kartini, E.; Talor, J.W.; Russina, M.: **Unique vibrational excitations in superionic conducting glass** The 3rd International Workshop on Complex Systems, Sendai, Japan, 16.11. - 18.11.2005	V3
Nakamura, M.; Iwase, H.; Arai, M.; Kartini, E.; Russina, M.; Yokoo, T.; Talor, J.W.: **Low energy vibrational excitations characteristic of superionic glass** International Conference on Neutron Scattering 2005, Sydney, Australia, 27.11. - 02.12.2005	V3

Seminars and Conference Contributions 2005

Peters, J.; Bleif, H.-J.; Kali, G.; Rosta, L.; Mezei, F.: **Performance of TOF powder diffractometers on reactor sources** International Conference on Neutron Scattering 2005, Sydney, Australia, 27.11. - 02.12.2005	
Peters, J.; Lieutenant, K.; Clemens, D.; Mezei, F:. **EXED, the new Extreme Environment Diffractometer at the HMI Berlin** Jahrestagung der Deutschen Gesellschaft für Kristallographie 2005, Köln, 28.02. - 03.03.2005	V15
Rack, A.; Haibel, A.; Manke, I.; Zabler, S.; Riesemeier, H.; Weidemann, G.; Goebbels, J.; Banhart, J.: **Chemical processes in commercial batteries studied by synchrotron-tomography and 3D image analysis** 69. Jahrestagung der DPG "Physik seit Einstein", Berlin, 04.03. - 09.03.2005	S5
Rack, A.; Knabe, C.; Gräber, H.G.; Stiller, M.; Apel, C.; Zabler, S.; Weidemann, G.; Riesemeier, H.; Goebbels, J.; Banhart, J.: **Regenerated bone tissue and human tooth tissue studied with high resolution synchrotron-tomography** BESSY User Meeting 2005, Berlin / Adlershof, 01.12. - 02.12.2005	S5
Rack, A.; Zabler, S.; Schladitz, K.; Godehardt, M.; Wiegmann, A.; Reif, S.; Haibel, A.; Manke, I.; Riesemeier, H.; Weidemann, G.; Goebbels, J.; Banhart, J.: **Analyse, Tomographie und Simulation von Mikrostrukturen** Industrietag HMI 2005, Berlin, Germany, 01.06. - 01.06.2005	S5
Rossner, H.H., Schmitz D., Imperia P., Maletta H., Krappe H.J., Rehr J.J.: **EXAFS and MEXAFS at overlapping L-edges** BESSY User Meeting 2005, Berlin / Adlershof, 01.12. - 02.12.2005	S1
Schmitz, D.; Imperia, P.; Maletta, H.; Tennant, D.A.; Goering, E.; Grüner, U.; Harlander, M.; Macke, S.; Schütz, G.: **Determination of magnetization depth profiles with X-Ray Resonant Magnetic Reflectometry** BESSY User Meeting 2005, Berlin / Adlershof, 01.12. - 02.12.2005	S1
Schmitz, D.; Imperia, P.; Rudorff, S.; Maletta, H.; Tennant, D.A.; Krzyzowski, M.A.; Wolfram, M.; Rohoff, M.; Einert, K.: **The new 7 T high magnetic field end station at UE46-PGM** BESSY User Meeting 2005, Berlin / Adlershof, 01.12. - 02.12.2005	S1
Schorr, S.; Hoebler, H.-J.; Tovar, M.: **Structure investigation of Kesterite-Stannite solid solution series** 83rd Annual Meeting of the German Mineralogical Society, Aachen, 09.09.2005 - 12.09.2005	E9
Schorr, S.; Wagner, G.; Goericke, D.; Tovar, M.: **Charakterisierung des 2-Phasengebietes in quaternären Halbleitermischkristallen mittels Neutronenbeugung und TEM-EDX** Sektionstreffen der Deutschen Mineralogischen Gesellschaft, München, 07.07. - 08.07.2005	E6
Schorr, S.; Wagner, G.; Tovar, M.; Stuesser, G.; Geandier, G.; Sheptyakov, D.: **Where the atoms are: cation disorder and anion displacement in DIIXVI-AIBIIIXVI2 semiconductors** International Conference on Neutron Scattering, Sydney, Australia, 27.11. - 02.12.2005	E6
Shin, T; Eltekov A.; Findenegg, G.H.; Keiderling U.; Brandt A.: **Adsorption and self-assembly of surfactants in MCM-41 type silicas studied by SANS** The 42nd Meeting of the German Colloid Society, Smart materials: foams, gels and microcapsules, Aachen, Germany, 26.09. - 28.09.2005	V4
Shin, T; Eltekov A.; Uredat S. ; Keiderling U. ; Findenegg, G.H.: **Adsorption and Self-Assembly of Surfactants in MCM-41 and SBA-15 Studied by SANS** 7th International Symposium on the Characterisation of Porous Solids, Aix-en-Provence, France, 25.05. - 28.05.2005	V4
Sikolenko, V.; Pomjakushina, E.; Zimmermann, U.; Gribanov, A. **μSR and neutron diffraction studies of $U(Ni_xCu_{1-x})_2Si_2$ magnetic structure** X International conference on muSR, Oxford, 08.08. - 12.08.2005	E1

Seminars and Conference Contributions 2005

Strunz, P., Schumacher, G.; Vassen, R., Wiedenmann, A.: **In-situ Small-angle Neutron Scattering Study of Novel Ceramic Materials for Thermal Barrier Coatings** EUROMAT 2005, Prague, 05.09. - 08.09.2005	V4
Teichert, A, Krist, T., Mezei, F: **Stress dependence in Si-FeCo multilayers on sputter parameters** International Conference on Neutron Scattering 2005, Sydney, Australia, 27.11. - 02.12.2005	V14
Tennant, D.A.; McLain, S.E.; Turner, J.F.C.; Barnes, T.: **Magnetic excitations in exotic silver(II)fluorides** International Conference on Neutron Scattering 2005, Sydney, Australia, 27.11. - 02.12.2005	
Tovar, M., Torabi, R., Welker, C., Fleischer, F.: **Structural and magnetic properties of Cu-Ni-Cr spinel oxides** International Conference on Neutron Scattering 2005, Sydney, Australia, 27.11. - 02.12.2005	
Wawrzynska, E.; Balanda, M.; Baran, S.; Gondek, L.; Hernandez-Velasco, J.; Kaczorowski, D.; Leciejewicz, J.; Penc, B.; Stuesser, N.; Szytula, A.: **Magnetic properties of RT_2Ge_2 (R=Pr and Nd; T=Cu, Ag or Fe)** XVII International School on Physics and Chemistry of Condensed Matter, Materials in Transition, Bialowieza, Poland, 20.06. - 29.06.2005	E6
Wawrzynska, E.; Balanda, M.; Baran, S.; Leciejewicz, J.; Penc, B.; Stuesser, N.; Szytula, A.: **Commensurate-incommensurate magnetic phase transitions in $PrCu_2Ge_2$ and $NdFe_2Ge_2$** Katowicko-Krakowskie Seminarium Fazy Skondensowanej, Krakow, Poland, 22.01. - 22.01.2005	E6
Wawrzynska, E.; Hernandez-Velasco, J.; Penc, B.; Szytula, A.; Tomala, K.: **Magnetic properties of $R_3Ag_4Sn_4$ (R=Pr, Nd) and $Nd_3Cu_4Ge_4$ compounds** Katowicko-Krakowskie Seminarium Fazy Skondensowanej, Krakow, Poland, 22.01. - 22.01.2005	E6 NMI3: 1027
Wawrzynska, E.; Szytula, A.: **Ordering schemes in $R_3T_4X_4$ (R-rare earth, T=Mn, Cu, Pd, X=Ge, Sn)** MAG-EL-MAT Members' Meeting, Bedlewo, Poland, 02.05. - 06.05.2005	E6 IHP II: 466 IHP II: 519 IHP II: 578 NMI3: 1027
Wiedenmann, A.; Keiderling, U.; May, R.P.; Dewhurst, C.: **Dynamics of Field Induced Ordering Processes in Ferrofluids Studied by Polarised Small Angle Neutron Scattering** International Conference on Neutron Scattering 2005, Sydney, Australien, 27.11. - 02.12.2005	V4
Wiedenmann, A.; May, R.P.; Dewhurst, C.; Haug, J.; Heinemann, A.; Kammel, M.; Keiderling, U.: **Time dependence of field induced ordering processes in Ferrofluids studied by Small Angle Neutron Scattering** DFG Kolloquium SPP 1104, Benediktbeuren, Germany, 28.11.2005	V4
Wollgarten, M., Hiller, S.; Vierke, J.; Haibel, A.; Schubert-Bischoff, P.; Sahoo, K.L.; Banhart, J.: **Study of the Microstructure of Rapidly Solidified Al-Ni-La-Zr Alloys by Synchrotron-Tomography and Transmission Electron Microscopy** Microscopy Conference, Dreiländertagung, Davos, Switzerland, 28.08. - 02.09.2005	S5 TEM
Zabler, S.; Haibel, A.; Rack, A.; Rueda, A.; Riesemeier, H.; Weidemann, G.; Goebbels, J.; Banhart, J.: **Study of semi-solid casting and processing with X-ray phase-sensitive tomography** DPG Tagung 2005, Berlin, Germany, 04.03. - 09.03.2005	S5
Zabler, S.; Rack, A.; Haibel, A.; Weidemann, G.; Riesemeier, H.; Goebbels, J.; Banhart, J. **Determination of partial transverse beam coherence at BAMline by means of Talbot imaging** BESSY User Meeting 2005, Berlin / Adlershof, 01.12. - 02.12.2005	S5

Contributions to the 13th BENSC Users' Meeting, September 2005

INVITED ORAL CONTRIBUTIONS

Alan Tennant, HMI Berlin
"SF2 in the future"

Ingwer Denks, HMI Berlin
"Presentation of the energy dispersive diffraction ('EDDI') beamline at BESSY"

Nikolay Kardjilov, HMI Berlin
"CONRAD - the new multifunctional tomography facility with cold neutrons at HMI"

Roberto Triolo, Univ. Palermo, I
"Combining SANS, USANS and neutron tomography to uniquely trace the source of white and polychromic marbles of archaeological interest"

Birgit Schröder-Smeibidl, HMI Berlin
"Cultural Heritage: Neutron autoradiography of paintings"

Arnaud Desmedt, Univ. Bordeaux, F
"Dynamics in clathrates hydrates"

Taegyu Shin, TU Berlin, Stranski Lab
"SANS study of surfactant adsorption in ordered masoporous silica"

Debora Berti, Univ. Firenze, I
"Amphiphilic self assemblies decorated by nucleobases"

Doreen Otto, MLU Halle
"New insights into the structure of the stratum corneum lipid model matrix by neutron diffraction"

Alexandra Buchsteiner, HMI Berlin
"QENS study of the water dynamics in graphite oxide"

Lev Smirnov, RF SSC ITEP Moscow & JINR, RU
"The crystal structure investigation of different phases of $[Rb_x(Nh_4)_{1-x}]_3H(SO_4)_2$ (neutron single crystal diffraction)"

Ewa Wawrzynska, Univ. Bristol, UK
"Magnetic structures of the $R_3T_4X_4$ rare earth intermetallics"

Blanka Janousova, CU Prague, CZ
"Magnetic structure of CePtSn"

Enrico Faulhaber, TU Dresden
"Setup of in-situ ac-suszeptibility measurement during neutron scattering"

Markus Hölzel, TU DA & TUM FRM II
"Ni-Fe-superalloys"

POSTER PRESENTATIONS

TAS Instruments E1, V2 (FLEX)

Flachbart, K.; Gabani, S. - IEP SAS Kosice, SK
Mataš, S., Shitsevalova, N. - NAS Kiev, UA
Paderno, Y.; Lonkai, T. - Uni Tübingen
N. Stüßer, N.; Prokeš, K. - HMI Berlin
Sikolenko, V.V.; Siemensmeyer, K. - HMI Berlin
Magnetism in HoB_{12} (E1, E2)

Rüegg, C. - UCL, UK & ETH PSI Zurich, CH
Furrer, A.; Thielemann, B. - ETH PSI Zurich
Krämer, K.; Güde, H.-U. - Univ. Bern, CH
Habicht, K.; Vorderwisch, P.; Gerischer, S.; Smeibidl, P.; Meissner, M.; Kiefer, K.; Wand, T. - HMI Berlin
Quantum phase transitions in dimer spin systems and novel organic quantum magnets (V2)

Fåk, B.; Niklowitz, P.G. - UCL, UK; Rüegg, C.; McMorrow, D.F. - ETH Zurich & PSI Villigen
Canfield, P.C.; Bud'ko, S.L.; Janssen, Y. - Univ. Bern, CH; Habicht, K.; Gerischer, S.; Smeibidl, P.; Meissner, M. - HMI Berlin
Study of the magnetic phase diagram and the spin fluctuations in a field-induced non-fermi liquid (V2)

Diffraction, Instruments E2, E9

Hoffmann, J.-U. - HMI Berlin
Amann, U.; Ihringer, J. - Uni Tübingen
The next generation of flat-cone diffraction (E2)

Hoffmann, J.-U. - Univ. Tübingen & HMI Berlin
Schneider, R. - HMI Berlin
New approach to international standardization in neutron instrument software (E2)

Raasch, S.; Dörr, M. - TU Dresden
Kreyssig, A.; Loewenhaupt, M. - TU Dresden
Rotter, M. - Univ. Wien, A
Hoffmann, J.-U. - HMI Berlin
Paramagnetic shape memory (P-MSM) in RCu_2 (E2)

Frontzek, M.; Kreyssig,A. - TU Dresden
Faulhaber, E.; Loewenhaupt, M. - TU Dresden
Hoffmann, J.-U. - HMI Berlin
Baehr, C.; Mazim, I. - IFW Dresden
Magnetic structure investigation of R_2PdSi_3 (R = Tb, Er, Tm) compounds (E2)

Frontzek, M.; Kreyssig, A. - TU Dresden
Doerr, M.; Loewenhaupt, M. - TU Dresden
Hoffmann, J.-U. - HMI Berlin
Bitterlich, H.; Behr, G. - IFW Dresden
Long and short-range magnetic order of Tb_2PdSi_3 in an applied magnetic field (E2)

Contributions to the 13th BENSC Users' Meeting, September 2005

Amann, U. - HMI Berlin; Ritter, C. - ILL Grenoble
Ihringer, J. - Univ. Tübingen
Magnetic phase transitions in electron-doped manganites (E2)

Vecchini, C.; Moze, O. - Univ. Modena, I
Argyriou, D. - HMI Berlin; Michels, - A. PSI & Uni Saarland; Weissmüller, J. - FZ Karlsruhe
The magnetic structure of nanocrystalline terbium (E9)

Auffermann, G.; Chemnitzer, R.; Kniep, R. - MPI CPfS Dresden
N. Stüßer, N.; Többens, D.M.; Tovar, M. - HMI Berlin
Using neutron diffraction for the localization of light elements (E9)

Schorr, S.; Kloess, G. - Univ. Leipzig
Tovar, M. - HMI Berlin
Geandier, G. - ESRF Grenoble, F
Nano- hematite in obsidian: a study using neutron and synchrotron diffraction (E9)

Schorr, S.; Höbler, H.-J. - Univ. Leibzig
Tovar, M. - HMI Berlin
Structure Investigation of the Kesterite-Stannite Series solid solution (E9)

Wolska. E.; Nowicki, W.; Darul, J.; Piszora, P. - AMU, Poznan, PL
Tovar, M. - HMI Berlin
Structural and magnetic studies of spinel oxides (E9)

Gilles, R. - TU München; Mukherji, D. - ETH / IAP Zürich, CH; Hoelzel, M. - TUM & TU Darmstadt
Strunz, P. - NPI, Rez/ Prague, CZ
Toebbens, D.M. - HMI Berlin
Barbier, B. - Dep. of Mineral. and Petrol., Bonn
Neutron and X-ray diffraction measurements on micro-and nano-sized precipitates embedded in a Ni-base superalloy and after their extraction from the alloy (E9)

Efimov, V. - JINP, Dubna, RU; Sikolenko, V.V. - HMI Berlin; Iakoubovskii, K. - KU Leuven, BE
Sternberg, A.; Kuzmin, A. - ISSP, Latvia
Neutron diffraction studies of the relaxor PLZT 8/65/35 powder irradiated by high-current pulsed electron beam (E9)

Hernandez-Velasco, J.; Argyriou, D. - HMI Berlin
Nunes-Bordallo, H. - ILL, Grenoble, F
Chapon, L. - ISIS, Chilton, UK
Landa-Canovas, A. - CSIC, ICM Madrid, E
Manson, J.L. - ORNL, US
Magnetic order and crystal disorder in the molecular magnet $Fe(NCS)_2pyz_2$ (E9)

Sazonov, A.P. - RWTH Aachen & ISSP, NAS, Minsk, BY; Troyanchuk, I.O. - ISSP, NAS, Minsk
Sikolenko, V.V. - HMI Berlin
Szymczak, H. - PAS Physics,Warsaw, PL
Crystal structure and magnetic properties of the $Nd_{1-x}Ba_xCoO_3$ system (E9)

Two Axis Diffractometer E4

Prokeš, K. - HMI Berlin
Manuel, P.; Adroja, D.T. - RAL ISIS, UK
Magnetic order in CePdAl single crystal: Effect of magnetic field (E4)

Kamarád, J.; Arnold, Z. - ASCR IP Prague, CZ
Prokhnenko, O.; Prokeš, K. - HMI Berlin
Magnetism in Y_2Fe_{17} under high pressure (E4)

Prchal, J.; Javorský, P. - CU Prague, CZ
Prokeš, K. - HMI Berlin
Andreev, A.V. - ASCR IP & CU Prague, CZ
Field-induced changes in magnetic structure of DyNiAl (E4)

Four Cycle Diffractometer E5

Smirnov, L.S. - RF SSC ITEP Moscow & JINR, RU
Natkaniec, I. - JINR Dubna, RU & IFJ, Krakow, PL
Loose, A. - HMI Berlin
Wozniak, K.; Dominiak, P. - Univ. Warsaw, PL
Zink, N.; Melnyk, G. - Uni Mainz
Pawlukojc, A. - JINR, Dubna, RU & SAA Warsaw, PL
Martinez Sarrion, M.L.; Mestres, L.; Herraiz, M. - Univ. Barcelona, E
The study of crystal structure and dynamics of the $K_{2-x}(NH_4)_xSeO_4$ mixed crystals by means of neutron scattering (E5)

Loose, A. - HMI Berlin
Smirnov, L.S. - RF SSC ITEP Moscow & JINR, Dubna, RU
Natkaniec, I. - JINR, Dubna, RU & IFJ, Krakow, PL
Dolbinina, V.V.; Yakovleva, L.M.; Grebenev, V.V. - RAS IC Moscow, RU
The ordering of ammonium in ferroelectric phase II of β-$LiNH_4SO_4$ (E5)

Reehuis, M.; Ulrich, C.; Keimer, B. - HMI Berlin
The influence of octahedral tilting and Jahn-Teller distortion in YTiO3: a neutron and x-ray diffraction study (E5)

Membrane Spectrometer V1

Kiselev, M.A.; Ryabova, N.Y.; Balagurov,A.M. - FLNP / JINR, Dubna, RU; Otto, D.; Neubert, R.H.H.; Wartewig, S. - MLU Halle
Dante, S.; Hauss, T. - HMI Berlin
Influence of ceramide 6 on the structure and hydration of multilamellar DPPC membrane (V1)

SANS Instrument V4

Ulbricht, A.; Bergner, F. - FZ Rossendorf
Heinemann, A. - HMI Berlin
Small-angle scattering applied to post-irradiation annealing of neutron-irradiated pressure vessel steels (V4)

Contributions to the 13th BENSC Users' Meeting, September 2005

Strunz, P. - NPI, Rež near Prague, CZ
Schumacher, G.; Wiedenmann, A. - HMI Berlin
Vassen, R. - FZ Jülich
In-situ small-angle neutron scattering study of LZO and SZO ceramics (V4)

Iolin, E.; Rusevich, L. - L.A.S., Riga, LV
Strobl, M.; Treimer, W. - HMI Berlin
Mikula, P. - NPI, Rež near Prague, CZ
Inelastic neutron scattering by ultrasound. Research by Bonse-Hart and DC diffractometers (V4 & V12b)

Morales-Flórez, V.; de la Rosa-Fox, N.; Piñero, M.; Toledo-Fernández, J.A.; Esquivias, L. - Univ. Cadiz, E
Hybrid organic/inorganic silica aerogels: control of mechanical behaviour (V4)

Wiedenmann, A.; Haug, J.; Heinemann, A.; Kammel, M.; Keiderling, U. - HMI Berlin
R.P. May, R.P.; Dewhurst, C. - ILL Grenoble, F
Time dependence of field induced ordering processes in Ferrofluids studied by SANS (V4)

Kammel, M.; Heinemann, A.; Wiedenmann, A. - HMI Berlin; Matoussevitch, N.; Bönnemann, H. - MPI für Kohlenforschung, Mühlheim a.d.R.
Evidence for oxide coating in air stable Co-ferrofluids (V4)

A. Heinemann, A.; Wiedenmann, A.; Kammel, M. - HMI Berlin; Buske, N.
SANS investigation of field induced structures in very high concentrated ferrofluids (V4)

Reflectometer V6

Gopinadhan, M.; Ahrens, H.; Günther, J.-U.; Helm, C.A. - EMAU Greifswald
Steitz, R. - HMI Berlin
Internal order in polyelectrolyte multilayers (V6)

Wesemann, A.; Ahrens, H.; Helm, C.A. - EMAU Greifswald; Steitz, R. - HMI Berlin
Förster, S. - Uni Hamburg
Temperature dependence of PEO brushes in PEE_{797}-PEO_{893} diblock copolymer monolayer at the air/water interface (V6)

Rehfeldt, F.; Tanaka, M. - TU München
Steitz, R. - HMI Berlin; von Klitzing, R. - CAU Kiel
Armes, S.P. - Univ. Sheffield, UK
Gast, A.P. - MIT Cambridge, US
Reversible activation of diblock copolymer monolayers by ph modulation - tuning membrane interactions at the solid/liquid interface (V6)

Wong, J.E. - RWTH Aachen
Steitz, R. - HMI Berlin; von Klitzing, R. - CAU Kiel
Kinetics of swelling in adsorbed polyelectrolyte multilayers (V6)

Mishra, N.C.; Müller, H.-J.; Möhwald, H.; Krastev, R. - MPI Potsdam
Interfacial effect on moisture absorption in thin polyelectrolyte film (V6)

Cold n Tomography CONRAD V7

Matsushima, U. - Iwate Univ., JP
Kawabata, Y. - Kyoto Univ., JP
Kardjilov, N. - HMI Berlin
Herppich, W. - ATB Potsdam
The potential of neutron and X-ray imaging to observe water transport in plants (V7)

Triolo, R.; Lo Celso, F.; Benfante, V.; Ruffo, I. - Univ. Palermo, I
Kardjilov, N.; Strobl, M.; Hilger, A. - HMI Berlin
Barker, J.; Butler, P. - Gaithersburg, USA
Applicatrion of Neutron Techniques in Archaeometry (V7)

Instrumental Developments and Other

Hoell, A.; Zizak, I; Haas, S.; Banhart, J. - HMI Berlin
Klobes, B. - Uni Bonn
The new SAXS instrument at BESSY - first results (S3: SAXS**)**

Keiderling, U. - HMI Berlin
New features of the "BerSANS-PC" software for reduction and handling of SANS data

Krist, T.; Hoffmann, J.-E.; Mezei, F. - HMI Berlin
Neutron Optical Elements from HMI Berlin (V14)

Genzel, C.; Stock, C.; Denks, I.; Klaus, M. - HMI Berlin
The High Energy Materials Research Beamline EDDI for Energy Dispersion Diffraction Analaysis (S4: EDDI**)**

Ohms, C.; Wimpory , R.; Schneider, R.; Poste, T. - HMI Berlin
The impact of grain size of residual stress measurement in welded components (E3)

Dudzik, E.; Feyerherm, R.; Wagner, G. - HMI Berlin
The synchrotrone beamlime MagS

AUTHOR INDEX

AUTHOR INDEX

author	page
A	
Abbas, S.	155
Abetz, V.	107
Adroja, D.T.	18, 53
Aeppli, G.	41
Alba, M.	55
Alff, L.	38
Aliotta, F.	101
Aliouane, N.	183, 184
Amann, U.	10, 11, 14, 58
Arai, M.	84, 85
Aranghel, D.	83
Aree, T.	93, 97
Argyriou, D.	29, 32, 35, 64, 66, 76, 183, 184
Arrighi, V.	100
Aso, N.	22
Auffermann, G.	63, 66
B	
Baglioni, P.	124
Banhart, J.	185, 190
Bansmann, J.	172
Baran, S.	28
Barla, A.	172
Bärner, K.	30, 35
Bartoll, J.	147
Bartolome, J.	37
Bauer, E.A.	53
Bedanta, S.	128
Behr, N.	171
Berthold, A.	190
Berti, D.	105
Betti, F.	105
Bianchi, A.D.	42
Bianco-Peled, H.	104
Blanco, J.A.	127
Bleif, H.J.	60, 61
Boeglin, C.	172
Bonarski, J.T.	59
Bonini, M.	124
Bordignon, E.	89
Borisov, S.	75
Borowiec, M.T.	8
Boschetti de Fierro, A.	107
Boue, F.	108
Braden, M.	49
Bradshaw, J.	90
Brakhman, E.V.	156
Brandt, A.	105, 109, 112
Bringezu, F.	86
Bryant, G.	106
Buchsteiner, A.	54, 82, 83, 93, 100, 101
Bulut, F.	172
C	
Calbucci, V.	132, 149
Campo, J.	37, 43, 127
Cantu, L.	96
Cartier dit Moulin, C.	174
Chatterji, T.	11
Christianson, A.	40
Christides, C.	64
Clemens, D.	108, 110, 170
Coldea, R.	6
Cornia, A.	174
Cosgrove, T.	110
Cousin, F.	108
D	
da Silva Wheeler, E.	6
Dahlborg, U.	141
Dai, P.	50, 52
Danilyan, A.S.	156
Danilyan, G.V.	156
Dante, S.	86, 87, 88, 91
Darul, J.	65, 68
Dathe, M.	92
de Beer, F.	164
De La Prida, V.	127
de la Rosa-Fox, N.	138
de Teresa Nogueras, J.M.	44
Dencher, N.	88
Denks, I.	187, 188, 189
Deriu, A.	96
Desmedt, A.	81
Dobner, B.	87
Donato, D.I.	150
Dudzik, E.	181, 182, 183, 184
E	
Efimov, V.	137
Eichelbaum, M.	185
Erne, B.	129
F	
Fak, B.	39
Faulhaber, E.	14
Feyerherm, R.	183, 184
Fiebig, M.	12
Fierro, D.	107
Findenegg, G.H.	112
Fiori, F.	132
Flachbart, K.	16, 19, 46
Flores Renteria, A.	139
Freidank, H.	190
Frontera, C.	5
Frontzek, M.	7, 14
Fujisawa, M.	3
G	
Gähler, R.	119, 158
Gamari-Seale, H.	31
Garab, G.	91, 95
Garcia-Matres, E.	43, 104, 127
García-Muñoz, J.L.	5
Garvey, C.J.	106
Gatteschi, D.	174
Genzel, C.	187, 188, 189
Gerdes, T.	125
Gerischer, S.	3
Getzlaff, M.	172
Giersig, M.	176
Gil Posada, J.	73
Gilles, R.	115, 140
Glaczytska, H.	176
Glavatskyy, I.	9
Goering, E.	179
Gradzielski, M.	107
Graf, H.A.	3
Griveau, J.-C.	17
Grüner, U.	179
Grünerbel, M.	142
Gruyters, M.	178
Gugiu, M.	83
Gummel, J.	108
H	
Haas, S.	185
Habicht, K.	39, 40, 41, 49, 50, 51, 52, 77, 78, 79, 119, 157, 158
Haibel, A.	190, 192
Hall, P.J.	73
Harlander, M.	179
Hartnig, C.	142
Haug, J.	42, 116, 117, 118, 139, 140, 141
Haußß, T.	86, 87, 88, 89, 90, 92
Heczko, O.	133
Heil, W.	159
Heinemann, A.	44, 45, 107, 122, 123, 128
Hernández-Velasco, J.	5, 28
Herppich, W.	98
Herrero-Albillos, J.	43
Hilger, A.	98, 142, 150, 161, 162, 163, 164
Hoell, A.	185
Hoffmann, J.-E.	171
Hoffmann, J.-U.	5, 6, 7, 8, 9, 10, 11, 12, 14, 56, 57, 58, 130
Hofmann, A.	90

AUTHOR INDEX

author	page
Hofmann, T.	103
Hohl, A.	74
Höhn, P.	63, 66
Hölzel, M.	115
Hoser, A.	1, 4, 10, 27
Hu, N.-J.	90
Huber, P.	103
Hütten, A.	128
I	
Iakoubovskii, K.	137
Ihringer, J.	130
Imperia, P.	172, 174, 176, 179
Irrgang, K.-D.	94, 95
J	
Jackisch, B.	147
Jardin, R.	17
K	
Kaczerowski, J.	142
Kaczorowski, D.	28
Kaden, R.	36
Kaiser-Bischoff, I.	56
Kamarád, J.	20, 21
Kammel, M.	42, 97, 122, 123, 125, 128, 149
Kandulski, W.	176
Kardjilov, N.	98, 142, 150, 151, 161, 162, 163, 164
Karpinsky, D.	30, 33, 45
Kartini, E.	84, 85
Kausche, S.	23
Keiderling, U.	74, 106, 111, 119, 120, 126, 138, 148, 158, 159, 160
Keimer, B.	24, 25, 26, 61, 78
Keller, T.	78
Kenzelmann, M.	42
Kiselev, M.	87
Klaus, M.	181, 182
Kleemann, W.	128
Kleibert, A.	172
Klenke, J.	2, 4, 47, 159
Klokkenburg, M.	129
Klösgen, B.	92
Klöß, G.	134
Kniep, R.	63, 66
Köbler, U.	4, 10, 27
Köhl, M.	130
Kolasi_ska, M.	114
Kosiorek, A.	176
Kouzmine, A.	93, 97
Kozhukharov, V.	69
Krakhotin, V.A.	156
Krastev, R.	114
Kremmin, B.	192
Kreyßig, A.	14
Krist, T.	171
Krockenberger, Y.	38
Krumova, S.	91, 95
Kucharik, M.	136
Kumar, P.	103
Kuzmin, A.	137
L	
Lake, A.B.	41, 60
Laurenze-Landsberg, C.	143, 144, 145, 146, 147
Lechner, R.	93, 97
Lenné, T.	106
Li, S.	50, 52
Lieutenant, K.	89
Liu, C.-T.	126
Lo Celso, F.	151, 154
Lobanovsky, L.	35
Lonkai, T.	8
M	
Macke, S.	179
Maier, B.	58
Majerowicz, M.	86
Malcherek, T.	70
Maletta, H.	176, 178, 179
Mançois, F.	81
Manescu, A.	132, 149, 153
Mangiapia, G.	109
Manke, I.	142, 167, 192
Mannini, M.	174
Manuel, P.	18
Matas, S.	16, 19, 46
Matsushima, U.	98
Mayorova, M.	102, 103
McMorrow, D.	39
Mehta, A.	63
Meiwes-Broer, K.H.	172
Mertens, L.A.	143, 144, 145, 146, 147
Mezei, F.	78, 84, 170
Mitsuda, S.	23
Mokrani, L.	170
Molnar, P.	135
Mondragon Rodriguez, C.G.	82
Morales-Flórez, V.	138
Movshovich, R.	42
Moze, O.	29, 47, 48
Mukherji, D.	115, 140
N	
Naberezhnov, A.	75
Nakajima, T.	23
Nakamura, M.	84, 85
Natali, F.	96
Natalia, B.	5
Nefeodova, E.	54
Neov, S.	69
Neubert, R.	87
Neumann, O.	167, 168
Niemann, A.	147
Niewa, R.	66
Niklowitz, P.	39
Novak, V.	135
Nowicki, W.	65, 68
O	
Odenbach, S.	125
Ohms, C.	131
Olek, W.	59
Onimaru, T.	22
Ono, T.	3
Otto, D.	87
P	
Paduano, L.	109
Panayiotou, C.	99
Pappas, C.	55
Park, J.-G.	53
Pavlov, V.S.	156
Perroud, O.	121
Peters, J.	59
Petracic, O.	128
Pieper, J.	80, 83, 94, 95, 96
Pissas, M.	32
Plugaru, N.	37
Poeste, T.	131
Pop, L.M.	125
Prager, M.	81
Pritula, O.	136
Prokes, K.	17, 18, 19, 20, 21, 22, 23, 133
Prokhnenko, O.	20, 21, 34, 35, 37, 68, 69, 72, 76
Psycharis, V.	64
Pulagam, V.L.P.	89
R	
Raasch, S.	7
Rademann, K.	185
Radulescu, A.	83
Rebizant, J.	17
Reehuis, M.	24, 25, 26, 38, 59, 60, 61
Reznik, D.	76
Rimke, M.	162
Ritzoulis, C.	99
Rösler, J.	140
Ross, K.	57
Rubin, J.	37
Rüegg, C.	39, 51
Ruffo, I.	152

AUTHOR INDEX

author	page
Rupp, A.	2, 159
Russina, M.	53, 73, 81, 84, 85, 102, 103, 156, 158, 170
Russina, O.	111
Ryabova, N.	87

S

Sadykov, R.	1
Saenger, W.	93, 97
Saija, F.	101
Sainctavit, P.	174
Saruhan-Brings, B.	82, 116, 117, 139
Sazonov, A.	30, 31
Schmidt, C.	143, 144, 145, 146
Schmidt, H.	130
Schmitz, D.	176, 178, 179
Schneider, R.	130
Schorr, S.	36, 71, 134
Schreiber, F.	58
Schröder-Smeibidl, B.	143, 144, 145, 146, 147
Schubert, H.	190
Senff, D.	49
Sessoli, R.	174
Shamai, K.	104
Shapiro, S.M.	77
Sharp, M.	110
Shatalov, P.	156
Sheptyakov, D.	24
Shin, T.	112
Siemensmeyer, K.	16, 19, 46, 54
Sikolenko, V.V.	1, 3, 4, 30, 31, 46, 48, 75, 137
Simon, P.	107
Sittner, P.	135
Skomorokhov, A.N.	80
Smeibidl, P.	6, 42
Smrcok, L.	136
So, J.-Y.	53
Sobolev, O.	80
Staack, K.	166
Stamopoulos, D.	32
Statescu, M.	83
Stefanopoulos, K.L.	31
Sternberg, A.	137
Stoica, A.D.	126
Stranzenbach, M.	82
Strobl, M.	99, 152, 153, 154, 155, 162, 163, 165, 166, 167, 168, 169
Strunz, P.	115, 118, 140
Stüßer, N.	1, 27, 28
Süllow, S.	2, 34, 72
Szymczak, H.	33, 45

T

Tanaka, H.	3
Tanchawanich, J.	100
Tatchev, D.	185
Tennant, D.A.	6, 60, 179
Thermann, K.	192
Thielemann, B.	51
Thillosen, N.	158
Tiden, N.	54
Tiedemann, J.	192
Titova, S.	80
Tovar, M.	33, 34, 35, 36, 37, 38, 62, 63, 65, 67, 68, 70, 71, 72, 115, 134, 135, 136
Treimer, W.	155, 162, 165, 166, 167, 168, 169
Triolo, A.	111
Triolo, R.	148, 151, 150, 152, 154
Tripadus, V.	83
Troyanchuk, I.O.	30, 31, 35

U

Ulrich, C.	24, 25, 26, 61
Urubkov, I.	9

V

Vasi, C.	101
Vecchini, C.	29, 47, 48
Velinov, N.	69
Vorderwisch, P.	77

W

Wagh, A.G.	155
Wallacher, D.	103
Wang, X.-L.	126
Warszynski, P.	114
Wawrzynska, E.	28
Weber, F.	76
Werner, F.	67
Wiedenmann, A.	42, 44, 116, 117, 119, 120, 121, 122, 123, 124, 125, 129, 139, 158, 159, 160
Wilpert, T.	156
Wilson, S.	50, 52
Wimpory, R.	131, 132
Winter, H.	178
Wolska, E.	65, 68
Woodward, A.	110

Y

Yusuf, S.M.	44

Z

Zabler, S.	192
Zhang, L.F.	57
Zizak, I.	185
Zobbi, L.	174
Zorn, R.	102, 103
Zrnik, J.	118